TD

Chemical analysis and in vitro cytotoxicity assessment of synthetic cathinones found in seized products

DOCTORAL THESIS

João Luís Jesus Gonçalves
DOCTORATE IN CHEMISTRY

UNIVERSIDADE da MADEIRA
A Nossa Universidade
www.uma.pt

December | 2022

FCT
Fundação para a Ciência e a Tecnologia
MINISTÉRIO DA EDUCAÇÃO E CIÊNCIA

Chemical analysis and in vitro cytotoxicity assessment of synthetic cathinones found in seized products

DOCTORAL THESIS

João Luís Jesus Gonçalves
DOCTORATE IN CHEMISTRY

ORIENTATION
José Sousa Câmara

COORIENTATION
Helena Maria de Sousa Ferreira e Teixeira

Chemical analysis and *in vitro* cytotoxicity assessment of synthetic cathinones found in seized products

A thesis presented to the University of Madeira to obtain the Doctoral degree in Chemistry

João Luís Jesus Gonçalves

Under the supervision of:

Professor Doutor José Sousa Câmara

Professora Doutora Helena Maria de Sousa Ferreira e Teixeira

The work presented in this dissertation was performed in Centro de Química da Madeira (CQM) of Universidade da Madeira supported by Fundação para a Ciência e a Tecnologia (FCT) through the PhD grant: SFRH/BD/116895/2016. The support of PROEQUIPRAM - Reforço do Investimento em Equipamentos e Infraestruturas Científicas na RAM (M1420-01-0145-FEDER000008), project M1420-01-0145-FEDER-000005-CQM+ (Madeira 14-20 Program), and FCT throught the CQM Projects: UID/QUI/00674/2015, PestOE/QUI/UI0674/2019. Base Fund UIDB/00674/2020 and Programmatic Fund UIDP/00674/2020, were also acknowledged.

Cofinanciado por:

ACKNOLEDGMENTS

This space is dedicated to all those who contributed, directly or indirectly, to this dissertation. To all of them I would like to express my sincere thanks.

My first words of thanks go to Professor Doctor Helena Teixeira, for her guidance, encouragement and constant support, despite the distance, she was always available to answer any questions, or solve any problems that arose throughout this work. I am very grateful for the attention, encouragement and understanding throughout the completion of this project.

I also express my gratitude to Professor Doctor José Sousa Câmara for his guidance, opportunity, availability, imparted knowledge and all the support provided to complete this work.

To Doctor Carlos Farinha and Doctor Maria João Caldeira of the Forensic Science Laboratory of Portuguese Criminal Police for their collaboration and for providing the samples and the analytical standards essential to this work.

To Professor Doctor Helena Tomás, for accepting me to perform part of the experimental work in the Laboratory of Biochemistry and Cellular Culture of the Centro de Química da Madeira. I would also like to express my gratitude to Doctor Mara Gonçalves for all the support, knowledge, help and patience during the cell culture assays.

To Professor Doctor João Rodrigues, for accepting me to carried out part of the experimental work in the in Laboratory of Nuclear Magnetic Resonance of the Centro de Química da Madeira. A special thanks to Doctors Cláudia Camacho, Dina Maciel and Ana Olival, for all the help and patience in the NMR analysis.

To Fundação para a Ciência e a Tecnologia (FCT) for funding the PhD scholarship (SFRH/BD/ 116895/2016) without which this project would not have been possible.

To the Universidade da Madeira and the Centro de Química da Madeira (CQM) for the conditions provided for the development of this project.

To Unidade de Tratamento de Toxicodependência do Serviço de Saúde da Região Autónoma da Madeira (SESARAM), especially to Doctor Daniel Neto, to Nurse José Manuel and all the nurses and auxiliary staff, I express my gratitude for their availability and collaboration in the development of this work. I would also like to express my gratitude and solidarity to all the patients who, although anonymous, made a fundamental contribution to make this study possible.

I would like to thank all colleagues of the Analytical Chemistry Laboratory of the Centro de Química da Madeira for their support, affection and good mood. A special thanks to Mariangie Castillo for her friendship, help and her funny stories that make me smile. To Doctor

Jorge Pereira and Doctor Rosa Perestrelo for their knowledge and help with equipment and analytical methods and for their availability to solve some problems that arose throughout these years.

I would also like to express a special word of appreciation and thanks to my colleague and friend Vera Alves, for the support, help, friendship, laughs, and encouragement throughout this long journey that we share with all its ups and downs.

Last but not least, I would like to express my deep gratitude to my family who were always there to support me. I am eternally grateful for your prayers, immense love, patience and trust that made it possible for me to continue this journey. In particular, to my parents, João Gonçalves and Delta Gonçalves, and my brothers for being models of courage, for their unconditional love and support, encouragement, friendship, patience and total help in overcoming the obstacles that along this journey have emerged. To my wife, Joselin Aguiar, for playing an important role in my life, for her love, constant support, encouragement, optimism and especially for making me smile on the greyest days. To all of them my deep and sincere thanks.

ABSTRACT

The abuse of synthetic cathinones (SCat) represents a serious public health problem, and despite the legislative efforts to control the availability and use of these substances, new derivatives continue to appear in the market. Monitoring these substances is a challenging task faced by forensic and toxicological laboratories, due to the closely related molecular structures that lead to similar analytical characteristics. Moreover, with the emergence of new substances, information about their potential toxicity is unknown and the effects can be dangerous and unpredictable.

The first purpose of this work was to chemically characterize fourteen seized products suspected to contained SCat, using several complementary analytical techniques, namely infrared spectroscopy (IR), gas chromatography coupled to mass spectrometry (GC-MS), ultrahigh performance liquid chromatography with photodiode array detector (UHPLC-PDA) and nuclear magnetic resonance (NMR). It was possible to identify nine SCat, namely methylone, methedrone, *N*-ethylcathinone, buphedrone, pentedrone, 3-fluoromethcathinone (3-FMC), 4-fluoromethcatinone (4-FMC), α-pyrrolidinohexanophenone (α-PHP) and 4-methyl-α-pyrrolidinohexanophenone (MPHP).

Subsequently, a new analytical methodology, based on the microextraction technique µSPEed® followed by UHPLC-PDA analysis, was developed for the determination of SCat in urine samples. Under the optimized conditions, the method showed satisfactory results in terms of linearity, with determination coefficients (R^2) > 0.998, within the studied concentration ranges, and low detection limits (LOD) ranging from 36.8 to 95.3 ng mL^{-1}. Once validated, the method was applied to real samples and α-PHP was detected in several samples.

The cytotoxic potential of SCat, individually and in the samples, was evaluated in HepG2 cells. The elucidation of the cellular mechanisms underlying the observed hepatotoxicity, particularly those involved in oxidative stress was also evaluated. MPHP and α-PHP were the most cytotoxic compounds, and all SCat were able to disrupt the balance between reactive oxygen and nitrogen species (ROS and RNS) generation and the scavenging capacity of the antioxidant system.

Keywords: Synthetic cathinones; Chemical characterization; µSPEed®; UHPLC-PDA; hepatotoxicity; HepG2 cells.

RESUMO

O abuso de catinonas sintéticas (SCat) representa um grave problema de saúde pública e apesar dos esforços legislativos para controlar a disponibilidade e utilização destas substâncias, novos derivados continuam a surgir no mercado. A monitorização destas substâncias é uma tarefa desafiadora enfrentada pelos laboratórios forenses e toxicológicos, devido às estruturas moleculares estreitamente relacionadas que conduzem a características analíticas muito semelhantes. Além disso, com o aparecimento de novas substâncias, a informação sobre a potencial toxicidade é desconhecida e os efeitos podem ser perigosos e imprevisíveis.

O primeiro objetivo deste trabalho foi caracterizar quimicamente catorze produtos apreendidos suspeitos de conterem SCat, utilizando várias técnicas analíticas, nomeadamente a espetroscopia de infravermelho (IR), a cromatografia gasosa acoplada à espetrometria de massa (GC-MS), a cromatografia líquida de ultra eficiência com detetor de fotodíodos (UHPLC-PDA) e a ressonância magnética nuclear (RMN). Neste estudo foi possível identificar nove SCat, nomeadamente a metilona, metedrona, *N*-etilcatinona, bufedrona, pentedrona, 3-fluorometcatinona (3-FMC), 4-fluorometcatinona (4-FMC), α-pirrolidinohexanofenona (α-PHP) e 4-metil-α-pirrolidinohexanofenona (MPHP).

Posteriormente desenvolveu-se uma nova metodologia analítica, baseada na técnica de microextração µSPEed® seguida de análise por UHPLC-PDA, para a determinação de SCat em amostras de urina. Nas condições otimizadas o método apresentou resultados satisfatórios em termos de linearidade com coeficientes de determinação (R^2) > 0,998, dentro das gamas de concentração estudadas, e baixos limites de deteção (LOD), variando de 36,8 a 95,3 ng mL^{-1}. Após validação, o método foi aplicado a amostras reais tendo sido detetada a α-PHP em várias amostras.

O potencial citotóxico das SCat, individualmente e nas amostras, foi avaliado em células HepG2. A elucidação dos mecanismos celulares subjacentes à hepatotoxicidade observada, particularmente os envolvidos no stress oxidativo também foram avaliados. A MPHP e a α-PHP foram os compostos mais citotóxicos, e todas as SCat foram capazes de perturbar o equilíbrio entre a produção de espécies reativas de oxigénio e azoto (ROS e RNS) e a defesa antioxidante.

Palavras-Chave: Catinonas sintéticas; Caracterização química; µSPEed®; UHPLC-PDA; hepatotoxicidade; células HepG2.

PUBLICATION OF RESULTS

Part of the original results obtained within the scope of this project have been published in the scientific community or in national and international conferences.

ARTICLES PUBLISHED IN INTERNATIONAL JOURNALS:

- **Gonçalves J.**, Alves V., Aguiar J., Teixeira H.M., Câmara J.S., Synthetic Cathinones: An Evolving Class of New Psychoactive Substances, *Critical Reviews in Toxicology* **2019**, 49, 549-566, DOI: 10.1080/10408444.2019.1679087.
- **Gonçalves J.**, Alves V., Aguiar J., Caldeira M.J., Teixeira H.M., Câmara J.S., Structure Assignment of Seized Products Containing Cathinone Derivatives Using High Resolution Analytical Techniques, *Metabolites* **2021**, 11, 144, DOI: 10.3390/metabo11030144.

ORAL COMMUNICATIONS

- **Gonçalves J.L.**, Alves V.L., Caldeira M.J., Teixeira H.M., Câmara J., Chemical Characterization of New Psychoactive Substances Belonging to the Class of Synthetic Cathinones in Seized Materials in Portugal. *11º Encontro Nacional de Cromatografia*, 9-11 December **2019**, Caparica, Portugal.
- **Gonçalves J.**, Alves V., Aguiar J., Caldeira M.J., Teixeira H.M., Câmara J., Chemical Characterization of Twelve Seized Products Suspected to Contain Synthetic Cathinones. *7th CQM Annual Meeting*, 21-22 September **2020**, Funchal, Madeira, Portugal.
- **Gonçalves J.**, Alves V., Câmara J.S., Teixeira H.M., Drogas Sintéticas: Prevalência e desafios analíticos na determinação de Catinonas e Canabinóides sintéticos. *Jornada de Reflexão sobre Novas Substâncias Psicoativas na RAM: Conhecer, intervir, prevenir, enfrentar…*, 15 October **2021**, Auditório do Departamento de Investigação Criminal da Madeira da Polícia Judiciária, Funchal, Madeira, Portugal.

POSTER COMMUNICATIONS

- **Gonçalves J.L.**, Alves V.L., Caldeira M.J., Câmara J.S., Teixeira H.M., Chemical Characterization Of New Psychoactive Substances Belonging To The Class Of Synthetic Cathinones In 'Legal High' Products. *57th Annual Meeting of the International Association of Forensic Toxicologists*, 2-6 September **2019**, Birmingham, UK.
- **Gonçalves J.**, Alves V., Caldeira M., Câmara J., Teixeira H.M., Caracterização Analítica de Catinonas Sintéticas em Produtos Apreendidos em Portugal. *18º Congresso Nacional de*

Medicina Legal e Ciências Forenses / 3ª Reunião da Rede de Serviços Médico-Legais de Língua Portuguesa, 21-23 November **2019**, Coimbra, Portugal.

- **Gonçalves J.**, Alves V., Caldeira M.J., Câmara J.S., Teixeira H.M., Desenvolvimento de um Método Analítico por Extração µSPEed® para a Determinação de Catinonas Sintéticas em Amostras de Urina. *19º Congresso Nacional de Medicina Legal e Ciências Forenses / 4ª Reunião da Rede de Serviços Médico-Legais de Língua Portuguesa*, 18-20 November **2021**, Coimbra, Portugal.

OTHER PUBLICATIONS/ CONTRIBUTIONS:

ARTICLES PUBLISHED IN INTERNATIONAL JOURNALS:

- Pereira J., **Gonçalves J.**, Porto-Figueira P., Figueira J., Alves V., Perestrelo R., Medina S., Câmara J.S., Current Trends on Microextraction by Packed Sorbent - Fundamentals, Application Fields, Innovative Improvements and Future Trends, *Analyst* **2019**, 144, 5048-5074, DOI: 10.1039/c8an02464b.
- Alves V., **Gonçalves J.**, Aguiar J., Teixeira H.M., Câmara J.S., The synthetic cannabinoids phenomenon: from structure to toxicological properties. A review, *Critical Reviews in Toxicology* **2020**, 50, 359-382, DOI: 10.1080/10408444.2020.1762539.
- Alves V., **Gonçalves J.**, Aguiar J., Caldeira M.J., Teixeira H.M., Câmara J.S., Highly sensitive screening and analytical characterization of synthetic cannabinoids in nine different herbal mixtures, *Analytical and Bioanalytical Chemistry* **2021**, 413, 2257-2273, DOI: 10.1007/s00216-021-03199-6.

ORAL COMMUNICATIONS

- Alves V., **Gonçalves J.**, Aguiar J., Caldeira M.J., Teixeira H.M., Câmara J., Rapid Screening and Analytical Characterization of Synthetic Cannabinoids in 'Herbal Incenses'. *7th CQM Annual Meeting*, 21-22 September **2020**, Funchal, Madeira, Portugal.

POSTER COMMUNICATIONS

- Alves V.L., **Gonçalves J.L.**, Caldeira M.J., Câmara J.S., Teixeira H.M., Characterization of Synthetic Cannabinoids In 'Herbal Incenses' Products. *57th Annual Meeting of the International Association of Forensic Toxicologists*, 2-6 September **2019**, Birmingham, UK.

- Alves V., **Gonçalves J.**, Caldeira M., Câmara J., Teixeira H.M., Identificação de Canabinóides Sintéticos em Extratos Metanólicos de Misturas Herbais por GC-MS e RMN. *18º Congresso Nacional de Medicina Legal e Ciências Forenses / 3ª Reunião da Rede de Serviços Médico-Legais de Língua Portuguesa*, 21-23 November **2019**, Coimbra, Portugal.
- Alves V., **Gonçalves J.**, Caldeira M., Câmara J., Teixeira H.M., Screening of 'Spice' Herbal Mixtures using GC-MS and NMR as Complementary Techniques. *11º Encontro Nacional de Cromatografia*, 9-11 December **2019**, Caparica, Portugal.

GENERAL CONTENT

ABSTRACT ..... **V**

RESUMO ..... **VI**

PUBLICATION OF RESULTS ..... **VII**

GENERAL CONTENT ..... **X**

LIST OF FIGURES ..... **XIV**

LIST OF TABLES ..... **XIX**

ABBREVIATIONS ..... **XXI**

PART I - LITERATURE REVIEW **27**

CHAPTER 1 - GENERAL INTRODUCTION **28**

1. Introduction 29

1.1. European Drug Market 30

1.2. New Psychoactive Substances 30

1.3. History and Abuse of Synthetic Cathinones 32

1.4. Patterns of Use and Legal Status of Synthetic Cathinones 36

1.5. Chemistry of Synthetic Cathinones 39

1.6. Mechanism of Action 41

1.7. Pharmacokinetic 44

1.7.1. Absorption, Distribution and Elimination 44

1.7.2. Metabolism 49

1.8. Adverse Effects 54

1.9. Treatment of intoxications 56

CHAPTER 2 - ANALYTICAL METHODOLOGIES USED FOR DETERMINATION OF SYNTHETIC CATHINONES **57**

2. Analytical Challenges 58

2.1. Nature of Samples 59

2.1.1. Seized materials 59

2.1.2. Biological samples 60

2.1.2.1. Blood, plasma and serum 61

2.1.2.2. Urine 62

2.1.2.3. Oral Fluid 63

2.1.2.4. Sweat 65

2.1.2.5. Hair 66

2.1.2.6. Other Alternative Biological Samples 67
2.2. Sample preparation techniques 68
2.2.1. Protein Precipitation 71
2.2.2. Liquid-Liquid Extraction (LLE) 72
2.2.3. Solid Phase Extraction (SPE) 73
2.2.3.1. Steps involved in the SPE technique 75
2.2.3.2. Extraction of Synthetic Cathinones by SPE 76
2.2.4. QuEChERS (Quick, Easy, Cheap, Effective, Rugged, and Safe) 77
2.2.5. Solid Phase Microextraction (SPME) 78
2.2.6. Dispersive Liquid-Liquid Microextraction (DLLME) 80
2.2.7. Microextraction by Packed Sorbent (MEPS) 81
2.3.7.1. MEPS configurations 85
2.3.7.2. Extraction of Synthetic Cathinones by MEPS 88
2.3. Analytical Methods used in the Determination of Synthetic Cathinones 91
2.3.1. Fourier Transform Infrared Spectroscopy (FTIR) 91
2.3.2. Chromatographic Techniques 96
2.3.2.1. Gas Chromatography coupled to mass spectrometry (GC-MS) 96
2.3.2.2. High Performance Liquid Chromatography (HPLC) 100
2.3.2.3. SCat analysis using chromatographic techniques 104
2.3.3. Nuclear Magnetic Resonance (NMR) 106

PART II - JUSTIFICATION AND AIMS OF THE STUDY 110

1. General Fundamentals 111
1.1. General Objectives and Specific Objectives 112

PART III - CHEMICAL ANALYSIS AND IN VITRO CYTOTOXICITY STUDIES 114

CHAPTER 1 - CHEMICAL CHARACTERIZATION OF SYNTHETIC CATHINONES FOUND IN SEIZED MATERIALS 115

1. Introduction 116
1.1. Materials and Methods 117
1.1.1. Reagents and Chemicals 117
1.1.2. Seized Samples 117
1.1.3. Chemical Characterization of Seized Materials 118
1.1.3.1. ATR-FTIR Analysis 118
1.1.3.2. GC-MS Analysis 118
1.1.3.3. UHPLC-PDA Analysis 119

1.1.3.4. NMR Analysis 119
1.2. Results and Discussion 120
1.2.1. ATR-FTIR Analysis 120
1.2.2. GC-MS Analysis 123
1.2.3. UHPLC-PDA Analysis 133
1.2.4. NMR Analysis 137
1.3. Conclusion 145
CHAPTER 2 - DETERMINATION OF SYNTHETIC CATHINONES IN URINE SAMPLES BY µSPEED®/ UHPLC-PDA METHODOLOGY 147
2. Introduction 148
2.1. Materials and Methods 149
2.1.1. Reagents, analytical standards and materials 149
2.1.2. Preparation of standard solutions 150
2.1.3. Urine samples 150
2.1.4. Sample preparation and optimization of µSPEed® conditions 150
2.1.5. UHPLC-PDA conditions 151
2.1.6. Method validation 152
2.1.6.1. Selectivity 152
2.2.6.2. Linearity 152
2.1.6.3. Limit of detection (LOD) and limit of quantification (LOQ) 154
2.1.6.4. Precision 155
2.1.6.5. Accuracy 156
2.1.6.6. Extraction efficiency 158
2.1.6.7. Matrix effect 158
2.1.6.8. Analyte stability 159
2.2. Results and Discussion 159
2.2.1. Optimization of µSPEed® 159
2.2.1.1. Nature of sorbent material and sample pH 160
2.2.1.2. Number of extraction cycles and sample volume 161
2.2.1.3. Washing conditions 162
2.2.1.4. Elution conditions 164
2.2.2. Method validation 165
2.2.2.1. Selectivity 165
2.2.2.2. Linearity 167
2.2.2.3. LOD and LOQ 167

2.2.2.4. Precision and Accuracy 169
2.2.2.5. Extraction Eficiency and Matrix Effect 170
2.2.2.6. Analyte stability 172
2.2.3. Application of the method to real samples 174
2.3. Conclusion 177
CHAPTER 3 - CYTOTOXICITY STUDIES OF SYNTHETIC CATHINONES IN HEPG2 CELL LINE 179
3. Introduction 180
3.1. Materials and Methods 182
3.1.1. Reagents, analytical standards and materials 182
3.1.2. Cell line and Culture 182
3.1.3. MTT reduction assay 182
3.1.4. Determination of intracellular reactive oxygen (ROS) and nitrogen (RNS) species 183
3.1.5. Determination of reduced (GSH) and oxidized (GSSG) glutathione levels 184
3.1.6. Determination of intracellular ATP levels 185
3.1.7. Determination of protein content 185
3.1.8. Statistical analysis 185
3.2. Results and Discussion 186
3.2.1. MTT reduction assay 186
3.2.2. Determination of intracellular ROS and RNS 190
3.2.3. Determination of intracellular levels of GSH and GSSG 193
3.2.4. Determination of intracellular levels of ATP 196
3.3. Conclusion 198
CHAPTER 4. FINAL CONCLUSIONS AND FUTURE PERSPECTIVES 201
REFERENCES 204
ANNEXES 242

LIST OF FIGURES

Figure 1. Classification of NPS based on their psychopharmacological effects [28]. 32

Figure 2. Numbers and categories of NPS notified to the EU Early Warning System for the first time between 2005 and October 2020 [89]. 36

Figure 3. General chemical structures of (A) SCat, and (B) phenylethylamines. Structures of (C) cathinone and (D) amphetamine (adapted from Tyrkko et al. [113]). 39

Figure 4. Classification of SCat based on their chemical structure (adapted from Valente et al. [32]). Abbreviation: MDPBP - 3,4-methylenedioxy-α-pyrrolidinobutiophenone, MDPV - 3,4-methylenedioxypyrovalerone and MDPPP - 3,4-methylenedioxy-α-pyrrolidinopropiophenone. 40

Figure 5. Schematic representation of the modes of action of SCat in the central nervous system (adapted from Almeida et al. [123]). Abbreviations: DA, dopamine; NA, noradrenaline; 5-HT, 5-hydroxytryptamine (serotonin); SCat: synthetic cathinones; DAT, dopamine transportes; NAT, noradrenaline transportes; SERT, serotonin transportes; $VMAT_2$, vesicular monoamine transporter-2. 42

Figure 6. General metabolic pathways for SCat: (A) N-alkyl cathinone derivatives with/without ring substituents; (B) 3,4-methylenedioxy cathinone derivatives (C) pyrrolidinophenone derivatives and (D) 3,4-methylenedioxypyrrolidinophenone derivatives (adapted from Tyrkko et al. [113]). 49

Figure 7. Major phase I metabolic pathways for mephedrone (adapted from Meyer et al. [167]). 50

Figure 8. Main metabolic pathways of methylone, ethylone and butylone (adapted from Zaitsu et al. [159]). Abbreviation: COMT catechol-O-methyltransferase. 51

Figure 9. Major phase I metabolic pathways for α-PVP (adapted from Nóbrega et al. [80]). 52

Figure 10. Major phase I metabolic pathways for MDPV (adapted from Zaitsu [160]). 53

Figure 11. General overview of drug detection times for different biological matrices (adapted from Hadland and Levy [226]). 60

Figure 12. General steps involved in the SPE (adapted from Pinto [287]). 75

Figure 13. Schematic representation of a typical QuEChERS method (adapted from Allcrom [298]). 77

Figure 14. Scheme of a syringe used in the SPME technique (adapted from Gonçalves [305]). 78

Figure 15. Modes of SPME extraction: (A) direct immersion (DI-SPME), (B) headspace (HS-SPME) and (C) membrane SPME (M-SPME). Adapted from Gonçalves [305]. 79

Figure 16. Schematic representation of a typical DLLME technique (adapted from Quigley et al. [313]). 81

Figure 17. Schematic overview of the MEPS syringe and MEPS-BIN (barrel insert and needle). The sorbent is packed and properly sealed inside the barrel to avoid leakage (adapted from Gonçalves [305]). 82

Figure 18. Typical MEPS procedure (adapted from Casado et al. [321]). 82

Figure 19. MEPS formats commercially available: manual (MEPS syringe), semi-automatic (eVol®) and on-line (several configurations available by CTC Analytics) (adapted from Pereira et al. [316]). 85

Figure 20. Volume range of eVol syringes (XCHANGE®) (adapted from SGE [326]). 86

Figure 21. Schematic representation of CDF MEPS. Position 1: the fluid is aspirated or dispensed across the MEPS bed; Position 2: Engaging position 2 the valve body is pulled down (black arrow) and this removes the MEPS bed from the fluid path. (adapted from SGE [328]) 87

Figure 22. µSPEed® cartridge (adapted from EPREP [330]). 87

Figure 23. digiVOL® Digital Syringe Driver (adapted from EPREP [331]). 88

Figure 24. Vibrational modes of chemical bonds (adapted from Cameron et al. [366]). 92

Figure 25. Schematic representation of a typical FTIR spectrophotometer (adapted from Skoog et al. [370]). 93

Figure 26. Scheme of a generic FTIR interferometer (adapted from InnovaTECH [373]). 94

Figure 27. Scheme of ATR-FTIR measurement principle (adapted from PerkinElmer [375]). 95

Figure 28. Basic gas chromatograph scheme and its main components (adapted from Aguiar [381]). 96

Figure 29. Schematic diagram of an injector (adapted from Dawling et al. [380]). 97

Figure 30. Chemical structure of some of the most common stationary phases available for GC. 98

Figure 31. Schematic diagram of a mass spectrometer (adapted from Neves and Freitas [382]). 99

Figure 32. Schematic diagram of chromatographic separation based on the differential migration of the constituents of a sample (adapted from Gonçalves [305]). 101

Figure 33. Schematic diagram of a typical HPLC (adapted from Gonçalves [305]). 102

Figure 34. Schematic diagram of a PDA detector (adapted from LCGC [390]). 104

Figure 35. Nuclear spin behavior (A) in absence of an external magnetic field and (B) under the influence of an external magnetic field (B_0). 107

Figure 36. Schematic diagram of the different spin states of a nucleus in a magnetic field (adapted from Course Hero [405]). 108

Figure 37. Schematic diagram of NMR setup (adapted from Pinto [287]). 109

Figure 38. General overview of the aims of this study. Abbreviations: ATP - adenosine triphosphate, GSH - reduced glutathione, GSSG - oxidized glutathione, MTT - 3-[4,5-dimethylthiazol-2-yl]-2,5 diphenyl tetrazolium bromide, ROS - reactive oxygen species, RNS - reactive nitrogen species. 112

Figure 39. FTIR spectra of seized products suspected to contain SCat. Products 3-7 show similar IR spectra. 122

Figure 40. Typical GC-MS chromatograms of seized products suspected to contain SCat. Products 3-7 show similar chromatographic profiles. Peak identification: (1) MPHP, (2) α-PHP, (3) *N*-ethylcathinone, (4) buphedrone, (5) methedrone, (6) ethylphenidate, (7) caffeine, (8) methylone, (9) 3-FMC, (10) 4-FMC, (11) isopentedrone and (12) pentedrone. 124

Figure 41. Mass spectra of compounds found in seized products. 126

Figure 42. General mass spectra fragmentation pattern of SCat under EI conditions (adapted from Zuba [429]). 127

Figure 43. General derivatization mechanism of SCat with the TFAA reagent. 128

Figure 44. Typical GC-MS chromatograms of seized products after derivatization with TFAA. Peak identification: (1) MPHP, (2) α-PHP, (3) buphedrone-TFAA derivative, (4) *N*-ethylcathinone-TFAA derivative, (5) methedrone-TFAA derivative, (6) ethylphenidate-TFAA derivative, (7) caffeine, (8) methylone-TFAA derivative, (9) 3-FMC-TFAA derivative, (10) 4-FMC-TFAA derivative, (11) pentedrone-TFAA derivative and (12) isopentedrone-TFAA derivative. 129

Figure 45. Mass spectra of SCat after derivatization with TFAA. 130

Figure 46. Probable fragmentation pathways of TFAA derivatives of (A) buphedrone and (B) *N*-ethylcathinone..... 132

Figure 47. Typical UHPLC-PDA chromatograms of seized products. Peak identification: (1) MPHP, (2) α-PHP, (3) *N*-ethylcathinone, (4) methedrone, (5) buphedrone, (6) caffeine, (7) methylone, (8) 3-FMC, (9) 4-FMC and (10) pentedrone. 134

Figure 48. UV spectra of compounds found in seized products. 135

Figure 49. Relative proportions of active substances other components detected in 14 seized products..... 145

Figure 50. Diagram of the µSPEed® procedure initially used to optimize the extraction process. 151

Figure 51. Comparison of the performance of 10 different sorbents materials and the influence of sample pH on the extraction efficiency of SCat in urine by µSPEeD®. Values expressed as average total area ± standard deviation (n= 3)..... 160

Figure 52. Influence of the number of extraction cycles and sample volume on µSPEeD® performance. 161

Figure 53. Influence of the washing conditions on µSPEeD® performance. (A) Total area and (B) recovery study obtained for each washing condition. 163

Figure 54. Typical chromatograms obtained by UHPLC-PDA from a urine sample spiked with SCat (A) without the sorbent washing step during µSPEed® extraction and (B) with the washing step constituted by 200 µL H_2O (0.1% FA), followed by 200 µL of H_2O:ACN (95:5 v/v). Peak identification: (1) 4-FMC, (2) methylone, (3) *N*-ethylcathinone, (4) methedrone, (5) buphedrone, (6) pentedrone, (7) α-PHP, (8) MPHP and (IS) internal standard. 164

Figure 55. Influence of different elution conditions on the extraction efficiency of µSPEed®. 164

Figure 56. Chromatograms of a typical µSPEeD®–UHPLC/PDA procedure of a (A) SCat standard solution, and (B-E) pooled blank urine samples. Peak identification: (IS) internal standard, (1) 4-FMC, (2) methylone, (3) *N*-ethylcathinone, (4) methedrone, (5) buphedrone, (6) pentedrone, (7) α-PHP and (8) MPHP. 166

Figure 57. Stability study of SCat in urine samples at low concentration (150 ng mL^{-1}). 172

Figure 58. Stability study of SCat in urine samples at medium concentration (750 ng mL^{-1})... 172

Figure 59. Stability study of SCat in urine samples at high concentration (1500 ng mL^{-1}). 173

Figure 60. Chromatographic profiles of real samples after extraction by µSPEed®/UHPLC-PDA methodology. 175

Figure 61. Chromatographic profiles of samples 1295 and 2230 after extraction by µSPEed®/UHPLC-PDA methodology. 176

Figure 62. Formation of 2''-oxo-α-PHP from parent compound (α-PHP) (adapted from Zaitsu [160]). 177

Figure 63. Dose-response curves obtained with MTT reduction assay for individual SCat and seized products in HepG2 cells after 24 h exposure at 37°C under humidified atmosphere containing 5% CO_2. The black dashed lines represent the 95% CI, while the dashed grey lines represent 50% and 100% effect. 188

Figure 64. Production of ROS and RNS in HepG2 cells after exposure to SCat at concentrations corresponding to EC_{25}, EC_{50} and EC_{75}, for 24 h at 37°C. Results were obtained from three independent experiments performed in five replicates and the statistical analysis of data was carried out using one-way ANOVA followed by Dunnett's test. * $p < 0.05$, ** $p < 0.01$ and *** $p < 0.001$ versus control. 192

Figure 65. Oxidation-reduction pathway of glutathione (adapted from Aoyama and Nakaki [516]). Hydrogen peroxide or hydroperoxides are degraded by GSH peroxidase to water and alcohols, respectively. During the GSH peroxidase-catalyzed reaction, GSH is converted to its oxidized disulfide form (GSSG). GSH in turn can be regenerated from GSSG by the GSSG reductase in the presence of NADPH. In this process NADPH is oxidized to $NADP^+$. NADPH is subsequently regenerated via the pentose phosphate pathway [517]. 194

Figure 66. Intracellular levels of GSH and GSSG, as well as the GSH/GSSG ratio in HepG2 cells after 24h of incubation with SCat at 37°C. Results were obtained from a single experiment performed in duplicate and the statistical analysis of data was carried out using one-way ANOVA followed by Dunnett's test. * $p < 0.05$, ** $p < 0.01$ and *** $p < 0.001$ versus control. 195

Figure 67. Intracellular levels of ATP in HepG2 cells after 24h of incubation with SCat at 37°C. Results were obtained from a single experiment performed in triplicate and the statistical analysis of data was carried out using one-way ANOVA followed by Dunnett's test. * $p < 0.05$, ** $p < 0.01$ and *** $p < 0.001$ versus control. 197

LIST OF TABLES

Table 1. Typical doses, routes of administration, onset of action and duration of effects of several SCat (adapted from Kerrigan [97]). 37

Table 2. General overview of pharmacokinetic studies involving SCat (adapted from Soares et al. [139]). 47

Table 3. Adverse effects of SCat consumption (adapted from Prosser [31] and Couto et al. [207]). 56

Table 4. General overview of the most commonly used sample preparation techniques for the analysis of SCat in biological samples..... 69

Table 5. General properties of several commercially available sorbents for MEPS (adapted from Pereira et al. [316])..... 83

Table 6. Application of MEPS for forensic drug analysis..... 89

Table 7. Main differences between packed and capillary columns (adapted from Pinto [287]). 98

Table 8. Main mechanisms of separation by liquid chromatography (adapted from Pinto [287]). 101

Table 9. Nuclear spin quantum number (*I*) of some common atomic nuclei (adapted from McGregor [402]). 107

Table 10. List of provided samples with the information about their chemical composition indicated on the product label. 117

Table 11. Active substances detected in seized products by GC-MS, with the respective retention times (RT), Kovats retention indices (KI), molecular formula (MF), molecular weight (MW), base peak and other characteristic ions. 126

Table 12. Chemical substances detected in seized products by GC-MS after derivatization with TFAA. 131

Table 13. Chemical substances detected in seized products by UHPLC-PDA, with the respective retention times (RT), molecular structure, molecular formula (MF) and UV maximum absorption wavelengths (λ_{max}). 136

Table 14. NMR assignments of SCat constituted by a pyrrolidine ring in the side chain or a methoxy or a methylenodioxy group attached to the aromatic ring..... 139

Table 15. NMR assignments of *N*-ethylcathinone, buphedrone, pentedrone, 3-FMC and 4-FMC found in seized materials. 140

Table 16. ^{1}H and ^{13}C NMR assignments of adulterants found in seized materials. 142

Table 17. Formulas used in the One-way ANOVA test [456, 457]. 155

Table 18. Calculation of variance for the experimental model used in the study of repeatability and intermediate precision [456, 457]. 156

Table 19. Washing solutions tested for µSPEeD® optimization. 162

Table 20. Linearity results obtained for determination of SCat from urine samples by µSPEed®/UHPLC-PDA methodology. 168

Table 21. LOD and LOQ values calculated for each SCat by µSPEed®/UHPLC-PDA. 169

Table 22. Results obtained for the study of precision and accuracy of the analytical method. 170

Table 23. Results obtained for extraction efficiency and matrix effect studies. 171

Table 24. Concentration of SCat found in real urine samples. 175

Table 25. Parameters derived from dose-response curves obtained during the MTT assay. .. 188

Table 26. Concentrations tested of each SCat for evaluating the production of reactive species in HepG2 cells. 191

ABBREVIATIONS

2C-E	2,5-dimetoxy-4-ethylphenetylamine
3-FMC	3-fluoromethcathinone
3-MMC	3-methylmethcathinone
3'-OH-4'-MeO	3'-hydroxy-4'-methoxymethcathinone
3,4-DMMC	3,4-dimethylmethcathinone
3,4-dimethoxy-α-PVP	3,4-dimethoxy-α-pyrrolidinopentiophenone
4-BEC	4-bromoethcathinone
4-Br-PVP	1-(4-bromophenyl)-2-(pyrrolidin-1-yl)pentan-1-one
4-Cl-α-EAPP	1-(4-chlorophenyl)-2-(ethylamino)pentan-1-one
4-Cl-α-PHP	1-(4-chlorophenyl)-2-(pyrrolidin-1-yl)hexan-1-one
4-Cl-PPP	1-(4-chlorophenyl)-2-(pyrrolidin-1-yl)propan-1-one
4-F-PBP	4'-fluoro-α-pyrrolidinobutyrophenone
4-F-α-PHPP	4-fluoro-α-pyrrolidinoheptanophenone
4-F-α-PVP	4-fluoro-α-pyrrolidinopentiophenone
4-FMC	4-fluoromethcathinone
4-MEC	4-methyl-*N*-ethylcathinone
4-MePPP	4-methyl-α-pyrrolidinopropiophenone
4-methoxy-α-PHPP	4-methoxy-α-pyrrolidinoheptanophenone
4-methoxy-α-POP	4-methoxy-α-pyrrolidinooctanophenone
4-methoxy-α-PVP	4-methoxy-α-pyrrolidinovalerophenone
4-MPD	4-methylpentedrone
4'-OH-3'-MeO	4'-hydroxy-3'-methoxymethcathinone
5-HT	Serotonin
6-APB	6-(2-aminopropyl)benzofuran
^{13}C NMR	Carbon-13 nuclear magnetic resonance
^{19}F NMR	Fluorine-19 nuclear magnetic resonance
^{1}H NMR	Proton nuclear magnetic resonance
α-EAPP	α-ethylaminopentiophenone
α-PBP	α-Pyrrolidinobutiophenone
α-PBT	α-pyrrolidinobutiothiophenone
α-PHP	α-pyrrolidinohexanophenone
α-PHPP	α-pyrrolidinoheptanophenone
α-PiHP	4-methyl-1-phenyl-2-(pyrrolidin-1-yl)pentan-1-one
α-POP	α-pyrrolidinooctanophenone
α-PPP	α-pyrrolidinopropiophenone
α-PVP	α-pyrrolidinopentiophenone
α-PVT	α-pyrrolidinopentiothiophenone
AA	Acetic anhydride
ACN	Acetonitrile
ANOVA	Analysis of variance

APS	Aminopropyl phase
ATP	Adenosine triphosphate
ATR	Attenuated total reflectance
BCA	Bicinchoninic acid solution
BIN	Barrel insert and needle
BSA	Bovine serum albumin
C_2	Ethylsilane
C_4	Butylsilane
C_6	Hexylsilane
C_8	Octylsilane
C_{18}	Octadecylsilane
$CHCl_3$	Chloroform
CLF2AA	Chlorodifluoroacetic anhydride
CK	Creatine kinase
CI	Confidence interval
Cl	Clearance
C_{max}	Maximum plasma concentration
CO	Carbon monoxide
COMT	Catechol O-methyltransferase
COSY	Correlation spectroscopy
CRM	Certified reference materials
CV	Coefficient of variation
CV_r	Coefficient of variation of repeatability
CV_{SI}	Coefficient of variation of the intermediate precision
CYP2D6	Cytochrome P450 2D6
D_2O	Deuterium oxide
DA	Dopamine
DAD	Diode array detector
DAT	Dopamine transporters
DC	Direct current
DCFH-DA	2',7'-dichlorofluorescin diacetate
DCM	Dichloromethane
DEA	Drug Enforcement Administration
DLLME	Dispersive liquid-liquid microextraction
DMSO	Dimethyl sulfoxide
DI-SPME	Direct immersion-solid phase microextraction
d-SPE	Dispersive solid phase extraction
DS^2	Difference of variances
DTT	Dithiothreitol
ECD	Electron capture detector
EDTA	Ethylenediaminetetraacetic acid
EDDP	2-ethylidene-1,5-dimethyl-3,3-diphenylpyrrolidine

EE	Extraction efficiency
EI	Electron ionization
EIA	Enzyme immunoassay
ELISA	Enzyme-linked immunosorbent assay
EMCDDA	European Monitoring Centre for Drugs and Drug Addiction
ESI	Electrospray ionization
EWS	EU Early Warning System
FA	Formic acid
FBS	Fetal bovine serum
FDA	Food and Drug Administration
FID	Flame ionization detector
FPIA	Fluorescent polarization immunoassay
FTIR	Fourier Transform Infrared Spectroscopy
GC	Gas chromatography
GC-MS	Gas chromatography coupled to mass spectrometry
GC-MS/MS	Gas chromatography tandem mass spectrometry
GC-NCI-MS	Gas chromatography coupled to mass spectrometry with negative chemical ionization mode
GLC	Gas-liquid chromatography
GSC	Gas-solid chromatography
GSH	Reduced glutathione
GSSG	Oxidized glutathione
HBSS	Hank's balanced salts solution
HFBA	Heptafluorobutyric anhydride
HMBC	Heteronuclear multiple bond correlation spectroscopy
HPLC	High performance liquid chromatography
HSQC	Heteronuclear single quantum correlation spectroscopy
HS-SPME	Headspace-solid phase microextraction
Hz	Hertz
IPA	Isopropanol
IR	Infrared
IS	Internal standard
J	Coupling constant
K_D	Distribution constant
KIMS	kinetic interaction of microparticles in solution
KOx	Potassium oxalate
LC	Liquid chromatography
LC-HRMS	Liquid chromatography coupled to high resolution mass spectrometry
LC-MS	Liquid chromatography coupled to mass spectrometry
LC-MS/MS	Liquid chromatography coupled with tandem mass spectrometry

LC-QTOF-MS	Liquid chromatography quadrupole time-of-flight mass spectrometry
LLE	Liquid-liquid extraction
LOD	Limit of detection
LOQ	Limit of quantification
Log P	Partition coefficient
LLOQ	Lower limit of quantification
LPC-PJ	Forensic Science Laboratory of Portuguese Criminal Police
LSD	Lysergic acid diethylamide
MBTFA	N-methyl-bis-(trifluoroacetamide)
MDMA	3,4-methylenedioxy-methamphetamine
MDPBP	3,4-methylenedioxy-α-pyrrolidinobutiophenone
MDPPP	3,4-methylenedioxy-α-pyrrolidinopropiophenone
MDPV	3,4-methylenedioxypyrovalerone
ME	Matrix effect
MEM	Minimum essential medium
MeOH	Methanol
MEPS	Microextraction by packed sorbent
MF	Molecular formula
MIPs	Molecularly imprinted polymers
MPHP	4-methyl-α-pyrrolidinohexanophenone
MS	Mass spectrometry
M-SPME	Membrane-solid phase microextraction
MSTFA	N-methyl-N-(trimethylsilyl)trifluoroacetamide
MTT	3-(4,5-Dimethylthiazol)-2,5-diphenyltetrazolium
MW	Molecular weight
m/z	mass-to-charge ratio
NA	Noradrenaline
NADPH	Nicotinamide adenine dinucleotide phosphate
NaF	Sodium fluoride
NAT	Noradrenaline transporters
NH_4OH	Ammonium hydroxide
NMR	Nuclear magnetic resonance
NPD	Nitrogen-phosphorus detector
NPS	New psychoactive substances
NRG-1	Energy-1
PBS	Phosphate buffered saline
PFPA	Pentafluoropropionic anhydride
PPA	Propionic anhydride
PDA	Photodiode array detector
PDMS/DVB	Polydimethylsiloxane/divinylbenzene
PFAS	Polyfluorinated alkyl substances

PFPA	Pentafluoropropionic anhydride
PGC	Porous graphitic carbon
pI	Isoelectric point
ppm	Parts per million
PS-DVB	Polystyrene-divinylbenzene
PTFE	Polytetrafluoroethylene
PV9	α-pyrrolidinooctanophenone
QuEChERS	Quick, easy, cheap, effective, rugged, and safe
QSM	Quaternary solvent manager
R	Coefficient of correlation
R^2	Coefficient of determination
R (%)	Extraction recovery
RIA	Radioimmunoassay
RAMs	Restricted-access matrix sorbents
R_F	Retention factor
RF	Radiofrequency
RI	Kováts retention index
ROS	Reactive oxygen species
RNS	Reactive nitrogen species
RSD	Relative standard deviation
RT	Retention time
SAX	Strong anion exchange
SALLE	Liquid-liquid extraction assisted by salting out
SAR	Structure-activity relationships
SBSE	Stir-bar sorptive extraction
SCat	Synthetic cathinones
SCX	Strong cation exchange
SD	Standard deviation
SEM	Standard error mean
SERT	Serotonin transporters
SESARAM	Serviço de Saúde da Região Autónoma da Madeira
SIL	Silica
SM	Sample manager
SPE	Solid phase extraction
SPME	Solid phase microextraction
S_r	Standard deviation of repeatability
SRM	Selected reaction monitoring
$S_{y/x}$	Residual standard deviation
$t_{1/2}$	Elimination half-life
t_{crit}	Two-tailed critical value
t_{exp}	*t*-Student test
TCD	Thermal conductivity detector

TFA	Trifluoroacetic acid
TFAA	Trifluoroacetic anhydride
tGSH	Total gluthatione
TMCS	Trimethylchlorosilane
TLC	Thin layer chromatography
T_{max}	Time of peak plasma concentration
TSD	Thermionic specific detector
TV	Test value
UHPSFC-MS	Ultrahigh performance supercritical fluid chromatography with mass spectrometry
UHPLC-MS/MS	Ultrahigh performance liquid chromatography coupled to tandem mass spectrometry
UHPLC-PDA	Ultrahigh performance liquid chromatography with photodiode array detector
UK	United Kingdom
UNODC	United Nations Office on Drugs and Crime
USA	United States of America
USSR	Union of Soviet Socialist Republics
UV-VIS	Ultraviolet/visible
$U_{\%\bar{R}}$	Uncertainty in average recovery
$VMAT_2$	Vesicular monoamine transporter-2
V_d	Volume of distribution
VWD	Variable wavelength detector
δ	Chemical shifts
λ_{max}	Maximum absorption wavelength

Part I

Literature Review

Chapter 1

General Introduction

1. Introduction

Drug use is a very old phenomenon in human history and constitutes a serious public health problem, with personal and social consequences [1]. Currently, it is known that the abusive consumption of psychoactive substances, including alcohol, cannabinoids, opioids, cocaine, among others, has grown in the last 10 years, constituting one of the most worrying problems in the world population. According to the World Drug Report 2021 [2], it is estimated that 275 million people worldwide have used drugs at least once in the previous year, and around 36 million people are estimated to be affected by drug use disorders. In fact, drug abuse is responsible for significant morbidity, and the treatment of drug dependence carries a huge burden to society [3].

Drug addiction or substance use disorder is a serious condition that affects a person's brain and behaviour, resulting from the compulsive use of one or more substances despite harmful consequence [4]. Although the terms "addiction" and "dependence" are often used interchangeably, they correspond to different concepts that should be defined for a better understanding. Drug addiction is considered a neuropsychiatric disease characterized by a compulsive desire to continue using drugs despite knowledge of possible adverse consequences, while dependence refers to the physiological adaptation to the usual drug consumption, being characterized by the symptoms of tolerance (the process by which the body requires increasingly larger doses to experience the same results) and withdrawal (symptoms that occur upon the abrupt discontinuation or decrease in drug intake) [4].

Several studies have shown that there is a high correlation between occasional use of drugs in adolescence and the possibility of becoming a drug addict in adulthood [5, 6]. During this period, adolescents have a strong inclination toward experimentation and curiosity and are more susceptible to peer pressure, which makes them vulnerable to drug abuse [7]. In addition, drug use at a very early age, led to a higher risk for reduced school performance, delinquency, teenage pregnancy, and depression [5]. On the other hand, accidental and intentional deaths that are related to drug use in the young population represent one of the main preventable causes of death for the group aged from 15 to 24 years old [4-6].

The internet is also a huge problem, as a mechanism for the rapid dissemination of new trends, and as a new marketplace to buy and sell drugs. In addition to drug exposure through marketing and advertising, some social media content contribute to the popularity of several psychoactive substances especially among young people [8].

1.1. European Drug Market

The illicit drug market is a dynamic system highly complex and adaptable, which change based on demand, competition, legislation and revenue [9]. Due to the clandestine nature of this market, it is difficult to estimate the total amount of money it generates, and published estimates are variable, covering different parts of the market and different geographical areas [10].

Europe is considered a reference in the drug market, based on its production and trafficking, it is an entry for drugs and precursors, mainly from South America, West Asia and North Africa [11]. Moreover, Europe is also known for its production of drugs, such as cannabis and synthetic drugs [11]. Although the production of the former is mostly for local consumption, some synthetic drugs are manufactured to be exported to other parts of the world [11].

At a national level, Portugal remains as an important destination of international drug trafficking. It is considered a transit country for cocaine and cannabis resin from Latin America and Morocco, respectively, destined for other European countries [12]. Most illicit drugs enter Portugal via sea routes, as a result of its large coastal area and its geographical position, while land and air routes are used to a lesser extent. [12]. Ecstasy or 3,4-methylenedioxy-methamphetamine (MDMA), for example, arrives predominantly from the Netherlands and is transported by air or overland in cars or lorries [13]. Heroin seized in Portugal comes mostly from the Netherlands, Spain and Belgium [13].

Currently, the use of postal services to transport drugs has expanded rapidly. With technological innovation and new forms of communication, the development of online markets has changed the dynamics of the buying and selling processes, opening the drug market to a wider audience [14]. In addition, most of these online markets provide a high level of anonymity, as they are hosted in the so-called “dark web”. Consumers may feel safer buying these substances on the internet, because there is less exposure, and drugs are delivered through the post, avoiding direct contact with drug dealers [14]. On the other hand, one of the main factors contributing to the growth of these markets is the wide range of psychoactive substances that are available, being many of them new to the market at more affordable prices than traditional drugs of abuse, in order to attract old and create new users.

1.2. New Psychoactive Substances

Over the last two decades, a tremendous change in the illicit drug market has become evident with the appearance of a “new generation” of psychoactive substances. Marketed as “legal highs”, “designer drugs” or “research chemicals”, the new psychoactive substances (NPS)

continue to increase, being a major problem to public health [15]. Compared to traditional drugs of abuse, NPS are cheap, easy to obtain, and their unregulated status in many countries makes them very attractive especially among young people [16, 17]. Usually, these substances are widely available on the Internet, in a variety of forms including powders, crystals, tablets, liquids, smoking blends and herbal mixtures [18]. Although many products are labelled "not for human consumption", NPS are intentionally marketed as replacements for illicit drugs, such as ecstasy, cocaine, amphetamine or cannabis [17]. In fact, most of these substances are developed by making designer substitutions to the chemical structures of existing psychoactive drugs, in order to create alternative psychoactive compounds and avoid drug legislation [17].

Despite the legislative efforts to regulate NPS, new derivatives continue to emerge on the recreational drugs market. Up to December 2021, more than 1120 NPS have been detected from over 130 countries and territories worldwide [19]. In Europe, at least one new substance is detected every week on the market. Presently, the European Monitoring Centre for Drugs and Drug Addiction (EMCDDA), through the EU Early Warning System (EWS), monitors more than 880 new substances, belonging to several chemical classes including, synthetic cannabinoids, SCat, phenethylamines, piperazines, ketamine- and phencyclidine-type substances, tryptamines, benzofurans, synthetic opioids (fentanyl analogues and compounds with a different chemical structure), benzodiazepines, among others [20, 21]. Based on their psychopharmacological activity, NPS are grouped into six major categories, namely, stimulants, synthetic cannabimimetics, hallucinogens, dissociatives, synthetic opioids and sedative/ hypnotics (Figure 1) [22].

While many of these substances often disappear from the market, some of them still continue on the market due to their popularity between drug users [23]. Among these substances, SCat are one of the most prevalent classes of designer drugs that became popular, due to the psychostimulant and hallucinogenic effects similar to cocaine, MDMA and amphetamines [24]. Usually, SCat are sold as "bath salts" or "plant food" and are labelled "not for human consumption" to avoid drug abuse legislation [25]. The chemical structure of cathinone, a naturally-occurring stimulant found in khat plant (*Catha edulis*), has been used as prototype for the development of several synthetic derivatives [17]. Like MDMA and cocaine, SCat exert their stimulant and sympathomimetic effects through the interaction with monoamine membrane transporters, leading to an increase on synaptic concentrations of dopamine (DA), noradrenaline (NA) and serotonin (5-HT) [26, 27].

Figure 1. Classification of NPS based on their psychopharmacological effects [28].

The resulting excessive monoamine levels in the synaptic cleft lead to overstimulation of postsynaptic DA, NA, and 5-HT receptors in the brain, which results in their psychological, behavioural and toxic effects [29]. Numerous intoxications and fatal cases involving SCat consumption have been reported, and the symptoms induced by their high dosages include hypertension, hyperthermia, tachycardia, seizures that in some cases culminate in multi-organ failure and consequent death [30, 31].

1.3. History and Abuse of Synthetic Cathinones

SCat encompass a large group of substances chemically related to cathinone, which can be found in the leaves of khat (*Catha edulis*), a shrub native of East Africa and the Arabian Peninsula [32]. Such as other psychoactive plants, khat has a long history of traditional use [33]. Historical references to the chewing of khat leaves for their euphoric and stimulant effects date of many centuries ago, and today this practice is prevalent in Somalia, Yemen, Kenya and Ethiopia [34]. The dried and powdered leaves are occasionally infused to prepare tea, known as Abyssinian, African or Arabian tea [35], or consumed as a paste with honey [36]. It is estimated that around 10 million people worldwide use khat on a daily basis [37].

Khat contains numerous compounds, including alkaloids, glycosides, tannins, amino acids, flavonoids, vitamins and minerals [38, 39]. Chewing khat releases these substances into the saliva, which are rapidly absorbed through the buccal mucosa and gastro-intestinal tract. Although its stimulant effect was initially attributed to cathine, extracts of fresh leaves of khat were shown to contain cathinone, which is an alkaloid 7- to 10-fold more potent than cathine

[32, 37]. However, cathinone is not very stable and breaks down to produce cathine and norephedrine, thus explaining the need to chew fresh khat leaves [32, 37].

The first SCat emerged in the beginning of the 20th century, with the synthesis of methcathinone, in 1928 [40], and mephedrone, in 1929 [41]. Although few SCat entered clinical trial for potential use as drugs, only bupropion (*m*-chloro-*N*-*ter*-butyl-cathinone) is currently used as a smoking cessation-aid, as well as to treat depression [31, 42]. Other cathinone derivatives have been investigated, but were unsuccessful due to severe side effects [43, 44]. Methcathinone, also known as ephedrone, was used, in the 1930s and 1940s, in Union of Soviet Socialist Republics (USSR), as an antidepressant, and a decade later the American pharmaceutical company Parke-Davis considered marketing this substance as an analeptic agent [45, 46]. In 1957, a USA patent was granted on the production process, but due to its strong addictive potential, this drug never went into commercial medical production [45, 47].

Concerns about the abuse of methcathinone began to emerge in the former USSR, from the 1970s and subsequently in the USA in the early 1990s, where this drug was known by the street names of “Jeff”, “Mulka” and “Cat” [48]. In 1994, the USA Government recommended the inclusion of methcathinone as a Schedule I controlled substance, in the UN Convention on Psychotropic Substances [49]. This Convention establishes an international control system for psychotropic substances, and Schedule I includes substances presenting a high risk of abuse, posing a particularly serious threat to public health, which are of very little or no therapeutic value [50, 51].

During the second half of the 20th century, other SCat continued to appear as potential medicines. Diethylcathinone, also known as amfepramone or diethylpropion, was introduced, in 1958, as an appetite suppressant [52]. Shortly after being patented, in 1961 [53], reports of its abuse began to emerge [54, 55]. In 1971, amfepramone was included in the list of controlled substances by the UN Convention on Psychotropic Substances [50].

Pyrovalerone is another cathinone derivative, which appeared in 1960s and was used in the treatment of chronic fatigue and as an appetite suppressant [56, 57]. However, few years after its discovery, pyrovalerone was withdrawn from the market and scheduled as a controlled substance, after reports of its intravenous abuse by polydrug users [58].

In 1996, methylone was synthetized for the first time, and was patented as antidepressant and anti-Parkinsonism agent [59], but never resulted in a commercialized pharmaceutical product due to its psychostimulant strength, closely related to MDMA [32, 60].

In the following decade, the scenario of cathinone derivatives began to change, appearing as “legal highs” in some countries. Around 2004, methylone emerged in the Japanese and European market, under the trade name ‘Explosion’, being one of the first products to be

marketed online and via smartshops (retail establishments specialized in selling psychoactive substances and related paraphernalia) [32, 61]. In Israel, the use of khat-extracted cathinone spread in the early 2000s. It was originally marketed as a natural psychostimulant and aphrodisiac named 'Hagigat', but was banned in 2004, after a large number of hospitalisations caused by its administration [62, 63].

In 2007, reports on mephedrone use started to emerge, first in Israel and then in other parts of the world, including Australia and Europe [49]. Finland was the first European country where mephedrone was detected, but rapidly spread to other countries, especially to UK [64, 65]. Besides mephedrone, a number of other SCat, including *N*-ethylcathinone, butylone, 3,4-methylenedioxypyrovalerone (MDPV), 4-FMC and its positional isomer, 3-FMC, were reported and used on the European drug scene [66]. The popularity of these substances, particularly mephedrone, suddenly increased in 2009, when an unprecedented decrease in ecstasy and cocaine purity and availability was observed [31, 67]. Consequently, many drug users switched to mephedrone, since it was cheaper and more powerful than the available 'traditional' stimulants [68]. In addition, its availability in internet and its legal status may have boosted its popularity [68].

A research project led by the National Addiction Centre, in London, at the end of 2009, disclosed that 41.7% of the surveyed people had tried mephedrone, 33.2% during the last month, making it the sixth most popular drug, after tobacco, alcohol, cannabis, ecstasy and cocaine [68, 69]. Also in the UK, a self-report questionnaire conducted in high schools, colleges and universities in Tayside (Scotland) revealed that 20.3% of the students had used mephedrone at least once, 4.4% reported daily use and 17.6% had already experienced addiction or dependence symptoms [70]. Given the growing concern about mephedrone safety, the UK government banned this substance and other cathinone derivatives, on April 2010, under the UK Misuse of Drugs Act 1971 [71].

In the USA, the rise in popularity of SCat started to become evident around 2010, when the first cases of exposure to products marketed as "legal highs" and "bath salts" were reported to US poison centres [72]. Approximately 98% of the SCat identified in toxicological investigations were primarily MDPV, mephedrone and methylone [27, 73]. Unlike the European experience, where many of the products were being purchased from a "dealer" or through internet, in the USA the majority of the "bath salt" products were being locally purchased in small independent stores, such as gas stations and "smartshops" [72]. The growing number of cases, along with the alarming severity of the effects caused by the abuse of SCat, promptly led the US Drug Enforcement Administration (DEA), in 2011, to classify these substances as Schedule I under the Controlled Substances Act [74].

Following legislative controls of the "first generation" cathinones, a new series of SCat emerged in the market. Naphyrone, also known as naphthylpyrovalerone, appeared in UK a few months after mephedrone was criminalized [75]. It was found in a product named "Energy-1" (NRG-1), which was advertised as the legal replacement of mephedrone [76]. Along with naphyrone, a number of other SCat, including butylone, pentylone, 4-methyl-*N*-ethylcathinone (4-MEC), 4-FMC, 4-methyl-α-pyrrolidinopropiophenone (4-MePPP), 3,4-methylenedioxy-α-pyrrolidinobutiophenone (MDPBP), and even the already known mephedrone and MDPV, were found in the same product group [76, 77].

At the same time, other SCat started appearing, first 3,4-dimethylmethcathinone (3,4-DMMC), and then pentedrone and α-pyrrolidinopentiophenone (α-PVP) [32]. This last one became very popular in the USA and in Europe, between 2011 and 2015, marketed as "flakka" or "gravel" [78, 79]. During this period, dozens of deaths and thousands of hospital emergency cases were associated with the use of α-PVP and, in 2016, it was placed under international control (Schedule II of the 1971 Convention) [80].

Meanwhile, between 2013 and 2014, a series of new cathinone derivatives, including 4-methoxy-α-pyrrolidinovalerophenone (4-methoxy-α-PVP), MPHP, α-pyrrolidinoheptanophenone (α-PHPP or PV8), α-pyrrolidinooctanophenone (α-POP or PV9), 3,4-dimethoxy-α-pyrrolidinopentiophenone (3,4-dimethoxy-α-PVP), 4-fluoro-α-pyrrolidinopentiophenone (4-F-α-PVP), α-ethylaminopentiophenone (α-EAPP), *N*-ethyl-4-methylpentedrone, α-PHP, 4-methoxy-α-pyrrolidinooctanophenone (4-methoxy-α-POP), 4-methoxy-α-pyrrolidinoheptanophenone (4-methoxy-α-PHPP) and 4-fluoro-α-pyrrolidinoheptanophenone (4-F-α-PHPP), emerged in the Japanese market, particularly in multicoloured liquids sold as "aroma liquids" and coloured powders advertised as "fragrance powders" [81-83].

In 2015, the chemical structure of 4'-fluoro-α-pyrrolidinobutyrophenone (4-F-PBP), was identified, for the first time, in Portugal [84]. This SCat was detected by the Portuguese Criminal Police, with the cutting agent myo-inositol, in two seized products [84]. In the same year, Doi et al. [85] reported the discovery of the first thienyl cathinone derivatives, namely α-pyrrolidinopentiothiophenone (α-PVT), α-pyrrolidinobutiothiophenone (α-PBT) and their bromothienyl analogues, in commercialized designer drugs. Gambaro et al. [86] also found a thienyl cathinone derivative (thiothinone) in seized products by the Financial Police of the Malpensa Airport, in Northern Italy.

In 2016, Liu et al. [87] identified nine SCat in seized materials, six of which, N-ethylhexedrone, 4-chloro-pentedrone, 1-(4-chlorophenyl)-2-(ethylamino)pentan-1-one (4-Cl-α-EAPP), propylone, 4-methyl-1-phenyl-2-(pyrrolidin-1-yl)pentan-1-one (α-PiHP) and 1-(4-

chlorophenyl)-2-(pyrrolidin-1-yl)hexan-1-one (4-Cl-α-PHP) were reported for the first time. In the following year, four novel substituted cathinones, specifically hexedrone, 4-bromoethcathinone (4-BEC), 1-(4-chlorophenyl)-2-(pyrrolidin-1-yl)propan-1-one (4-Cl-PPP), and 1-(4-bromophenyl)-2-(pyrrolidin-1-yl)pentan-1-one (4-Br-PVP), were identified in seized products prior to being sold in the market [88].

Currently, the total number of SCat monitored by EMCDDA is 162, being the second largest group of NPS monitored by this agency [21]. Figure 2 shows the number of NPS notified to EU Early Warning System for the first time between 2005-2020.

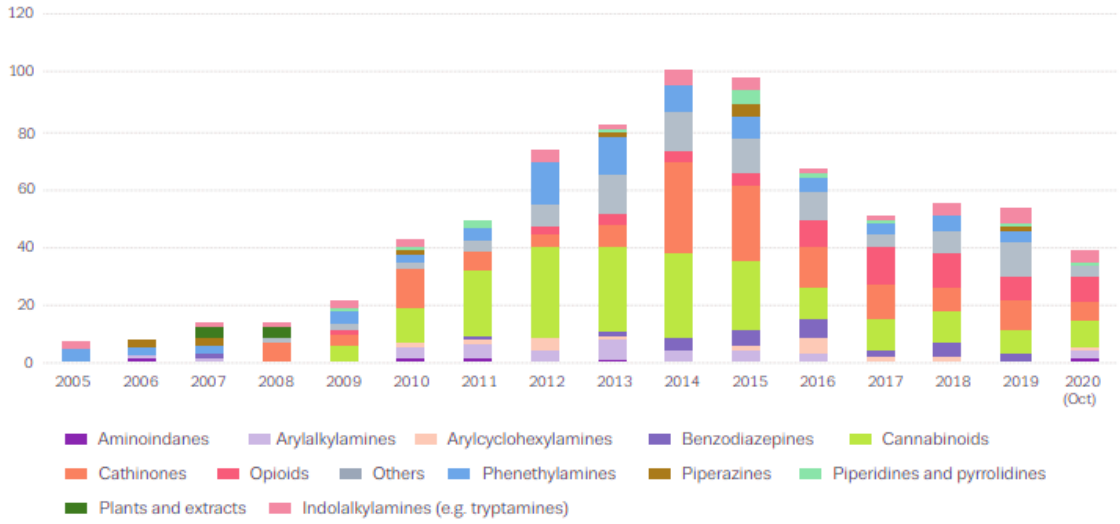

Figure 2. Numbers and categories of NPS notified to the EU Early Warning System for the first time between 2005 and October 2020 [89].

According to these data, the number of new SCat has reached peak levels in 2014 and 2015, and since then, the number has been decreasing. The causes of this decreasing are unclear, but may in part be due to measures taken by national governments in Europe to prohibit new substances. In addition, control measures and law enforcement operations in China (one of the major sources of NPS) targeting laboratories producing new substances may be an important factor [90].

1.4. Patterns of Use and Legal Status of Synthetic Cathinones

SCat are commonly found in the form of powder and can be administered by different pathways, the primary routes of administration being nasal insufflation ("snorting") and oral ingestion [91]. Users frequently practice "bombing", where the powder is wrapped in a cigarette paper and swallowed, or "keying", that is, the practice of dipping a key into powder and then insufflating [31]. Inhalation, intramuscular and intravenous injection, rectal administration and

gingival delivery, have also been reported, but are less common routes [92]. There have been occasional reports of SCat being placed on the eye cornea, sometimes referred to as “eyeballing” [64, 93]. Furthermore, multiple routes of administration have also been reported in a single session [94, 95].

In general, self-reported doses range from a few milligrams to over 1 g of powder [31, 96]. However, due to the unknown purity of “legal highs”, as well as the exact composition, the dose is difficult to assess [31]. Table 1 summarizes typical doses, routes of administration and duration of effects of several SCat.

Table 1. Typical doses, routes of administration, onset of action and duration of effects of several SCat (adapted from Kerrigan [97]).

Synthetic Cathinone	Typical Dosage (mg)	Routes of Administration	Onset of Action (min)	Duration of Effects (h)	REF.
Mephedrone	50-250	Oral	45-120	2-4	[32, 68, 91, 98, 99]
	5-75	Nasal	–	0.5-1	
	50-75	Intravenous	–	0.25-0.5	
MDPV	3-30	Oral	15-30	2.5-3	[32, 91, 93, 99]
	3-20	Nasal	< 30	6-8	[32]
Methylone	50-250	Oral	15-30	2-5	[32, 91, 99]
4-MEC	100-300	Oral	30-45	2-4	[96]
Butylone	80-250	Oral	15-30	4-6	[32, 91]
Methedrone	50-500	Oral	–	0.75-2	[100]
Buphedrone	20-150	Oral	–	2.5-4	[91, 101]
	5-30	Nasal	2-4	0.5-1	
Methcathinone	60-250	Intravenous, Nasal and Oral	–	–	[49]
Pyrovalerone	20	–	–	–	[102]
Ethylone	175	–	–	–	[102]
α-PVP	1-25	Oral	10-40	–	[80, 103]
	1-20	Nasal	–	–	[80, 104]
	10-400	Inhalation (smoked/vaporized)	–	–	[80]
α-PVT	50-60	Oral	–	–	[104]
	50-70	Nasal	–	–	
Naphyrone	10-50	Oral	30-60	4	[91, 105]
	10-50	Nasal	5-10	0.5-2	[105]
3,4-MDPBP	50-100	Oral	–	–	[104]
3,4-MDPPP	Up to 75	Oral	–	–	[104]
	10-25	Nasal	–	–	

Desired effects reported by SCat users include euphoria, increased sociability, intensification of sensory experiences, sexual arousal and well-being [27]. However, numerous negative physical and psychiatric effects have been associated with the use of SCat, and for this reason several countries have applied new control mechanisms with accelerated ways to curtail the free sale and distribution of these substances [106]. In general, countries affected by a limited number of NPS, often control NPS on a substance-by-substance basis (*i.e.* individual listing) [107]. Despite this measure to have the advantage that there is no ambiguity about whether a substance is covered, or not, by the control measures, the major drawback of this approach is that adding substance by substance to the schedules of national drug laws can become a lengthy procedure, which may not provide a fitting response to the current fast-paced nature of the synthetic drug market [22].

In order to overcome this problem, countries affected by a high number of NPS have adopted different types of legislation that go beyond placing individual substances under control. These include legislation that enable the control of NPS that are chemically similar to a drug already controlled (analogue control) or of whole groups of NPS (generic control), without the need to refer to each individual substance in the legislation [107, 108]. Generic controls on NPS groups have been applied in Europe and North America, where a wide variety of NPS has been reported [107]. On the other hand, some countries have resorted to the use of consumer protection laws and/or drug legislation to control NPS [109]. These measures have helped to reduce the supply of NPS by seizing stock, and closing down retail outlets, at least temporarily [110]. However, products containing these substances are often labelled as “not for human consumption” and sold as “research chemicals” to bypass existing consumer legislation [110].

Given the complexity and highly dynamic nature of the NPS market, some countries have adopted specific legislation to stop the rapid proliferation of NPS. These legislative approaches range from a general prohibition on the distribution of NPS to pre-market approval regulatory regimes and controls on psychoactive substances which are intended for human consumption and capable of producing a psychoactive effect [107].

Despite these innovative measures against the NPS problem, each approach has its benefits and limitations. Differences in country-specific legislation and its capacity to implement them open opportunities for trafficking NPS and pose a major obstacle for effective law enforcement interventions [110]. In Portugal, the commercialization of NPS has been outlawed since 2013, after the introduction of the Decree-Law no. 54/2013, of 17 April, which defines the legal framework for the prevention and protection against the advertising and commerce of the NPS and forbids the production, importation, exportation, publicity, distribution, possession and

selling of 159 NPS, including 34 SCat [111]. These measures have helped to reduce the supply of NPS by seizing stock and closing down the so-called “smartshops”.

1.5. Chemistry of Synthetic Cathinones

Chemically SCat are phenylalkylamine derivatives, which resemble the molecule of amphetamine, differing only by the presence of a carbonyl group at the β-position of the side chain (Figure 3) [112].

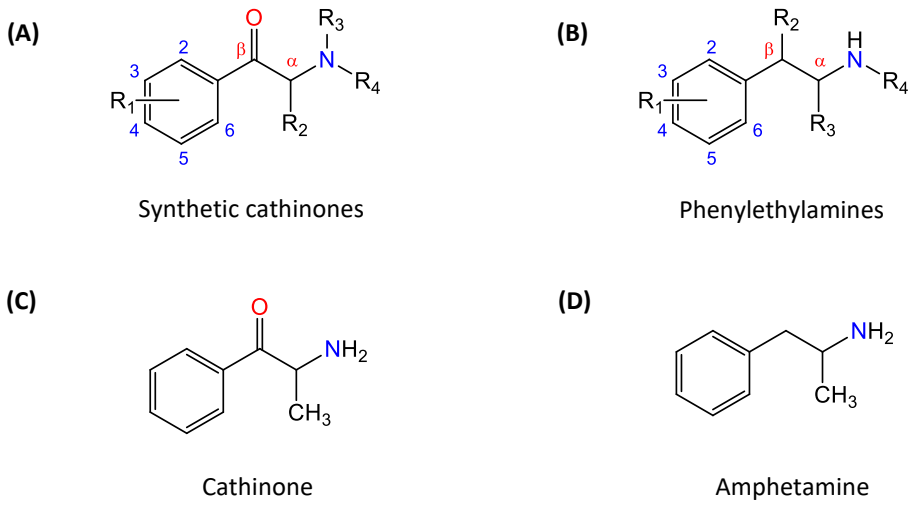

Figure 3. General chemical structures of (A) SCat, and (B) phenylethylamines. Structures of (C) cathinone and (D) amphetamine (adapted from Tyrkko et al. [113]).

Designer modifications of the basic structure of cathinone, in general, take place in three distinct regions of the molecule, namely the aromatic ring, the alkyl side chain and the amino group that lead to a multitude of derivatives, which can be separated into different groups, based on the substitution made [32]. The most basic derivatives are the N-alkyl derivatives or those with an alkyl or halogen substituent at any position of the aromatic ring (Figure 4). The majority of the first SCat fall into this group, and they include methcathinone, *N*-ethylcathinone, mephedrone, 4-FMC, buphedrone, and pentedrone [112]. When a methylenedioxy group is added to the aromatic ring, cathinones structurally similar to MDMA are produced [114]. Methylone, ethylone, butylone and pentylone are some examples of substances that belong to this group. Another group of SCat is the pyrrolidinophenone-like family, which is characterized by a pyrrolidinyl substitution at the nitrogen atom [115]. These compounds are derivatives of *α*-pyrrolidinopropiophenone (*α*-PPP), and are the most frequently encountered in the designer drug market [32, 112]. From the combination of the last two groups, appears the SCat family that has both the 3,4-methylenedioxy ring substitution and the *N*-pyrrolininyl moiety [32].

Members of this class include 3,4-methylenedioxy-α-pyrrolidinopropiophenone (MDPPP), MDPBP and MDPV.

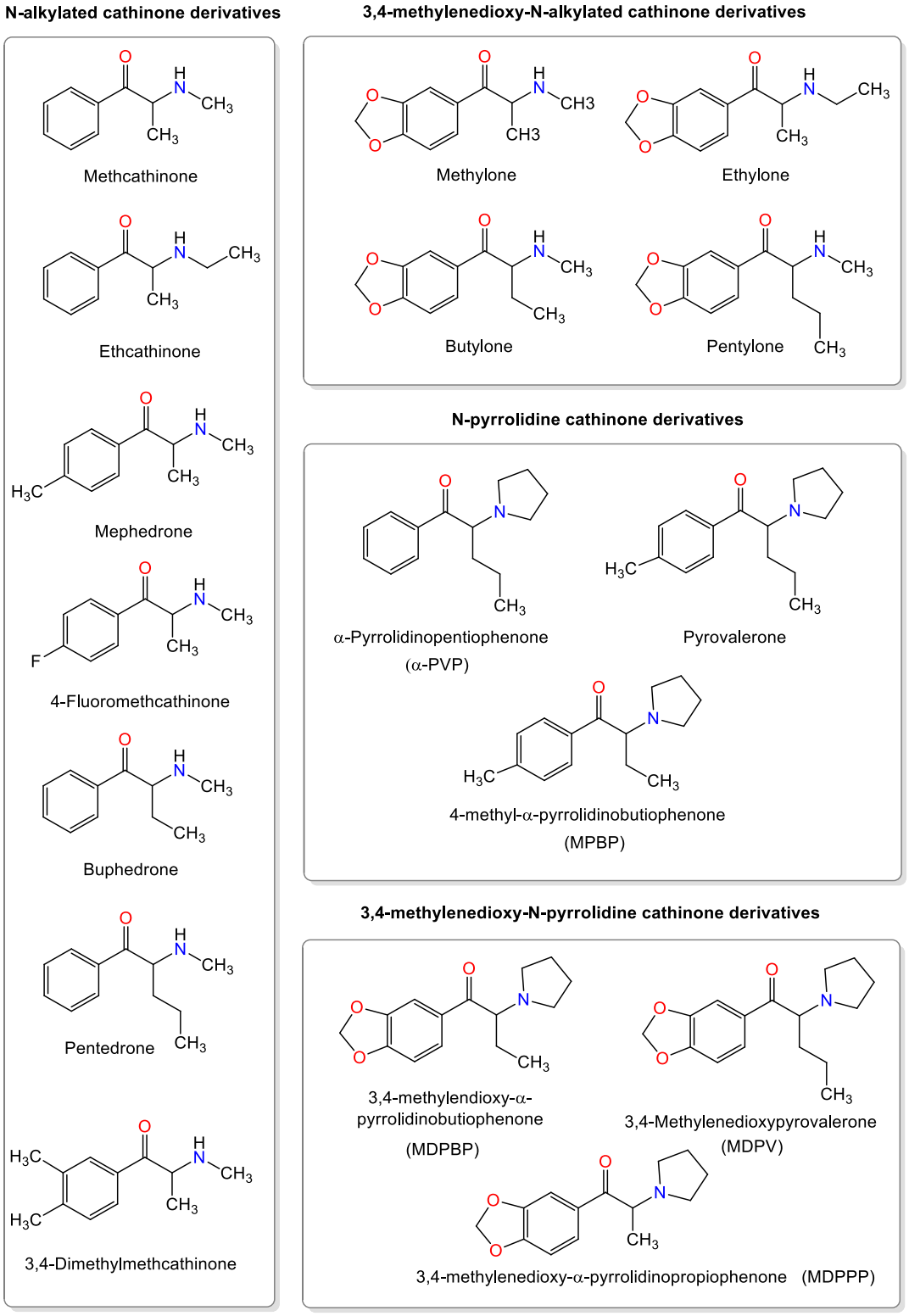

Figure 4. Classification of SCat based on their chemical structure (adapted from Valente et al. [32]). Abbreviation: MDPBP - 3,4-methylenedioxy-α-pyrrolidinobutiophenone, MDPV - 3,4-methylenedioxypyrovalerone and MDPPP - 3,4-methylenedioxy-α-pyrrolidinopropiophenone.

It is important to note that cathinones presenting a unique structure have also been described. It is the case of naphyrone which shows a naphthyl ring, instead of phenyl and is not present in other cathinone derivatives [32]. Recently, other cathinone derivatives, such as α-PVT, α-PBT and thiothinone, appeared with a thienyl group, instead of the benzoyl moiety [85, 86]. Furthermore, like other phenethylamines, substituted cathinones are chiral molecules and can exist in two stereoisomeric forms that may differ in their potency and receptor affinity [30, 32, 116].

1.6. Mechanism of Action

SCat are generally considered to be less pharmacologically active when compared with amphetamines, due to their higher hydrophilicity given the presence of the β-keto group [117]. In general, the ketone group increases the polarity of SCat and, consequently, reduces the ability to cross the blood-brain barrier, thereby reducing the potency of these compounds over amphetamines [116]. To obtain equipotent effect, the doses of SCat reported by users are commonly higher than those reported for the related amphetamines, and for some cathinone derivatives, there is often the need to repeat the dose shortly after the first intake [32, 118, 119].

SCat with a pyrrolidine ring in its chemical structure tend to be an exception to this rule. The high lipophilicity of the pyrrolidine ring increases permeability through the blood-brain barrier, and hence, increased potency and abuse potential [30, 120, 121]. Simmler et al. [122] showed, in an *in vitro* study, the ability of four cathinone derivatives (mephedrone, methylone, ethylone and MDPV) to cross the blood-brain barrier. Among the four derivatives, the blood-brain barrier was most permeable to MDPV, followed by mephedrone, methylone and methcathinone, and evidences suggest that the first one is actively transported into the brain via specific blood-brain influx carriers [122].

Similar to other illicit substances, SCat seem to exert their psychostimulant effects through the interaction with monoamine membrane transporters, namely dopamine transporters (DAT), noradrenaline transporters (NAT) and serotonin transporters (SERT), leading to an increase of synaptic concentrations of these biogenic amines [26, 27]. In general, these interactions can occur through inhibition of the mononamine reuptake from the synaptic cleft, and/or promotion of the release of monoamines (e.g., by inhibition of the vesicular monoamine transporter-2 ($VMAT_2$)) (Figure 5) [123]. However, the affinity and type of interaction towards these transporters vary among SCat [122]. Considering the relative potency of their inhibition of DA, NA and 5-HT reuptake, as well as their ability to liberate these neurotransmitters Simmler et al. [122] classified them into three major groups. The first group includes cathinones that act

very closely to cocaine and MDMA, and it is represented as the "cocaine-MDMA-mixed cathinone" group [112]. Substances belonging to this group, including mephedrone, methylone, ethylone, butylone and naphyrone, show non-selective inhibition of monoamine reuptake, in a way that resembles cocaine, with an affinity for DA transporter up to 5-times higher than the affinity for 5-HT transporter [122]. In addition, these substances, with the exception of naphyrone, also induce the release of 5-HT in a manner similar to MDMA [112, 122].

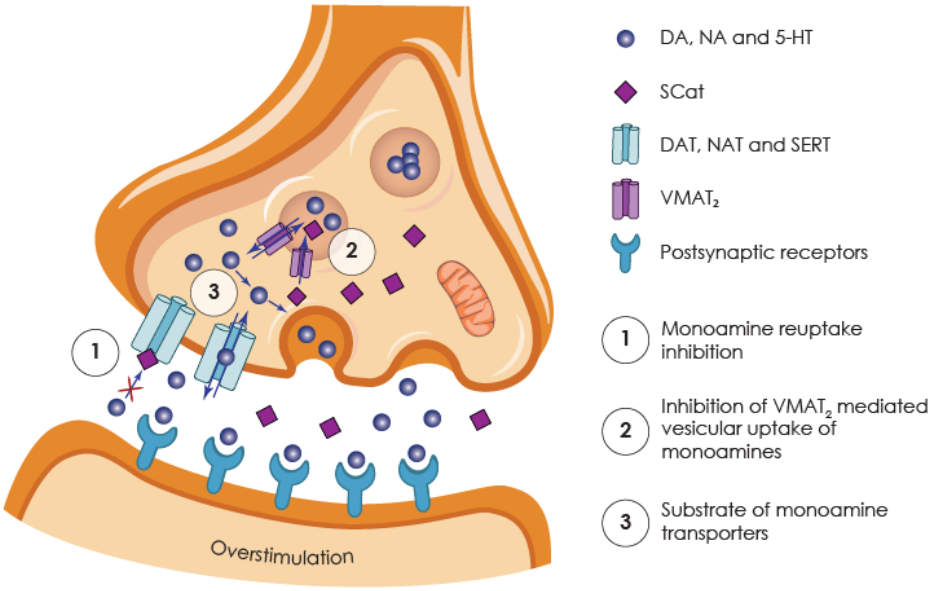

Figure 5. Schematic representation of the modes of action of SCat in the central nervous system (adapted from Almeida et al. [123]). Abbreviations: DA, dopamine; NA, noradrenaline; 5-HT, 5-hydroxytryptamine (serotonin); SCat: synthetic cathinones; DAT, dopamine transportes; NAT, noradrenaline transportes; SERT, serotonin transportes; $VMAT_2$, vesicular monoamine transporter-2.

The second group, represented as "methamphetamine-like cathinones", include cathinones that act as preferential catecholamine (DA and NA) reuptake inhibitors and DA releasers. *In vitro* studies have shown that cathinone and methcathinone exhibit a relative monoamine transporter inhibition profile very similar to amphetamine and methamphetamine, with high inhibitory potencies at the DA and low potencies at the 5-HT transporters [122, 124, 125]. In addition, cathinone and methcathinone are also potent releasers of DA, similar to their non-β-keto analogues [122]. *N*-ethylcathinone, 4-FMC and its positional isomer 3-FMC also belongs to this group, showing monoamine uptake transporter inhibition profiles that resemble methamphetamine [122, 126]. With exception of *N*-ethylcathinone, 4-FMC and 3-FMC are also DA releasers [122, 126].

"Pyrovalerone-cathinones" are the third group, being characterized by very potent and selective inhibitors of the catecholamine reuptake, which do not promote the release of

neurotransmitters. Pyrovalerone and its derivative MDPV are very potent and selective DA transporter inhibitors, at least 10-fold more potent than cocaine and methamphetamine [122, 127]. In contrast to naphyrone (pyrovalerone derivative), MDPV and pyrovalerone are weak inhibitors of the 5-HT transporter, resulting in high DA transporter selectivity, with DA/5-HT transporter inhibition ratios over 100, revealing a high abuse potential [122, 128]. In addition, both cathinone derivatives are potent NA transporter inhibitors, but unlike amphetamines, do not promote monoamine release [122, 129, 130]. Some *in vitro* studies have demonstrated that α-PVP and 4-MePPP act in a similar way to MDPV [131, 132].

Investigations of structure-activity relationships (SAR) of SCat have been fundamental to understand the effect of chemical structure, and its alterations, on a particular pharmacological action, and to explore trends in the action of a series of related agents [133]. In an informative SAR study, Kolanos et al. [134] analysed the MDPV molecule to determine which structural features govern activity at DA transporter. They found that the bulky pyrrolidine ring and the α-carbon chain are critical attributes for potent uptake inhibition at DA transporter, whereas the 3,4-methylenedioxy ring moiety has a minimal contribution [134].

Marusich et al. [131] examined truncation of the α-PVP n-propyl side chain to its ethyl and methyl counterparts (i.e., α-PBP and α-PPP, respectively) and found that shortening the chain resulted in reduced potency at DA and NA transporters. Similar results were also reported for the DA transporter, by Kolanos et al. [135].

Using microdialysis in conscious rats, a number of studies showed that depending on the substituent in *para* position of the phenyl unit of methcathinone, the compound can produce different effects on extracellular DA or 5-HT levels. Suyama et al. [136] showed that halogenated methcathinone analogues (-F, -Cl or -Br) increased DA and 5-HT release with different potencies. 4-FMC and 4-bromomethcathinone preferentially increased extracellular 5-HT levels, while 4-chloromethcathinone increased, more efficiently, extracellular DA levels. On the other hand, the addition of a *para*-methoxy group (i.e. methedrone) displayed an increased potency to raise 5-HT over DA extracellular levels [136].

Although the SAR studies of SCat are still in their infancy, it is clear that simple structural changes can have a substantial impact on the potency and selectivity of SCat [133]. In addition, several studies have demonstrated that, similarly to other drugs of abuse, the affinity of SCat toward NA transporter may be associated with sympathomimetic effects, while the potency to inhibit DA transporter may be related with their psychostimulant effects and addictive potential [32]. Symptoms of paranoia and hallucinations, similar to those observed with classic hallucinogenic drugs (e.g. psilocybin, mescaline and LSD) have been associated with the great

affinity for 5-HT transporter [137]. On the other hand, symptoms of depression and anhedonia could be resultant from both 5-HT and DA putative depletion induced by these substances [68].

1.7. Pharmacokinetic

1.7.1. Absorption, Distribution and Elimination

SCat can be introduced into the body by several routes of administration, as previously described. Generally, they are rapidly absorbed, reaching peak concentrations within 1.5 h after administration [138]. However, the rate of absorption depends on the substance form, administration route or even factors related to the user [139].

Once they reach the systemic circulation, these substances are first distributed to highly irrigated organs, including brain, lungs, liver and kidneys [140]. It is in this phase that the entrance of SCat on the brain is dependent on their ability to permeate the blood-brain barrier and, consequently, to promote the first effects [139]. Following that, the substances are distributed to other parts of the body, including muscle, fat and skin, being responsible for the redistribution phenomenon observed for some drugs [139]. The distribution process is influenced by a number of factors, including the substance ability to bind to plasma proteins and tissues, blood flow and capillary permeability, and local pH [139]. In general, SCat tend to poorly bind to plasma proteins, as demonstrated in several studies [141, 142]. On the other hand, cathinone and its synthetic derivatives can undergo metabolism although almost all SCat may be partially excreted unchanged in urine [139].

In vivo studies aiming to investigate pharmacokinetics properties of SCat have been mainly performed in animal models, being the overwhelming majority in rodent models. To date only a few studies have been performed in humans [143, 144]. In 2014, Namera et al. [145] investigated the time-course profile of urinary excretion of α-PVP and α-pyrrolidinobutiophenone (α-PBP) in one individual, after intravenous administration of an unknown dose. After the patient's admission to the hospital, urine was daily collected for 1 month to examine the excretion profile. The concentrations of both SCat were highest in the first sample collected, at least 32 h after administration, and the values found were 1.2 μg mL^{-1} for α-PVP and 1.6 μg mL^{-1} for α-PBP. The urinary concentration gradually decreased, day by day, reaching almost imperceptible values 10 days after drug administration. According to the results, during the initial 5 days after drug administration, the elimination half-life ($t_{1/2}$) was estimated to be 22 h and 11 h, for α-PVP and α-PBP, respectively. During the second half period, i.e., 6 to 10 days after drug administration, the estimated $t_{1/2}$ was 40 h for α-PVP and 30 h for α-PBP. According to the authors, the $t_{1/2}$ difference may be attributed to the hydrophobicity of

these substances. In this study, the authors also proved that the urinary excretion rate of amphetamine-type substances is remarkably influenced by the pH of urine, as acidified urine facilitates the elimination of this substances from the body [145].

In 2016, Papaseit et al. [144] evaluated for the first time the pharmacokinetic properties of mephedrone in healthy and recreational drug abusers. After the oral administration of 200 mg of mephedrone to the subjects, an average maximum plasma concentration (C_{max}) value of 134.6 μg L^{-1} was obtained at 1.25 h (T_{max}). Following the absorption phase, concentrations declined to mean values of 6.1 ng mL^{-1} at 12h, being undetectable 24 h post-administration. The average $t_{1/2}$ was 2.15 h. The pharmacokinetic findings obtained in this investigation, are consistent with the quick onset and brief duration of effects described for mephedrone abuse in recreational scenarios [139].

In a similar study performed by Olesti et al. [143], 150 mg of mephedrone was orally administrated in healthy and recreational drug abusers. Peak plasma concentration (C_{max} = 122.6 ng mL^{-1}) was reached at 1-hour post-drug administration, and the $t_{1/2}$ was 2.2 h. The renal clearance, which reflects how quickly a substance is removed from plasma by the kidney and excreted in urine, was 5.6 L h^{-1}, while the absolute volume of distribution (V_d), which represents the apparent volume of a drug distributed based on the dose of the drug administered and describes the relationship between the dose and the resulting serum concentration, was 123.5 L (calculated considering a hypothetical bioavailability of 10%).

In a study performed with Landrace pigs, the pharmacokinetic profile of the 3-methylmethcathinone (3-MMC) was explored, a positional isomer of mephedrone. This SCat was administrated as a single intravenous dose (0.3 mg kg^{-1}), followed by a multiple oral dose administration (3 mg kg^{-1}) for five days. After the oral administration, 3-MMC displayed rapid absorption with a C_{max} of 27 μg L^{-1} at a T_{max} of 0.08 h. However, the bioavailability was about 7%. The authors also determined a total clearance of 199 L h^{-1}, an apparent V_d of 240 L and an average $t_{1/2}$ of 0.8 h. Moreover, most of 3-MMC was quickly excreted, with plasma concentrations barely detectable 4 h after administration [146].

The pharmacokinetic of SCat has also been studied in rat models. In 2013, Martinez-Clemente et al. [141] administered mephedrone intravenously to Sprague-Dawley rats (10 mg kg^{-1}), as well as orally (30 and 60 mg kg^{-1}). When administered via intravenous route, mephedrone had a C_{max} of 7221 ng mL^{-1}, a $t_{1/2}$ of 0.37 h, a total plasma clearance of approximately 1.69 L h^{-1} and an apparent V_d at steady state of about 0.58 L. In addition, the concentration of mephedrone in plasma was almost undetectable 4 h after its administration. For oral dosing conditions, the C_{max} values (dose 30 mg kg^{-1}: C_{max} = 331.2 ng mL^{-1}; dose 60 mg kg^{-1}: C_{max} = 960.0 ng mL^{-1}) were archived rapidly, showing a T_{max} within 0.93 h for the lower dose

and 0.43 h for the highest dose. Both administrated doses showed a $t_{1/2}$ of 0.55 h. In addition, after oral administration, mephedrone bioavailability was about 7.3% (at the dose of 30 mg kg^{-1}) and 11.2% (at the dose of 60 mg kg^{-1}), and plasma concentration decrease to undetectable levels 9 h post-administration.

López-Arnau et al. [142] also used Sprague-Dawley rats to study the pharmacokinetic of methylone, and this substance was administered intravenously (10 mg kg^{-1}) and orally (15 and 30 mg kg^{-1}). For oral dosing conditions, C_{max} values (dose 15 mg kg^{-1}: C_{max} = 1456.7 ng mL^{-1}; dose 30 mg kg^{-1}: C_{max} = 1896.0 ng mL^{-1}) were achieved rapidly, usually within 0.5 to 1 h, and declined to undetectable levels at 24 h. Both administered doses showed a $t_{1/2}$ of 0.55 h, and the total plasma clearance was 0.53 L h^{-1}. On the other hand, the apparent V_d at steady state was about 0.43 L for the 15 mg kg^{-1} dose, and the bioavailability range from 78% for the highest dose and 89% for the lower dose. With regard to intravenous administration, methylone had a C_{max} of 3483.8 ng mL^{-1}, a $t_{1/2}$ of 0.95 h, and a total plasma clearance similar to that of orally administered doses (0.53 L h^{-1}). On the other hand, the apparent V_d at steady state was higher than that observed for the oral route of administration (about 0.54 L).

Recently, another study using Sprague-Dawley rats, evaluated the plasma and central nervous system (CNS) pharmacokinetic parameters of three SCat, namely methylone, butylone and pentylone [147]. In this study, SCat (20 mg kg^{-1}) were administered by the subcutaneous route. Plasma pharmacokinetic parameters displayed significantly differences between drugs. Pentylone, the most lipophilic SCat, demonstrated the highest C_{max} value (5735.7 µg L^{-1}), followed by butylone (1844.6 µg L^{-1}) and, finally, methylone (949.9 µg L^{-1}), the SCat with the shortest α-alkyl chain studied. All SCat showed a T_{max} of 0.5 h, while $t_{1/2}$ was 0.69 h for methylone, 1.37 h for butylone and 4.22 h for pentylone. The apparent V_d and the total plasma clearance were also determined in this study, and the values were as follow: methylone: V_d = 4.23 L and clearance = 4.44 L h^{-1}; butylone: V_d = 2.36 L and clearance = 1.2 L h^{-1}; pentylone: V_d = 3.68 L and clearance = 0.59 L h^{-1}. Regarding the CNS pharmacokinetic parameters, C_{max} values for methylone was 12215 µg L^{-1}, for butylone 13458 µg L^{-1} and for pentylone 7425.6 µg L^{-1}. All SCat showed a T_{max} of 1 h, while $t_{1/2}$ values was 2.25 h for methylone, 1.17 h for butylone and 1.40 h for pentylone.

Currently, there are several pharmacokinetic studies performed in SCat. Table 2 provides an overview of the most recent pharmacokinetic studies involving SCat.

Table 2. General overview of pharmacokinetic studies involving SCat (adapted from Soares et al. [139]).

Synthetic Cathinones	Dose (mg kg^{-1})	Route of administration	Sample	C_{max} (µg L^{-1})	T_{max} (h)	$t_{1/2}$ (h)	Cl (L h^{-1})	V_d (L)	$AUC_{0-\infty}$ (µg h L^{-1})	REF.
Human										
Mephedrone	200 mg	Oral	Plasma	134.6	1.25	2.15	n.a.	n.a.	556.2	[144]
Mephedrone	150 mg	Oral	Plasma	122.6	1.0	2.2	Renal: 5.6 Plasma: 41.1[a]	123.5[a]	460.9	[143]
Landrace pigs										
3-MMC	0.3	Intravenous	Plasma	n.a.	n.a.	0.83	199[b]	240[c]	48	[146]
	3	Oral		27	0.08	n.a.	n.a.	n.a.	31	
Sprague–Dawley rats										
Mephedrone	10	Intravenous	Plasma	7221	n.a.	0.37	1.69[b]	0.58[d]	1331.8	[141]
	30	Oral		331.2	0.93	0.55	1.30[e]	n.a.	294.5	
	60	Oral		960.0	0.43	0.55	0.38[e]	n.a.	895.4	
Methylone	3	Subcutaneous	Plasma	620	0.25	0.80	n.a.	n.a.	446.7	[148]
	6			1410		0.95			1138.3	
	12			3170		1.10			3350	
Methylone	10	Intravenous	Plasma	5271.6	n.a.	0.95	0.53[b]	0.54[d]	4251.9	[142]
	15	Oral		1456.7	0.50	0.55	0.53[b]	0.43[d]	5740.3	
	30	Oral		1896.0	0.97	0.55	0.53[b]	n.a.	9988.8	
Methylone, Butylone and Pentylone	20	Subcutaneous	Plasma	MET: 949.9 BUT: 1844.6 PENT: 5735.7	0.5	MET: 0.69 BUT: 1.37 PENT: 4.22	MET: 4.44 BUT: 1.20 PENT: 0.59	MET: 4.23[c] BUT: 2.36[c] PENT: 3.68[c]	MET: 1205.6 BUT: 4060.7 PENT: 8923.8	[147]
			CFS	MET: 12215 BUT: 13458 PENT: 7425.6	1.0	MET: 2.25 BUT: 1.17 PENT: 1.40	n.a.	n.a.	MET: 47646.7 BUT: 28990 PENT: 18530	
MDPV	0.5	Subcutaneous	Plasma	74.2	0.26	1.63	n.a.	n.a.	89.9	[149]
	1.0			165	0.22	1.30			188.0	
	2.0			271	0.31	1.40			386.1	
MDPV	0.5	Intraperitoneal	Plasma	20	0.17	1.53	n.a.	n.a.	18.6	[150]
	1.0			54		1.32			47.6	
	2.0			135		1.65			145.4	
MDPV	1.0	Subcutaneous	Striatum	0.95 µg g^{-1}	0.41	1.02	n.a.	n.a.	6192.7	[151]

Table 2. (Continuation)

Synthetic Cathinone	Dose (mg kg^{-1})	Route of administration	Sample	C_{max} (µg L^{-1})	T_{max} (h)	$t_{1/2}$ (h)	Cl (L h^{-1})	V_d (L)	$AUC_{0-\infty}$ (µg h L^{-1})	REF.
Wistar rats										
Mephedrone	5.0	Subcutaneous	Serum	826.2	0.5	n.a.	n.a.	n.a.	n.a.	[152]
			Brain	0.77 µg g^{-1}	0.5					
			Liver	≈ 0.20 µg g^{-1}	0.5					
			Lungs	1.04 µg g^{-1}	0.5					
Methylone	10	Subcutaneous	Serum	≈ 2000	0.5	n.a.	n.a.	n.a.	n.a.	[153]
			Brain	≈ 10.0 µg g^{-1}	0.5					
MDPV	2.0	Subcutaneous	Serum	140	0.5	n.a.	n.a.	n.a.	n.a.	[154]
			Brain	0.26 µg g^{-1}	0.5					
			Lungs	0.53 µg g^{-1}	0.5					
β-Naphyrone	10	Subcutaneous	Serum	269	0.5	n.a.	n.a.	n.a.	n.a.	[155]
			Brain	0.0017 µg g^{-1}	0.5					
			Lungs	0.0030 µg g^{-1}	1					
			Liver	0.00042 µg g^{-1}	1					
CD-1 mice										
β-Naphyrone	30	Intraperitoneal	Plasma	3992	0.08–0.17	0.3	0.37[b]	0.29[d]	n.a.	[156]

Abbreviations: 3-MMC: 3-methylmethcathinone; $AUC_{0-\infty}$: area under the concentration–time curve; BUT: butylone; CFS: cerebrospinal fluid; *Cl*: clearance; C_{max}: maximum concentration; MET: methylone; n.a.: not available; PENT: pentylone; REF: references; $t_{1/2}$: elimination half-life; T_{max}: time of occurrence of maximum concentration; V_d: volume of distribution.

[a] Values calculated with a hypothesized bioavailability of 10%

[b] Total plasma clearance

[c] Apparent volume of distribution

[d] Apparent volume of distribution at steady state

[e] Metabolic clearance

1.7.2. Metabolism

Metabolism studies play an important role in clinical and forensic toxicology, since metabolites may have pharmacodynamic or toxicological activity in addition to being appropriate targets for drug screening in humans [92, 157].

Studies in rats and humans have shown that SCat can be metabolized by multiple pathways, which can vary according to their molecular structure [158-160]. In general, metabolic reactions can be divided into phase I or functionalization reactions, such as hydroxylation or dealkylation and phase II or conjugation reactions, in which the parent drug or phase I metabolites are conjugated with certain moieties such as glucuronic acid, sulfonic acid, or methyl moieties [161]. Figure 6 shows common metabolic pathways of SCat.

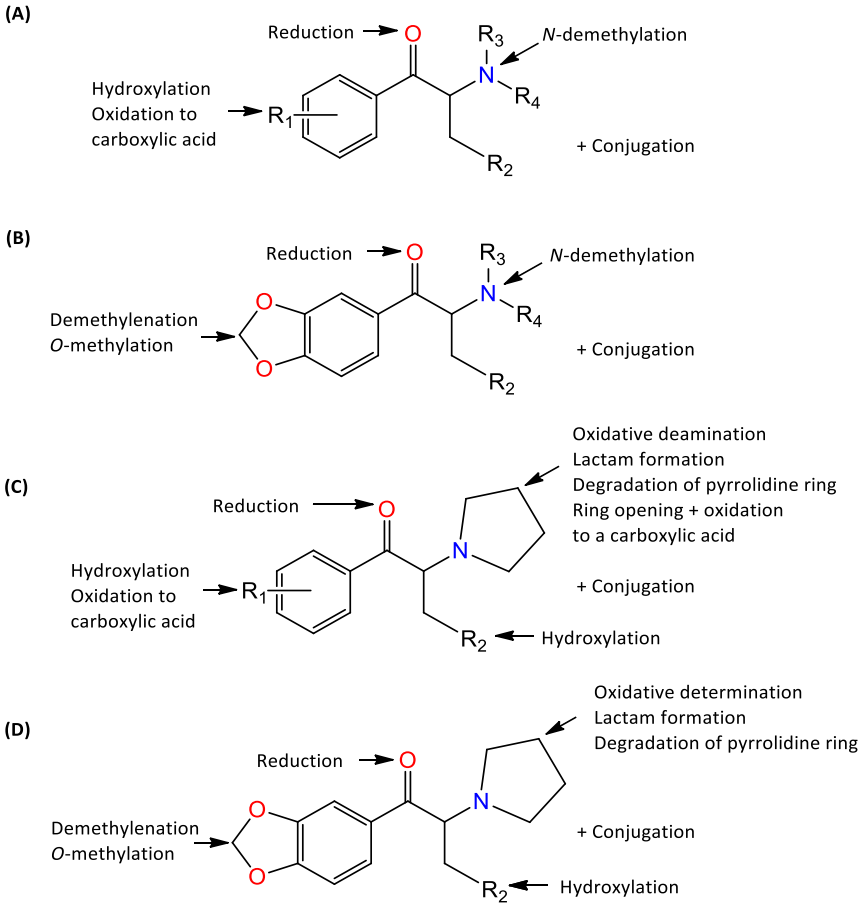

Figure 6. General metabolic pathways for SCat: (A) N-alkyl cathinone derivatives with/without ring substituents; (B) 3,4-methylenedioxy cathinone derivatives (C) pyrrolidinophenone derivatives and (D) 3,4-methylenedioxypyrrolidinophenone derivatives (adapted from Tyrkko et al. [113]).

Generally, phase I metabolic reactions include *N*-dealkylation to the primary amine, reduction of the β-keto group to the corresponding alcohol, and in case of alkyl substituted

cathinones at phenyl ring, oxidation of the alkyl moiety to the corresponding alcohol and carboxylic acid [93, 113]. Since the β-ketone group is a common structure among SCat, almost all SCat showed reduction of the ketone group to a hydroxyl group [160].

Cathinone and methcathinone are known to be metabolized partly by reduction of the ketone group to the corresponding amino alcohols, which are similar compounds to norephedrine and ephedrine [160, 162, 163]. The metabolism of cathinone has been shown to be stereoselective with the principal metabolite of S-(−)-cathinone being norephedrine, whilst R-(+)-cathinone is metabolized to cathine [164]. This stereoselectivity metabolism was also demonstrated for methcathinone and dimethylpropion to the corresponding β-ketone-reduced hydroxyl metabolites [165, 166]. In addition, methcathinone and dimethylpropion are also metabolized by N-dealkyl reaction [160, 165].

For ring and side-chain-substituted cathinones, N-dealkylation is also a common metabolic pathway [121]. Based on the analysis of rat and human urine, Meyer et al. [167] showed that mephedrone is metabolised by three phase I pathways. Besides the N-demethylation to the primary amine, mephedrone can undergo oxidation in the 4'-methyl moiety of the phenyl ring, producing an alcohol that can be further oxidized to give a carboxylic acid metabolite (Figure 7) [167].

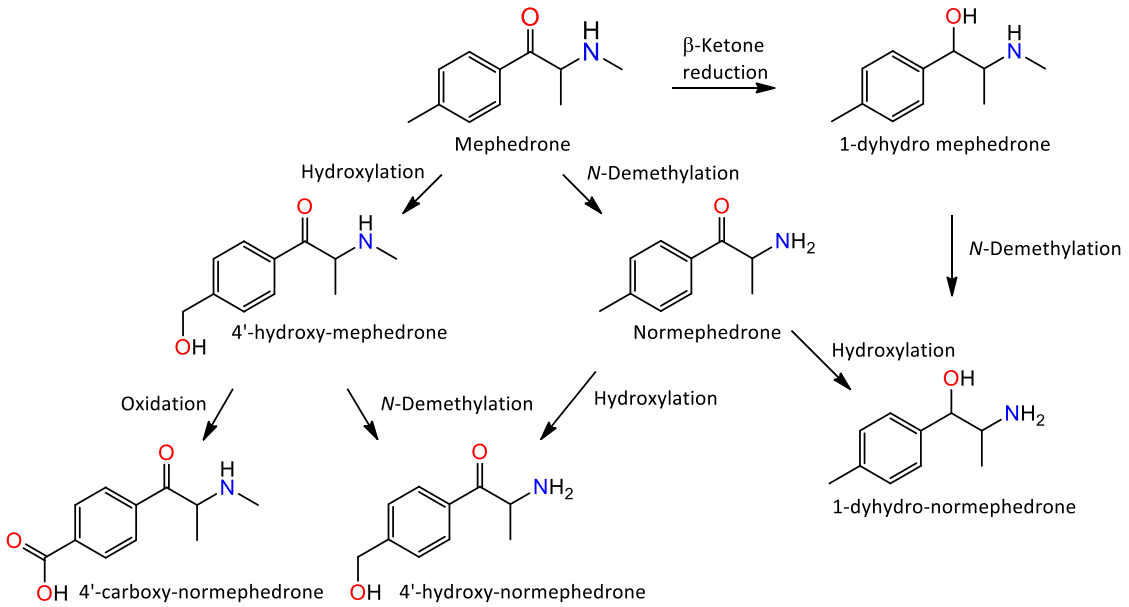

Figure 7. Major phase I metabolic pathways for mephedrone (adapted from Meyer et al. [167]).

Recent evidences suggest that cytochrome P450 2D6 (CYP2D6) is the main responsible enzyme for the *in vitro* phase I metabolism of mephedrone, with some minor contribution from other NAPDH-dependent enzymes [108]. On the other hand, it should be noted that

mephedrone itself was found in rat and human urine, which indicates that it is not metabolised to a very high extent [167, 168].

Regarding to the metabolism of 3,4-methylenedioxy ring-substituted cathinones, demethylenation of the 3,4-methylenedioxy moiety to dihydroxy metabolite, followed by O-methylation are the major metabolic pathways of these compounds [158, 159]. Studies on methylone, ethylone and butylone metabolism have shown that these substances seem to be almost metabolized by the same pathways (Figure 8) [159, 169].

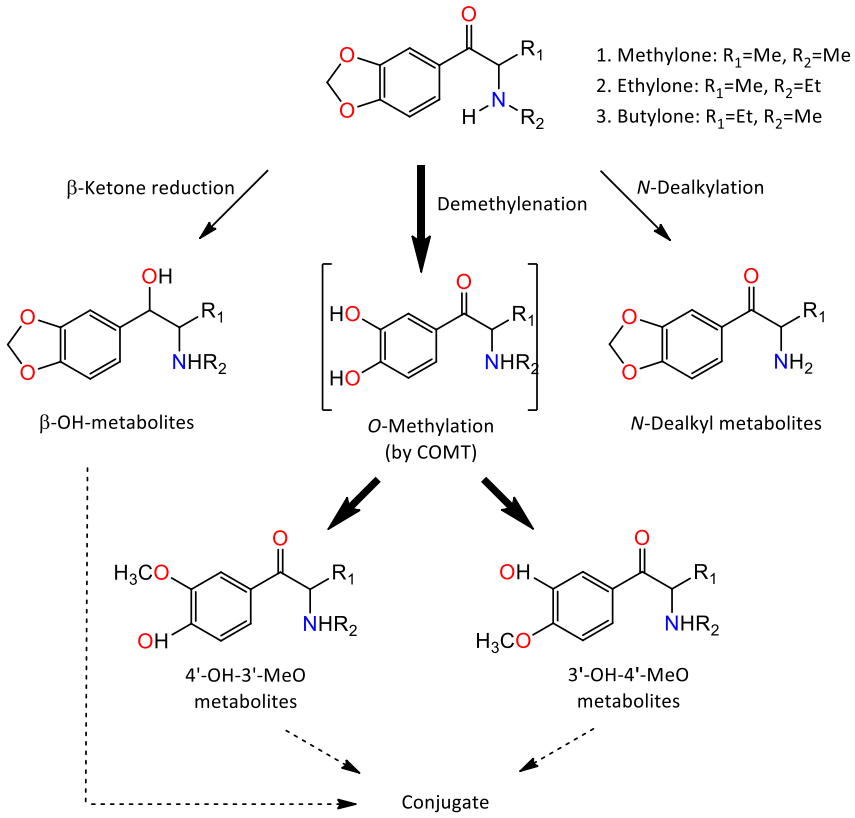

Figure 8. Main metabolic pathways of methylone, ethylone and butylone (adapted from Zaitsu et al. [159]). Abbreviation: COMT catechol-O-methyltransferase.

Primary metabolism begins with demethylation of methylenedioxy ring, followed by catechol O-methyltransferase (COMT) mediated O-methylation into 4'-hydroxy-3'-methoxy (4'-OH-3'-MeO) or 3'-hydroxy-4'-methoxymethcathinone (3'-OH-4'-MeO) [158, 169]. These metabolites are partially conjugated with glucuronides and sulfates and excreted in urine, along with the unmetabolized drugs [31, 158, 169]. Reduction of the β-ketone group and the N-dealkylation are other possible pathways for metabolism of these substances, but it seems to play a minimal role [31, 159].

The metabolism of a number of pyrrolidine cathinone derivatives has also been investigated over the last years [170-172]. Sauer et al. [170] were the first authors to study and

demonstrate the extensive metabolism of α-PVP via different pathways. Eleven metabolites of α-PVP were identified in rat urine, suggesting the following metabolic steps: (i) hydroxylation of the side chain followed by dehydrogenation to the corresponding ketone; (ii) hydroxylation of the 2''-position of the pyrrolidine ring followed by dehydrogenation to the corresponding lactam; (iii) degradation of the pyrrolidine ring to the corresponding primary amine; (iv) hydroxylation of the phenyl ring, most probably in the 4'-position and (*v*) ring opening of the pyrrolidine ring to the corresponding carboxylic acid [170, 173]. Figure 9 shows the main phase I metabolic pathways of α-PVP.

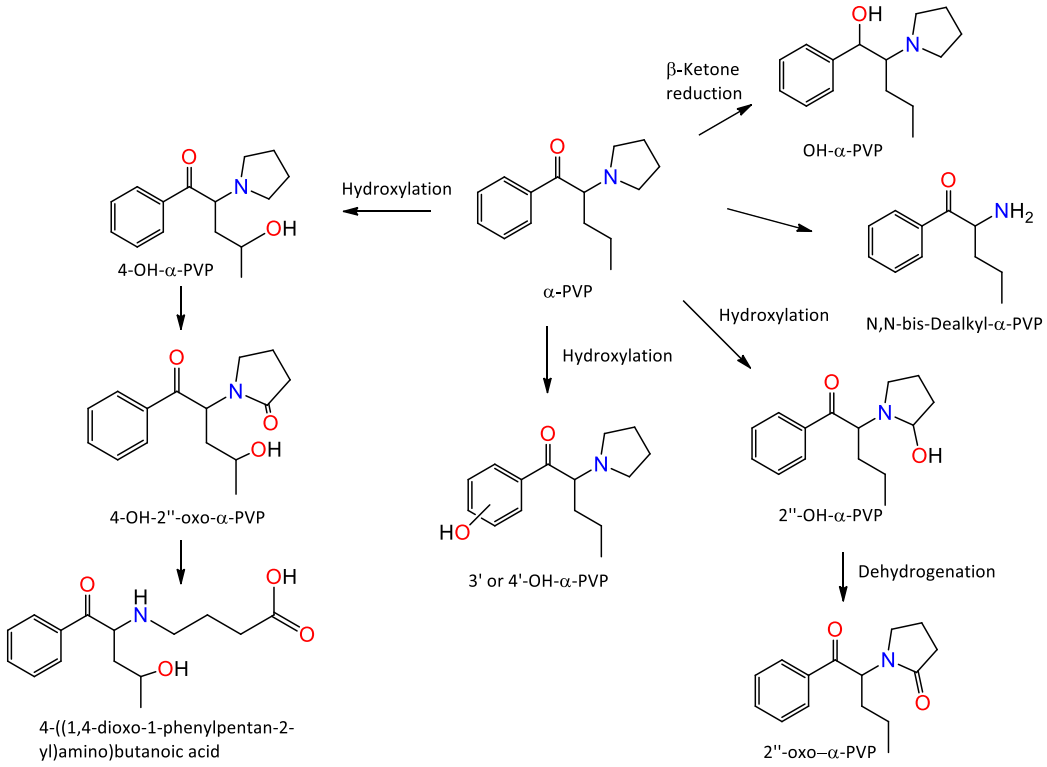

Figure 9. Major phase I metabolic pathways for α-PVP (adapted from Nóbrega et al. [80]).

Hydroxylation of the propyl side chain of α-PVP is mainly catalysed by the human isoenzymes CYP2B6, 2C19, 2D6 and 3A4 [170]. The formation of phase II metabolites was investigated in human liver microsomes and cytosol by Negreira et al. [174], and two glucuronidated metabolites of α-PVP were identified.

Recent studies have shown that the main metabolic pathway of α-pyrrolidinophenones significantly change, depending on the alkyl chain length of the parent molecule in humans [172, 175]. Shima et al. [175] showed that the metabolism of α-pyrrolidinooctanophenone (PV9) differed, remarkably, from α-PVP and α-PBP. In this sense, the metabolic pathways of PV9 involved reduction of the ketone group to the corresponding alcohol, oxidation of the pyrrolidine ring to the corresponding pyrrolidone, aliphatic oxidation of the terminal carbon

atom to the corresponding carboxylate, and hydroxylation at the penultimate carbon atom to the corresponding alcohols followed by further oxidation to ketones, and combinations of these steps [175]. Matsuta [172] also found remarkably differences between α-pyrrolidinophenones. For α-pyrrolidinophenones with shorter alkyl side chain, such as α-PBP, the reduction of the ketone group is the predominant metabolism, and it decreases with elongation of the side chain. For the oxidation of pyrrolidine ring (to form the 2″-oxo metabolite), it was revealed that its relative abundance is highest for α-PHP and decreases with a longer or shorter side chain. For α-pyrrolidinophenones with longer side chain, such as α-PHP, α-PHPP and PV9, oxidation of the side chain of the terminal carbon or at the penultimate carbon atom becomes more significant [172].

3,4-Methylenedioxypyrrolidinophenones are structurally a combination of methylenedioxy derivatives and pyrrolidinophenones, and undergo similar metabolism at the methylenedioxy moiety and pyrrolidino ring system as the other synthetic cathinone with corresponding structures [113]. Studies on the biotransformation of MDPV were described by Meyer et al. [176] in rat and human, and Negreira et al. [174] reported the *in vitro* metabolism of MDPV by human liver microsomes and human liver cytosol. As with MDPPP, MDPV is mainly metabolized by reduction of the β-ketone group, demethylenation followed by O-methylation and hydroxylation of 2″-position of the pyrrolidine ring, and then by dehydrogenation to the corresponding lactam (Figure 10) [160]. Besides CYP2D6, the isoenzyme CYP2C19 plays an essential role in the metabolism of both substances [176, 177]. In addition, in an *in vitro* phase II metabolism study, demethylenated metabolites were conjugated to glucuronides and/ or sulfates [174].

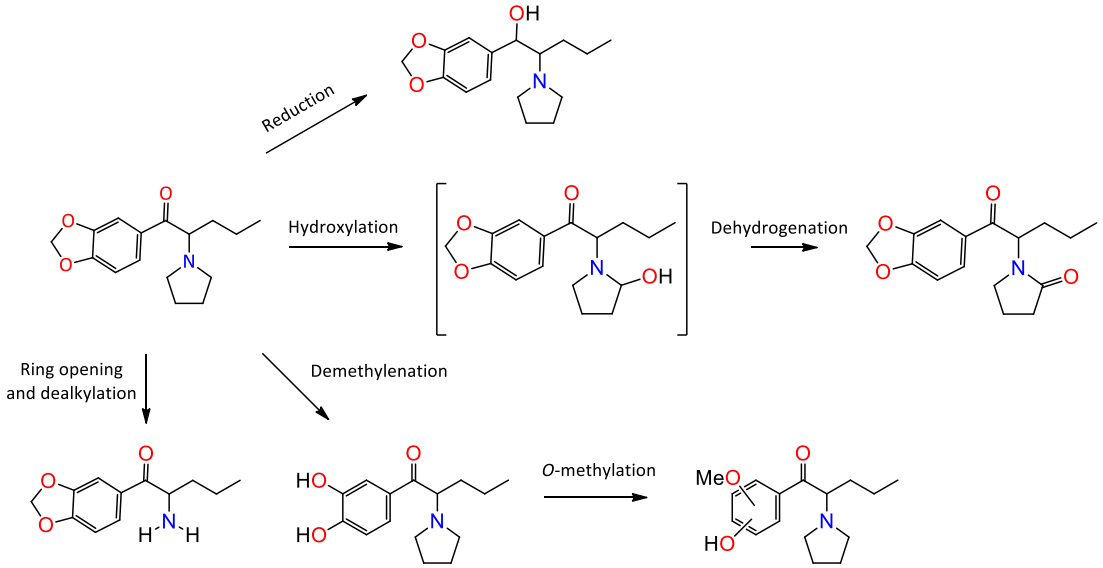

Figure 10. Major phase I metabolic pathways for MDPV (adapted from Zaitsu [160]).

1.8. Adverse Effects

The use of SCat is associated with a wide spectrum of unwanted effects, with cardiac, psychiatric and neurological symptoms being the most commonly reported adverse effects [31]. In general, patients intoxicated with SCat tend to be aggressive, violent and often suffer from auditory and visual hallucinations, tremors, severe anxiety as well as paranoia [178, 179]. Other usual signs of intoxication include headaches, nausea, palpitations, peripheral vasoconstriction and convulsions [94].

The cardiovascular effects of SCat are similar to those of amphetamine/cocaine and include tachycardia, hypertension with a subsequent risk of myocardial infarction, stroke, and upon prolonged abuse, dilated cardiomyopathy [117].

Hyponatremia is another possible complication associated with the use of SCat [180], being a well-known feature among MDMA users, but it is also occasionally associated with mephedrone and methylone intoxications [181, 182], and thought to result from an increase of 5-HT-mediated antidiuretic hormone secretion, with consequent decrease of sodium concentration in the blood [32, 181].

Severe toxicity signs compatible with excessive serotonin activity, such as hyperthermia, metabolic acidosis and prolonged rhabdomyolysis, have also been observed [91]. Hyperthermia is a toxicological effect that has been associated with the consumption of several SCat, including mephedrone, methylone, butylone, methedrone and MDPV [32, 183-185]. Hyperthermia is a significant cause of mortality as high temperatures can lead to metabolic acidosis, rhabdomyolysis, renal failure, disseminated intravascular coagulation, coma and death [185].

Rhabdomyolysis is a disorder caused when damaged muscle releases substances, such as creatine kinase (CK) and myoglobin, into the bloodstream. Acute renal failure is the most severe complication of rhabdomyolysis, whose prognosis depends on the degree to which renal function is compromised [186]. Although rhabdomyolysis may be one of the major causes leading to acute renal failure, there are several possible mechanisms that may contribute to this condition [180]. Adebamiro and Perazella [187] describe a case of acute renal failure after the ingestion of SCat, where acute tubular necrosis seems to be the cause of renal failure. According to these authors, tubular damage in patients intoxicated with SCat results from severe renal vasospasm, induced by these vasoactive substances. SCat may promote severe renal arteriolar vasospasm in a manner similar to cocaine, thereby producing renal hypoperfusion and renal ischemia, resulting in acute tubular necrosis [180, 187].

Acute liver failure is another complication associated with SCat intoxications. Fröhlich et al. [183] described a case of a 28-year-old male who presented hepatic failure after the

ingestion of 12 stimulant tablets, containing butylone and MDPV. At the emergency he had tachycardia, hypertension, hyperpyrexia and profuse sweating. Two days after the ingestion, he developed acute liver failure. Following treatment with N-acetylcysteine infusion, for 3 days, liver indices slowly returned to normal, and the patient was discharged into psychiatric care. *In vitro* studies have demonstrated that mitochondrial dysfunction and oxidative stress may contribute to hepatic injury associated with these substances [114, 188].

Regarding to neurological effects, some evidences suggest that SCat induce neurocognitive dysfunction and cytotoxicity, which are dependent on drug type, dose, frequency and time following exposure [189]. Habitual khat users exhibit some deficits in learning, memory, psychomotor speed, cognitive set-shifting and response inhibition [190-193]. Similar degrees of cognitive dysfunction have also been observed in common SCat users. Three separated studies demonstrated that regular mephedrone users may exhibit impaired verbal recall and fluency, as well as short-term memory deficits [194-196]. Other studies involving laboratory animals, such as mice, rats and monkeys, showed that repeated exposure to SCat produces impaired cognitive function in the domains of spatial working and recognition memory [197-200].

In addition to neurocognitive disfunctions, several *in vitro* studies showed that SCat may exhibit neurotoxic properties. Martínez-Clemente et al. [201] demonstrated the cytotoxic effect of mephedrone against cortical neurons isolated from mouse embryos. Siedlecka-Kroplewska et al. [202] revealed the ability of 3-FMC to inhibit growth and induce cell cycle arrest in HT22 immortalized mouse hippocampal cells. More recently, Wojcieszak et al. [203] demonstrated that pyrovalerone and its derivatives reduced the viability of human neuroblastoma SH-SY5Y cells. Despite the exact mechanisms of their action have not been fully elucidated, there are evidences indicating that SCat induce oxidative stress, autophagy and apoptosis in neuronal cells [204-206].

Beside all the adverse effects described so far, several other effects may be associated with SCat intoxication. Table 3 lists common adverse effects resulting from SCat intoxication.

It is important to note that specific effects of cathinones are sometimes difficult to assess, since they are often consumed in combination with other substances such as alcohol, tobacco, MDMA, cannabis and cocaine [31].

Table 3. Adverse effects of SCat consumption (adapted from Prosser [31] and Couto et al. [207]).

Group	Symptoms
Psychiatric	Agitation, hallucinations, anxiety/panic attacks, confusion, anterograde amnesia, psychosis, aggressive behavior, delusions
Neurological	Dizziness, loss of consciousness, somnolence, anesthesia/paresthesia, muscle cramps/fasciculations, seizures, headache, ataxia, tremor, irritability
Cardiovascular	Tachycardia, arterial hypertension, ST-segment alterations, chest pain, hypotension, bradycardia, cardiac ischemia
Pulmonary	Dyspnea, hyperventilation
Gastrointestinal	Nausea/vomiting
Metabolic	Hyperglycemia, hypoalemia, other electrolyte changes
Hepatic	Coagulopathy, hepatic failure, hepatitis, thrombocytopenia
Renal	Renal failure
Cutaneous	Xerostomia, diaphoresis, pallor
Muscular	Creatine kinase (CK) elevation, myalgia, rhabdomyolysis
Ocular	Mydriases, blurred vision, nystagmus
Others	Fever, hyperthermia

1.9. Treatment of Intoxications

To date, there is no specific antidote for the treatment of synthetic cathinone intoxications, and for this reason, clinical management is generally orientated towards providing symptomatic and supportive care [23]. Hydration with intravenous fluids should be initiated along with measures to actively cool patients if they are hyperthermic [91]. Hypertonic saline or water restriction should be prescribed if the patient becomes hyponatremic [31, 91].

Benzodiazepines are typically the first-line treatment for the agitation, aggression, seizures, hypertension and tachycardia due to its rapid onset of action and its duration time [178, 208]. However, if symptoms of agitation or aggression persist, antipsychotics could be an effective alternative therapeutic [178, 209]. In the case of persistent hypertension, the administration of vasodilators, such as sodium nitroprusside and nitroglycerin is recommended [210]. Beta blockers should be avoided due to the potential to cause unopposed alpha-adrenergic stimulation, worsening the hypertension [210].

All moderately to severe symptomatic patients should be monitored at cardiac level and body temperature. It should be also performed the evaluation of biochemical markers of muscle damage, electrolytes, renal and hepatic function, cardiac enzymes, as well as screening tests for drugs [37, 210]. Patients monitoring must remain until symptoms resolution and stabilization of vital signs [210].

Chapter 2

Analytical Methodologies Used for Determination of Synthetic Cathinones

2. Analytical Challenges

Since their appearance in the illicit drug market, the number of NPS continue to increase, leading to analytical challenges for both clinical and forensic laboratories [211]. What was initially thought to be a small subset of illicit drugs, has now turned into a series of new substances comprised of a variety of chemical structures, each with its own pharmacological effects, thus representing a significant threat to public health. Additionally, since the potency and composition of these products are highly variable, rapid and comprehensive drug screening approaches are absolutely necessary to enable accurate and timely identification of these emerging novel substances [212].

There are several significant factors that can make difficult the effective detection and identification of NPS, such as the huge number of substances that reach the market, even within a specific chemical class, the lack of reference standards, the scarce analytical information about these substances, and the inefficiency of several immunoassays used for drug screening routine to detect NPS in biological matrices [213].

Generally, when a suspected drug arrives in a forensic laboratory, the forensic chemist/toxicologist performs a screening test, which intends to indicate the probable identity of the unknown substance [214]. This presumptive test is usually colorimetric, where changes in the colour can indicate the presence or absence of a suspect substance [214]. Thin layer chromatography (TLC) and microcrystalline tests are other types of techniques that can often been used to identify controlled substances. While TLC is a separation technique that offers the advantage of the solubility and physical properties of the controlled substance to separate and distinguish compounds in a mixture, microcrystalline tests are used to identify specific controlled substances by observing the morphology and colour of the crystals that are formed when the substance is mixed with a specific reagent [214]. Usually, this last test is performed under a compound microscope [214].

When a positive result is obtained in a screening test, the substance structure must be confirmed [215]. In this step, the use of reliable analytical equipment, such as infrared (IR) spectroscopy or even mass spectrometry (MS), combined with separation techniques (*e.g.* gas chromatography (GC) or liquid chromatography (LC)) is mandatory. In some cases, specially involving NPS, the identification of unknown substances requires the use of advanced analytical methods, such as nuclear magnetic resonance (NMR), which allows to determine the exact structure of the molecule.

In the field of clinical and forensic toxicology, screening, identification, and quantification of drugs in biological samples are more challenging than the analysis of seized

materials, due to the extremely low concentrations found in the samples, as well as the diverse metabolic alterations of the parent compounds [216]. Thus, appropriate sample selection is a critical step of any toxicological investigation, and it is up to the toxicologist to select the most appropriate specimen(s), according to their availability and the nature of the investigation [217]. Normally, drug testing is mainly performed using whole blood, plasma, and urine; however, other alternative biological specimens, including hair, sweat and oral fluid have been studied and used [218, 219].

The appropriate sample preparation and the choice of instrumentation technique, is another key step in any toxicological analysis [220, 221].

The most frequently used techniques for the extraction of NPS, including SCat, from biological specimens are liquid-liquid extraction (LLE) and solid phase extraction (SPE) [221]. However, with the introduction of new methodologies, such as QuEChERS, a technique known for being quick, easy, cheap, effective, rugged and safe, or even miniaturized techniques such as microextraction by packed sorbent (MEPS), allowed to redesign the analytical process, making it simpler, faster and more environmentally friendly [222]. Furthermore, it is possible to get at least some degree of automation, when using these microextraction techniques, thus allowing their use in routine laboratory analysis [222].

Regarding to analytical instrumentation, MS-based techniques have become routine tools in most toxicology laboratories due to their exceptional sensitivity, thus enabling the detection and quantification of small amounts of analytes in complex matrices, such as biological samples [222]. The combination of modern analytical instrumentation and sample preparation techniques have allowed to perform rapid measurements on small sample volumes, and this assumes a special relevance in forensic toxicology, since sample availability is often limited and several analysis need to be performed using the same sample [222].

2.1. Nature of Samples

2.1.1. Seized materials

Forensic laboratories perform chemical profiling of a large volume of seized products. Suspected materials can arrive in a variety of forms, including powders, crystals, tablets, herbal mixtures, e-liquids, and even edibles. Typically, NPS are found in colored packaging, under a wide variety of brand names. The packages may describe a list of ingredients, and commonly have the advertence “not for human consumption”. Products containing SCat are usually found in the form of white, yellowish or brown powder or fine crystals, but less frequently as tablets or capsules [223]. They are known by their trade names such as “Ivory Wave”, “Purple wave”,

"Cloud Nine", "Bloom", "Bliss", "Vanilla Sky", "Red Dove", "Blue Silk", among others [209]. The packages generally contain one or more SCat, and are often mixed with other substances, such as caffeine, topical anesthetics, binding and cutting agents and other illicit drugs [24, 27, 224, 225].

2.1.2. Biological samples

Drug testing in forensic toxicology has been traditionally performed in whole blood, plasma, and urine specimens; however, in the last decades alternative or unconventional matrices have become increasingly important, as a result of the numerous advantages that these samples offer over 'conventional' ones [219]. Among these alternative matrices, hair, oral fluid, sweat, and meconium are some of the most regularly used samples, being easily collected and noninvasively. In addition, their adulteration is more difficult, and they can allow larger detection windows for certain drugs [219]. Figure 11 shows a general overview of drug detection windows for different biological specimens.

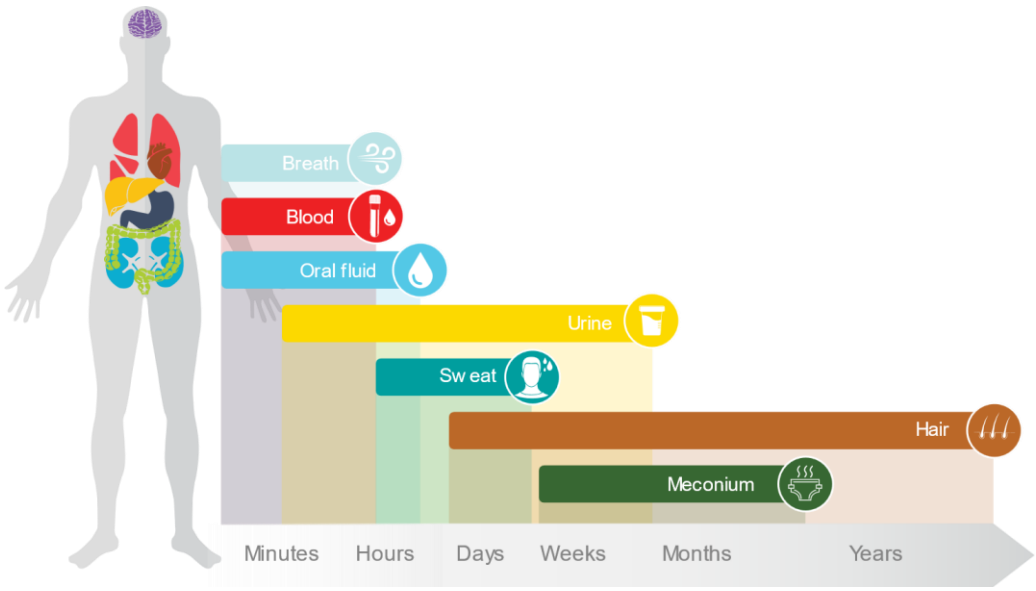

Figure 11. General overview of drug detection times for different biological matrices (adapted from Hadland and Levy [226]).

Selection of the appropriate sample in a toxicological investigation depends on several aspects, including detection time, sample volume, stability of the drug(s) in the specimen, matrix effects, among others [217]. When a drug is ingested, it is absorbed by the gastrointestinal tract and distributed through the body. However, substances that are injected, snorted or inhaled can avoid gastrointestinal absorption and liver first-pass effect and are delivered directly to tissues [226]. Blood and breath reflect moment-to-moment serum levels of a consumed drug and offer

the earliest and shortest detection windows [226]. Oral fluid and sweat, in turn, reflect the presence of a substance within the body, several hours after consumption, while urine offers a slightly longer detection window, typically ranging from several hours after consumption to several weeks [226]. Hair and meconium have the longest detection windows, which can range from weeks to months [226]. Despite the different characteristics, each sample has its own strengths and weaknesses, which need to be considered.

2.1.2.1. Blood, plasma and serum

Blood is a complex biological fluid, mostly constituted by water (80%), soluble proteins, fats, salts and suspended cells, that circulates through the body [227]. It has many different functions, including transporting oxygen and nutrients to cells and tissues, and removes carbon dioxide and other waste products from cells. Despite its complexity, blood is undoubtedly the biological matrix of choice for the main clinical and toxicological investigations, since it provides unique advantages over other matrices.

One of the great advantages of this sample is the possibility of establishing a correlation between the concentration of the drug in the blood with the pharmacological or toxic effects [227]. In addition, the use of the parent drug/metabolite ratio can be very useful in predicting the period that has elapsed since its administration [227].

In general, drugs of abuse appear in the blood shortly after being injected or inhaled, and within a few hours after ingestion [228]. As drugs can be rapidly metabolized, depending on the half-life of the substance, and eliminated from the body, blood analysis offers a restricted detection window [227]. An additional limitation is that obtaining blood samples requires venipuncture, which is an invasive procedure and requires specialized training [226].

During blood collection, the addition of anticoagulant and preservative is essential to prevent clotting and minimize biochemical changes. However, the choice of anticoagulant depends on the analytes to be investigated [227]. Ethylenediaminetetraacetic acid (EDTA), potassium oxalate (KOx), heparin and citrate are some anticoagulants commonly used in various clinical and forensic applications [229]. It is known that heparin can interact with some drugs, while EDTA is a complexing agent, not indicated in cases where the analytes are metals or organometallic compounds [227]. Some anticoagulants are frequently combined with a preservative such as sodium fluoride (NaF) to inhibit glycolysis via inhibition of enolase [229]. Additionally, the NaF may inhibit the activity of several other enzymes including cholinesterase, urease, and also bacterial proliferation, thus reducing losses of nitroaromatic compounds [229].

Recently, several studies have shown that the addition of a preservative in blood samples increase SCat stability. Busardò et al. [230] tested the stability of mephedrone in both

antemortem and post-mortem blood samples using different preservatives. In their study, mephedrone was spiked in unpreserved blood samples or preserved with 3% EDTA, or with 1.67%/0.2% NaF/KOx. The stability was assessed over 6 months at −20°C, 4°C, and 20°C. According to the results, both antemortem and post-mortem samples that were preserved with NaF/KOx were more stable than with EDTA and without preservative throughout the 6-month period. In addition, the authors concluded that the addition of NaF/KOx as a preservative and storage at −20°C is the most suitable storage condition.

Sørensen [231] studied the stability of several cathinones and ephedrines in whole blood samples preserved with NaF/KOx (pH 7.4) and NaF/citrate buffer (pH 5.9). The stability was assessed over 6 days at 5°C and 20°C. After 5 days of storage at 20°C, the concentrations of cathinone, methcathinone, *N*-ethylcathinone, mephedrone and 4-FMC, in blood samples preserved with NaF/KOx, were lost more than 70%, compared with less than 40% loss in samples with NaF/citrate buffer. The other SCat, namely butylone, methedrone, methylone and amfepramone also decomposed but less rapidly. At a storage temperature of 5°C, the decomposition is markedly lower, but after 3 days of storage it was possible to observe a trend towards samples preserved with NaF/KOx. Notably, under the same storage and preservation conditions, all ephedrine analytes were stable over the whole study, which allowed to conclude that the presence of a hydroxyl group in ephedrines confers greater stability to the compounds than SCat which contain a β-keto group.

Depending on the purpose of the analysis, drugs may be determined in plasma or serum. Both plasma and serum are commonly obtained from clinical samples, as blood cells can be easily separated from liquid components to create a “cleaner” sample and reduce matrix effects [232]. However, many drugs show differences in concentration between whole blood and plasma or serum [233]. If the objective is the quantification of the drug, the evaluation in a whole blood sample is more indicated, because the drugs have different affinities for proteins and, since they have a considerable affinity, they can be discarded if investigated only in a plasma or serum sample [227].

The analysis of post-mortem specimens present additional challenges. The concentration of many drugs are affected by post-mortem redistribution through the vascular system from the major organs, by direct post-mortem diffusion from organ to organ, and sometimes by incomplete distribution [234].

2.1.2.2. Urine

Urine is produced by the renal system, in order to remove unwanted substances from the body, and is normally composed of approximately 95% water and 5% waste products,

inorganic ions (e.g. sodium, potassium), proteins, metabolites and other organic molecules (e.g. urea, uric acid, carbohydrates) [235]. It is widely used in toxicological analysis and is considered a matrix of choice for toxicological screening [236]. The ease of collection, the volume available and the presence of a high number of products from the metabolic pathways are some of the factors that make this sample so attractive. In addition, the concentrations of drugs and/or metabolites in the urine are relatively higher and can remain for longer time, when compared to other biological matrices [226]. On the other hand, due to renal filtration, urine has a low protein and lipid content, making it a less complex matrix than blood or plasma, allowing a wide variety of preliminary tests to be carried out and easy to apply in several extraction techniques [237].

Urine drug testing often used require about 30 mL of urine, and the samples are collected into a plastic container with screw cap (without preservative) [238, 239], designed for safe collection and transportation of biological specimens for laboratory evaluation. The conservation of urine samples in refrigerated/ frozen conditions is strongly recommended [240].

Reports of SCat stability in urine are still relatively limited, and just a small number of cathinones have been characterized. In the early 2000s, Paul and Cole [165] were the first to study the stability of cathinone and methcathinone in urine over three months, at 4°C and –18 °C. According to their results, both substances were stable for two months at –18°C, and for 3 days when refrigerated at 4°C. Recently, Glicksberg and Kerrigan [241] evaluated the influence of several factors on the stability of SCats in urine samples, such as temperature, concentration, pH and analyte structure. In this study, a total of 22 SCat were evaluated at 100 ng mL^{-1} and 1000 ng mL^{-1} in pH 4 and pH 8 over six months. Urine samples were stored at temperatures of -20°C, 4°C, 20°C, and 32°C. According to the obtained results, the authors concluded that the stability of SCat is highly dependent on urine pH and storage temperature, with SCat being considerably more stable in acidic urine at low temperature. In addition, a significant structural influence was also observed. SCat containing a tertiary amine (pyrrolidine group) were significantly more stable than secondary amines. The methylenedioxy group also exerted a significant stabilizing effect on tertiary and secondary amines. On the other hand, the position of the ring substitution can influence stability of cathinones, as in the case of 3-FMC which degraded much more extensively than its ring-substituted counterparts (4-FMC).

2.1.2.3. Oral Fluid

Oral fluid is the liquid found in the oral cavity and is mainly produced by the three pairs of major salivary glands (sublingual, submaxillary and parotid), a great number of minor salivary glands, the oral mucosa and gingival crevices [219].

In recent years, oral fluid has been gaining attention as an alternative sample in drug testing, due to the inherent advantages it has over other matrices [242]. The fact that the sample is collected noninvasively under direct supervision, reducing the possibility of providing an invalid specimen (e.g. sample adulteration or substitution), is one of the main advantages of oral fluid testing [243]. In addition, it is thought that drug concentrations in this specimen can be related to free drug concentrations in plasma and, therefore, to the pharmacological effects [242, 243]. However, several factors can affect drug concentration in this matrix, such as route of administration, molecular size, pK_a, degree of protein binding, and lipophilicity of the drug [219, 220].

In general, drugs are incorporated into oral fluid by oral contamination (chewing or smoking) or from the bloodstream, where different mechanisms can be involved in drug transport [244]. Passive diffusion through the membrane, active processes against a concentration gradient, filtration through pores in the membrane and pinocytosis are the main mechanisms involved [243]. However, the most common mechanism of drug transport is passive diffusion, which is dependent on physicochemical properties of the substance or class of substances (e.g. pK_a and molecular weight), the degree of binding to plasma proteins and the pH of both oral fluid and blood [219, 243]. Commonly, oral secretions have a lower pH than blood (pH 5.8–6.8), and this affects the partition of drugs between blood and saliva [228, 245]. As a result, drugs that are basic in nature, such as amphetamines, methamphetamine, cocaine, and opiates tend to have higher concentrations in oral fluid, while acidic drugs such as benzodiazepines tend to have higher concentrations in blood [245].

As with blood drug testing, oral fluid testing is only useful for detecting very recent drug use, as drug levels in the oral fluid rapidly decline and drug concentrations stop being detected hours after the last drug use [228]. Currently, there are several methods for oral fluid collection, with or without stimulation, which include suction, draining, spiting and collection on absorbent materials [243]. However, care should be taken as the collection procedure may affect the concentration of the drugs [243].

Although oral fluid offers many benefits compared to other matrices, it has some drawbacks. Drugs that are ingested orally or smoked may be detected in high concentrations in this matrix after recent use, due to residual amounts of drug remaining in the oral cavity [243]. In this sense, the results for these drugs may not be accurate, since their concentration in the oral fluid may not reflect the blood drug concentration [243]. On the other hand, the limited amount of saliva produced by the examinee and the limited time in which drugs can be detected are other major drawbacks in oral fluid analysis [243].

Despite these limitations, oral fluid continues being one of the most suitable alternative matrices for the assessment of recent exposure of psychoactive drugs [245]. In recent years, the oral fluid analysis of individuals suspected of driving under the influence of drugs is considered one of the most important applications of this sample [219, 245]. In a study developed by Richeval et al. [246], the authors tested oral fluid specimens in drivers, in order to assess the prevalence of NPS consumption. According to this study, NPS were detected in 17 of the 229 collected samples, and 3 of them contained SCat. Another study published by Richeval et al. [247] also revealed the presence of NPS in drivers. In this study, a total of 391 oral fluid specimens were collected and high the NPS were detected in 33 samples, the vast majority being cathinone derivatives. According to the authors, these results was comparable to the available blood data observed in the previous year in similar populations.

2.1.2.4. Sweat

Sweat is another alternative biological sample that has been gaining prominence in toxicological analysis. This slightly acidic biofluid is produced by the eccrine and apocrine sweat glands and is mainly constituted by water (approximately 99%), electrolytes, amino acids, carbohydrates, and other organic compounds [219, 248]. On average, the volume of sweat excreted per day in healthy individuals ranges from 300 to 700 mL [219]. The mechanisms involved in the transportation of substances to sweat remain not fully elucidated, and it is believed that drugs are incorporated into sweat by passive diffusion and transdermal migration [227, 245]. The physicochemical properties of drugs such as molecular mass, pKa, lipophilicity, and even the degree of binding to plasma proteins influence this incorporation [227, 245]. Commonly, parent drugs are found in sweat at higher concentrations than their corresponding hydrophilic metabolites [245]. In addition, as sweat pH is more acidic than blood, basic drugs tend to preferentially concentrate in this fluid rather than acid substances [245].

Unlike other biofluids, sweat possesses many advantages, including its non-invasive sampling, which can be performed in a simple and safe manner with a low risk of adulteration [227]. Due to its characteristics, sweat analysis is considered a rapid and easy process compared to blood, and in some cases, it provides longer time-detection windows (up to 14 days after exposure) [245, 249]. However, despite these advantages, this biological matrix also has some limitations, including the lack of information concerning dose-response relationships [219]. In addition, sweat is not suitable for quantitative drug analysis due to the impossibility of knowing accurately the volume of sample really collected [219]. On the other hand, the low concentration of analytes demands the use of more sensitive analytical techniques [245].

Sweat samples are usually collected using an absorbent patch that is placed on the skin over an extended period of time, which can range from a few days to even weeks [237]. The patch design allows carbon dioxide, oxygen, and water vapor to escape while the non-volatile components, such as drugs of abuse are retained in the absorbent material [245]. To minimise contamination from the external environment and reduce the possibility of bacterial growth, the skin is usually cleaned with an alcohol (e.g. 70% isopropanol (IPA)) prior to patch placement [219, 245].

Although the use of sweat for drug testing has some drawbacks, it has been successfully applied to several drugs of abuse, such as cocaine [250], amphetamines [251] and cannabinoids [252]. However, the literature on NPS analysis in sweat remains scarcely explored.

2.1.2.5. Hair

Hair is an interesting and very useful matrix in forensic toxicology since it provides valuable information regarding drug addiction history [253]. Although hair appears to be a fairly uniform structure, it has two distinct regions: the follicle and the hair shaft.

The exact mechanisms involved in the drug incorporation into hair are still unclear, however the most accepted model assumes that drugs and their metabolites enter the hair by passive diffusion through blood capillaries to the growing cells at the base of the hair follicle [245]. Other possible mechanisms involve the indirect incorporation through the diffusion of drugs from sweat or sebum into the hair, or even through contamination from the external environment (e.g. smoke or physical transfer from contaminated hands) [245].

Hair analysis presents several advantages over other biological matrices, namely the fact that sample collection is performed in a less invasive manner, with a low risk of sample adulteration or substitution [254]. In addition, the large detection window, which can range from days to months or even years, depending on the length of the hair, makes it possible to assess the individual drug abuse history through segmental analysis [245, 254]. In general, one centimetre of hair reflects approximately a period of one month, where the proximal centimetres reflect the most recent consumption periods [255].

Despite these advantages, there are, some limitations associated with hair analysis. One of the most important issues is the environmental contamination, which can generate false positive results [219]. For this reason, the first step in hair drug testing is a decontamination step with organic solvents, surfactants or phosphate buffer, in order to remove externally bounded contaminants [237, 256]. Another important limitation of this sample is recent drug exposure. Generally, hair is not a suitable sample to document recent drug exposure [238]. Furthermore,

drug concentrations in hair are often small, in the order of ng mg^{-1} of hair, which requires for highly sensitive techniques [227, 257].

Currently, several studies have used hair analysis to detect NPS consumption. The use of SCat, especially mephedrone, among MDMA and other drugs users was confirmed by Kintz [258]. According to the author, out of the 112 samples analysed, mephedrone was detected in 24 samples, in concentrations ranging from 0.10 to 86.8 ng mg^{-1} hair. MDMA was also detected in 16 from these 24 specimens. Larabi et al. [259] also presented a study describing the prevalence of NPS and conventional drugs of abuse in high risk populations. In this study, 141 patients (29%) tested positive for NPS, being mephedrone (24 cases) and 4-MEC (24 cases) the most detected cathinones, followed by methylone (15 cases) and MDPV (7 cases). The concentrations found ranged from 0.001 to 169 ng mg^{-1} hair. Both studies highlighted the importance of including SCat hair analyses in the routine workflow of forensic toxicology laboratories.

2.1.2.6. Other Alternative Biological Samples

The development of sophisticated analytical techniques, as well as the introduction of new forms of sample preparation, has allowed exploring other biological matrices for drug testing. Despite being less routinely used in toxicology, several alternative biological samples can provide useful information, such as cerebrospinal fluid, breast milk, amniotic fluid, umbilical cord blood and tissue, meconium, gastric content, vitreous humour, bile, human tissues, bones and bone marrow, teeth and nails [219, 253].

Currently, several studies have used alternative biological matrices to detect SCat consumption. In a fatal intoxication case involving the consumption of 4-methylpentedrone (4-MPD), along with cocaine, sildenafil, bromazepam and nevirapine, Cartiser et al. [260] used several biological fluids for toxicological analysis. The results revealed that urine was the sample with the highest concentration of 4-MPD (>10,000 ng mL^{-1}), followed by peripheral blood (1285 ng mL^{-1}), bile (1187 ng mL^{-1}), cardiac blood (1128 ng mL^{-1}), and vitreous humor (875 and 734 ng mL^{-1} in right and left samples, respectively). Bottinelli et al. [261] also reported a fatal case involving the consumption of SCat. For toxicological analysis several biological samples, including blood, urine, vitreous humor and bile were collected. 3-MMC was found in all biological samples, with urine being the sample with the highest concentration (29,694 ng mL^{-1}), followed by vitreous humor (2988 ng mL^{-1}), bile (1291 ng mL^{-1}), cardiac blood (609 ng mL^{-1}) and peripheral blood (249 ng mL^{-1}). In both cases the toxicological findings, associated with the autopsy observations and the circumstances of death, led the pathologists to diagnose drug intoxication as the cause of death.

2.2. Sample Preparation Techniques

Generally, the analysis of drugs and other chemical substances in biological samples require several sample preparation steps, prior to their identification by an analytical instrument, highlighting the complexity of the matrices involved, its incompatibility with analytical instruments (e.g. chromatographic systems) and the fact that many of the compounds are in residual concentrations [253].

Although the sample pre-treatment is the most laborious part of the analytical procedure, reaching up to 80% of the total analysis time, this is considered a crucial step in toxicological analyses, as it is in this phase that isolation and recovery of the analyte are carried out, making it a more suitable sample for instrumental analysis [262].

There are a large number of sample preparation techniques available that, from the historical point of view and the frequency of use, can be divided into two main groups: (1) the conventional sample preparation techniques, which are simultaneously techniques most used in routine analysis and which may include protein precipitation, LLE and SPE; (2) and the second group, which corresponds to the sample preparation techniques more recently to solve some drawbacks of conventional techniques, such as the high solvents consumption, the large amount of sample needed for analysis and the low selectivity [253, 262].

The selection of an appropriate sample preparation technique is carried out taking into account the nature of the sample, the available amount, the analyte type, the selectivity and sensitivity of the method, the solvent consumption, the extraction time, and the automation possibility [262].

Regarding the extraction of SCat in biological matrices, the sample preparation techniques commonly used are LLE [263, 264], SPE [213, 265], protein precipitation [266] and, in some cases, a dilution followed by direct injection [267, 268]. However, other techniques, such as SPME [269], QuEChERS [270, 271], bar adsorptive microextraction (BAμE) [272], and MEPS [273, 274], have been successfully applied in the extraction of these substances, in biological matrices. Table 4, shows a general overview of the most commonly used sample preparation techniques for the analysis of SCat in biological samples.

Table 4. General overview of the most commonly used sample preparation techniques for the analysis of SCat in biological samples.

Synthetic Cathinones	Sample (amount)	Sample Preparation	Analytical Technique	LOD/LOQ (ng mL^{-1})	Recovery (%)	REF.
4-CEC, α-PVP, 4-Cl-PVP, MDPV	Blood (500 µL)	SPE (Oasis MCX® 60 mg)	GC-MS	LOD: 5 - 25 LOQ: 25	87.3 - 116.5	[213]
CAT, 4-FMC, BUPH, α-PVP, MET, ETH, PTL, MDPV	Blood (250 µL)	SPE (Oasis MCX® 60 mg)	GC-MS	LOD: 5 - 40 LOQ: 5 - 40	71.5 - 116.6	[275]
α-PVP, 3,4-DMMC, 4-MEC, 4-MPPP, βk-2C-B, BUPH, BUT, ETH, CAT, 4-CMC, ETCAT, 4-FMC, MDPV, 3-MMC, 4-MMC, 4-MeOMC, MET, NPY, PENT, PTL, BUT	Blood (500 µL)	PP (MeOH) followed by DLLME ($CHCl_3$:MeOH 1:2.5 v/v, as extracting and disperser solvent)	UHPLC-MS/MS	LOD: 0.2 - 1 LOQ: n.a.	10.0 - 81.0	[276]
MET, ETH, NEP	Blood (250 µL)	PP (acetonitrile)	LC-MS/MS	LOD: 0.8 - 1.4 LOQ: 5.0	61.4 - 77.3	[266]
CAT, ETCAT, 2-MMC, 3-MMC, 4-MMC, PENT, 3-CMC, 4-CMC, 4-MEC, 4-EMC, 3,4-DMMC, 4-MPD, N-PPT, 3-CEC, 4-CEC, 4-MeOMC, Hex-en, 4-CPD, α-PVP, MET, α-PiHP, 4-F-PHP, α-PHP, BUT, bk-EBDB, PTL, 4-Cl-α-PVP, NEP, MPHP, PV9, MDPBP, MDPV, 3,4-MDPHP, NPY	Blood (200 µL; AM and PM)	LLE (ethyl acetate)	GC-MS/MS	LOD: 0.02 - 0.72 LOQ: 1.0 - 2.5	85.9 - 105.8	[277]
MET, 4-MMC, MDPV	Plasma (300 µL)	MEPS (C_8/SCX sorbent)	UHPLC-PDA	LOD: 5 - 25 LOQ: 10 - 50	85.2 - 101	[274]
MDPV, 4-MMC, 4-MeOMC, MET, α-PVP	Serum (1 mL)	LLE (diethyl ether:ethyl acetate, 1:1 v/v)	LC-QTOF-MS GC-MS	LOD: 2 - 25 LOQ: n.a.	> 75	[278]
α-PHP	Serum (500 µL)	QuEChERS	LC-MS/MS	LOD: 0.2 LOQ: 1.0	75 - 77	[270]
4-FMC, CAT, 3-MMC, 4-MMC, PENT, 4-MEC, 4-MeOMC, MET, ETH, BUT, PTL, α-PVP, MDPV	Blood (2.0 mL)	PP (MeOH) followed by DLLME ($CHCl_3$:MeOH 1:2.5 v/v, as extracting and disperser solvent)	GC-MS	LOD: 2 - 10 LOQ: 5 - 50	82.6 - 106.5	[279]
	Urine (2.0 mL)	DLLME ($CHCl_3$:MeOH 1:2.5 v/v, as extracting and disperser solvent)	GC-MS	LOD: 2 - 10 LOQ: 2 - 50	95.6 - 116.0	
3,4-DMMC	Blood (500 µL)	QuEChERS	LC-MS/MS	LOD: 1.03 LOQ: 5.00	85.9 - 89.4	[271]
	Urine (500 µL)	QuEChERS	LC-MS/MS	LOD: 1.37 LOQ: 5.38	95.8 - 101	
CAT, 4-FMC, 4-FEC, BUPH, 3-MMC, 3-MBP, 4-MBP, 3-EMC, 3-EEC, 4-EEC, 3,4-DMEC, 2,3-MDMC, BUT, PTL	Plasma (1 mL)	SPE (200 mg Clean Screen® CSDAU203 cartridges)	GC-NCI-MS	LOD: 0.26 - 0.34 LOQ: 0.89 - 1.12	89.0 - 99.9	[280]
	Urine (3 mL)	SPE (200 mg Clean Screen® CSDAU203 cartridges)	GC-NCI-MS	LOD: 0.26 - 0.76 LOQ: 0.89 - 2.34	87.8 - 99.9	
4-MMC, MET, 4-MeOMC, ETH, BUT, bk-DMBDB, 4-CEC, 4-Cl-α-PPP, NEP, 4-EMC, α-PVP, MDPV, 4-MPD, NEH, 4-F-PHP, 4-Cl-α-PVP	Urine (500 µL)	LLE (1-chlorobutane)	LC-MS/MS	LOD: 0.09 - 0.37 LOQ: 1	n.a.	[263]
4-MEC, α-PVP, MDPV, 4-MMC, MET	Urine (10 µL)	Dilution (H_2O:MeOH, 85:15 v/v)	UHPLC-MS/MS	LOD: 0.3 LOQ: 1.0	83 - 102	[267]

Table 4. (Continuation)

Synthetic Cathinones	Sample (amount)	Sample Preparation	Analytical Technique	LOD/LOQ (ng mL^{-1})	Recovery (%)	REF.
CAT, BUPH, 3-MMC, 3-FMC, 4-FMC, 4-MEC, 4-MeOMC, MET, ETH, BUT, NPY	Urine (200 µL)	Dilution (MeOH)	UHPLC-MS	LOD: 0.01 - 1.04 LOQ: 0.02 - 3.16	63.6 - 139.1	[268]
		Dilution (propan-2-ol)	UHPSFC-MS	LOD: 0.02 - 5.15 LOQ: 0.07 - 15.6	67.5 - 91.0	
4-MMC, MET, ETH, BUPH, MCAT	Urine (2 mL)	LLE (1-chlorobutane:DCM, 9:1 v/v)	GC-MS	LOD: 25 - 50 LOQ: n.a.	n.a.	[264]
2-MMC, 3,4-DMMC, 4-FMC, 4-MEC, 4-MMC, α-PVP, PENT, BUPH, BUT, MDPV, ETCAT	Urine (2.5 mL)	SPE (Oasis MCX® cartridge)	LC-HRMS	LOD: 0.04 - 0.16 LOQ: 0.05 - 0.2	69 - 125	[265]
			LC-MS/MS	LOD: 0.005 - 0.035 LOQ: 0.02 - 0.05	53 - 98	
	Oral fluid (n.a.)	Centrifugation, dilution, evaporation and reconstitution	LC-HRMS	LOD: 0.01 - 0.035 ng g^{-1} LOQ: 0.075 - 0.10 ng g^{-1}	41 - 55	
			LC-MS/MS	LOD: 0.003 - 0.030 ng g^{-1} LOQ: 0.075 ng g^{-1}	50 - 66	
α-PVT, α-PVP, MDPV	Oral fluid (500 µL)	BAµE-µLD (Strata-X sorbent)	GC-MS	LOQ: 30 LOQ: 90	43.1 - 52.3	[272]
MET, 4-FMC, ETCAT, ETH, BUT, 4-MMC, PENT, MDPV, PRV	Oral fluid (300 µL)	PP (MeOH) MEPS (mixed-mode C_8/SCX sorbent)	UHPLC-MS/MS	LOD: 0.25 LOQ: 0.5 - 1.0	75 - 125	[273]
CAT, MCAT, MET, 4-FMC, 4-MeOMC, BUT, 4-MMC, 4-MEC, PENT, α-PVP, MPBP, MDPV, NPY	Oral fluid (100 µL)	PP (acetonitrile)	LC-MS/MS	LOD: 1.0 LOQ: 2.5	n.a.	[281]
MET, ETCAT, BUPH, Amfepramone, BUT, 4-MMC, 4-MEC, PENT, α-PVP, MDPV, BPP	Hair (25 mg)	Washing (DCM), pulverization and incubation (55°C for 15h)	UHPLC-MS/MS	LOD: 2.0 - 4.2 pg mg^{-1} LOQ: 4.0 - 8.4 pg mg^{-1}	79 - 115	[282]

Abbreviations: 2-MMC - 2-methylmethcathinone; 2,3-MDMC - 2,3-methylenedioxymethcathinone; 3-CEC - 3-chloroethcathinone; 3-CMC - 3-chloromethcathinone; 3-EEC - 3-ethylethcathinone; 3-EMC - 3-ethylmethcathinone; 3-MBP - 3-Methylbuphedrone; 3-MMC - 3-methylmethcathinone; 4-CEC - 4-chloroethcathinone; 4-Cl-α-PPP - 4-chloro-α-pyrrolidinopropiophenone; 4-Cl-α-PVP - 4-Chloro-alpha-pyrrolidinovalerophenone; 4-CMC - 4-chloromethcathinone; 4-CPD - 4-chloropentedrone; 4-EEC - 4-ethylethcathinone; 4-EMC - 4-ethylmethcathinone; 4-FEC - 4-fluoroethcathinone; 4-FMC - 4-Fluormethcathinone; 4-F-PHP - 4-fluoro-α-pyrrolidinohexanophenone; 4-MBP - 4-Methylbuphedrone; 4-MEC - 4-methyl-*N*-ethylcathinone; 4-MeOMC - methedrone; 4-MMC - 4-methylmethcathinone (mephedrone); 4-MPD - 4-methylpentedrone; 4-MPPP - 4-methylphenylpyrrolidinylpropanone; 3,4-MDPHP - 3,4-methylenedioxy-α-pyrrolidinohexanophenone; 3,4-DMEC - 3,4-dimethylethcathinone; 3,4-DMMC - 3,4-dimethylmethcathinone; α-PHP - α-pyrrolidinohexanophenone; α-PiHP - α-pyrrolidinoisohexanophenone; α-PVP - α-pyrrolidinopentiophenone; α-PVT - α-pyrrolidinopentiothiophenone; βk-2C-B - 2-Amino-1-(4-bromo-2,5-dimethoxyphenyl)ethan1-one; AM - antemortem; BAµE-µLD - bar adsorptive microextraction followed by microliquid desorption; bk-DMBDB - Dibutylone; bk-EBDB - Eutylone; BPP - Bupropion; BUPH - buphedrone; BUT - butylone; CAT - cathinone; $CHCl_3$ - chloroform; DCM - dichloromethane; DLLME - Dispersive Liquid-Liquid Microextraction; ETCAT - ethylcathinone; ETH - ethylone; Hex-en - N-ethylhexedrone; GC-MS - gas chromatography coupled to mass spectrometry; GC-MS/MS - gas chromatography tandem mass spectrometry; GC-NCI-MS - gas chromatography coupled to mass spectrometry with negative chemical ionization mode; LC-HRMS - liquid chromatography coupled with high-resolution mass spectrometry; LC-MS - liquid chromatography coupled to mass spectrometry; LC-MS/MS - liquid chromatography coupled to tandem mass spectrometry; LC-QTOF-MS - liquid chromatography quadrupole time-of-flight mass spectrometry; LLE - liquid-liquid extraction; MCAT - methcathinone; MDPBP - 3,4-methylenedioxy-α-pyrrolidinobutiophenone; MDPV - 3,4-methylenedioxypyrovalerone; MEPS - microextraction by packed sorbent; MeOH - methanol; MET - methylone; MPBP - 4-Methyl-α-pyrrolidinobutiophenone; MPHP - 4-methyl-α-pyrrolidinohexanophenone; n.a. - not available; NEH - N-ethylhexedrone; NEP - N-ethylpentylone; N-PPT - N-propylpentedrone; NPY - Naphyrone; PENT - pentedrone; PM - post-mortem; PP - protein precipitation; PRV - Pyrovalerone; PTL - Pentylone; PV9 - α-pyrrolidinooctanophenone; SPE - solid phase extraction; UHPLC-MS/MS - ultrahigh performance liquid chromatography coupled to tandem mass spectrometry; UHPLC-PDA - ultrahigh performance liquid chromatography with photodiode array detector; UHPSFC-MS - ultrahigh performance supercritical fluid chromatography with mass spectrometry.

2.2.1. Protein Precipitation

Removal of proteins by precipitation or denaturation is a very common sample preparation strategy [283]. The content of these compounds in biological fluids and tissues is considerable, and their removal is essential when it comes to chromatographic analysis.

Proteins are macromolecules composed of amino acids linked to each other by peptide bonds in a sequence that is unique for each protein. The conformational integrity of a protein is maintained by a proper balance of forces established not only between elements of the chain itself (e.g. hydrogen bonds, electrostatic interactions, disulfide bridges, and hydrophobic interactions) but also with the surrounding environment, on which the physicochemical properties and biological activity depend [284]. Any condition that changes its native conformation, either temporarily or permanently, can lead to protein denaturation.

Loss of protein solubility is a common indicative of protein denaturation [285]. However, this decrease in solubility varies from protein to protein and can be influenced by several extrinsic factors, such as pH, ionic strength, temperature, and type of solvent.

Generally, samples with high protein content are often removed by precipitation before chromatographic analysis, since proteins solubility is considered a critical factor. The percentage of the organic solvent in the mobile phase of LC, can lead to protein denaturation and consequent precipitation, which can cause several problems, including obstruction and rapid deterioration of the column and, consequently, loss of chromatographic efficiency. In order to avoid these drawbacks, proteins are removed by precipitation before chromatographic analysis. Currently, several methods have been used to reduce the solubility of proteins and facilitate their removal from biological samples. These involve the use of precipitating agents such as salts, acids, organic solvents, and metal ions that act by specific mechanisms on proteins [283].

Regardless of the method used for protein precipitation, in general, after the addition of the precipitating agent, the sample is subjected to agitation and centrifugation, allowing the separation of the protein precipitate and the supernatant, used for toxicological analysis [227]. In this process there is no extraction or pre-concentration of the sample [227], it provides only a minimal clean-up of the sample, that can be sufficient for many clinical applications. Due to its simplicity, this technique is widely used in the determination of drugs in biological fluids. Particularly in the analysis of SCat, protein precipitation is often induced with organic solvents, with ACN [266, 281] and MeOH [276, 279] being the most used solvents.

2.2.2. Liquid-Liquid Extraction (LLE)

LLE, also known as solvent extraction, is a versatile extraction technique based on the distribution of an analyte between two immiscible or partially miscible liquids. Commonly, one of the solvents is water or an aqueous mixture and the other is a nonpolar organic solvent (organic phase) [286]. The distribution or partition of the analyte between phases is governed by the Nernst's distribution law, which considers that a substance is distributed between two immiscible liquid phases, depending on its solubility in each one [287]. When equilibrium is reached, the concentration ratio of the substance in the two phases is constant for a given temperature and solvent system. This constant is called the distribution coefficient or distribution constant (K_D) and can be expressed by the following equation:

$$K_D = \frac{C_{org}}{C_{aq}} \quad (1)$$

where C_{org} is the analyte concentration in the organic phase and C_{aq} the analyte concentration in the aqueous phase.

The distribution coefficient is an expression of the relative preference of the solute for the solvents [286]. A large value for K_D indicates that the extraction of the analyte into the organic phase (extracting solvent) is favourable [287]. When the K_D value is very low, it can be increased either by replacing the extraction solvent or by adjusting the pH, to prevent the ionization of acidic or basic compounds, or by adding neutral salts, in order to decrease the solubility of the organic compounds in the aqueous phase, providing the occurrence of the salting out effect [286, 287]. In some cases, the extraction efficiency and selectivity can be enhanced by multiple extraction procedures [283, 287].

In general, the choice of extraction solvent is one of the most critical points of LLE, since it will depend on the nature of the analyte to be extracted [288]. In this sense, the solubility, polarity, volatility, toxicity, degree of purity and chemical reactivity are parameters that must necessarily be evaluated before performing the extraction [288]. Once the extraction solvent is selected, this is added to the sample containing the analytes, followed by mechanical agitation to promote maximum contact between the organic and aqueous phases [227]. Subsequently, the mixture is subjected to centrifugation to optimize the separation between the phases and then the phase of interest is collected for analysis [227].

Although LLE is a relatively simple extraction technique and has some advantages, such as the availability of a large number of organic solvents, which provide a wide range of solubility and selectivity, this technique also has several limitations [283]. One of the major problems in LLE is the formation of emulsions that are very difficult to break [283]. This causes loss of analyte by occlusion within the emulsion [283]. In addition, the use large volume of extracting solvents

associated with a long analysis time, automation difficulties and the low analyte recovery are some disadvantages of this technique [283]. Currently, there are a several extraction techniques that overcome some of these drawbacks, however, LLE still has a large field of application in toxicology. As an example, we can highlight the extraction of SCat from blood [277] and urine [263].

2.2.3. Solid Phase Extraction (SPE)

SPE is a solid-liquid separation technique that is based on classical liquid chromatography. It has become one of the most popular sample preparation techniques due to its versatility, effectiveness, and relatively low solvent usage. Typically, SPE is mainly used to remove interferences and for extraction and/or preconcentration of analytes present in complex matrices prior to analysis. The basic principles of SPE are similar to LLE, involving the partition of the analytes between two phases. However, instead of two immiscible liquid phases, SPE involves the partition of analytes between a liquid phase (sample) and a solid phase (sorbent) [289].

The retention and elution mechanisms of the analytes in the solid phase are analogous to those involved in LC, where intermolecular forces assume special relevance. Depending on the characteristics of the solid phase and the nature of the sample, the SPE can be divided into four groups according to the extraction mechanism: reverse phase, normal phase, ion exchange and mixed mode [290].

The reversed phase separation mode is probably the most used, where the analytes are separated based on their polarity. This type of extraction involves a polar matrix (usually aqueous) and a non-polar or hydrophobic solid phase, such as C_{18}, C_8, C_6, C_4, C_2, phenyl, cyclohexyl, and cyanopropyl [287, 290]. Typically, the interaction between the analyte and sorbent surface occurs through van der Waals forces or dispersion forces [290]. This interaction is facilitated by polar solvents, since the analyte is attracted to the surface of the sorbent, and the solution phase is repelled [290]. On the other hand, elution solvents are generally nonpolar to break the interactions that bind the analyte to the sorbent.

In contrast to the reversed phase, the normal phase SPE is used for the extraction of polar analytes from nonpolar matrices [290]. The sorbent surface is covered by polar functional groups, such as aminopropyl, cyanopropyl and diol [290]. Alumina, silica and Florisil are also SPE sorbents commonly used in normal phase [290]. In this SPE mode, the analytes are retained by polar interaction with the sorbent, which can include hydrogen bounding, dipole-dipole interactions, induced dipole-dipole interactions and π-π interactions [287]. To maximize analyte–sorbent interaction, nonpolar solvents should be used in this extraction mode [290].

Thus, compounds containing amines, carbonyl groups, hydroxyl groups, aromatic rings, double bounds, or heteroatoms such as nitrogen, oxygen, sulphur or phosphorous can be extracted by normal phase SPE. Regarding the elution of the analytes, it is usually performed with polar solvents that allow the breaking these interactions between the functional group of the analyte and the surface of the stationary phase [287].

Analytes containing ionic groups, such as acids or bases, can be extracted from aqueous samples or polar organic solvents by ion exchange SPE [287, 291]. The main type of interaction in ion exchange SPE is ionic interactions between ionic groups on the analyte and ionic groups on the sorbent phase [291]. For ion exchange to occur, the solid phase and sample must be at a pH where both are in their ionized form [287]. Anionic analytes are negatively charged and can be extracted using anion exchange sorbents, which are positively charged (e.g. quaternary amines) [291]. In contrast, cationic analytes are positively charged and can be extracted using cation exchange sorbents, which contain negatively charged groups, such as sulphonic acid or carboxylic acid groups [291]. In this since, cation exchange works best for basic analytes, while anion exchange works best for acidic analytes. During the SPE process, the most common elution strategy is by pH manipulation in order to neutralize the functional groups of the analyte and/or the sorbent and break the electrostatic interactions. Another common strategy used for elution of the analytes is to use a counter-ion to compete for ion-exchange binding sites [287].

Mixed-mode SPE phases have become very popular since it combines two retention mechanisms to simultaneously extract a broad range of compounds. Commonly, mixed-mode sorbents combine the use of reversed-phase and ion-exchange modes into a single SPE cartridge [290]. They can be used to isolate and separate acidic, basic and neutral compounds from complex matrices, and for this reason they are being used increasingly in drug analysis [292].

Currently, there are other types of sorbent materials used in SPE, which include restricted-access matrix sorbents (RAMs), immunosorbents and molecularly imprinted polymers (MIPs). Generally, RAMs are constituted by porous silica particles with a hydrophilic moiety on the outer surface and hydrophobic groups on the inner surface that retain small drugs through a reversed-phase mechanism [293]. This type of sorbents is very useful for the removal of matrix components, such as proteins, from complex biological samples including blood, serum and urine [293, 294]. MIPs are other type of modern sorbents that are constituted by synthetic polymers, which have a predetermined selectivity for a single analyte or group of structurally related analytes [294]. The selectivity of this type of sorbent is introduced during its synthesis by the imprinting method against template molecule to create artificial recognition sites on polymer matrices that complement the template in terms of size, shape, and spatial arrangement of functional groups [295]. Another type of high selective SPE sorbents is the

immunosorbents. This type of sorbent is obtained by covalently binding antibodies to an appropriate sorbents, such as silica and the extraction is based on molecular recognition [293]. Although antibodies can be specific compounds, they sometimes cross-react with structural analogues and are denatured by contact with organic solvents. For this reason, these sorbents should be used under mild SPE conditions, with regard to pH and organic content [293].

2.2.3.1. Steps involved in the SPE technique

Although the SPE sometimes requires a laborious procedure, the extraction process can be divided into four main steps, which include the conditioning of the solid phase, the adsorption of the analyte in the sorbent, washing of the stationary phase (elimination of interferences) and finally the analyte recovery by elution. This type of extraction sometimes requires two additional steps, namely evaporation and reconstitution, in order to concentrate the analytes prior instrumental analysis. Figure 12 shows the main steps involved in the SPE.

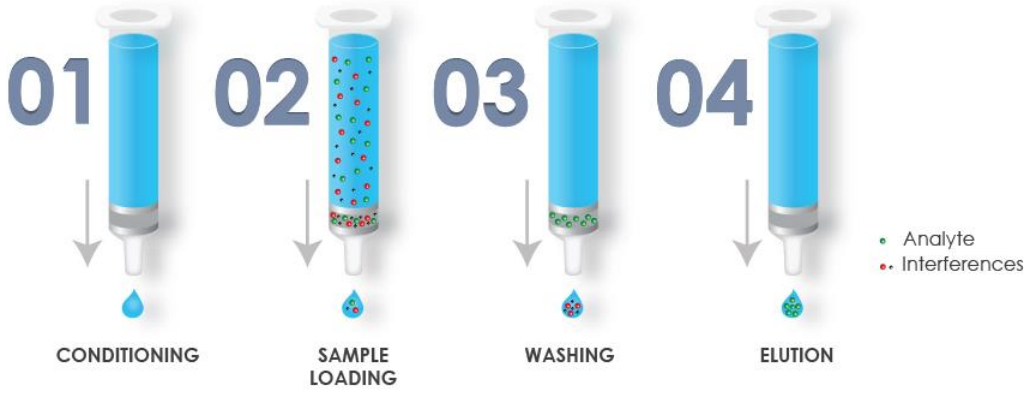

Figure 12. General steps involved in the SPE (adapted from Pinto [287]).

In a first step, the solid phase is conditioned with a suitable solvent, in order to remove any impurity from the production process and activates the sorbent surface to promote analyte interaction [290]. Once the cartridge has been conditioned, the sample is then loaded in the SPE cartridge. During this step, the passage of the sample through the sorbent results in the retention of the analytes, concentrating them on the solid support, while other components of the sample are eluted. This strategy is commonly used when the analyte is present in low concentrations, or when the matrix contains multiple components of different polarities [287]. The inverse process, i.e. the retention of other components in the sample while the analyte of interest is eluted, can also be used as a way of cleaning the sample (clean-up) before instrumental analysis [287]. This strategy is particularly useful when the analyte is in high concentrations [287]. In both cases, controlling the pH or ionic strength of the sample can be

advantageous for a more effective retention of the analytes or interferences [296]. In addition, during the passage of the sample, the flow rate must be controlled, since it can influence the retention process [296].

The third step of SPE is optional and consists of washing the solid sorbent with an appropriate solvent to remove unwanted interference compounds. Commonly, the washing solvent has a higher elution strength than the sample solvent, but is weaker than the elution solvent in order to ensure that analytes are not eluted [294].

To complete the SPE process, the last step consists in the elution of the analytes from the solid phase and should be performed with a suitable solvent capable to disrupt all retentive interactions between the analyte and the sorbent [294]. Often, the solvent volume should be adjusted, in order to recover the analytes in the smallest volume possible [296].

2.2.3.2. Extraction of Synthetic Cathinones by SPE

Due to its versatility and selectivity, SPE is widely used in forensic toxicology to isolate drugs of abuse from biological fluids. A brief review of the literature revealed that, mixed-mode sorbents are the most used solid phases for SCat extraction from biological fluids.

Antunes et al. [213] used a mixed-mode cation exchange sorbent (Oasis MCX®) for the extraction of 4 SCat in whole blood samples. Before the SPE procedure the samples were diluted with a buffered solution (pH 6), homogenized and centrifuged. The resulting solution was added to SPE cartridge, which was previously conditioned with MeOH and H_2O. The sorbent was then washed with a series of solvents to remove as many interference compounds as possible, and the SCat were eluted with a DCM:IPA:NH_4OH (78:20:2, v/v/v) solution. The extraction efficiency achieved with this methodology was higher than 85% for all analytes.

Cláudia et al. [275], also used a very similar procedure to extract of 11 NPS, including 8 SCat in whole blood samples, and the recoveries obtained ranged from 70.3% to 116.6%.

Another study used SPE for the simultaneous determination of SCat enantiomers in plasma and urine samples [280]. As in the previous works, the samples were pre-treated and for the SPE a mixed mode sorbent was used (Clean Screen® CSDAU203 SPE cartridges). After the passage of the sample, the sorbent was washed with three distinct solvents and the analytes were eluted with a DCM:IPA:NH_4OH (78:20:2, v/v/v) solution. The recovery study, expressed in terms of percent error, was within the acceptable range and the values obtained ranged between 0.05% and 12.25% for urine and between 0.06% and 10.98% for plasma.

2.2.4. QuEChERS (Quick, Easy, Cheap, Effective, Rugged, and Safe)

QuEChERS is a relatively recent sample preparation technique, which has become very popular in the analysis of pesticide residues in food and agricultural products, due to its simplicity and speed, making the extraction process inexpensive, compared to classic methods [297]. In general, the extraction process is divided into two steps: the liquid-liquid extraction assisted by salting out (SALLE) and the clean-up of the organic extract, using the dispersive solid phase extraction (d-SPE). Figure 13 shows a schematic representation of a standard QuEChERS method.

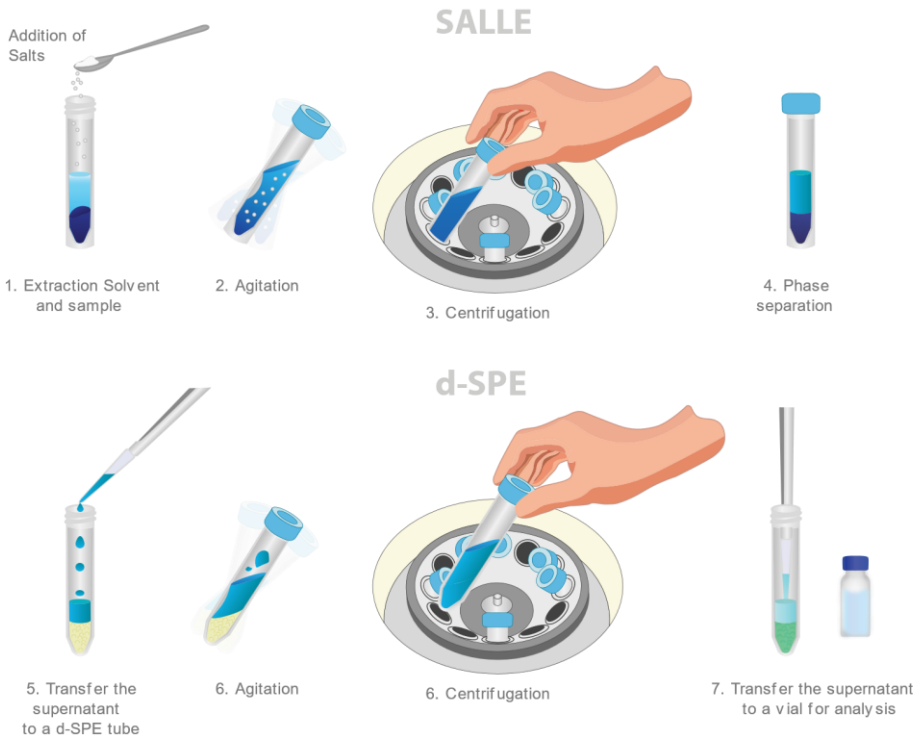

Figure 13. Schematic representation of a typical QuEChERS method (adapted from Allcrom [298]).

In the first step, the sample is extracted with an organic solvent, usually miscible with water (e.g. ACN), in the presence of large amounts of salts (e.g. sodium chloride and magnesium sulfate), and/or buffering agents (e.g. citrate sodium) to induce the separation of the liquid phase and stabilize acidic or basic analytes [299]. The addition of salts, in this step, promotes the effect of salting out, which is based on the decrease of the solubility of the compounds in the aqueous phase by adding a salt, forcing them to migrate to the organic phase, providing good percentages of analyte recovery. After shaking and centrifugation, an aliquot of the organic phase is subjected to an additional clean-up using d-SPE [299]. In contrast to traditional methods using SPE cartridges, d-SPE is carried out in a clean-up tube that allows, the removal of interference and the reduction of residual water. The dispersive component allows the

distribution of the salts to diffuse throughout the sample for a more complete extraction [300]. After sample clean-up, the mixture is centrifuged, and the supernatant is ready for analysis.

In recent years, some changes in the original methodology proposed by Anastassiades et al. [297] were being carried out, allowing their application in a wide variety of analytes and matrices. Currently, there are several studies that used QuEChERS methodology for the extraction of drugs of abuse [301, 302] and NPS [270, 271, 303] from biological matrices.

Usui et al. [271] used a QuEChERS procedure to extract 3,4-DMMC from blood and urine. For both samples, the percentage of analyte recovery ranged from 85.9% to 89.4% for blood and 95.8% to 101% for urine. Fujita et al. [270] also used a similar procedure for the extraction of α-PHP from serum samples, and QuEChERS provided good percentage of analyte recovery with values ranging from 75-77%.

2.2.5. Solid Phase Microextraction (SPME)

SPME is a singular sample preparation technique that is based on sorptive extraction. This technique has shown itself to be very promising and fits precisely in the concept of "green chemistry". Preserving all the SPE advantages, including simplicity, ease of use and possibility of automation, this solvent-free extraction technique was developed to address the need for rapid sample preparation both in the laboratory and on-site [304]. In SPME, the analytes from a liquid or gaseous sample are retained in a fused silica fibre, covered with a thin layer of sorbent, which is part of the syringe needle (Figure 14).

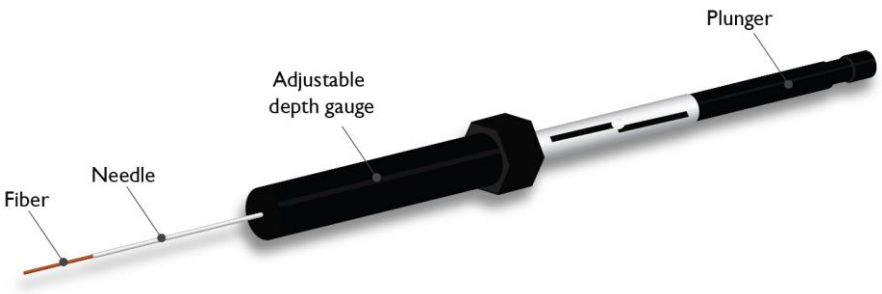

Figure 14. Scheme of a syringe used in the SPME technique (adapted from Gonçalves [305]).

In general, this extraction technique comprises two fundamental steps: the partition of the analytes between the fibre and the matrix, and the desorption of the analytes in a chromatographic system. In the first step, the fibre is exposed directly in the sample or in the headspace (vapor phase above the sample), which causes a partition of the analytes from the sample to the fibre. The selection of the extraction mode should be based on the sample composition and the volatility of the analyte. In direct immersion SPME (DI-SPME), the fibre is

directly immersed in the sample and the analytes are distributed between the matrix and the extractive phase (Figure 15A). This mode is ideally used to extract low volatile analytes from less complex matrices [306]. Regarding to headspace SPME (HS-SPME), the analytes need to be volatilized before being adsorbed/absorbed by the fibre coating, since the extraction occurs in the vapor phase (Figure 15B). This extraction mode is more selective than direct immersion, avoiding low volatile interference and substances with high molecular weight (e.g. proteins), which may be present in the sample [306]. In addition, the headsapce mode allows the modification of the sample, such as the pH adjustment, without damaging the fibre, thus extending its lifetime [306]. Membrane SPME (M-SPME) is another mode of extraction close similar to direct immersion, differing only in the fact that the fibre is protected by a semi-permeable membrane (Figure 15C). This type of extraction is suitable for "dirty" matrices, in cases where headspace extraction is not possible (e.g. low-volatile analytes) [306]. Moreover, this extraction method is advantageous since the membrane protects the fibre, thus prolonging its useful life and, depending on the material that makes up the membrane, it can add a certain degree of selectivity to the extraction process [306].

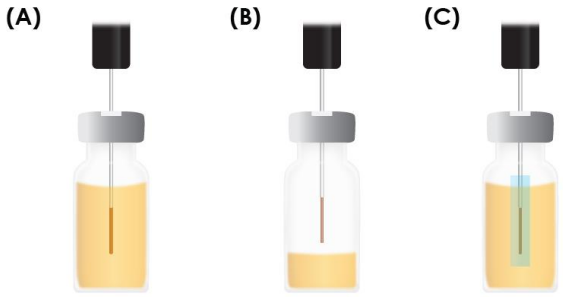

Figure 15. Modes of SPME extraction: (A) direct immersion (DI-SPME), (B) headspace (HS-SPME) and (C) membrane SPME (M-SPME). Adapted from Gonçalves [305].

Generally, several parameters, including fibre type, extraction time, ionic strength, sample pH, extraction temperature and sample agitation, need to be optimized, in order to maximize the extraction efficiency [307]. The process is considered finished when the concentration of the analytes reaches the balance of distribution between the matrix and the fibre coating. Once the extraction is complete, the fibre is removed and transferred to the analytical instrument where the analyte desorption and analysis takes place.

Due to the inherent advantages over other sample preparation methodologies, SPME has been successfully applied in several fields, including environmental [308], food [309], forensic [310] and pharmaceutical [311] analysis.

Despite the wide application of SPME, the literature on SCat analysis remains little explored. Only one study was found, where SPME was used to extract this type of compounds. LaPointe et al. [269] used DI-SPME to extract 3 SCat and their metabolites from urine samples. After the optimization of the fibre type, the authors rapidly concluded that C_{18} and polydimethylsiloxane/divinylbenzene (PDMS/DVB) were the best fibres to extract the studied compounds, however, PDMS/DVB demonstrated better specificity for the metabolites than the C_{18} sorbent. Moreover, the use of SPME increased the signals of both drugs and metabolites, compared with direct analysis, and provided cleaner spectra devoid of the major peaks associated with urine that oftentimes dominate such samples [269].

2.2.6. Dispersive Liquid-Liquid Microextraction (DLLME)

DLLME, is a recent sample preparation technique that allows simultaneous extraction and pre-concentration of analytes using a ternary solvent system constituted by an aqueous phase, a nonpolar water immiscible high-density solvent that acts as extraction phase, and a disperser solvent [279, 312]. Like LLE, DLLME is based on the process of partitioning analytes between two immiscible liquid phases, however, this microextraction technique is more environmentally friendly, as it requires less consumption of organic solvents with volumes in the microliter range [313].

A typical DLLME procedure comprises two fundamental steps as shown in Figure 16. The first step involves the injection of a suitable mixture of extracting and dispersing solvents into the aqueous sample containing the analytes [314]. In this step, the extraction solvent is dispersed in the aqueous phase in microdroplets creating a cloudy solution. This dispersion is favoured by the dispersing solvent, which must be soluble in the aqueous sample and in the organic phase [314]. On the other hand, due to the large surface area created by the numerous microdroplets, partitioning of analytes into the extraction phase is instantaneous, and the equilibrium state is reached quickly, which is one of the main advantages of this method [313, 314]. Finally, the last step of this microextraction technique consists of centrifuging the cloudy solution to break the emulsion in a two-phase system allowing easy recovery of the extraction solvent for analysis [313].

In DLLME, there are several factors that influence the extraction efficiency that must be optimized prior to analysis. These include the volume and type of extraction and dispersive solvent, pH of the aqueous phase, ionic strength, extraction time, and centrifugation time must be optimized to ensure quantitative extraction of analytes [313].

Figure 16. Schematic representation of a typical DLLME technique (adapted from Quigley et al. [313]).

Although DLLME is a relatively recent methodology, it has been successful applied to the extraction of SCat from biological fluids. Odoardi et al. [276] used DLLME for the screening of 78 different NPS, including 21 SCat from blood samples. Before extraction, the samples were pre-treated, in order to remove proteins from the matrix. For the DLLME procedure, a mixture of $CHCl_3$:MeOH (1:2.5, v/v) was used as the extractant and the disperser solvent, respectively. The recovery values obtained for SCat ranged from 10% to 81%.

Mercieca et al. [279] also used DLLME for the extraction of several NPS, including 13 SCat from blood and urine samples. As in the previous study, a mixture of $CHCl_3$:MeOH (1:2.5, v/v) was used as the extractant and the disperser solvent, respectively, and the recovery values for SCat ranged from 95.6% to 114.9% in urine, and from 82.6% and 106.5% in blood.

2.2.7. Microextraction by Packed Sorbent (MEPS)

MEPS is one of the most recent sample preparation techniques, which was created in 2004 as a miniaturization of the conventional SPE technique by Abdel-Rehim et al. [315], in order to reduce the volume of solvents and sample needed and provide an automated method through its easy interface to chromatographic systems. In this technique, sample extraction, concentration and clean-up are performed in a single device composed by two parts: the MEPS syringe and the MEPS cartridge, also known as barrel insert and needle (BIN) (Figure 17) [316, 317].

In contrast to the conventional SPE technique, where the sorbent is packed in a column, in MEPS the sorbent material is integrated directly into a micro-syringe needle that can be reused up to 100 extraction or more depending on the sample matrix [318, 319]. The small quantity of extraction sorbent (1-4 mg) in the MEPS cartridge can be washed between samples to remove impurities and carryover, which is a significant advantage over the conventional SPE

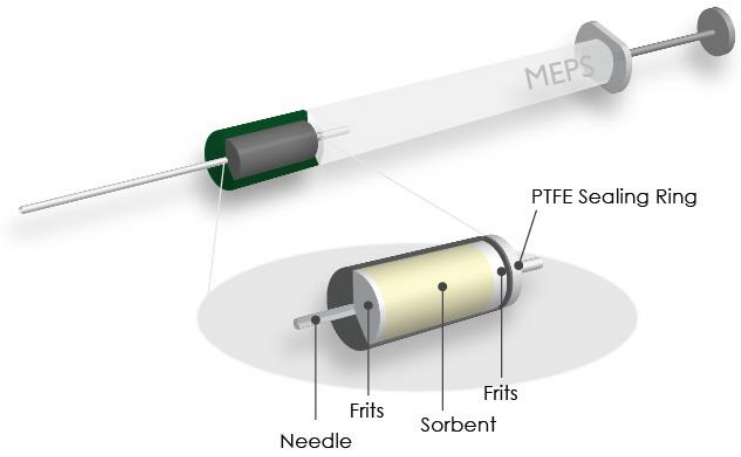

Figure 17. Schematic overview of the MEPS syringe and MEPS-BIN (barrel insert and needle). The sorbent is packed and properly sealed inside the barrel to avoid leakage (adapted from Gonçalves [305]).

column that is used only once [318, 319]. In addition, the low quantity of sorbent reduces the sample volume from millilitre to microliter, which assumes particular relevance in forensic toxicology, since sample availability is often limited and several exams need to be performed on the same sample [222, 274]. On the other hand, the reduced solvent consumption makes MEPS more environment-friendly than SPE and other extraction techniques, which also results in a reduction in analysis time and costs [274].

The MEPS experimental layout is very simple and usually follows the conventional 4-step SPE procedure: sorbent conditioning, sample loading, washing and elution (Figure 18). Despite this simplicity, MEPS involves a wide range of optimization steps, including the type of sorbent material, washing and elution solvents, number of extraction cycles, sample volume, washing solvent volume and elution solvent volume, that allow a fine tuning of the extraction efficiency [319, 320].

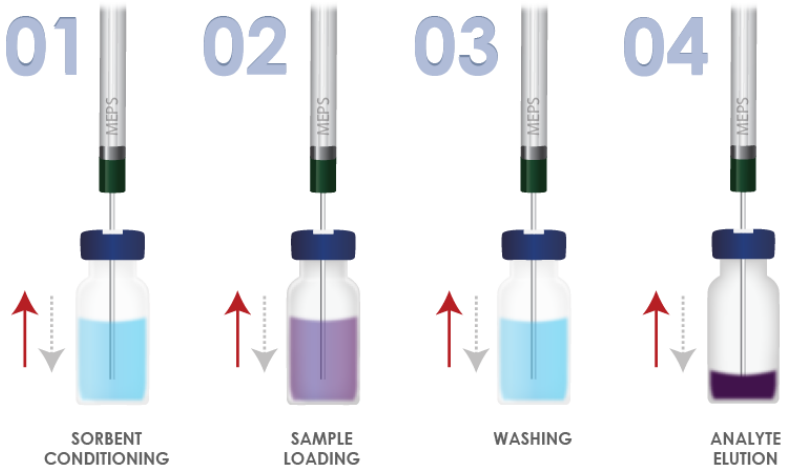

Figure 18. Typical MEPS procedure (adapted from Casado et al. [321]).

One of the critical parameters that determine the success of MEPS is the choice of the sorbent material. Depending on the analytes to be extracted, the sorbent material must have specific characteristics that allow obtaining the highest extraction efficiency [316, 321]. Currently, there are several MEPS sorbent materials available, including reverse phase (C_{18}, C_8 and C_2), normal phase (silica), ion exchange materials (SAX and SCX), mixed mode (C_8/SCX), and polymeric sorbents based on the polystyrene-divinylbenzene (PS-DVB). Materials featuring specific extraction capability such as porous graphitic carbon (PGC), molecular imprinted polymers (MIPs), and monoclonal antibodies for immunoaffinity sorbents were also reported for MEPS application [322, 323]. Table 5 shows some characteristics of the most common sorbents commercially available for MEPS.

Table 5. General properties of several commercially available sorbents for MEPS (adapted from Pereira et al. [316]).

Sorbent	Chemistry	Properties
Silica	Normal Phase	– highly polar sorbent retaining polar analytes (as those that contain amino groups from nonpolar matrices)
C_2	Reverse phase	– fairly non-polar sorbent (short chain length of functional group) – alternative to C_8 and C_{18} if analytes are retained too strongly
C_8	Reverse phase	– less retentive than C_{18} for non-polar compounds – lower carbon loading than C_{18}
C_{18}	Reverse phase	– highest hydrophobic and least selective sorbent – extremely retentive for non-polar compounds, retaining most organic analytes from aqueous matrices – suitable for the simultaneous extraction of analytes with diverse structures
APS	Ion Exchange and Reverse phase	– very polar silica-bonded aminopropyl phase used as an ion-exchanger in both normal-phase and ion-exchange applications – allows the rapid release of very strong anions such as sulfonic acids that may be retained irreversibly on SAX
SCX	Ion Exchange and Reverse phase	– Strong Cation Exchange: silica bonded benzene ring offering mixed-mode capabilities (hydrophobic interactions) – very low pK_a (<1.0) due to H^+ counter ion from the benzene sulfonic acid excellent capacity; suitable for weakly basic compounds
SAX	Ion Exchange and Reverse phase	– Strong Anion Exchange: remains charged at all pH levels due to the quaternary amine bonded to silica – selectivity can be modified by changing the counter ion with the appropriate buffer during conditioning suitable for weakly acidic compounds
C_8/SCX (M1 or Verify CX)	Mixed-mode	– Mixture of C_8 and SCX phases – dual retention mechanisms broaden retention for a range of neutral, basic, acidic and zwitterionic compounds – higher selectivity for basic compounds from biological fluids
C_8/SAX (Verify AX)	Mixed-mode	– non-polar and cationic characteristics for improved analysis of acidic drugs of abuse and metabolites from biological matrices (including THC and its metabolites) and moderately polar to non-polar and ionized and charged compounds

Table 5. (Continuation)

Sorbent	Chemistry	Properties
Hypercarb	Reverse phase	– 100% porous graphitic carbon material – retention of extremely polar compounds – recommended for pesticides extraction from different matrices
SDVB	Reverse phase	– hydrophobic polystyrene-divinylbenzene copolymer; highly retention of non-polar compounds; poor retention of polar compounds
HDVB	Reverse phase	– highly cross-linked polystyrene divinylbenzene copolymer (PS-DVB); hydrophobic polymeric sorbent offering 100% reversed phase interaction
Retain PEP	Mixed-mode	– polymeric PS-DVB modified with urea functional groups to give balanced retention of polar and non-polar analytes. – ideal for a wide range of applications, such as drugs and metabolites in biological fluids
Retain-CX	Ion Exchange	– polymeric PS-DVB material partially functionalized with sulfonic acid groups to give balanced retention of basic and non-polar analytes – ideal for the retention of a wide range of drugs of abuse, including basic and neutral drugs
Retain-AX	Ion Exchange	– polymeric PS-DVB material partially functionalized with quaternary amine groups to give balanced retention of acidic and non-polar analytes. – ideal for the retention of THC and its metabolites

In MEPS, the sample can be drawn through the needle into the syringe, once or several times (draw-eject), in order to maximize the retention of the target analytes on the extracting material [319, 320]. Commonly, these extraction cycles can be performed by two different extraction procedures: the first method called "draw-eject", which consists of a sequence of cycles of aspirations and injections in the same vial, and the second one, called "extract-discard", which consists of a similar cycle sequence, but the aspired sample in this case is discarded into waste [222, 324]. The optimization of the number of extraction cycles is crucial since it can compromise the absolute recovery of the analytes. In general, a higher number of extraction cycles is often considered necessary for complex matrices, such as biological fluids, including blood, plasma and urine. In addition, complex samples should be processed accordingly to optimize the extraction of the target analytes by favouring a better interaction between sample analytes and the sorbent [320]. This may involve the dilution of sample (to reduce the sample viscosity), pH adjustment, deprotonation, or even sample loading speed [316, 320].

Upon the target analyte retention in the solid phase, the washing step is usually considered to remove matrix interferents. This is an important part of the MEPS procedure that should be optimized since it is intended to discard undesired contaminant species [319]. The solvent used in this step, in general has a higher elution strength than the sample solvent, but

lower than the elution solvent to ensure that the analytes are not eluted, which would lead to low recovery.

The last step of MEPS procedure consists on elution of the target analytes using an appropriate solvent, which must be capable of disrupting all of the retentive interactions between the analyte and sorbent. Typically, this step is performed with an organic solvent, such as ACN, MeOH or IPA, pure or mixed with acidic or basic solutions (0.1–3%) and the maximum amount of analyte should be eluted using the smallest volume of the solvent possible, thus increasing the target analyte concentration [319, 320]. Moreover, very small elution volumes allow MEPS to be used for direct injection in chromatography systems [317].

2.3.7.1. MEPS configurations

Since its introduction in 2004, MEPS has gone through several improvements mainly affecting its technical configuration. Currently, MEPS is commercially available in off-line and on-line formats as shown in Figure 19.

Figure 19. MEPS formats commercially available: manual (MEPS syringe), semi-automatic (eVol®) and on-line (several configurations available by CTC Analytics) (adapted from Pereira et al. [316]).

The simplest and most often reported format is the manual MEPS, where the MEPS syringe containing the BIN are manually operated [316]. The BIN is used with a 100 µl or 250 µl gas tight MEPS syringe that allows fluid handling at normal SPE pressures [325].

The semi-automatic MEPS version, constituted by the programmable digital syringe eVol®, was a breakthrough in MEPS extraction, allowing a significant automation of the experimental procedure which became very close to what an autosampler can offer, but at a more affordable price [319]. The eVol® has a digital interface very intuitive and easy-to-use with a touch wheel controller and a full-colour screen [326]. The numerous withdraw–dispense operation cycles are performed automatically by the electronic syringe after simple programming [318]. The eVol syringes (XCHANGE®) are available for the maximum capacities 5 µL, 50 µL, 100 µL, 500 µL and 1000 µL, which allow higher flexibility in terms of sample/solvent

volume (Figure 20). Moreover, the ease of replacing eVol syringes (XCHANGE®), preventing cross contamination between solvents/samples, as well as the ease of calibration by the user in order to ensure accurate and precise measurements, are some of the factors that make this tool very attractive from an analytical point of view [326]. For these reasons, eVol®-MEPS extraction is more reliable than manual MEPS, exhibiting better reproducibility and repeatability [319].

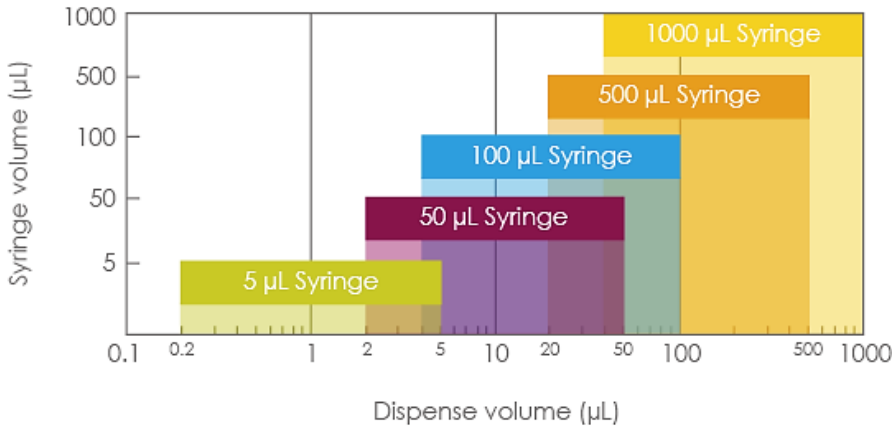

Figure 20. Volume range of eVol syringes (XCHANGE®) (adapted from SGE [326]).

The last MEPS format is the online and fully automated MEPS approaches that can be easily achieved using the same MEPS XCHANGE® syringes on autosamplers (e.g. CTC Analytics auto-injectors) [316, 318]. With a typical volume of a few microliters, the MEPS elution is compatible with the liquid and gas chromatography (LC and GC) systems, making it possible to prepare samples online [317]. In addition, these autosamplers bring together several technological innovations, being an asset for routine analysis, thus increasing laboratory productivity. Despite these advantages, fully automatic MEPS versions are still very expensive and are not accessible to many laboratories.

In any MEPS formats, the samples and solvents are loaded and discarded through the same channel [319]. The two-directional flow (up and down), which provides repetition of each step, enhances the sample-sorbent contact and improves the method's efficiency [321]. However, for target analytes with weak interactions with the sorbent, this may be particularly critical, since these analytes can be partially eluted and lost during the sample withdrawal and washing steps [319]. On the other hand, elution leads to sample dilution, with the analyte mixed throughout the entire solvent volume, and this can make the method prone to sample carryover [327]. To overcome this problem, the integration of a two-way valve into the barrel of the MEPS syringe to control the direction of liquid flow (controlled directional flow - CDF) was developed by SGE Analytical Science in collaboration with the Australian Centre for Research On Separation Science [327, 328]. This allows, for example, the loading of the elution solvent directly from the

top of the sorbent bed, therefore reducing the possibility of dilution, carryover and any other contamination made during the bidirectional flow [319]. Figure 21 shows a schematic representation of the CDF MEPS.

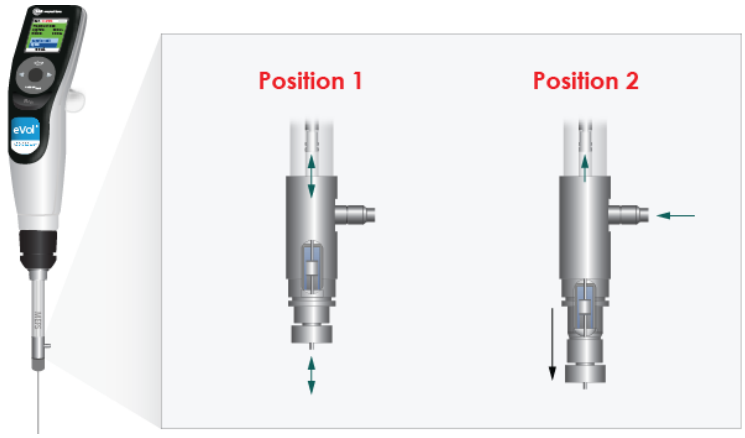

Figure 21. Schematic representation of CDF MEPS. Position 1: the fluid is aspirated or dispensed across the MEPS bed; Position 2: Engaging position 2 the valve body is pulled down (black arrow) and this removes the MEPS bed from the fluid path. (adapted from SGE [328])

More recently, an innovative improvement in the µ-SPE techniques was achieved by the EPREP company (Victoria, Australia) with the introduction of the µSPEed® cartridges [319]. In contrast to MEPS, this system was designed to provide a single way flow path through the sorbent bed in every step of the extraction protocol. Using an efficient pressure-driven one-way check valve, the sample and solvents are aspirated through the cartridge into the syringe barrel, without passing through the sorbent bed [329]. Then pushing the syringe plunger, the sample passes through the sorbent where the analytes are retained. Figure 22 shows the operation of a typical µSPEed® cartridge.

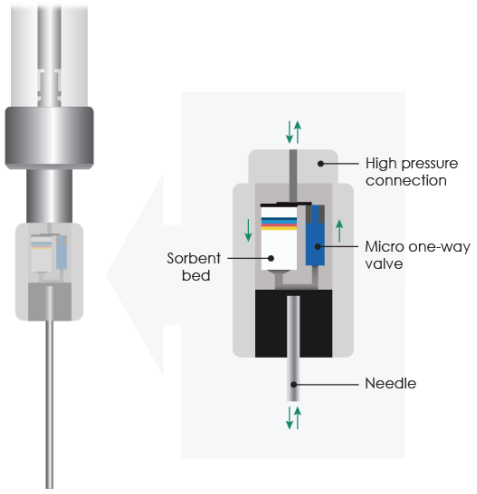

Figure 22. µSPEed® cartridge (adapted from EPREP [330]).

The simple design of µSPEed® cartridges does not require additional tubes and fittings, since the whole microextraction system is integrated into a single cartridge [319, 329]. Moreover, µSPEed® cartridges resemble a short high-performance liquid chromatography column (HPLC; < 1 cm long), due to the small sorbent particles (≤ 3 µm) used, instead of the 50 µm diameter particles used in SPE, the efficient pressure-driven one-way check valve, and ultra-low dead volume connection [319, 329]. On the other hand, the constant, high pressure (up to 1600 psi) and single direction flow through the small particle size sorbent, allow more efficient extractions of the target analytes [319, 329].

It should also be noted that the standard eVol® syringe and the new digiVOL® Digital Syringe Driver (EPREP) are fully compatible with µSPEed® cartridges [329]. The EPREP system can cope with higher backpressures than the standard eVol® syringe, which can be very advantageous for the extraction of complex samples, such as biological fluids, that often cause sorbent clogging [319, 329]. However, unlike the cordless eVol®, the digiVOL® requires a continuous power connection to operate [319, 329]. Figure 23 shows a typical digiVOL® system.

Figure 23. digiVOL® Digital Syringe Driver (adapted from EPREP [331]).

2.3.7.2. Extraction of Synthetic Cathinones by MEPS

Although MEPS is a relatively recent methodology, it has been gaining ground against traditional sample preparation methodologies. Due to its versatility, MEPS has been successfully applied in numerous environmental [332, 333], food [334, 335], clinical [336, 337], and forensic applications [273, 338]. A brief review of the literature reveals, that to date, there are few studies that have used MEPS in the determination of SCat in biological matrices. Fernández et al. [274] developed a simple method based on MEPS for quantitative determination of three SCat and seven conventional drugs of abuse and metabolites in human plasma. In their work, the influence of several extraction parameters was evaluated, and the best experimental

conditions were obtained using 300 µL of pre-treated plasma, loading 10 × 100 µL through the C_8/SCX sorbent. The washing step was performed using 150 µL of H_2O:MeOH (90:10, v/v), followed by drying for 0.5 min and the elution of the analytes was carried out with 200 µL DCM:IPA:NH_4OH (78:20:2, v/v/v).

Ares et al. [273] also developed a fast bioanalytical method based on MEPS for determination of eleven SCat, six opiates, scopolamine, cocaine and two metabolites in oral fluid. The influence of several variables such as the phase type, number of extraction cycles, pH, washing solution and eluent volumes was investigated and the best conditions were obtained using 100 µL of pre-treated oral fluid, loading six times at 10 µL s^{-1} through the C_8/SCX sorbent. Then, the sorbent was washed with 50 µL of H_2O:MeOH (90:10, v/v) at 20 µL s^{-1} to remove interferences and dried for 0.5 min. The analytes were eluted with 90 µL of DCM:IPA:NH_4OH (78:20:2, v/v/v) at 10 µL s^{-1}.

Rocchi et al. [339] also used MEPS for simultaneous screening and quantification of 31 NPS, including 10 SCat, in oral fluid. After conditioning C_{18} sorbent with 3 × 250 µL of MeOH and 3 × 250 µL H_2O:MeOH (75:25, v/v), the pre-treated sample (200 µL) was loaded 5 times followed by washing with 3 × 200 µL H_2O:MeOH (90:10, v/v). The elution of the analytes was carried out with 5 × 100 µL of MeOH containing 10 mM of formic acid (FA).

Although few studies have used MEPS as extraction technique in the determination of SCat, in recent years MEPS has been successfully applied to the extraction of several classes of drugs of abuse, including amphetamines [340, 341], cocaine and its metabolites [342, 343], opioids [274, 344], cannabinoids [345, 346], as well as numerous classes of NPS [339, 347, 348]. Table 6 summarizes the most recent applications of MEPS for the determination of drugs and their metabolites in a forensic context.

Table 6. Application of MEPS for forensic drug analysis.

Compounds	Sample (amount)	MEPS sorbent	Analytical technique	Extraction Recovery	LOD/LOQ (ng mL^{-1})	REF.
AMP, MAMP, MDA, MDMA, MBDB and MDEA	Urine (200 µL)	C_{18}	GC-MS	19 - 71%	LLOQs: 25 - 50	[341]
MOR, 6-MAM, COC, COCET, BZE, METHA, EDDP, MDPV, MEP, MET, BUP, NAL, PENT, ETH, BUT, ETCAT, ETCATEP, METEP, PRV, FLE and SCO	Oral fluid (300 µL)	C_8/SCX	UPLC-MS/MS	75 - 125%	LOQ: 0.5 - 1.0	[273]
AMP, METHA	Urine (100 µL)	C_8	Direct injection-MS/MS	92 - 107%	LOD: 1.5 - 6.0 LOQ: 5 - 20	[349]
AMP, MAMP	Hair (5 mg)	C_{18}	GC-MS	64 - 74%	LOQ: 0.20	[340]
Salvinorin A	Urine (200 µL)	C_{18}	GC-MS/MS	71 - 80%	LOD: 5 LOQ: 20	[350]
BZP, *m*-CPP, TFMPP, *p*-MeOPP	Urine (100 µL)	C_8/SCX	HPLC-DAD	52 - 100%	LOD: 50 - 100 LLOQ: 100	[351]

Table 6. (Continuation)

Compounds	Sample (amount)	MEPS sorbent	Analytical technique	Extraction Recovery	LOD/LOQ (ng mL^{-1})	REF.
KET, NKET	Plasma (250 µL) Urine (250 µL)	C_8/SCX	GC-MS/MS	63 - 101%	LOD: 5 LOQ: 10	[352]
11-OH-THC, THC-COOH, THC	Plasma (250 µL)	C_8/SCX	GC-MS/MS	53 - 78%	LLOQ: 0.1	[345]
11-OH-THC, THC-COOH, CBD, CBN, THC	Oral Fluid (125 µL)	C_{18}	LC-MS/MS	50 - 105%	LOD: 0.008 - 0.12 LOQ: 0.02 - 0.40	[338]
BZE, COC, EME	Urine (200 µL)	C_8/SCX	GC-MS	14 - 83%	LLOQ: 25	[343]
BZE, COC, COCET, EME	Urine (–)	Clean Screen DAU material	DART-TOF/MS	–	LOD: 4.0 - 23.7 LLOQ: 65 - 95	[342]
BZE, COC, COCET, EDDP, 6-AM, METHA, MOR, MDPV, MEP, MET	Plasma (300 µL)	C_8/SCX	UHPLC-PDA	80 - 104%	LOD: 5 - 25 LOQ: 10 - 50	[274]
AMP, MAMP, MDA, MDMA, MDEA, KET, PCP, BZE, COC, EME, NCOC, EDDP, 6-MAM, BUP, COD, DAM, MSC, METHA, MOR, NBUP	Oral fluid (120 µL)	C_{18}	LC-MS/MS	18 - 102%	LOD: 0.2 - 10 LOQ: 0.5 - 30	[344]
2C-B, MDBZP, *p*-MeOPP, AB-005, AM-1220, JWH-018, JWH-018 N-COOH, JWH-018 N-5-OH, JWH-073, JWH-081, JWH-122, JWH-200, JWH-250, MAM-2201, MAM-2201 N-COOH, UR-144, UR-144 N-5-OH, XLR-11, XLR-11 N-4-OH, MDPV, 4-MEC, α-PVP, BUPH, BUT, MET, MEP, ETCAT, 4-MeOMC, DMC	Oral Fluid (90 µL)	C_{18}	UHPLC-MS/MS	31 - 96%	LOD: 0.005 - 0.850 LOQ: 0.015 - 2.600	[353]
Zopiclone, Zolpidem, Nifoxipam, Deschloroetizolam, Zaleplon, Clonazolam, Flubromazolam, Meclonazepam	Plasma (300 µL)	HyperSep Retain PEP	UHPLC-MS/MS	61 - 123%	LOD: 0.5 - 5 LOQ: 1 - 10	[354]

Abbreviations: 2C-B - 2,5-dimethoxy-4-bromophenethylamine; 4-MEC - 4-methyl-*N*-ethylcathinone; 4-MeOMC - methedrone; 6-AM - 6-acetylmorphine; 6-MAM - 6-monoacetylmorphine; 11-OH-THC - 11-Hydroxy-Δ^9-tetrahydrocannabinol; α-PVP - α-pyrrolidinopentiophenone; AB-005 - [1-[(1-methyl-2-piperidinyl)methyl]-1H-indol-3-yl](2,2,3,3-tetramethylcyclopropyl)-methanone; AM-1220 - [1-[(1-methyl-2-piperidinyl)methyl]-1H-indol-3-yl]-1-naphthalenyl-methanone; AMP - amphetamine; BUP - buprenorphine; BUPH - buphedrone; BUT - butylone; BZE - benzoylecgonine; BZP - 1-benzylpiperazine; CBD - cannabidiol; CBN - cannabinol; COC - cocaine; COCET - cocaethylene; COD - codeine; DAM - diacetylmorphine; DMC - dimethylcathinone; EDDP - 2-ethylidene-1,5-dimethyl-3,3-diphenylpyrrolidine; EME - ecgonine methyl ester; ETCAT - ethylcathinone; ETCATEP - ethylcathinone ephedrine metabolite; ETH - ethylone; FLE - flephedrone; JWH-018 - 1-pentyl-3-(1-naphthoyl)índole; JWH-018 N-5-OH - JWH-018 N-(5-hydroxypentyl) metabolite; JWH-018 N-COOH - JWH-018 N-pentanoic acid metabolite; JWH-073 - 1-Butyl-3-(1-naphthoyl)índole; JWH-081 - 1-Pentyl-3-[1-(4-methoxynaphthoyl)]índole; JWH-122 - 1-Pentyl-3-(4-methyl-1-naphthoyl)índole; JWH-200 - [1-[2-(4-morpholinyl)ethyl]-1H-indol-3-yl]-1-naphthalenyl-methanone; JWH-250 - 1-pentyl-3-(2-methoxyphenylacetyl)índole; KET - ketamine; MAM-2201 - [1-(5-fluoropentyl)-1H-indol-3-yl](4-methyl-1-naphthalenyl)-methanone; MAM-2201 N-COOH - MAM-2201 N-pentanoic acid metabolite; MAMP - methamphetamine; MBDB - 3,4-methylenedioxy-N-methyl-α-ethylfenilethylamine; *m*-CPP - 1-(3-chlorophenyl) piperazine; MDA - 3,4-methylenedioxyamphetamine; MDBZP - 1-(3,4-methylenedioxybenzyl)piperazine; MDEA - 3,4-methylenedioxy-*N*-ethylamphetamine; MDMA - 3,4-methylenedioxyethylmethamphetamine; MDPV - 3,4-methylenedioxypyrovalerone; MEP - mephedrone; MET - methylone; METEP - methylephedrine metabolite; METHA - methadone; MOR - morphine; MSC - mescaline; NAL - naloxone; NBUP - norbuprenorphine; NCOC - norcocaine; NKET- norketamine; PCP - phencyclidine; PENT - pentedrone; *p*-MeOPP - 1-(4-methoxyphenyl) piperazine; PRV - pyrovalerone; TFMPP - 1-(3-trifluoromethylphenyl) piperazine; THC - tetrahydrocannabinol; THC-COOH - 11-Nor-9-carboxy-Δ^9-tetrahydrocannabinol; SCO - scopolamine; UR-144 - (1-pentyl-1H-indol-3-yl)(2,2,3,3-tetramethylcyclopropyl)-methanone; UR-144 N-5-OH - UR-144 N-(5-hydroxypentyl) metabolite; XLR-11

- (1-(5-fluoropentyl)-1H-indol-3-yl)(2,2,3,3-tetramethylcyclopropyl)methanone; XLR-11 N-4-OH - XLR-11 N-(4-hydroxypentyl) metabolite.

2.3. Analytical Methods used in the Determination of Synthetic Cathinones

The identification of drugs of abuse in seized materials and in biological samples, generally follows a sequence of techniques designed to obtain reliable results in an effective way. Generally, the identification begins with the application of screening tests (presumptive), which aim to provide preliminary data on the presence or absence of a certain class of compounds [355]. An ideal tool for such presumptive testing is colour testing, which utilizes a chemical reaction between a drug and a reagent to produce a readily observable coloured product [356]. These tests are well established and have been applied to many drug classes; however, the emergence of NPS has posed a new challenge [356]. Currently, there are few commercially available colour tests that claim to detect SCat. Unfortunately, these tests are often not specific towards cathinones alone, or do not fully screen for the most common SCat derivatives [357].

In the field of toxicology, routine immunoassays for drug screening also present limitations in the analysis of NPS. Due to the structural similarity of several NPS and traditional drugs of abuse, limits their analysis due to cross-reactivity [207, 242]. As a result, the routine immunoassay drug testing may become less effective due to an increased occurrence of false positive and false negative results [358]. Moreover, the use of immunoassays for NPS screening is limited by the need to develop antibodies specific to an ever-increasing range of new drugs entering the market.

Due to the several limitations of presumptive tests, the detection and determination of NPS in seized materials and in biological samples requires the use of more sophisticated analytical techniques, which may include the IR spectroscopy, GC-MS and NMR.

2.3.1. Fourier Transform Infrared Spectroscopy (FTIR)

IR spectroscopy is a rapid and non-destructive analytical tool used typically to identify the functional groups of organic compounds. This technique has proven to be very useful in the forensic analysis of a wide variety of evidence types including, fibre identification [359], ink analysis [360], gunshot residues [361], biological samples [362], controlled substances [363, 364], among others.

In IR spectroscopy, a sample is irradiated with an IR source, and the intensity of the transmitted or reflected radiation is measured as a function of frequency. When the frequency of the radiation matches the vibrational frequency of an interatomic bond, the molecule absorbs

the energy, causing a change in the amplitude of molecular vibration [365]. This generates signals whose frequency corresponds the vibration of a specific bond, which is very useful for determining the molecular structure of a substance [287].The simplest types, or modes, of vibrational motion in a molecule are the stretching and bending modes. While symmetric or asymmetric stretching alters the bond length, bending vibrations change the bond angle, through twisting, rocking, wagging, and scissoring (Figure 24) [366].

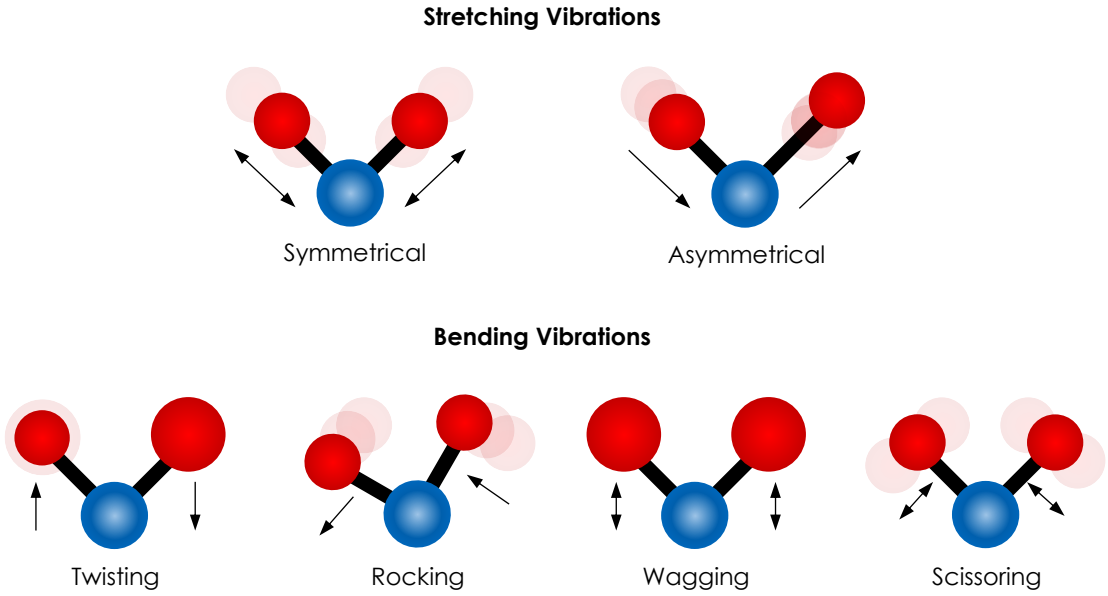

Figure 24. Vibrational modes of chemical bonds (adapted from Cameron et al. [366]).

These characteristic vibrations are a good way to detect the existence of functional groups in a chemical compound [367]. Practically the most useful IR region lies between 4000-400 cm^{-1} (middle IR region), since molecules can absorb radiations in this region to induce the vibrational excitation of functional groups [365]. Generally, it is not possible to assign specific molecular vibrations to all bands in an IR spectrum. However, it is helpful to divide an IR spectrum into two regions: the functional group region and the fingerprint region. The region from 4000cm^{-1} to approximately 1500 cm^{-1} is called functional group region [365]. The characteristic stretching frequencies for important functional groups such as OH, NH, and C=O occur in this region of the spectrum. Alternately, in the region of the spectrum below 1500 cm^{-1}, known as the fingerprint region, the absorption bands are numerous and differ for each compound [365, 368]. These are deformation vibrations of both the bonds and the skeleton and are difficult to assign with accuracy [368]. Small changes in the chemical structure of a molecule will result in significant changes in the appearance and distribution of absorption peaks in this

region [288]. However, the fingerprint region is very useful for comparing the spectrum of an unknown compound with the spectra of a known compound for identification purposes.

IR spectra can be complex, and the frequency characteristics vary with the physical state of the molecule, with the precise position of a functional group in the spectrum being influenced by steric effects and the relative size of the charge of neighboring groups [288]. Thus, the exact interpretation of the spectra is not always possible due to its complexity, a fact that also makes it unique [288]. As auxiliary measures in the interpretation, there are correlation tables, spectrum catalogues and digital libraries [288].

Regarding to the IR spectrometers, most commercial instruments separate and measure IR radiation using dispersive spectrometers or Fourier transform spectrometers [369]. Fourier transform IR spectrometers (FTIR) have recently replaced dispersive instruments for most applications due to their superior speed and sensitivity [369]. Essentially a FTIR spectrometer is composed by three major parts, namely radiation source, interferometer, and detector [369]. A simplified overview of a typical FTIR spectrometer is illustrated in Figure 25.

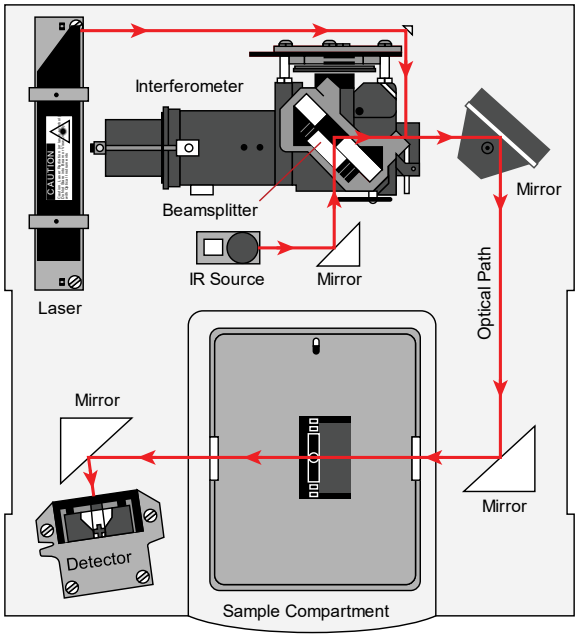

Figure 25. Schematic representation of a typical FTIR spectrophotometer (adapted from Skoog et al. [370]).

The source generates radiation which passes the sample through the interferometer and reaches the detector. Generally, the IR source is an inert solid, such as globar, a silicon carbide rod which is electrically heated to about 1300 K [371]. This source emits radiation in the mid-IR region [371]. For shorter wavelengths of the near-IR, a tungsten-halogen lamp is typically

required, while for far-IR, a mercury discharge lamp gives a larger throughout than a thermal source [372].

IR energy emitted from the source enters the interferometer where a special type of signal - interferogram - is produced. The interferometer is an optical device composed of a beamsplitter, a fixed mirror and a moving mirror and is considered the key part of any FTIR spectrophotometer [369]. The beamsplitter divides an incoming beam of radiation into two parts, such that half the beam is transmitted to a moving mirror and the other half is reflected to a fixed mirror (Figure 26) [370]. The splitted beams are then recombined back at the beamsplitter and steered toward the sample. The difference in the path of the mirrors causes constructive and destructive interference depending upon the position of the mirror and the frequency of the radiation [369]. This resulting interference pattern are known as interferogram. When this interference beam is passed through the sample, part of the energy is absorbed, and part is transmitted and reaches the detector [369]. It is important to note that, FTIR spectrophotometer use a reference laser, typically a helium neon (HeNe) laser, for precise wavelength calibration, mirror position control and data acquisition timing.

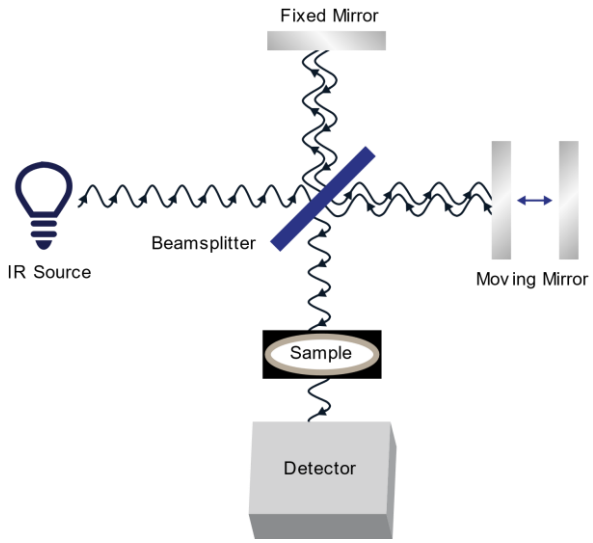

Figure 26. Scheme of a generic FTIR interferometer (adapted from InnovaTECH [373]).

Once the interferogram is collected, it is subsequently converted into a spectrum by Fourier transform. In simple terms, Fourier transform is a mathematical operation that can be used to transform a function from one real variable to another. In this sense, the raw signal (interferogram), represented as the intensity of light (y axis) versus the mirror position (x axis), which in turn is a function of time (as the mirror is in motion at a constant velocity) is converted by Fourier transform to produce the more familiar IR representation of intensity as a function of wavenumber [369].

IR analysis can be used on solid, liquid or gaseous samples, being this one of the great advantages of this technique. In recent years, attenuated total reflectance (ATR) has become the preferred sampling technique in FTIR spectroscopy, since it enables samples to be examined directly in the solid or liquid state without further preparation. In ATR-FTIR spectroscopy the sample is in contact with the ATR crystal (Figure 27). An incident IR beam travels through the crystal and interacts with the sample on the surface in contact with the ATR crystal [374]. Due to the differences in refractive indices of both materials, total internal reflection occurs. This reflection forms the evanescent wave which extends into the sample, typically by a few micrometers [374].

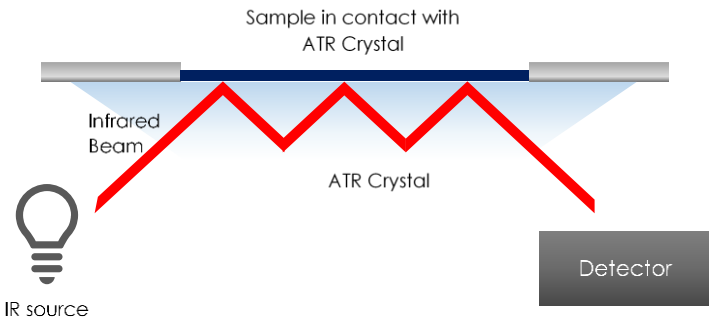

Figure 27. Scheme of ATR-FTIR measurement principle (adapted from PerkinElmer [375]).

Depending on the sample's composition, some of the IR radiation is absorbed when the evanescent wave interacts with the sample, resulting in a slightly attenuated total reflection [374].

Numerous studies have shown that ATR-FTIR is a suitable method for drug analysis. Zancajo et al. [376] used ATR-FTIR for the analytical profile of products containing SCat. For this purpose, 20 mg of each product was placed directly in the instrument and IR spectra were obtained in the range of 4000 - 600 cm^{-1}. All spectra were consistent with the molecular structure of SCat, showing the characteristic band corresponding to the carbonyl group, the bands with low relative intensity corresponding to an amine group, and the C=C band corresponding to the aromatic ring. Piorunska-Sedlak and Stypulkowska [364] also used ATR-FTIR for the identification of NPS in illicit samples. In this work, a total of 31 NPS, including 13 SCat, 4 synthetic cannabinoids, 3 phenylethylamines, 1 opioid, 1 piperazine derivative, 1 arylcyclohexylamine and 8 substances from other groups, were identified in 45 samples. As in the previous work, the samples were measured in the ATR unit, without any pre-treatment. In addition, the authors concluded that the developed analytical strategy, based on ATR-FTIR spectroscopy, offers a fast, easy and little costs alternative for the screening process of NPS in samples.

2.3.2. Chromatographic Techniques

2.3.2.1. Gas Chromatography coupled to Mass Spectrometry (GC-MS)

Currently, GC-MS constitutes one of the most versatile analytical techniques, finding wide application in forensic analysis. It has been considered the "gold standard" in forensic trace evidence analysis because of its ability to separate, identify and quantify components in complex mixtures [377]. In drug testing, GC-MS is employed to establish the identity of unknown drugs. It has been routinely used to make the final, confirmatory identification of a wide range of drugs including amphetamines, barbiturate, cannabis, codeine, hashish, heroin, methadone, morphine, opiates, psilocin, and steroids [378].

The basic operating principle of GC involves volatilization of the sample in a heated inlet port (injector) of the gas chromatograph, followed by separation of the components of the sample using a column coated with a solid or liquid stationary phase [379]. An important aspect of GC is the use of a carrier gas as mobile phase to transfer the sample from the injector to the column, and finally to the detector [379]. Separation of the analytes is determined by the distribution of each component between the carrier gas and the stationary phase [288, 379]. Thus, the analytes that have greater affinity for the stationary phase spend more time retained in the chromatographic column and, consequently, take longer to reach the detector, than those with a lower affinity [380].

A typical gas chromatograph comprises a gas supply system, an injector, a chromatographic column placed in a heating oven, a detector and a data acquisition and processing system [287]. Figure 28 shows a schematic diagram of the components of a typical gas chromatograph.

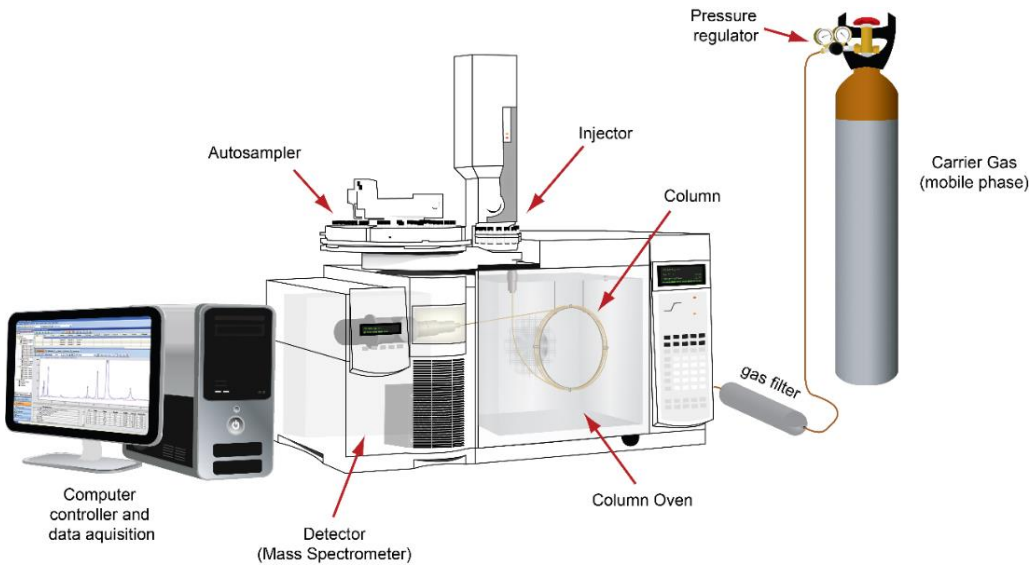

Figure 28. Basic gas chromatograph scheme and its main components (adapted from Aguiar [381]).

In general, the carrier gas for GC should be an inert gas that does not react with the sample components. Commonly, helium, nitrogen or hydrogen are used as the carrier gas, however, the choice of the gas is often dependent upon the type of detector which is used [287]. The gas flow conditions at the injector inlet are controlled by pressure regulators and gas metering valves [382].

The injector contains a heated chamber containing a glass liner into which the sample is injected through the septum (Figure 29). Frequently, the injector temperature is high in order to vaporize all components of the sample, which are carried by the carrier gas directly to the chromatographic column where they are separated [287].

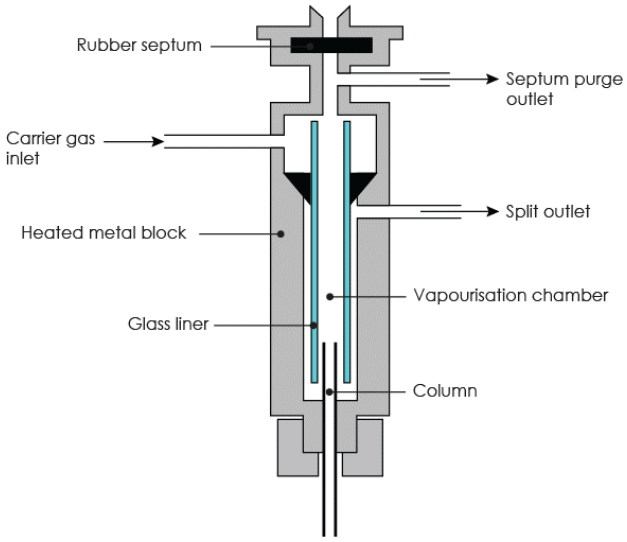

Figure 29. Schematic diagram of an injector (adapted from Dawling et al. [380]).

In GC there are two general types of columns: packed columns, in which the stationary phase is packed into the cavity of the column and capillary columns, where the stationary phase coats the inner surface of the column. Depending on the state of the stationary phase, GC can be classified in gas-liquid chromatography (GLC), where the stationary phase is a liquid, and gas-solid chromatography (GSC), that uses a solid as stationary phase. In general, solid stationary phases are less versatile and less used than liquid stationary phases [287]. In addition, the mechanisms of analyte retention in the column are different. In GLC, the analyte is partitioned between the gaseous mobile phase and the liquid stationary phase, while in GSC, the retention of analytes is the consequence of its physical adsorption onto a solid stationary phase [383]. Table 7 shows the main differences between packed and capillary columns.

Table 7. Main differences between packed and capillary columns (adapted from Pinto [287]).

Packed Column	Capillary Column
A column that contains a fully-packed stationary phase made up of fine particles	Stationary phase is coated on the inner wall of the column
Applicable for both GSC and GLC	Applicable only for GLC
Require large amount of sample	Requires only a small amount of sample
Have high pressures inside the column	Have less pressure inside the column
Short length (1.5 - 10 m)	Long length (15 - 100 m)
Internal diameter can be several millimeters (2 - 4 mm)	Internal diameter of a few tenths of a millimeter (0.1 - 0.7 mm)
Efficiency is low	Efficiency is high
Give comparatively a poor resolution	Give a higher resolution
Less expensive	More expensive

The number and variety of columns and stationary phases for GC currently available on the market is enormous, and it is even possible to find columns and stationary phases developed for specific applications [287]. Figure 30 shows some of the most common GC column stationary-phase chemistries.

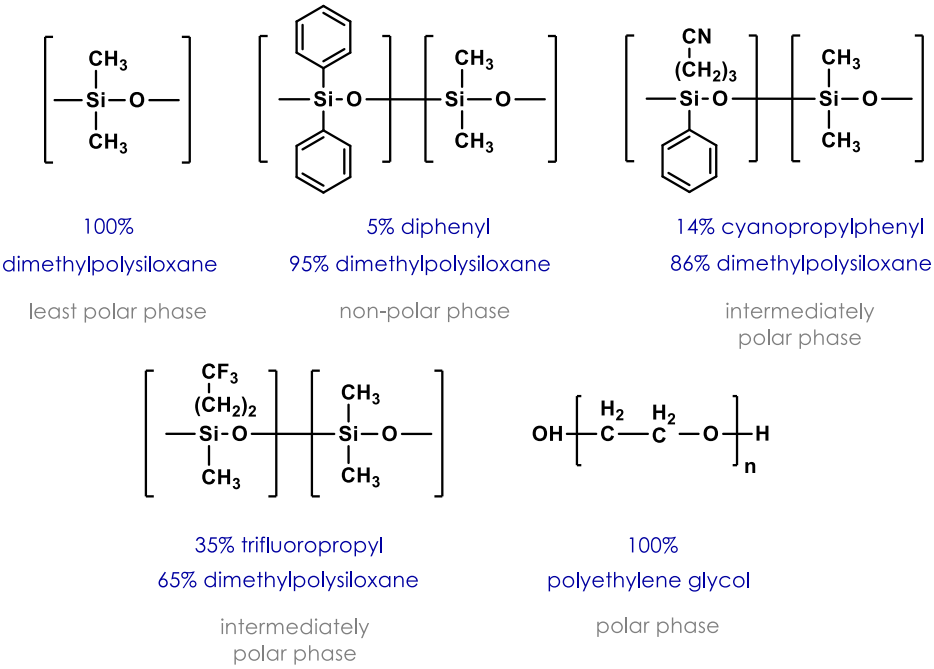

Figure 30. Chemical structure of some of the most common stationary phases available for GC.

Temperature is a very important parameter that influences chromatographic separation. For this reason, the GC column is located inside a temperature-controlled oven that can be operated either at constant temperature (isothermal) or using a series of temperature

holds and ramps (temperature programming or gradient elution). This allows the separation of individual sample components to be controlled and optimized.

The final part of a gas chromatograph is the detector. This is probably the most expensive and sophisticated component of the chromatographic system that continuously measures some physical or chemical property of the sample, and sends a recording signal, usually directly proportional to the concentration of the component in the sample [288]. Among the most common detectors, we can highlight the flame ionization detector (FID), thermal conductivity detector (TCD), electron capture detector (ECD), nitrogen-phosphorus detector (NPD) also known as thermionic specific detector (TSD), and MS detector [288].

MS is probably the most used detector in confirmatory toxicological analysis, given the low detection limit, the high discriminatory power of the technique and the availability of mass spectral libraries, which increases the confidence in identification when analysing complex samples [288]. The basic function of a mass spectrometer is to generate ions from the sample under investigation, separate these ions according to their mass-to-charge ratio (m/z) and to detect them qualitatively and quantitatively by their respective m/z and abundance. Despite the wide variety of mass spectrometers currently available on the market, with specific features and designs, all they have three fundamental components: an ion source, a mass analyser, and a detector. Figure 31 shows a schematic overview of a mass spectrometer.

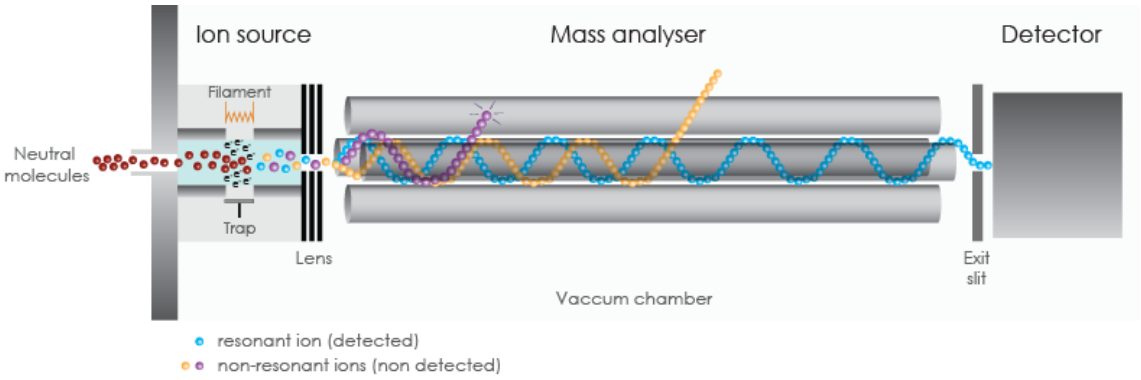

Figure 31. Schematic diagram of a mass spectrometer (adapted from Neves and Freitas [382]).

The ion source is intended to create electrically charged particles (“ions”) from the molecules in the sample. Electron ionization (EI), also known as electron impact ionization, is one of the most common ionization methods to convert neutral molecules in the gas phase to ionized molecules [384]. Ionization is induced through the interaction of the gas-phase sample molecules with high-energy electrons emitted from a resistively heated filament [385]. Typically, these electrons are accelerated by a potential of around 70 eV when collision with sample molecules occurs [382]. In this process, an electron from the analyte is removed during the

collision process to convert the molecule to a positive ion with an odd number of electrons (Equation 2). This first formed ion is termed the molecular ion and has a mass nominally equivalent to the molecular mass of the analyte [385].

$$M + e^- \longrightarrow M^{+\cdot} + 2e^- \quad (2)$$

where M is the analyte molecule being ionized, e^- is the electron and $M^{+\cdot}$ is the resulting molecular ion.

Following ionization, the excess energy transferred causes fragmentation of the molecular ion, yielding a series of fragment ions that are unique to that molecule under those ionization conditions [385]. Once formed, the ions are electrostatically directed into a mass analyser where they are separated according to m/z. There are many different kinds of mass analysers, currently available, that can be used for the separation of ions in a mass spectrometer. Quadrupole mass analyser is probably the most used. It is constituted of four parallel cylindrical metal rods (electrodes with a hyperboloidal interior surface) inside a vacuum chamber, positioned equidistant from the centre axis. The rods are charged by direct current (DC) and radiofrequency (RF) voltages, with the opposite pairs of rods carrying like charges. Oscillating electrical fields are used to selectively stabilize or destabilize ions, as they pass through an RF quadrupole field. Only ions with a selected m/z value are able to achieve a stable trajectory, allowing them to reach the detector. Ions with different m/z values have an unstable trajectory and consequently collide with the rods, or are expelled from the analyser (Figure 31) [386].

Detecting ions in GC-MS is mostly performed using an electron multiplier. The operation of electron multipliers is fundamentally based on the concepts of "dynodes" and "secondary emission". A "dynode" is essentially an electrode in a vacuum that emits electrons when an ion or electron with sufficient kinetic energy hits it. This process of emitting electrons is called "secondary emission" [387]. Basically, electron multipliers link a series of dynodes so that the secondary emission happens repeatedly, amplifying the number of electrons exponentially at each step along the way, and in the end, it will provide enough signal to be detected [387]. The amplified signal is then sent to a computer for processing.

2.3.2.2. High Performance Liquid Chromatography (HPLC)

HPLC is one of the separation techniques most frequently used in forensic toxicology. It is an advance form of LC used in separating complex mixtures of molecules. Like all chromatographic techniques, HPLC is based on selective distribution of the analyte molecules between two different phases: a liquid mobile phase and a stationary phase, made up of small particles with a large surface area packed inside a column [287]. The samples are dissolved in a

suitable solvent and analysed in solution which is then introduced into the chromatographic system and dragged by the mobile phase under high pressure along the stationary phase [287]. As the mobile phase advances through the stationary phase, the sample components are separated according to differences in affinity for each phase (Figure 32). The wide variety of combinations between mobile and stationary phases makes LC an extremely versatile technique.

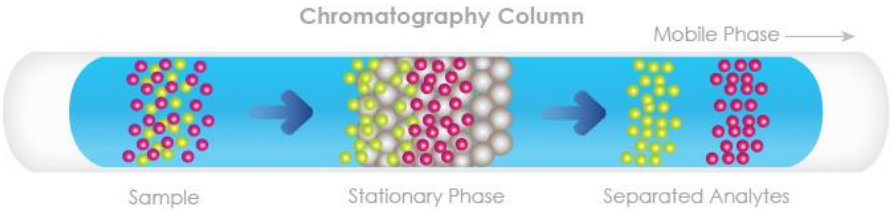

Figure 32. Schematic diagram of chromatographic separation based on the differential migration of the constituents of a sample (adapted from Gonçalves [305]).

There are several mechanisms that can influence chromatographic separation. Depending on the type of stationary phase used, separations are achieved by partition, adsorption, exclusion, or ion-exchange processes. Table 8 presents the main characteristics of each separation mechanisms.

Table 8. Main mechanisms of separation by liquid chromatography (adapted from Pinto [287]).

Separation mechanisms	Description
Adsorption	In adsorption chromatography the stationary phase is an adsorbent and the separation is based on repeated adsorption/desorption processes.
Partition	In partition chromatography, the stationary phase is a liquid that coats small diameter silica particles, and the separation depends essentially on the differential solubility of the analytes in the stationary phase and mobile phase. This type of chromatography is based on the principle of "like dissolves like" and there are two main types of partition chromatography: normal phase chromatography and reversed phase chromatography. The main difference between them is that normal phase chromatography has a very polar stationary phase and a non-polar mobile phase whereas reverse phase chromatography has a non-polar stationary phase and a polar mobile phase.
Ion-exchange	In ion exchanged chromatography, retention is based on the attraction between the solute ions and charged sites bound to stationary phase. Columns used for ion exchange are characterized by the presence of charged groups covalently attached to the stationary phase. Anionic exchangers contain bound positive groups, whereas cation exchangers contain bound negative groups. This technique is used exclusively with ionic or ionizable samples.

Table 8. (Continuation)

Separation mechanisms	Description
Exclusion	In exclusion chromatography, the stationary phase is made up of a material with pores of a precise size and separation occurs according to the molecular size of the analytes: larger molecules do not fit in the pores and are eluted first, and the molecules smaller ones penetrate the pores and are eluted later.

HPLC is a form of LC that requires an appropriated equipment constituted of various of components, including the solvent reservoir, a high-pressure pump, an injector system, a column, a detector, and a workstation (Figure 33). The reservoir contains the solvent that constitutes the mobile phase. A pump is used to generate a specified flow of the mobile phase which supplies the LC system. Although manual injection of samples is still possible, most HPLCs are now fully automated. The injector, or auto sampler, introduces a precise volume of the liquid sample into the flow stream of the mobile phase that carries it into the HPLC column, where separation takes place. The column can be placed inside an oven, allowing the use of temperature to optimize chromatographic separation [287].

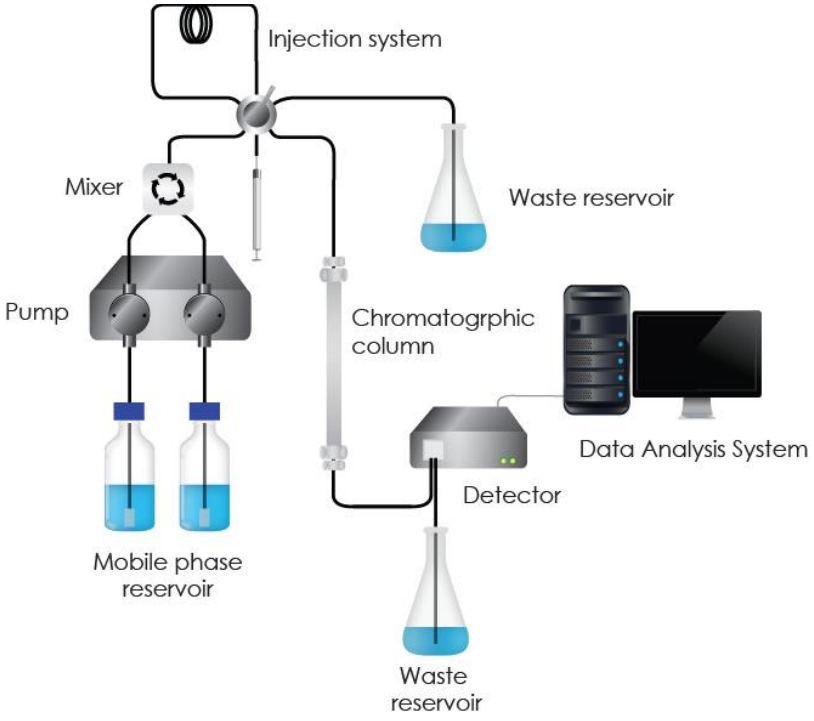

Figure 33. Schematic diagram of a typical HPLC (adapted from Gonçalves [305]).

At the end of the chromatographic column, there is a detector which provides a quantitative measurement of the components of the sample as they elute. The main characteristics desired when choosing a detector are high sensitivity and selectivity, low

detection limit and stability against changes in mobile phase composition and temperature [388].

Currently, LC in combination with MS detection is considered by many laboratories the method of choice for the determination of drugs in biological samples. It is an exceptional technique to identify unknown components in a sample, or confirming their presence, and its major advantage is its high sensitivity. However, despite this advantages MS is a very expensive equipment and generally has a higher operating cost, which limits the access of this analytical technique to many laboratories.

As an alternative to mass spectrometers, absorbance detectors are much less expensive and relatively simple to use. Ultraviolet/visible spectrophotometric detectors (UV-VIS) are one of the most commonly used detectors for LC and operate by passing visible and UV light through a sample in a flow cell. The amount of light absorbed provides information on the properties of the sample of interest. UV-VIS detectors are considered non-destructive chromatography detectors and are selective for molecules that have chromophores.

Currently, there are three types of equipment available that work according to this principle, namely, fixed wavelength UV-VIS detector, variable wavelength detector (VWD) and photodiode array detector (PDA), also known as diode array detector (DAD) [388]. In a fixed wavelength detector, as its name implies, absorbance of only one given wavelength is monitored by the system. It is the simplest and cheapest type of detector but is limited in terms of flexibility and the type of compounds that can be used to monitor.

Like the fixed wavelength detector, the VWD also monitors a single wavelength. However, in contrast to the first one, where changing the detection wavelength requires changing the lamp and associated filters, the VWD uses a monochromator (slits and a grating) to select one wavelength to pass through the flow cell [389]. This has a great advantage in that the optimal detection wavelength can be selected for each analyte during the course of the chromatographic run, thus improving the sensitivity of the detector [389].

PDA detector uses the same principles of operation as a VWD. However, the array of diodes enables simultaneous acquisition across a range of wavelengths, rather than just a single one. This offers the benefit of obtaining full spectral information of each analyte which can be of use quantitatively to determine whether a chromatographic peak is derived from the analyte or not. Figure 34 shows a schematic diagram of a typical PDA detector.

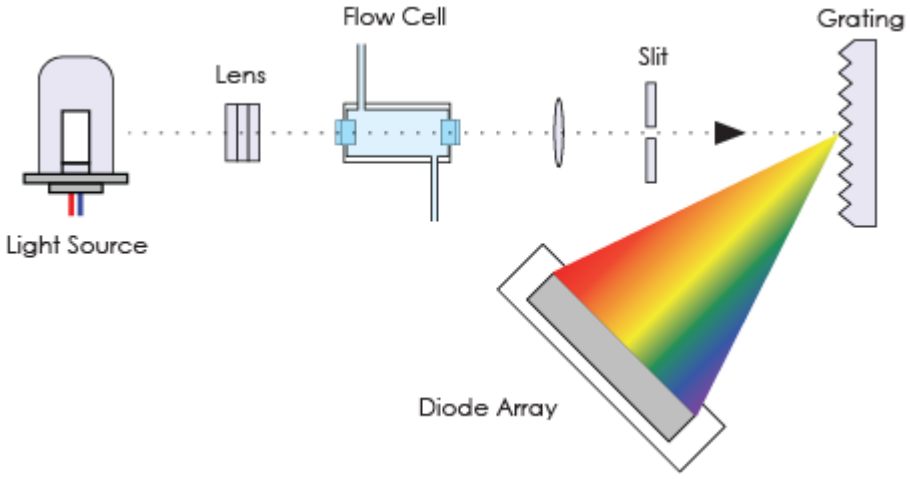

Figure 34. Schematic diagram of a PDA detector (adapted from LCGC [390]).

The PDA detector continuously passes the entire spectral range of interest through the flow cell. The lighting exiting from the flow cell is then spread out by diffraction grating, which impinges on a linear array of photodiodes [389]. This allows the spectra to be taken continuously. The output of a PDA detector is a three-dimensional chromatogram with retention time in one axis, absorbance signal intensity on a second axis, and wavelength on the third axis [389]. PDA detectors are extensively used in several areas and when coupled to MS detectors, represent one of the most powerful methods of drug analysis [389].

2.3.2.3. Synthetic Cathinone Analysis using Chromatographic Techniques

The versatility and resolving power of chromatographic systems, has made chromatography an excellent analytical technique for forensic drug analysis. Currently, this separation technique, in its most diverse configurations, has been widely used for SCat analysis, either in seized materials [391-393] or in biological specimens [213, 265, 272, 282].

GC-MS is currently a primary means for qualitative seized-drug analysis, and one of the most common for SCat investigation [394]. Typically, GC-MS analysis of SCat mostly involves the usage of derivatizing agents, since these compounds suffer partial thermal degradation during chromatographic analysis [395, 396]. Generally, derivatization involves the chemical modification of functional groups, replacing polar groups of the molecule with less polar ones, forming derivatives suitable for instrumental analysis [288]. This procedure is particularly useful to improve the volatility, adsorption and stability characteristics of the analyte, as well as the resolution and symmetry of the chromatographic peaks [288]. In addition, this procedure is also used to reduce detection limits, to increase the precision and selectivity of the method, to facilitate the separation of enantiomers and to confirm the identity of an analyte in the MS detector [288]. Araújo et al. [17] during the chemical analysis of 'legal high' packages containing

SCat used the derivatization to confirm the identities of the compounds. In a first step, the methanolic extracts of each sample were directly injected into the GC-MS system, where it was possible to identify several SCat. Then, in order to confirm the identity of the compounds, the methanolic extracts were derivatized with trifluoroacetic anhydride (TFAA) and analysed. According to the results, the authors concluded that the derivatization is an effective methodology to confirm the identities of SCat, allowing to obtain more specific structural information about these compounds. In addition, the derivatization allowed to obtain cleaner chromatograms and better separations with increased resolution and response [17].

More recently, some studies have compared the efficacy of several derivatizing agents for SCat analysis. Alsenedi and Morrison [397] compared the efficacy of six derivatizing agents for the determination of 9 SCat using GC-MS. In this study, the derivatizing agents, namely propionic anhydride (PPA), acetic anhydride (AA), pentafluoropropionic anhydride (PFPA), heptafluorobutyric anhydride (HFBA), chlorodifluoroacetic anhydride (CLF_2AA) and TFAA were optimized for incubation time and temperature. The peak area values of the target ions of SCat were more evident using reaction conditions of 25 minutes at 70°C, with the exception of PFPA and TFAA derivatives which showed better responses at room temperature [397]. According to the authors, all reagents proved to be suitable for SCat analysis with precision and accuracy values below 20% under the optimized conditions. However, PFPA, HFBA and TFAA gave the best results. Mohamed and Bakdash [398] also compare three derivatization reagents, namely HFBA, PFPA, and TFAA, for the determination of 10 amphetamines and SCat in oral fluid by GC-MS. The three methods have suitable linearity, sensitivity, accuracy, and precision. However, based on sensitivity, PFPA was the best derivatizing agent for the target compounds.

Although derivatization is a common approach to improve thermal stability and mass spectral properties of SCat, it is also pertinent the development of methodologies without derivatization since they provide more comprehensive and faster results [272].

LC-MS based techniques, such as LC-MS/MS or LC-QTOF-MS may be highly advantageous and provide much needed sensitivity for the toxicological detection of SCat in biological evidence. In fact, LC-MS systems are ideal for applications involving drugs, which generally are polar and nonvolatile molecules [399]. In addition, separation and ion generation can be accomplished without derivatizing the analytes [399]. Most SCat analysis by LC-MS are performed in tandem MS mode with electrospray ionization (ESI) source in positive ion mode [112, 400]. The use of two or more mass analysers in series, with a collision cell to promote ion fragmentations between them, allows additional 'purification' by selecting specific precursor molecular ions from a mixture for further analysis and characterization [401].

Olesti et al. [267], used an UHPLC-MS/MS system for the quantification of 14 common NPS, including 5 SCat, in urine samples for doping control analysis. In this study, the separation was achieved at 55°C using an Acquity UPLC BEH C_{18} column (2.1 mm × 100 mm, 1.7 µm) and the mobile phase composed by 1 mM ammonium formate with FA (0.01% v/v) in MeOH (phase A) and 1 mM ammonium formate with FA (0.01% v/v) in water (phase B). The flow rate was kept at 0.3 mL min^{-1} and the total run time was 10 min. The triple quadrupole mass spectrometer was equipped with an ESI source operated in positive ionization mode. Analytes were determined by a selected reaction monitoring (SRM) method by acquiring two transitions for each compound, in order to facilitate the confirmation of the identity [267]. Low limits of detection (LOD) were achieved with the developed method, with values ranging from 0.3 to 0.5 ng mL^{-1}. The validated method was then applied to samples collected from volunteers after the self-administration of methylone, mephedrone, 6-(2-aminopropyl)benzofuran (6-APB), and 2,5-dimetoxy-4-ethylphenetylamine (2C-E).

A less frequently employed detection system for SCat analysis is the UV-Vis detectors. With this detection system, one can record the UV-Vis spectra of the investigated compounds and establish the absorption wavelength characteristics of each SCat [112]. These data can be added to a library, thus providing physicochemical characteristics of individual cathinone species, that can be used later in quantitative analyses [112, 400]. Fernández et al. [274], successfully used an UHPLC-PDA system for quantitative determination of 3 SCat and 7 conventional drugs of abuse and metabolites. The drugs separation was achieved using an ACQUITY BEH Shield RP18 column (2.1 mm × 100 mm, 1.7 µm) and the mobile phase composed of 0.1% aqueous FA and 0.1% FA in ACN. During separation, the column oven temperature was set at 55 °C, and the flow rate was kept at 0.4 mL min^{-1}. The total run time was 4 min. The PDA allowed the wavelength range from 200 to 400 nm to be scanned to obtain three-dimensional (wavelength x absorbance x time) chromatograms. Low LOD and limits of quantification (LOQ) was achieved with this method, with values ranged from 5 to 25 ng mL^{-1} for LOD and 10 to 50 ng mL^{-1} for LOQ. In addition, the method was successfully applied for primary screening of 24 real plasma samples obtained from intoxications related to drugs of abuse.

2.3.3. Nuclear Magnetic Resonance (NMR)

NMR spectroscopy is an extremely powerful analytical tool that is routinely used to identify and structurally elucidate molecules of interest. The principle behind NMR is based on the absorption of radio frequencies by certain nuclei of a molecule when subjected to a strong magnetic field. To explain the properties of certain nuclei, it is necessary to understand that they are positively charged and spin on an axis, creating a tiny magnetic field.

The nuclear spin is defined by a quantic number (*I*), which varies depending on the considered isotope [402]. The rules for determining nuclear spin may be related to the nucleon composition of a nucleus. If the nuclei containing even numbers of both protons and neutrons, then the nucleus has no overall spin (*I* = 0). If the number of protons and the number of neutrons are both odd, then the nucleus has an integer spin (*I* = 1, 2, 3, …). If the number of neutrons plus the number of protons is an odd number, then the nucleus has a half-integer spin (*I* = $^{1}/_{2}$, $^{3}/_{2}$, $^{5}/_{2}$, …). Table 9 shows the nuclear spin quantum number of some of the most common nuclei.

Table 9. Nuclear spin quantum number (*I*) of some common atomic nuclei (adapted from McGregor [402]).

I	Nucleus
0	^{12}C, ^{16}O
$^{1}/_{2}$	^{1}H, ^{13}C, ^{15}N, ^{19}F, ^{29}Si, ^{31}P
1	^{2}H, ^{14}N
$^{3}/_{2}$	^{11}B, ^{23}Na, ^{35}Cl
$^{5}/_{2}$	^{17}O
3	^{10}B

Not all atomic nuclei are suitable for NMR analysis. Only those with $I \neq 0$, such as ^{1}H, ^{13}C, ^{15}N, ^{19}F, among others are detectable by NMR spectroscopy. These NMR active nuclei have magnetic moments and behave as tiny magnets, which can interact with an external magnetic field. On the other hand, atomic nuclei such as ^{12}C or even ^{16}O, have spins paired against each other, such that the nucleus has no overall spin (*I* = 0), and in these cases, they are not detected by NMR spectroscopy [403]. In the absence of an external magnetic field the direction of the spin of the nuclei will be randomly oriented. However, when these nuclei are place in an external magnetic field, the nuclear spins will adopt specific orientations (Figure 35).

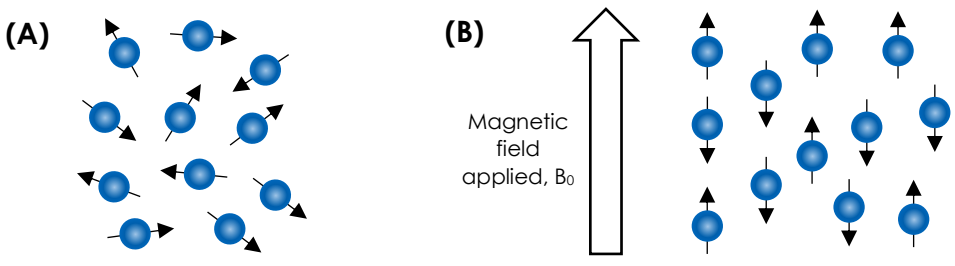

Figure 35. Nuclear spin behavior (A) in absence of an external magnetic field and (B) under the influence of an external magnetic field (B_0).

According to quantum mechanics a nucleus of spin *I* will have 2*I* + 1 possible orientations [402]. In this sense, atoms that possess a spin $^{1}/_{2}$ nucleus, as in the case of ^{1}H and ^{13}C, which are the most commonly used NMR nuclei, are able to adopt two different orientations when they align to an external magnetic field [402]. One orientation corresponds to the lowest energy level of the nucleus called α-spin state (parallel to the external magnetic field), and the other one is associated to the highest energy level of the nucleus called β-spin state (antiparallel to the external magnetic field) [404]. The application of radio waves at just the right frequency will cause these nuclei to absorb energy and "flip" from the α to the β spin state (Figure 36) [404]. When the spin returns to its base level, energy is emitted at the same frequency. The signal corresponding to this transfer is then measured and processed to produce an NMR spectrum for the nucleus concerned [404].

It is important to note that the energy difference between the two spin states (α and β spin state) depends on the strength of the magnetic field [404]. In addition, the greater the operating frequency and the stronger the magnet the better is the resolution of the NMR spectrum [402].

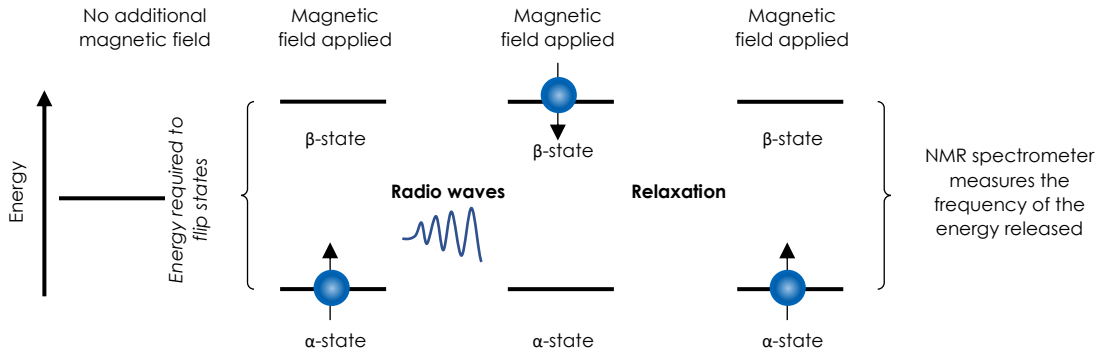

Figure 36. Schematic diagram of the different spin states of a nucleus in a magnetic field (adapted from Course Hero [405]).

Generically, an NMR equipment consists of the association of a magnet, capable of creating a homogeneous field, and a radiofrequency source that emits radiation through a spiral circuit that surrounds the sample (Figure 37) [287]. The static magnetic field is produced by a liquid helium cooled super conducting magnet consisting of complex twined coils [406]. These coils induce a homogenous magnetic field, which is required during NMR analysis. Deviation from this ideal can introduce various line shape distortions, compromising both sensitivity and resolution. When applying short pulsed electromagnetic radiation (radio frequency in this case), the nuclei absorb energy, and the measurement is made during the subsequent relaxation [406].

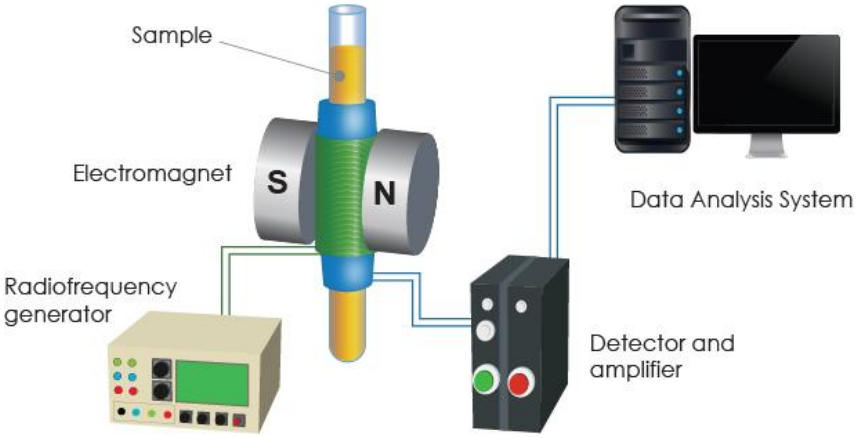

Figure 37. Schematic diagram of NMR setup (adapted from Pinto [287]).

The NMR spectra are unique to each kind of molecule and for this reason, NMR spectroscopy analysis is commonly used to confirm the identity of an organic chemical or even organic mixtures [407]. Different functional groups are distinguishable from one another and identical functional groups with differing neighbouring substituents give distinguishable signals, which makes this technique particularly useful to identify structural isomers [407]. Moreover, this method not only makes it possible to definitively identify a compound, but also to confirm the absence of other organic compounds and to determine the purity of a product [408]. Another major advantage is that NMR can quickly and accurately provide a wealth of structural information about compounds without destroying the properties of the compound [409]. As NMR is a non-destructive technique, the same sample can be analysed repeatedly [410]. For these reasons, NMR has been widely used for forensic purposes, especially as a tool for unambiguous structure determination of unknown NPS.

Part II

Justification and aims of the study

1. General Fundamentals

Drug use has been one of the most serious social and public health problems worldwide. The continued diffusion, diversification and use of NPS remain a major challenge faced by healthcare professionals, law enforcement and judicial authorities as well as drug testing and toxicology laboratories. Despite the legislative efforts to control these substances, new derivatives continue to emerge on the drugs market, with more than 1120 NPS having been reported to the United Nations Office on Drugs and Crime (UNODC) [19].

Monitoring NPS use is an arduous task and different sources of information are required to gain greater insight of their prevalence and diffusion [411]. The characterization of NPS in commercially available products and drug seizures is an important source of information [411]. Since reference standards are often unavailable, a combination of several techniques, including NMR, FTIR, GC-MS, LC-MS, among other techniques, is normally applied for unambiguous confirmation of the identity of the substances [411]. Although, there is a correlation between the identification of NPS in seized products and the prevalence of use, the identification of new substances in seized products mainly provides information about the NPS available on the drug market [411]. In this sense, the analysis of biological samples can be considered the frontline in the detection of NPS consumption. However, due to the complexity of the samples and the low concentrations of analytes normally found, different analytical strategies are required to deal with this type of samples [411]. Currently, microextraction techniques offers several advantages over traditional sample preparation techniques. The use of small sample volumes, assumes particular relevance in forensic toxicology, since sample availability is often limited and several exams need to be performed on the same sample [222].

In addition to monitoring the use of NPS, it is important to assess the toxicity of these substances. Since the consumption of NPS is relatively recent, there are still not many studies regarding the toxicity of these substances. Cytotoxicity assays are a quick way to assess the effects of a particular chemical compound on a given human cell line. These studies are essential to evaluate the toxicity of a compound when it is intended for human use, for example, when new pharmaceutical compounds appear, their cytotoxic effects must be evaluated before they are placed on the market. The same happens with NPS, it is important to know the cytotoxic effects of these compounds that are available in different forms and without knowledge of their purity, or the true content of what is marketed [412].

1.1. General Objectives and Specific Objectives

In view of the foregoing, the main objectives of this study were the chemical characterization of seized products suspected to contain SCat, the second largest group of NSP currently seized in Portugal, as well as the development of an analytical methodology based on µSPEed®/UHPLC-PDA, for determination of SCat in urine samples. Due to the scarcity of cytotoxicity studies relating to NPS, the third major objective of this study was to evaluate the cytotoxicity of SCat found in seized products in HepG2 cell line. Figure 38 shows a general overview of the aims of this study.

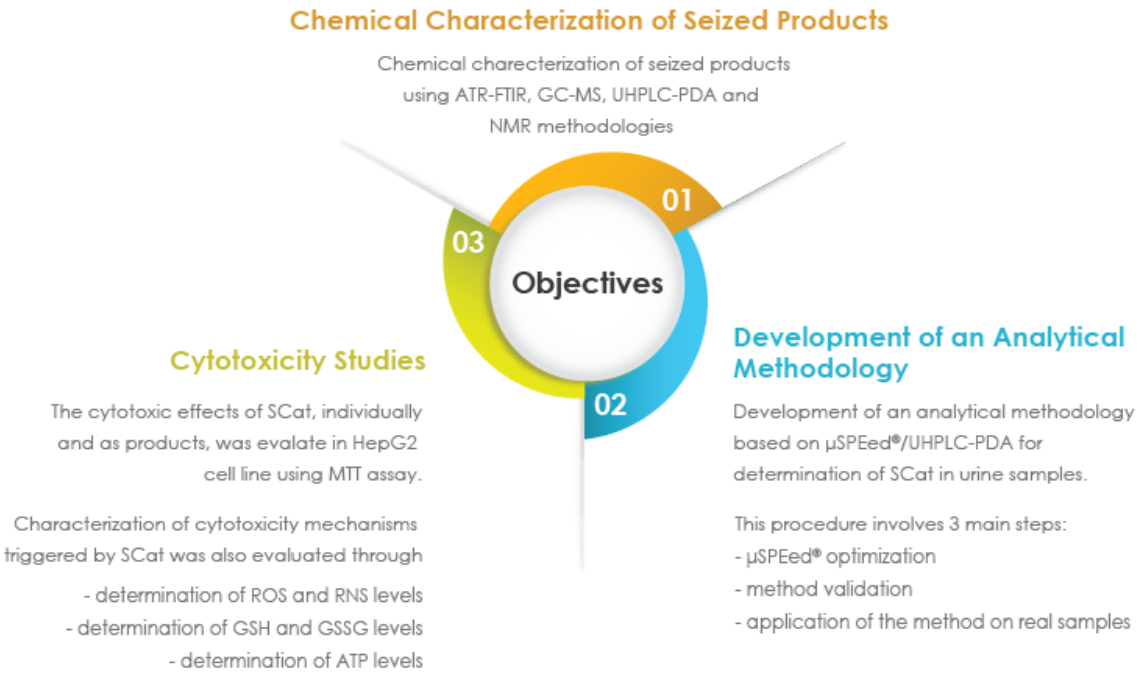

Figure 38. General overview of the aims of this study. Abbreviations: ATP - adenosine triphosphate, GSH - reduced glutathione, GSSG - oxidized glutathione, MTT - 3-[4,5-dimethylthiazol-2-yl]-2,5 diphenyl tetrazolium bromide, ROS - reactive oxygen species, RNS - reactive nitrogen species.

The first part of this work consisted in the chemical analysis of seized products, suspected to contain SCat, as well as potential adulterants that can also have harmful effects, using highly powerful methodologies, such as ATR-FTIR, GC-MS, UHPLC-PDA and NMR. The purity of the products was assessed calculating the mass fraction (% m/m) of each compound in the seized products.

Once the characterization of the products was carried out, the second part aimed to develop and validate a new analytical methodology, based on µSPEed® followed by UHPLC-PDA analysis, for detection and quantification of SCat in urine samples. For this purpose, several

experimental parameters were evaluated, in order to obtain the best experimental conditions for the simultaneous identification and quantification of all substances under study. In this context, the studies conducted included:

- Evaluation of the best separation conditions by UHPLC-PDA, in terms of chromatographic column selection, column temperature, mobile phase and flow rate;
- Evaluation of the different parameters that influence the extraction of SCat by µSPEed®, namely, the nature of the sorbent, the sample volume, the number of extraction cycles, the pH of the sample, the washing solution, the elution solvent, and the elution volume;
- Validation of the µSPEed®/UHPLC-PDA methodology, in terms of selectivity, linearity, LOD and LOQ, extraction efficiency, accuracy, intra- and inter-day precision, matrix effect and stability;
- Application of the developed methodology to real samples from synthetic drug users.

The last part of the present work consisted in the evaluation of cytotoxic potential of SCat, individually and as products, in HepG2 cells. The elucidation of the cellular mechanisms underlying the observed hepatotoxicity, particularly those involved in oxidative stress, was also evaluated. From the experimental point of view, several tests were carried out, in order to access the toxicity of these substances. These studies included:

- Evaluation of the cytotoxicity of SCat and seized products using the MTT assay;
- Evaluation of the oxidative stress through the determination of the intracellular formation of ROS and RNS and the levels of the reduce (GSH) and oxidized (GSSG) glutathione levels;
- Determination of the intracellular levels of adenosine triphosphate (ATP) for assessing the energetic homeostasis of the cells after SCat exposure.

Part III

Chemical Analysis and *in vitro* cytotoxicity studies

Chapter 1

Chemical Characterization of Synthetic Cathinones Found in Seized Materials

1. Introduction

The innovation of the illicit drugs market requires the rapid identification of new substances that can be a risk to public health, in order to reduce its use damage. Among these substances, SCat have, in recent years, received particular attention due to several intoxication events and deaths associated to its consumption [413, 414].

In fact, many efforts and some progresses have been made to control the sale and distribution of these substances, and from temporary banning orders, to consumer legislation, governments are working in order to avoid the free sale and distribution of these products [415]. In Portugal, the commercialization of SCat has been outlawed since 2013, after the introduction of the Decree-Law no. 54/2013, of 17 April, which prohibits the production, export, advertisement, distribution and sale of 159 NPS, including 34 SCat [111].

Despite these measures that have helped to reduce the supply of NPS, by closing down the so-called 'smartshops', SCat continue to appear in the drug market and its abuse still represents a public health issue.

The ever-evolving nature of these substances has created many analytical challenges for forensic laboratories, due to the large number of potential compounds to be investigated, and for many of which there is no available reference standards [416, 417].

Although it is possible to routinely analyse the already identified substances using appropriate instrumentation, such as LC-MS and GC-MS, the identification of unknown substances generally requires a structural elucidation before being included in routine methods [418]. Typically, this process requires the use of NMR spectroscopy to identify the chemical structure of the compound. However, some known substances, such as the SCat, may offer analytical challenges, since many of them exhibit structural similarities (e.g. positional isomerism of a ring substituent), which make the analysis particularly difficult. In such situations, the selection of analytical techniques can be challenging, since each technique has its own advantages, that may be more or less suitable, depending on the situations. This highlight the importance of using complementary analytical techniques to confirm the identity of a substance [418].

In this context, the present work describes and discusses the analytical assays performed to identify the components of 14 products seized in Portugal, suspected to contain SCat. Compounds structure elucidation was carried out by ATR-FTIR, GC-MS, UHPLC-PDA and NMR spectroscopy.

1.1. Materials and Methods

1.1.1. Reagents and Chemicals

All used chemicals were of analytical grade. MeOH was obtained from Fisher Scientific (Loughborough, UK), while ethyl acetate was provided by Riedel-de Haën (Seelze, Germany). TFAA (≥ 99.0%), maleic acid (99.0%), trifluoroacetic acid (TFA, 99.0%), methylamine hydrochloride (≥ 98.0%), cellulose microcrystalline (20 μm) and deuterium oxide (99.9%) were obtained from Sigma-Aldrich (St. Louis, MO, USA), while pure caffeine was purchased from Merck (Darmstadt, Germany). The reference SCat (methylone, pentedrone, buphedrone, *N*-ethylcathinone, methedrone, MPHP and α-PHP) were kindly provided by the Forensic Science Laboratory of Portuguese Criminal Police (LPC-PJ).

1.1.2. Seized Samples

Fourteen seized products suspected to contain illicit substances were provided by the LPC-PJ, under a special authorization. The products were presented in different forms, including powders, crystals and tablets, packed in small plastic bags with striking designs or, occasionally, in see-through plastic bags. Some of the products were labelled as "plant feeders" with the indication "not for human consumption". Table 10 shows the list of provided substances, with the respective information about their composition indicated on the product label.

Table 10. List of provided samples with the information about their chemical composition indicated on the product label.

Sample Number	Product Name	Description	Appearance	Quantity (g)	Composition indicated on the label
1	Unknown	n.a.[1]	White powder	1	n.a.
2	Flakka	n.a.	Brownish crystal	5	n.a.
3	Bloom	Plant feeder	White powder	1	94 % Ketones, 5 % caffeine, 1 % glucose
4	Bloom	Plant feeder	White powder	1	94 % Ketones, 5 % caffeine, 1 % glucose
5	Bloom	Plant feeder	White powder	1	94 % Ketones, 5 % caffeine, 1 % glucose
6	Bloom	Plant feeder	White powder	1	94 % Ketones, 5 % caffeine, 1 % glucose
7	Bloom	Plant feeder	White powder	1	94 % Ketones, 5 % caffeine, 1 % glucose
8	Charlie	Plant feeder	Light yellow powder	1	100 % Ketones
9	Bliss	Plant feeder	White powder	1	94 % Ketones, 5 % caffeine, 1 % glucose
10	Bliss	Plant feeder	White powder	1	94 % Ketones, 5 % caffeine, 1 % glucose
11	Bliss	Plant feeder	White tablets	5 tablets	Per Pill: 120 mg lactose, 20 mg magnesium stearate, 100 mg corn starch, 160 mg ketones, 50 mg calcium stearate, 4 mg E142, 6 mg E132, 20 mg E124
12	Blast	Plant feeder	White powder	1	89 % Ketones, 10 % caffeine, 1 % glucose
13	Blast	Plant feeder	White powder	1	89 % Ketones, 10 % caffeine, 1 % glucose
14	Kick	Plant feeder	White powder	1	94 % Ketones, 5 % caffeine, 1 % glucose

Abbreviation: n.a. - not available.

1.1.3. Chemical Characterization of Seized Materials

1.1.3.1. ATR-FTIR Analysis

A PerkinElmer® Spectrum Two FTIR Spectrometer (Massachusetts, USA) equipped with a DuraSamplIR™ diamond ATR unit (Smiths Detection, London, UK) was used for IR spectroscopy analysis. Approximately 20 mg of powder sample was placed on the small ATR crystal area, and the IR spectra were collected in the range from 4000 to 600 cm^{-1}, with 32 scans at 4 cm^{-1} resolution. Spectra were obtained in triplicate, and a PerkinElmer Spectrum IR software, version 10.6.0, was used for processing and visualizing the spectra.

1.1.3.2. GC-MS Analysis

For GC-MS analysis, each sample was homogenized and dissolved in MeOH to a final concentration of 1 mg mL^{-1}. Before the GC-MS analysis, each solution was filtered through 0.22 µm polytetrafluoroethylene (PTFE) membrane filters (Millipore, Milford, MA, USA), and 2 µL of the sample was directly injected into the GC-MS.

Derivatization with TFAA was also performed, according to the method developed by Araújo, et al. [17]. Each sample was prepared to a final concentration of 100 µg mL^{-1} by dilution of the initial methanolic solution (1 mg mL^{-1}), and was evaporated to dryness under nitrogen flow. Then 100 µL of TFAA/ethyl acetate (1:1, v/v) was added to the dried residue, and the incubation was performed at 70°C, for 30 min. After cooling at room temperature, the solvent was evaporated to dryness, under a nitrogen stream, and the residues were reconstituted in 100 µL of ethyl acetate. A 2 µL aliquot of the resulting solution was injected into the GC-MS system.

GC-MS analysis was performed with an Agilent 6890N GC system (Palo Alto, CA, USA), equipped with a 5975 Mass Selective Detector (Agilent Technologies, Palo Alto, CA, USA).

The samples were performed using an Agilent J&W HP-5 capillary column (30 m × 0.32 mm ID, 0.25 µm film thickness), and helium (Air Liquid, Portugal) was used as the carrier gas, at a constant flow of 1.3 mL min^{-1}. The injections were performed in split mode, with a ratio of 40:1. The injector port was heated to 250°C and 2 µL of sample was injected in the GC system. The initial column temperature was set to 60°C for 4 min, followed by a temperature ramp of 15°C min^{-1} to 150°C held for 5 min and 20°C min^{-1} to 290°C held for 10 min. The mass spectrometer was operated in EI mode at 70 eV. For the MS system, the temperatures of the transfer line, quadrupole and ionization source were 250, 150 and 230 °C, respectively. The ionization was maintained off during the first 4 min, to avoid solvent overloading. The mass spectra were recorded in the range 40–500 m/z, and acquisition was made in Full Scan mode, with a scan rate of 6 scans/s. All mass spectra were compared with NIST 14 MS library and

SWGDRUG MS library version 3.4. The compounds identification was also performed comparing the GC retention times and mass spectra, with the available standards. The Kováts retention index (RI) was also determined through injection of a series of C7–C40 straightchain *n*-alkanes (concentration of 1000 µg mL^{-1} in *n*-hexane) and the values were compared with the values reported in the literature for similar chromatographic columns.

1.1.3.3. UHPLC-PDA Analysis

The UHPLC-PDA analysis were carried out on a Waters Ultra Performance Liquid Chromatographic Acquity system (UPLC, Acquity H-Class) (Milford, MA, USA), equipped with a quaternary solvent manager (QSM), a sample manager (SM), a column heater, a 2996 PDA detector, and a degassing system. The whole configuration was driven by Empower software v2.0 from Waters Corporation. Optimum separation was achieved with an Acquity UPLC™ strength silica HSS T3 analytical column (100 mm × 2.1 mm, 1.8 µm particle size), protected with an Acquity UPLC™ HSS T3 VanGuard™ Pre-column (Waters, Milford, MA, USA). Column temperature was maintained at 40°C, and a binary mobile phase composed of (A) water with 0.1% FA, and (B) MeOH were used for the separation of the analytes. The 12 min gradient started with 90% eluent A (0-4 min), then decreased to 85% A (5-6 min), 36 % (9 min), 10% (10-10.5 min), and finally increased to 90% (11-12 min). The system was re-equilibrated with the initial composition for 3 min, prior to next injection. The flow rate was maintained at 350 µL min^{-1}, giving a maximum back pressure of 10.000 psi, which is within the skills of the UHPLC system. Two µL of methanolic solutions of each sample were directly injected into the Waters Acquity UPLC system. The identification of target analytes was based on the comparison of retention time and spectral characteristics with the chemical standards.

1.1.3.4. NMR Analysis

For NMR analysis, 10 mg of sample was dissolved in 500 µL of deuterium oxide (D_2O), containing maleic acid as the internal standard (5 mg mL^{-1}). The resulting mixture was transferred to a 5 mm NMR tube and the NMR spectra were acquired in a Brucker Avance II 400 MHz Spectrometer (Bruker BioSpin GmbH, Rheinstetten, Germany), operating at 400.13 MHz for ^{1}H NMR and 100.61 MHz for ^{13}C NMR. Chemical shifts (δ) were expressed as parts per million (ppm) and referenced to the signal of maleic acid (δH = 6.42, δC = 132.16). Coupling constants (*J*) were reported in units of Hertz (Hz). The structure's identification with the respective assignment of the carbon and proton signals was based on the analysis of NMR spectra obtained by 1D (^{1}H and ^{13}C) and 2D (COSY, HMBC and HSQC) techniques. For products 12 and 13, a ^{19}F

NMR spectrum (376.5 MHz) was also recorded, and the chemical shifts were referenced to the TFA resonance at -78.0 ppm.

For NMR purity assessment, the ^{1}H signal integration for each compound was calculated calibrating for 100 the area of maleic acid resonance peak. The purity of the products was assessed calculating the mass fraction (% *m/m*) of each compound in the seized products, using the following equation:

$$\%compound = \frac{I_X}{I_{IS}} \times \frac{N_{IS}}{N_X} \times \frac{M_X}{M_{IS}} \times \frac{m_{IS}}{m_{sample}} \times P_{IS} \quad (3)$$

where I_X and I_{IS} are the integrated area of the compound of interest (*X*) and the internal standard (*IS*), N_X and N_{IS} are the numbers of protons generating the selected signals for integration, M_X and M_{IS} are the molecular weights in g mol^{-1}, m_{sample} and m_{IS} are the masses of the sample and the internal standard, respectively, and P_{IS} is the purity of maleic acid.

1.2. Results and Discussion

The products identification containing NPS is a challenging task, as the present substances do not generally correspond to the label, and can contain a wide range of impurities and/or adulterants [419].

The products were presented in brightly coloured packaging or, occasionally, in see-through plastic bags with the trade name, the supposed composition, the product quantity along with the warning “not for human consumption”. Most products (85.7%) were in powder form, and only two products were presented in the crystal (product 2) and tablets (product 11) forms (Table 10). The predominant colour of the powders and tablets were white, whereas the crystal had a brownish colour. Regarding the composition indicated on the packaging, all had "ketones" in the list of ingredients, presumably indicative of the presence of SCat, except for products 1 and 2. In addition, most powder products also referred the presence of caffeine and glucose. The composition indicated on the packaging of the tablets was more elaborated, with the information of the active principle and of other excipients related to the production of the tablets.

1.2.1. ATR-FTIR Analysis

The IR spectra of all seized materials were consistent with the molecular structure of SCat (Figure 39). All spectra showed a prominent absorption band around 1700–1674 cm^{-1} that corresponded to the carbonyl group stretching (C=O). The intensity of this band exhibited variation among the samples, but was the major peak in many cases. Bands observed at 3063–3024 cm^{-1} and 2952–2711 cm^{-1} can be assigned to aryl C-H and alkyl C-H stretch vibration,

respectively. On the other hand, the medium/strong band observed at 1605-1580 cm^{-1} can indicate stretch aromatic ring vibrations (C=C), while a set of bands in the range of 2700-2400 cm^{-1} can be assigned to the amine salt [418, 420].

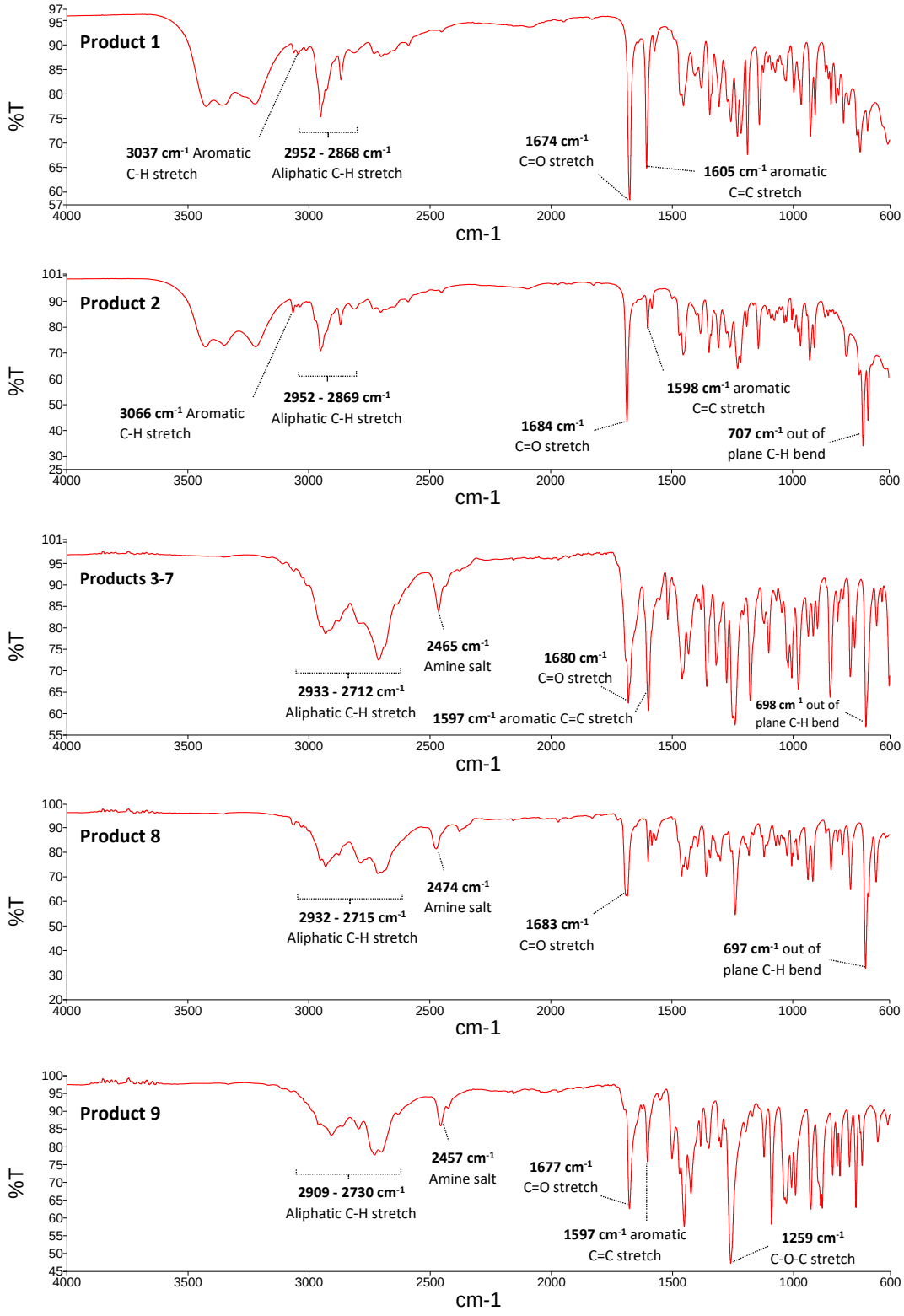

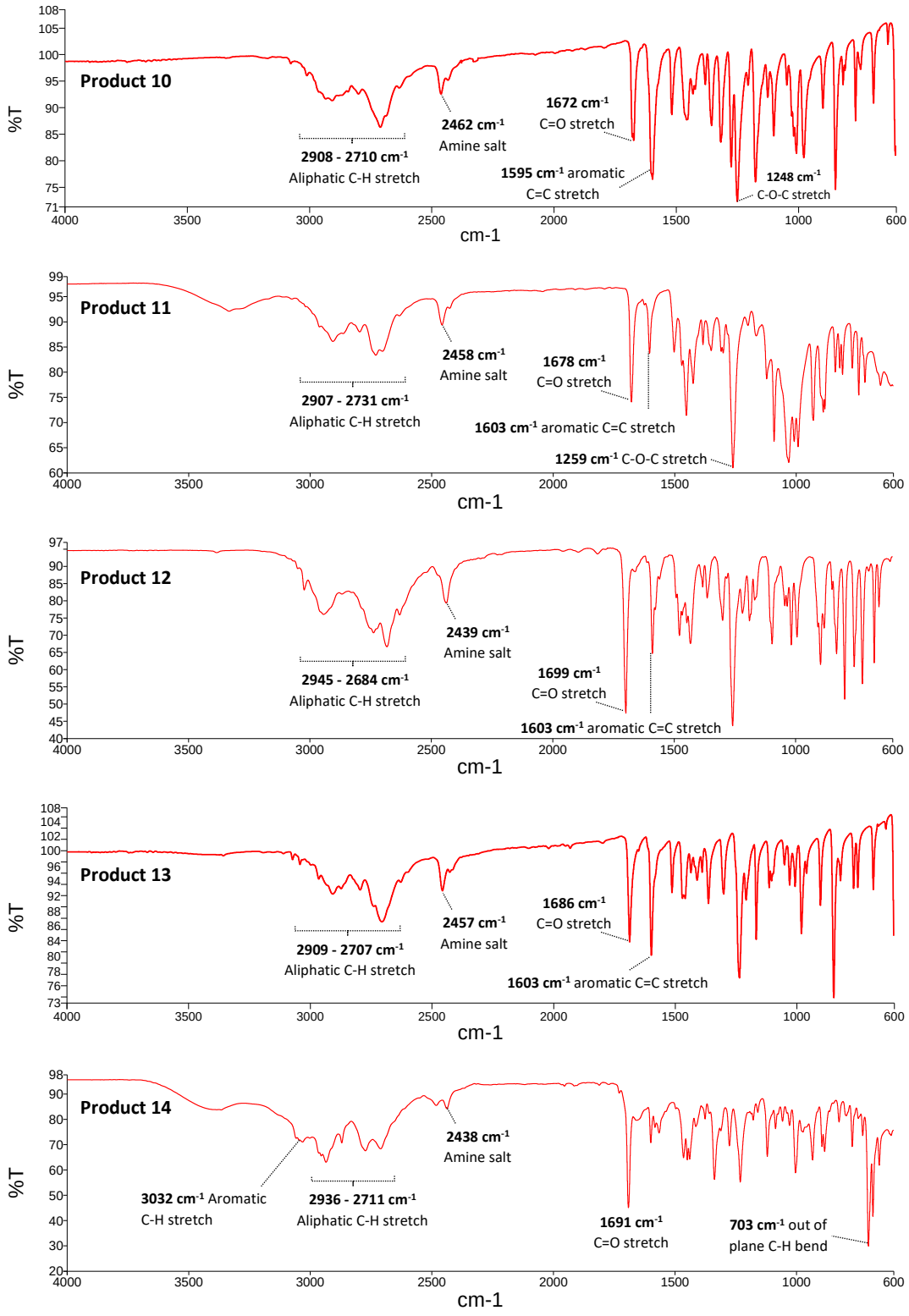

Figure 39. FTIR spectra of seized products suspected to contain SCat. Products 3-7 show similar IR spectra.

For absorptions below 1500 cm^{-1}, the differences between samples were more significant. A strong band observed in products 9, 10 and 11 at 1248-1259 cm^{-1} dominates the IR spectrum and can indicate a C-O-C stretching [421, 422]. In fact, products 9 and 11 show an

IR spectrum very similar to that of methylone, while IR spectrum of product 10 is very similar to that of methedrone (Figure S1 supporting information).

In general, the out-of-plane C–H bending bands in the region of 675-900 cm^{-1} are used to differentiate between substituted aromatic compounds [423, 424]. For monosubstituted benzene rings, out-of-plane C-H bending bands are between 770-730 cm^{-1} and 710-690 cm^{-1} and are often the most intense bands in the spectra [423, 425]. In this sense, products 2-8 and 14 showed a pattern consistent with these characteristics, indicating that we may be facing compounds with monosubstituted aromatic rings. It is important to note that "Bloom" products (products 3-7) had identical IR spectra, which may indicate that they have the same chemical composition.

1.2.2. GC-MS Analysis

Methanolic solutions of the seized materials were directly analysed by GC-MS, resulting in different chromatographic profiles (Figure 40). The EI mass spectra for most compounds were consistent with the fragmentation pattern of SCat, showing the presence of iminium cations as the base peak and small or absent intensities of the molecular ions (Figure 41). Table 11 shows the identified compounds, their molecular formulas, retention time, the base peak and other characteristic ions for the identified compounds.

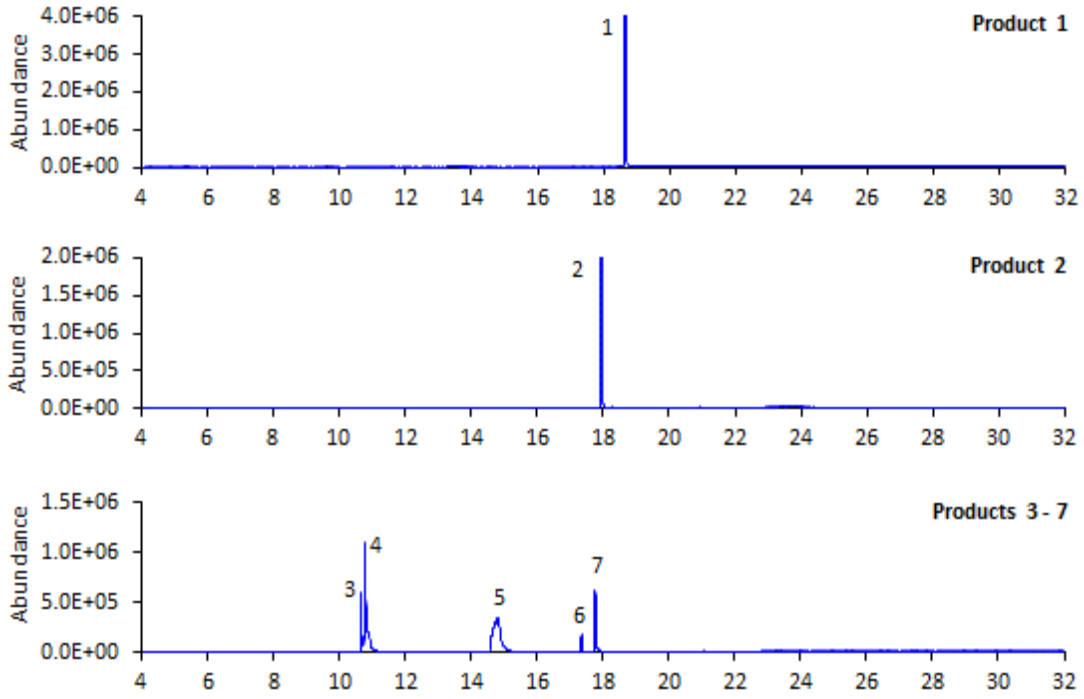

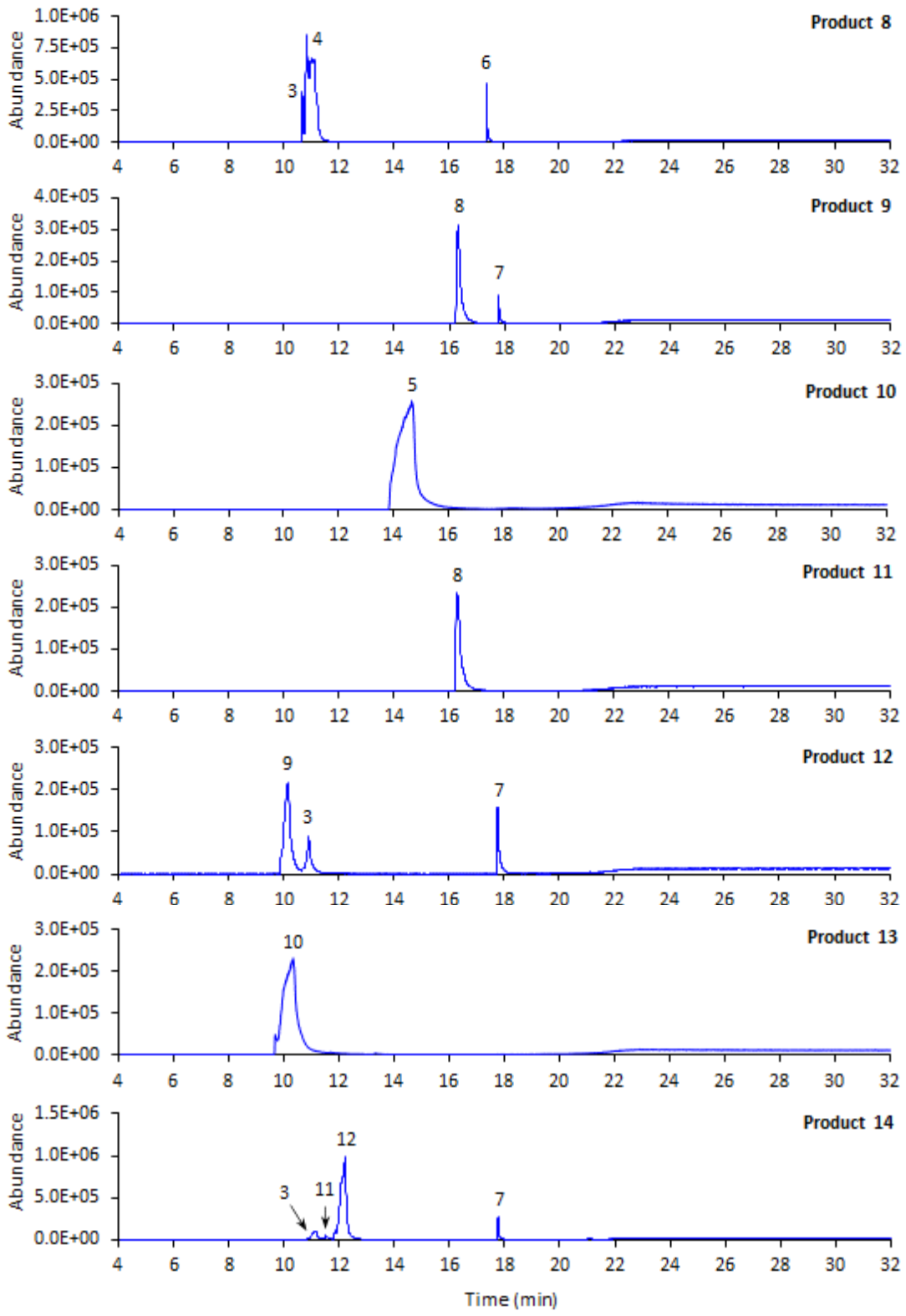

Figure 40. Typical GC-MS chromatograms of seized products suspected to contain SCat. Products 3-7 show similar chromatographic profiles. Peak identification: (1) MPHP, (2) α-PHP, (3) *N*-ethylcathinone, (4) buphedrone, (5) methedrone, (6) ethylphenidate, (7) caffeine, (8) methylone, (9) 3-FMC, (10) 4-FMC, (11) isopentedrone and (12) pentedrone.

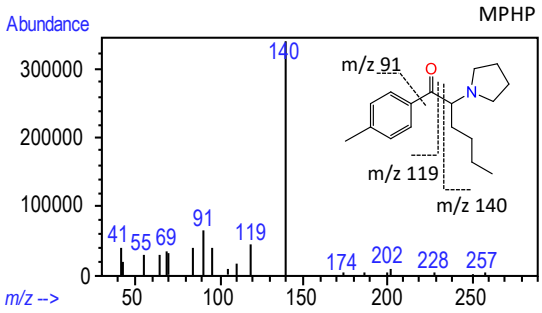
MPHP
Abundance
m/z -->
140
91
119
41
55
69
174
202
228
257
m/z 91
m/z 119
m/z 140

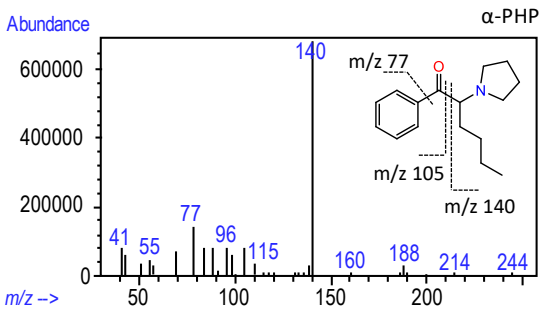
α-PHP
Abundance
m/z -->
140
77
96
41
55
115
160
188
214
244
m/z 77
m/z 105
m/z 140

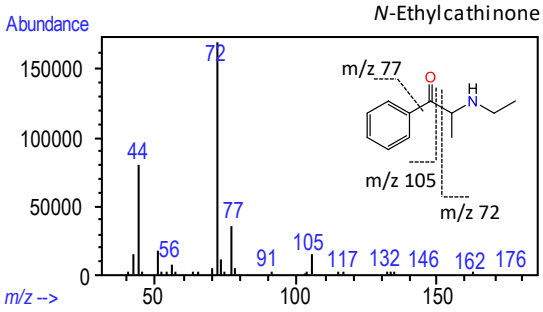
N-Ethylcathinone
Abundance
m/z -->
72
44
77
56
91
105
117
132
146
162
176
m/z 77
m/z 105
m/z 72

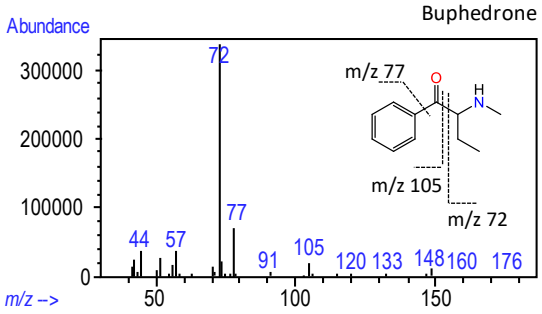
Buphedrone
Abundance
m/z -->
72
77
44
57
91
105
120
133
148
160
176
m/z 77
m/z 105
m/z 72

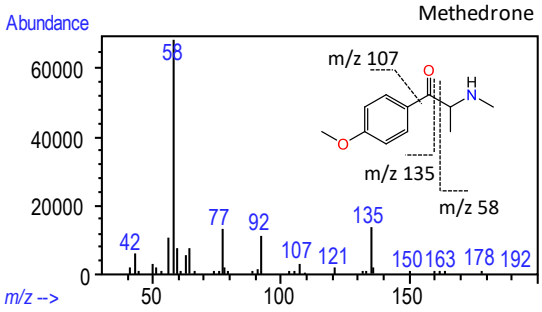
Methedrone
Abundance
m/z -->
58
77
92
135
42
107
121
150
163
178
192
m/z 107
m/z 135
m/z 58

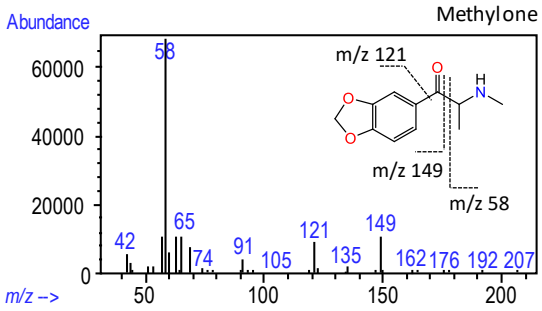
Methylone
Abundance
m/z -->
58
65
42
91
121
149
74
105
135
162
176
192
207
m/z 121
m/z 149
m/z 58

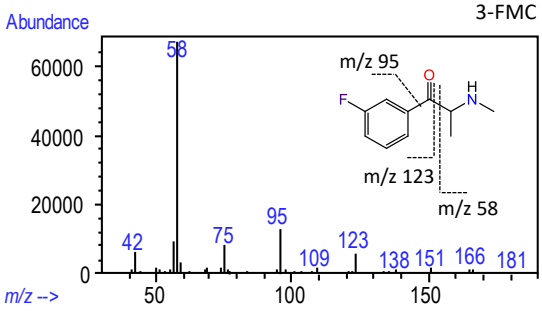
3-FMC
Abundance
m/z -->
58
95
42
75
123
109
138
151
166
181
m/z 95
m/z 123
m/z 58

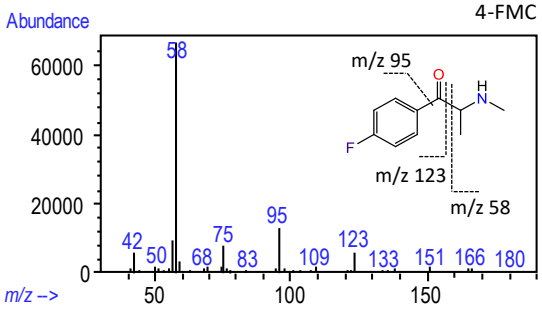
4-FMC
Abundance
m/z -->
58
95
42
50
75
68
83
109
123
133
151
166
180
m/z 95
m/z 123
m/z 58

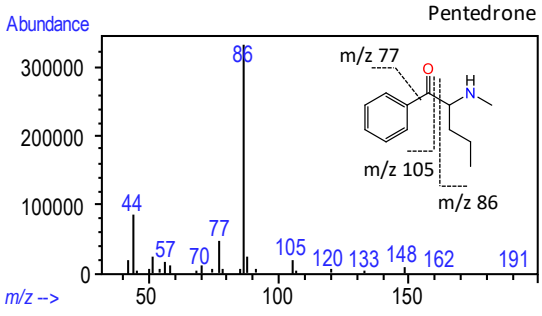
Pentedrone
Abundance
m/z -->
86
44
77
57
70
105
120
133
148
162
191
m/z 77
m/z 105
m/z 86

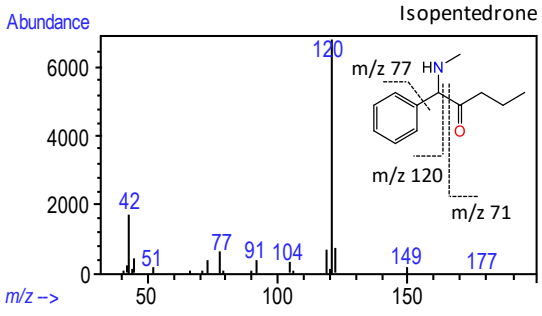
Isopentedrone
Abundance
m/z -->
120
42
77
91
104
51
149
177
m/z 77
m/z 120
m/z 71

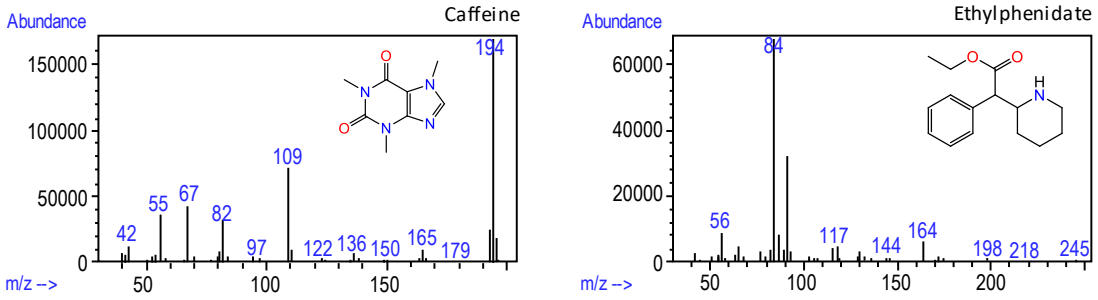

Figure 41. Mass spectra of compounds found in seized products.

Table 11. Active substances detected in seized products by GC-MS, with the respective retention times (RT), Kovats retention indices (KI), molecular formula (MF), molecular weight (MW), base peak and other characteristic ions.

RT (min)	KI_{calc}	$KI_{Lit.}$	Compound name	MF	MW	Ions (m/z)
10.007	1339	1336[a]	3-FMC*	$C_{10}H_{12}FNO$	181	**58**, 95, 75, 123
10.256	1366	1380[a]	4-FMC*	$C_{10}H_{12}FNO$	181	**58**, 95, 75, 123
10.658	1407	1399[b]	*N*-Ethylcathinone	$C_{11}H_{15}NO$	177	**72**, 44, 77, 105
10.785	1417	1410[b]	Buphedrone	$C_{11}H_{15}NO$	177	**72**, 77, 44, 105
11.516	1477	-	Isopentedrone	$C_{12}H_{17}NO$	191	**120**, 42, 118, 91
12.083	1516	1519[a]	Pentedrone	$C_{12}H_{17}NO$	191	**86**, 44, 77, 105
14.820	1654	1651[a]	Methedrone	$C_{11}H_{15}NO_2$	193	**58**, 135, 77, 92
16.314	1730	1739[a]	Methylone	$C_{11}H_{13}NO_3$	207	**58**, 149, 65, 121
17.357	1809	-	Ethylphenidate	$C_{14}H_{19}NO_2$	233	**84**, 91, 56, 164
17.775	1855	1820[c]	Caffeine	$C_8H_{10}N_4O_2$	194	**194**, 109, 67, 55
17.950	1874	1880[a]	α-PHP	$C_{17}H_{25}NO$	245	**140**, 77, 96, 105
18.654	1943	2001[a]	MPHP	$C_{17}H_{25}NO$	259	**140**, 91, 119, 41

* Identification of 3-FMC and 4-FMC was performed after NMR confirmation.
[a] Sisco et al. [426]
[b] Matsuta et al. [427]
[c] Menezes et al. [428]
Bold numbers represent the base peak ion.

As reported by Zuba [429], the α-cleavage process is a key feature of the mass spectral fragmentation of SCat. This process results in the formation of the iminium ion, by fragmentation of the C–C bond, between the α and β carbon atoms, under EI conditions (Figure 42). In the case of cathinones with a straight-chained aliphatic side ring, the structural formula of the base iminium ion is represented by $C_nH_{2n+2}N^+$ (n = 1, 2, …), resulting in a base peak of mass-to-charge ratio (m/z) 44, 58, 72, 86, 100 and so on, depending on the number of carbon atoms contained in the iminium ion [429, 430].

N-Ethylcathinone, buphedrone, pentedrone, methedrone, methylone, 3-FMC and 4-FMC are SCat that produce typical $C_nH_{2n+2}N^+$ iminium ions. For cathinones with a pyrrolidine ring in the side chain, such as MPHP and α-PHP, fragmentation leads to the formation of characteristic ions represented by the structural formula $C_nH_{2n}N^+$ (n = 5, 6,…), which corresponds

to $R_3CH=N^+(C_4H_8)$ species [429]. The consequent fragmentation of the pyrrolidine ring leads to the formation of characteristic ions m/z 70, 55, 42 and 41 [429, 431].

Another common reaction observed in SCat under EI condition is the formation of the acylium ion. In general, this process takes place at the same location as for the formation of the iminium ion, and involves the dissociation of the C_α–C_β bond, leaving behind an acylium ion [430]. The consequent loss of carbon monoxide (CO) from the acylium ion results in the formation of the phenyl cation, as indicated in Figure 42. The phenyl (m/z 77), methylphenyl (m/z 91), and fluorophenyl (m/z 95) cations are some representative examples of ions produced by the loss of carbon monoxide from the corresponding acylium ions at m/z 105 (benzoyl ion), 119 (methylbenzoyl ion) and 123 (fluorobenzoyl ion). Although these fragmentation patterns in the mass spectra provide structural information about the elemental composition, they do not differentiate structural isomers with different substitution patterns on the aromatic ring.

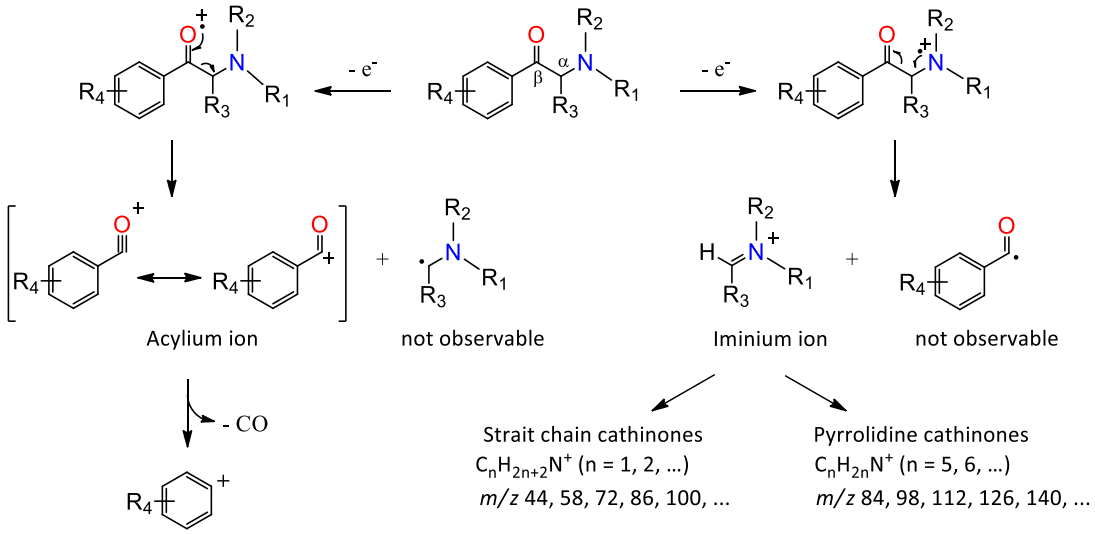

Figure 42. General mass spectra fragmentation pattern of SCat under EI conditions (adapted from Zuba [429]).

Unfortunately, the EI method is often limited to differentiate structurally similar cathinones. The similar fragmentation pattern in some of these compounds, associated with the absence of molecular ion peak, may produce ambiguous mass spectra. However, the differentiation of these compounds can be achieved using an alternative approach, such as chemical derivatization, which can represent a straightforward and cost-effective way to improve the capability of compound identification [432, 433].

TFAA is one of the most widely used derivatizing agents, known to react with the primary and secondary amine groups of the amphetamine-type stimulants [397, 434]. Derivatives are

formed via acylation, where the amine hydrogen is replaced by a trifluoroacyl group (Figure 43) [435].

Not all substituted cathinones can be directly derivatized using TFAA, which requires, at least, one hydrogen atom in the amino group or an active hydrogen atom from other functional groups (*e.g.* -OH, -COOH).

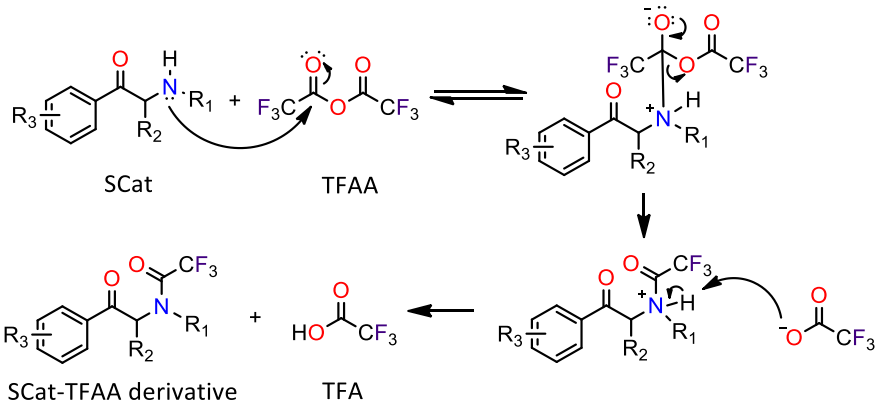

Figure 43. General derivatization mechanism of SCat with the TFAA reagent.

After derivatization, and knowing the molecular weight and ions resulting from fragmentation, it was possible to identify the chemical structures of the formed compounds. Figure 44 shows the typical GC-MS chromatograms of the seized products after derivatization with TFAA, and Figure 45 describes the respective mass spectra of SCat after derivatization. Table 12 shows the identified TFAA derivative compounds, their molecular formulas, retention time, the base peak and other characteristic ions for the identified compounds.

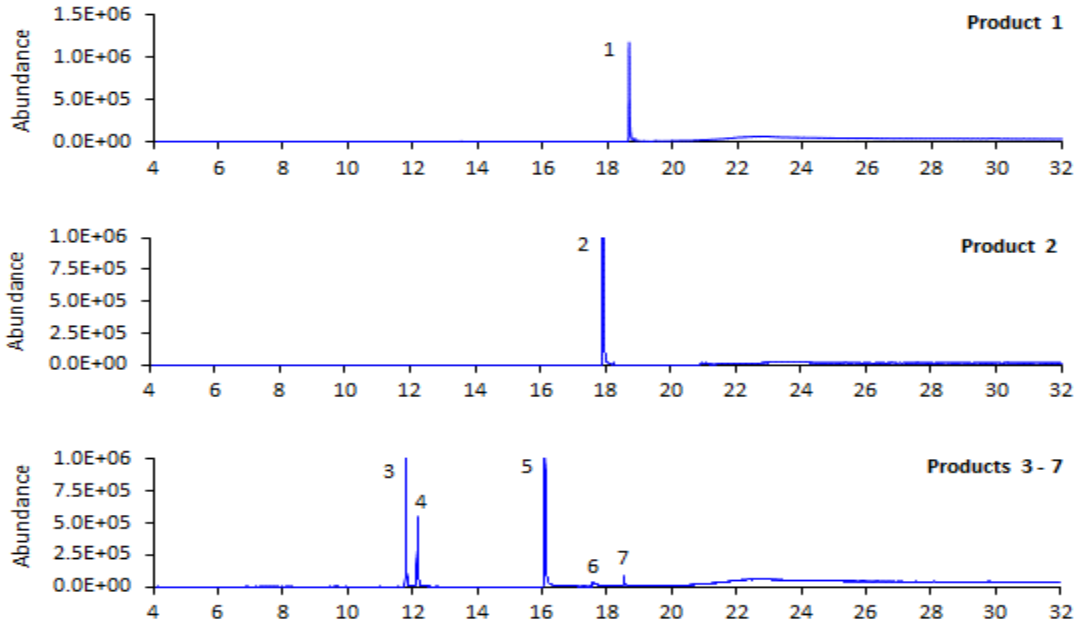

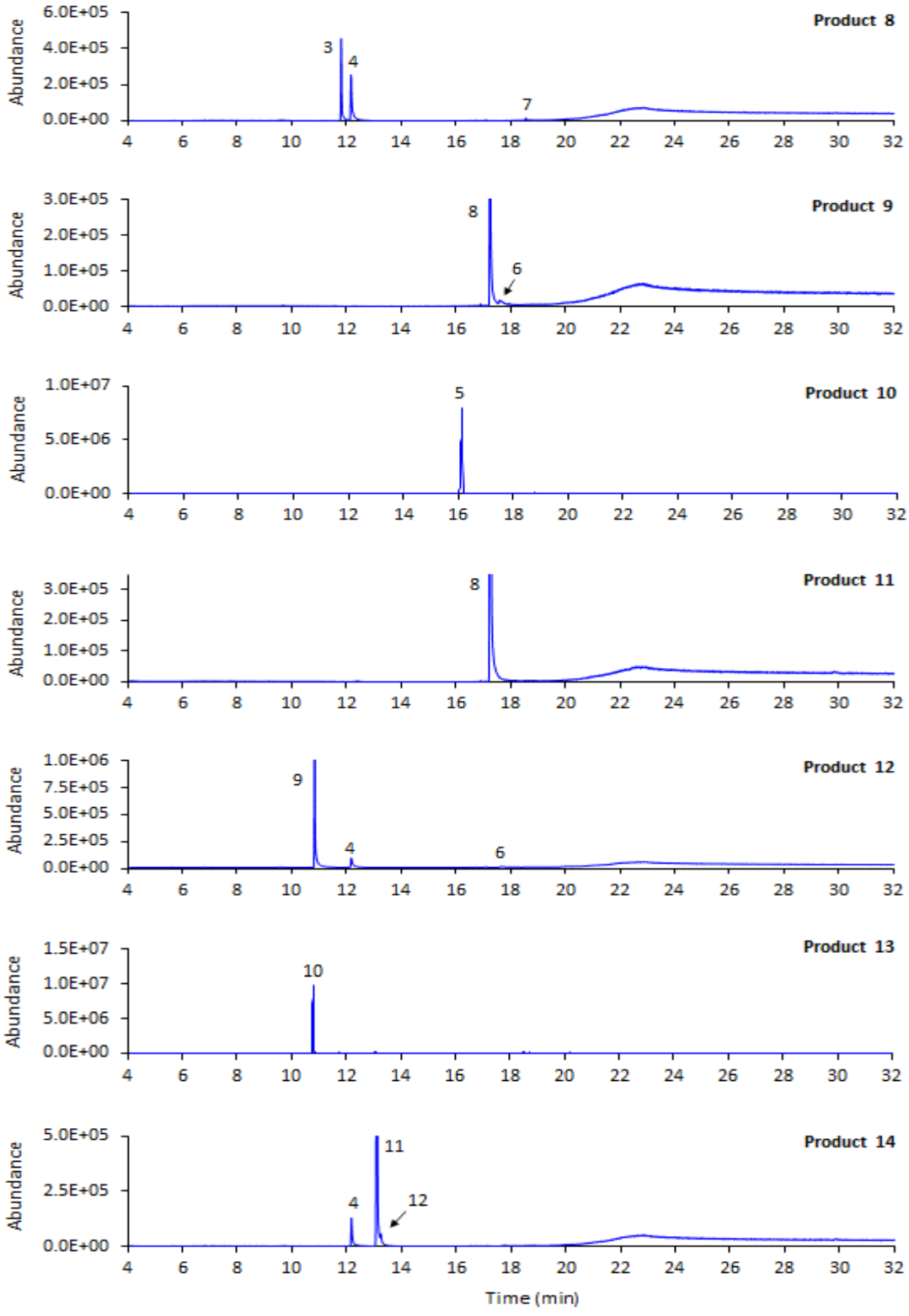

Figure 44. Typical GC-MS chromatograms of seized products after derivatization with TFAA. Peak identification: (1) MPHP, (2) α-PHP, (3) buphedrone-TFAA derivative, (4) *N*-ethylcathinone-TFAA derivative, (5) methedrone-TFAA derivative, (6) ethylphenidate-TFAA derivative, (7) caffeine, (8) methylone-TFAA derivative, (9) 3-FMC-TFAA derivative, (10) 4-FMC-TFAA derivative, (11) pentedrone-TFAA derivative and (12) isopentedrone-TFAA derivative.

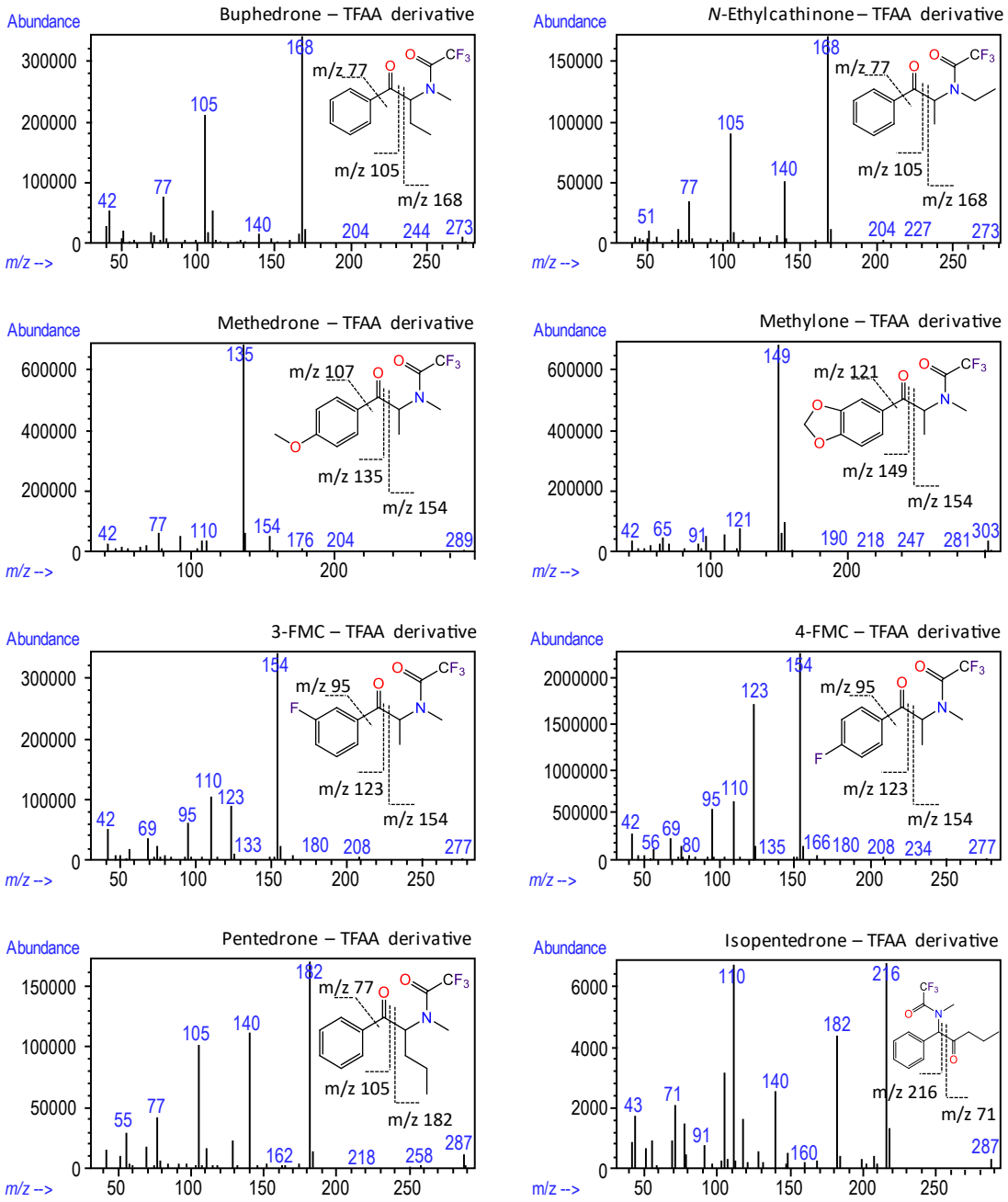

Figure 45. Mass spectra of SCat after derivatization with TFAA.

Derivatization of SCat with TFAA produced a better chromatographic resolution and increased mass spectral abundances for molecular and fragment ions. Before derivatization, products containing *N*-ethylcathinone and buphedrone (products 3-8) had a poor resolution, and the fragmentation patterns observed on the mass spectra of both compounds were very similar. After derivatization, these SCat showed better chromatographic separation, with larger, narrower, and more symmetric chromatographic peaks, and the mass fragmentation pattern of both compounds were readily distinguished by the different relative abundance of two common fragment ions (m/z 140 and 110). In general, SCat with a methyl substituent on the nitrogen

Table 12. Chemical substances detected in seized products by GC-MS after derivatization with TFAA.

RT (min)	KI_{calc}	$KI_{Lit.}$	Compound name	MF	MW	Ions (m/z)
10.799	1418	-	4-FMC-TFFA derivative	$C_{12}H_{11}F_4NO_2$	277	**154**, 123, 110, 95
10.837	1421	-	3-FMC-TFFA derivative	$C_{12}H_{11}F_4NO_2$	277	**154**, 110, 123, 95
11.813	1501	1507[a]	Buphedrone-TFFA derivative	$C_{13}H_{14}F_3NO_2$	273	**168**, 105, 77, 110
12.173	1521	1528[a]	*N*-Ethylcathinone-TFFA derivative	$C_{13}H_{14}F_3NO_2$	273	**168**, 105, 140, 77
13.098	1575	1582[a]	Pentedrone-TFFA derivative	$C_{14}H_{16}F_3NO_2$	287	**182**, 140, 105, 77
13.239	1583	-	Isopentedrone-TFFA derivative	$C_{14}H_{16}F_3NO_2$	287	**110**, 216, 182, 140
16.096	1714	1720[a]	Methedrone-TFFA derivative	$C_{13}H_{14}F_3NO_3$	289	**135**, 77, 154, 92
17.239	1798	1813[a]	Methylone-TFFA derivative	$C_{13}H_{12}F_3NO_4$	303	**149**, 154, 121, 110
17.775	1855	1820[c]	Caffeine*	$C_8H_{10}N_4O_2$	194	**194**, 109, 67, 55
17.950	1874	1880[c]	α-PHP*	$C_{17}H_{25}NO$	245	**140**, 77, 96, 105
18.538	1932	-	Ethylphenidate-TFFA derivative	$C_{17}H_{20}F_3NO_3$	343	**180**, 164; 67; 55
18.654	1943	2001[c]	MPHP*	$C_{17}H_{25}NO$	259	**140**, 91, 119, 41

Abbreviations: RT - retention time; KI - Kovats retention indices; MF - molecular formula; MW - molecular weight.
*Derivatization did not occur
[a] Matsuta et al. [427]
[b] Menezes et al. [428]
[c] Sisco et al. [426]

atom, such as buphedrone, have a characteristic ion at m/z 110 ($[CH_3–N{\equiv}C–CF_3]^+$). This cation may be formed from the decomposition reaction of the TFAA imine specie at m/z 168 (Figure 46A). *N*-Ethylcathinone with an ethyl substituent in the amino group produced analogous cation at m/z 124 corresponding to $[C_2H_5–N{\equiv}C–CF_3]^+$ (Figure 46B), with low relative abundance (2%). In addition, both compounds showed a characteristic ion at m/z 140. This cation is more abundant in *N*-ethylcathinone (29%) than in buphedrone (4%) and is probably originated from a rearrangement of the ethyl group of the m/z 168 cation to lose ethylene.

We were able to conclude, based on these results, and considering the number of potential compounds to be investigated and the existence of a wide diversity of isomers with identical fragmentation patterns under EI conditions, that the derivatization with TFAA showed to be an effective strategy to confirm the identity of these substances, allowing us to obtain more specific structural information of these compounds. Thus, through the GC-MS analysis it was possible to identify a total of 12 different substances, belonging most of them, to the class of SCat. MPHP was identified as the main compound in product 1, while α-PHP was the main component in product 2. Both substances showed characteristic mass spectral fragmentation pattern with SCat containing a pyrrolidine ring in the side chain. Methylone was identified as the main component in product 11, together with caffeine in product 9. Methedrone and 4-FMC were identified as the main components in products 10 and 13, respectively.

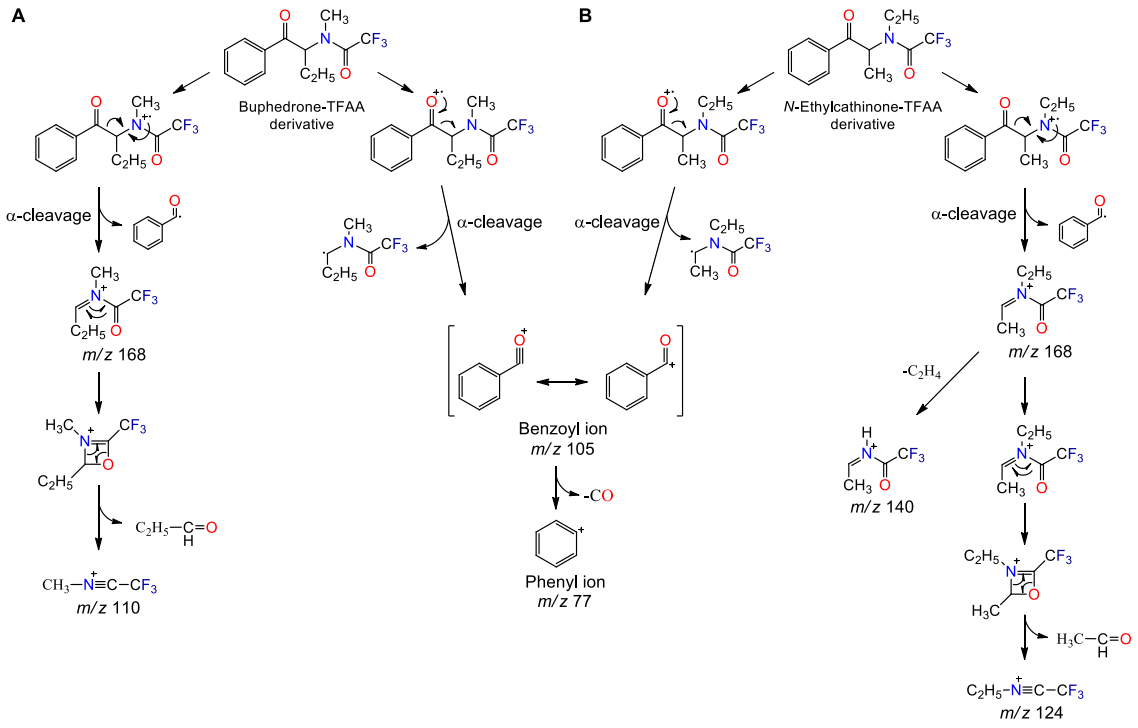

Figure 46. Probable fragmentation pathways of TFAA derivatives of (A) buphedrone and (B) *N*-ethylcathinone.

"Bloom" products (products 3-7) had a similar chromatographic profile and identical chemical composition, which means that they probably belong to the same batch. *N*-Ethylcathinone, buphedrone, methedrone, caffeine and ethylphenidate were the identified substances in these samples. It was also confirmed by GC-MS that products 8, 12 and 14 contained *N*-ethylcathinone, making this SCat the most frequently detected psychoactive substance (57 % of the total analysed products). On the other hand, 3-FMC and pentedrone were the main compounds in products 12 and 14, respectively.

In product 14, it was also present, an isomeric impurity identified as isopentedrone (1-methylamino-1-phenylpentan-2-one), a by-product of the pentedrone synthesis, in which the amino moiety and keto group changed their position in the molecule. Regarding the adulterant compounds found in these products, caffeine was the most frequently detected substance (57 % of the total analysed products), followed by ethylphenidate (43% of the total analysed products). It is also important to note that the identification of compounds was performed by comparing the GC retention times and mass spectra, with the available standards (Figure S2 and Figure S3, supporting information).

1.2.3. UHPLC-PDA Analysis

Methanolic solutions of the seized materials were also analysed by UHPLC-PDA, resulting in different chromatographic profiles (Figure 47). The absorption spectra in the UV region were recorded in the range of 200-400 nm for each compound (Figure 48) and compared with the available standards (Figure S4 and Figure S5, supporting information). Table 13 summarizes the respective retention times, molecular structures, and the UV maximum absorption wavelengths (λ_{max}).

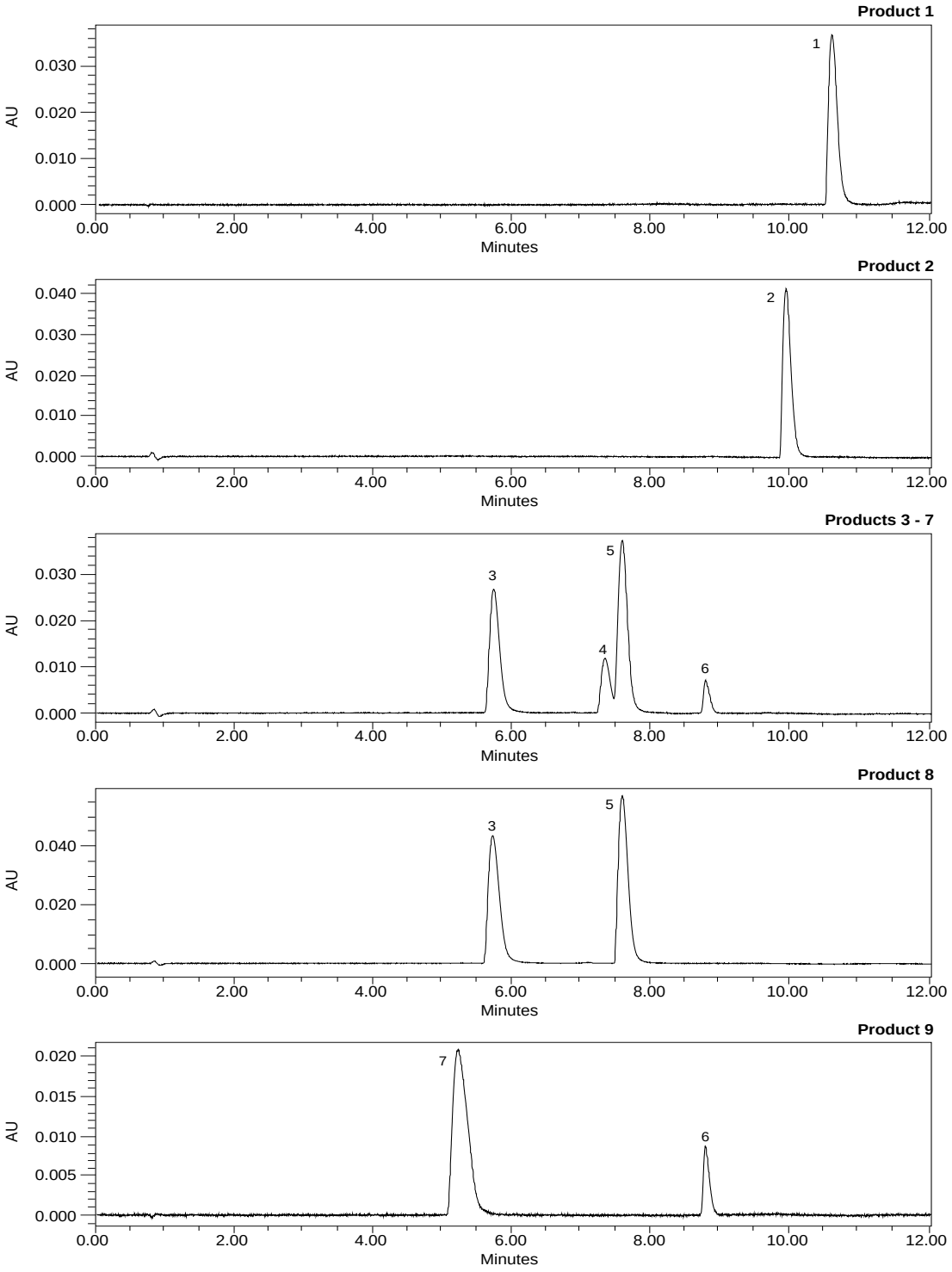

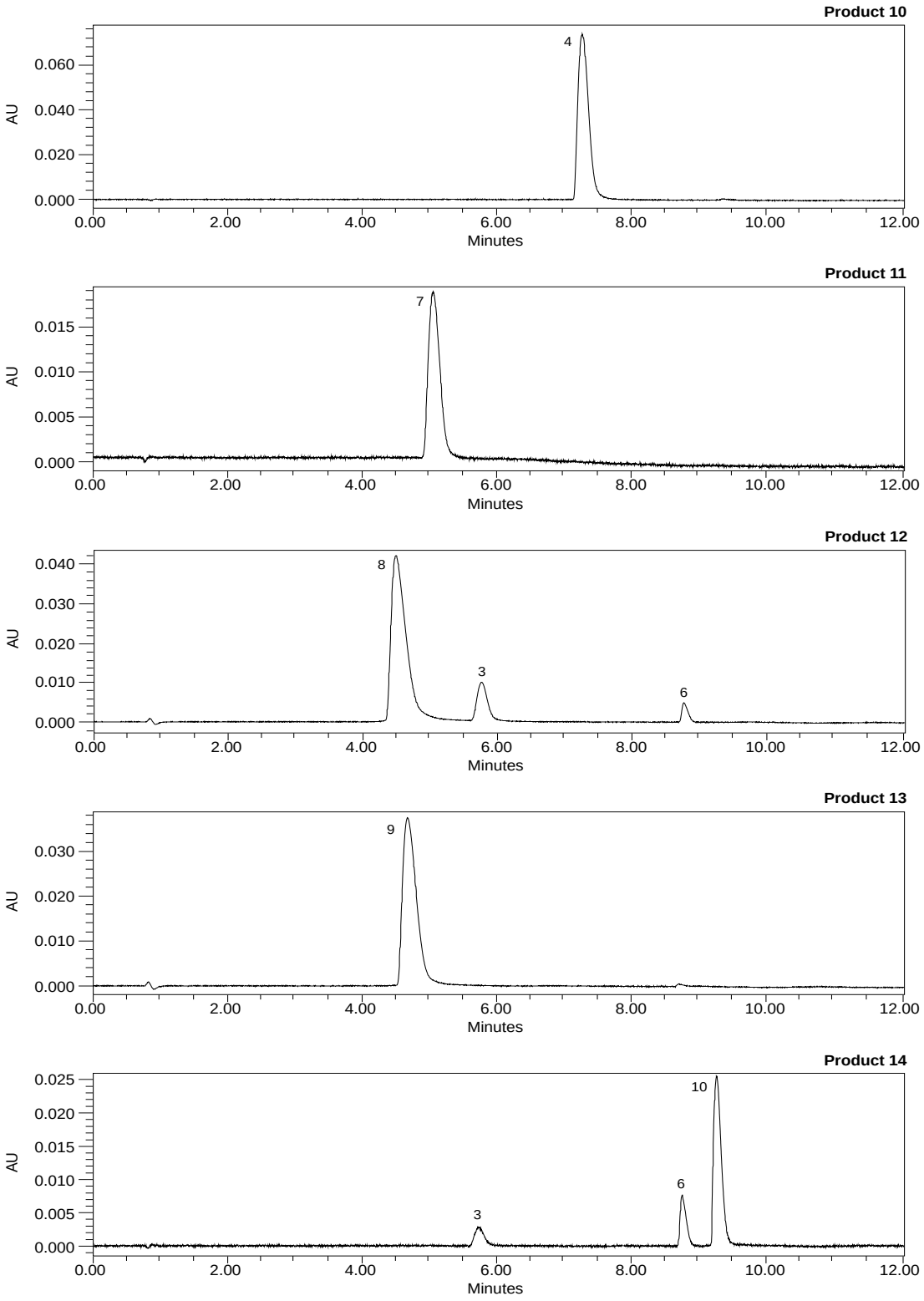

Figure 47. Typical UHPLC-PDA chromatograms of seized products. Peak identification: (1) MPHP, (2) α-PHP, (3) *N*-ethylcathinone, (4) methedrone, (5) buphedrone, (6) caffeine, (7) methylone, (8) 3-FMC, (9) 4-FMC and (10) pentedrone.

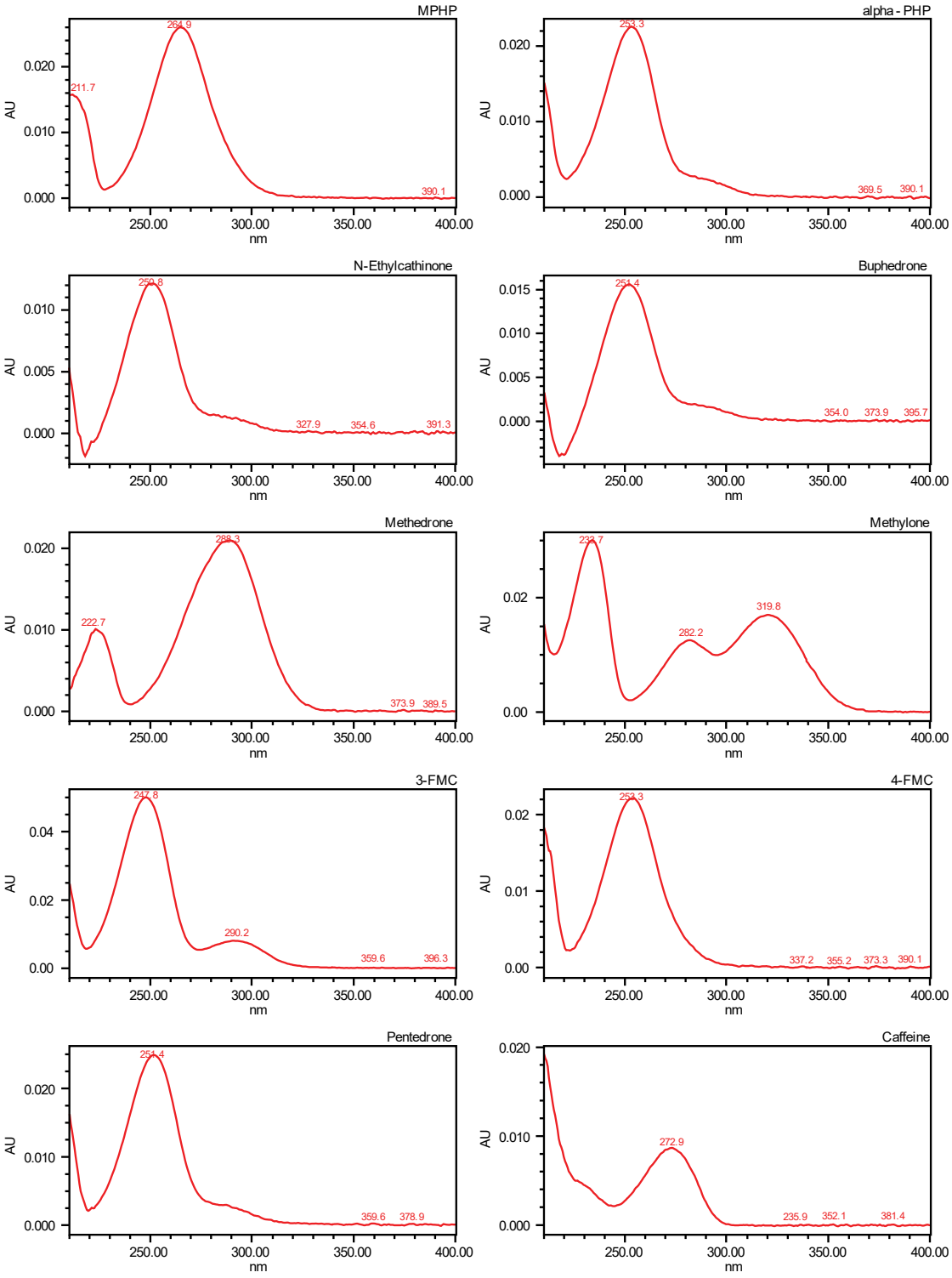

Figure 48. UV spectra of compounds found in seized products.

Significant differences in UV spectra, in terms of spectral shape and λ_{max}, arise due to substitutions on the benzene ring. For example, the presence of a methyl group at the *para* position of the benzene ring in MPHP causes the absorption peak to appear at a longer wavelength compared to α-PHP. The fluoromethcathinone isomers also present differences in their λ_{max}. The 4-fluor substituent has a slightly higher absorption maximum (253 nm) compared

Table 13. Chemical substances detected in seized products by UHPLC-PDA, with the respective retention times (RT), molecular structure, molecular formula (MF) and UV maximum absorption wavelengths (λ_{max}).

RT (min)	Compound name	Structure	MF	λ_{max} (nm)
4.532	3-FMC	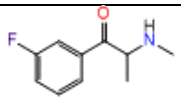	$C_{10}H_{12}FNO$	248, 290
4.650	4-FMC	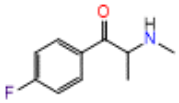	$C_{10}H_{12}FNO$	253
5.179	Methylone	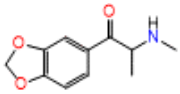	$C_{11}H_{13}NO_3$	234, 320, 282
5.699	*N*-Ethylcathinone	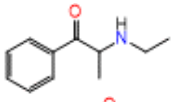	$C_{11}H_{15}NO$	251
7.342	Methedrone	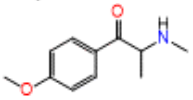	$C_{11}H_{15}NO_2$	288, 223
7.688	Buphedrone	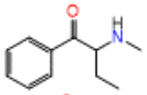	$C_{11}H_{15}NO$	251
8.737	Caffeine	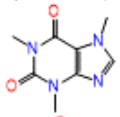	$C_8H_{10}N_4O_2$	273
9.228	Pentedrone	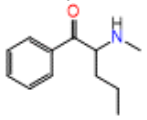	$C_{12}H_{17}NO$	251
9.983	α-PHP	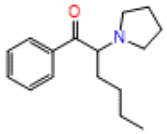	$C_{17}H_{25}NO$	253
10.701	MPHP	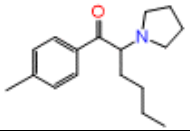	$C_{17}H_{25}NO$	265, 212

with 3-fluor counterpart (248 nm), which makes possible to distinguish these positional isomers. On the other hand, the presence of a methoxy group in the *para* position of the benzene ring, as in the case of methedrone, produces a significant increase in λ_{max}, mostly likely due to the electron releasing effect on the π-electrons of the aromatic ring [436]. Regarding to 3,4-methylenedioxy SCat, such as methylone, these substances produce a characteristic pattern that differentiates them from other types of substituents [437].

Finally, the compounds belonging to the N-alkylated cathinone derivatives class, namely *N*-ethylcathinone, buphedrone and pentedrone showed a very similar UV spectra, with λ_{max} of 251 nm. These results were consistent with the results reported by Li and Lurie [437] and by

Rowe et al. [438], and we can conclude that alkyl substitutions away from the aromatic ring do not produce significant changes in the spectrum of these SCat.

UHPLC-PDA methodology showed to be useful in the identification of SCat, since the shapes of the UV spectra, including the location of the maxima and relative intensity of the spectral bands, depend on the position and type of substitution [400]. This aspect is fundamental to distinguish positional isomers that contain differences in the substitution around the benzene ring [400]. Another advantage of UHPLC-PDA is the repeatability and stability of analytical signal, which makes this technique a good choice for quantitative purposes [400]. Moreover, in the analysis of seized materials, the UHPLC-PDA provides information complementary to EI-MS, where the latter technique cannot distinguish some types of positional isomers, such as 3-FMC and 4-FMC.

1.2.4. NMR Analysis

In order to complement the FTIR, GC-MS and UHPLC-PDA results, NMR analyses were performed for a correct structural elucidation.

The ^{1}H and ^{13}C NMR spectra of all substances were registered at 400 and 100 MHz, respectively. Signals assignments were based on chemical shifts (δ, ppm) of ^{1}H and ^{13}C, on the multiplicity patterns of proton resonances depicted by the *J* couplings (Hz), and on data of homonuclear ^{1}H-^{1}H COSY and heteronuclear ^{1}H-^{13}C HMBC and HSQC (Figure S6 to Figure S16, supporting information). The NMR experiments and the signals assignments were made for all compounds and presented in Tables 14, 15 and 16. For products 12 and 13, which contains a fluoromethcathinone, a ^{19}F NMR spectrum (Figure S8, supporting information) was also recorded and the respective signal assignment was presented in Table 15.

The NMR spectra of pyrovalerone derivatives (Figure S6 and Figure S7, supporting information), namely MPHP and α-PHP, identified in products 1 and 2, respectively, showed many similarities, but also some differences that allowed unequivocal identification of both compounds.

MPHP is a 1,4-disubstituted aromatic compound with a symmetric distribution of protons on the aromatic ring, and, for this reason, the ^{1}H NMR signal of the aromatic protons exhibits a characteristic splitting pattern constituted by two doublets at 7.96 ppm (H-2'/H-6') and 7.47 ppm (H-3'/H-5'). The methyl group attached to the *para* position of the benzene ring (H-7') produced a large singlet at 2.46 ppm, which was also observed by Westphal et al. [115]. In contrast to MPHP, the ^{1}H NMR spectrum of α-PHP showed a typical phenyl pattern at 7.65 ppm (*meta*, appears as a 2H triplet), 7.81 ppm (*para*, appears as a 1H triplet), and 8.06 ppm (*ortho*, appears as a 2H doublet), which is consistent with the values reported in the literature [83, 392].

The methine proton (H-2) of both pyrovalerone derivatives showed a triplet signal at around 5.3 ppm, and the protons of the alkyl side chain were found between 2.18 ppm (H-3) and 0.76 ppm (H-6). The multiplets of the methylene protons H-1'' and H-4'' of the pyrrolidine-ring appeared as separated signals, centred at 3.07 ppm (1H from H-4''), 3.36 ppm (1H from H-1'') and 3.74 ppm (two overlapped protons; 1H from H-4'' and 1H from H-1''), while the proton signals of H-2'' and H-3'' appeared between 2.01 and 2.30 ppm, and were partially overlapped with the methylene protons H-3 of the alkyl side chain. Due to their structural similarities, it was also possible to observe several common characteristics in the ^{13}C NMR spectra, including the signals for the carbon of the carbonyl group (C-1) around 198 ppm, the chiral carbon C-2 at 70 ppm and the carbons of the aliphatic side chain C-3, C-4, C-5 and C-6 between 13.2 ppm and 30.2 ppm. The carbons C-1'' and C-4'' of pyrrolidine moiety resonate at 52.6 ppm and 55.8 ppm, respectively, while C-2'' and C-3'' signals are partially overlap at 23.3 ppm, in both compounds. The six aromatic carbons appearing as four signals for these pyrovalerone derivatives showed some differences, thus indicating chemical and structural differences between compounds. By the attachment of a substituent group to the benzene ring, the electronic density and, consequently, the chemical shifts of the carbon atoms, will increase or decrease depending on the electronic nature of the substituent and its position in the aromatic ring [439]. In this sense, the presence of a methyl group in the *para* position of the aromatic ring of MPHP leads to a downfield shift of 12 ppm of the C-4' resonance in comparison with α-PHP. In addition, the carbon of the methyl group C-7' attached to the aromatic ring produced a signal at around 21 ppm, which is in agreement with the results obtained by Westphal et al. [115].

For products 9 and 11, the NMR analysis confirmed the presence of methylone in both samples. Methylone is a 1,3,4-trisubstituted aromatic compound characterized by one double doublet at 7.70 ppm (H-6') and two doublets at 7.47 (H-2') and 7.04 ppm (H-5') on ^{1}H NMR spectrum. The methylenedioxy group attached to aromatic ring was identified by the singlet at 6.14 ppm (H-7'), while the methine proton (H-2) located between the carbonyl group and the nitrogen atom were observed at 5.06 ppm (appears as a 1H quartet), which is in agreement with the results reported in the literature [424, 440, 441].

The singlet at 2.82 ppm integrates 3 protons and belongs to the *N*-methyl group (H-1''), while the doublet at 1.64 ppm corresponds to the terminal methyl group of the alkyl side chain (H-3) that were confirmed by the COSY experiment (Figure S11, supporting information). In the ^{13}C NMR spectrum, the signals from the eleven carbon atoms were assigned, based on two-dimensional experiments ^{1}H-^{13}C HSQC and HMBC (Figure S15, supporting information). The carbon signals, corresponding to the phenyl ring, were observed at 108.5 (C-2'), 109.1 (C-5'), 127.0 (C-6'), 127.3 (C-1'), 148.9 (C-3') and 154.1 ppm (C-4'), while the methylenedioxy group

Table 14. NMR assignments of SCat constituted by a pyrrolidine ring in the side chain or a methoxy or a methylenodioxy group attached to the aromatic ring.

Position	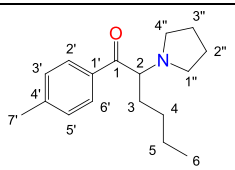 MPHP		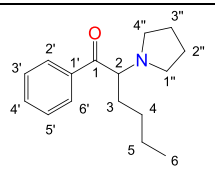 α-PHP		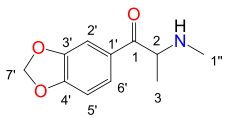 Methylone		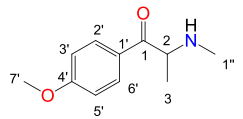 Methedrone	
	^{13}C (δ/ppm)	^{1}H (δ/ppm, protons, multiplicity[a], coupling constants)	^{13}C (δ/ppm)	^{1}H (δ/ppm, protons, multiplicity [1], coupling constants)	^{13}C (δ/ppm)	^{1}H (δ/ppm, protons, multiplicity[a], coupling constants)	^{13}C (δ/ppm)	^{1}H (δ/ppm, protons, multiplicity[a], coupling constants)
1	197.9	-	198.4	-	195.9	-	196.4	-
2	69.9	5.27, 1H, t, *J* = 5.06 Hz	70.0	5.31, 1H, t, *J* = 5.06 Hz	59.9	5.06-5.01, 1H, q, *J* = 7.23 Hz	59.9	5.11-5.05, 1H, q, *J* = 7.21 Hz
3	30.2	2.18-2.01, 2H, m	30.0	2.18-2.01, 2H, m	16.3	1.64, 3H, d, *J* = 7.24 Hz	16.2	1.64, 3H, d, *J* = 7.24 Hz
4	25.8	1.28-1.22, 1H, m 1.15-1.11, 1H, m	25.3	1.28-1.18, 1H, m 1.15-1.11, 1H, m	-	-	-	-
5	22.4	1.28-1.21, 2H, m	22.3	1.28-1.18, 2H, m	-	-	-	-
6	13.3	0.76, 3H, t, *J* = 6.92 Hz	13.2	0.76, 3H, t, *J* = 7.02 Hz	-	-	-	-
1’	131.6	-	134.1	-	127.3	-	125.8	-
2’	129.7	7.96, 1H, d, *J* = 8.16 Hz	129.5	8.06, 1H, d, *J* = 7.52 Hz	108.5	7.47, 1H, d, *J* = 1.64 Hz	132.2	8.04, 1H, at, *J* = 8.84 Hz
3’	130.6	7.47, 1H, d, *J* = 8.08 Hz	129.9	7.65, 1H, t, *J* = 7.82 Hz	148.9	-	115.1	7.14, 1H, d, *J* = 8.96 Hz
4’	148.4	-	136.3	7.81, 1H, t, *J* = 7.46 Hz	154.1	-	165.4	-
5’	130.6	7.47, 1H, d, *J* = 8.08 Hz	129.9	7.65, 1H, t, *J* = 7.82 Hz	109.1	7.04, 1H, d, *J* = 8.28 Hz	115.1	7.14, 1H, d, *J* = 8.96 Hz
6’	129.7	7.96, 1H, d, *J* = 8.16 Hz	129.5	8.06, 1H, d, *J* = 7.52 Hz	127.0	7.70-7.68, 1H, dd, *J* = 8.32, 1.72 Hz	132.2	8.04, 1H, at, *J* = 8.84 Hz
7’	21.6	2.46, 3H, s	-	-	103.2	6.14, 2H, s	56.3	3.48, 3H, s
1’’	52.6	3.80-3.69, 1H, m 3.39-3.32, 1H, m	52.6	3.80-3.70, 1H, m 3.40-3.32, 1H, m	31.5	2.82, 3H, s	31.6	2.83, 3H, s
2’’	23.3	2.18-2.01, 2H, m	23.3	2.18-2.01, 2H, m	-	-	-	-
3’’	23.4	2.30-2.23, 1H, m 2.18-2.01, 1H, m	23.4	2.27-2.21, 1H, m 2.18-2.01, 1H, m	-	-	-	-
4’’	55.8	3.80-3.69, 1H, m 3.10-3.04, 1H, m	55.8	3.80-3.70, 1H, m 3.12-3.06, 1H, m	-	-	-	-

[a]abbreviations: s = singlet, d = doublet, t = triplet, q = quartet, m = multiplet, at = apparent triplet, dd = doublet of doublets.

Table 15. NMR assignments of *N*-ethylcathinone, buphedrone, pentedrone, 3-FMC and 4-FMC found in seized materials.

Position	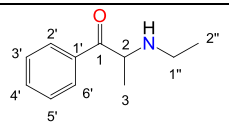		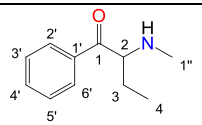		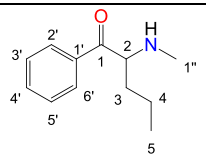		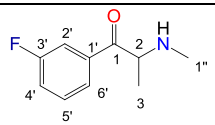			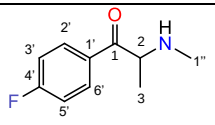		
	N-Ethylcathinone		Buphedrone		Pentedrone		3-FMC			4-FMC		
	^{13}C (δ/ppm)	^{1}H (δ/ppm, protons, multiplicity[a], coupling constants)	^{13}C (δ/ppm)	^{1}H (δ/ppm, protons, multiplicity[a], coupling constants)	^{13}C (δ/ppm)	^{1}H (δ/ppm, protons, multiplicity[a], coupling constants)	^{19}F (δ/ppm)	^{13}C (δ/ppm)	^{1}H (δ/ppm, protons, multiplicity[a], coupling constants)	^{19}F (δ/ppm)	^{13}C (δ/ppm)	^{1}H (δ/ppm, protons, multiplicity[a], coupling constants)
1	198.2	-	197.8	-	197.8	-		196.9, d, *J* = 2.15 Hz	-		196.7	-
2	58.6	5.22-5.16, 1H, m	65.0	5.22-5.16, 1H, m	64.2	5.19, 1H, t, *J* = 5.26 Hz		60.4	5.14-5.09, 1H, q, *J* = 7.28 Hz		60.2	5.14-5.09, 1H, q, *J* = 7.27 Hz
3	16.1	1.63, 3H, d, *J* = 7.4 Hz	23.6	2.24-2.05, 2H, m	32.4	2.12-1.95, 2H, m		15.7	1.65, 3H, d, *J* = 7.28 Hz		15.9	1.64, 3H, d, *J* = 7.28 Hz
4	-	-	7.9	0.89, 3H, t, *J* = 7.58 Hz	17.6	1.41-1.32, 1H, m 1.29-1.17, 1H, m		-	-		-	-
5	-	-	-	-	13.4	0.86, 3H, t, *J* = 7.28 Hz		-	-		-	-
1’	132.9	-	133.7	-	136.0	-		134.9, d, *J* = 6.75 Hz	-		132.7, d, *J* = 10.1 Hz	-
2’	129.5	8.06, 1H, d, *J* = 8.20 Hz	129.4	8.06, 1H, d, *J* = 8.20 Hz	129.4	8.05, 1H, d, *J* = 7.40 Hz		115.9, d, *J* = 23.0 Hz	7.86, 1H, d, *J* = 7.76		129.5, d, *J* = 2.78 Hz	8.13-8.09, 1H, m
3’	129.9	7.65, 1H, at, *J* = 7.62 Hz	129.9	7.65, 1H, at, *J* = 7.62 Hz	129.8	7.64, 1H, t, *J* = 7.82 Hz	-114.3	162.0, d, *J* = 244.8 Hz	-		117.1, d, *J* = 22.2 Hz	7.36, 1H, t, *J* = 8.80 Hz

4’	136.0	7.81, 1H, at, *J* = 7.44 Hz	136.1	7.81, 1H, at *J* = 7.44 Hz	133.6	7.80, 1H, t, *J* = 7.48 Hz	122.8, d, *J* = 21.4 Hz	7.53, 1H, dt, *J* = 8.30, 2.13Hz	-104.6	167.4, d, *J* = 254.26 Hz	-
5’	129.9	7.65, 1H, at, *J* = 7.62 Hz	129.9	7.65, 1H, at, *J* = 7.62 Hz	129.8	7.64, 1H, t, *J* = 7.82 Hz	131.8, d, *J* = 7.94 Hz	7.68-7.62, 1H, m		117.1, d, *J* = 22.2 Hz	7.36, 1H, t, *J* = 8.80 Hz
6’	129.5	8.06, 1H, d, *J* = 8.20 Hz	129.4	8.06, 1H, d, *J* = 8.20 Hz	129.4	8.05, 1H, d, *J* = 7.40 Hz	125.6, d, *J* = 2.89 Hz	7.78, 1H, d, *J* = 9.28 Hz		129.5, d, *J* = 2.78 Hz	8.13-8.09, 1H, m
1’’	41.9	3.31-3.22, 1H, m 3.22-3.13, 1H, m	32.2	2.82, 3H, s	32.3	2.81, 3H, s	31.5	2.85, 3H, s		31.6	2.84, 3H, s
2’’	11.3	1.39, 3H, t, *J* = 7.32 Hz	-	-	-	-	-	-		-	-

[a]abbreviations: s = singlet, d = doublet, t = triplet, q = quartet, m = multiplet, at = apparent triplet, dt = double triplet.

Table 16. ^{1}H and ^{13}C NMR assignments of adulterants found in seized materials.

Position	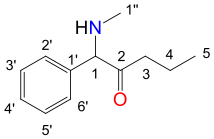 Isopentedrone		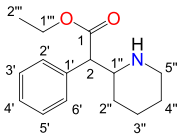 Ethylphenidate		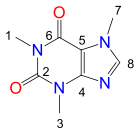 Caffeine		 Methylamine	
	^{13}C (δ/ppm)	^{1}H (δ/ppm, protons, multiplicity[a], coupling constants)	^{13}C (δ/ppm)	^{1}H (δ/ppm, protons, multiplicity[a], coupling constants)	^{13}C (δ/ppm)	^{1}H (δ/ppm, protons, multiplicity[a], coupling constants)	^{13}C (δ/ppm)	^{1}H (δ/ppm, protons, multiplicity[a], coupling constants)
1	69.9	5.29, 1H, s	173.3	-	28.6	3.26, 3H, s	25.1	2.62, 3H, s
2	206.8	-	54.4	4.02, 1H, d, *J* = 9.0 Hz	152.8	-	-	-
3	41.7	2.56-5.52, 1H, m 2.47-2.38, 1H, m	-	-	30.5	3.43, 3H, s	-	-
4	16.9	1.58-1.49, 3H, m	-	-	148.6	-	-	-
5	13.0	0.70, 3H, t, *J* = 7.44 Hz	-	-	108.0	-	-	-
6	-	-	-	-	156.3	-	-	-
7	-	-	-	-	34.2	3.91, 3H, s	-	-
8	-	-	-	-	144.0	7.92, 1H, s	-	-
1’	130.6	-	133.9	-	-	-	-	-
2’	129.5	All aromatic signals at 7.46-7.44, 5H, m	129.2	7.36, 1H, ad, *J* = 7.7 Hz	-	-	-	-
3’	129.6		130.0	7.48, 1H, at, *J* = 6.2 Hz	-	-	-	-
4’	129.4		129.2	7.44, 1H, at, *J* = 6.2 Hz	-	-	-	-
5’	129.6		130.0	7.48, 1H, at, *J* = 6.2 Hz	-	-	-	-
6’	129.5		129.2	7.36, 1H, ad, *J* = 7.7 Hz	-	-	-	-
1’’	31.2	2.99, 3H, s	58.5	3.86, 1H, at, *J* = 10.2 Hz	-	-	-	-
2’’	-	-	26.8	1.48-1.45, 1H, m 1.68, 1H, m	-	-	-	-
3’’	-	-	21.8	1.84-1.79, 1H, m 1.57-1.50, 1H, m	-	-	-	-
4’’	-	-	22.3	1.91, 1H, d, *J* = 14.2 Hz 1.68, 1H, m	-	-	-	-
5’’	-	-	46.2	3.49, 1H, bd, *J* = 12.9 Hz 3.10, 1H, m	-	-	-	-
1’’’	-	-	63.6	4.29-4.20, 2H, m	-	-	-	-
2’’’	-	-	13.6	1.21, 3H, t, *J* = 7.16 Hz	-	-	-	-

[a]abbreviations: s = singlet, d = doublet, t = triplet, m = multiplet, ad = apparent doublet, at = apparent triplet, bd = broad doublet.

(C-7') produced a signal at around 103 ppm. The carbonyl carbon (C-1) was found at 195.9 ppm, and the methine carbon (C-2) and the two methyl groups C-1'' and C-3 appeared at 59.9, 31.5 and 16.3 ppm, respectively.

Analytical data for products 3 to 7 revealed the presence of methedrone together with other cathinones, namely *N*-ethylcathinone and buphedrone. Methedrone is a methcathinone derivative only differing by the presence of a methoxy group in the *para* position of the aromatic ring. Hydrogens belonging to the methoxy group were identified in the ^{1}H NMR spectrum as a singlet at 3.48 ppm, while the proton attached to chiral carbon (H-2) was identified as a quartet at 5.11 ppm, which is in accordance with the results obtained by Zancajo et al. [376]. An apparent triplet at 8.04 ppm (due to overlap with buphedrone and *N*-ethylcathinone signals) and a doublet at 7.14 ppm, with coupling constants of 8.84 Hz and 8.96 Hz, supported substitution in *para* position. The methyl groups H-3 and H-1'' produce a doublet at 1.64 ppm and a singlet at 31.6 ppm, respectively.

N-Ethylcathinone and buphedrone have a close similar chemical structure, and for this reason, the protons corresponding to the aromatic ring were found overlapped. The protons in the *ortho* position (H-2' and H-6') appeared as a doublet at 8.06 ppm with a coupling constant of 8.20 Hz, while *meta* (H-3' and H-5') and *para* (H-4') protons appear as two apparent triplets at 7.65 ppm and 7.81 ppm with coupling constants of 7.62 Hz and 7.44 Hz, respectively. As achieved by Zancajo et al. [376], both compounds showed the signal corresponding to the protons from chiral carbon atoms (H-2) overlapped and appeared as a multiplet at around 5.19 ppm. The *N*-ethyl side chain of *N*-ethylcathinone yielded two multiplets for methylene protons (H-1'') centred at 3.27 ppm and 3.17 ppm and one triplet for the terminal methyl group H-2'' at 1.39 ppm, which are in agreement with the results obtained by Kuś et al. [442]. For buphedrone the *N*-methyl moiety resonates as a large singlet at 2.82 ppm, and the alkyl side chain presents a multiplet centred at 2.14 ppm for the methylene protons H-3 and a triplet at 0.89 ppm for the terminal methyl group (H-4).

Regarding product 14, the NMR data supported the previous findings of GC-MS, and confirmed the presence of pentedrone. As expected, the ^{1}H NMR results obtained for this SCat were very similar to the ^{1}H NMR results for buphedrone, since both substances have similar chemical structures, differing only in the length of the alkyl chain. Pentedrone is constituted by one more methylene group than buphedrone. The methinic proton of pentedrone was observed at 5.19 ppm, and the triplet was more defined than that verified for buphedrone. The two multiplets observed at 1.37 and 1.23 ppm corresponded to the diastereotopic protons H-4, while the methylene protons H-3 appeared at 2.04 ppm as a multiplet. The protons corresponding to the terminal methyl group H-5 remained relatively unchanged at around 0.86 ppm. Maheux and

Copeland [420] obtained similar results during the chemical characterization of pentedrone and buphedrone in their study.

For products 12 and 13, the NMR analysis confirmed the presence of 3-FMC and 4-FMC, respectively. The observed ^{1}H signals of the aliphatic portion of both fluoromethcathinone isomers, are similar to those observed for methedrone and methylone. However, the signals pattern observed in the aromatic region was distinct from these previous ones. For 3-FMC, the two doublets observed at 7.86 ppm and 7.78 ppm corresponded to the protons at *ortho* position H-2' and H-6', respectively, while the multiplet centred at 7.65 ppm and the double triplet at 7.53 ppm belonged to the protons in the *meta* (H-5') and *para* (H-4') positions. Moreover, the doublet splitting of the carbon atom signals at position 1' to 6' and the spin-spin coupling constants ($^{1}J_{C3'-F}$ = 244.8 Hz, $^{2}J_{C2'-F}$ = 23.0 Hz, $^{2}J_{C4'-F}$ = 21.4 Hz, $^{3}J_{C5'-F}$ = 7.94 HZ, $^{3}J_{C1'-F}$ = 6.75 Hz, $^{4}J_{C6'-F}$ = 2.89 Hz) were characteristic for fluorine–carbon interactions, which supported the assignment of the 3'-position for the fluorine atom [443]. Regarding to 4-FMC, the ^{1}H NMR analysis showed a symmetric distribution of protons on the aromatic ring constituted by a triplet at 7.36 ppm corresponding to the protons in the *meta* position (H-3' and H-5') and a multiplet centred at 8.11 ppm belonging to the protons H-2' and H-6'. In addition, the doublet splitting of the carbon atom signals at position 1' to 6' and the spin-spin coupling constants ($^{1}J_{C4'-F}$ = 254.4 Hz, $^{2}J_{C3'-F}$ = 22.2 Hz, $^{3}J_{C5'-F}$ = 22.2 HZ, $^{4}J_{C1'-F}$ = 10.1 Hz, $^{5}J_{C2'-F}$ = 2.78 Hz, $^{6}J_{C6'-F}$ = 2.78 Hz) were also consistent with the fluorine–carbon interactions of 4-FMC. On the other hand, the ^{19}F NMR chemical shift value for the 3-FMC was -114.3 ppm, while for the 4-FMC was -104.6 ppm, which is close related with the reported in the literature [443].

Regarding to the purity of these products, Figure 49 shows the mass fraction (% *m/m*) of each compound found in the seized products. Some of the analysed products only presented one active substance (*e.g.* product 1, 2, 10, 11 and 13), while most of them were mixtures of psychoactive substances with a high number of constituents, for example products 3 to 7 ("Bloom") or product 14 ("Kick").

As verified by GC-MS, caffeine and ethylphenidate were the main adulterants found in these samples. The respective assignments of ^{1}H and ^{13}C signals are described in Table 16. The presence of isopentedrone in product 14 was also confirmed by NMR, being this the minor compound detected in this product (2.3%). Additionally, in the same product, NMR analysis allowed the identification of methylamine, which is commonly used in the synthesis of *N*-methyl cathinones, and is not detected in the GC-MS analysis due to its volatility [17]. The presence of methylamine in these products was not surprising, since it was previously reported in other works [17, 443].

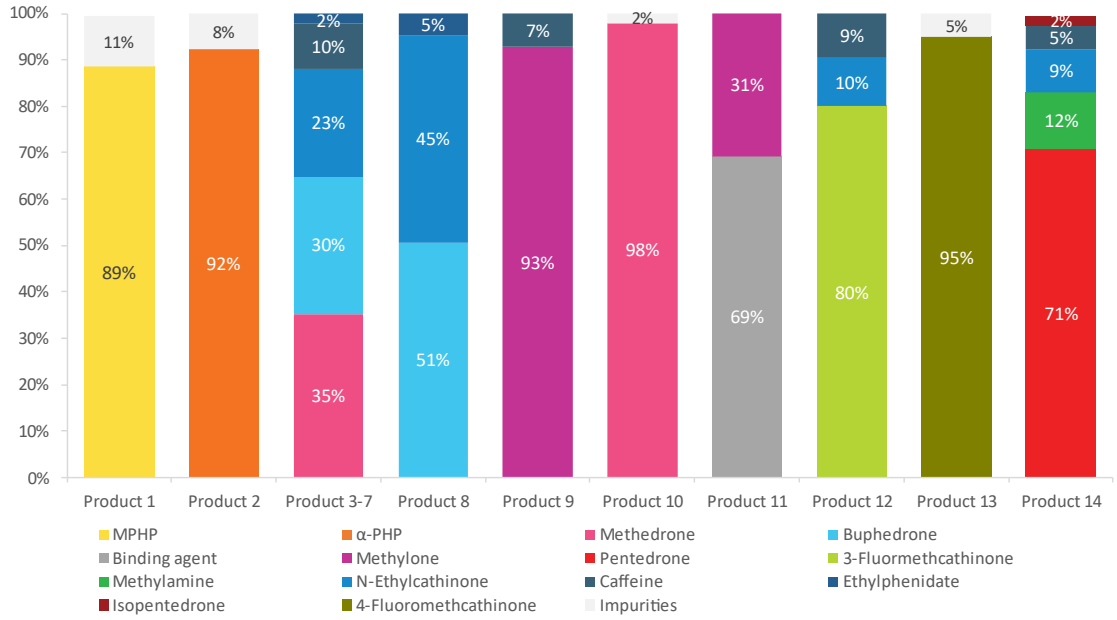

Figure 49. Relative proportions of active substances other components detected in 14 seized products.

For product 11, only 31% of the analysed tablets contained methylone in their composition. In fact, during the preparation of this sample for chromatographic and NMR analysis, an insoluble material was observed and was removed from the solution through filtration, and then analysed by ATR-FTIR. The results are present in Figure S20 and the substance was identified as microcrystalline cellulose, which was probably used as a binding agent, for direct tablet compression or even added to increase the substance amount (bulking agent) [444].

1.3. Conclusion

The present work describes the identification of 9 SCat as the key constituents found in 14 seized products.

In general, the products showed different compositions between them, although very similar for the products labelled with the same name, as in the case of bloom products (products 3 to 7).

Among the identified SCat, 7 of them, methylone, methedrone, *N*-ethylcathinone, buphedrone, pentedrone, 3-FMC and 4-FMC, belong to the "classic cathinone group", analogues of amphetamines, being considered as the first generation of SCat. Pyrovalerone derivatives, a particular class of SCat, characterized by the presence of a pyrrolidine ring in their chemical structures, were also identified in two distinct products with a high degree of purity. MPHP was found in product 1 with a purity of 89%, while α-PHP was found in product 2 with a purity of 92%. Among the adulterants, caffeine, an active ingredient commonly found in illicit drugs, was

the most frequently detected substance (57 % of the total analysed products), followed by ethylphenidate (43% of the total analysed products). Both substances are probably added to these products, since they are cheap and potentiate the stimulating effect.

Regarding the analytical techniques, the combination of ATR-FTIR, GC-MS, UHPLC-PDA and NMR techniques proved to be an effective methodology to unequivocally identify the molecular structure of the SCat present in “plant feeders”. While ATR-FTIR provided a quick and presumptive identification of the seized drugs without destroying evidence, chromatographic analysis allowed the precise identification of the substances, being an excellent tool for confirmatory tests. On the other hand, NMR spectroscopy proved to be of great importance for structural elucidation, allowing the positional isomers distinction, and the identification of compounds not detected by other techniques, such as methylamine.

Chapter 2

Determination of Synthetic Cathinones in Urine Samples by µSPEed®/UHPLC-PDA methodology

2. Introduction

SCat represent a new trend in the recreational drug market and several cases of abuse, dependence, intoxication, and deaths related to their consumption have been reported in the literature [31, 32, 414, 445, 446]. In order to detect them, comprehensive bioanalytical methods are needed and, for this reason, forensic and clinical laboratories worldwide need to constantly update their analytical procedures for the identification and quantification of these new drugs in several biological matrices [447].

Currently, chromatographic techniques play a key role to identify and accurately quantify SCat in a wide range of different biological samples, including blood [213, 276], urine [263, 264], oral fluid [272, 273], cerebrospinal fluid [448], hair [282], among others. Although recent advances in analytical instrumentation have allowed the introduction of increasingly sensitive systems, sample pre-treatment is a crucial step in the analytical process, as it allows the extraction and/or concentration of the compounds of interest, thus improving the analytical performance [222]. Among the large number of sample preparation methodologies available, LLE and SPE remain the most widely used extraction techniques for drug analysis [222]. However, both methodologies involve time-consuming procedures and need relatively large volumes of organic solvents and sample [222].

Recently, novel analytical procedures based on microextraction techniques were proposed for quantitative determination of SCat in different biological matrices [272, 274, 279]. These microextraction techniques have gained attention due to their many advantages over conventional approaches, including the minimal use of organic solvents, the low amount of sample required and the user-friendly systems. Among the available sample preparation techniques, µSPEed® has emerged as an alternative to conventional extraction techniques, which use small sorbent particles of <3 µm, instead of the 50-60 µm particles normally used in SPE and MEPS. These smaller particles, which are available in the equivalent MEPS chemistries, provide higher surface area, and thus a more efficient sorption of the analytes [319, 449]. In addition, µSPEed® cartridge architecture contains an efficient pressure-driven one-way check valve, allowing a single direction flow in every step of the extraction protocol, reducing the risk of carryover [319, 450]. Currently, several studies have shown the potential of µSPEed® extraction technique. González-Gómez et al. [451] successfully used this technique to extract atropine and scopolamine in tea and herbal tea infusions, with recovery values ranging between 94 and 106%. Casado et al. [449] also demonstrated the effectiveness of µSPEed® during the extraction of phenolic compounds from baby food samples. In this study, the authors compared the performance of µSPEed® and MEPS and rapidly concluded that µSPEed® is more sensitive,

selective and efficient for the extraction of these compounds than MEPS. Porto-Figueira et al. [450], also successfully used µSPEed® for the analysis of phenolic compounds in teas, showing good recovery values (≥ 89 %).

To date, no references have been found in the literature regarding the applicability of µSPEed® to extract SCat or other classes of NPS from biological matrices. Therefore, the main goal of this study was to evaluate the performance of µSPEed® followed by UHPLC-PDA analysis for the quantification of 8 SCat, namely MPHP, α-PHP, 4-FMC, methylone, methedrone, *N*-ethylcathinone, buphedrone and pentedrone in urine samples. For this purpose, the influence of several factors that affect µSPEed® performance, such as the nature of sorbent material, the washing and elution solvent system, the number of extraction cycles (extract–discard), the sample and eluting volume, and the sample pH, were evaluated. The method was then validated and applied to 15 urine samples from drug users who were assisted at the medical service after consuming NPS.

2.1. Materials and Methods

2.1.1. Reagents, analytical standards and materials

HPLC gradient grade MeOH and ACN were purchased from Fisher Scientific (Loughborough, UK), while FA, acetic acid and potassium dihydrogen phosphate (KH_2PO_4) were obtained from Panreac (Barcelona, Spain). Ammonium hydroxide solution (32%) was acquired from Riedel-de Haën (Seelze, Germany), while dipotassium hydrogen phosphate (K_2HPO_4) was supplied by Merck (Darmstadt, Germany). Ultrapure water (18 MΩ cm at 23°C) used for preparing the mobile phase and other aqueous solutions, was obtained from a Milli-Q water purification system (Millipore, Milford, MA, USA). The SCat standards, methylone, pentedrone, buphedrone, *N*-ethylcathinone, methedrone, MPHP and α-PHP were kindly provided by the LPC-PJ, while 4-FMC was used from product 13, since it has a high degree of purity. The IS, 3-(dimethylamino)propriophenone hydrochloride, was obtained from Sigma-Aldrich (St. Louis, MO, USA). It is important to note that all chromatographic solvents used in this work were filtered through a 0.20 µm membrane nylon filter and all solutions and samples extracts were filtered using a 0.22 µm PTFE syringe filter (BGB, Rheinfelden, Germany). The digiVOL® hand-held automated analytical syringe and the µSPEed® cartridges were kindly provided by EPREP company (Victoria, Australia).

2.1.2. Preparation of standard solutions

Individual stock standard solutions (1000 µg mL^{-1}) were prepared in MeOH and stored at −20°C in darkness. A multicomponent working standard solution of 100 µg mL^{-1} were also prepared by proper dilution of the stock standard solutions with MeOH. This working solution was used to spike a blank urine sample, in order to perform the assays for optimization of extraction conditions and for the method validation study.

2.1.3. Urine samples

Drug-free urine samples (blank samples) were obtained from 20 healthy volunteers, with ages ranging from 18 to 61 years old. These urine samples were used for µSPEed® optimization and for the method validation study. To demonstrate the applicability of the method, 15 urine samples from synthetic drug users were obtained through Unidade de Tratamento de Toxicodependência do Serviço de Saúde da Região Autónoma da Madeira (SESARAM) and analysed. All urine samples were stored in appropriate polypropylene sterile flasks at −20°C until analysis.

2.1.4. Sample preparation and optimization of µSPEed® conditions

Before the extraction procedure, urine samples were thawed at room temperature and centrifuged at 3500 rpm for 15 min. Then 600 µL of urine spiked with SCat (1500 ng mL^{-1}) and IS (500 ng mL^{-1}) was mixed with 400 µL of phosphate buffer (50 mM, pH 6).

The µSPEed® technique was performed with a digiVOL® automated analytical syringe (1.25 mL) and starting from a generic procedure (Figure 50) each parameter that affect µSPEed® performance was evaluated and optimized. For this purpose, the extraction efficiency of ten available sorbents, namely silica, C_4, C_8, C_{18}, C_{18} RPS, SCX, SAX, DVB RP, PS-DVB and PFAS was evaluated and compared. The effect of sample pH at three different levels (pH 6, 7 and 8) was also consider in this study. To optimize the number of extraction cycles (extract-discard) and sample volume, aliquots of 250, 500 and 1000 µL of pre-treated sample were pumped up and down 1, 3, 5, 8 and 10 times. In order to remove as many compounds as possible that could interfere with the analytical method, 16 washing solutions at two distinct volumes (100 and 200 µL) were evaluated. Finally, to obtain the highest extraction efficiency for the target analytes, different elution solvents, such as MeOH, MeOH (0.1% FA), MeOH (5% NH_4OH), ACN, ACN (0.1% FA) and ACN (5% NH_4OH), at three distinct volumes (250, 500 and 1000 µL) were investigated. All optimization procedures were carried out in triplicate. It is also important to note that, in all

µSPEed® assays the aspiration flow rate was automatically set to about 20 µL s^{-1} to prevent cavitation.

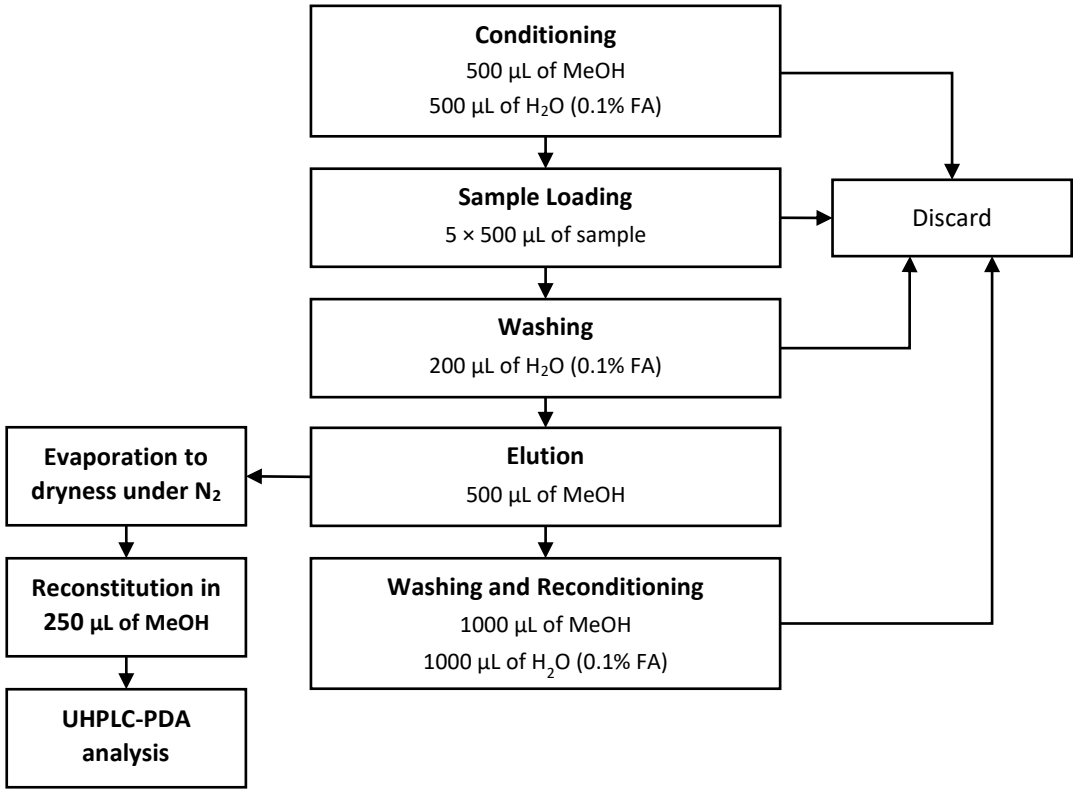

Figure 50. Diagram of the µSPEed® procedure initially used to optimize the extraction process.

2.1.5. UHPLC-PDA conditions

The analysis of SCat were carried out on a Waters Acquity H-Class UPLC system (Milford, MA, USA) equipped with a quaternary solvent manager, a column heater, a degassing system, a sample manager, and a 2996 PDA detector. After optimizing the chromatographic conditions, the best separation was achieved using an Acquity UPLC™ strength silica HSS T3 analytical column (100 mm × 2.1 mm, 1.8 µm particle size), protected with an Acquity UPLC™ HSS T3 VanGuard™ pre-column (Waters, Milford, MA, USA). Column temperature was maintained at 40°C and a binary mobile phase composed of water with 0.1% FA (solvent A) and MeOH (solvent B) at constant flow rate of 350 µL min^{-1} were used for the separation of the analytes. The gradient elution started with 90% eluent A (0-4 min), then decreased to 85% A (5-6 min), 36 % (9 min), 10% (10-10.5 min), and finally increased to 90% (11-12 min). The system was re-equilibrated with the initial composition for 3 min, prior to next injection. The samples were kept at 20°C in the sample manager, and 2 µL of extract were injected into the Waters Acquity UPLC system. The identification of target analytes was based on the comparison of retention

time and spectral characteristics with the chemical standards. For quantification purposes, the PDA detection was set to the maximum absorbance wavelength of each SCat and IS.

2.1.6. Method validation

The reliability of analytical results is of extreme importance in analytical chemistry, as it is an essential requirement for the correct interpretation of results. Thus, the validation process must include all parameters necessary to demonstrate that an analytical technique intended for the quantitative determination of one or more analytes in a given sample is suitable. Taking into account these assumptions, the analytical parameters evaluated in the validation of the µSPEed®/UHPLC-PDA methodology were selectivity, linearity, LOD and LOQ, precision, accuracy, extraction efficiency, matrix effect and analyte stability. It is important to note that the quantitative analysis was performed using the internal standardization method, which consists of adding a known substance (IS) at a constant concentration to the samples. The addition of the IS aims to correct or compensate analyte losses during sample preparation including transfer loss, adsorption loss, evaporation loss and variation in injection volume [452]. In this work, 3-(dimethylamino)propriophenone was used as IS since it has similar physicochemical properties and show similar behaviour to the analytes when extracted or run through the analytical column or detection in the analytical system.

2.1.6.1. Selectivity

Selectivity corresponds to the ability of an analytical method to distinguish a particular analyte in a complex matrix without interference from other elements that may be present in the sample. To evaluate the selectivity of the method, drug-free urine samples from 20 healthy volunteers were collected and randomly mixed in groups of 5, to obtain 4 pooled urine samples. Then each pool was analysed by µSPEed®/UHPLC-PDA methodology and compared with the same pool fortified with SCat and with a standard solution of SCat. The selectivity of the method was assessed by the absence of interfering peaks at the retention times of the SCat.

2.2.6.2. Linearity

Linearity is defined as the ability of the analytical method to provide results directly proportional to the concentration of the analyte, within a given working range. For most analytical techniques, linearity is expressed as the correlation between instrument response (e.g. chromatographic peak area or peak height) and analyte concentration, and can be graphically represented by a calibration curve.

To evaluate the linearity of the method a blank urine sample spiked at final concentrations ranging from 150 to 1500 ng mL^{-1}, for each SCat was prepared and analysed by the previously described procedure. The concentration range used for this study were selected according to the sensitivity of the UHPLC-PDA system as well as the expected amount in the samples. Calibration curves were obtained by plotting the peak area ratio between each analyte and the IS (peak $area_{analyte}$/peak $area_{IS}$) against the analyte concentration. The line that best fits the set of experimental results was carried out by using the least squares method.

The coefficients of correlation (R) and determination (R^2) are frequently used to express the linearity of the calibration curve, and these should be close to 1 to guarantee a better adjustment of the results (less dispersion of the set of experimental points and less uncertainty of the estimated regression coefficients). Several authors considered this evidence sufficient to conclude that the calibration curve is linear [452]. However, the magnitude of such coefficients only indicates the degree of adjustment of the data to the calibration curve, which by themselves are not enough to establish linearity, and for this reason, some statistical tests need to be performed to demonstrate the linearity of the method [453]. In this sense, the Mandel's fitting test and residual analysis, should be part of this study.

The Mandel's fitting test compare the fit of two models: the fit of a linear model with the fit of the nonlinear model (e.g. polynomial second-order function). For each model, the residual standard deviation is determined using the follow equations:

$$S_{y/x} = \sqrt{\frac{\sum(y_i - \hat{y}_{i1})^2}{N-2}} \quad (4)$$

$$S_{y^2} = \sqrt{\frac{\sum(y_i - \hat{y}_{i2})^2}{N-3}} \quad (5)$$

Where, $S_{y/x}$ is the residual standard deviation calculated for the linear model, S_{y^2} is the residual standard deviation calculated for the nonlinear model (polynomial of second degree), y_i is the experimental signal value for a given concentration of analyte, $\hat{y}_i$ is the estimated response for a given concentration of analyte obtained by the linear calibration function ($\hat{y}_{i1}$) or nonlinear calibration function ($\hat{y}_{i2}$) and *N* is the number of calibration points.

The difference of variances (DS^2) is then determined using the residual standard deviation $S_{y/x}$ and S_{y^2} through the equation 6.

$$DS^2 = (N-2) \times S^2_{y/x} - (N-3) \times S^2_{y^2} \quad (6)$$

Where, $S^2_{y/x}$ is the linear residual variance, $S^2_{y^2}$ is the nonlinear residual variance from the second-order calibration function and *N* is the number of calibration points.

The test value (*TV*) is then calculated using the equation 7 and compared with the value obtained from the table F (f_1 = 1, f_2 = N – 3) for a determined confidence level (e.g. 95%):

$$TV = \frac{DS^2}{S_{y^2}^2} \quad (7)$$

If *TV* ≤ *F*, the second-order calibration function will not provide a significant better fit, meaning that the calibration function is linear. Otherwise, i.e. TV > F, the calibration function is nonlinear. In this case, reducing the working range should be attempt in order to maintain sufficient linearity. If this is not possible, a nonlinear calibration function must be used [454].

Residual analysis is another useful tool used to assess the appropriateness of a linear regression model. It is based on the evaluation of the distance between the experimental y_i values and the estimated $\hat{y}_i$ values of the calibration curve [454].

$$d_i = \hat{y}_i - y_i \quad (8)$$

A graphic representation of the residual values will allow to detect problems in the curve fitting such as, for example, deviations from linearity, presence of atypical samples, heteroscedasticity (occurrence of non-constant variances in the residuals), dependence, among other errors [453]. A well-fitting calibration curve should present errors with uniform distribution, constant variance (homoscedasticity) and absence of atypical samples [453].

Therefore, during the validation of the analytical method, the linearity of the calibration curve was evaluated based on R^2, residual analysis and Mandel's fitting test.

2.1.6.3. Limit of detection (LOD) and limit of quantification (LOQ)

LOD and LOQ are two parameters that play a very important role in the validation of analytical procedures since they reflect the ability of the method to detect and quantify low concentrations of an analyte. LOD is generally defined as the lowest amount of analyte present in a sample that can be reliable detected but not necessarily quantified by a particular analytical method, while LOQ expresses the lowest concentration of analyte that can be accurately and precisely quantified [452, 455]. Both limits are expressed in concentration units and can be determined by signal to noise ratio or by calibration curve parameters. In this study, LOD and LOQ were established based on the calibration curve parameters, according to the following formulas:

$$LOD = \frac{3.3 \times S_{y/x}}{b} \quad (9)$$

$$LOQ = \frac{10 \times S_{y/x}}{b} \quad (10)$$

Where, $S_{y/x}$ represents the residual standard deviation and *b* the slope of the calibration curve.

2.1.6.4. Precision

Precision of an analytical method expresses the degree of agreement between a series of measurements of an analyte under the same conditions [452]. It is usually specified in terms of standard deviation (SD) or relative standard deviation (RSD) and can be defined in terms of repeatability, intermediate precision and reproducibility [453]. Repeatability or intra-day precision expresses the precision of a method under the same operating conditions, i.e. on the same sample, by the same analyst, in the same laboratory, and during the same series of tests carried out in a short period of time. Intermediate precision, also known as inter-day precision, defines the precision within the same laboratory for measurements obtained by different analysts, different days, or by different equipment [453]. On the other hand, reproducibility expresses the precision between measurement results obtained with the same method, on identical test items, but in different laboratories, with different operators, using different equipment [453]. In this work, the precision was evaluated in terms of repeatability and intermediate precision. To perform this study, blank urine samples spiked with SCat were prepared at three distinct concentration levels, namely low level (150 ng mL^{-1}), medium level (750 ng mL^{-1}) and high level (1500 ng mL^{-1}). Repeatability was determined by performing five replicate analyses of spiked samples for each concentration level on the same day, while intermediate precision was accessed through the analysis of three replicate of each concentration level during five non-consecutive days (n = 15). All samples were prepared freshly on the day of analysis, and the results were expressed as RSD, also known as coefficient of variation (CV).

For each compound and concentration level, the estimates of variance of repeatability (S_r^2) and intermediate precision (S_i^2) were determined by the analysis of variance (ANOVA) test. The expressions required for the calculation are represented in tables 17 and 18.

Table 17. Formulas used in the One-way ANOVA test [456, 457].

Source	Sum of Squares (*SS*)	Mean Squares (*MS*)	Degrees of Freedom
Between groups	$SS_{run} = n\sum_{i=1}^{p}(\overline{X}_i - \overline{\overline{X}})^2$	$MS_{run} = \frac{n\sum_{i=1}^{p}(\overline{X}_i - \overline{\overline{X}})^2}{p-1}$	$p-1$
Within groups	$SSr = \sum_{i=1}^{p}\sum_{j=1}^{n}(X_{ij} - \overline{X}_i)^2$	$MSr = \frac{\sum_{i=1}^{p}\sum_{j=1}^{n}(X_{ij} - \overline{X}_i)^2}{p(n-1)}$	$p(n-1)$
Total	SS_T	$MS_T = \frac{SS_T}{n-1}$	$pn-1$

Where p is the number of analytical sequences for each concentration level (one sequence per day); n is the number of replicates performed in each sequence; X_{ij} represents an individual replicated (replicated j) obtained in sequence i; $\overline{X}_i$ represents the average of n replicates obtained in sequence i; $\overline{\overline{X}}$ is the average of the averages of p sequences.

Table 18. Calculation of variance for the experimental model used in the study of repeatability and intermediate precision [456, 457].

Variance	Expression
Repeatability Variance ($\boldsymbol{S_r^2}$)	$S_r^2 = MS_r$
Precision Variance ($\boldsymbol{S_{run}^2}$)	$S_{run}^2 = \frac{MS_{run} - MS_r}{n}$
Intermediate Precision Variance ($\boldsymbol{S_i^2}$)	$S_i^2 = (S_r^2) + (S_{run}^2)$

The determination of the coefficient of variation of repeatability (CV_r), expressed in percentage and defined as the ratio of the standard deviation of repeatability (S_r) in relation to the mean value ($\overline{X}$) (equation 11), allowed estimate the repeatability of the analytical method for each concentration range.

$$CV_r = \frac{S_r}{\overline{\overline{X}}} \times 100 \quad (11)$$

Likewise, the estimate of the coefficient of variation of the intermediate precision (CV_{si}) given by equation 12, is also expressed in percentage.

$$CV_{si} = \frac{S_i}{\overline{\overline{X}}} \times 100 \quad (12)$$

Where, S_i is the standard deviation of intermediate precision and $\overline{X}$ the mean of the obtained results.

2.1.6.5. Accuracy

Accuracy is one of the most important validation parameters, since it shows the degree of agreement between the test results generated by the method and the true value [452]. It is a measurement of the systematic errors affecting the method and there are several ways to determine the accuracy of a method, including the analysis of certified reference materials (CRM), the comparison of results with reference methods or through interlaboratory tests [455, 458]. However, when a CRM or a reference procedure is not available and given the impossibility of interlaboratory tests, the accuracy of the analytical method can be evaluated through the absolute recovery values obtained from the analysis of fortified samples with a known

concentration of analyte [459]. It is recommended the determination of the accuracy by analysing samples spiked at three different concentrations (low, medium, high) covering the entire working range [455].

For the evaluation of this validation parameter, the procedure used in this work was similar to that of the intermediate precision (section 2.2.6.4). After determination of the relative areas for the different analytes in relation to the IS, accuracy was determined as relative bias, for each concentration level or as percentage recovery. Bias reflects the difference between observed measurements and a true value and can be easily determined by the equations 13 and 14.

$$Bias = \bar{x} - x_{ref} \tag{13}$$

$$Relative\ Bias\ (\%) = \frac{(\bar{x} - x_{ref})}{x_{ref}} \times 100 \tag{14}$$

Where, $\bar{x}$ is the average of results obtained and x_{ref} is the reference value.

The recovery of the method (R_i) was determined in percentage by the ratio between the observed value (C_{obs}) and the expected value (C_{fort}) as shown in equation 15. Then, the average recovery ($\bar{R}$) was calculated for each concentration level, according to equation 16.

$$R_i\ (\%) = \frac{C_{obs}}{C_{fort}} \times 100 \tag{15}$$

$$\bar{R} = \frac{\sum_{i=1}^{p} R_i}{p} \tag{16}$$

Where, R_i is the average recovery of *n* replicates obtained under repeatability conditions, and p represents the number of groups (days).

For each concentration level, the *t*-student test was applied in order to verify whether the mean recovery was statistically different from the unit (which corresponds to 100%) [456]. The t_{exp} was determined by equation 17 and compared against the value obtained from the two-tailed critical value (t_{crit}), for $p - 1$ degrees of freedom and 95% of confidence level.

$$t_{exp} = \frac{|1 - \bar{R}|}{U_{\%\bar{R}}} \tag{17}$$

$$U_{\%\bar{R}} = \frac{S_{exp}}{\sqrt{p}} \tag{18}$$

Where, $U_{\%\bar{R}}$ represents the uncertainty in average recovery, S_{exp} is the standard deviation of p values of R_i obtained under intermediate precision conditions.

If $t_{exp} \leq t_{crit}$, then $\bar{R}$ is not significantly different from 100% and the relative standard uncertainty ($U_{\bar{R}}$) can be determined by the following equation:

$$U_{\bar{R}} = \frac{U_{\%\bar{R}}}{\bar{R}} \quad (19)$$

On the other hand, if $t_{exp} > t_{crit}$, then $\bar{R}$ is significantly different from 100% and the $U_{\bar{R}}$ is calculated according to equation 18.

$$U_{\bar{R}} = \frac{\sqrt{(U_{\%\bar{R}})^2 + \left(\frac{1 - \bar{R}}{k}\right)^2}}{\bar{R}} \quad (20)$$

Where, k is the coverage factor, which was used to calculate the expanded uncertainty.

2.1.6.6. Extraction efficiency

Extraction efficiency is defined as the percentage of the analyte removed from a sample solution after extraction. The process is more efficient the closer to 100%. In order to evaluate the extraction efficiency of the method, two sets of blank urine samples were prepared. In the first set, the samples were spiked with the analytes under study at three concentration levels, namely low level (150 ng mL^{-1}), medium level (750 ng mL^{-1}) and high level (1500 ng mL^{-1}), being later subjected to extraction. In the second set, the blank urine samples were subjected to extraction and the resulting extracts were spiked with SCat in the three concentration ranges mentioned above. The extraction efficiency was then calculated according to the following equation:

$$EE\ (\%) = \frac{C_{BE}}{C_{AE}} \times 100 \quad (21)$$

Where, EE is the extraction efficiency, C_{BE} represents the concentration of SCat spiked before µSPEed® extraction and C_{AE} represents the concentration of SCat spiked after µSPEed® extraction.

2.1.6.7. Matrix effect

Matrix effect is the effect on an analytical method caused by all components of the sample except the analyte to be analysed [460]. This effect can dramatically influence analysis performance, and it is commonly observed as a loss in response, which produces an underestimation of the measured values of the target analyte, or as an increase in response, producing an overestimated result. The evaluation of the matrix effect can be easily performed by comparing a solvent-based calibration curve with the matrix-matched calibration curve. The slope of calibration analysed in the matrix is then divided by the slope of calibration curve prepared in the solvent and the result is expressed in percentage, according to the following equation:

$$ME\ (\%) = \frac{m_{Matrix}}{m_{Solvent}} \times 100 \quad (22)$$

Where, ME represents the matrix effect, m_{Matrix} is the slope of calibration curve prepared in matrix and $m_{Solvent}$ is the slope of calibration curve prepared in solvent.

In this work, matrix effect was determined by comparing the slopes of standard curves dissolved in solvent and matrix-matched calibration curves. For this purpose, seven different concentrations of standards were analysed in solvent and the resulting calibration curves were compared with the calibration curves prepared in matrix. If ME > 100% matrix results in overestimation, otherwise, i.e. ME < 100%, tested matrix leads to signal suppression.

2.1.6.8. Analyte stability

The stability of a drug in biological matrices is an important part of bioanalytical method validation, so that analytical findings can be properly interpreted [461]. Often biological samples cannot be assayed immediately after collection for several reasons, including laboratory workload, instrumentation downtime, delay in shipment, or if a second analysis or a counter-test is requested after some time [462]. This delay in the analysis can be a problem if the analytes are not stable in the biological samples [462]. In this context, a stability study was carried out in the present work, to investigate the effect of temperature on the stability of SCat in urine samples. For this purpose, a blank urine sample was fortified with SCat at three concentration levels, namely low level (150 ng mL^{-1}), medium level (750 ng mL^{-1}) and high level (1500 ng mL^{-1}), and then aliquoted into 1.5 mL eppendorf tubes and storage over a maximum period of 3 months at four different temperatures (−80°C, −20°C, 4°C and room temperature). On the day of analysis, IS solution was added and samples were analysed as described previously. Each sample was analysed in triplicate.

2.2. Results and Discussion

2.2.1. Optimization of µSPEed®

To maximize µSPEeD® extraction efficiency, the influence of several experimental parameters including the nature of sorbent material, sample pH, sample volume, number of extraction cycles, and washing and elution conditions, were evaluated. The entire optimization process was performed using a blank urine sample spiked with target analytes at 1500 ng mL^{-1}. The extraction efficiency was determined by the average total peak area response observed on UHPLC-PDA.

2.2.1.1. Nature of sorbent material and sample pH

The selection of an appropriated sorbent phase is of major importance to achieve a good extraction efficiency. In this context, the performance of ten commercially available solid phases for µSPEeD®, including silica phases functionalized with butyl (C_4), octyl (C_8) and octadecyl (C_{18}) groups, unmodified silica (SIL), ion exchange resins (SCX and SAX), and polymeric phases (DVB-RP, PS-DVB and PFAS), as well as an octadecyl-polymeric base sorbent (C_{18} RPS) were evaluated for their performance in the extraction of SCat from urine samples. The influence of sample pH on the extraction process was also evaluated for each tested sorbent material. Figure 51 shows the obtained results in the optimization of the various sorbents at different pH.

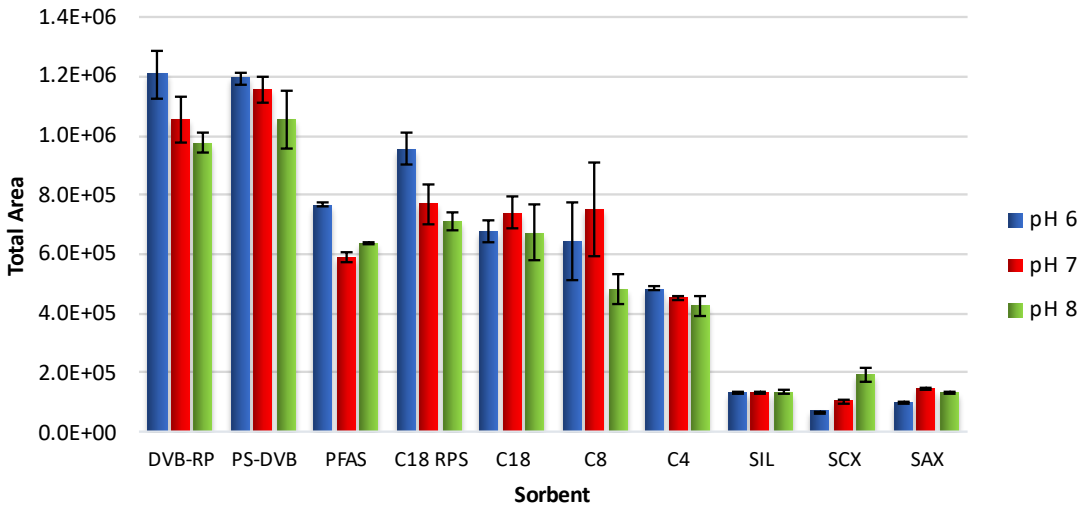

Figure 51. Comparison of the performance of 10 different sorbents materials and the influence of sample pH on the extraction efficiency of SCat in urine by µSPEeD®. Values expressed as average total area ± standard deviation (n= 3).

The performance of each sorbent material was evaluated in terms of intensity of the response (peak area) and reproducibility. The results of each sorbent phase in relation to the individual compounds are presented in Figure S21 (supporting information). According to the results, DVB-RP and PS-DVB sorbents provided the highest chromatographic response, while SIL, SCX and SAX provided lower or even unsatisfactory retention for the selected SCat. Generally, C_2–C_{18} phases are suitable for lipophilic analytes, while polymeric phases, such as DVB with ionic groups chemically bounded (ionic exchange) or even the mixed mode phases are suitable for polar analytes, such as acidic and basic compounds [463]. SCat are characterized as small polar molecules bearing in their structure an aromatic moiety and an amine group. Commonly, DVB and PS-DVB sorbents have a hydrophobic structure constituted by several benzyl groups, which

can interact with the analytes through the Van der Waals forces and π-π interactions of the aromatic rings. Although PS-DVB is able to display the π-π type of interactions, the small pores of this sorbent may have probably allowed for improved extraction of the aforementioned compounds, as in the work developed by Liu et al. [464] during the extraction of phenylalanine, tryptophan and adenine. González-Gómez et al. [451] also demonstrated that PS-DVB phase was the best sorbent to extract atropine and scopolamine by µSPEeD® from tea and tea infusions.

Regarding the pH of the sample, it was found that the retention of analytes is favored at pH values between 6 and 7, while at higher pH values retention is not as efficient. In this context, the best extraction conditions were obtained with PS-DVB sorbent and a pH of sample 6.

2.2.1.2. Number of extraction cycles and sample volume

In µSPEeD®, the extraction efficiency is influenced by the number of loading cycles or extraction cycles. The sample can be drawn through the needle into the syringe once or several times (cycles), allowing the retention of the analytes [450]. Commonly, when the sample passes several times through the sorbent, the interaction of the analytes with the solid phase is greater, enabling a higher extraction efficiency. It is important in this step to maintain a slow flow rate through the device to allow sufficient interaction between the analyte and the binding/retention sites in the sorbent.

As in MEPS, the multiple extraction cycles in µSPEeD® can be carried out from the same aliquot (draw–eject in the same vial) or by drawing up from an aliquot and discarding as waste (extract–discard) [450]. The first option was selected in this work, and the optimization of the number of extraction cycles and sample volume was performed by testing 1, 3, 5, 8 and 10 extraction cycles on aliquots of 250, 500 and 1000 µL of spiked urine samples. Figure 52 shows the obtained results.

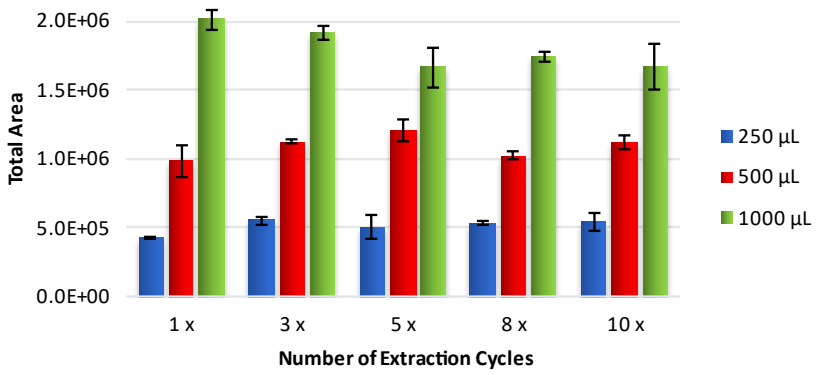

Figure 52. Influence of the number of extraction cycles and sample volume on µSPEeD® performance.

According to the results, it was found that when the number of cycles increased the extraction efficiency increased slightly, especially for the lower sample volumes (250 and 500 µL). However, for a larger sample volume (1000 µL), a single extraction cycle was sufficient for the sorbent to reach its saturation point and no significant improvement was expected from this point. In fact, there was a decreasing trend in extraction efficiency from this point, which may indicate that analytes with weak interactions by the sorbent may be partially eluted and lost during sample withdrawal. This trend was verified for almost all analytes (Figure S22 supporting information), and for this reason 1 × 1000 µL was selected as it provided the highest chromatographic area.

2.2.1.3. Washing conditions

The selection of the best washing conditions is a critical factor in the extraction process, since the analytes cannot be eluted together with the interferents and must remain retained in the solid phase. This step is usually performed with the same solvent used to equilibrate the sorbent in the first step [465]. However, the optimization of this parameter is a necessary requirement to eliminate the largest number of compounds from the matrix that can interfere with the analytical method. In this context, several washing solutions were tested in two different volumes (100 and 200 µL) in order to obtain the best washing conditions. Table 19 shows the different solutions tested.

Table 19. Washing solutions tested for µSPEeD® optimization.

Test Number	Washing solutions
1	H_2O
2	H_2O (0.1% FA)
3	Acetic acid (0.1M)
4	H_2O:MeOH (95:5 v/v)
5	H_2O:MeOH (90:10 v/v)
6	H_2O:MeOH (80:20 v/v)
7	H_2O:ACN (95:5 v/v)
8	H_2O:ACN (90:10 v/v)
9	NH_4OH (0.1%)
10	NH_4OH (2%)
11	NH_4OH (5%)
12	H_2O + H_2O:MeOH (95:5 v/v)
13	H_2O + H_2O:MeOH (90:10 v/v)
14	H_2O + H_2O:MeOH (80:20 v/v)
15	H_2O + H_2O:ACN (95:5 v/v)
16	H_2O + H_2O:ACN (90:10 v/v)
17	Without washing

Abbreviations: ACN - acetonitrile, FA - formic acid, MeOH - methanol.

The performance of each washing condition was evaluated in terms of intensity of total peak area and reproducibility (Figure 53A). In addition, a recovery study was performed to establish the best washing conditions and the results are presented in Figure 53B.

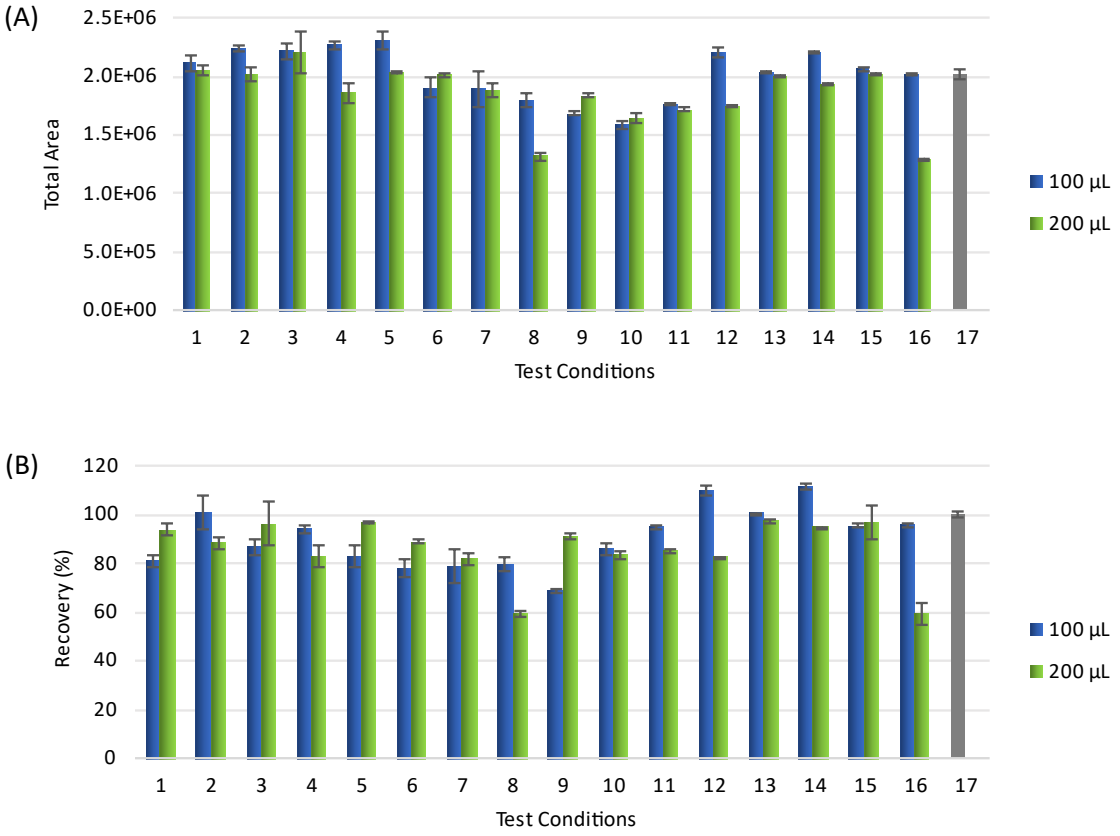

Figure 53. Influence of the washing conditions on µSPEeD® performance. (A) Total area and (B) recovery study obtained for each washing condition.

After the chromatographic analysis of each conditions (Figure S23 supporting information) and taking into account the results presented above, the best washing conditions was 200 µL of water, followed by 200 µL of a solution of H_2O:ACN (95:5 v/v) (condition 15). This solution removed most of the interferences in the matrix and provided a good recovery of the analytes (96.7% ± 7.2%). Figure 54 shows the chromatograms obtained from a urine sample spiked with SCat (A) without the sorbent washing step during µSPEed® extraction and (B) with the best washing conditions.

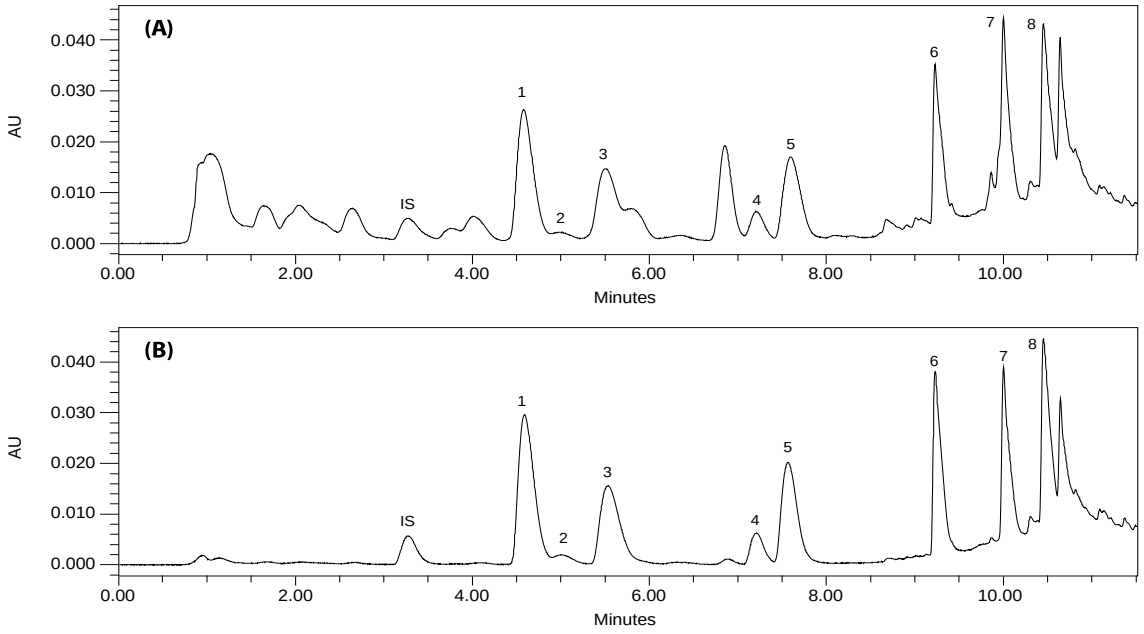

Figure 54. Typical chromatograms obtained by UHPLC-PDA from a urine sample spiked with SCat (A) without the sorbent washing step during µSPEed® extraction and (B) with the washing step constituted by 200 µL H_2O, followed by 200 µL of H_2O:ACN (95:5 v/v). Peak identification: (1) 4-FMC, (2) methylone, (3) *N*-ethylcathinone, (4) methedrone, (5) buphedrone, (6) pentedrone, (7) α-PHP, (8) MPHP and (IS) internal standard.

2.2.1.4. Elution conditions

The selection of the elution solvents is an important parameter since the target analytes should be efficiently eluted in the smallest volume possible. In this work, several elution solvents including MeOH, MeOH (0.1% FA), 5% NH_4OH in MeOH, ACN, ACN (0.1% FA) and 5% NH_4OH in ACN, were evaluated. For determination of suitable volume of elution solvent, different volumes (250, 500 and 1000 µL) were tested and the results are shown in Figure 55. For the elution volumes 500 and 1000 µL, the eluate was evaporated to dryness under a gentle stream of nitrogen and dissolved in 250 µL of MeOH.

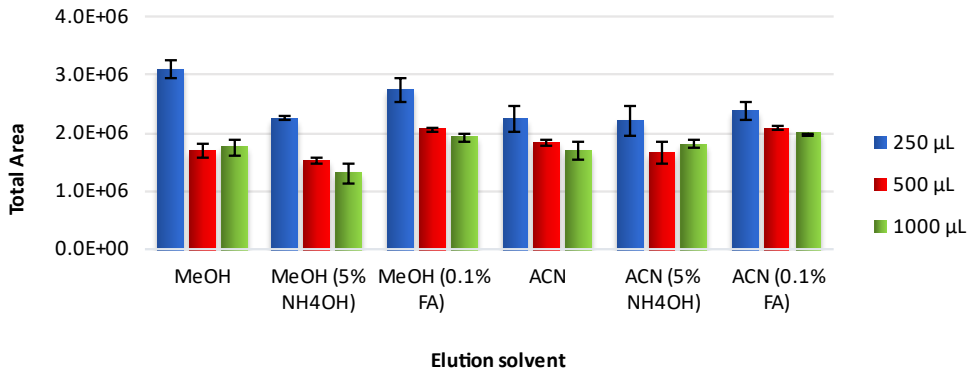

Figure 55. Influence of different elution conditions on the extraction efficiency of µSPEed®.

The results indicate that the best extraction efficiency was obtained using 250 µL of MeOH. This elution condition was the best for almost all analytes (Figure S24 supporting information). For higher elution volumes (500 and 1000 µL) it was observed a decreased in the total area, which may indicate that the analytes can be partial lost during the evaporation and reconstitution process. In this sense, 250 µL of MeOH was selected as elution solvent as it provided the highest chromatographic area.

Therefore, the best µSPEeD® experimental conditions for analysis of the studied SCat were as follows: PS-DVB sorbent, one draw–eject cycle (1 × 1000 µL of sample), sample pH of 6.0, a washing step constituted by 200 µL H_2O, followed by 200 µL of H_2O:ACN (95:5 v/v) and finally the elution of the analytes carried out with 250 µL of MeOH.

2.2.2. Method validation

The good performance of any analytical technique essentially depends on two parameters: the quality of the instrumental measurements and the statistical reliability of the calculations involved in their processing [453]. For this purposed, the optimized µSPEed®/UHPLC-PDA methodology was validated in terms of selectivity, linearity, LOD and LOQ, precision, accuracy, extraction efficiency, matrix effect and analyte stability.

2.2.2.1. Selectivity

Method selectivity reflects the ability to identify the target analytes in the presence of matrix components. This parameter was evaluated through analysis of peak shape, retention time and chromatographic purity of the spectrum, in order to detect possible interferences. The analysis of pool urine samples revealed the presence of interferences in the same retention times of some target analytes (Figure S25 supporting information).

To overcome this issue, the UHPLC mobile phase gradient was slightly adjusted, in order to separate these interferences from the target analytes. In this sense, the best separation was achieved with following gradient elution: 90% eluent A (0-4 min), then decreased to 85% A (5-6 min), 60 % (9-10 min), 45% (11-12 min), 30% (13 min) and finally increased to 90% (14-15 min). Then each pool was analysed with the best separation conditions and the results are presented in Figure 56. It is possible to verify that all SCat are clearly separated and do not coelute with interfering compounds present in the samples, thus demonstrating the selectivity of the method.

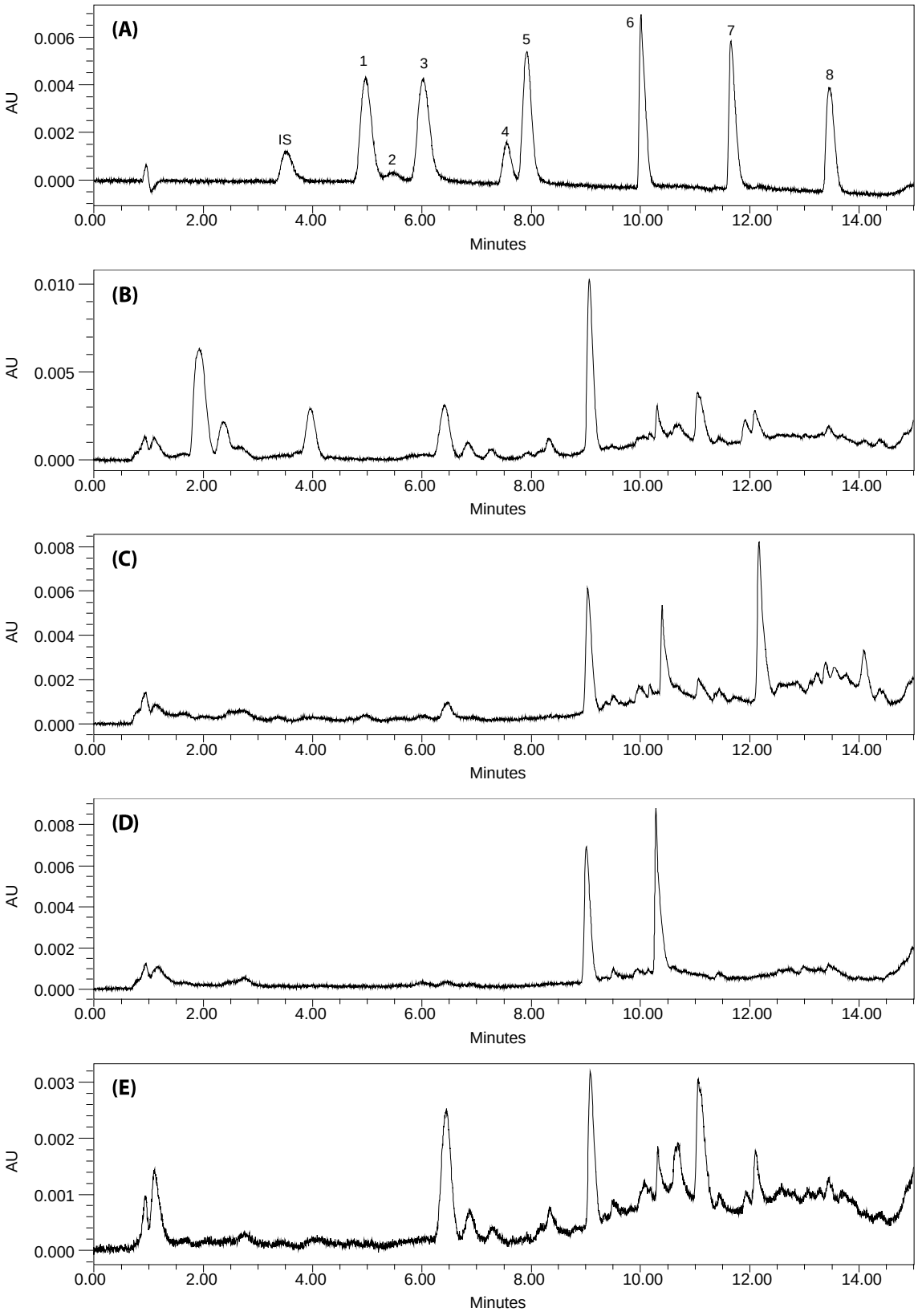

Figure 56. Chromatograms of a typical µSPEeD®–UHPLC/PDA procedure of a (A) SCat standard solution, and (B-E) pooled blank urine samples. Peak identification: (IS) internal standard, (1) 4-FMC, (2) methylone, (3) *N*-ethylcathinone, (4) methedrone, (5) buphedrone, (6) pentedrone, (7) α-PHP and (8) MPHP.

2.2.2.2. Linearity

For linearity evaluation, 8 calibration curves were performed, one for each analyte, with 7 calibration points, in a concentration range from 150 to 1500 ng mL^{-1}. Each calibration curve was obtained in triplicate by plotting the peak area ratio between each analyte and the IS against analyte concentration (peak $area_{analyte}$/peak $area_{IS}$ vs. concentration). Once the regression equation is determined, the linearity of the method can be demonstrated through the statistical study of the parameters of the calibration curve. Commonly, in linear calibration method, the slope should be statistically different from 0, the intercept should not be statistically different from 0 and the regression coefficient should not be statistically different from 1 [452]. In case of having a significant non-zero intercept, the accuracy of the method must be demonstrated [452]. On the other hand, in addition to regression analysis, the application of the Mandel's fitting test and the residual analysis should be part of this study. Table 20 summarises the obtained results for the linearity study, while the statistical regression and residual analysis are presented in supporting information.

According to the results, the linear regression analysis by the least squares method showed values of *R* and R^2 greater than 0.995 for all SCat, the slopes were statistically different from 0, and the intercept was close to 0, considering a 95% confidence interval. Regarding to the residual analysis (supporting information), no trends were observed, i.e. the residues showed an uniform distribution presenting a deviation ≤10%, thus guaranteeing the homoscedasticity of the results. Moreover, the results of the Mandel's fitting test, showed that the *TV* values calculated for a 95% confidence level were lower than those reported in the tabulated F, indicating that the linear model provided the best adjustment to the points of the calibration curve, thus proving the linearity of the analytical method.

2.2.2.3. LOD and LOQ

Commonly, the calibration curve parameters, such as slope and residual standard deviation can be used to estimate the LOD and LOQ of the assay. In this sense, the LOD and LOQ were calculated based on equations 6 and 7 and the results are presented in Table 21.

According to the results, it was found that the LOQ values obtained for almost all SCat were higher than the lowest standard of the calibration curve (150 ng mL^{-1}). However, according to the Food and Drug Administration (FDA) [466], the lowest standard of the calibration curve can be accepted as the lower limit of quantification (LLOQ) if the response produced by the analyte is at least 5 times the baseline response obtained by the blank and if the analyte peak is identifiable, discrete and reproducible with a precision of up to 20% and an accuracy ± 20% of

Table 20. Linearity results obtained for determination of SCat from urine samples by µSPEed®/UHPLC-PDA methodology.

Compound	Rt (min)[a]	λ_{max} (nm)[b]	Conc. range (ng mL^{-1})	Linear				Polynomial				Mandel's test	
				Regression equation	R[c]	R^2[d]	$S_{y/x}$[e]	Regression equation	R	R^2	S_{y^2}[f]	TV[g]	$F_{(0.95;1;N-3)}$[h]
4-FMC	4.95	254	150 - 1500	$y = 0.0037x - 0.2758$	0.9993	0.9987	0.0752	$y = 3\times10^{-7}x^2 + 0.0032x - 0.1575$	0.9997	0.9994	0.0539	5.74	7.71
Methylone	5.50	320	150 - 1500	$y = 0.0021x - 0.1353$	0.9992	0.9984	0.0462	$y = -9\times10^{-8}x^2 + 0.0023x - 0.1751$	0.9994	0.9987	0.0469	0.86	7.71
N-Ethylcathinone	6.02	250	150 - 1500	$y = 0.0043x - 0.4333$	0.9995	0.9990	0.0736	$y = 2\times10^{-7}x^2 + 0.0040x - 0.3550$	0.9996	0.9993	0.0704	1.47	7.71
Methedrone	7.52	289	150 - 1500	$y = 0.0049x - 0.3162$	0.9998	0.9996	0.0547	$y = -3\times10^{-8}x^2 + 0.0049x - 0.3298$	0.9998	0.9996	0.0606	0.06	7.71
Buphedrone	7.93	251	150 - 1500	$y = 0.0038x - 0.2104$	0.9995	0.9990	0.0652	$y = -1\times10^{-7}x^2 + 0.0040x - 0.2615$	0.9996	0.9992	0.0674	0.68	7.71
Pentedrone	10.0	251	150 - 1500	$y = 0.0023x + 0.0133$	0.9987	0.9973	0.0669	$y = -2\times10^{-7}x^2 + 0.0027x - 0.0850$	0.9993	0.9987	0.0521	4.23	7.71
α-PHP	11.7	253	150 - 1500	$y = 0.0023x - 0.0870$	0.9987	0.9973	0.0668	$y = 1\times10^{-7}x^2 + 0.0021x - 0.0293$	0.9989	0.9978	0.0677	0.86	7.71
MPHP	13.6	265	150 - 1500	$y = 0.0027x + 0.1421$	0.9991	0.9982	0.0639	$y = 2\times10^{-7}x^2 + 0.0024x + 0.2338$	0.9995	0.9991	0.0511	3.83	7.71

[a] Retention time.
[b] Maximum absorbance values obtained in the PDA system detection.
[c] Correlation coefficient.
[d] Determination coefficient.
[e] residual standard deviation calculated for the linear model.
[f] residual standard deviation calculated for the nonlinear model (polynomial of second degree).
[g] Test value.
[f] Value of Fisher theoretical determined for 95% of confidence.

Table 21. LOD and LOQ values calculated for each SCat by µSPEed®/UHPLC-PDA.

Compound	LOD (ng mL^{-1})	LOQ (ng mL^{-1})
4-FMC	67.3	204.1
Methylone	72.4	219.4
N-Ethylcathinone	56.9	172.5
Methedrone	36.8	111.6
Buphedrone	56.9	172.4
Pentedrone	95.3	288.9
α-PHP	94.6	286.6
MPHP	77.1	233.7

the nominal concentration value. Considering this criterion and after the determination of the precision and accuracy of the method (see section 2.3.2.4), the lowest standard of the calibration curve was defined as the LLOQ for all SCat under study.

2.2.2.4. Precision and Accuracy

Precision and accuracy are considered two of the most relevant validation parameters, as they allow the estimation of errors and variations associated with the analytical results. In this work, the precision was assessed in terms of repeatability and intermediate precision. To perform this study, blank urine samples spiked with SCat were prepared at three different concentration levels, namely low, medium, and high levels, covering the entire working range. For each of these concentrations, five replicates were performed in the same day to assess repeatability, while for intermediate precision and accuracy, three replicates of each level were analysed for five non-consecutive days (n = 15). The results of this study are described in the Table 22.

According to the results, it was possible to verify that the precision was very satisfactory, with values below the maximum described in guidelines (CV ≤ 20% at LLOQ and CV ≤ 15% for the others concentration levels) [466]. The repeatability values ranged from 0.74 to 7.28% while intermediate precision values varied between 0.97 and 18.2%. As with the precision tests, the bias values obtained in the accuracy test remained within the regulated values of ±15% of the nominal concentrations except for the LLOQ which should be up to ±20%. The analytical method also showed good values for recovery for all SCat, ranging between 85.1 (pentedrone) and 107.9% (MPHP). Additionally, the presence of systematic errors (trends) was also investigated for this parameter. For this purpose, the *t*-student test was applied, in order to verify if the average recovery was statistically different from the unit. The results revealed that $t_{exp} < t_{crit}$ for

Table 22. Results obtained for the study of precision and accuracy of the analytical method.

Compound	Conc. (ng mL^{-1})	Repeatability CV_r (%)	Intermediate precision CV_{Si} (%)	Accuracy				
				Bias (%)	$\bar{R}$	t_{exp}	t_{crit} (N-1, 0.95)	$U_{\bar{R}}$
4-FMC	150	2.73	7.07	6.38	106.4	2.00	2.78	0.03
	750	4.39	4.44	-2.30	97.7			0.01
	1500	0.97	0.97	0.51	100.5			0.003
Methylone	150	5.30	15.1	-0.28	99.7	0.04	2.78	0.06
	750	5.60	6.93	0.10	100.1			0.02
	1500	1.80	1.87	-0.02	100.0			0.01
N-Ethylcathinone	150	4.65	10.6	5.62	105.6	1.21	2.78	0.04
	750	3.07	4.58	-2.02	98.0			0.02
	1500	1.41	1.42	0.45	100.4			0.004
Methedrone	150	5.49	8.62	-7.94	92.1	2.62	2.78	0.03
	750	3.83	3.92	2.86	102.9			0.01
	1500	0.74	0.82	-0.63	99.4			0.002
Buphedrone	150	2.64	10.2	-0.81	99.2	0.18	2.78	0.04
	750	1.63	3.78	0.29	100.3			0.02
	1500	0.98	1.12	-0.10	99.9			0.004
Pentedrone	150	3.97	14.6	-14.9	85.1	2.76	2.78	0.06
	750	6.18	6.52	5.38	105.4			0.02
	1500	0.88	1.21	-1.20	98.8			0.004
α-PHP	150	2.98	18.2	-9.73	90.3	1.33	2.78	0.08
	750	4.93	6.95	3.50	103.5			0.03
	1500	1.85	2.00	-0.78	99.2			0.01
MPHP	150	7.28	11.5	7.91	107.9	1.66	2.78	0.04
	750	2.98	4.63	-2.85	97.2			0.02
	1500	1.40	1.42	0.63	100.6			0.004

a 95% confidence level for all SCat, concluding absence of systematic errors, thus proving the accuracy of the method.

2.2.2.5. Extraction efficiency and Matrix Effect

Most extraction processes lead to the loss of analytes by incomplete partition or adsorption, making it essential to evaluate the extraction efficiency of the analytical process. In this context, the extraction efficiency of each SCat was carried out at three different concentration levels and the results are presented in Table 23. In parallel with this study, the effect of the of endogenous compounds present in sample on the analytical performance (matrix effect) was also investigated and the results are shown in Table 23.

Table 23. Results obtained for extraction efficiency and matrix effect studies.

Compound	Concentration (ng mL^{-1})	Extraction Efficiency (%)	Matrix Effect (%)
4-FMC	150	104.9 ± 4.8	79.0
	750	81.7 ± 5.7	
	1500	94.7 ± 4.1	
Methylone	150	107.4 ± 7.9	104.3
	750	81.3 ± 5.1	
	1500	91.2 ± 2.0	
N-Ethylcathinone	150	105.5 ± 9.9	122.2
	750	93.0 ± 6.4	
	1500	98.2 ± 8.2	
Methedrone	150	115.5 ± 6.8	93.4
	750	82.8 ± 3.7	
	1500	96.6 ± 4.5	
Buphedrone	150	118.8 ± 11.2	88.1
	750	81.5 ± 5.4	
	1500	97.5 ± 4.2	
Pentedrone	150	109.3 ± 12.1	94.4
	750	88.4 ± 10.1	
	1500	99.5 ± 6.6	
α-PHP	150	101.2 ± 11.6	102.4
	750	89.8 ± 6.4	
	1500	84.4 ± 2.9	
MPHP	150	98.1 ± 12.6	75.7
	750	62.1 ± 6.9	
	1500	65.8 ± 4.7	

According to the results, the analytical method showed good extraction efficiency for almost all SCat with values ranging from 62.1% (MPHP) and 118.8% (buphedrone). In general, the results were acceptable with no significant loss of each analyte in the extraction process, thus indicating, that the proposed µSPEed®/UHPLC-PDA methodology is suitable for the extraction of SCat from urine samples.

Regarding to the matrix effect, this study was performed by comparing the slope of the calibration curve obtained for each analyte in the matrix and the slope of the calibration curve prepared in solvent. Figure S26 (supporting information) shows the comparison of both calibration curves. From the obtained results it can be assumed that there is a slight matrix effect with values ranging between 75.7% (MPHP) and 122.2% (*N*-ethylcathinone). However, taking

into account the high complexity of urine samples the effect of matrix was considered acceptable.

2.2.2.6. Analyte stability

The stability of SCat in urine samples was also investigated in this work. To perform this study, blank urine samples spiked with SCat were prepared at three distinct concentration levels and storage over a maximum period of 3 months at four different temperatures, namely −80°C, −20°C, 4°C and room temperature. Figures 57, 58 and 59 shows the obtained results for this study.

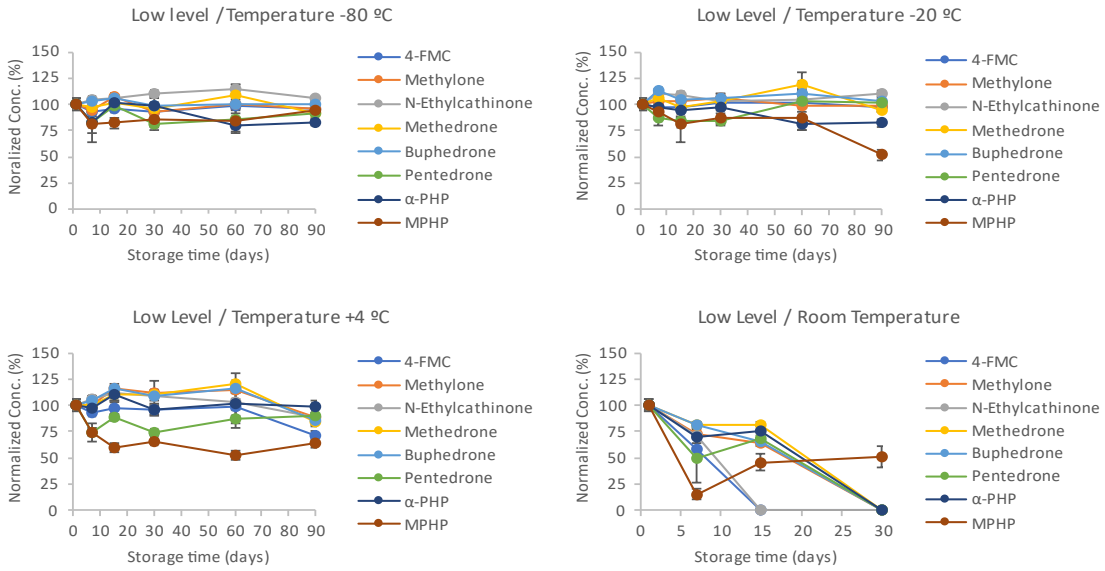

Figure 57. Stability study of SCat in urine samples at low concentration (150 ng mL^{-1}).

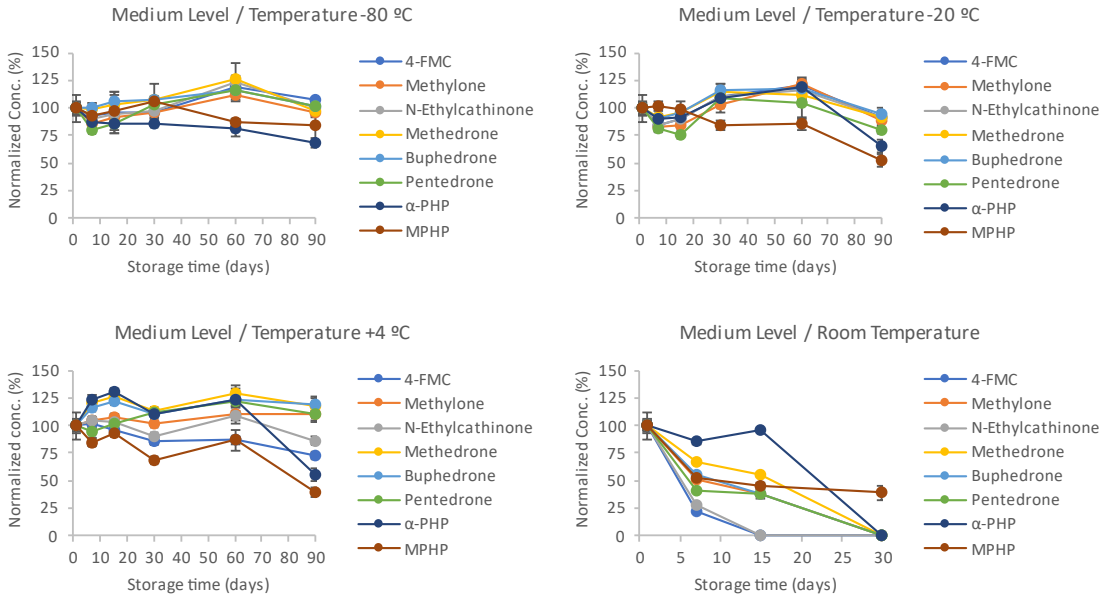

Figure 58. Stability study of SCat in urine samples at medium concentration (750 ng mL^{-1}).

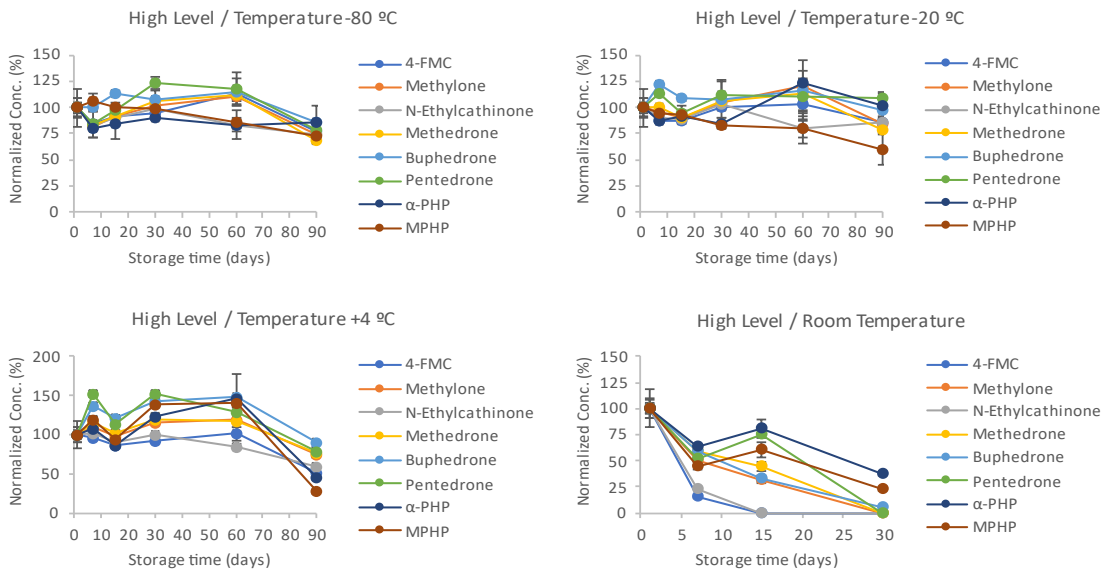

Figure 59. Stability study of SCat in urine samples at high concentration (1500 ng mL^{-1}).

During this study, the concentration of each SCat was determined based on the calibration curve obtained in the linearity. Baseline concentration (T0) was averaged and regarded as 100% and the percentage remaining for each time point was compared to baseline concentration. Concentrations deviating ±20% from baseline concentration at each sampling point were considered unstable. According to the results, it was possible to verify that at low temperatures (−80°C and −20°C) the analytes slightly decreased over time, but at a slower rate of degradation in comparison to room temperature or at 4°C. For samples stored at room temperature most SCat are almost undetectable after 30 days, while at frozen conditions the analytes were stable for 60 days, with values above 80%. After this period, some analytes showed some degree of instability, as in the case of methedrone that, at higher concentration, the deviation of the baseline concentration is greater than 30% for −80°C and 20% for −20°C (Table S1 and S2 supporting information). MPHP and α-PHP also show some degradation after 60 days especially for high concentrations. It was expected that these SCat were stable in frozen conditions for 90 days as demonstrated in several studies [241, 467]. Commonly, cathinones bearing a tertiary amine, such as pyrrolidine derivatives are more stable than the secondary amine counterparts, due to their inability to undergo oxidative deamination [241, 467]. However, as demonstrated by Glicksberg and Kerrigan [241], the pH of samples also has a significant impact on stability of SCat. At alkaline pH, SCat tend to be more unstable and easily suffer degradation, in comparison with low pH [241]. Typically, decreasing pH, SCat tend to be more stable for a long period of time [241, 468]. In this work the effect of pH of the sample on the stability of SCat was not evaluated, however it was possible to verify that SCat remain stable

for 60 days at frozen conditions. Therefore, we can conclude that a temperature ≤ −20°C is the most suitable to store this type of samples for SCat determination.

2.2.3. Application of the method to real samples

One of the main objectives of this work was to demonstrate the applicability of the developed methodology for the analysis of SCat in real samples. In this sense, 15 urine samples from synthetic drug users were obtained through Unidade de Tratamento de Toxicodependência do Serviço de Saúde da Região Autónoma da Madeira (SESARAM) and analysed by the optimized and validated methodology. The patients were under observation and treatment in this health unit and, in order to ensure maximum confidentiality, only the age and gender of the patients were provided, and an internal code was applied to each sample. Figure 60 shows the chromatographic profile of urine samples where it was possible to identify SCat, while Table 24 presents the concentrations found.

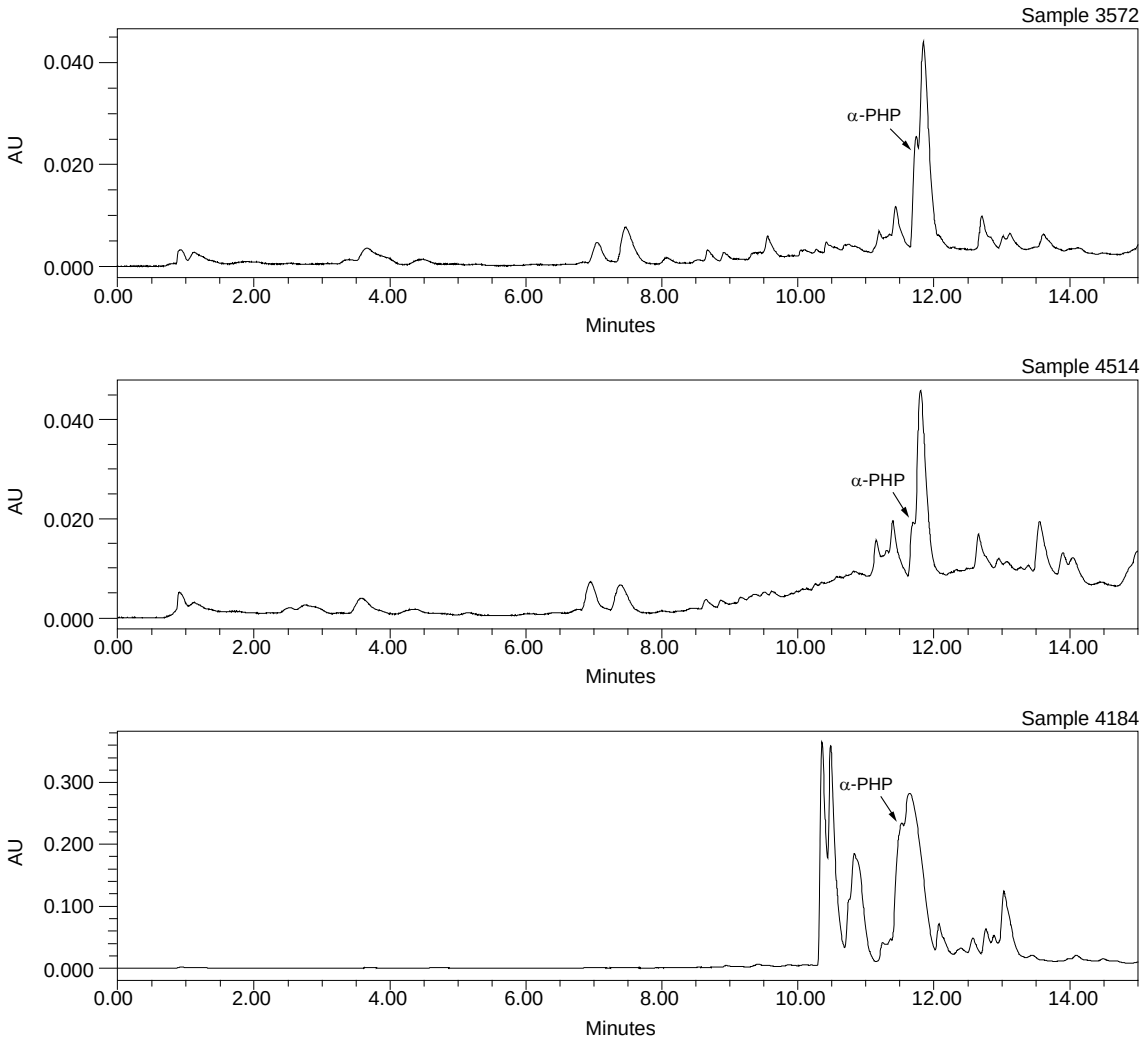

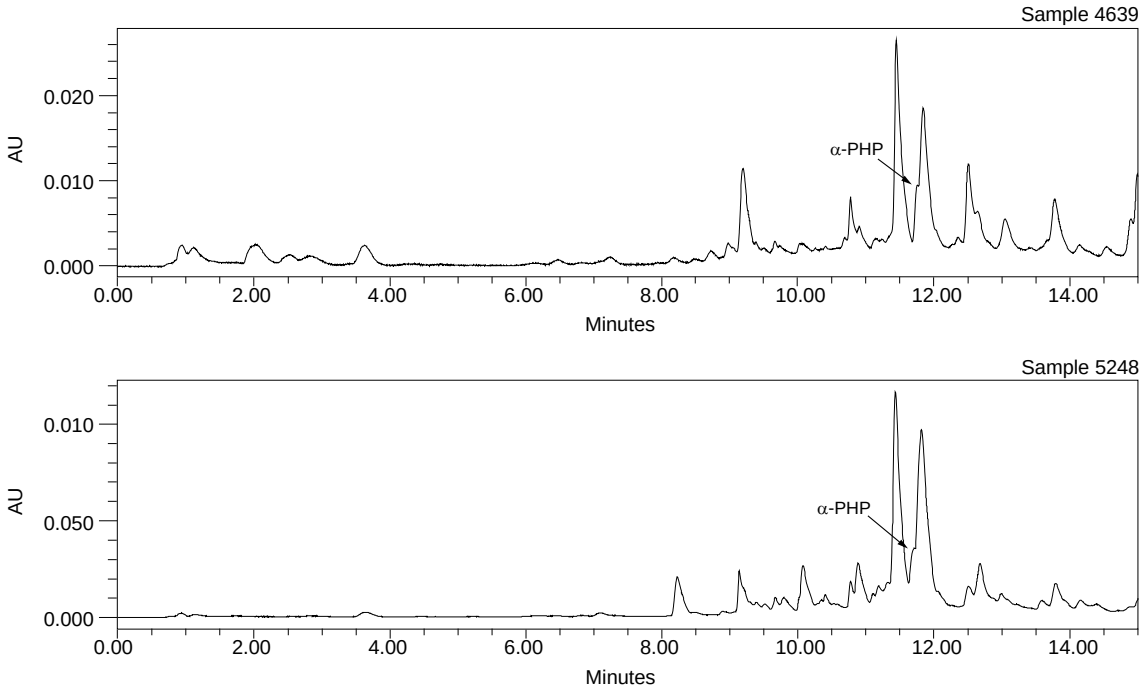

Figure 60. Chromatographic profiles of real samples after extraction by µSPEed®/UHPLC-PDA methodology.

Table 24. Concentration of SCat found in real urine samples.

Sample	Gender	Age	Concentration (ng mL^{-1})							
			4-FMC	Methylone	N-EtCat	Methedrone	Buphedrone	Pentedrone	α-PHP	MPHP
752	Male	25	n.d.	n.d.	n.d.	n.d.	n.d.	n.d.	n.d.	n.d.
2230	Male	20	n.d.	n.d.	n.d.	n.d.	n.d.	n.d.	n.d.	n.d.
4514	Male	29	n.d.	n.d.	n.d.	n.d.	n.d.	n.d.	< LOD	n.d.
7088	Male	23	n.d.	n.d.	n.d.	n.d.	n.d.	n.d.	n.d.	n.d.
6947	Male	44	n.d.	n.d.	n.d.	n.d.	n.d.	n.d.	n.d.	n.d.
1829	Male	53	n.d.	n.d.	n.d.	n.d.	n.d.	n.d.	n.d.	n.d.
4184	Male	45	n.d.	n.d.	n.d.	n.d.	n.d.	n.d.	18813 ± 402.2	n.d.
5584	Male	17	n.d.	n.d.	n.d.	n.d.	n.d.	n.d.	n.d.	n.d.
3572	Male	28	n.d.	n.d.	n.d.	n.d.	n.d.	n.d.	588 ± 30.7	n.d.
1295	Male	25	n.d.	n.d.	n.d.	n.d.	n.d.	n.d.	n.d.	n.d.
6754	Male	49	n.d.	n.d.	n.d.	n.d.	n.d.	n.d.	n.d.	n.d.
2588	Male	21	n.d.	n.d.	n.d.	n.d.	n.d.	n.d.	n.d.	n.d.
5248	Male	31	n.d.	n.d.	n.d.	n.d.	n.d.	n.d.	156 ± 15.4	n.d.
5218	Male	24	n.d.	n.d.	n.d.	n.d.	n.d.	n.d.	n.d.	n.d.
4639	Male	44	n.d.	n.d.	n.d.	n.d.	n.d.	n.d.	303 ± 26.1	n.d.

n.d. – not detected

After chromatographic analysis it was possible to identify α-PHP in 5 urine samples, whose concentration ranged from 116 to 18813 ng mL^{-1}, and which is in agreement with values reported in the literature for intoxications with SCat [469-471]. Very high concentrations, such

as those found in sample 4184, were also reported by Willeman et al. [469] during a case of recurrent acute α-PHP intoxications in a chronic drug abuser. The concentrations found in urine samples by the authors ranged between 8500 and 20100 ng mL^{-1} [469]. Regarding to the shape of chromatographic peak observed for α-PHP, it was found the presence of an interfering compound that coelutes with α-PHP and has a very similar UV spectrum whose maximum absorption wavelength is 252 nm. Probably this compound should be a metabolite of α-PHP which has a close similar chemical structure with the parent compound and ends up co-eluting with the target analyte. Samples 2230 and 1295 also showed an intense chromatographic peak at the same retention time of α-PHP but with an absorption maximum of 252 nm (Figure 61).

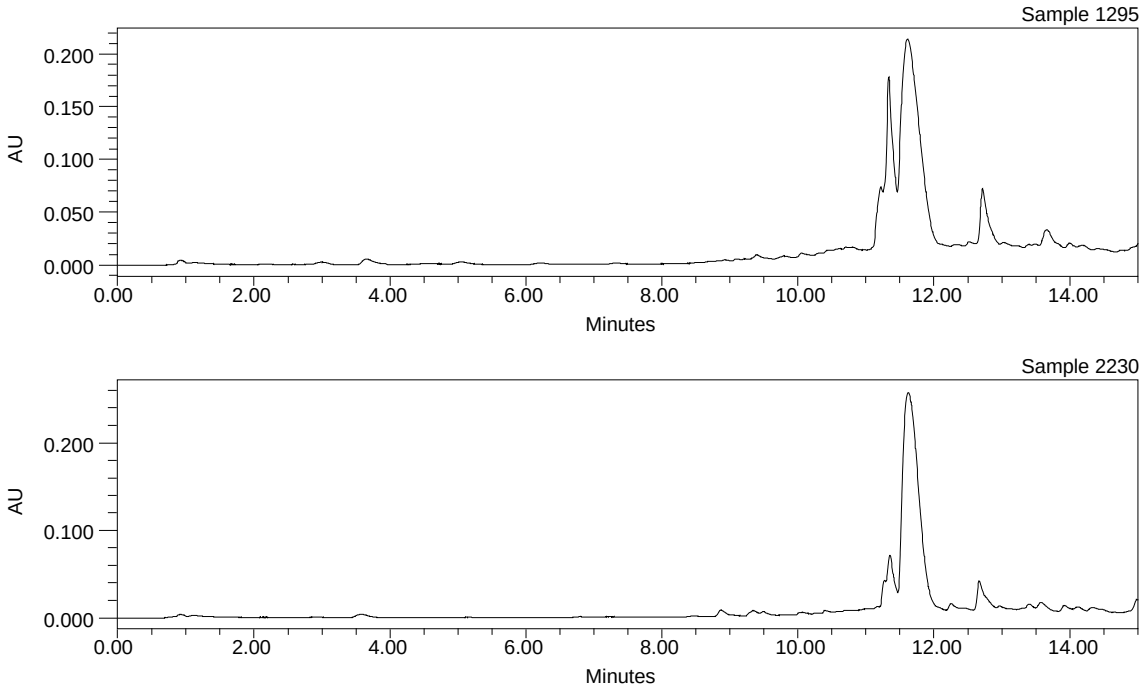

Figure 61. Chromatographic profiles of samples 1295 and 2230 after extraction by µSPEed®/UHPLC-PDA methodology.

In order to identify the possible interferences, the urine samples were analysed by GC-MS and the results are shown in Table S5 (supporting information). α-PHP and its metabolite 2''-oxo-α-PHP were identified in samples 2230, 4514, 4184, 3572, 1295, 4639 and 5248. 2''-oxo-α-PHP has been frequently detected in urine samples and is formed via oxidation of the pyrrolidine ring to the corresponding pyrrolidone (Figure 62) [160].

In addition to the presence of α-PHP and its 2''-oxo metabolite, it was also detected in sample 1295, the presence of bupropion, which is a cathinone derivative that carries a medical indication, mainly for the treatment of major depression disorder and to support smoking cessation.

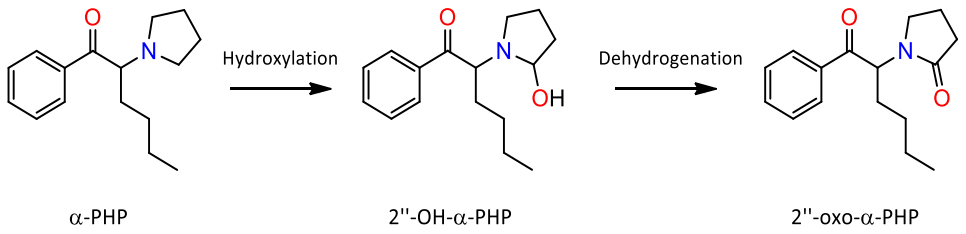

Figure 62. Formation of 2''-oxo-α-PHP from parent compound (α-PHP) (adapted from Zaitsu [160]).

Methadone and its main metabolite 2-ethylidene-1,5-dimethyl-3,3-diphenylpyrrolidine (EDDP) were also found in several urine samples (4184, 4639, 6947 and 6754). Methadone is a prescription medication that is commonly used in the treatment of opioid dependence, such as heroin, oxycodone or fentanyl. Other medications were also detected in some urine samples, such venlafaxine and its metabolite norvenlafaxine found in sample 5218 and mirtazapine in sample 6754.

Regarding sample 2230, although α-PHP and its metabolite were found in this sample, 2''-oxo-α-PHP was the main component identified by GC-MS, corresponding to 95% of the total area of all compounds identified. α-PHP was present only at trace levels in this sample.

2.3. Conclusion

The present work describes a novel methodology based on µSPEed®/UHPLC-PDA for the simultaneous determination of 8 SCat in urine samples. The extraction procedure was optimized and after a careful selection of the sorbent type, the washing and elution conditions, the number of extraction cycles and the pH of the sample, the method was validated in terms of selectivity, linearity, LOD and LOQ, precision, accuracy, extraction efficiency, matrix effect and stability. The validated method showed a satisfactory performance with linearity ranging from 150 and 1500 ng mL^{-1} and R^2 values > 0.995. Low detection limits were achieved with values ranging between 36.8 and 95.3 ng mL^{-1}, while LLOQ was 150 ng mL^{-1}, corresponding to the lowest standard of the calibration curve. The method also showed satisfactory results for accuracy and precision, with relative bias values ranging from -14.9% and 7.91% for accuracy and CV values ranging from 0.74 and 18.2% for precision. The extraction efficiency of the µSPEed®/UHPLC-PDA methodology were found between 62.1% (MPHP) and 118.8% (buphedrone). Regarding to the application of the methodology to real samples, despite the short number of samples analysed, it was possible to demonstrate the ability of the method to identify and quantify this type of substances. However, it was found that the presence of some interferences in the samples coelute with α-PHP and, for this reason, the method should be improved. Knowledge of SCat metabolism is

crucial for the analytical detection of drug intake in the urine. The identification of target metabolites can increase the chances of detecting drug ingestion and may increase the detection window in biological matrices [471]. In this context, the method should also include the analysis of metabolites in order to make the methodology more effective.

As far as we know, this is the first time that µSPEed® is applied to the extraction of SCat from biological fluids. The results are very promising, and this new approach can offer simplicity, reduced sample preparation and analysis time, low-cost and minimum extraction solvent consumption, thus constituting an alternative to conventional extraction methodologies. On the other hand, the combination of a short analysis time with a low flow, obtained by the UHPLC system, can drastically reduce the consumption of solvents, making this methodology attractive from an analytical, economic, and environmental point of view. In addition, PDA detection is a more economical alternative when compared to more sophisticated and expensive equipment, such as the MS detector, making this methodology more accessible to many laboratories.

Therefore, once improved, this methodology can be applied to the analysis of SCat in urine samples. Moreover, the methodology could potentially be extended to other biological matrices and to the analysis of other compounds of clinical and toxicological interest.

Chapter 3

Cytotoxicity Studies of Synthetic Cathinones in HepG2 cell line

3. Introduction

The abuse of SCat has raised serious public health concerns due to its high addiction potential and the number of intoxications and deaths associated with the consumption of these substances [31, 32, 414, 445, 446]. Information on the toxicological properties of these drugs is still unknown or very limited, but several adverse effects, including hypertension, tachycardia, seizures, that may result in multi-organ failure and death have been reported [32, 472].

Liver is a vulnerable target for many illicit drugs, including amphetamines [473-475], cocaine [476, 477] and even cathinone and its synthetic derivatives [183, 478, 479]. As ingestion is one of the main routes of administration for this NPS class, the first-pass effect makes the liver more susceptible to toxic injury, as demonstrated by clinical evidences of SCat-induced hepatic dysfunction [183, 472, 480] and organ accumulation [481, 482]. In addition, some *in vitro* studies associated with these compounds have shown that oxidative stress and mitochondrial dysfunction contribute to hepatic injury [114, 483, 484].

Currently, several liver-derived *in vitro* models have been extensively used in the investigation of the potential adverse effects of drugs and other chemical compounds [485]. These *in vitro* liver preparations are commonly used as surrogate models to hepatotoxicity *in vivo*, due to the many advantages, such as the reduced number of animals and costs associated to animal maintenance and care, as well as the small quantity of compound required for testing [485, 486]. In addition, these models have been shown to be fast and reliable [485, 486].

Primary hepatocytes and immortalized cell lines are two of the most widely used *in vitro* models for liver toxicity testing [485, 486]. Hepatocytes are specialized epithelial cells that account approximately 60 % of the total liver cells and 80 % of the total liver volume [487]. They are responsible for the majority of the physiological and biochemical functions of the liver playing a vital role in metabolism (e.g. carbohydrates, lipids, and xenobiotics), detoxification, and protein synthesis [487, 488]. Hepatocytes directly isolated from liver tissue are called primary hepatocytes. The functionality of primary human hepatocytes in culture is very similar to that of *in vivo* hepatocytes, and for this reason they are considered the gold standard for drug metabolism screening and toxicity study [489, 490]. However, due to their restricted availability, inter-individual variability, phenotypic instability, limited life span and high costs have prevented their widespread use [491-493].

In order to circumvent major drawbacks of primary human hepatocytes, hepatoma cell lines have been explored as an alternative model [492]. HepaRG cell line is one of the most used *in vitro* models to assess drug-induced hepatotoxicity, since it exhibits many characteristics of primary human hepatocytes including morphology, the activity of many drug-metabolizing

enzymes, and the functionality of several important mechanisms that regulate their expression [490, 492]. However, this human hepatocarcinoma cell line has some limitations, such as the availability of only one human donor, the complex time-consuming cellular differentiation procedure and the high cost [492, 494]. HepG2 cells are another human hepatoma cell line widely used in drug testing assays, since they are easy to handle and provide rapid, reproducible, and cost-effective feedback to identify possible hepatotoxic compounds [492, 495]. In addition, extensive data on the toxic effects of a large number of compounds to HepG2 cells are available in the literature [492, 495]. Despite this advantages, HepG2 cell line also has some drawbacks as it shows a poor expression of key drug-metabolizing enzymes compared with primary hepatocytes, which limits its ability to identify metabolism-dependent toxicity [492, 495].

Selecting the most appropriate cellular model can be challenging, since each has its own advantages and limitations. Currently, hepatotoxicity studies of SCat have been performed in different *in vitro* models. Valente et al. [114] used primary rat hepatocytes and HepaRG cells to investigate the effects and mechanisms underlying the hepatotoxicity of four SCat belonging to different chemical families, namely methylone, pentedrone, MDPV and 4-MEC. Their results revealed that all cathinone derivatives were hepatotoxic but at a different extent according to the specific chemical structure. MDPV and pentedrone were the more toxic compounds, while methylone was the least cytotoxic compound. Moreover, primary rat hepatocytes revealed to be the most sensitive experimental model. Bravo et al. [484] also used primary rat hepatocytes and two human cell lines (HepaRG and HepG2) to characterized the hepatotoxicity of three commonly abused SCat (butylone, buphedrone and 3,4-DMMC). Primary rat hepatocytes were, as in the previous study, the most sensitive cell model and the 3,4-DMMC was the most toxic compound for all the hepatocyte models. The cell lines HepaRG and HepG2 were also used in another study to evaluate the hepatocellular toxicity of bupropion, naphyrone, mephedrone, methedrone, methylone and MDPV [483]. The results revealed that all SCat were cytotoxic in both cell lines, but HepaRG cells were less sensitive to the SCat exposure. Other studies have been developed in human HepG2 cell line as hepatocyte model to investigate the effects of several SCat [203, 496]. Wojcieszac et al. [203] explored the effects of different pyrovalerone derivatives using this cellular model and the results showed that pyrovalerone, MDPV and 2,3-MDPV has low to moderate cytotoxicity, while α-PVP and PV9 were the most potent cytotoxic compounds. Gaspar et al. [496] also used HepG2 cells to investigate the potential hepatotoxicity of 21 SCat and the results revealed that N,N-dimethylbuphedrone and N,N-dimethylpentedrone α-dimethylaminopentiophenone were the more cytotoxic compounds.

Therefore, bearing all of this in mind, the main objective of the present work was to evaluate of the cytotoxic potential of 8 SCat and 5 real samples in the human hepatic cell line

HepG2 and elucidate cellular mechanisms behind the observed hepatotoxicity, with special focus on the oxidative stress.

3.1. Materials and Methods

3.1.1. Reagents, analytical standards and materials

Hank's balanced salts solution (HBSS) from Biowest and dimethyl sulfoxide (DMSO) from Fisher Scientific were acquired from VWR (Carnaxide, Portugal). Antibiotic mixture of penicillin/streptomycin, fetal bovine serum (FBS), minimum essential medium (MEM), phosphate buffered saline (PBS), and trypsin were purchased from Gibco Invitrogen (Barcelona, Spain). Trypan blue solution, Triton X-100, 3-(4,5-Dimethylthiazol)-2,5-diphenyltetrazolium (MTT), bicinchoninic acid solution (BCA), bovine serum albumin (BSA), 2',7'-dichlorofluorescin diacetate (DCFH-DA), and copper (II) sulfate solution 4% (w/v) were purchased from Sigma-Aldrich (St. Louis, MO, USA). Adenosine triphosphate (ATP) determination kit from Invitrogen™ was purchased from Thermo Fisher Scientific (Waltham, Massachusetts, USA), while the Amplite™ Fluorimetric Glutathione GSH/GSSG Ratio Assay Kit *Green Fluorescence* from AAT Bioquest was obtained from Deltaclon (Madrid, Spain). The perchloric acid 70-72% and the potassium hydrogen carbonate were supplied by Merck (Darmstadt, Germany). The SCat methylone, pentedrone, buphedrone, *N*-ethylcathinone, methedrone, MPHP, α-PHP, 4-FMC and the seized products were kindly provided by the LPC-PJ.

3.1.2. Cell line and Culture

The HepG2 cell line (Elabscience® - EP-CL-0103) was obtained from Quimigen (Alverca do Ribatejo, Portugal) and cultured in MEM supplemented with 10% FBS and 1% penicillin/streptomycin (10,000 U/mL; 10,000 µg mL^{-1}), in plastic petri dishes, at 37°C under humidified atmosphere containing 5% CO_2 and subjected to regular medium changes (every 2-3 days). Upon reaching 80% confluence, cells were sub-cultured by trypsinization up to a maximum of 10 passages.

3.1.3. MTT reduction assay

The cytotoxicity of SCat in HepG2 cells was indirectly determined by measuring the metabolic activity of cells using the MTT reduction assay. The underlying principle of this colorimetric assay is based on the reduction of the yellow tetrazolium MTT salt by the mitochondrial dehydrogenases (in particular succinate-dehydrogenase) into water-insoluble purple formazan crystals that accumulates within metabolically active cells [497]. The resulting

formazan crystals can be solubilized and quantified spectrophotometrically, and the total amount of formazan produced is directly proportional to the number of viable cells in the culture [498].

For the MTT reduction assay, HepG2 cells were seeded in 96-well plates, at a density of 80,000 cells/well, in a volume of 100 µL of complete medium, and left to adhere overnight. After incubation, the complete culture medium was gently aspired and replaced by the solutions of the tested compounds prepared in complete medium at concentrations ranging from 0.1 to 50 mM. Some seized products that were previously characterized (Chapter I), namely products 3, 8, 9, 12 and 14 were also tested in this study. For these products, working solutions were prepared in such a way that the range of concentrations corresponds to the major SCat presented in each sample. After incubation for 24 h, the solutions were removed and 200 µL of 0.5 mg mL^{-1} MTT prepared in fresh culture medium was added to each well. The cells were further incubated at 37°C under humidified atmosphere containing 5% CO_2 for 2.5 h. Then the MTT solution was removed, and the intracellular formazan crystals were dissolved in 100 µL of DMSO. Finally, the absorbance of the coloured solution was measured at 550 nm, using a microplate reader (Perkin Elmer Victor^3 1420). In order to reduce interexperimental variability, data were normalized to positive (1% Triton X-100) and negative (culture medium only) controls, through the equation 23 [499].

$$Citototixity\ (\%) = \frac{A_{sample} - A_{negative}}{A_{positive} - A_{negative}} \quad (23)$$

where A_{sample} is the absorbance of the tested sample, $A_{negative}$ is the absorbance of the untreated control cells (negative control) and $A_{positive}$ is the absorbance of the positive control (1% Triton X-100).

The results were obtained from three independent experiments, with each test plate containing five replicates of increasing concentrations of the tested compounds.

3.1.4. Determination of intracellular reactive oxygen (ROS) and nitrogen (RNS) species

Intracellular generation of ROS and RNS was monitored using the DCFH-DA fluorescence assay as described by da Silva et al. [500]. For this determination, HepG2 cells were seeded in black 96-well plates, at a density of 80,000 cells/well, in a volume of 100 µL of complete medium, and left to adhere overnight. After incubation, the culture medium was removed and rinsed twice with 100 µL of HBSS, and pre-incubated with 10 µM DCFH-DA for 30 min at 37°C under humidified atmosphere containing 5% CO_2. It is important to note that DCFH-DA is a non-water-soluble powder, and for this reason it was initially prepared as a 20 mM stock solution in DMSO. Immediately before each experiment, the 10 µM DCFH-DA solution was prepared in fresh

culture medium and the final concentration of DMSO did not exceed 0.05%. The cells were then washed twice with 100 µL of HBSS and incubated for 24 h with each tested drug at concentrations that produced 25%, 50% and 75% of the maximum cytotoxicity effect determined in the MTT assay, i.e. concentrations corresponding to EC_{25}, EC_{50} and EC_{75}. Fluorescence was then recorded on a microplate reader (Perkin Elmer Victor^3 1420), set to 485 nm excitation and 530 nm emission. Data were obtained from three independent experiments, with each concentration tested in five replicates within each experiment. The results were normalized to negative controls (cells with no treatment) and presented as fold increase over control conditions.

3.1.5. Determination of reduced (GSH) and oxidized (GSSG) glutathione levels

Determination of GSH and GSSG was performed through a fluorimetric GSH/GSSG assay kit (AAT Bioquest), which uses a proprietary nonfluorescent dye that becomes strongly fluorescent upon reacting with thiol group of GSH [501]. For this assessment, cells were prepared as described by da Silva et al. [500] with some modifications. Briefly, HepG2 cells were seeded in 6-well plates, at a density of 2×10^6 cells/well and left to adhere overnight at 37°C under humidified atmosphere containing 5% CO_2. After this period, the medium was removed, and the cells were incubated for 24 h with the tested drugs at concentrations corresponding to EC_{25}, EC_{50} and EC_{75} determined in the MTT assay. After drug exposure, the cells were washed twice with 1 mL HBSS, and then precipitated with 500 µL of 5% $HClO_4$ (w/v). The cells were scrapped, and the obtained suspension was transferred to 1.5 mL tubes and centrifuged at 10,000 g at 4°C for 5 min. The supernatants were collected and stored at –80°C until further analyses, while the cell pellets were used to determine the total amount of protein through the BCA protein assay.

On the day of experiment, the acidic supernatants stored at –80°C were thawed and neutralized using an equal volume of 0.76M $KHCO_3$ and then centrifuged at 10,000 g for 5 min at 4°C. The GSH and GSSG levels were then determined using the fluorimetric GSH/GSSG assay kit (AAT Bioquest), following the manufacturer's instructions. In a black 96-well plate, 50 µL of the neutralized supernatants were mixed with 50 µL of the GSH working solution, or 50 µL of the total GSH (tGSH) working solution, respectively. Then, the mixture was incubated at room temperature protected from light and the fluorescence (excitation: 485 nm/emission: 535 nm) was monitored for 60 min. For calculating the concentration of reduced and oxidized GSH, a standard series of GSH (0.16 - 10 µM) and GSSG (0.078 - 5 µM) were used to construct the calibration curves. The results were obtained from a single experiment, run in duplicate and data

were normalized to the total protein amount and expressed as nmol GSH or GSSG per mg of protein.

3.1.6. Determination of intracellular ATP levels

Determination of intracellular ATP levels was performed through a bioluminescence luciferase-based assay (Invitrogen™), according to the manufacturer's instructions. For this assessment, samples were prepared as described previously for determination of GSH and GSSG content. The acidic supernatants stored at –80°C were thawed and neutralized using an equal volume of 0.76M $KHCO_3$ and then centrifuged at 10,000 g for 5 min at 4°C. 10 µL of each supernatant, ATP standard or blank were transferred to a white 96-well plate and 90 µL of luciferin-luciferase standard reaction solution were added and the luminescence was measured using a microplate reader (Perkin Elmer Victor^3 1420). The luciferin-luciferase standard reaction solution consisted of 0.5 mM D-luciferin, 1.25 µg mL^{-1} of firefly luciferase, 25 mM tricine buffer, 5 mM $MgSO_4$, 100 µM EDTA, 100 µM sodium azide and 1 mM dithiothreitol (DTT). The ATP concentrations in the samples were determined by interpolation from a standard calibration curve (0–1000 nM). Results were obtained from one experiment, run in triplicate and data were normalized to the total protein amount and expressed as nmol ATP mg^{-1} protein.

3.1.7. Determination of protein content

The protein content of each sample was determined by the BCA protein assay, also known as the Smith assay. The principle behind of the method is the reduction of Cu^{2+} to Cu^{+} by proteins in an alkaline environment (biuret reaction). In a second step, the BCA chelates with the reduced copper producing a stable purple complex, which can be measured spectrophotometrically [502]. For determination of protein content, the cell pellets obtained during the sample preparation for the ATP and GSH/GSSG measurements were resuspended in 0.3 M NaOH. In a 96-well plate, 10 µL of sample was mixed with 190 µL of BCA working reagent, consisting of 50 parts of BCA solution with 1 part of copper (II) sulfate solution 4% (w/v). The mixture was then incubated at 37°C for 60 min and the absorbance was recorded on a microplate reader (Perkin Elmer Victor^3 1420) at 550 nm. The protein content in the samples were determined by interpolation from a standard calibration curve with BSA (0 to 5 µg $µL^{-1}$).

3.1.8. Statistical analysis

Dose-response curves of normalized MTT data were constructed and analysed for each SCat as described by Valente et al. [114], using the GraphPad Prism 8 software. The logit function that best fitted the experimental values (equation 24) allowed the determination of the half-

maximal effective concentration (EC_{50}) for each SCat. The MTT results were presented including the 95% confidence intervals (CI) of the mean values.

$$Y = \theta_{max} / \left(1 + exp\left(-\theta_1 - \theta_2 \times log(x)\right)\right) \quad (24)$$

where Y corresponds the drug response, θ_{max} is the maximal observed effect, θ_1 is the parameter for the location, θ_2 is the slope parameter and x is the concentration of the test drug. For the remaining assays, the results of test drugs and control were presented as means ± standard error mean (SEM). The normality of data distribution was evaluated by the Shapiro-Wilk normality test, and statistical comparisons between test drugs and control were performed through one-way ANOVA, followed by a Dunnett's test. *P*-values < 0.05 were considered statistically significant.

3.2. Results and Discussion

3.2.1. MTT reduction assay

The potential cytotoxic effect of eight SCat and five seized materials was evaluated *in vitro* in the human HepG2 cell line using the MTT reduction assay. This cell line was selected, since they have been commonly used as a model to study the impact of NPS on human liver cells [203, 496, 503]. In addition, HepG2 cells represent a simple and suitable alternative to primary human hepatocytes whose use is limited by the restricted availability and high variability during cultivation [496].

In this work, HepG2 cells were exposed to different concentrations of SCat, and after a 24 h exposure period, all tested substances induced cell death in a concentration-dependent manner. Dose-response curves including the 95% CI were constructed for each tested drug and presented in Figure 63. The parameters related to dose-response curves, namely the maximal effect (θ_{max}), the location parameter (θ_1), the Hill slope (θ_2) and the concentration that elicited 50% of cell death (EC_{50}) were summarized in Table 25.

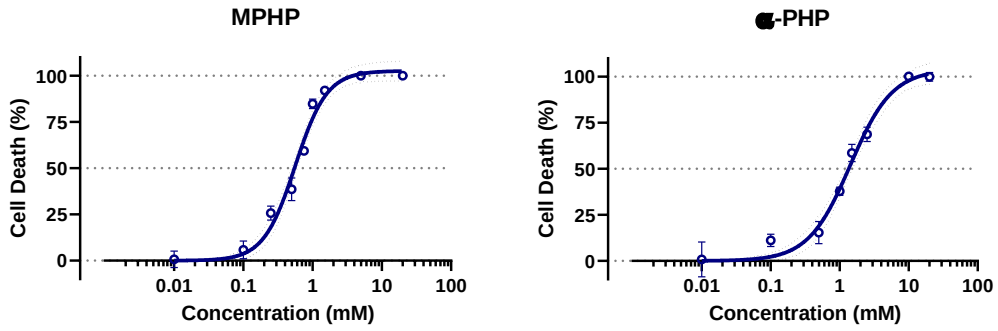

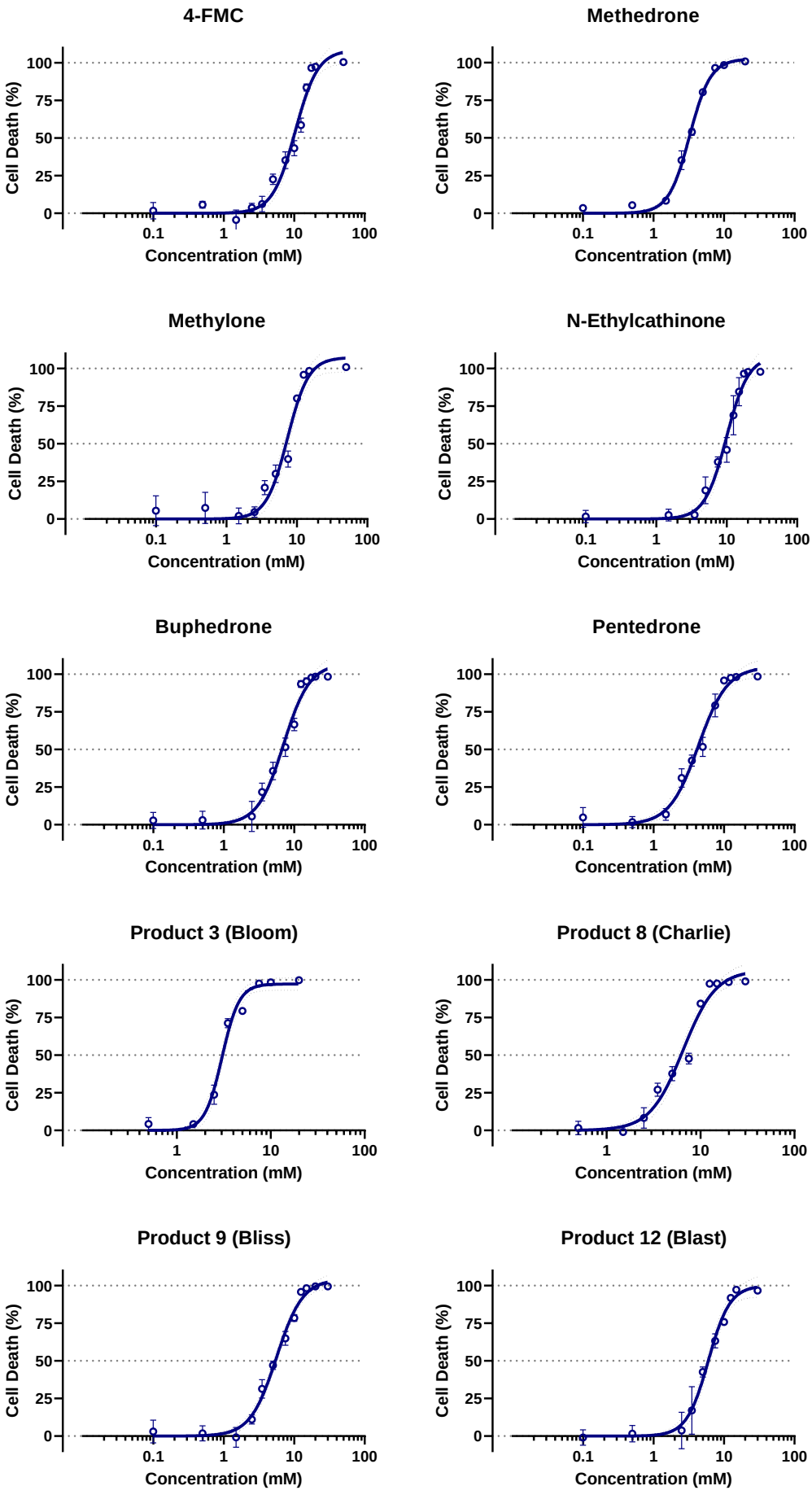
4-FMC
Methedrone
Methylone
N-Ethylcathinone
Buphedrone
Pentedrone
Product 3 (Bloom)
Product 8 (Charlie)
Product 9 (Bliss)
Product 12 (Blast)
Cell Death (%)
Concentration (mM)
0
25
50
75
100
0.1
1
10
100

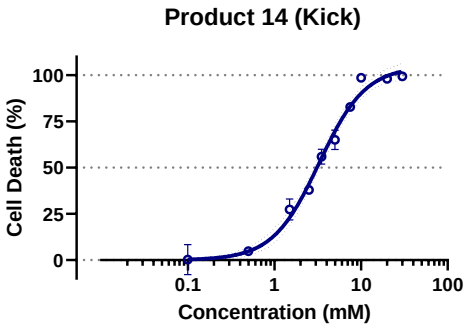

Figure 63. Dose-response curves obtained with MTT reduction assay for individual SCat and seized products in HepG2 cells after 24 h exposure at 37°C under humidified atmosphere containing 5% CO_2. The black dashed lines represent the 95% CI, while the dashed grey lines represent 50% and 100% effect.

Table 25. Parameters derived from dose-response curves obtained during the MTT assay.

Compound/ Product	Conc. range (mM)	Estimated parameters of dose-response curves			EC_{50} (mM)
		θ_1 [a]	θ_2 [b]	θ_{max} [c]	
SCat					
MPHP	0.01 – 20	-0.2496	1.898	102.7	0.56
α-PHP	0.01 – 20	0.1543	1.427	103.9	1.43
4-FMC	0.1 – 50	1.014	2.694	108.5	10.3
Methedrone	0.1 – 20	0.5129	3.201	101.4	3.26
Methylone	0.1 – 50	0.8669	2.895	107.4	7.36
N-Ethylcathinone	0.1 – 30	0.9963	2.802	108.2	9.92
Buphedrone	0.1 – 30	0.8505	2.358	107.1	7.09
Pentedrone	0.1 – 30	0.6367	2.117	104.9	4.33
Products					
Product 3 - Bloom MTD (35%), BUPH (30%), ETCAT (23%), CAF (10%) and ETPH (2%)	0.5 – 20	0.4820	4.754	97.31	3.03
Product 8 - Charlie BUPH (51%), %), ETCAT (45%), CAF (7%)	0.5 – 30	0.8139	2.488	106.5	6.51
Product 9 - Bliss MET (93%), CAF (7%)	0.1 – 30	0.7482	2.338	104.4	5.60
Product 12 - Blast 3-FMC (80%), ETCAT (10%), CAF (9%)	0.1 – 30	0.7773	2.832	100.0	5.99
Product 14 - Kick PENT (71%), MA (12%), ETCAT (9%), CAF (5%)	0.1 – 30	0.5159	1.621	104.9	3.28

Abbreviations: 3-FMC - 3-fluoromethcathinone; BUPH - buphedrone; CAF - caffeine; ETCAT - *N*-ethylcathinone; ETPH - ethylphenidate; MA - methylamine; MET - methylone; MTD - methedrone; PENT - pentedrone.
[a] Location parameter
[b] Slope parameter
[c] Maximal effect, expressed as % of cell death.

The regression lines of the dose-response curves for the tested substances were relatively similar in shape, slope and plateau, but exhibited different individual potencies. The pyrrolidine-type cathinone derivatives, MPHP and α-PHP, were the most cytotoxic compounds with EC_{50} values of 0.56 mM and 1.43 mM, respectively. These results were somehow expected and can be explained in part by the chemical structures and properties of the substances under study. As reported by Valente et al. [114], the presence of a pyrrolidine ring in SCat significantly reduces their polarity, resulting in a greater diffusion of these compounds through cell membranes. In fact, MPHP and α-PHP have the highest partition coefficient values (log P; Table S6, supporting information) of all cathinones in study, which indicates higher lipophilicity. Furthermore, the existence of a substituent group on the aromatic ring of this class of cathinones seems to play an important role in the cytotoxic effect, since the presence of a methyl group on the aryl moiety of MPHP increased the toxicity almost three times when compared to α-PHP.

The length of the alkyl side chain of SCat, also seems to influence the cytotoxicity of these drugs. Comparing the EC_{50} values obtained for buphedrone (7.09 mM) and pentedrone (4.33 mM), it was found that increasing the alkyl side chain increases the toxicity of the compound. On the other hand, the effect of the substitution of the amine moiety also appears to have influence on the cytotoxicity of SCat. Buphedrone and *N*-ethylcathinone are two structural isomers, which differs in the position of the ethyl group. Buphedrone is an α-ethyl substituted cathinone, while *N*-ethylcathinone has its ethyl-substitution on the nitrogen atom. Comparing the EC_{50} values obtained for these compounds, *N*-ethylcathinone (9.92 mM) has a slightly higher EC_{50} than buphedrone (7.09 mM), thus reflecting lower cytotoxicity.

Regarding to methcathinone derivatives, namely methedrone, methylone and 4-FMC, differences were also found in the cytotoxic potency of these compounds. Methedrone (EC_{50} 3.26 mM) showed a potency approximately 2 times higher than methylone (EC_{50} 7.36 mM) and about 3 times higher than 4-FMC (EC_{50} 10.32 mM). In addition, methedrone was the compound that showed a dose-response curve with greater steepness, indicating that the cytotoxicity increases more intensely for small increases in concentration. On the other hand, 4-FMC with an EC_{50} 10.32 mM, shares a similar potency with *N*-ethylcathinone (EC_{50} 9.92 mM) and these two compounds were the least cytotoxic.

After the characterization of the dose-response curves for individual SCat, the effects of five real samples were also evaluated. Product 3 (Bloom) and Product 14 (Kick) showed the highest cytotoxicity with EC_{50} values of 3.03 mM and 3.28 mM, respectively, while product 8 (Charlie) was the least cytotoxic (EC_{50} 6.51 mM). Compared to the individual compounds, it appears that the mixture of SCat showed higher cytotoxicity, as the EC_{50} values are somewhat lower than the individual SCat. It is important to note that the presence of other components in

the samples, such as caffeine and methylphenidate, may also contribute to the increased cytotoxicity. This was particularly observed in product 9 (Bliss), where caffeine seems to potentiate the cytotoxic effect of methylone in HepG2 cells. This sample, which consisted of 93% methylone and 7% caffeine (assessed by NMR analysis), had an EC_{50} 5.60 mM value that was significantly lower ($p < 0.01$ determined by one-way ANOVA vs methylone) than that observed for methylone alone (EC_{50} 7.36 mM). However, further studies are necessary to understand if the interactions between drugs and/or chemicals found in samples, cause additive, synergistic, or antagonistic effects.

Comparing our results with previous studies, it was found that the EC_{50} values obtained in HepG2 cells for buphedrone was approximately two times lower than that reported by Bravo et al. [484] (EC_{50} 13.7 mM) and almost 2.5 times higher than that reported by Gaspar et al. [496] (EC_{50} 2.92 mM). Pentedrone and *N*-ethylcathinone also showed some differences when compared with the results obtained by Gaspar et al. [496], who reported EC_{50} values two times lower for pentedrone and five times lower for *N*-ethylcathinone. Despite these differences, the concentrations used to determine cytotoxicity in any of these studies were higher than those found in blood or urine from intoxication cases with SCat [101, 472, 504, 505]. However, due to the distribution and tissue accumulation, the drug concentration to which the liver is really exposed may be substantially higher than that observed in the blood, as demonstrated in several studies. In a fatal case involving the consumption of SCat, Sykutera and co-authors [482] shown that, α-PVP and pentedrone reach liver-to-blood ratios up to 2.9 and 11, respectively. Another study on to the distribution of methylone in four postmortem cases showed that drug concentrations in the liver were higher than in the blood, with liver-to-blood ratios ranging from 1.19 to 4.66 [506]. Furthermore, HepG2 cells have been demonstrated to be more resistant to toxicants than primary human hepatocytes, and for this reason the presence of susceptibility factors may shift the dose-response curve to lower concentrations [483, 507].

3.2.2. Determination of intracellular ROS and RNS

Oxidative and nitrosative stress reflects disruption of the redox balance between the production of ROS/RNS and the scavenging capacity of the antioxidant system in favour of the former [508]. ROS and RNS are byproducts of the normal cellular metabolism which in low concentrations are involved in beneficial cell signalling and regulation, while at high concentrations lead to the formation of damaging species [509, 510].The overproduction of reactive species and the resulting oxidative stress is a common mechanism involved in the hepatotoxicity of several drugs, including amphetamines [500], piperazines [511] and some SCat [114, 188]. In order to evaluate the role of oxidative stress in SCat-induced hepatotoxicity, the

formation of these reactive species was measure in HepG2 cells exposed to SCat at concentrations corresponding to EC_{25}, EC_{50} and EC_{75}, calculated based on the MTT assay (Table 26). The results are presented in Figure 64.

Table 26. Concentrations tested of each SCat for evaluating the production of reactive species in HepG2 cells.

Compound	EC_{25} (mM)	EC_{50} (mM)	EC_{75} (mM)
MPHP	0.32 ± 0.03	0.56 ± 0.02	1.00 ± 0.08
α-PHP	0.66 ± 0.07	1.43 ± 0.07	3.08 ± 0.07
4-FMC	6.86 ± 0.88	10.3 ± 0.65	15.5 ± 0.43
Methedrone	2.23 ± 0.14	3.26 ± 0.13	4.73 ± 0.11
Methylone	5.04 ± 0.59	7.36 ± 0.45	10.8 ± 0.09
N-Ethylcathinone	6.70 ± 0.94	9.92 ± 1.31	14.7 ± 1.88
Buphedrone	4.45 ± 0.41	7.09 ± 0.63	11.3 ± 0.98
Pentedrone	2.58 ± 0.13	4.33 ± 0.21	7.28 ± 0.75

* ECx concentration (mM) producing x % of the maximal effect in the MTT assay.

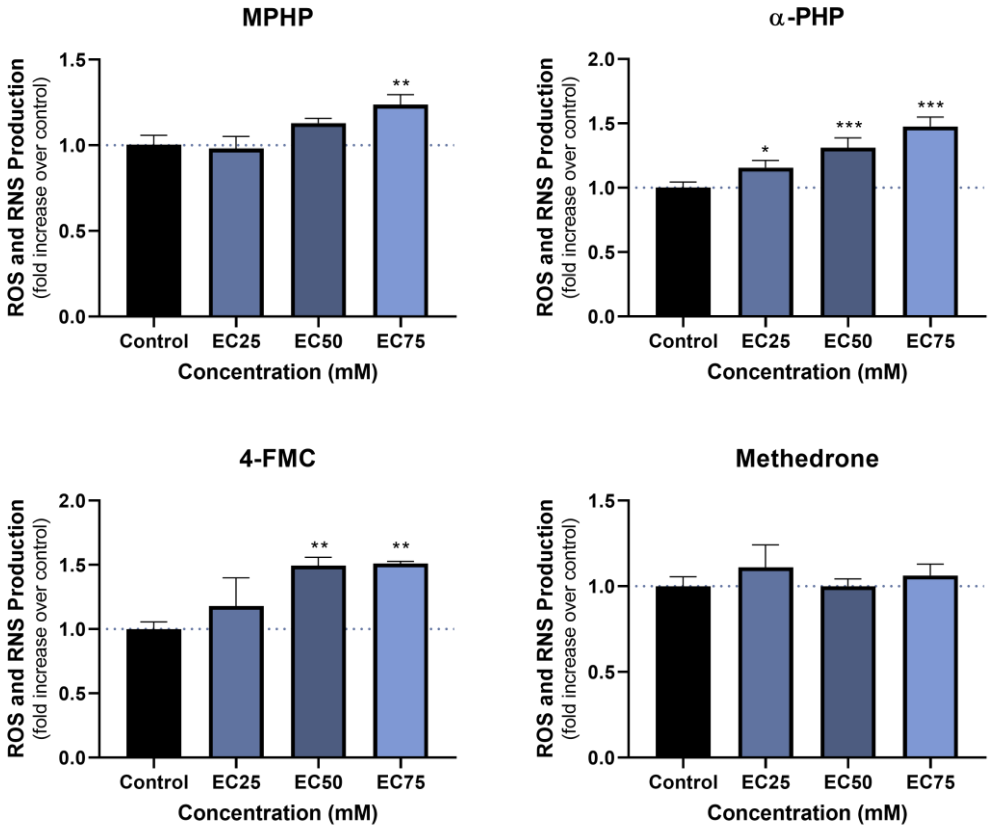

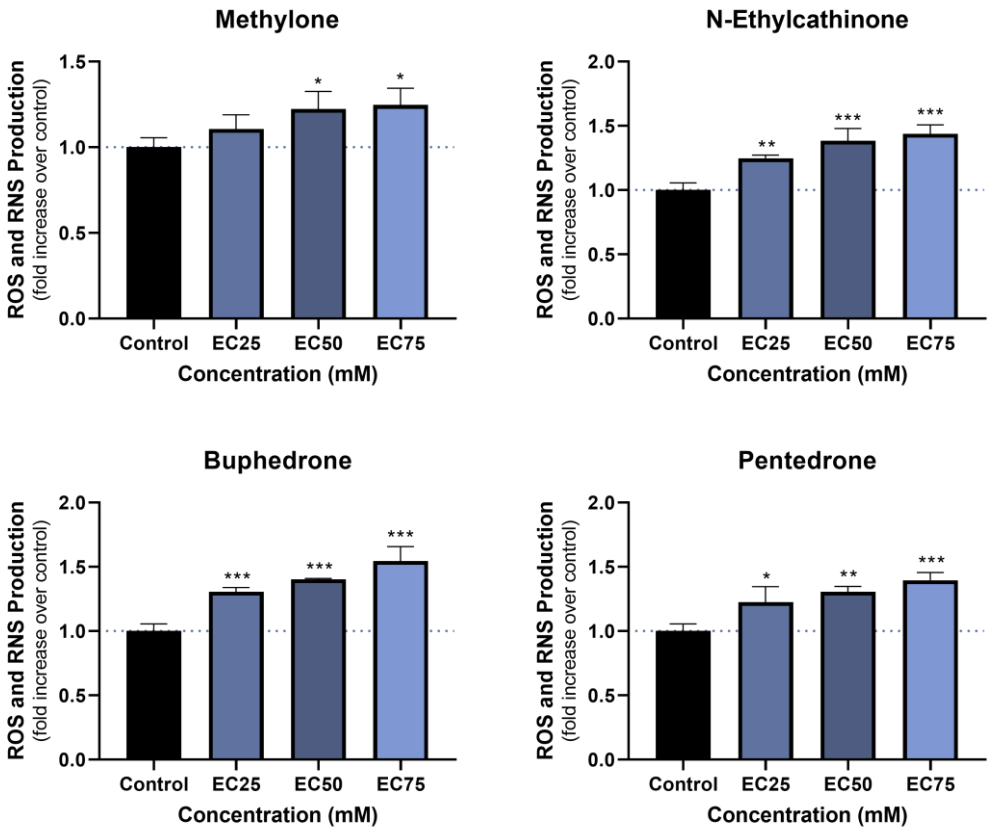

Figure 64. Production of ROS and RNS in HepG2 cells after exposure to SCat at concentrations corresponding to EC_{25}, EC_{50} and EC_{75}, for 24 h at 37°C. Results were obtained from three independent experiments performed in five replicates and the statistical analysis of data was carried out using one-way ANOVA followed by Dunnett's test. * $p < 0.05$, ** $p < 0.01$ and *** $p < 0.001$ versus control.

The DCFH-DA assay demonstrated that after 24 h of SCat exposure, almost all SCat significantly increased the production of reactive species in a concentration-dependent manner. Buphedrone elicited the highest production of reactive species, with a 1.55 ± 0.11-fold increase over control cells at the highest concentration ($p < 0.001$ vs control). 4-FMC also elicited a high production of ROS and RNS that increased significantly as the exposure concentration increased, with both EC_{50} and EC_{75} causing the maximal effect (about 1.50-fold increase over control). It was also found that α-PHP, pentedrone, *N*-ethylcathinone and buphedrone induced a significant increase of ROS and RNS production even at their lowest tested concentration, while methylone only induced a significant increase of reactive species at concentrations that elicited 50% and 75% cell death. MPHP also produced a concentration-dependent effect, causing a significant increase of reactive species only at the higher concentration tested (1.24 ± 0.06- fold increase over control, $p < 0.01$). On the other hand, methedrone was the least effective compound as it did not show a significant difference from the control.

Over the last few years, several studies have demonstrated the effect of SCat on the production of ROS and RNS. Valente et al. [114] showed the ability of 4 cathinone derivatives and MDMA of stimulating the production of ROS and RNS in primary rat hepatocytes. After a 24h exposure period, the authors observed a significant increase of ROS and RNS production in a concentration-dependent manner. Pentedrone, methylone and 4-MEC induced a significant increase of ROS and RNS at concentrations as low as 0.4 mM, while MDPV and MDMA were the least effective compounds, showing an identical increase of reactive species, but only significant at the highest concentration tested. Bravo et al. [484] also observed a significative increase in intracellular levels of ROS and RNS after primary rat hepatocytes were exposed to SCat for 24h. In this study, 3,4-DMMC caused the formation of reactive species that increased remarkably as the exposure concentration increased. Buphedrone also showed a similar concentration-dependent effect, where the highest concentration tested induced the most significant increase in ROS/RNS (1.98 ± 0.21-fold increase over control) of all compounds tested. Butylone, in turn was the SCat tested that elicited the lower ROS/RNS effect. Similar levels of disturbance in production of ROS and RNS was also reported by Dias da Silva et al. [512] for 3-MMC.

In an interestingly study performed by Valente et al. [188], the authors investigated the *in vitro* mechanisms of hepatotoxicity induced by MDPV under normothermic and hyperthermic conditions. For this purpose, primary cultures of rat hepatocytes were exposed to MDPV for 48 h, at 37°C or 40.5°C to simulate the rise in body temperature that follows MDPV intake. After the exposure period, the authors observed that the formation of reactive species were significantly potentiated when MDPV was incubated at 40.5°C. Dias da Silva et al. [500] also obtained similar results when study the role of oxidative stress in HepG2 cells exposed to different amphetamines (MDMA, D-amphetamine, methamphetamine and 4-methylthioamphetamine) under hyperthermic conditions. According to these results, the authors concluded that hyperthermia can aggravate the oxidant effect of these drugs, and that these substances, directly or through the production of reactive metabolites, can disrupt the pro-oxidant/antioxidant cellular status, in favour of the first [500].

3.2.3. Determination of intracellular levels of GSH and GSSG

Glutathione is an important tripeptide thiol (γ-L-glutamyl-L-cysteinyl-glycine) antioxidant that plays a key role in protecting cells from oxidative damage induced by reactive species. In cells, glutathione exists in two different forms, one being the reduced form (GSH) and the other the oxidised form (GSSG) [513]. The ratio between reduced and oxidized glutathione (GSH/GSSG) has been used as an important indicator of the cellular redox balance and consequently of oxidative stress [514]. Generally, the ratio is kept in balance through

oxidation/reduction reactions involving GSH peroxidase and GSH reductase (Figure 65) [515]. However, when cells are exposed to increased levels of oxidative stress, intracellular GSSG will accumulate and the GSH/GSSG ratio will decrease [513].

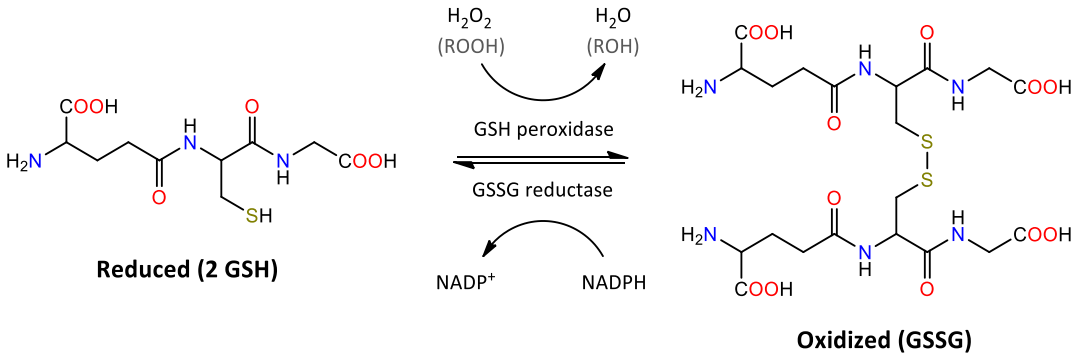

Figure 65. Oxidation-reduction pathway of glutathione (adapted from Aoyama and Nakaki [516]). Hydrogen peroxide or hydroperoxides are degraded by GSH peroxidase to water and alcohols, respectively. During the GSH peroxidase-catalyzed reaction, GSH is converted to its oxidized disulfide form (GSSG). GSH in turn can be regenerated from GSSG by the GSSG reductase in the presence of NADPH. In this process NADPH is oxidized to $NADP^+$. NADPH is subsequently regenerated via the pentose phosphate pathway [517].

In order to assess the influence of SCat on gluthatione intracellular content, the concentrations of GSH and GSSG were investigated by a fluorescence-based assay. Figure 66 shows the gluthatione levels in HepG2 cells following SCat exposure.

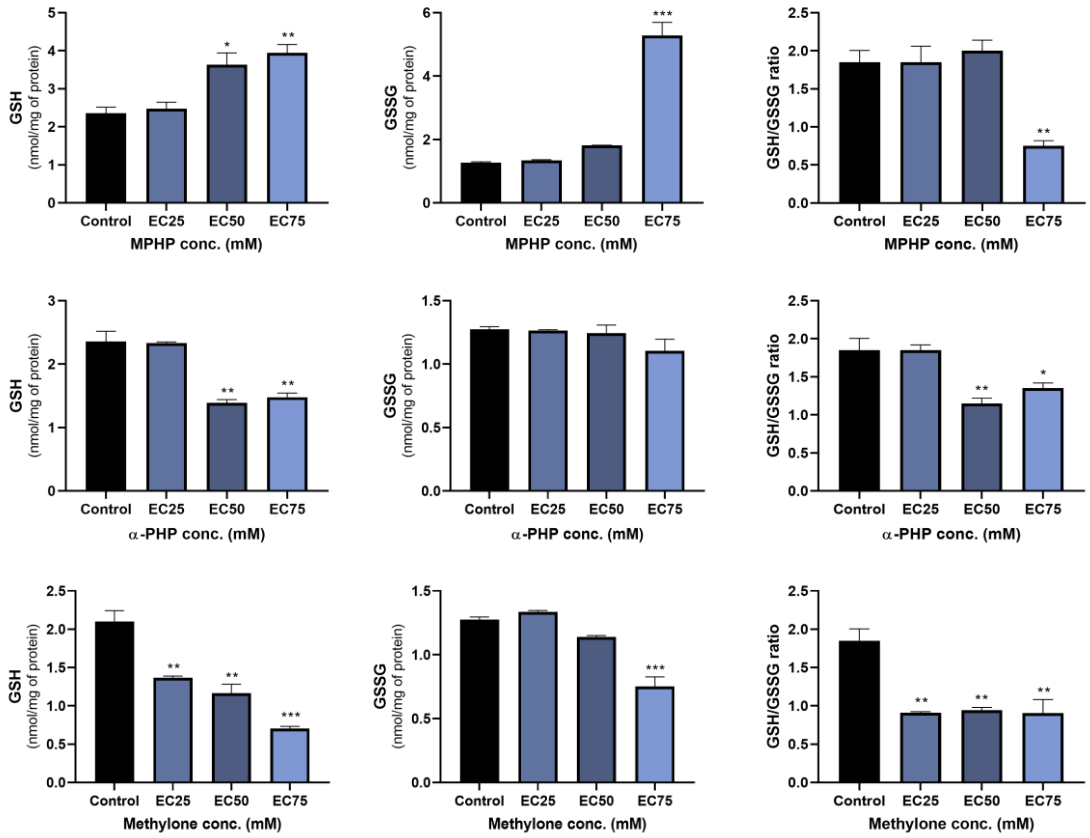

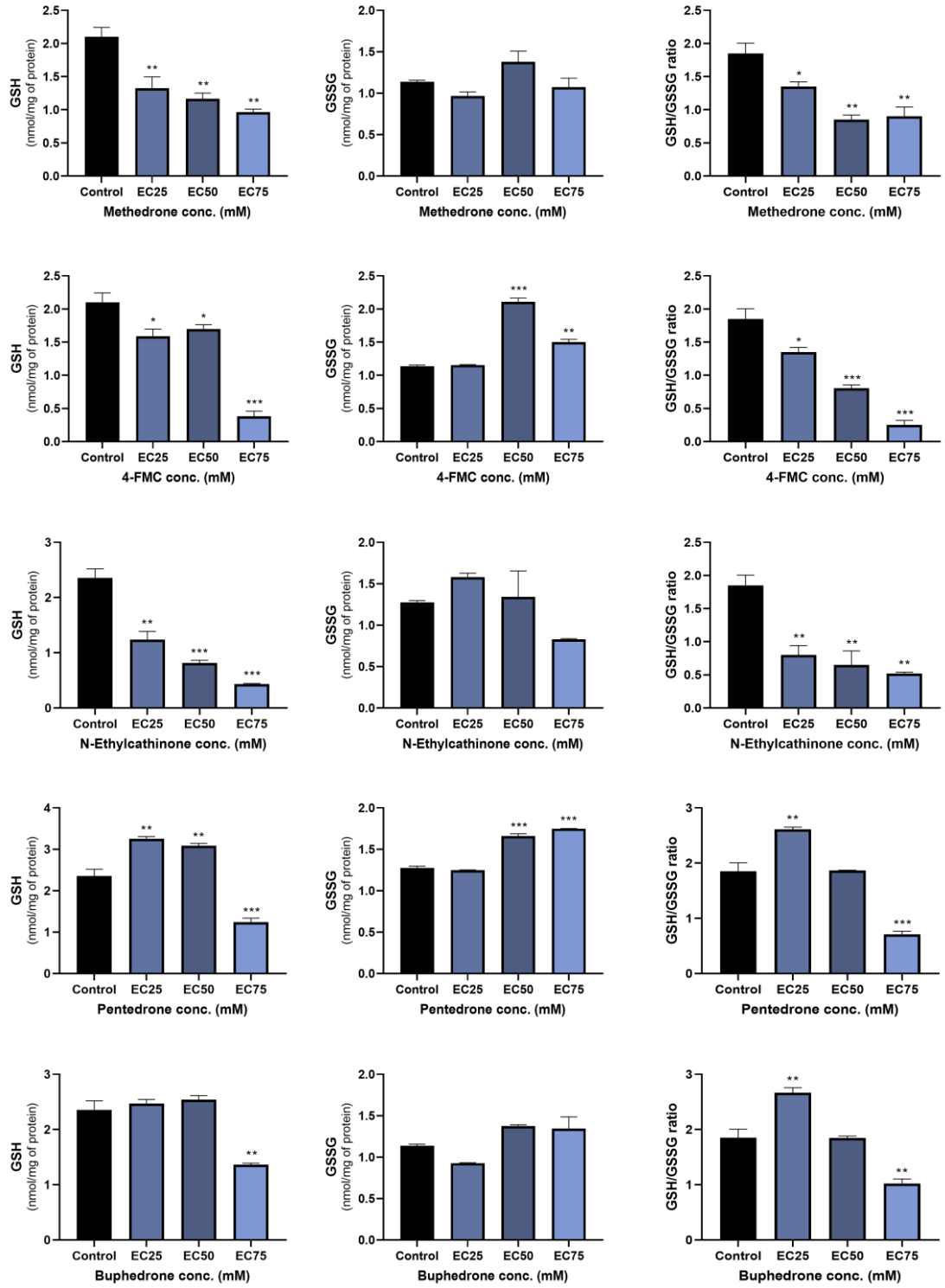

Figure 66. Intracellular levels of GSH and GSSG, as well as the GSH/GSSG ratio in HepG2 cells after 24h of incubation with SCat at 37°C. Results were obtained from a single experiment performed in duplicate and the statistical analysis of data was carried out using one-way ANOVA followed by Dunnett's test. * $p < 0.05$, ** $p < 0.01$ and *** $p < 0.001$ versus control.

According to the results, almost all SCat induced a decrease in GSH levels in an apparent concentration-dependent manner. For most compounds, these results are in agreement with the production of reactive species, since the highest GSH depletion, observed for the highest tested concentrations (EC_{75}) also induced the highest production of reactive species. *N*-Ethylcathinone was the compound that caused the most significant decrease in GSH levels even at the lowest tested concentration (EC_{25}). However, this decrease was not accompanied with the expected increase in GSSG levels. In fact, for most compounds, the GSH depletion was not accompanied with an increase in GSSG levels. Only MPHP showed a significant increase in intracellular levels of GSSG, when HepG2 cells were exposed to EC_{75}, a concentration at which the drug also increased significantly the GSH levels. This divergence between the respective decrease and increase of GSH and GSSG levels, were also observed for amphetamines and a number of SCat [188, 484, 500]. According to Bravo et al. [484], a plausible explanation for this disparity of values is the extrusion of GSSG for the extracellular medium, as a protective response of cells from damage derived from oxidative stress. Another possible explanation for the observed discrepancies in terms of decrease of GSH that was not compensated by the increase in GSSG, is the formation of glutathione conjugated metabolites, which has already been described for some amphetamines [475, 484, 512, 518]. As demonstrated by Carvalho and co-authors [475, 518], MDMA and MDA can undergo extensive hepatic metabolism to produce catechols, which in turn can be oxidized to form *ortho*-quinones. These unstable molecules can enter the redox cycle inducing massive formation of ROS, including the superoxide anion, the hydrogen peroxide and hydroxyl radical [475, 518]. In the presence of GSH, the *ortho*-quinones can react with it to form the corresponding GSH conjugate [475, 518]. Due to structural similarities to amphetamines, it is thought that SCat may undergo a similar mechanism. In fact, a study performed by Meyer et al. [519], the authors identified the formation of glutathionyl adducts with the demethylated metabolites of several methylenedioxy designer drugs, including MDPV and methylone. Despite these findings, there is currently no evidence to support the ability of other SCat groups, i.e. SCat without a methylenedioxy ring, to undergo metabolic pathways that result in the formation of conjugates with GSH [114, 512].

3.2.4. Determination of intracellular levels of ATP

Mitochondria play an important role in several cellular functions, including the synthesis of ATP which is the main source of energy for cells. ATP is a key metabolite that participate in a variety of cellular activities, including cellular energetics, signaling and metabolic regulation [520]. Since all cells need ATP to remain alive and perform their specific functions, ATP levels has been used as a tool for the functional integrity of living cells [520]. In order to assess the

effect of SCat on the intracellular ATP levels in HepG2 cells, the concentration of ATP was determined using a bioluminescence-based assay and the results are shown in Figure 67.

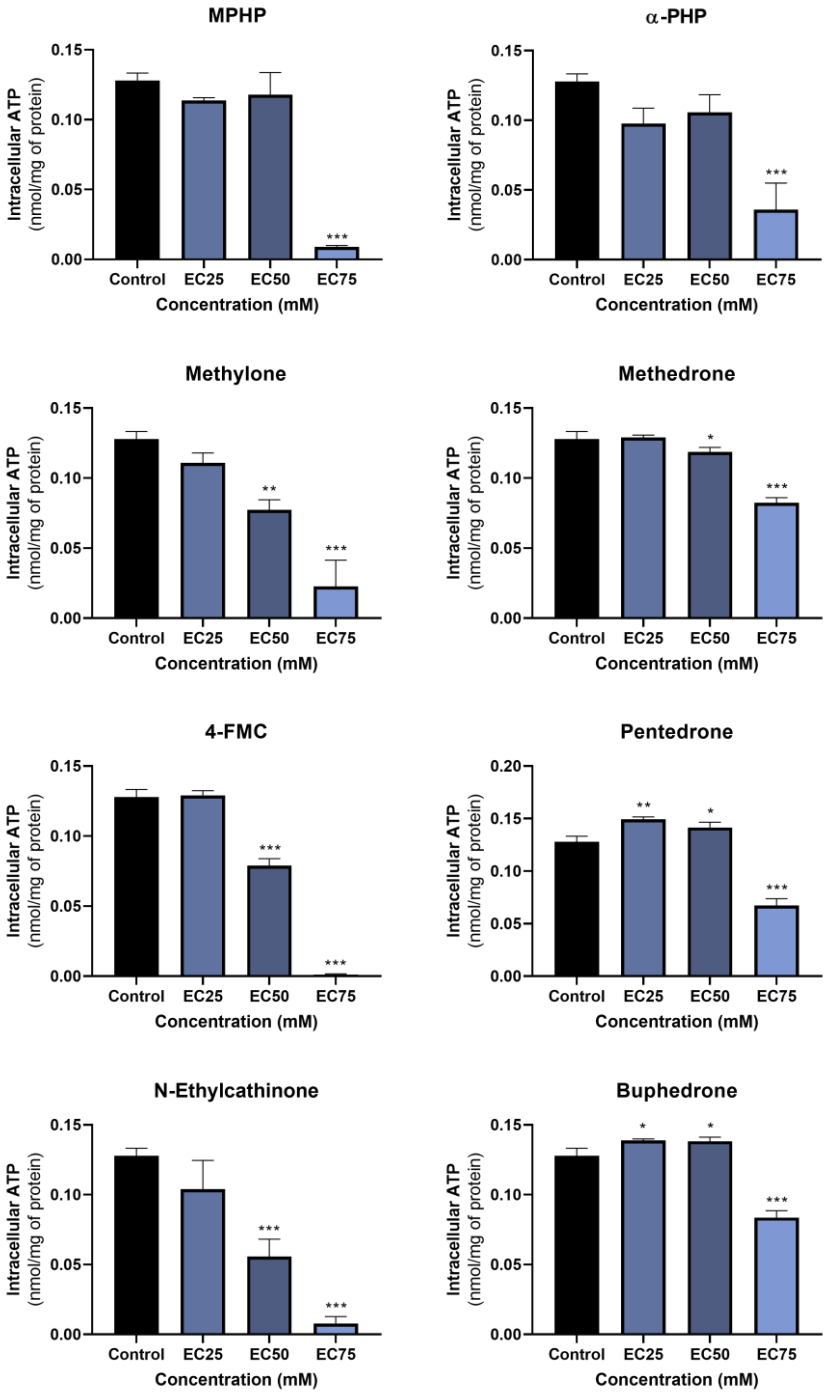

Figure 67. Intracellular levels of ATP in HepG2 cells after 24h of incubation with SCat at 37°C. Results were obtained from a single experiment performed in triplicate and the statistical analysis of data was carried out using one-way ANOVA followed by Dunnett's test. * $p < 0.05$, ** $p < 0.01$ and *** $p < 0.001$ versus control.

As showed in Figure 67, after 24h exposure, all SCat decrease the cellular ATP content in a concentration-dependent manner. 4-FMC and *N*-ethylcathinone were the most effective SCat, inducing a decrease of ATP levels from $1.3\times10^{-1} \pm 5.3\times10^{-3}$ nmol ATP mg^{-1} of protein in control cells to $1.1\times10^{-3} \pm 0.5\times10^{-3}$ nmol ATP mg^{-1} of protein for 4-FMC and $7.7\times10^{-3} \pm 5.1\times10^{-3}$ nmol ATP mg^{-1} of protein for *N*-ethylcathinone at the highest concentration tested (EC_{75}). Methylone and methedrone also induced a significant ATP depletion with the highest concentrations causing the most significant effects ($p < 0.001$ vs control). Regarding to pyrovalerone derivatives, namely MPHP and α-PHP, it was also observed a significant decrease in ATP levels, but only at the higher concentration. On the other hand, pentedrone and buphedrone, showed a very similar effect, with a slight increase in ATP levels at the lowest concentrations tested (EC_{25} and EC_{50}) followed by a significant decrease in relation to the control at the highest concentration (EC_{75}). Dias da Silva et al. [512] also observed a similar effect, when primary cultures of rat hepatocytes were exposed to a lower concentration of 3-MMC. According to the authors, this slightly increase may be associated with an attempt by cells to respond to the drug insult by activating pro-survival mechanisms [512].

In general, our results showed that all SCat tested were able to affect energetic homeostasis, as they significantly decrease the intracellular ATP content. For almost all compounds, this decrease occurred at concentrations where the GSH depletion and the production of reactive species were significantly increased, suggesting that oxidative stress may play a role in mitochondrial dysfunction. These results are in agreement with those reported in the literature for other SCat in primary cultured rat hepatocytes [114, 188, 484, 512] and HepG2 cells [483].

3.3. Conclusion

The present work provided evidence of the cytotoxic potential of 8 SCat and several seized products in HepG2 cells. MPHP and α-PHP, were the most cytotoxic compounds with EC_{50} values of 0.56 mM and 1.43 mM, respectively, while 4-FMC and *N*-ethylcathinone were the least cytotoxic. Regarding the seized products, the results showed a slight increase in the cytotoxic effect compared to the individual SCat, with products 3 (“Bloom”) and 14 (“Kick”) showing the highest cytotoxic effect. However, further studies should be performed in order to understand the type of interaction between drugs and/or chemicals found in samples (i.e. additive, synergistic or antagonistic effect), as it can provide useful information that may help explain the cause of death in fatal intoxication cases, as well as aid in the diagnosis and treatment of non-fatal intoxications. Furthermore, the results obtained in this study also suggest that oxidative stress plays a central role in the toxicity of these substances, since with the increase in drug

concentration there was a significant increase in ROS and RNS production and a depletion in GSH. Moreover, all tested SCat were able to affect energetic homeostasis, as the intracellular levels of ATP decreased significantly with increasing drug concentration. It is also important to note that to further increase the confidence in the obtained results the number of independent experiments for ATP determination as well as GSH/GSSG should be increased. However, these results can provide important information regarding to SCat and their effects on users, with special focus on the hepatotoxicity.

Chapter 4

Final Conclusions and Future Perspectives

4. Final Conclusions and Future Perspectives

With the ever-changing drug landscape, there is a growing need to develop methods for the rapid identification and quantitative determination of new substances entering the drug market. In this context, the present work aimed to identify the chemical composition of products seized from the drug market and, based on that identification, develop an analytical methodology that would allow its detection and quantification in biological samples. In parallel, it also projected the contribution to the knowledge of its potential hepatotoxic effect, through an *in vitro* study using HepG2 cells. Based on the obtained results throughout this work, it was possible to conclude the following:

- The combination of complementary analytical techniques, such as ATR-FTIR, GC-MS, UHPLC-PDA and NMR, proved to be an effective strategy for the unequivocal identification of SCat found in seized products from the illicit drug market.
- The diversity in the composition of these products is one of the biggest problems related to the NPS phenomenon. As demonstrated in our results, the product's composition is variable and products with the same trade name can have different substances (for example, "Bliss" and "Blast" products), which puts users at high risk as they do not know what they are consuming. In addition, the high purity of some products (≥ 89%), can have serious consequences.
- The development of analytical strategies that allow the simultaneous detection and quantification of NPS in biological samples is another important source of information about the prevalence of use of this type of drugs. In this context, an analytical methodology based on the µSPEed® followed by UHPLC-PDA analysis was developed, for the detection and quantification of SCat in urine samples.
- The µSPEed® performance was optimized and the best extraction conditions were obtained using the PS-DVB sorbent, one draw–eject cycle (1 × 1000 µL of sample), sample pH of 6.0, a washing step constituted by 200 µL H_2O (0.1% FA), followed by 200 µL of H_2O:ACN (95:5 v/v) and finally the elution of the analytes carried out with 250 µL of MeOH.
- The method was validated and showed satisfactory results in terms of linearity, with R^2 ≥ 0.998, within the studied concentration ranges. Regarding the LOD's, it had also satisfactory results, with values ranging from 36.8 to 95.3 ng mL^{-1}, whereas the LLOQ was 150 ng mL^{-1}, corresponding to the lowest concentration of the standard curve. Precision and accuracy were also very satisfactory, with values below the maximum described in guidelines. In addition, the method showed good extraction efficiencies

with values ranging from 62.1% (MPHP) to 118.8% (buphedrone) and the matrix effect was considered acceptable, with values ranging from 75.7% (MPHP) to 122.2% (*N*-ethylcathinone).

- The concentrations of SCat analysed in real samples, allowed to demonstrate the ability of the method to identify and quantify this kind of substances. However, the method should be improved in order to reduce the interferences that occurred during the analysis of some real samples, and also include the analysis of metabolites, in order to make it more effective. Moreover, these results suggest that this methodology could potentially be extended to the analysis of other compounds of clinical and toxicological interest.
- The present work also provided evidence of the hepatotoxic potential of SCat, individually and as products, using HepG2 cells as *in vitro* model. The results showed that after 24h exposure period, all SCat induced cytotoxicity in a concentration-dependent manner, in the following order of potency: MPHP > α-PHP > methedrone > pentedrone > buphedrone ≈ methylone > *N*-ethylcathinone ≈ 4-FMC. Compared to the individual compounds, it seems that products containing SCat show higher cytotoxicity, as the EC_{50} values are somewhat lower than the individual components.
- The results obtained in this work also suggest that oxidative stress and alterations on energy homeostasis may have an important role on the observed effects.

Despite these promising results, it is important to conduct further studies in order to fully understand the mechanisms of action and physiological consequences of these substances. In addition, the chemical characterization of new substances that appear in the market and the improvement of the analytical methodology developed for the determination of this type of substances in biological samples should be part of these studies, in order to assist researchers, public health agents and police forces who work in this area on a daily basis. In this sense, as main future perspectives we can highlight:

- Improve the developed analytical methodology in order to include the metabolites of the studied SCat and extend the methodology to other biological matrices (e.g. blood and oral fluid) and/or other NPS classes.
- Explore the role of metabolites of the SCat tested in the hepatoxicity.
- Investigate the potential toxic effects of the SCat and its metabolites on other target organs, such as the kidneys, as the renal excretion is the main route of elimination of these substances and some studies have shown that SCat can induced nephrotoxicity.

REFERENCES

References

1. Second Street Rehabilitation Center. What changes come in behavior if someone takes drugs? [accessed December 7, 2021]. Available from: https://www.secondstreet.in/drug-rehabilitation-centre-in-thane/.

2. UNODC. World Drug Report 2021. [accessed February 20, 2022]. Available from: https://www.unodc.org/unodc/en/data-and-analysis/wdr2021.html.

3. UNODC. World Drug Report 2012. [accessed March 3, 2022]. Available from: https://www.unodc.org/documents/data-and-analysis/WDR2012/WDR_2012_web_small.pdf.

4. Dinis-Oliveira RJ, Vieira-Coelho MA, Carvalho FD. Introdução às Toxicodependências. Toxicologia Forense. Lisboa: Pactor - Edições de Ciências Sociais, Forenses e da Educação, 2015. p. 131-139.

5. Belcher HME, Shinitzky HE. Substance Abuse in Children: Prediction, Protection, and Prevention. Arch. Pediatr. Adolesc. Med. 1998; 152: 952-960.

6. Dinis-Oliveira RJ. Licit and Ilicit Uses of Medicines. Acta Med. Port. 2014; 27: 755-766.

7. Nawi AM, Ismail R, Ibrahim F, Hassan MR, Manaf MRA, Amit N, et al. Risk and protective factors of drug abuse among adolescents: a systematic review. BMC Public Health 2021; 21: 2088.

8. Miliano C, Margiani G, Fattore L, De Luca MA. Sales and Advertising Channels of New Psychoactive Substances (NPS): Internet, Social Networks, and Smartphone Apps. Brain Sci. 2018; 8: 123.

9. Krausz RM, Westenberg JN, Mathew N, Budd G, Wong JSH, Tsang VWL, et al. Shifting North American drug markets and challenges for the system of care. Int. J. Ment. Health Syst. 2021; 15: 86.

10. EMCDDA-Europol. EU Drug Markets Report 2019. [accessed February 26, 2022]. Available from: https://www.europol.europa.eu/sites/default/files/documents/drug_markets_report_2019_pdf.pdf.

11. EMCDDA. European Drug Report 2019: Trends and Developments. [accessed February 23, 2022]. Available from: https://www.emcdda.europa.eu/system/files/publications/11364/20191724_TDAT19001ENN_PDF.pdf.

12. EMCDDA. Country Drug Report 2017 - Portugal. [accessed February 26, 2022]. Available from: https://www.emcdda.europa.eu/system/files/publications/4508/TD0116918ENN.pdf.

13. EMCDDA. Portugal Country Drug Report 2019. [accessed Februrary 26, 2022]. Available from: https://www.emcdda.europa.eu/system/files/publications/11331/portugal-cdr-2019_0.pdf.

14. EMCDDA. The internet and drug markets. [accessed February 28, 2022]. Available from: https://www.emcdda.europa.eu/system/files/publications/2155/TDXD16001ENN_FINAL.pdf.

15. Guirguis A. New psychoactive substances: a public health issue. Int. J. Pharm. Pract. 2017; 25: 323-325.

16. Dolengevich-Segal H, Rodríguez-Salgado B, Gómez-Arnau J, Sánchez-Mateos D. An approach to the new psychoactive drugs phenomenon. Salud Ment. 2017; 40: 71-82.

17. Araújo AM, Valente MJ, Carvalho M, Dias da Silva D, Gaspar H, Carvalho F, et al. Raising awareness of new psychoactive substances: chemical analysis and in vitro toxicity screening of 'legal high' packages containing synthetic cathinones. Arch. Toxicol. 2015; 89: 757-771.

18. Dasgupta A. 3 - Designer drugs including bath salts and spices. Alcohol, Drugs, Genes and the Clinical Laboratory: Academic Press, 2017. p. 53-73.

19. UNODC. Early Warning Advisory on New Psychoactive Substances. [accessed March 26, 2022]. Available from: https://www.unodc.org/LSS/Announcement/Details/40df1bf0-4f70-4862-844e-20536e0d95fd.

20. EMCDDA. European Drug Report 2021: Trends and Developments. [accessed February 24, 2022]. Available from: https://www.drugsandalcohol.ie/34349/1/EMCDDA_2021_report.pdf.

21. EMCDDA. European Commission adopts measures to control two harmful new drugs amidst health concerns and surge in supply. [accessed March 26, 2022]. Available from: https://www.emcdda.europa.eu/news/2022/3/european-commission-adopts-measures-control-two-harmful-new-drugs_en.

22. UNODC. Understanding the synthetic drug market: the NPS factor, Global SMART Update. [accessed September 20, 2018]. Available from: https://www.unodc.org.

23. Zawilska JB, Wojcieszak J. Novel Psychoactive Substances: Classification and General Information. In: Zawilska JB, editor. Synthetic Cathinones: Novel Addictive and Stimulatory Psychoactive Substances. Cham: Springer International Publishing, 2018. p. 11-24.

24. German CL, Fleckenstein AE, Hanson GR. Bath salts and synthetic cathinones: An emerging designer drug phenomenon. Life Sci. 2014; 97: 2-8.

25. Concheiro M, Anizan S, Ellefsen K, Huestis MA. Simultaneous quantification of 28 synthetic cathinones and metabolites in urine by liquid chromatography-high resolution mass spectrometry. Anal. Bioanal. Chem. 2013; 405: 9437-9448.

26. Gołembiowska K, Kamińska K. Effects of Synthetic Cathinones on Brain Neurotransmitters. In: Zawilska JB, editor. Synthetic Cathinones: Novel Addictive and Stimulatory Psychoactive Substances. Cham: Springer International Publishing, 2018. p. 117-124.

27. Watterson LR, Olive MF. Synthetic cathinones and their rewarding and reinforcing effects in rodents. Advances in Neuroscience (Hindawi) 2014; 2014: 209875.

28. Gonçalves JL, Alves VL, Aguiar J, Teixeira HM, Câmara JS. Synthetic cathinones: an evolving class of new psychoactive substances. Crit. Rev. Toxicol. 2019; 49: 549-566.

29. Musselman ME, Hampton JP. "Not for Human Consumption": A Review of Emerging Designer Drugs. Pharmacotherapy 2014; 34: 745-757.

30. Coppola M, Mondola R. Synthetic cathinones: Chemistry, pharmacology and toxicology of a new class of designer drugs of abuse marketed as "bath salts" or "plant food". Toxicol. Lett. 2012; 211: 144-149.

31. Prosser JM, Nelson LS. The Toxicology of Bath Salts: A Review of Synthetic Cathinones. J. Med. Toxicol. 2012; 8: 33-42.

32. Valente MJ, Guedes de Pinho P, Bastos MdL, Carvalho F, Carvalho M. Khat and synthetic cathinones: a review. Arch. Toxicol. 2014; 88: 15-45.

33. Lemieux AM, Li B, al'Absi M. Khat use and appetite: an overview and comparison of amphetamine, khat and cathinone. J. Ethnopharmacol. 2015; 160: 78-85.

34. Capriola M. Synthetic cathinone abuse. Clin. Pharmacol. 2013; 5: 109-115.

35. Dasgupta A. Chapter Five - Challenges in Laboratory Detection of Unusual Substance Abuse: Issues with Magic Mushroom, Peyote Cactus, Khat, and Solvent Abuse. In: Makowski GS, editor. Advances in Clinical Chemistry: Elsevier, 2017. p. 163-186.

36. Rätsch C, Hofmann A. The Encyclopedia of Psychoactive Plants: Ethnopharmacology and Its Applications: Inner Traditions/Bear, 2005.

37. Dunne FJ, Jaffar K, Hashmi S. Legal Highs - Not so new and still growing in popularity. Br. J. Med. Pract. 2015; 8: a801.

38. Halbach H. Medical aspects of the chewing of khat leaves. Bull. World Health Organ. 1972; 47: 21-29.

39. Wabe NT. Chemistry, pharmacology, and toxicology of khat (catha edulis forsk): a review. Addict. Health 2011; 3: 137-149.

40. Hyde JF, Browning E, Adams R. Synthetic Homologs of D,L-Ephedrine. J. Am. Chem. Soc. 1928; 50: 2287-2292.

41. Sanchez SdB. Sur un homologue de l'éphédrine (On an analogue of ephedrine). Bul.l Soc. Chim. Fr. 1929; 45: 284-286.

42. Abouchedid R, Wood DM. Cathinones. In: Brent J, Burkhart K, Dargan P, Hatten B, Megarbane B, Palmer R, editors. Critical Care Toxicology: Springer International Publishing, 2016. p. 1-40.

43. Wiegand TJ. Designer Drugs: Focus on Cathinones (Bath Salts) and Synthetic Cannabinoids (K2 or Spice). Emerg. Med. Rep. 2012.

44. Corazza O, Roman-Urrestarazu A. Handbook of Novel Psychoactive Substances: What Clinicians Should Know about NPS: Taylor & Francis, 2018.

45. Sikk K, Taba P. Chapter Twelve - Methcathinone “Kitchen Chemistry” and Permanent Neurological Damage. In: Taba P, Lees A, Sikk K, editors. International Review of Neurobiology: Academic Press, 2015. p. 257-271.

46. Barceloux DG. Methcathinone, Mephedrone, and Methylone. Medical Toxicology of Drug Abuse: Synthesized Chemicals and Psychoactive Plants: John Wiley & Sons, Inc., 2012. p. 120-125.

47. L’Italien Y, Park H, Rebstock L. Methylaminopropiophenone compounds and methods for producing the same. United States Patent Office (1957). [accessed April 25, 2018]. Available from: https://patentimages.storage.googleapis.com/bf/7b/0c/4680ba84af1e79/US2802865.pdf.

48. Emerson TS, Cisek JE. Methcathinone: A russian designer amphetamine infiltrates the rural midwest. Ann. Emerg. Med. 1993; 22: 1897-1903.

49. Kelly JP. Cathinone derivatives: A review of their chemistry, pharmacology and toxicology. Drug Test. Anal. 2011; 3: 439-453.

50. UN. Convention on Psychotropic Substances, 1971. UN Doc. No. A/RES/3443 [accessed October 29, 2018]. Available from: https://www.unodc.org.

51. UNODC. Terminology and Information on Drugs - Third Edition. [accessed May 7, 2019]. Available from: https://www.unodc.org.

52. Angrist B, Sudilovsky A. Central Nervous System Stimulants: Historical Aspects and Clinical Effects. In: Iversen L, editor. Stimulants. New York: Springer US, 2012. p. 99-165.

53. Werke T. Anorexigenic Propiophenones. United States Patent Office (1961). [accessed April 25, 2018]. Available from: https://worldwide.espacenet.com/publicationDetails/originalDocument?CC=US&NR=3001910A&KC=A&FT=D&ND=&date=19610926&DB=&locale=en_EP.

54. Clein LJ, Benady DR. Case of diethylpropion addiction. Br. Med. J. 1962; 2: 456-456.

55. Kuenssberg EV. Diethylpropion. Br. Med. J. 1962; 2: 729-730.

56. Gardos G, Cole JO. Evaluation of pyrovalerone in chronically fatigued volunteers. Curr. Ther. Res. Clin. Exp. 1971; 13: 631-635.

57. Goldberg J, Gardos G, Cole JO. A controlled evaluation of pyrovalerone in chronically fatigued volunteers. Int. Pharmacopsychiatry 1973; 8: 60-69.

58. Deniker P, Loo H, Cuche H, Roux JM. [Abuse of pyrovalerone by drug addicts]. Ann. Med. Psychol. (Paris) 1975; 2: 745-748.

59. Jacob P, Shulgin AT. Novel N-Substituted-2-Amino-3’,4’-Methylenedioxy Propiophenone. World Intelectual Property Organization (1996). [accessed April 26, 2018]. Available from: https://patentimages.storage.googleapis.com/66/e4/41/78d0d55fdbdae1/WO1996039133A1.pdf.

60. Dal Cason TA, Young R, Glennon RA. Cathinone: An Investigation of Several N-Alkyl and Methylenedioxy-Substituted Analogs. Pharmacol. Biochem. Behav. 1997; 58: 1109-1116.

61. Bossong MG, Van Dijk JP, Niesink RJ. Methylone and mCPP, two new drugs of abuse? Addict. Biol. 2005; 10: 321-323.

62. Bentur Y, Bloom-Krasik A, Raikhlin-Eisenkraft B. Illicit cathinone ("Hagigat") poisoning. Clin. Toxicol. 2008; 46: 206-210.

63. Power M. Drugs Unlimited: The Web Revolution That's Changing How the World Gets High. New York: St. Martin's Press, 2014.

64. Karila L, Megarbane B, Cottencin O, Lejoyeux M. Synthetic Cathinones: A New Public Health Problem. Curr. Neuropharmacol. 2015; 13: 12-20.

65. Oyemade A. Meow meow or miaow miaow: a new drug of concern. Psychiatry (Edgmont). 2010; 7: 10.

66. EMCDDA-Europol. EMCDDA-Europol 2008 annual report on the implementation of council decision 2005/387/JHA. [accessed November 12, 2018]. Available from: http://www.emcdda.europa.eu/.

67. Measham F, Moore K, Newcombe R, Z. Tweaking, bombing, dabbing and stockpiling: the emergence of mephedrone and the perversity of prohibition. Drugs and Alcohol Today 2010; 10: 14-21.

68. Schifano F, Albanese A, Fergus S, Stair JL, Deluca P, Corazza O, et al. Mephedrone (4-methylmethcathinone; 'meow meow'): chemical, pharmacological and clinical issues. Psychopharmacology 2011; 214: 593-602.

69. Winstock AR, Mitcheson LR, Deluca P, Davey Z, Corazza O, Schifano F. Mephedrone, new kid for the chop? Addiction 2011; 106: 154-161.

70. Dargan PI, Albert S, Wood DM. Mephedrone use and associated adverse effects in school and college/university students before the UK legislation change. QJM-INT. J. MED. 2010; 103: 875-879.

71. Morris K. UK places generic ban on mephedrone drug family. Lancet 2010; 375: 1333-1334.

72. Spiller HA, Ryan ML, Weston RG, Jansen J. Clinical experience with and analytical confirmation of "bath salts" and "legal highs" (synthetic cathinones) in the United States. Clin. Toxicol. 2011; 49: 499-505.

73. Watterson LR, Burrows BT, Hernandez RD, Moore KN, Grabenauer M, Marusich JA, et al. Effects of α-Pyrrolidinopentiophenone and 4-Methyl-N-Ethylcathinone, Two Synthetic Cathinones Commonly Found in Second-Generation "Bath Salts," on Intracranial Self-Stimulation Thresholds in Rats. Int. J. Neuropsychopharmacol. 2015; 18: pyu014-pyu014.

74. Drug Enforcement Administration, Department of Justice. Drug Enforcement Administration, Schedules of controlled substances: temporary placement of three synthetic cathinones in Schedule I. Final Order. Fed Regist 2011; 76: 65371-65375.

75. Vardakou I, Pistos C, Dona A, Spiliopoulou C, Athanaselis S. Naphyrone: a “legal high” not legal any more. Drug Chem. Toxicol. 2012; 35: 467-471.

76. Brandt SD, Sumnall HR, Measham F, Cole J. Analyses of second-generation ‘legal highs’ in the UK: Initial findings. Drug Test. Anal. 2010; 2: 377-382.

77. Brandt SD, Freeman S, Sumnall HR, Measham F, Cole J. Analysis of NRG ‘legal highs’ in the UK: identification and formation of novel cathinones. Drug Test. Anal. 2011; 3: 569-575.

78. Crespi C. Flakka-Induced Prolonged Psychosis. Case Rep. Psychiatry 2016; 2016: 3460849-3460849.

79. Castellanos D, Menendez B, Logan BK, Mohr ALA, Ayer D, Thomas M, et al. "Flakka" Intoxication: What have We Learned? J. Drug Abuse 2018; 4: 1-6.

80. Nóbrega L, Dinis-Oliveira RJ. The synthetic cathinone α-pyrrolidinovalerophenone (α-PVP): pharmacokinetic and pharmacodynamic clinical and forensic aspects. Drug Metab. Rev. 2018; 50: 125-139.

81. Uchiyama N, Matsuda S, Kawamura M, Shimokawa Y, Kikura-Hanajiri R, Aritake K, et al. Characterization of four new designer drugs, 5-chloro-NNEI, NNEI indazole analog, α-PHPP and α-POP, with 11 newly distributed designer drugs in illegal products. Forensic Sci. Int. 2014; 243: 1-13.

82. Uchiyama N, Matsuda S, Kawamura M, Kikura-Hanajiri R, Goda Y. Identification of two new-type designer drugs, piperazine derivative MT-45 (I-C6) and synthetic peptide Noopept (GVS-111), with synthetic cannabinoid A-834735, cathinone derivative 4-methoxy-α-PVP, and phenethylamine derivative 4-methylbuphedrine from illegal products. Forensic Toxicol. 2014; 32: 9-18.

83. Uchiyama N, Shimokawa Y, Kawamura M, Kikura-Hanajiri R, Hakamatsuka T. Chemical analysis of a benzofuran derivative, 2-(2-ethylaminopropyl)benzofuran (2-EAPB), eight synthetic cannabinoids, five cathinone derivatives, and five other designer drugs newly detected in illegal products. Forensic Toxicol. 2014; 32: 266-281.

84. Gaspar H, Bronze S, Ciríaco S, Queirós CR, Matias A, Rodrigues J, et al. 4F-PBP (4’-fluoro-α-pyrrolidinobutyrophenone), a new substance of abuse: Structural characterization and purity NMR profiling. Forensic Sci. Int. 2015; 252: 168-176.

85. Doi T, Asada A, Takeda A, Tagami T, Katagi M, Matsuta S, et al. Identification and characterization of α-PVT, α-PBT, and their bromothienyl analogs found in illicit drug products. Forensic Toxicol. 2016; 34: 76-93.

86. Gambaro V, Casagni E, Dell’Acqua L, Roda G, Tamborini L, Visconti GL, et al. Identification and characterization of a new designer drug thiothinone in seized products. Forensic Toxicol. 2016; 34: 174-178.

87. Liu C, Jia W, Li T, Hua Z, Qian Z. Identification and analytical characterization of nine synthetic cathinone derivatives N-ethylhexedrone, 4-Cl-pentedrone, 4-Cl-α-EAPP, propylone, N-ethylnorpentylone, 6-MeO-bk-MDMA, α-PiHP, 4-Cl-α-PHP, and 4-F-α-PHP. Drug Test. Anal. 2017; 9: 1162-1171.

88. Błażewicz A, Bednarek E, Sitkowski J, Popławska M, Stypułkowska K, Bocian W, et al. Identification and structural characterization of four novel synthetic cathinones: α-methylaminohexanophenone (hexedrone, HEX), 4-bromoethcathinone (4-BEC), 4-chloro-α-pyrrolidinopropiophenone (4-Cl-PPP), and 4-bromo-α-pyrrolidinopentiophenone (4-Br-PVP) after their seizures. Forensic Toxicol. 2017; 35: 317-332.

89. EMCDDA. New Psychoactive Substances: Global Markets, Glocal Threats and the COVID-19 Pandemic-An Update from the EU Early Warning System. [accessed March 29, 2022]. Available from: https://www.emcdda.europa.eu/publications/rapid-communication/new-psychoactive-substances-global-markets-glocal-threats-and-covid-19-pandemic_en.

90. EMCDDA. European Drug Report 2018: Trends and Developments. [accessed January 19, 2019]. Available from: http://www.emcdda.europa.eu/.

91. Paillet-Loilier M, Cesbron A, Le Boisselier R, Bourgine J, Debruyne D. Emerging drugs of abuse: current perspectives on substituted cathinones. Subst. Abuse Rehabil. 2014; 5: 37-52.

92. Calinski DM, Kisor DF, Sprague JE. A review of the influence of functional group modifications to the core scaffold of synthetic cathinones on drug pharmacokinetics. Psychopharmacology 2018; 236: 881–890.

93. Zawilska JB, Wojcieszak J. Designer cathinones—An emerging class of novel recreational drugs. Forensic Sci. Int. 2013; 231: 42-53.

94. James D, Adams RD, Spears R, Cooper G, Lupton DJ, Thompson JP, et al. Clinical characteristics of mephedrone toxicity reported to the U.K. National Poisons Information Service. Emerg. Med. J. 2011; 28: 686-689.

95. Carhart-Harris RL, King LA, Nutt DJ. A web-based survey on mephedrone. Drug Alcohol Depend. 2011; 118: 19-22.

96. Gil D, Adamowicz P, Skulska A, Tokarczyk B, Stanaszek R. Analysis of 4-MEC in biological and non-biological material—Three case reports. Forensic Sci. Int. 2013; 228: e11-e15.

97. Kerrigan S. Improved Detection of Synthetic Cathinones in Forensic Toxicology Samples: Thermal Degradation and Analytical Considerations. U.S. Department of Justice, 2015.

98. Dargan PI, Sedefov R, Gallegos A, Wood DM. The pharmacology and toxicology of the synthetic cathinone mephedrone (4-methylmethcathinone). Drug Test. Anal. 2011; 3: 454-463.

99. Rosenbaum CD, Carreiro SP, Babu KM. Here today, gone tomorrow...and back again? A review of herbal marijuana alternatives (K2, Spice), synthetic cathinones (bath salts), kratom, Salvia divinorum, methoxetamine, and piperazines. J. Med. Toxicol. 2012; 8: 15-32.

100. Wikstrom M, Thelander G, Nystrom I, Kronstrand R. Two fatal intoxications with the new designer drug methedrone (4-methoxymethcathinone). J. Anal. Toxicol. 2010; 34: 594-598.

101. Zuba D, Adamowicz P, Byrska B. Detection of buphedrone in biological and non-biological material – Two case reports. Forensic Sci. Int. 2013; 227: 15-20.

102. Miotto K, Striebel J, Cho AK, Wang C. Clinical and pharmacological aspects of bath salt use: A review of the literature and case reports. Drug Alcohol Depend. 2013; 132: 1-12.

103. Karila L, Lafaye G, Scocard A, Cottencin O, Benyamina A. MDPV and α-PVP use in humans: The twisted sisters. Neuropharmacology 2018; 134: 65-72.

104. Zawilska JB, Wojcieszak J. α-Pyrrolidinophenones: a new wave of designer cathinones. Forensic Toxicol. 2017; 35: 201-216.

105. Zawilska JB. "Legal Highs" – An Emerging Epidemic of Novel Psychoactive Substances. In: Taba P, Lees A, Sikk K, editors. International Review of Neurobiology: Academic Press, 2015. p. 273-300.

106. Weinstein AM, Rosca P, Fattore L, London ED. Synthetic Cathinone and Cannabinoid Designer Drugs Pose a Major Risk for Public Health. Front. Psychiatry 2017; 8.

107. Commission on Narcotic Drugs. New psychoactive substances: overview of trends, challenges and legal approaches. [accessed December 12, 2018]. Available from: https://www.unodc.org/.

108. Pedersen AJ, Reitzel LA, Johansen SS, Linnet K. In vitro metabolism studies on mephedrone and analysis of forensic cases. Drug Test. Anal. 2013; 5: 430-438.

109. Uchtenhagen A. Which policy for new psychoactive drugs? Addiction 2017; 112: 32-33.

110. Tettey JN, Levissianos S. The Global Emergence of NPS: An Analysis of a New Drug Trend. In: Corazza O, Roman-Urrestarazu A, editors. Novel Psychoactive Substances: Policy, Economics and Drug Regulation. Cham: Springer International Publishing, 2017. p. 1-12.

111. DRE. Decree Law No. 54/2013 of 17 April 2013, Administrative Rule 154/2013.: Diário da República n.º 75/2013, Série I de 2013-04-17; 2013 [accessed July 24, 2020]. Available from: https://dre.pt/pesquisa/-/search/260421/details/.

112. Majchrzak M, Celiński R, Kuś P, Kowalska T, Sajewicz M. The newest cathinone derivatives as designer drugs: an analytical and toxicological review. Forensic Toxicol. 2018; 36: 33-50.

113. Tyrkko E, Andersson M, Kronstrand R. The Toxicology of New Psychoactive Substances: Synthetic Cathinones and Phenylethylamines. Ther. Drug Monit. 2016; 38: 190-216.

114. Valente MJ, Araújo AM, Bastos MdL, Fernandes E, Carvalho F, Guedes de Pinho P, et al. Editor's Highlight: Characterization of Hepatotoxicity Mechanisms Triggered by Designer Cathinone Drugs (β-Keto Amphetamines). Toxicol. Sci. 2016; 153: 89-102.

115. Westphal F, Junge T, Rösner P, Fritschi G, Klein B, Girreser U. Mass spectral and NMR spectral data of two new designer drugs with an α-aminophenone structure: 4'-Methyl-

α-pyrrolidinohexanophenone and 4’-methyl-α-pyrrolidinobutyrophenone. Forensic Sci. Int. 2007; 169: 32-42.

116. Coppola M, Mondola R, Oliva F, Picci RL, Ascheri D, Trivelli F. Treating the Phenomenon of New Psychoactive Substances: Synthetic Cannabinoids and Synthetic Cathinones. In: Preedy VR, editor. Neuropathology of Drug Addictions and Substance Misuse. San Diego: Academic Press, 2016. p. 679-686.

117. Mladěnka P, Applová L, Patočka J, Costa VM, Remiao F, Pourová J, et al. Comprehensive review of cardiovascular toxicity of drugs and related agents. Med. Res. Rev. 2018; 38: 1332-1403.

118. Winder GS, Stern N, Hosanagar A. Are "Bath Salts" the next generation of stimulant abuse? J. Subst. Abuse Treat. 2013; 44: 42-45.

119. Gibbons S, Zloh M. An analysis of the ‘legal high’ mephedrone. Bioorg. Med. Chem. Lett. 2010; 20: 4135-4139.

120. Coppola M, Mondola R. 3,4-Methylenedioxypyrovalerone (MDPV): Chemistry, pharmacology and toxicology of a new designer drug of abuse marketed online. Toxicol. Lett. 2012; 208: 12-15.

121. Ellefsen KN, Concheiro M, Huestis MA. Synthetic cathinone pharmacokinetics, analytical methods, and toxicological findings from human performance and postmortem cases. Drug Metab. Rev. 2016; 48: 237-265.

122. Simmler LD, Buser TA, Donzelli M, Schramm Y, Dieu LH, Huwyler J, et al. Pharmacological characterization of designer cathinones *in vitro*. Br. J. Pharmacol. 2013; 168: 458-470.

123. Almeida AS, Silva B, Pinho PGd, Remião F, Fernandes C. Synthetic Cathinones: Recent Developments, Enantioselectivity Studies and Enantioseparation Methods. Molecules 2022; 27: 2057.

124. Fleckenstein AE, Haughey HM, Metzger RR, Kokoshka JM, Riddle EL, Hanson JE, et al. Differential effects of psychostimulants and related agents on dopaminergic and serotonergic transporter function. Eur. J. Pharmacol. 1999; 382: 45-49.

125. Cozzi NV, Sievert MK, Shulgin AT, Jacob P, Ruoho AE. Inhibition of plasma membrane monoamine transporters by β-ketoamphetamines. Eur. J. Pharmacol. 1999; 381: 63-69.

126. Simmler LD, Rickli A, Hoener MC, Liechti ME. Monoamine transporter and receptor interaction profiles of a new series of designer cathinones. Neuropharmacology 2014; 79: 152-160.

127. Meltzer PC, Butler D, Deschamps JR, Madras BK. 1-(4-Methylphenyl)-2-pyrrolidin-1-yl-pentan-1-one (Pyrovalerone) analogues: a promising class of monoamine uptake inhibitors. J. Med. Chem. 2006; 49: 1420-1432.

128. Katz DP, Bhattacharya D, Bhattacharya S, Deruiter J, Clark CR, Suppiramaniam V, et al. Synthetic cathinones: “A khat and mouse game”. Toxicol. Lett. 2014; 229: 349-356.

129. Baumann MH, Partilla JS, Lehner KR. Psychoactive "bath salts": not so soothing. Eur. J. Pharmacol. 2013; 698: 1-5.

130. Baumann MH, Partilla JS, Lehner KR, Thorndike EB, Hoffman AF, Holy M, et al. Powerful Cocaine-Like Actions of 3,4-Methylenedioxypyrovalerone (MDPV), a Principal Constituent of Psychoactive 'Bath Salts' Products. Neuropsychopharmacology 2012; 38: 552-562.

131. Marusich JA, Antonazzo KR, Wiley JL, Blough BE, Partilla JS, Baumann MH. Pharmacology of novel synthetic stimulants structurally related to the "bath salts" constituent 3,4-methylenedioxypyrovalerone (MDPV). Neuropharmacology 2014; 87: 206-213.

132. Saha K, Partilla JS, Lehner KR, Seddik A, Stockner T, Holy M, et al. 'Second-generation' mephedrone analogs, 4-MEC and 4-MePPP, differentially affect monoamine transporter function. Neuropsychopharmacology 2015; 40: 1321-1331.

133. Glennon RA, Dukat M. Synthetic Cathinones: A Brief Overview of Overviews with Applications to the Forensic Sciences. Ann. Forensic Res. Anal. 2017; 4: 1040.

134. Kolanos R, Solis E, Jr., Sakloth F, De Felice LJ, Glennon RA. "Deconstruction" of the abused synthetic cathinone methylenedioxypyrovalerone (MDPV) and an examination of effects at the human dopamine transporter. ACS Chem. Neurosci. 2013; 4: 1524-1529.

135. Kolanos R, Sakloth F, Jain AD, Partilla JS, Baumann MH, Glennon RA. Structural Modification of the Designer Stimulant α-Pyrrolidinovalerophenone (α-PVP) Influences Potency at Dopamine Transporters. ACS Chem. Neurosci. 2015; 6: 1726-1731.

136. Suyama JA, Sakloth F, Kolanos R, Glennon RA, Lazenka MF, Negus SS, et al. Abuse-Related Neurochemical Effects of Para-Substituted Methcathinone Analogs in Rats: Microdialysis Studies of Nucleus Accumbens Dopamine and Serotonin. J. Pharmacol. Exp. Ther. 2016; 356: 182-190.

137. McGraw M, McGraw L. Bath Salts: Not as Harmless as They Sound. J. Emerg. Nurs. 2012; 38: 582-588.

138. Soria ML. New psychoactive substances: Popular and dangerous. Span. J. Leg. Med. 2018; 44: 64-72.

139. Soares J, Costa VM, Bastos MdL, Carvalho F, Capela JP. An updated review on synthetic cathinones. Arch. Toxicol. 2021; 95: 2895-2940.

140. Simão AY, Antunes M, Cabral E, Oliveira P, Rosendo LM, Brinca AT, et al. An Update on the Implications of New Psychoactive Substances in Public Health. Int. J. Environ. Res. Public Health 2022; 19: 4869.

141. Martínez-Clemente J, López-Arnau R, Carbó M, Pubill D, Camarasa J, Escubedo E. Mephedrone pharmacokinetics after intravenous and oral administration in rats: relation to pharmacodynamics. Psychopharmacology (Berl) 2013; 229: 295-306.

142. López-Arnau R, Martínez-Clemente J, Carbó Ml, Pubill D, Escubedo E, Camarasa J. An integrated pharmacokinetic and pharmacodynamic study of a new drug of abuse, methylone, a synthetic cathinone sold as "bath salts". Prog. Neuropsychopharmacol. Biol. Psychiatry 2013; 45: 64-72.

143. Olesti E, Pujadas M, Papaseit E, Pérez-Mañá C, Pozo ÓJ, Farré M, et al. GC–MS Quantification Method for Mephedrone in Plasma and Urine: Application to Human Pharmacokinetics. J. Anal. Toxicol. 2016; 41: 100-106.

144. Papaseit E, Pérez-Mañá C, Mateus J-A, Pujadas M, Fonseca F, Torrens M, et al. Human Pharmacology of Mephedrone in Comparison with MDMA. Neuropsychopharmacology 2016; 41: 2704-2713.

145. Namera A, Konuma K, Kawamura M, Saito T, Nakamoto A, Yahata M, et al. Time-course profile of urinary excretion of intravenously administered α-pyrrolidinovalerophenone and α-pyrrolidinobutiophenone in a human. Forensic Toxicol. 2014; 32: 68-74.

146. Shimshoni JA, Britzi M, Sobol E, Willenz U, Nutt D, Edery N. 3-Methyl-methcathinone: Pharmacokinetic profile evaluation in pigs in relation to pharmacodynamics. J. Psychopharmacol. 2015; 29: 734-743.

147. Grecco GG, Kisor DF, Magura JS, Sprague JE. Impact of common clandestine structural modifications on synthetic cathinone “bath salt” pharmacokinetics. Toxicol. Appl. Pharmacol. 2017; 328: 18-24.

148. Elmore JS, Dillon-Carter O, Partilla JS, Ellefsen KN, Concheiro M, Suzuki M, et al. Pharmacokinetic Profiles and Pharmacodynamic Effects for Methylone and Its Metabolites in Rats. Neuropsychopharmacology 2017; 42: 649-660.

149. Anizan S, Concheiro M, Lehner KR, Bukhari MO, Suzuki M, Rice KC, et al. Linear pharmacokinetics of 3,4-methylenedioxypyrovalerone (MDPV) and its metabolites in the rat: relationship to pharmacodynamic effects. Addict. Biol. 2016; 21: 339-347.

150. Baumann MH, Bukhari MO, Lehner KR, Anizan S, Rice KC, Concheiro M, et al. Neuropharmacology of 3,4-Methylenedioxypyrovalerone (MDPV), Its Metabolites, and Related Analogs. Curr. Top. Behav. Neurosci. 2017; 32: 93-117.

151. Novellas J, López-Arnau R, Carbó ML, Pubill D, Camarasa J, Escubedo E. Concentrations of MDPV in rat striatum correlate with the psychostimulant effect. J. Psychopharmacol. 2015; 29: 1209-1218.

152. Šíchová K, Pinterová N, Židková M, Horsley RR, Lhotková E, Štefková K, et al. Mephedrone (4-Methylmethcathinone): Acute Behavioral Effects, Hyperthermic, and Pharmacokinetic Profile in Rats. Front. Psychiatry 2018; 8: 306-306.

153. Štefková K, Židková M, Horsley RR, Pinterová N, Šíchová K, Uttl L, et al. Pharmacokinetic, Ambulatory, and Hyperthermic Effects of 3,4-Methylenedioxy-N-Methylcathinone (Methylone) in Rats. Front. Psychiatry 2017; 8: 232-232.

154. Horsley RR, Lhotkova E, Hajkova K, Feriancikova B, Himl M, Kuchar M, et al. Behavioural, Pharmacokinetic, Metabolic, and Hyperthermic Profile of 3,4-Methylenedioxypyrovalerone (MDPV) in the Wistar Rat. Front. Psychiatry 2018; 9: 144-144.

155. Pinterova-Leca N, Horsley RR, Danda H, Žídková M, Lhotková E, Šíchová K, et al. Naphyrone (naphthylpyrovalerone): Pharmacokinetics, behavioural effects and thermoregulation in Wistar rats. Addict. Biol. 2021; 26: e12906.

156. Mégarbane B, Gamblin C, Roussel O, Bouaziz-Amar E, Chevillard L, Callebert J, et al. The neurobehavioral effects of the designer drug naphyrone – an experimental investigation with pharmacokinetics and concentration/effect relationship in mice. Psychopharmacology 2020; 237: 1943-1957.

157. Richter LHJ, Flockerzi V, Maurer HH, Meyer MR. Pooled human liver preparations, HepaRG, or HepG2 cell lines for metabolism studies of new psychoactive substances? A study using MDMA, MDBD, butylone, MDPPP, MDPV, MDPB, 5-MAPB, and 5-API as examples. J. Pharm. Biomed. Anal. 2017; 143: 32-42.

158. Kamata HT, Shima N, Zaitsu K, Kamata T, Miki A, Nishikawa M, et al. Metabolism of the recently encountered designer drug, methylone, in humans and rats. Xenobiotica 2006; 36: 709-723.

159. Zaitsu K, Katagi M, Tatsuno M, Sato T, Tsuchihashi H, Suzuki K. Recently abused β-keto derivatives of 3,4-methylenedioxyphenylalkylamines: a review of their metabolisms and toxicological analysis. Forensic Toxicol. 2011; 29: 73-84.

160. Zaitsu K. Metabolism of Synthetic Cathinones. In: Zawilska JB, editor. Synthetic Cathinones: Novel Addictive and Stimulatory Psychoactive Substances. Cham: Springer International Publishing, 2018. p. 71-96.

161. Peters FT, Meyer MR. *In vitro* approaches to studying the metabolism of new psychoactive compounds. Drug Test. Anal. 2011; 3: 483-495.

162. Toennes SW, Kauert GF. Excretion and Detection of Cathinone, Cathine, and Phenylpropanolamine in Urine after Kath Chewing. Clin. Chem. 2002; 48: 1715-1719.

163. Brenneisen R, Mathys K, Geisshüsler S, Fisch HU, Koelbing U, Kalix P. Determination of S-(-)-Cathinone and Its Main Metabolite R,S-(-)-Norephedrine In Human Plasma By High-Performance Liquid Chromatography and Photodiode Array Detection. J. Liq. Chromatogr. 1991; 14: 271-286.

164. Mathys K, Brenneisen R. Determination of (S)-(−)-cathinone and its metabolites (R,S)-(−)-norephedrine and (R,R)-(−)-norpseudoephedrine in urine by high-performance liquid chromatography with photodiode-array detection. J. Chromatogr. A 1992; 593: 79-85.

165. Paul BD, Cole KA. Cathinone (Khat) and Methcathinone (CAT) in Urine Specimens: A Gas Chromatographic-Mass Spectrometric Detection Procedure. J. Anal. Toxicol. 2001; 25: 525-530.

166. Schreiber EC, Min BH, Zeiger AV, Lang JF. Metabolism of diethylpropion-1-C^{14} hydrochloride by the human. J. Pharmacol. Exp. Ther. 1968; 159: 372-378.

167. Meyer MR, Wilhelm J, Peters FT, Maurer HH. Beta-keto amphetamines: studies on the metabolism of the designer drug mephedrone and toxicological detection of mephedrone, butylone, and methylone in urine using gas chromatography–mass spectrometry. Anal. Bioanal. Chem. 2010; 397: 1225-1233.

168. Ciechomska M, Woźniakiewicz M, Wietecha-Posłuszny R. Activity and Biotransformation of Three Synthetic "Legal Highs": Mephedrone, Methylone and 3,4-methylenodioxypyrovalerone. Prob. Forensic Sci. 2012; 89: 71-85.

169. Zaitsu K, Katagi M, Kamata HT, Kamata T, Shima N, Miki A, et al. Determination of the metabolites of the new designer drugs bk-MBDB and bk-MDEA in human urine. Forensic Sci. Int. 2009; 188: 131-139.

170. Sauer C, Peters FT, Haas C, Meyer MR, Fritschi G, Maurer HH. New designer drug α-pyrrolidinovalerophenone (PVP): studies on its metabolism and toxicological detection in rat urine using gas chromatographic/mass spectrometric techniques. J. Mass Spectrom. 2009; 44: 952-964.

171. Springer D, Fritschi G, Maurer HH. Metabolism of the new designer drug α-pyrrolidinopropiophenone (PPP) and the toxicological detection of PPP and 4′-methyl-α-pyrrolidinopropiophenone (MPPP) studied in rat urine using gas chromatography-mass spectrometry. J. Chromatogr. B 2003; 796: 253-266.

172. Matsuta S, Shima N, Kakehashi H, Kamata H, Nakano S, Sasaki K, et al. Metabolism of α-PHP and α-PHPP in humans and the effects of alkyl chain lengths on the metabolism of α-pyrrolidinophenone-type designer drugs. Forensic Toxicol. 2018; 36: 486-497.

173. Katselou M, Papoutsis I, Nikolaou P, Spiliopoulou C, Athanaselis S. α-PVP (“flakka”): a new synthetic cathinone invades the drug arena. Forensic Toxicol. 2016; 34: 41-50.

174. Negreira N, Erratico C, Kosjek T, van Nuijs ALN, Heath E, Neels H, et al. In vitro Phase I and Phase II metabolism of α-pyrrolidinovalerophenone (α-PVP), methylenedioxypyrovalerone (MDPV) and methedrone by human liver microsomes and human liver cytosol. Anal. Bioanal. Chem. 2015; 407: 5803-5816.

175. Shima N, Kakehashi H, Matsuta S, Kamata H, Nakano S, Sasaki K, et al. Urinary excretion and metabolism of the α-pyrrolidinophenone designer drug 1-phenyl-2-(pyrrolidin-1-yl)octan-1-one (PV9) in humans. Forensic Toxicol. 2015; 33: 279-294.

176. Meyer MR, Du P, Schuster F, Maurer HH. Studies on the metabolism of the α-pyrrolidinophenone designer drug methylenedioxy-pyrovalerone (MDPV) in rat and human urine and human liver microsomes using GC–MS and LC–high-resolution MS and its detectability in urine by GC–MS. J. Mass Spectrom. 2010; 45: 1426-1442.

177. Springer D, Staack RF, Paul LD, Kraemer T, Maurer HH. Identification of cytochrome P450 enzymes involved in the metabolism of 3′,4′-methylenedioxy-α-pyrrolidinopropiophenone (MDPPP), a designer drug, in human liver microsomes. Xenobiotica 2005; 35: 227-237.

178. Gries RR, Straw K. Manifestations and treatment of central nervous system complications associated with synthetic cathinone (“bath salts”) toxicities. Mental Health Clinician 2013; 3: 309-312.

179. Loeffler G, Penn A, Ledden B. "Bath salt"-induced agitated paranoia: a case series. J. Stud. Alcohol Drugs 2012; 73: 706.

180. Romolo FS, Fiore PA, Bottoni E, Cappelletti S, Aromatario M, Ciallella C. Mephedrone and Mephedrone-Based Cocktails: Market, Analysis, Mechanisms of Action, and Toxicity. In: Preedy VR, editor. Neuropathology of Drug Addictions and Substance Misuse. San Diego: Academic Press, 2016. p. 40-49.

181. Boulanger-Gobeil C, St-Onge M, Laliberté M, Auger PL. Seizures and hyponatremia related to ethcathinone and methylone poisoning. J. Med. Toxicol. 2012; 8: 59-61.

182. Karila L, Billieux J, Benyamina A, Lançon C, Cottencin O. The effects and risks associated to mephedrone and methylone in humans: A review of the preliminary evidences. Brain Res. Bull. 2016; 126: 61-67.

183. Fröhlich S, Lambe E, O'Dea J. Acute liver failure following recreational use of psychotropic "head shop" compounds. Ir. J. Med. Sci. 2011; 180: 263-264.

184. Borek HA, Holstege CP. Hyperthermia and Multiorgan Failure After Abuse of "Bath Salts" Containing 3,4-Methylenedioxypyrovalerone. Ann. Emerg. Med. 2012; 60: 103-105.

185. Garrett G, Sweeney M. The serotonin syndrome as a result of mephedrone toxicity. BMJ Case Reports 2010; 2010: bcr0420102925.

186. Valga-Amado F, Monzón-Vázquez TR, Hadad F, Torrente-Sierra J, Pérez-Flores I, Barrientos-Guzmán A. Rhabdomyolysis with acute renal failure secondary to taking methadone. Nefrología 2012; 32: 262-263.

187. Adebamiro A, Perazella MA. Recurrent Acute Kidney Injury Following Bath Salts Intoxication. Am. J. Kidney Dis. 2012; 59: 273-275.

188. Valente MJ, Araújo AM, Silva R, Bastos MdL, Carvalho F, Guedes de Pinho P, et al. 3,4-Methylenedioxypyrovalerone (MDPV): in vitro mechanisms of hepatotoxicity under normothermic and hyperthermic conditions. Arch. Toxicol. 2016; 90: 1959-1973.

189. Leyrer-Jackson JM, Nagy EK, Olive MFJP. Cognitive deficits and neurotoxicity induced by synthetic cathinones: is there a role for neuroinflammation? Psychopharmacology 2019; 236: 1079-1095.

190. Khattab NY, Amer G. Undetected neuropsychophysiological sequelae of khat chewing in standard aviation medical examination. Aviat. Space Environ. Med. 1995; 66: 739-744.

191. Colzato LS, Ruiz MJ, van den Wildenberg WPM, Bajo MT, Hommel B. Long-term effects of chronic khat use: impaired inhibitory control. Front. Psychol. 2011; 1: 219-219.

192. Colzato LS, Ruiz MJ, van den Wildenberg WPM, Hommel B. Khat use is associated with impaired working memory and cognitive flexibility. PloS one 2011; 6: e20602-e20602.

193. Ismail AA, El Sanosy RM, Rohlman DS, El-Setouhy M. Neuropsychological Functioning Among Chronic Khat Users in Jazan Region, Saudi Arabia. Substance Abuse 2014; 35: 235-244.

194. Freeman TP, Morgan CJA, Vaughn-Jones J, Hussain N, Karimi K, Curran HV. Cognitive and subjective effects of mephedrone and factors influencing use of a 'new legal high'. Addiction 2012; 107: 792-800.

195. Herzig DA, Brooks R, Mohr C. Inferring about individual drug and schizotypy effects on cognitive functioning in polydrug using mephedrone users before and after clubbing. Hum. Psychopharmacol Clin. Exp. 2013; 28: 168-182.

196. Homman L, Seglert J, Morgan MJJP. An observational study on the sub-acute effects of mephedrone on mood, cognition, sleep and physical problems in regular mephedrone users. Psychopharmacology 2018; 235: 2609-2618.

197. Wright J, MJ, Vandewater S, Angrish D, Dickerson T, Taffe M. Mephedrone (4-methylmethcathinone) and d-methamphetamine improve visuospatial associative memory, but not spatial working memory, in rhesus macaques. Br. J. Pharmacol. 2012; 167: 1342-1352.

198. Sewalia K, Watterson LR, Hryciw A, Belloc A, Ortiz JB, Olive MF. Neurocognitive dysfunction following repeated binge-like self-administration of the synthetic cathinone 3,4-methylenedioxypyrovalerone (MDPV). Neuropharmacology 2018; 134: 36-45.

199. Daniel JJ, Hughes RN. Increased anxiety and impaired spatial memory in young adult rats following adolescent exposure to methylone. Pharmacol. Biochem. Behav. 2016; 146-147: 44-49.

200. Naseri G, Fazel A, Golalipour MJ, Haghir H, Sadeghian H, Mojarrad M, et al. Exposure to mephedrone during gestation increases the risk of stillbirth and induces hippocampal neurotoxicity in mice offspring. Neurotoxicol. Teratol. 2018; 67: 10-17.

201. Martínez-Clemente J, López-Arnau R, Abad S, Pubill D, Escubedo E, Camarasa J. Dose and time-dependent selective neurotoxicity induced by mephedrone in mice. PloS one 2014; 9: e99002-e99002.

202. Siedlecka-Kroplewska K, Szczerba A, Lipinska A, Slebioda T, Kmiec Z. 3-Fluoromethcathinone, a structural analog of mephedrone, inhibits growth and induces cell cycle arrest in HT22 mouse hippocampal cells. J. Physiol. Pharmacol. 2014; 65: 241-246.

203. Wojcieszak J, Andrzejczak D, Woldan-Tambor A, Zawilska JB. Cytotoxic Activity of Pyrovalerone Derivatives, an Emerging Group of Psychostimulant Designer Cathinones. Neurotox. Res. 2016; 30: 239-250.

204. Valente MJ, Amaral C, Correia-da-Silva G, Duarte JA, Bastos MdL, Carvalho F, et al. Methylone and MDPV activate autophagy in human dopaminergic SH-SY5Y cells: a new insight into the context of β-keto amphetamines-related neurotoxicity. Arch. Toxicol. 2017; 91: 3663-3676.

205. Matsunaga T, Morikawa Y, Kamata K, Shibata A, Miyazono H, Sasajima Y, et al. α-Pyrrolidinononanophenone provokes apoptosis of neuronal cells through alterations in antioxidant properties. Toxicology 2017; 386: 93-102.

206. Siedlecka-Kroplewska K, Wrońska A, Stasiłojć G, Kmieć Z. The Designer Drug 3-Fluoromethcathinone Induces Oxidative Stress and Activates Autophagy in HT22 Neuronal Cells. Neurotox. Res. 2018; 34: 388-400.

207. Couto RAS, Gonçalves LM, Carvalho F, Rodrigues JA, Rodrigues CMP, Quinaz MB. The Analytical Challenge in the Determination of Cathinones, Key-Players in the Worldwide Phenomenon of Novel Psychoactive Substances. Crit. Rev. Anal. Chem. 2018; 48: 372-390.

208. Pourmand A, Mazer-Amirshahi M, Chistov S, Li A, Park M. Designer drugs: Review and implications for emergency management. Hum. Exp. Toxicol. 2018; 37: 94-101.

209. Mas-Morey P, Visser MHM, Winkelmolen L, Touw DJ. Clinical Toxicology and Management of Intoxications With Synthetic Cathinones ("Bath Salts"). J. Pharm. Pract. 2012; 26: 353-357.

210. Rosenbaum CD, Carreiro SP, Babu KM. Here today, gone tomorrow…and back again? A review of herbal marijuana alternatives (K2, Spice), synthetic cathinones (bath salts), kratom, Salvia divinorum, methoxetamine, and piperazines. J. Med. Toxicol. 2012; 8: 15-32.

211. Salerno TMG, Donato P, Frison G, Zamengo L, Mondello L. Gas Chromatography—Fourier Transform Infrared Spectroscopy for Unambiguous Determination of Illicit Drugs: A Proof of Concept. Front. Chem. 2020; 8.

212. SCIEX. Novel psychoactive substances: staying ahead of the curve. Screening, identifying, and quantifying with mass spectrometry. [accessed February 15, 2022]. Available from: https://sciex.com/content/dam/SCIEX/pdf/brochures/forensic-ebook.pdf.

213. Antunes M, Sequeira M, de Caires Pereira M, Caldeira MJ, Santos S, Franco J, et al. Determination of Selected Cathinones in Blood by Solid-Phase Extraction and GC-MS. J. Anal. Toxicol. 2021; 45: 233-242.

214. Girard JE. Criminalistics: Forensic Science, Crime, and Terrorism. Massachusetts: Jones & Bartlett Learning, 2021.

215. Bruni A, Rodrigues C, dos Santos C, de Castro J, Mariotto L, Sinhorini L. Analytical Challenges for Identification of New Psychoactive Substances: A Literature-Based Study for Seized Drugs. Braz. J. Anal. Chem. 2021; 9: 52-78.

216. Wagmann L, Maurer HH. Bioanalytical Methods for New Psychoactive Substances. Handb. Exp. Pharmacol. 2018; 252: 413-439.

217. Kerrigan S. Sampling, Storage and Stability. In: Negrusz A, Cooper G, editors. Clarke's Analytical Forensic Toxicology: Pharmaceutical Press, 2013. p. 335-356.

218. Maurer HH. Analytical toxicology. Anal. Bioanal. Chem. 2007; 388: 1311-1311.

219. Gallardo E, Queiroz JA. The role of alternative specimens in toxicological analysis. Biomed. Chromatogr. 2008; 22: 795-821.

220. Jones S, McGowan C, Boyle S, Ke Y, Chan CHM, Hwang H. An overview of sample preparation in forensic toxicology. WIREs Forensic Sci. 2022; 4: e1436.

221. Simão AY, Antunes M, Marques H, Rosado T, Soares S, Gonçalves J, et al. Recent bionalytical methods for the determination of new psychoactive substances in biological specimens. Bioanalysis 2020; 12: 1557-1595.

222. Barroso M, Moreno I, da Fonseca B, Queiroz JA, Gallardo E. Role of microextraction sampling procedures in forensic toxicology. Bioanalysis 2012; 4: 1805-1826.

223. Salomone A. Chapter 11 - Detection of New Psychoactive Substances. In: Kintz P, Salomone A, Vincenti M, editors. Hair Analysis in Clinical and Forensic Toxicology. Boston: Academic Press, 2015. p. 301-336.

224. Zuba D, Byrska B. Prevalence and co-existence of active components of 'legal highs'. Drug Test. Anal. 2013; 5: 420-429.

225. Miserez B, Ayrton O, Ramsey J. Analysis of purity and cutting agents in street mephedrone samples from South Wales. Forensic Toxicol. 2014; 32: 305-310.

226. Hadland SE, Levy S. Objective Testing: Urine and Other Drug Tests. Child Adolesc. Psychiatr. Clin. N. Am. 2016; 25: 549-565.

227. Bordin DCM, Monedeiro F, Campos EGd, Alves MNR, Bueno LHP, Martinis BSd. Técnicas de preparo de amostras biológicas com interesse forense. Scientia Chromatographica 2015; 7: 125-143.

228. Vearrier D, Curtis JA, Greenberg MI. Biological testing for drugs of abuse. In: Luch A, editor. Molecular, Clinical and Environmental Toxicology. Experientia Supplementum. Basel: Birkhäuser Basel, 2010. p. 489-517.

229. Aldubayyan AA, Castrignanò E, Elliott S, Abbate V. Stability of synthetic cathinones in clinical and forensic toxicological analysis—Where are we now? Drug Test. Anal. 2021; 13: 44-68.

230. Busardò FP, Kyriakou C, Tittarelli R, Mannocchi G, Pantano F, Santurro A, et al. Assessment of the stability of mephedrone in ante-mortem and post-mortem blood specimens. Forensic Sci. Int. 2015; 256: 28-37.

231. Sørensen LK. Determination of cathinones and related ephedrines in forensic whole-blood samples by liquid-chromatography–electrospray tandem mass spectrometry. J. Chromatogr. B 2011; 879: 727-736.

232. Saar E, Gerostamoulos D, Drummer OH, Beyer J. The Analysis of Antipsychotic Drugs in Human Biosamples by LC-MS. In: Xu QA, Madden TL, editors. LC-MS in Drug Bioanalysis. Boston, MA: Springer US, 2012. p. 177-195.

233. Drummer OH. Pharmacokinetics and metabolism. In: Jickells S, Negrusz A, editors. Clarke's Analytical Forensic Toxicology. London: Pharmaceutical Press, 2008. p. 13-42.

234. Jones GR. Interpretation of Postmortem Drug Levels. In: Karch SB, editor. Postmortem Toxicology of Abused Drugs. Florida: CRC Press, 2007. p. 113-127.

235. Guthrie JW. 3.01 - General Considerations when Dealing with Biological Fluid Samples. In: Pawliszyn J, editor. Comprehensive Sampling and Sample Preparation. Oxford: Academic Press, 2012. p. 1-19.

236. Allen KR. Screening for drugs of abuse: which matrix, oral fluid or urine? Ann. Clin. Biochem. 2011; 48: 531-541.

237. Kabir A, Furton KG. Forensic Sampling and Sample Preparation. In: Paixão TRLC, Coltro WKT, Salles MO, editors. Forensic Analytical Methods. United Kingdom: Royal Society of Chemistry, 2019. p. 7-35.

238. Dinis-Oliveira RJ, Vieira DN, Magalhães T. Guidelines for Collection of Biological Samples for Clinical and Forensic Toxicological Analysis. Forensic Sci. Res. 2017; 1: 42-51.

239. Stimpf T, Muller K, Gergov M, LeBeau M, Polettini A, Sporkert F, et al. Recommendations on Sample Collection. TIAFT; Bulletin XXIX - Number 1: 1-7.

240. Pellegrini M, Graziano S, Mastrobattista L, Minutillo A, Busardo FP, Scarsella G. Stability of Drugs of Abuse in Urine Samples at Room Temperature by Use of a Salts Mixture. Curr. Pharm. Biotechnol. 2017; 18: 815-820.

241. Glicksberg L, Kerrigan S. Stability of Synthetic Cathinones in Urine. J. Anal. Toxicol. 2018; 42: 77-87.

242. Amaratunga P, Lorenz Lemberg B, Lemberg D. Quantitative Measurement of Synthetic Cathinones in Oral Fluid. J. Anal. Toxicol. 2013; 37: 622-628.

243. Gallardo E, Barroso M, Queiroz JA. Current technologies and considerations for drug bioanalysis in oral fluid. Bioanalysis 2009; 1: 637-667.

244. Truver MT, Palmquist KB, Swortwood MJ. Oral Fluid and Drug Impairment: Pairing Toxicology with Drug Recognition Expert Observations. J. Anal. Toxicol. 2019; 43: 637-643.

245. de Campos EG, da Costa BRB, dos Santos FS, Monedeiro F, Alves MNR, Santos Junior WJR, et al. Alternative matrices in forensic toxicology: a critical review. Forensic Toxicol. 2022; 40: 1-18.

246. Richeval C, Dumestre-Toulet V, Wiart JF, Vanhoye X, Humbert L, Nachon-Phanithavong M, et al. New psychoactive substances in oral fluid of drivers around a music festival in south-west France in 2017. Forensic Sci. Int. 2019; 297: 265-269.

247. Richeval C, Wille SMR, Nachon-Phanithavong M, Samyn N, Allorge D, Gaulier JM. New psychoactive substances in oral fluid of French and Belgian drivers in 2016. Int. J. Drug Policy 2018; 57: 1-3.

248. de Castro MDL. Sweat as a clinical sample: what is done and what should be done. Bioanalysis 2016; 8: 85-88.

249. Jadoon S, Karim S, Akram MR, Kalsoom Khan A, Zia MA, Siddiqi AR, et al. Recent developments in sweat analysis and its applications. Int. J. Anal. Chem. 2015; 2015: 164974-164974.

250. Kacinko SL, Barnes AJ, Schwilke EW, Cone EJ, Moolchan ET, Huestis MA. Disposition of Cocaine and Its Metabolites in Human Sweat after Controlled Cocaine Administration. Clin. Chem. 2005; 51: 2085-2094.

251. Barnes AJ, Smith ML, Kacinko SL, Schwilke EW, Cone EJ, Moolchan ET, et al. Excretion of methamphetamine and amphetamine in human sweat following controlled oral methamphetamine administration. Clin. Chem. 2008; 54: 172-180.

252. Huestis MA, Scheidweiler KB, Saito T, Fortner N, Abraham T, Gustafson RA, et al. Excretion of Delta9-tetrahydrocannabinol in sweat. Forensic Sci. Int. 2008; 174: 173-177.

253. Manousi N, Samanidou V. Green sample preparation of alternative biosamples in forensic toxicology. Sustain Chem Pharm 2021; 20: 100388.

254. Barroso M, Gallardo E, Vieira DN, López-Rivadulla M, Queiroz JA. Hair: a complementary source of bioanalytical information in forensic toxicology. Bioanalysis 2011; 3: 67-79.

255. Matey JM, Montalvo G, García-Ruiz C, Zapata F, López-Fernández A, Martínez MA. Prevalence study of drugs and new psychoactive substances in hair of ketamine consumers using a methanolic direct extraction prior to high-resolution mass spectrometry. Forensic Sci. Int. 2021; 329: 111080.

256. Usman M, Naseer A, Baig Y, Jamshaid T, Shahwar M, Khurshuid S. Forensic toxicological analysis of hair: a review. Egypt. J. Forensic Sci. 2019; 9: 17.

257. Barroso M, Gallardo E. Hair analysis for forensic applications: is the future bright? Bioanalysis 2014; 6: 1-3.

258. Kintz P. Evidence of 2 Populations of Mephedrone Abusers by Hair Testing. Application to 4 Forensic Expertises. Curr. Neuropharmacol. 2017; 15: 658-662.

259. Larabi IA, Fabresse N, Etting I, Nadour L, Pfau G, Raphalen JH, et al. Prevalence of New Psychoactive Substances (NPS) and conventional drugs of abuse (DOA) in high risk populations from Paris (France) and its suburbs: A cross sectional study by hair testing (2012–2017). Drug Alcohol Depend. 2019; 204: 107508.

260. Cartiser N, Sahy A, Advenier A-S, Franchi A, Revelut K, Bottinelli C, et al. Fatal intoxication involving 4-methylpentedrone (4-MPD) in a context of chemsex. Forensic Sci. Int. 2021; 319: 110659.

261. Bottinelli C, Cartiser N, Gaillard Y, Boyer B, Bévalot F. A fatal case of 3-methylmethcathinone (3-MMC) poisoning. Toxicol. Anal. Clin. 2017; 29: 123-129.

262. Nováková L. Advances in Sample Preparation for Biological Fluids. LCGC Supplements 2016; 29: 9-15.

263. Aldubayyan AA, Castrignanò E, Elliott S, Abbate V. A Quantitative LC-MS/MS Method for the Detection of 16 Synthetic Cathinones and 10 Metabolites and Its Application to Suspicious Clinical and Forensic Urine Samples. Pharmaceuticals 2022; 15: 510.

264. Reidy L, Junquera P, Dijck K, Steele B, Salloum M. The Use of Synthetic Cathinones and Tryptamines in a Psychiatric Population. J. Forensic Toxicol. Pharmacol. 2013; 2: 1-4.

265. Pascual-Caro S, Borrull F, Aguilar C, Calull M. Determination of Synthetic Cathinones in Urine and Oral Fluid by Liquid Chromatography High-Resolution Mass Spectrometry and Low-Resolution Mass Spectrometry: A Method Comparison. Separations 2020; 7: 53.

266. Leal Cunha R, da Silva Lima Oliveira C, Lima de Oliveira A, Maldaner AO, P. Pereira PA. Fast determination of amphetamine-type stimulants and synthetic cathinones in whole blood samples using protein precipitation and LC-MS/MS. Microchem. J. 2021; 163: 105895.

267. Olesti E, Pascual JA, Ventura M, Papaseit E, Farré M, de la Torre R, et al. LC-MS/MS method for the quantification of new psychoactive substances and evaluation of their

urinary detection in humans for doping control analysis. Drug Test. Anal. 2020; 12: 785-797.

268. Borovcová L, Pauk V, Lemr K. Analysis of new psychoactive substances in human urine by ultra-high performance supercritical fluid and liquid chromatography: Validation and comparison. J. Sep. Sci. 2018; 41: 2288-2295.

269. LaPointe J, Musselman B, O'Neill T, Shepard JR. Detection of "bath salt" synthetic cathinones and metabolites in urine via DART-MS and solid phase microextraction. J. Am. Soc. Mass Spectrom. 2015; 26: 159-165.

270. Fujita Y, Mita T, Usui K, Kamijo Y, Kikuchi S, Onodera M, et al. Toxicokinetics of the Synthetic Cathinone α-Pyrrolidinohexanophenone. J. Anal. Toxicol. 2018; 42: e1-e5.

271. Usui K, Aramaki T, Hashiyada M, Hayashizaki Y, Funayama M. Quantitative analysis of 3,4-dimethylmethcathinone in blood and urine by liquid chromatography–tandem mass spectrometry in a fatal case. Leg. Med. 2014; 16: 222-226.

272. Segurado AM, Ahmad SM, Neng NR, Maniés-Sequeira MM, Gaspar H, Nogueira JMF. Simple Analytical Strategy for Screening Three Synthetic Cathinones (α-PVT, α-PVP, and MDPV) in Oral Fluids. Analytica 2022; 3: 14-23.

273. Ares AM, Fernández P, Regenjo M, Fernández AM, Carro AM, Lorenzo RA. A fast bioanalytical method based on microextraction by packed sorbent and UPLC–MS/MS for determining new psychoactive substances in oral fluid. Talanta 2017; 174: 454-461.

274. Fernández P, González M, Regenjo M, Ares AM, Fernández AM, Lorenzo RA, et al. Analysis of drugs of abuse in human plasma using microextraction by packed sorbents and ultra-high-performance liquid chromatography. J. Chromatogr. A 2017; 1485: 8-19.

275. Cláudia M, Pedro A, Tiago R, Francisco CR, Eugenia G. Determination of New Psychoactive Substances in Whole Blood Using Microwave Fast Derivatization and Gas Chromatography/Mass Spectrometry. J. Anal. Toxicol. 2019; 44: 92-102.

276. Odoardi S, Fisichella M, Romolo FS, Strano-Rossi S. High-throughput screening for new psychoactive substances (NPS) in whole blood by DLLME extraction and UHPLC–MS/MS analysis. J. Chromatogr. B 2015; 1000: 57-68.

277. Woźniak MK, Banaszkiewicz L, Wiergowski M, Tomczak E, Kata M, Szpiech B, et al. Development and validation of a GC–MS/MS method for the determination of 11 amphetamines and 34 synthetic cathinones in whole blood. Forensic Toxicol. 2020; 38: 42-58.

278. Grapp M, Kaufmann C, Streit F, Binder L. Systematic forensic toxicological analysis by liquid-chromatography-quadrupole-time-of-flight mass spectrometry in serum and comparison to gas chromatography-mass spectrometry. Forensic Sci. Int. 2018; 287: 63-73.

279. Mercieca G, Odoardi S, Cassar M, Strano Rossi S. Rapid and simple procedure for the determination of cathinones, amphetamine-like stimulants and other new psychoactive substances in blood and urine by GC–MS. J. Pharm. Biomed. Anal. 2018; 149: 494-501.

280. Alremeithi R, Meetani MA, Alaidaros AA, Lanjawi A, Alsumaiti K. Simultaneous Quantitative Determination of Synthetic Cathinone Enantiomers in Urine and Plasma Using GC-NCI-MS. J. Anal. Methods Chem. 2018; 2018: 4396043.

281. Williams M, Martin J, Galettis P. A Validated Method for the Detection of 32 Bath Salts in Oral Fluid. J. Anal. Toxicol. 2017; 41: 659-669.

282. Salomone A, Gazzilli G, Di Corcia D, Gerace E, Vincenti M. Determination of cathinones and other stimulant, psychedelic, and dissociative designer drugs in real hair samples. Anal. Bioanal. Chem. 2016; 408: 2035-2042.

283. Jain R. Thin-Layer Chromatography in Clinical Chemistry. In: Fried B, editor. Practical Thin-Layer Chromatography: A Multidisciplinary Approach: CRC Press, 2017. p. 131-152.

284. Sun PD, Foster CE, Boyington JC. Overview of protein structural and functional folds. Curr. Protoc. Protein Sci. 2004; 35: 1711-171189.

285. Ruchi S. Bioinformatics: Genomics and Proteomics. India: Vikas Publishing House, 2015.

286. Berk Z. Chapter 11 - Extraction. In: Berk Z, editor. Food Process Engineering and Technology (Third Edition): Academic Press, 2018. p. 289-310.

287. Pinto MMM. Manual de Trabalhos Laboratoriais de Química Orgânica e Farmacêutica. Lisboa: Lidel, 2011.

288. Mariotti KdC, Ortiz RS, Limberger RP. Sequência Analítica em Toxicologia Forense. In: Dinis-Oliveira RJ, Carvalho FD, Bastos MdL, editors. Toxicologia Forense. Lisbon: Pactor, 2015. p. 109-130.

289. Abd-Talib N, Mohd-Setapar SH, Khamis AK. The Benefits and Limitations of Methods Development in Solid Phase Extraction: Mini Review. J. Teknol. 2014; 69: 69-72.

290. Raynie DE, Watson DW. Understanding and Improving Solid-Phase Extraction. LCGC 2014; 32: 908-915.

291. Hansen SH, Pedersen-Bjergaard S, Rasmussen K. Introduction to Pharmaceutical Chemical Analysis. United Kingdom: John Wiley & Sons, 2011.

292. Walker V, Mills GA. Solid-phase extraction in clinical biochemistry. Ann. Clin. Biochem. 2002; 39: 464-477.

293. Kataoka H. Recent Advances in Online Column-Switching Sample Preparation. Reference Module in Chemistry, Molecular Sciences and Chemical Engineering: Elsevier, 2018. p.

294. Majors RE, Watson DW, Raynie DE. Understanding and Improving Solid-Phase Extraction. LCGC 2014; 27: 645-652.

295. Hasanah AN, Safitri N, Zulfa A, Neli N, Rahayu D. Factors Affecting Preparation of Molecularly Imprinted Polymer and Methods on Finding Template-Monomer Interaction as the Key of Selective Properties of the Materials. Molecules 2021; 26: 5612.

296. Almeida C, Rosário P, Serôdio P, Nogueira JMF. Novas perspectivas na preparação de amostras para análise cromatográfica. Química 2004; 95: 69-77.

297. Anastassiades M, Lehotay SJ, Stajnbaher D, Schenck FJ. Fast and easy multiresidue method employing acetonitrile extraction/partitioning and "dispersive solid-phase extraction" for the determination of pesticide residues in produce. J. AOAC Int. 2003; 86: 412-431.

298. Allcrom. roQ QuEChERS. [accessed June 26, 2022]. Available from: https://www.allcrom.com.br/produto/roq-quechers/.

299. Majors RE. QuEChERS - A New Technique for Multiresidue Analysis of Pesticides in Foods and Agricultural Samples. LCGC 2007; 20: 574–581.

300. Westland JL, Dorman FL. QuEChERS extraction of benzodiazepines in biological matrices. J. Pharm. Anal. 2013; 3: 509-517.

301. Anzillotti L, Odoardi S, Strano-Rossi S. Cleaning up blood samples using a modified "QuEChERS" procedure for the determination of drugs of abuse and benzodiazepines by UPLC-MSMS. Forensic Sci. Int. 2014; 243: 99-106.

302. Dulaurent S, El Balkhi S, Poncelet L, Gaulier J-M, Marquet P, Saint-Marcoux F. QuEChERS sample preparation prior to LC-MS/MS determination of opiates, amphetamines, and cocaine metabolites in whole blood. Anal. Bioanal. Chem. 2016; 408: 1467-1474.

303. Hou W, Wang YY, Zhang Y, Zhang LP, Xin GB, Qin SY, et al. Determination of Three Types of New Psychoactive Tryptamines in Blood by QuEChERS Combined with UPLC-MS/MS. Fa Yi Xue Za Zhi 2021; 37: 516-523.

304. Pawliszyn J. Chapter 13 Solid phase microextraction. Comprehensive Analytical Chemistry: Elsevier, 2002. p. 389-477.

305. Gonçalves JLJ. Quantificação de Antipsicóticos em Urina, recorrendo à Microextração por Sorvente Empacotado combinada com a Cromatografia Líquida de Ultra Eficiência. Dissertação apresentada na Faculdade de Medicina da Universidade de Coimbra para a obtenção do grau de Mestre. 2015.

306. Gallardo E, Costa S, Barroso M. A microextracção em fase sólida como técnica de preparação de amostras em quimíca analítica e toxicologia: Teoria e aplicações. Revista Lusófona de Ciências e Tecnologias da Saúde 2009; 6: 105-124.

307. Bogialli S, Di Corcia A, Nazzari M. Chapter 9 - Extraction procedures. In: Picó Y, editor. Food Toxicants Analysis. Amsterdam: Elsevier, 2007. p. 269-297.

308. Grandy JJ, Lashgari M, Heide HV, Poole J, Pawliszyn J. Introducing a mechanically robust SPME sampler for the on-site sampling and extraction of a wide range of untargeted pollutants in environmental waters. Environ. Pollut. 2019; 252: 825-834.

309. Aguiar J, Gonçalves JL, Alves VL, Câmara JS. Relationship between Volatile Composition and Bioactive Potential of Vegetables and Fruits of Regular Consumption—An Integrative Approach. Molecules 2021; 26: 3653.

310. Meng L, Dai Y, Chen C, Zhang J. Determination of amphetamines, ketamine and their metabolites in hair with high-speed grinding and solid-phase microextraction followed by LC-MS. Forensic Sci. Res. 2021; 6: 273-280.

311. Szultka M, Szeliga J, Jackowski M, Buszewski B. Development of novel molecularly imprinted solid-phase microextraction fibers and their application for the determination of antibiotic drugs in biological samples by SPME-LC/MSn. Anal. Bioanal. Chem. 2012; 403: 785-796.

312. Wang Q, Chen R, Shatner W, Cao Y, Bai Y. State-of-the-art on the technique of dispersive liquid-liquid microextraction. Ultrasonics Sonochemistry 2019; 51: 369-377.

313. Quigley A, Cummins W, Connolly D. Dispersive Liquid-Liquid Microextraction in the Analysis of Milk and Dairy Products: A Review. J. Chem. 2016; 2016: 4040165.

314. Zanella R, Martins M, Primel E, Caldas S, Prestes O, Adaime M. Microextração líquido-líquido dispersiva: fundamentos e aplicações. Scientia Chromatographica 2012; 4: 35-51.

315. Abdel-Rehim M, Altun Z, Blomberg L. Microextraction in packed syringe (MEPS) for liquid and gas chromatographic applications. Part II—Determination of ropivacaine and its metabolites in human plasma samples using MEPS with liquid chromatography/tandem mass spectrometry. J. Mass Spectrom. 2004; 39: 1488-1493.

316. Pereira J, Gonçalves J, Alves V, Câmara JS. Microextraction using packed sorbent as an effective and high-throughput sample extraction technique: Recent applications and future trends. Sample Preparation 2013; 1: 38-53.

317. Pereira J, Câmara JS, Colmsjö A, Abdel-Rehim M. Microextraction by packed sorbent: an emerging, selective and high-throughput extraction technique in bioanalysis. Biomed. Chromatogr. 2014; 28: 839-847.

318. He Y, Concheiro-Guisan M. Microextraction sample preparation techniques in forensic analytical toxicology. Biomed. Chromatogr. 2019; 33: e4444.

319. Pereira JAM, Gonçalves J, Porto-Figueira P, Figueira JA, Alves V, Perestrelo R, et al. Current trends on microextraction by packed sorbent – fundamentals, application fields, innovative improvements and future applications. Analyst 2019; 144: 5048-5074.

320. Silva C, Cavaco C, Perestrelo R, Pereira J, Câmara JS. Microextraction by Packed Sorbent (MEPS) and Solid-Phase Microextraction (SPME) as Sample Preparation Procedures for the Metabolomic Profiling of Urine. Metabolites 2014; 4: 71-97.

321. Casado N, Gañán J, Morante-Zarcero S, Sierra I. New Advanced Materials and Sorbent-Based Microextraction Techniques as Strategies in Sample Preparation to Improve the Determination of Natural Toxins in Food Samples. Molecules 2020; 25: 702.

322. Kabir A, Locatelli M, Ulusoy HI. Recent Trends in Microextraction Techniques Employed in Analytical and Bioanalytical Sample Preparation. Separations 2017; 4: 36.

323. Prieto A, Schrader S, Bauer C, Möder M. Synthesis of a molecularly imprinted polymer and its application for microextraction by packed sorbent for the determination of fluoroquinolone related compounds in water. Anal. Chim. Acta 2011; 685: 146-152.

324. Quinto M, Spadaccino G, Nardiello D, Palermo C, Amodio P, Li D, et al. Microextraction by packed sorbent coupled with gas chromatography–mass spectrometry: A comparison between "draw-eject" and "extract-discard" methods under equilibrium conditions for the determination of polycyclic aromatic hydrocarbons in water. J. Chromatogr. A 2014; 1371: 30-38.

325. Ellefsen KN, Anizan S, Castaneto MS, Desrosiers NA, Martin TM, Klette KL, et al. Validation of the only commercially available immunoassay for synthetic cathinones in urine: Randox Drugs of Abuse V Biochip Array Technology. Drug Test. Anal. 2014; 6: 728-738.

326. SGE. eVol® XR Automated Analytical Syringe – User Manual. [accessed March 21, 2021]. Available from: https://www.bgb-info.com/knowhow/literature/evol/MN-0807-S-eVol-XR-Manual_SP.pdf.

327. Candish E, Gooley A, Wirth H-J, Dawes PA, Shellie RA, Hilder EF. A simplified approach to direct SPE-MS. J. Sep. Sci. 2012; 35: 2399-2406.

328. SGE. eVol® MEPS® CDF: Introductory Information - Prototypes. [accessed Mach 24, 2021]. Available from: https://cdn.shopify.com/s/files/1/0767/9441/files/MN-0878-M.pdf?14558841128445666688.

329. Dugheri S, Marrubini G, Mucci N, Cappelli G, Bonari A, Pompilio I, et al. A review of micro-solid-phase extraction techniques and devices applied in sample pretreatment coupled with chromatographic analysis. Acta Chromatogr. 2021; 33: 99-111.

330. EPREP. µSPEed Cartridges Brochure. [accessed March 27, 2021]. Available from: https://www.eprep-analytical.com/product-literature.

331. EPREP. digiVOL Digital Syringe Driver Brochure. [accessed April 1, 2021]. Available from: https://www.eprep-analytical.com/product-literature.

332. Grueiro Noche G, Fernández Laespada ME, Pérez Pavón JL, Moreno Cordero B, Muniategui Lorenzo S. Determination of chlorobenzenes in water samples based on fully automated microextraction by packed sorbent coupled with programmed temperature vaporization–gas chromatography–mass spectrometry. Anal. Bioanal. Chem. 2013; 405: 6739-6748.

333. Sánchez MdN, Santos PM, Sappó CP, Pavón JLP, Cordero BM. Microextraction by packed sorbent and salting-out-assisted liquid–liquid extraction for the determination of aromatic amines formed from azo dyes in textiles. Talanta 2014; 119: 375-384.

334. Silva P, Silva CL, Perestrelo R, Nunes FM, Câmara JS. A useful strategy based on chromatographic data combined with quality-by-design approach for food analysis applications. The case study of furanic derivatives in sugarcane honey. J. Chromatogr. A 2017; 1520: 117-126.

335. Perestrelo R, Silva CL, Câmara JS. Quantification of furanic derivatives in fortified wines by a highly sensitive and ultrafast analytical strategy based on digitally controlled microextraction by packed sorbent combined with ultrahigh pressure liquid chromatography. J. Chromatogr. A 2015; 1381: 54-63.

336. Alves V, Gonçalves J, Conceição C, Teixeira HM, Câmara JS. An improved analytical strategy combining microextraction by packed sorbent combined with ultra high pressure liquid chromatography for the determination of fluoxetine, clomipramine and their active metabolites in human urine. J. Chromatogr. A 2015; 1408: 30-40.

337. Magiera S, Gülmez Ş, Michalik A, Baranowska I. Application of statistical experimental design to the optimisation of microextraction by packed sorbent for the analysis of nonsteroidal anti-inflammatory drugs in human urine by ultra-high pressure liquid chromatography. J. Chromatogr. A 2013; 1304: 1-9.

338. Sergi M, Montesano C, Odoardi S, Mainero Rocca L, Fabrizi G, Compagnone D, et al. Micro extraction by packed sorbent coupled to liquid chromatography tandem mass spectrometry for the rapid and sensitive determination of cannabinoids in oral fluids. J. Chromatogr. A 2013; 1301: 139-146.

339. Rocchi R, Simeoni MC, Montesano C, Vannutelli G, Curini R, Sergi M, et al. Analysis of new psychoactive substances in oral fluids by means of microextraction by packed sorbent followed by ultra-high-performance liquid chromatography–tandem mass spectrometry. Drug Test. Anal. 2018; 10: 865-873.

340. Miyaguchi H, Iwata YT, Kanamori T, Tsujikawa K, Kuwayama K, Inoue H. Rapid identification and quantification of methamphetamine and amphetamine in hair by gas chromatography/mass spectrometry coupled with micropulverized extraction, aqueous acetylation and microextraction by packed sorbent. J. Chromatogr. A 2009; 1216: 4063-4070.

341. Malaca S, Rosado T, Restolho J, Rodilla JM, Rocha PMM, Silva L, et al. Determination of amphetamine-type stimulants in urine samples using microextraction by packed sorbent and gas chromatography-mass spectrometry. J. Chromatogr. B Analyt. Technol. Biomed. Life Sci. 2019; 1120: 41-50.

342. Jagerdeo E, Abdel-Rehim M. Screening of Cocaine and Its Metabolites in Human Urine Samples by Direct Analysis in Real-Time Source Coupled to Time-of-Flight Mass Spectrometry After Online Preconcentration Utilizing Microextraction by Packed Sorbent. J. Am. Soc. Mass Spectrom. 2009; 20: 891-899.

343. Rosado T, Gonçalves A, Margalho C, Barroso M, Gallardo E. Rapid analysis of cocaine and metabolites in urine using microextraction in packed sorbent and GC/MS. Anal. Bioanal. Chem. 2017; 409: 2051–2063.

344. Montesano C, Simeoni MC, Curini R, Sergi M, Lo Sterzo C, Compagnone D. Determination of illicit drugs and metabolites in oral fluid by microextraction on packed sorbent coupled with LC-MS/MS. Anal. Bioanal. Chem. 2015; 407: 3647-3658.

345. Rosado T, Fernandes L, Barroso M, Gallardo E. Sensitive determination of THC and main metabolites in human plasma by means of microextraction in packed sorbent and gas chromatography–tandem mass spectrometry. J. Chromatogr. B 2017; 1043: 63-73.

346. Sartore DM, Vargas Medina DA, Costa JL, Lanças FM, Santos-Neto ÁJ. Automated microextraction by packed sorbent of cannabinoids from human urine using a lab-made device packed with molecularly imprinted polymer. Talanta 2020; 219: 121185.

347. da Cunha KF, Rodrigues LC, Huestis MA, Costa JL. Miniaturized extraction method for analysis of synthetic opioids in urine by microextraction with packed sorbent and liquid chromatography—tandem mass spectrometry. J. Chromatogr. A 2020; 1624: 461241.

348. Sorribes-Soriano A, Monedero A, Esteve-Turrillas FA, Armenta S. Determination of the new psychoactive substance dichloropane in saliva by microextraction by packed sorbent – Ion mobility spectrometry. J. Chromatogr. A 2019; 1603: 61-66.

349. Vlčková H, El-Beqqali A, Nováková L, Solich P, Abdel-Rehim M. Determination of amphetamine and methadone in human urine by microextraction by packed sorbent coupled directly to mass spectrometry: An alternative for rapid clinical and forensic analysis. J. Sep. Sci. 2014; 37: 3306-3313.

350. Moreno I, Fonseca B, Oppolzer D, Martinho A, Barroso M, Cruz A, et al. Analysis of Salvinorin A in urine using microextraction in packed syringe and GC–MS/MS. Bioanalysis 2013; 5: 661-668.

351. Moreno IED, da Fonseca BM, Barroso M, Costa S, Queiroz JA, Gallardo E. Determination of piperazine-type stimulants in human urine by means of microextraction in packed sorbent and high performance liquid chromatography-diode array detection. J. Pharm. Biomed. Anal. 2012; 61: 93-99.

352. Moreno I, Barroso M, Martinho A, Cruz A, Gallardo E. Determination of ketamine and its major metabolite, norketamine, in urine and plasma samples using microextraction by packed sorbent and gas chromatography-tandem mass spectrometry. J. Chromatogr. B 2015; 1004: 67-78.

353. Rocchi R, Simeoni MC, Montesano C, Vannutelli G, Curini R, Sergi M, et al. Analysis of new psychoactive substances in oral fluids by means of microextraction by packed sorbent followed by ultra-high-performance liquid chromatography–tandem mass spectrometry. Drug Test. Anal. 2018; 10: 865-873.

354. Ares-Fuentes AM, Lorenzo RA, Fernández P, Carro AM. An analytical strategy for designer benzodiazepines and Z-hypnotics determination in plasma samples using ultra-high performance liquid chromatography/tandem mass spectrometry after microextraction by packed sorbent. J. Pharm. Biomed. Anal. 2021; 194: 113779.

355. Maurer HH. Systematic toxicological analysis procedures for acidic drugs and/or metabolites relevant to clinical and forensic toxicology and/or doping control. J. Chromatogr. B Biomed. Appl. 1999; 733: 3-25.

356. Toole K, Philp M, Krayem N, Fu S, Shimmon R, Taflaga S. Color Tests for the Preliminary Identification of New Psychoactive Substances. Methods Mol. Biol. 2018; 1810: 1-11.

357. Philp M, Shimmon R, Tahtouh M, Fu S. Development and validation of a presumptive color spot test method for the detection of synthetic cathinones in seized illicit materials. Forensic Chem. 2016; 1: 39-50.

358. Beck O, Rausberg L, Al-Saffar Y, Villen T, Karlsson L, Hansson T, et al. Detectability of new psychoactive substances, 'legal highs', in CEDIA, EMIT, and KIMS immunochemical screening assays for drugs of abuse. Drug Test. Anal. 2014; 6: 492-499.

359. Meleiro PP, García-Ruiz C. Spectroscopic techniques for the forensic analysis of textile fibers. Appl. Spectrosc. Rev. 2016; 51: 278-301.

360. Sharma S, Garg D, Chophi R, Singh R. On the spectroscopic investigation of stamp inks using ATR-FTIR and chemometrics: Application in forensic document examination. Forensic Chem. 2021; 26: 100377.

361. Álvarez Á, Yáñez J. Screening of Gunshot Residue in Skin Using Attenuated Total Reflection Fourier Transform Infrared (ATR FT-IR) Hyperspectral Microscopy. Appl. Spectrosc. 2020; 74: 400-407.

362. Ewelina M, Igor KL. FT-IR Spectroscopy for Identification of Biological Stains for Forensic Purposes. Spectroscopy 2018; 33: 8–19.

363. da Silva AF, Grobério TS, Zacca JJ, Maldaner AO, Braga JWB. Cocaine and adulterants analysis in seized drug samples by infrared spectroscopy and MCR-ALS. Forensic Sci. Int. 2018; 290: 169-177.

364. Piorunska-Sedlak K, Stypulkowska K. Strategy for identification of new psychoactive substances in illicit samples using attenuated total reflectance infrared spectroscopy. Forensic Sci. Int. 2020; 312: 110262.

365. Agarwal M, Prakash S. Engineering Chemistry: Concepts in Chemistry for Engineering: Khanna Book Publishing, 2018.

366. Cameron JM, Bruno C, Parachalil DR, Baker MJ, Bonnier F, Butler HJ, et al. Chapter 10 - Vibrational spectroscopic analysis and quantification of proteins in human blood plasma and serum. In: Ozaki Y, Baranska M, Lednev IK, Wood BR, editors. Vibrational Spectroscopy in Protein Research: Academic Press, 2020. p. 269-314.

367. Drake A. Infrared spectroscopy. In: Jickells S, Negrusz A, editors. Clarke's Analytical Forensic Toxicology. London: Pharmaceutical Press, 2008. p. 421-454.

368. Rouessac F, Rouessac A. Chemical Analysis: Modern Instrumentation Methods and Techniques. 2nd ed: John Wiley & Sons, 2013.

369. Hsu SCP. Infrared Spectroscopy. In: Settle FA, editor. Handbook of Instrumental Techniques for Analytical Chemistry. New Jersey: Prentice Hall PTR, 1997. p. 247-283.

370. Skoog DA, Crouch, Holler FJ, West DM. Fundamentos de Química Analítica. 8th ed: Thomson Learning, 2010.

371. Kafle BP. Chapter 7 - Infrared (IR) spectroscopy. In: Kafle BP, editor. Chemical Analysis and Material Characterization by Spectrophotometry: Elsevier, 2020. p. 199-243.

372. Christy AA, Ozaki Y, Gregoriou VG. Instrumentation. In: Barceló D, editor. Comprehensive Analytical Chemistry: Elsevier, 2001. p. 105-129.

373. InnovaTECH. How Does FTIR Work? [accessed January 30, 2022]. Available from: https://www.innovatechlabs.com/newsroom/672/stuff-works-ftir-analysis/.

374. Anton Paar. Attenuated total reflectance (ATR). [accessed February 3, 2022]. Available from: https://wiki.anton-paar.com/en/attenuated-total-reflectance-atr/.

375. PerkinElmer. Technical Note, FT-IR Spectroscopy Attenuated Total Reflectance (ATR). [accessed February 3, 2022]. Available from: https://cmdis.rpi.edu/sites/default/files/ATR_FTIR.pdf.

376. Zancajo VMR, Brito J, Carrasco MP, Bronze MR, Moreira R, Lopes A. Analytical profiles of "legal highs" containing cathinones available in the area of Lisbon, Portugal. Forensic Sci. Int. 2014; 244: 102-110.

377. Bridge CM, Jones K, Maric M. GC×GC–MS for Forensic Analysis. The Column 2018; 14: 25-30.

378. Imwinkelried EJ, Gin J. Gas Chromatography-Mass Spectrometer (GC/MS): In Scientific Evidence, Even "Gold Standard" Techniques Have Limitations. 2018.

379. Kitson FG, Larsen BS, McEwen CN. Gas Chromatography and Mass Spectrometry: A Pratical Guide. New York: Academic Place, 1996.

380. Dawling S, Jickells S, Negrusz A. Gas chromatography. In: Jickells S, Negrusz A, editors. Clarke's Analytical Forensic Toxicology. London: Pharmaceutical Press, 2008. p. 469-511.

381. Aguiar JMV. Determinação de Compostos Bioativos em Frutas e Vegetais Consumidos na Região Autónoma da Madeira. Dissertação apresentada na Universidade da Madeira para obtenção do grau de Mestre, 2017.

382. Neves HJC, Freitas AMC. Introdução À Cromatografia Gás-Líquido de Alta Resolução. Portugal: Dias de Sousa, Lda., 1996.

383. Falaki F. Sample Preparation Techniques for Gas Chromatography. In: Kusch P, editor. Gas Chromatography - Derivatization, Sample Preparation, Application: IntechOpen, 2019. p.

384. Saitman A. Chapter 13 - Overview of Analytical Methods in Drugs of Abuse Analysis: Gas Chromatography/Mass Spectrometry, Liquid Chromatography Combined With Tandem Mass Spectrometry and Related Methods. In: Dasgupta A, editor. Critical Issues in Alcohol and Drugs of Abuse Testing (Second Edition): Academic Press, 2019. p. 157-171.

385. Smith RW. Mass Spectrometry. In: Siegel JA, Saukko PJ, Houck MM, editors. Encyclopedia of Forensic Sciences (Second Edition). Waltham: Academic Press, 2013. p. 603-608.

386. Thomas SN. Chapter 10 - Mass spectrometry. In: Clarke W, Marzinke MA, editors. Contemporary Practice in Clinical Chemistry (Fourth Edition): Academic Press, 2019. p. 171-185.

387. Mass Spec Pro. Electron Multiplier. [accessed January 7, 2022]. Available from: http://www.massspecpro.com/detectors/electron-multiplier.

388. Cass QB, Degani ALG. Desenvolvimento de métodos por HPLC: fundamentos, estratégias e validação: EdUFSCar, 2001.

389. Hacker M, Messer WS, Bachmann KA. Bionalytical Tools for Drug Analysis. Pharmacology: Principles and Practice. London: Elsevier Science, 2009. p. 279-302.

390. LCGC. The LCGC Blog: Diode Array Detector Settings - Five Minutes to Change Your Chromatography Forever. [accessed January 13, 2022]. Available from: https://www.chromatographyonline.com/view/lcgc-blog-diode-array-detector-settings-five-minutes-change-your-chromatography-forever.

391. Gwak S, Arroyo-Mora LE, Almirall JR. Qualitative analysis of seized synthetic cannabinoids and synthetic cathinones by gas chromatography triple quadrupole tandem mass spectrometry. Drug Test. Anal. 2015; 7: 121-130.

392. Majchrzak M, Rojkiewicz M, Celiński R, Kuś P, Sajewicz M. Identification and characterization of new designer drug 4-fluoro-PV9 and α-PHP in the seized materials. Forensic Toxicol. 2016; 34: 115-124.

393. Dei Cas M, Casagni E, Arnoldi S, Gambaro V, Roda G. Screening of new psychoactive substances (NPS) by gas-chromatography/time of flight mass spectrometry (GC/MS-TOF) and application to 63 cases of judicial seizure. Forensic Science International: Synergy 2019; 1: 71-78.

394. Levitas MP, Andrews E, Lurie I, Marginean I. Discrimination of synthetic cathinones by GC–MS and GC–MS/MS using cold electron ionization. Forensic Sci. Int. 2018; 288: 107-114.

395. Alsenedi K. The analysis and long-term stability of amphetamine-type stimulants and synthetic cathinones in urine using novel extraction methods and GC-MS. University of Glasgow, 2018.

396. Kerrigan S, Savage M, Cavazos C, Bella P. Thermal Degradation of Synthetic Cathinones: Implications for Forensic Toxicology. J. Anal. Toxicol. 2016; 40: 1-11.

397. Alsenedi KA, Morrison C. Comparison of six derivatizing agents for the determination of nine synthetic cathinones using gas chromatography-mass spectrometry. Anal. Methods 2017; 9: 2732-2743.

398. Mohamed KM, Bakdash A. Comparison of 3 Derivatization Methods for the Analysis of Amphetamine-Related Drugs in Oral Fluid by Gas Chromatography-Mass Spectrometry. Anal. Chem. Insights 2017; 12: 1-16.

399. Schug KA. The LCGC Blog: Forensic Drug Analysis: GC–MS versus LC–MS.: LCGC; 2018 [accessed June 29, 2022]. Available from: https://www.chromatographyonline.com/view/lcgc-blog-forensic-drug-analysis-gc-ms-versus-lc-ms.

400. Zuba D, Adamowicz P. Analytical Methods Used for Identification and Determination of Synthetic Cathinones and Their Metabolites. In: Zawilska JB, editor. Synthetic Cathinones: Novel Addictive and Stimulatory Psychoactive Substances. Cham: Springer International Publishing, 2018. p. 41-69.

401. Guilhaus M. MASS SPECTROMETRY | Time-of-Flight. In: Worsfold P, Townshend A, Poole C, editors. Encyclopedia of Analytical Science (Second Edition). Oxford: Elsevier, 2005. p. 412-423.

402. McGregor M. Nuclear Magnetic Resonance Spectroscopy. In: Settle FA, editor. Handbook of Instrumental Techniques for Analytical Chemistry. USA: Prentice Hall PTR, 1997. p. 309-337.

403. Lambert JB, Mazzola EP. Nuclear Magnetic Resonance Spectroscopy: An Introduction to Principles, Applications, and Experimental Methods: Pearson Education, 2004.

404. Starkey LS. Introduction to Nuclear Magnetic Resonance (NMR) Spectroscopy Pomona: California State Polytechnic University; [accessed January 18, 2022]. Available from: https://www.cpp.edu/~lsstarkey/courses/CHM424/NMR_handouts.pdf.

405. Course Hero. Nuclear Magnetic Resonance (NMR) Spectroscopy. [accessed January 18, 2022]. Available from: https://www.coursehero.com/sg/organic-chemistry/nuclear-magnetic-resonance-nmr-spectroscopy/#nuclear-magnetic-resonance-nmr-spectroscopy.

406. Carlsson A. Synthesis and spectroscopic characterization of emerging synthetic cannabinoids and cathinones. Sweden: Linköping University, 2016.

407. Speight JG. Chapter 5 - Properties of Organic Compounds. In: Speight JG, editor. Environmental Organic Chemistry for Engineers: Butterworth-Heinemann, 2017. p. 203-261.

408. Ameline A, Garnier D, Gheddar L, Richeval C, Gaulier J-m, Raul J-s, et al. Identification and analytical characterization of seven NPS, by combination of 1H NMR spectroscopy, GC–MS and UPLC–MS/MS®, to resolve a complex toxicological fatal case. Forensic Sci. Int. 2019; 298: 140-148.

409. Zhong Y, Huang K, Luo Q, Yao S, Liu X, Yang N, et al. The Application of a Desktop NMR Spectrometer in Drug Analysis. Int. J. Anal. Chem. 2018; 2018: 3104569.

410. Emwas A-H, Szczepski K, Poulson BG, Chandra K, McKay RT, Dhahri M, et al. NMR as a "Gold Standard" Method in Drug Design and Discovery. Molecules 2020; 25: 4597.

411. Bijlsma L, Bade R, Been F, Celma A, Castiglioni S. Perspectives and challenges associated with the determination of new psychoactive substances in urine and wastewater – A tutorial. Anal. Chim. Acta 2021; 1145: 132-147.

412. Oliveira CC. Síntese de Catinonas Psicoativas e Avaliação da sua Hepatotoxicidade. Universidade de Lisboa, 2017.

413. Pieprzyca E, Skowronek R, Czekaj P. Toxicological Analysis of Intoxications with Synthetic Cathinones. J. Anal. Toxicol. 2021; 46: 705–711.

414. Zaami S, Giorgetti R, Pichini S, Pantano F, Marinelli E, Busardò FP. Synthetic cathinones related fatalities: an update. Eur. Rev. Med. Pharmacol. Sci. 2018; 22: 268-274.

415. EURAD. Psychoactive Substances: Issues for policy makers. [accessed December 4, 2019]. Available from: https://www.unodc.org/documents/ungass2016/Contributions/Civil/EURAD/Psychoactive_Substances_Exec_Summary.pdf.

416. Liu C, Jia W, Li T, Hua Z, Qian Z. Identification and analytical characterization of nine synthetic cathinone derivatives N-ethylhexedrone, 4-Cl-pentedrone, 4-Cl-α-EAPP, propylone, N-ethylnorpentylone, 6-MeO-bk-MDMA, α-PiHP, 4-Cl-α-PHP, and 4-F-α-PHP. Drug Test Anal 2017; 9: 1162-1171.

417. Antunes M, Sequeira M, de Caires Pereira M, Caldeira MJ, Santos S, Franco J, et al. Determination of Selected Cathinones in Blood by Solid-Phase Extraction and GC–MS. Journal of Analytical Toxicology 2020; 00: 1-10.

418. Carlsson A, Sandgren V, Svensson S, Konradsson P, Dunne S, Josefsson M, et al. Prediction of designer drugs: Synthesis and spectroscopic analysis of synthetic cathinone analogs that may appear on the Swedish drug market. Drug Test. Anal. 2018; 10: 1076-1098.

419. Assi S, Guirguis A, Halsey S, Fergus S, Stair JL. Analysis of 'legal high' substances and common adulterants using handheld spectroscopic techniques. Anal. Methods 2015; 7: 736-746.

420. Maheux CR, Copeland CR. Chemical analysis of two new designer drugs: buphedrone and pentedrone. Drug Test. Anal. 2012; 4: 17-23.

421. Maheux CR, Alarcon IQ, Copeland CR, Cameron TS, Linden A, Grossert JS. Identification of polymorphism in ethylone hydrochloride: synthesis and characterization. Drug Test. Anal. 2016; 8: 847-857.

422. Westphal F, Junge T, Girreser U, Greibl W, Doering C. Mass, NMR and IR spectroscopic characterization of pentedrone and pentylone and identification of their isocathinone by-products. Forensic Sci. Int. 2012; 217: 157-167.

423. Smith BC. Infrared Spectral Interpretation: A Systematic Approach. New York: Taylor & Francis, 1998.

424. Kavanagh P, O'Brien J, Fox J, O'Donnell C, Christie R, Power JD, et al. The analysis of substituted cathinones. Part 3. Synthesis and characterisation of 2,3-methylenedioxy substituted cathinones. Forensic Sci. Int. 2012; 216: 19-28.

425. Coates J. Interpretation of Infrared Spectra, A Practical Approach. In: Meyers RA, McKelvy ML, editors. Encyclopedia of Analytical Chemistry: John Wiley & Sons, 2006. p.

426. Sisco E, Burns A, Moorthy AS. Development and evaluation of a synthetic cathinone targeted gas chromatography mass spectrometry (GC-MS) method. J. Forensic Sci. 2021; 66: 1919-1928.

427. Matsuta S, Katagi M, Nishioka H, Kamata H, Sasaki K, Shima N, et al. Structural characterization of cathinone-type designer drugs by EI mass spectrometry. Jpn. J. Forensic Sci. Tech. 2014; 19: 77-89.

428. Menezes JCd, Borges GBV, Gomes FdCO, Vieira MdLA, Marques AR, Machado AMdR. Volatile compounds and quality analysis in commercial medicinal plants of Camellia sinensis. Cienc. Rural 2019; 49: e20180548.

429. Zuba D. Identification of cathinones and other active components of 'legal highs' by mass spectrometric methods. Trends Analyt. Chem. 2012; 32: 15-30.

430. Kohyama E, Chikumoto T, Tada H, Kitaichi K, Horiuchi T, Ito T. Differentiation of the Isomers of N-Alkylated Cathinones by GC-EI-MS-MS and LC-PDA. Anal. Sci. 2016; 32: 831-837.

431. Paillet-Loilier M, Cesbron A, Le Boisselier R, Bourgine J, Debruyne D. Emerging drugs of abuse: current perspectives on substituted cathinones. Subst. Abuse Rehabil. 2014; 5: 37-52.

432. Lum BJ, Hibbert DB, Brophy J. Identification of Substituted Cathinones (β-keto phenethylamines) by Heptafluorobutyric Anhydride (HFBA) Chemical Derivatization and Gas Chromatography Mass Spectrometry. SWAFS Journal 2013; 34: 7-30.

433. Moldoveanu SC, David V. Derivatization Methods in GC and GC/MS. In: Kusch P, editor. Gas Chromatography - Derivatization, Sample Preparation, Application: IntechOpen, 2018. p.

434. Kumazawa T, Hara K, Hasegawa C, Uchigasaki S, Lee X-P, Seno H, et al. Fragmentation Pathways of Trifluoroacetyl Derivatives of Methamphetamine, Amphetamine, and Methylenedioxyphenylalkylamine Designer Drugs by Gas Chromatography/Mass Spectrometry. Int. J. Spectrosc. 2011; 2011: 318148.

435. Ash J, Hickey L, Goodpaster J. Formation and identification of novel derivatives of primary amine and zwitterionic drugs. Forensic Chem. 2018; 10: 37-47.

436. Berger J, Staretz ME, Wood M, Brettell TA. Ultraviolet absorption properties of synthetic cathinones. Forensic Chem. 2020; 21: 100286.

437. Li L, Lurie IS. Screening of seized emerging drugs by ultra-high performance liquid chromatography with photodiode array ultraviolet and mass spectrometric detection. Forensic Sci. Int. 2014; 237: 100-111.

438. Rowe WF, Marginean I, Carnes S, Lurie IS. The role of diode array ultraviolet detection for the identification of synthetic cathinones. Drug Test. Anal. 2017; 9: 1512-1521.

439. Balci M. ^{13}C Chemical Shifts of Organic Compounds. Balci M, editor. Amestardan: Elsevier Science, 2005.

440. Souza LF, Vieira TS, Alcantara GB, Lião LM. HR-MAS NMR for Rapid Identification of Illicit Substances in Tablets and Blotter Papers Seized by Police Department. J. Braz. Chem. Soc. 2016; 27: 2141-2148.

441. Maheux CR, Copeland CR, Pollard MM. Characterization of Three Methcathinone Analogs: 4-Methylmethcathinone, Methylone, and bk-MBDB. Microgram J. 2010; 7: 42-49.

442. Kuś P, Kusz J, Książek M, Pieprzyca E, Rojkiewicz M. Spectroscopic characterization and crystal structures of two cathinone derivatives: N-ethyl-2-amino-1-phenylpropan-1-one (ethcathinone) hydrochloride and N-ethyl-2-amino-1-(4-chlorophenyl)propan-1-one (4-CEC) hydrochloride. Forensic Toxicol. 2017; 35: 114-124.

443. Archer RP. Fluoromethcathinone, a new substance of abuse. Forensic Sci. Int. 2009; 185: 10-20.

444. Guirguis A, Girotto S, Berti B, Stair JL. Identification of new psychoactive substances (NPS) using handheld Raman spectroscopy employing both 785 and 1064nm laser sources. Forensic Sci. Int. 2017; 273: 113-123.

445. Sadeg N, Darie A, Vilamot B, Passamar M, Frances B, Belhadj-Tahar H. Case Report of Cathinone-Like Designer Drug Intoxication Psychosis and Addiction With Serum Identification. Addict. Disord. Their Treat. 2014; 13.

446. Daveluy A, Labadie M, Titier K, Courtois A, Penouil F, Castaing N, et al. Poisoning by synthetic cathinones: Consumption behaviour and clinical description from 11 cases recorded by the Addictovigilance Centre of Bordeaux. Toxicol. Anal. Clin. 2017; 29: 34-40.

447. Gerace E, Caneparo D, Borio F, Salomone A, Vincenti M. Determination of several synthetic cathinones and an amphetamine-like compound in urine by gas chromatography with mass spectrometry. Method validation and application to real cases. J. Sep. Sci. 2019; 42: 1577-1584.

448. Thornton SL, Lo J, Clark RF, Wu AH, Gerona RR. Simultaneous detection of multiple designer drugs in serum, urine, and CSF in a patient with prolonged psychosis. Clin. Toxicol. (Phila) 2012; 50: 1165-1168.

449. Casado N, Perestrelo R, Silva CL, Sierra I, Câmara JS. Comparison of high-throughput microextraction techniques, MEPS and µ-SPEed, for the determination of polyphenols in baby food by ultrahigh pressure liquid chromatography. Food Chem. 2019; 292: 14-23.

450. Porto-Figueira P, Figueira JA, Pereira JAM, Câmara JS. A fast and innovative microextraction technique, µSPEed, followed by ultrahigh performance liquid chromatography for the analysis of phenolic compounds in teas. J. Chromatogr. A 2015; 1424: 1-9.

451. González-Gómez L, Pereira JAM, Morante-Zarcero S, Câmara JS, Sierra I. Green extraction approach based on µSPEed® followed by HPLC-MS/MS for the determination of atropine and scopolamine in tea and herbal tea infusions. Food Chem. 2022; 394: 133512.

452. Moosavi SM, Ghassabian S. Linearity of Calibration Curves for Analytical Methods: A Review of Criteria for Assessment of Method Reliability. In: Stauffer MT, editor. Calibration and Validation of Analytical Methods - A Sampling of Current Approaches. London: IntechOpen, 2018. p. 109-127.

453. Ribeiro FAdL, Ferreira MMC, Morano SC, da Silva LR, Schneider RP. Planilha de validação: Uma nova ferramenta para estimar figuras de mérito na validação de métodos analíticos univariados. Quim. Nova 2008; 31: 164-171.

454. Funk W, Dammann V, Donnevert G, Iannelli S, Iannelli E. Quality Assurance in Analytical Chemistry: Applications in Environmental, Food and Materials Analysis, Biotechnology, and Medical Engineering. 2 ed. Germany: John Wiley & Sons, 2007.

455. Araujo P. Key aspects of analytical method validation and linearity evaluation. J. Chromatogr. B 2009; 877: 2224-2234.

456. Maroto A, Boqué R, Riu J, Rius FX. Measurement uncertainty in analytical methods in which trueness is assessed from recovery assays. Anal. Chim. Acta 2001; 440: 171-184.

457. Maroto A, Riu J, Boqué R, Xavier Rius F. Estimating uncertainties of analytical results using information from the validation process. Anal. Chim. Acta 1999; 391: 173-185.

458. Relacre (Associação de Laboratórios Acreditados de Portugal). *Validação de métodos internos de ensaio em análise química - Guia Relacre nº 13*. Lisboa: Relacre: 2000.

459. Marson BM, Concentino V, Junkert AM, Fachi MM, Vilhena RO, Pontarolo R. Validation of analytical methods in a pharmaceutical quality system: An overview focused on HPLC methods. Quim. Nova 2020; 43: 1190-1203.

460. Smeraglia J, Baldrey SF, Watson D. Matrix effects and selectivity issues in LC-MS-MS. Chromatographia 2002; 55: S95-S99.

461. Adamowicz P, Malczyk A. Stability of synthetic cathinones in blood and urine. Forensic Sci. Int. 2019; 295: 36-45.

462. Miller B, Kim J, Concheiro M. Stability of synthetic cathinones in oral fluid samples. Forensic Sci. Int. 2017; 274: 13-21.

463. Queiroz ME. Microextração em sorvente empacotado (MEPS) para a determinação de fármacos em fluidos biológicos. Scientia Chromatographica 2011; 3: 223-229.

464. Liu JW, Murtada K, Reyes-Garcés N, Pawliszyn J. Systematic Evaluation of Different Coating Chemistries Used in Thin-Film Microextraction. Molecules 2020; 25: 3448.

465. Moein MM, Abdel-Rehim A, Abdel-Rehim M. Microextraction by packed sorbent (MEPS). Trends Analyt. Chem. 2015; 67: 34-44.

466. Food and Drug Administration (FDA). Guidance for Industry - Bioanalytical Method Validation. [accessed September 9, 2022]. Available from: https://www.fda.gov/media/70858/download.

467. Alsenedi KA, Morrison C. Determination and long-term stability of twenty-nine cathinones and amphetamine-type stimulants (ATS) in urine using gas chromatography–mass spectrometry. J. Chromatogr. B 2018; 1076: 91-102.

468. Tsujikawa K, Mikuma T, Kuwayama K, Miyaguchi H, Kanamori T, Iwata YT, et al. Degradation pathways of 4-methylmethcathinone in alkaline solution and stability of methcathinone analogs in various pH solutions. Forensic Sci. Int. 2012; 220: 103-110.

469. Willeman T, Revol B, Fouilhé N, Stanke-Labesque F. Recurrent acute poisoning with synthetic cathinone α-pyrrolidinohexanophenone (α-PHP) in a chronic drug abuser. Toxicol. Anal. Clin. 2022; 34: 283-288.

470. Franzén L, Bäckberg M, Beck O, Helander A. Acute Intoxications Involving α-Pyrrolidinobutiophenone (α-PBP): Results from the Swedish STRIDA Project. J. Med. Toxicol. 2018; 14: 265-271.

471. Grapp M, Kaufmann C, Schwelm HM, Neukamm MA, Blaschke S, Eidizadeh A. Intoxication cases associated with the novel designer drug 3',4'-methylenedioxy-α-

pyrrolidinohexanophenone and studies on its human metabolism using high-resolution mass spectrometry. Drug Test. Anal. 2020; 12: 1320-1335.

472. Pearson JM, Hargraves TL, Hair LS, Massucci CJ, Clinton Frazee C, III, Garg U, et al. Three Fatal Intoxications Due to Methylone. J. Anal. Toxicol. 2012; 36: 444-451.

473. Kamijo Y, Soma K, Nishida M, Namera A, Ohwada T. Acute liver failure following intravenous methamphetamine. Vet. Hum. Toxicol. 2002; 44: 216-217.

474. Atayan Y, Çağın YF, Erdoğan MA, Harputluoglu MM, Bilgic Y. Ecstasy induced acute hepatic failure. Case reports. Acta Gastroenterol. Belg. 2015; 78: 53-55.

475. Carvalho M, Pontes H, Remiao F, L. Bastos M, Carvalho F. Mechanisms Underlying the Hepatotoxic Effects of Ecstasy. Curr. Pharm. Biotechnol. 2010; 11: 476-495.

476. Paiva JHHGL, Medeiros VN, Brasil IRC. Acute hepatitis secondary to abuse of cocaine, associated with severe rhabdomyolysis. Rev. Med. (São Paulo) 2020; 99: 189-196.

477. Kanel GC, Cassidy W, Shuster L, Reynolds TB. Cocaine-induced liver cell injury: Comparison of morphological features in man and in experimental models. Hepatology 1990; 11: 646-651.

478. Palacios Argueta P, Attar B, Sikavi C, Alagiozian-Angelova V, Mishra S. Drug-Induced Liver Injury Caused by “Khat,” an Herbal Stimulant. ACG Case Rep. J. 2020; 7: e00480.

479. Sauer C, Hoffmann K, Schimmel U, Peters FT. Acute poisoning involving the pyrrolidinophenone-type designer drug 4’-methyl-alpha-pyrrolidinohexanophenone (MPHP). Forensic Sci. Int. 2011; 208: e20-e25.

480. Gavriilidis G, Kyriakoudi A, Tiniakos D, Rovina N, Koutsoukou A. "Bath Salts" intoxication with multiorgan failure and left-sided ischemic colitis: a case report. Hippokratia 2015; 19: 363-365.

481. Marinetti LJ, Antonides HM. Analysis of synthetic cathinones commonly found in bath salts in human performance and postmortem toxicology: method development, drug distribution and interpretation of results. J. Anal. Toxicol. 2013; 37: 135-146.

482. Sykutera M, Cychowska M, Bloch-Boguslawska E. A Fatal Case of Pentedrone and α-Pyrrolidinovalerophenone Poisoning. J. Anal. Toxicol. 2015; 39: 324-329.

483. Luethi D, Liechti ME, Krähenbühl S. Mechanisms of hepatocellular toxicity associated with new psychoactive synthetic cathinones. Toxicology 2017; 387: 57-66.

484. Bravo RR, Carmo H, Valente MJ, Silva JP, Carvalho F, Bastos MdL, et al. From street to lab: in vitro hepatotoxicity of buphedrone, butylone and 3,4-DMMC. Arch. Toxicol. 2021; 95: 1443-1462.

485. Soldatow VY, Lecluyse EL, Griffith LG, Rusyn I. In vitro models for liver toxicity testing. Toxicol Res. (Camb.) 2013; 2: 23-39.

486. Guillouzo A, Corlu A, Aninat C, Glaise D, Morel F, Guguen-Guillouzo C. The human hepatoma HepaRG cells: a highly differentiated model for studies of liver metabolism and toxicity of xenobiotics. Chem. Biol. Interact. 2007; 168: 66-73.

487. Tanaka M, Miyajima A. Liver regeneration and fibrosis after inflammation. Inflamm. Regen. 2016; 36: 19.

488. Zhou Z, Xu M-J, Gao B. Hepatocytes: a key cell type for innate immunity. Cell Mol. Immunol. 2016; 13: 301-315.

489. Silva B, Rodrigues JS, Almeida AS, Lima AR, Fernandes C, Guedes de Pinho P, et al. Enantioselectivity of Pentedrone and Methylone on Metabolic Profiling in 2D and 3D Human Hepatocyte-like Cells. Pharmaceuticals 2022; 15: 368.

490. Castell JV, Jover R, Martnez-Jimnez CP, Gmez-Lechn MJ. Hepatocyte cell lines: their use, scope and limitations in drug metabolism studies. Expert Opin. Drug Metab. Toxicol. 2006; 2: 183-212.

491. Donato MT, Lahoz A, Castell JV, Gómez-Lechón MJ. Cell lines: a tool for in vitro drug metabolism studies. Curr. Drug Metab. 2008; 9: 1-11.

492. Tolosa L, Gómez-Lechón MJ, López S, Guzmán C, Castell JV, Donato MT, et al. Human Upcyte Hepatocytes: Characterization of the Hepatic Phenotype and Evaluation for Acute and Long-Term Hepatotoxicity Routine Testing. Toxicol. Sci. 2016; 152: 214-229.

493. Szabo M, Veres Z, Baranyai Z, Jakab F, Jemnitz K. Comparison of Human Hepatoma HepaRG Cells with Human and Rat Hepatocytes in Uptake Transport Assays in Order to Predict a Risk of Drug Induced Hepatotoxicity. PLOS ONE 2013; 8: e59432.

494. Wang Z-Y, Li W-J, Li Q-G, Jing H-S, Yuan T-J, Fu G-B, et al. A DMSO-free hepatocyte maturation medium accelerates hepatic differentiation of HepaRG cells in vitro. Biomed. Pharmacother. 2019; 116: 109010.

495. Gómez-Lechón MJ, Tolosa L, Donato MT. Upgrading HepG2 cells with adenoviral vectors that encode drug-metabolizing enzymes: application for drug hepatotoxicity testing. Expert Opin. Drug Metab. Toxicol. 2017; 13: 137-148.

496. Gaspar H, Bronze S, Oliveira C, Victor BL, Machuqueiro M, Pacheco R, et al. Proactive response to tackle the threat of emerging drugs: Synthesis and toxicity evaluation of new cathinones. Forensic Sci. Int. 2018; 290: 146-156.

497. Saravanan BC, Sreekumar C, Bansal GC, Ray D, Rao JR, Mishra AK. A rapid MTT colorimetric assay to assess the proliferative index of two Indian strains of Theileria annulata. Vet. Parasitol. 2003; 113: 211-216.

498. Rai Y, Pathak R, Kumari N, Sah DK, Pandey S, Kalra N, et al. Mitochondrial biogenesis and metabolic hyperactivation limits the application of MTT assay in the estimation of radiation induced growth inhibition. Sci. Rep. 2018; 8: 1531.

499. Rajapakse N, Silva E, Scholze M, Kortenkamp A. Deviation from Additivity with Estrogenic Mixtures Containing 4-Nonylphenol and 4-tert-Octylphenol Detected in the E-SCREEN Assay. Environ. Sci. Technol. 2004; 38: 6343-6352.

500. Dias da Silva D, Silva E, Carmo H. Combination effects of amphetamines under hyperthermia - the role played by oxidative stress. J. Appl. Toxicol. 2014; 34: 637-650.

501. Bioquest A. Amplite™ Fluorimetric Glutathione GSH/GSSG Ratio Assay Kit *Green Fluorescence*. In: Bioquest A, editor. 2011.

502. Huang T, Long M, Huo B. Competitive Binding to Cuprous Ions of Protein and BCA in the Bicinchoninic Acid Protein Assay. Open Biomed. Eng. J. 2010; 4: 271-278.

503. Richter LHJ, Beck A, Flockerzi V, Maurer HH, Meyer MR. Cytotoxicity of new psychoactive substances and other drugs of abuse studied in human HepG2 cells using an adopted high content screening assay. Toxicol. Lett. 2019; 301: 79-89.

504. Glicksberg L, Bryand K, Kerrigan S. Identification and quantification of synthetic cathinones in blood and urine using liquid chromatography-quadrupole/time of flight (LC-Q/TOF) mass spectrometry. J. Chromatogr. B 2016; 1035: 91-103.

505. Adamowicz P, Gieroń J, Gil D, Lechowicz W, Skulska A, Tokarczyk B. The prevalence of new psychoactive substances in biological material - a three-year review of casework in Poland. Drug Test. Anal. 2016; 8: 63-70.

506. Cawrse BM, Levine B, Jufer RA, Fowler DR, Vorce SP, Dickson AJ, et al. Distribution of Methylone in Four Postmortem Cases. J. Anal. Toxicol. 2012; 36: 434-439.

507. Gerets HH, Tilmant K, Gerin B, Chanteux H, Depelchin BO, Dhalluin S, et al. Characterization of primary human hepatocytes, HepG2 cells, and HepaRG cells at the mRNA level and CYP activity in response to inducers and their predictivity for the detection of human hepatotoxins. Cell Biol. Toxicol. 2012; 28: 69-87.

508. Chen Z, Tian R, She Z, Cai J, Li H. Role of oxidative stress in the pathogenesis of nonalcoholic fatty liver disease. Free Radic. Biol. Med. 2020; 152: 116-141.

509. Zhang J, Wang X, Vikash V, Ye Q, Wu D, Liu Y, et al. ROS and ROS-Mediated Cellular Signaling. Oxid. Med. Cell. Longev. 2016; 2016: 4350965.

510. Ayla O, Metin O. Biochemistry of Reactive Oxygen and Nitrogen Species. In: Sivakumar Joghi Thatha G, editor. Basic Principles and Clinical Significance of Oxidative Stress. Rijeka: IntechOpen, 2015. p. Ch. 3.

511. Dias-da-Silva D, Arbo MD, Valente MJ, Bastos ML, Carmo H. Hepatotoxicity of piperazine designer drugs: Comparison of different in vitro models. Toxicol. In Vitro 2015; 29: 987-996.

512. Dias da Silva D, Ferreira B, Roque Bravo R, Rebelo R, Duarte de Almeida T, Valente MJ, et al. The new psychoactive substance 3-methylmethcathinone (3-MMC or metaphedrone) induces oxidative stress, apoptosis, and autophagy in primary rat hepatocytes at human-relevant concentrations. Arch. Toxicol. 2019; 93: 2617-2634.

513. Rahman I, Kode A, Biswas SK. Assay for quantitative determination of glutathione and glutathione disulfide levels using enzymatic recycling method. Nat. Protoc. 2006; 1: 3159-3165.

514. Sentellas S, Morales-Ibanez O, Zanuy M, Albertí JJ. GSSG/GSH ratios in cryopreserved rat and human hepatocytes as a biomarker for drug induced oxidative stress. Toxicol. In Vitro 2014; 28: 1006-1015.

515. Xiong Y, Uys JD, Tew KD, Townsend DM. S-glutathionylation: from molecular mechanisms to health outcomes. Antioxid. Redox Signal. 2011; 15: 233-270.

516. Aoyama K, Nakaki T. Inhibition of GTRAP3-18 may increase neuroprotective glutathione (GSH) synthesis. Int. J. Mol. Sci. 2012; 13: 12017-12035.

517. Higuchi M. Chapter 15 - Antioxidant Properties of Wheat Bran against Oxidative Stress. In: Watson RR, Preedy VR, Zibadi S, editors. Wheat and Rice in Disease Prevention and Health. San Diego: Academic Press, 2014. p. 181-199.

518. Carvalho M, Milhazes N, Remião F, Borges F, Fernandes E, Amado F, et al. Hepatotoxicity of 3,4-methylenedioxyamphetamine and α-methyldopamine in isolated rat hepatocytes: formation of glutathione conjugates. Arch. Toxicol. 2004; 78: 16-24.

519. Meyer MR, Richter LHJ, Maurer HH. Methylenedioxy designer drugs: Mass spectrometric characterization of their glutathione conjugates by means of liquid chromatography-high-resolution mass spectrometry/mass spectrometry and studies on their glutathionyl transferase inhibition potency. Anal. Chim. Acta 2014; 822: 37-50.

520. Arbo MD, Silva R, Barbosa DJ, da Silva DD, Rossato LG, Bastos MdL, et al. Piperazine designer drugs induce toxicity in cardiomyoblast h9c2 cells through mitochondrial impairment. Toxicol. Lett. 2014; 229: 178-189.

521. Phillips AM, Logan BK, Stafford DT. Further applications for capillary gas chromatography in routine quantitative toxicological analyses. J. High Resolut. Chromatogr. 1990; 13: 754-758.

Annexes

Supporting Information

Chemical Characterization of Synthetic Cathinones Found in Seized Materials

1. FTIR Analysis

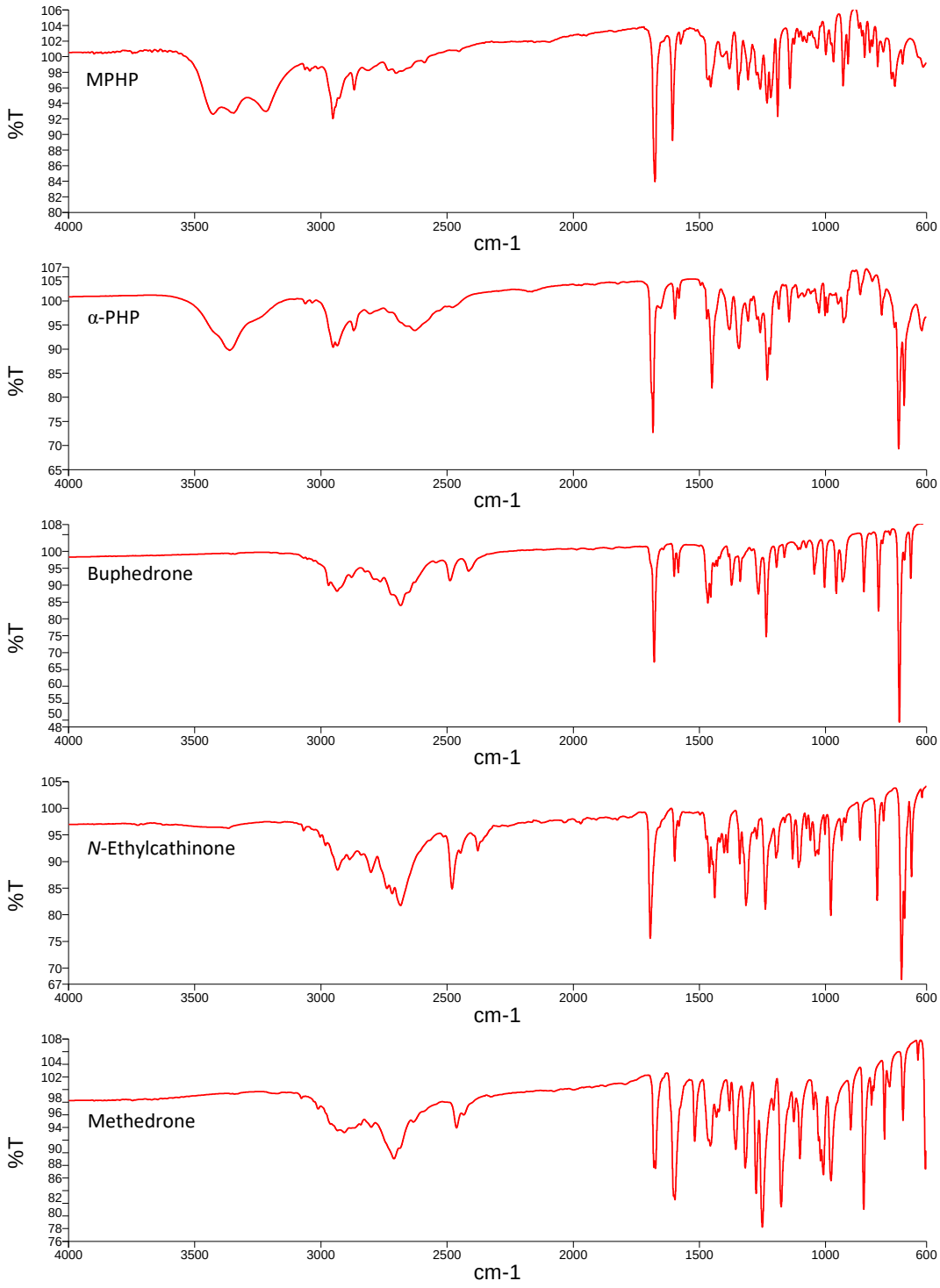

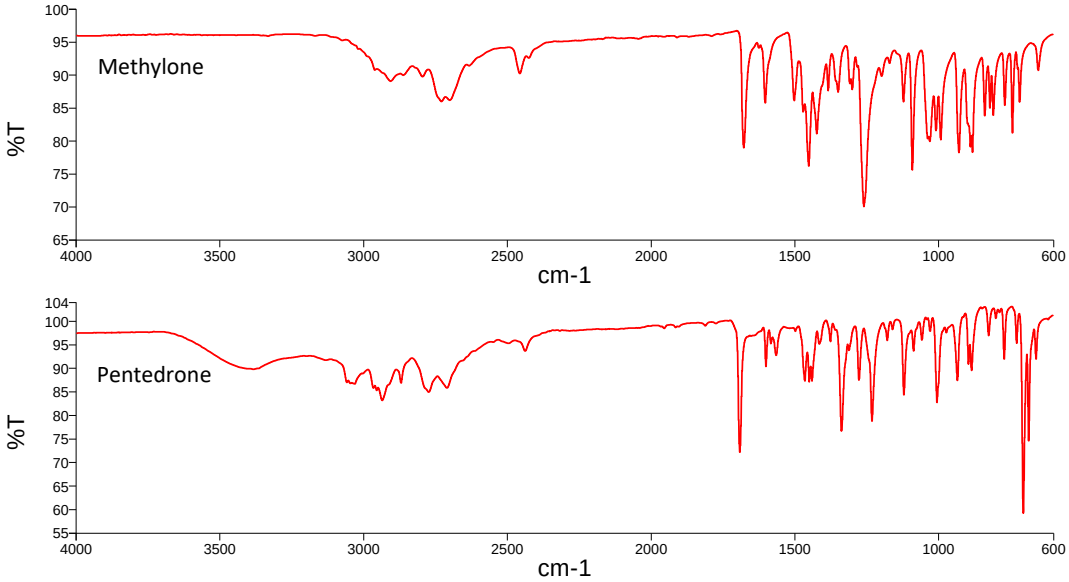

Figure S1. FTIR spectra of SCat standards.

2. GC-MS Analysis

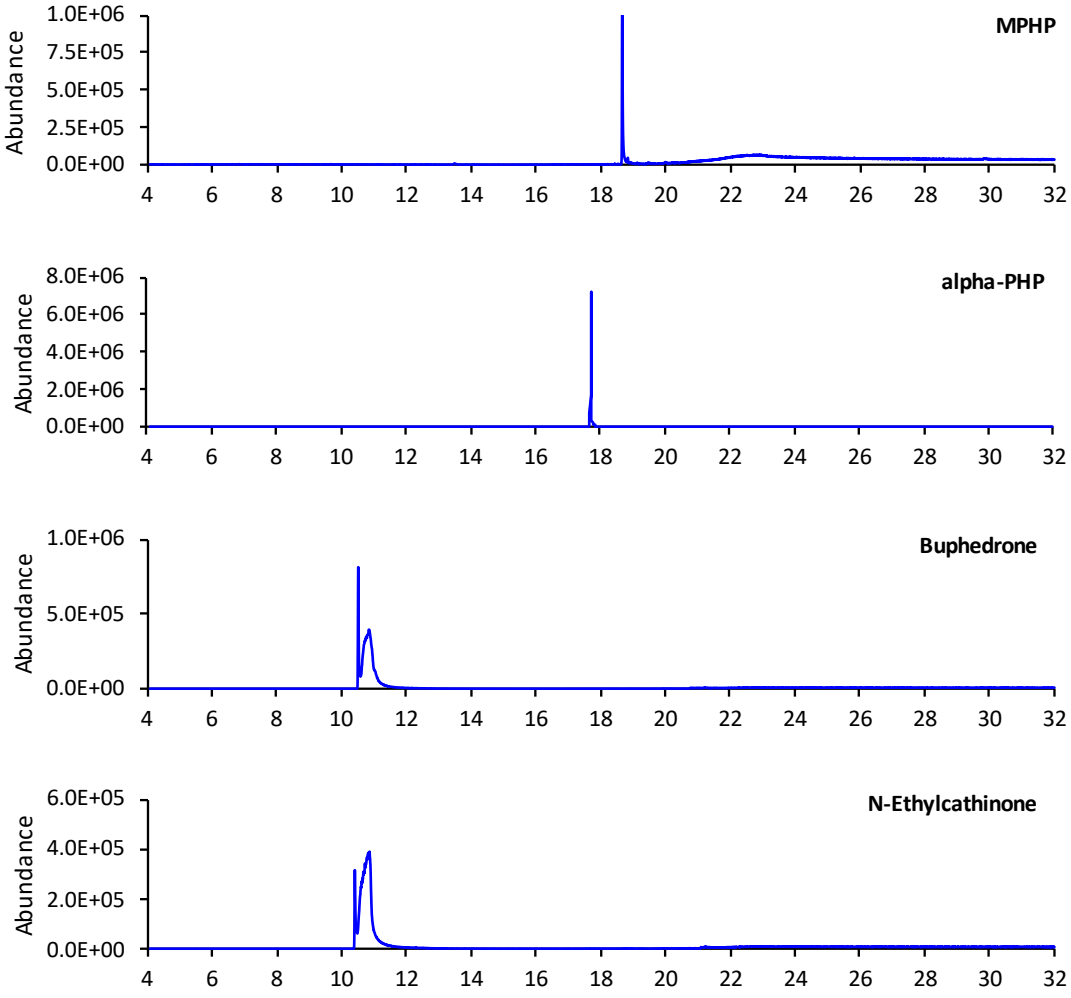

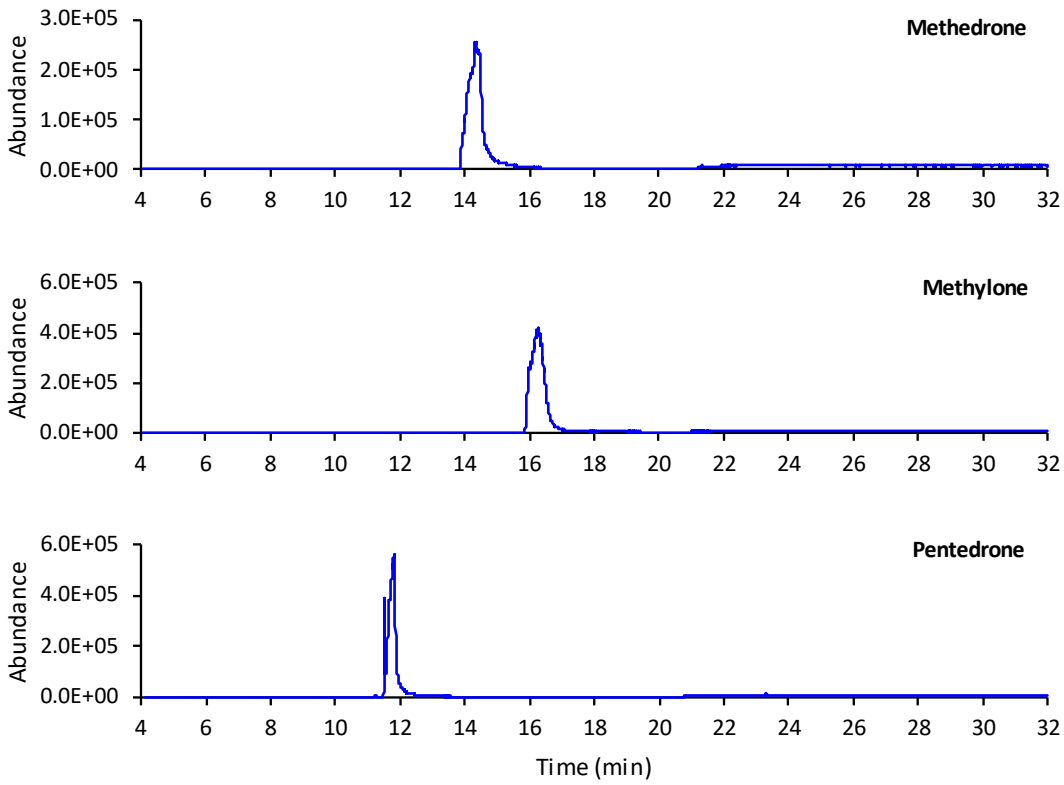

Figure S2. Typical GC-MS chromatograms of SCat standards.

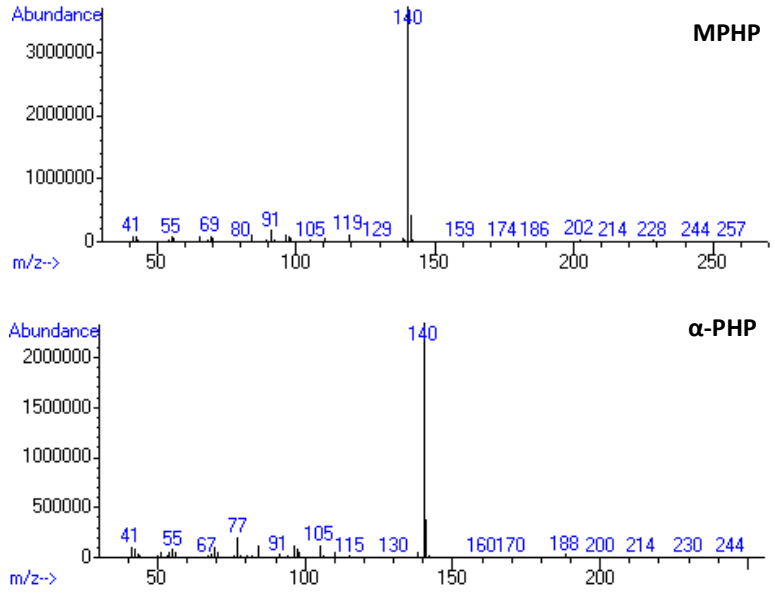

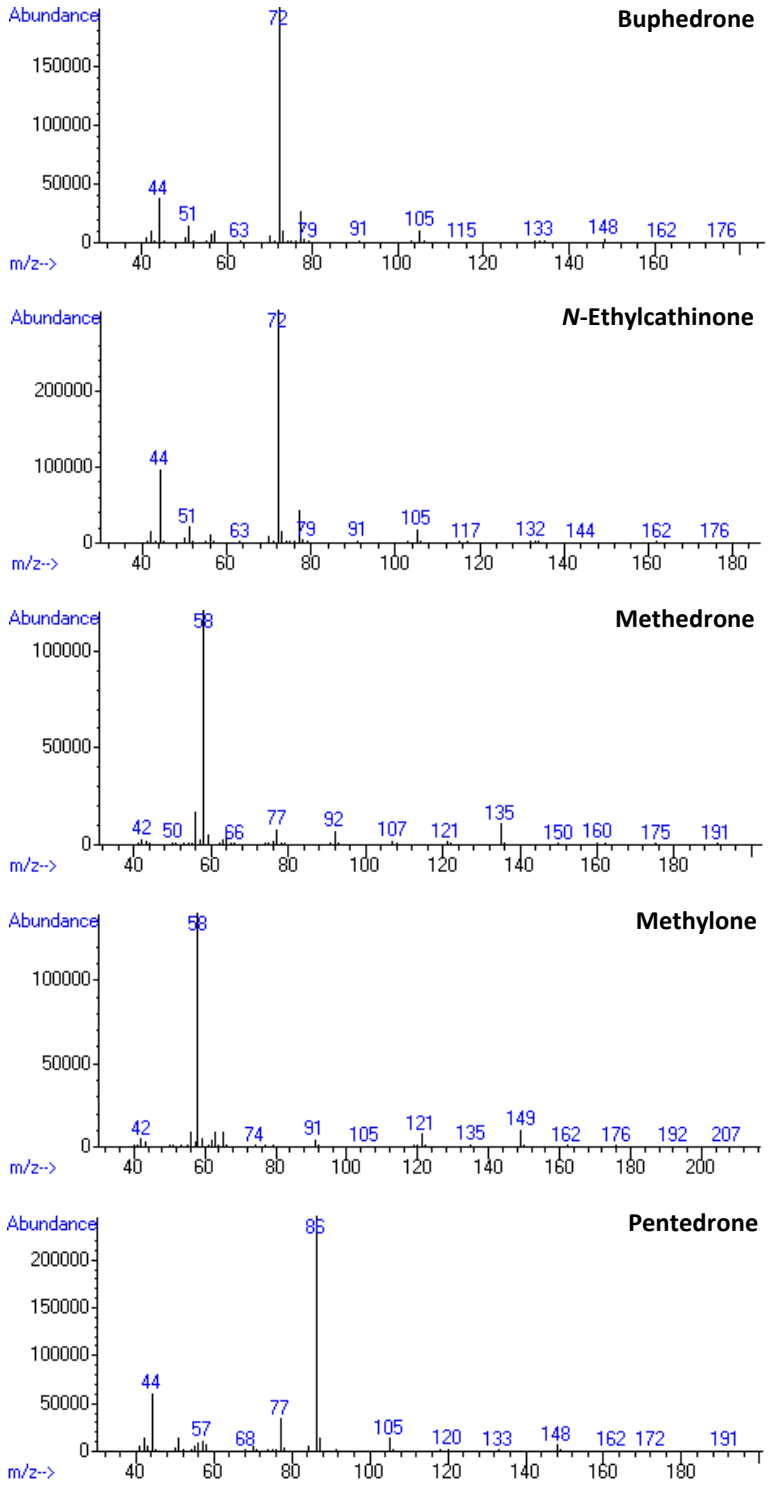

Figure S3. Mass spectra of SCat standards.

3. UHPLC-PDA analysis

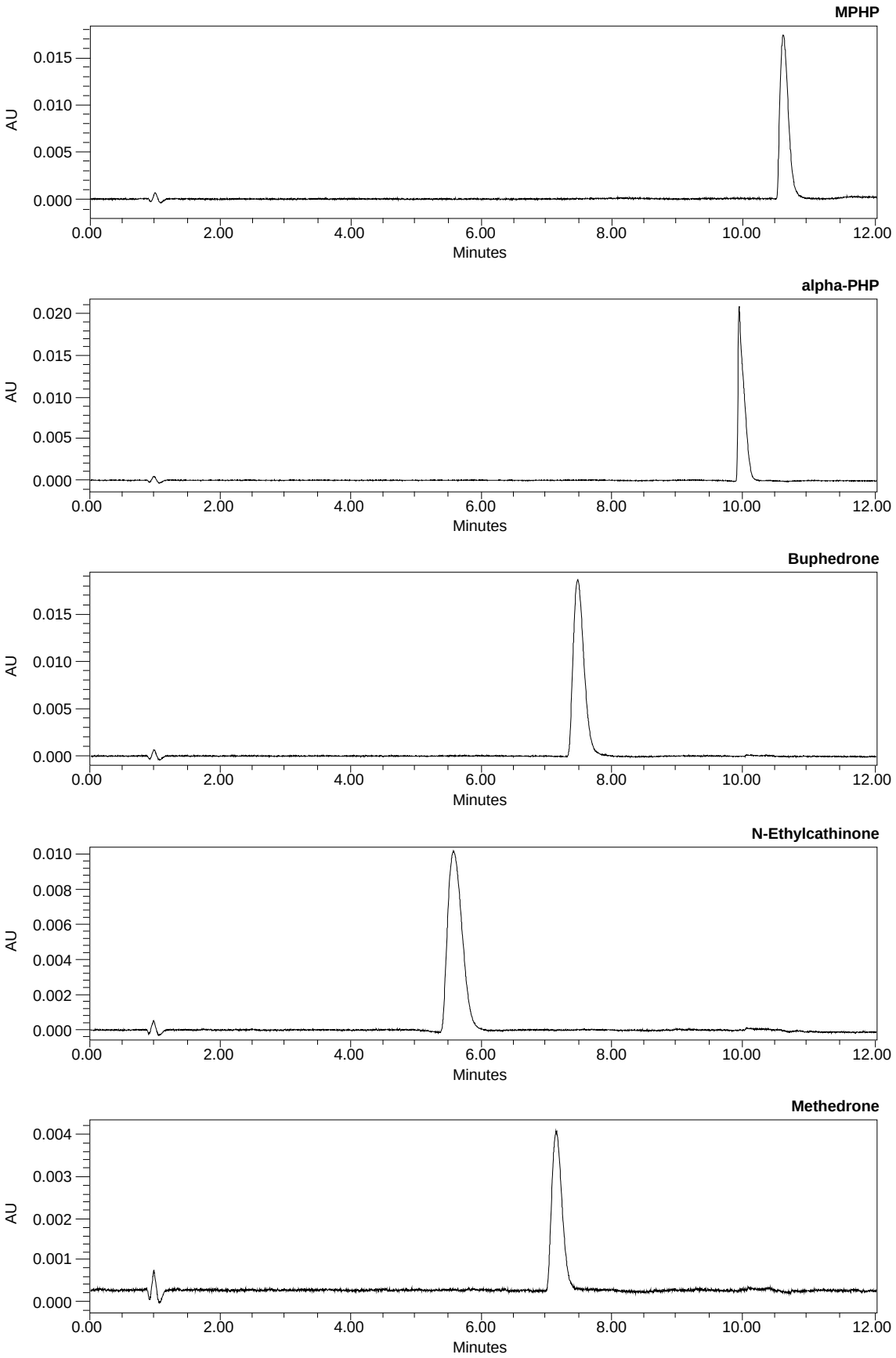

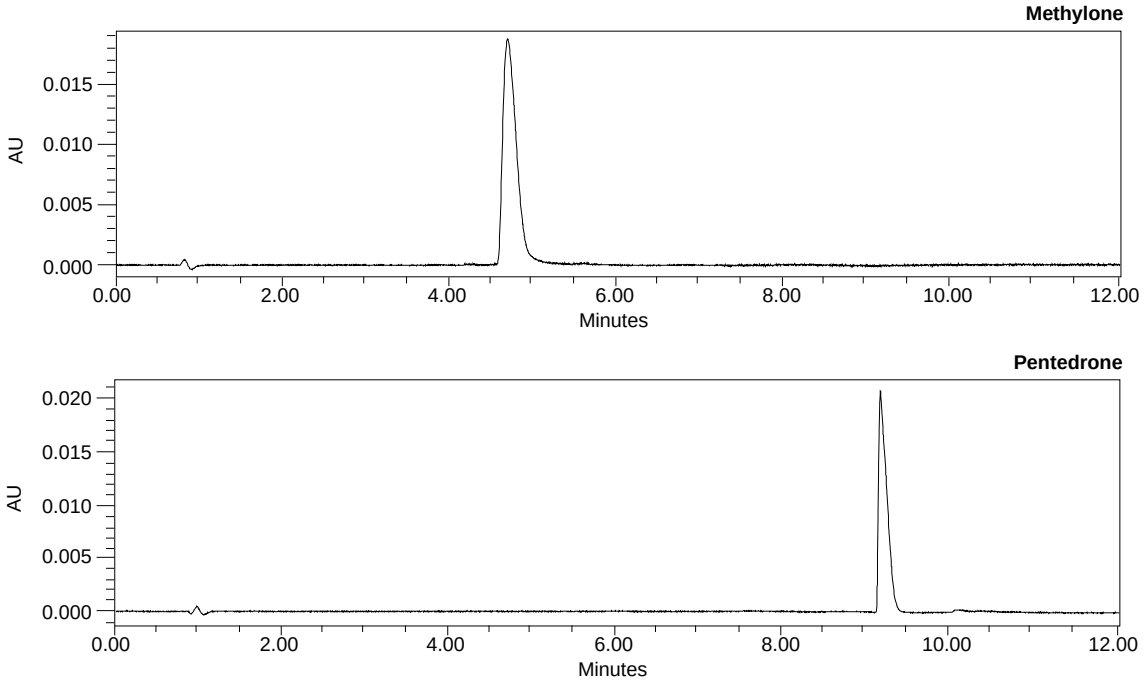

Figure S4. Typical UHPLC-PDA chromatograms of SCat standards.

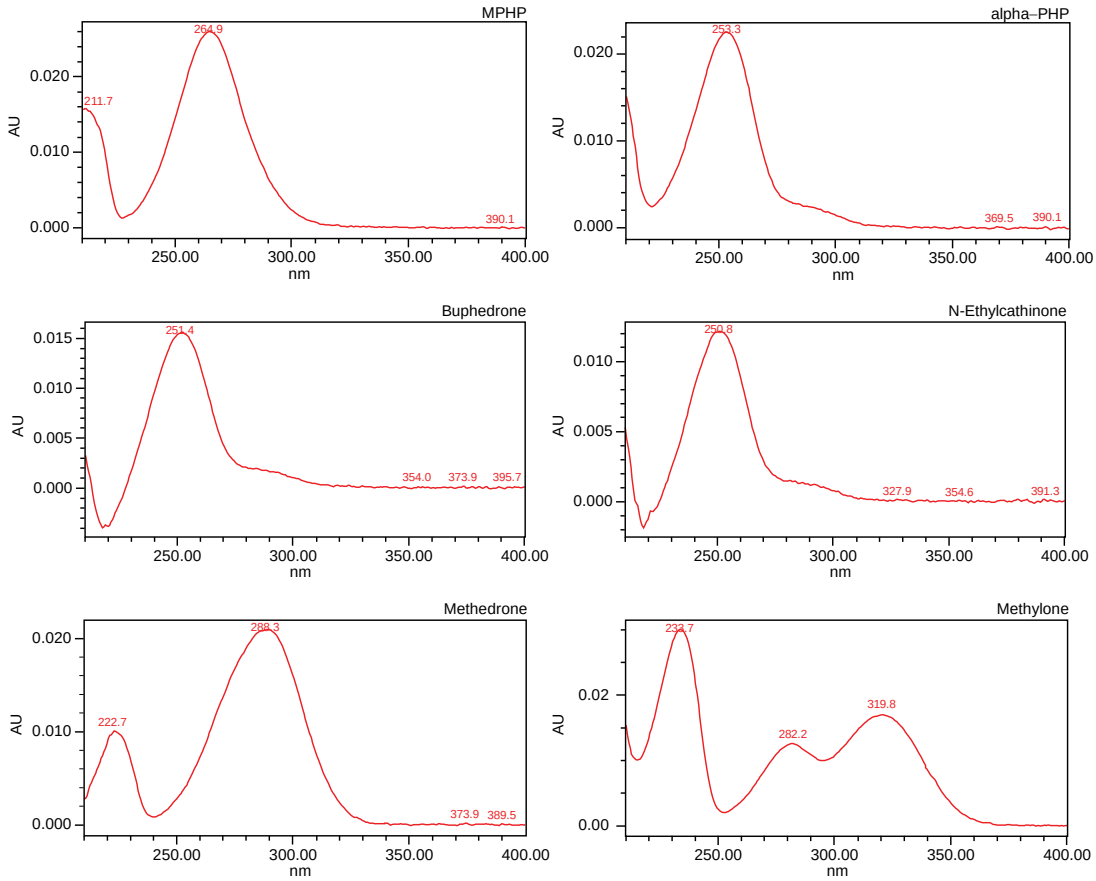

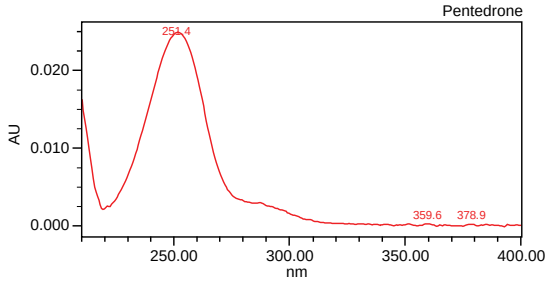

Figure S5. UV spectra of SCat standards.

4. NMR analysis

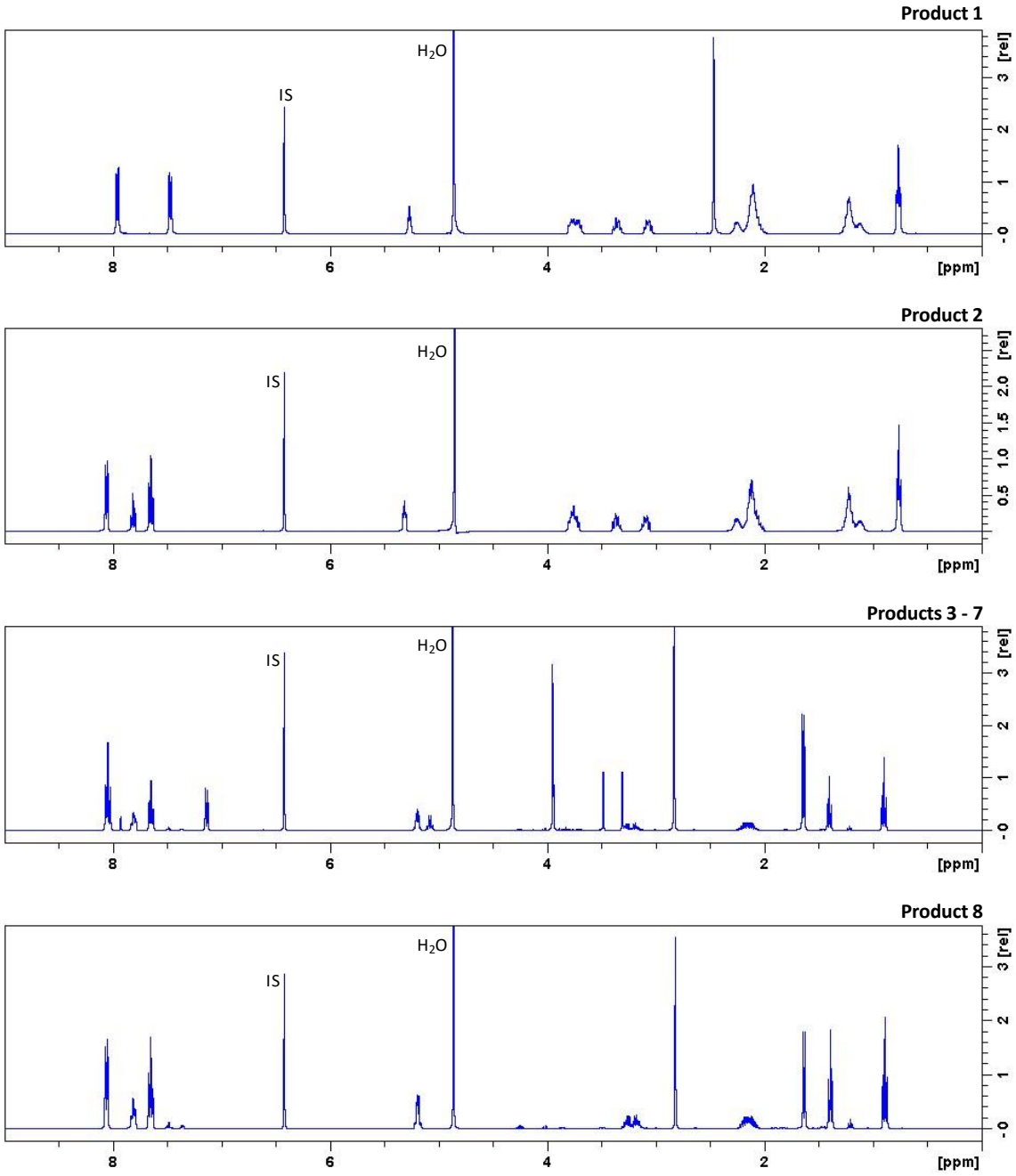

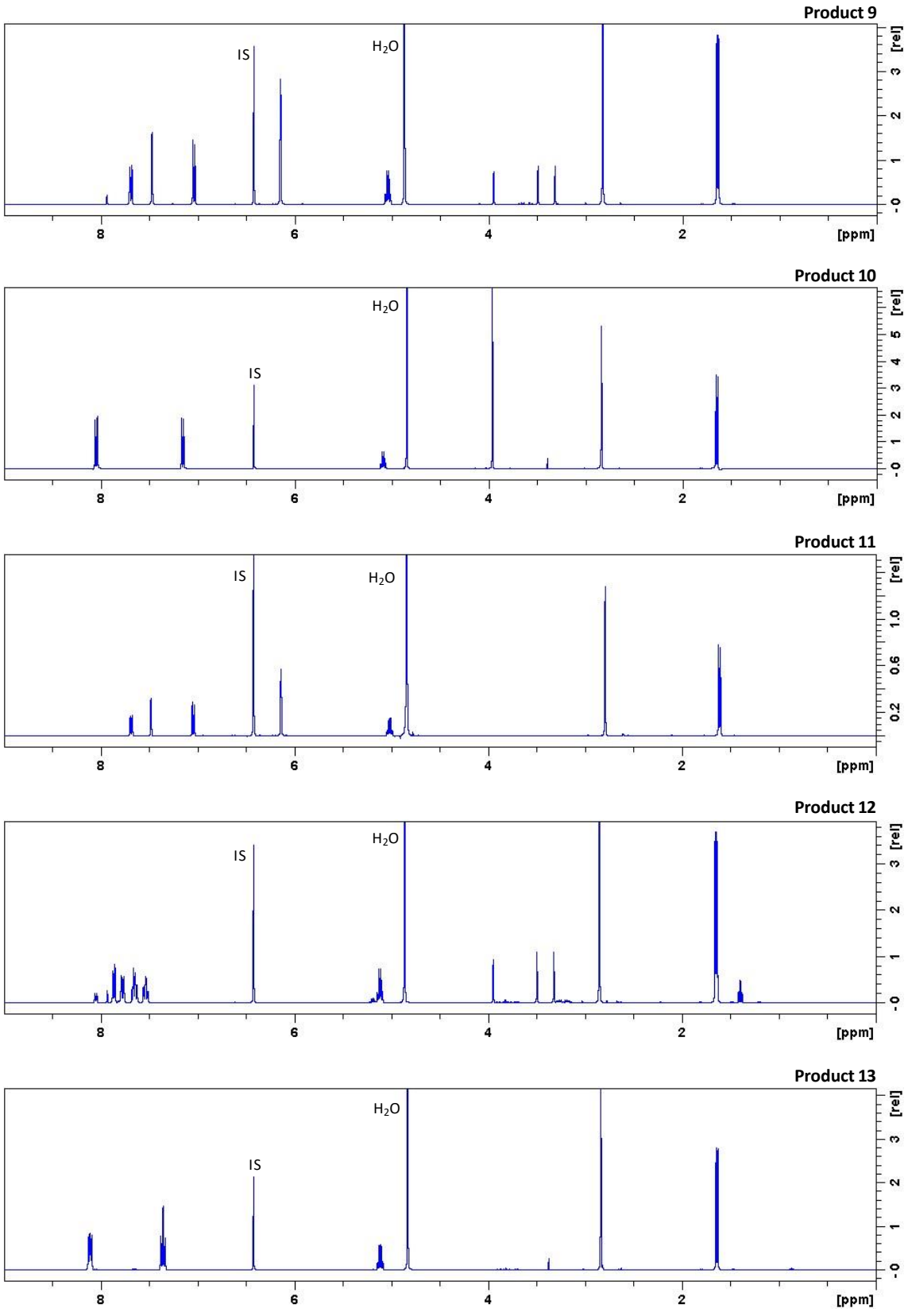
Product 9
IS
H2O
[rel]
[ppm]
Product 10
H2O
IS
[rel]
[ppm]
Product 11
IS
H2O
[rel]
[ppm]
Product 12
H2O
IS
[rel]
[ppm]
Product 13
H2O
IS
[rel]
[ppm]

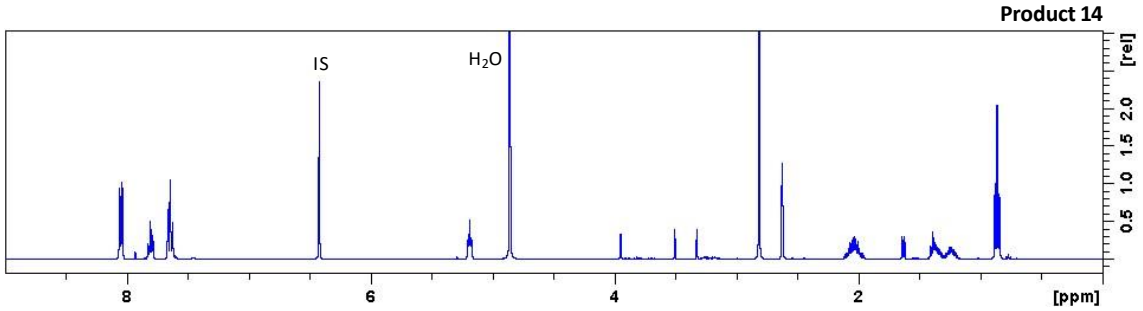

Figure S6. ^{1}H NMR spectra of seized products.

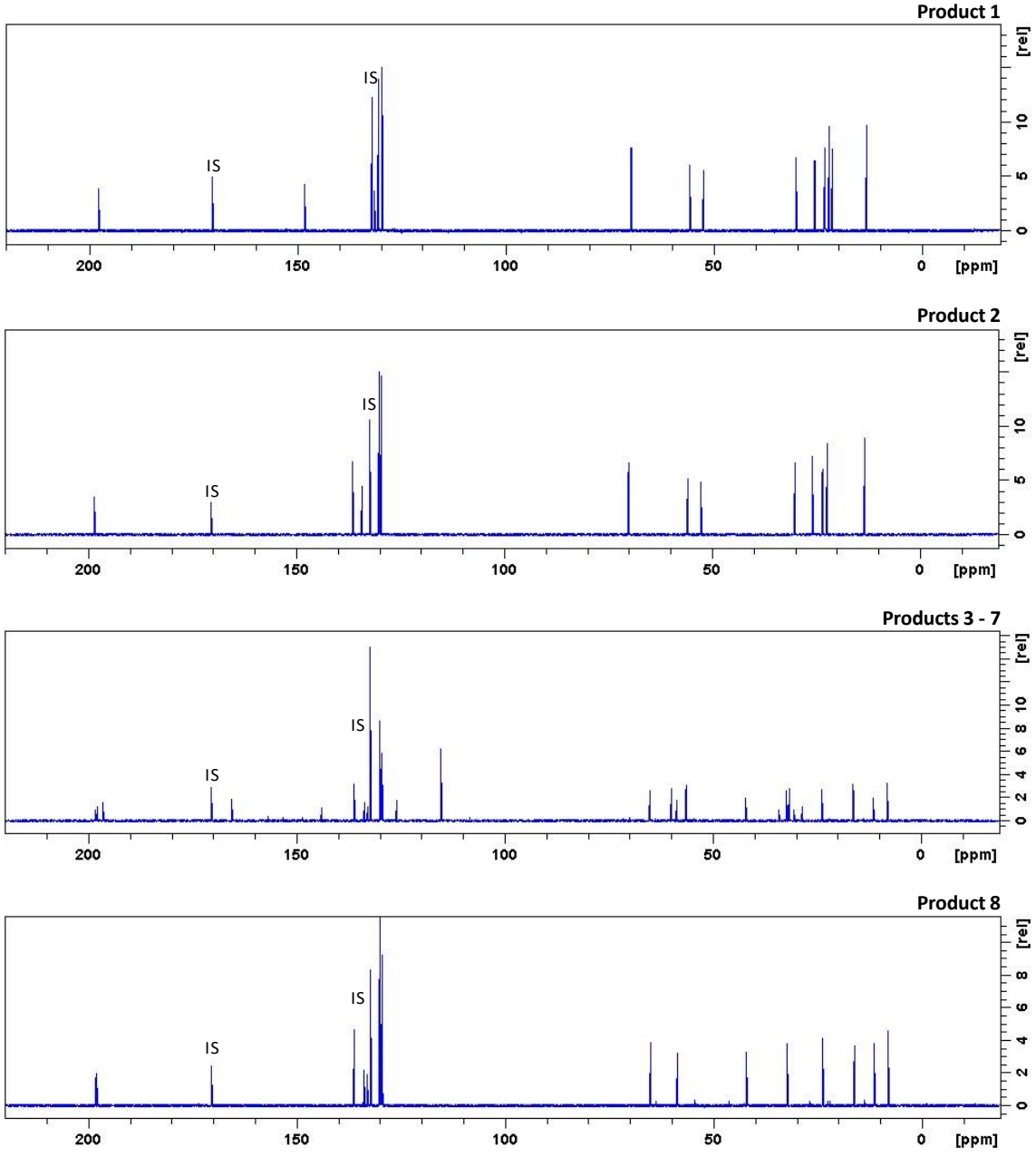

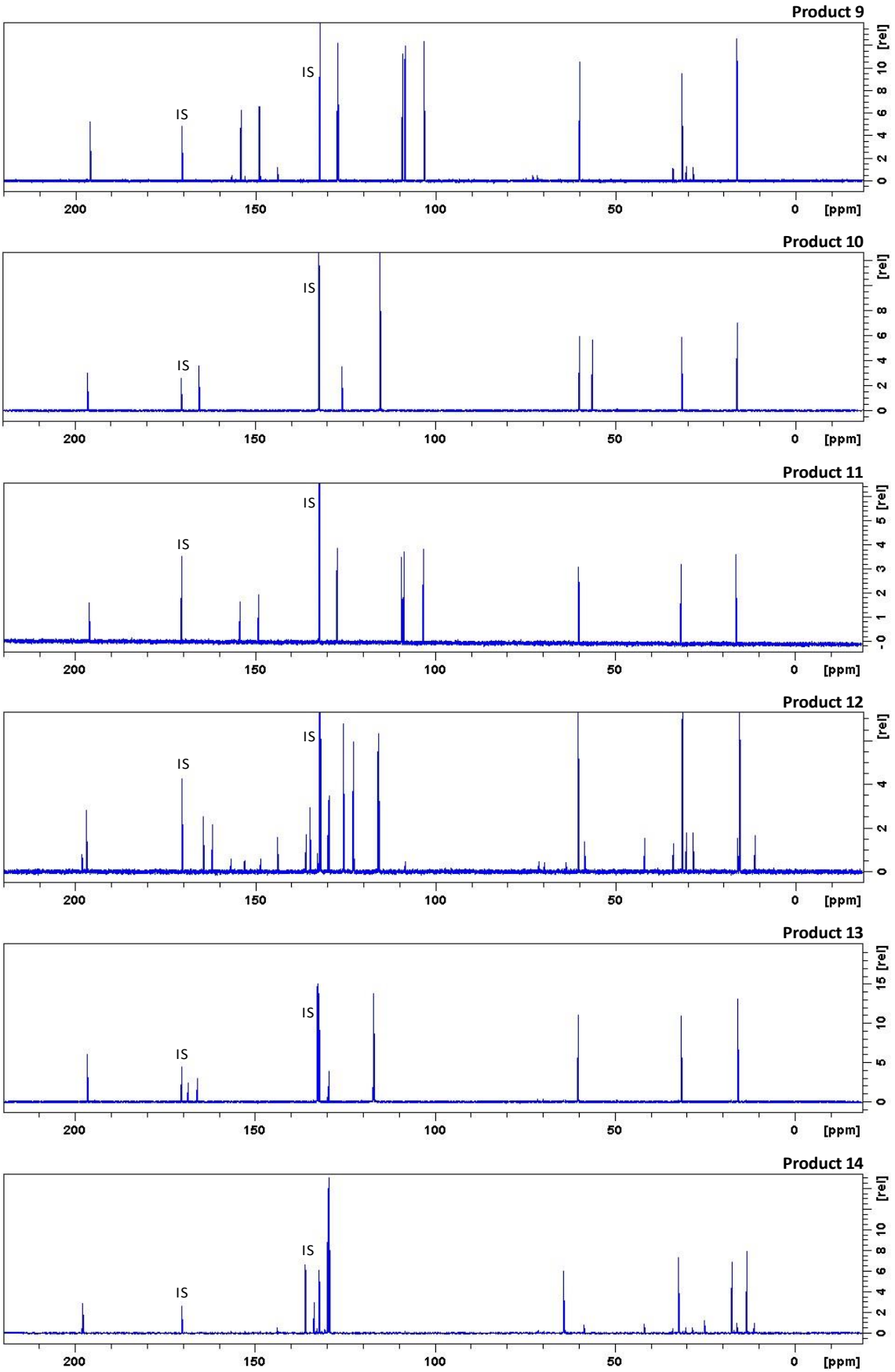

Figure S7. ^{13}C NMR spectra of seized products.

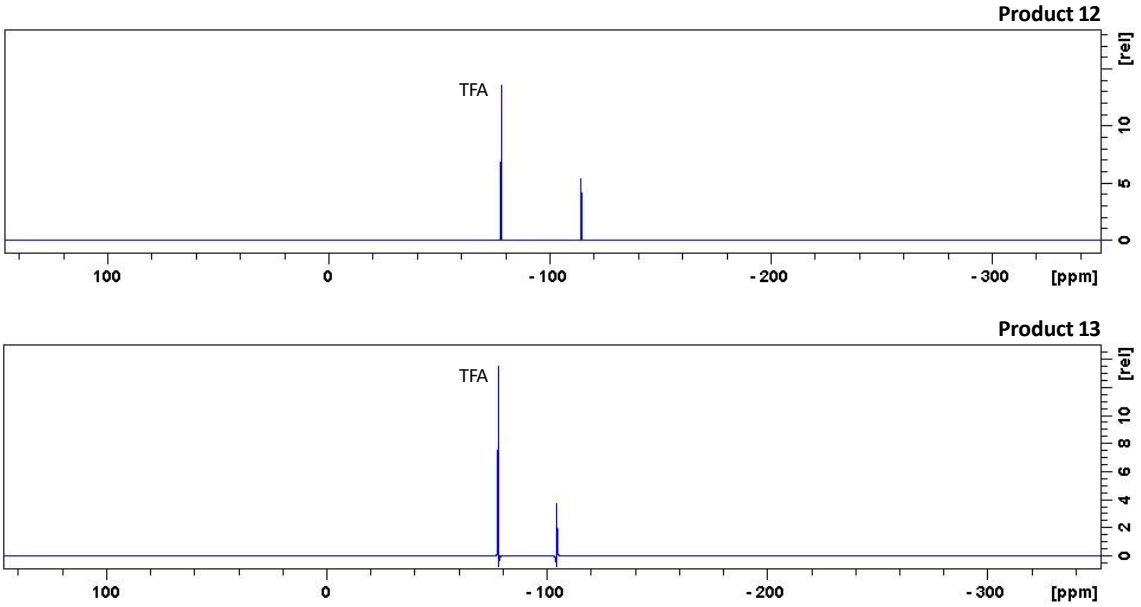

Figure S8. ^{19}F NMR spectra of products 12 and 13.

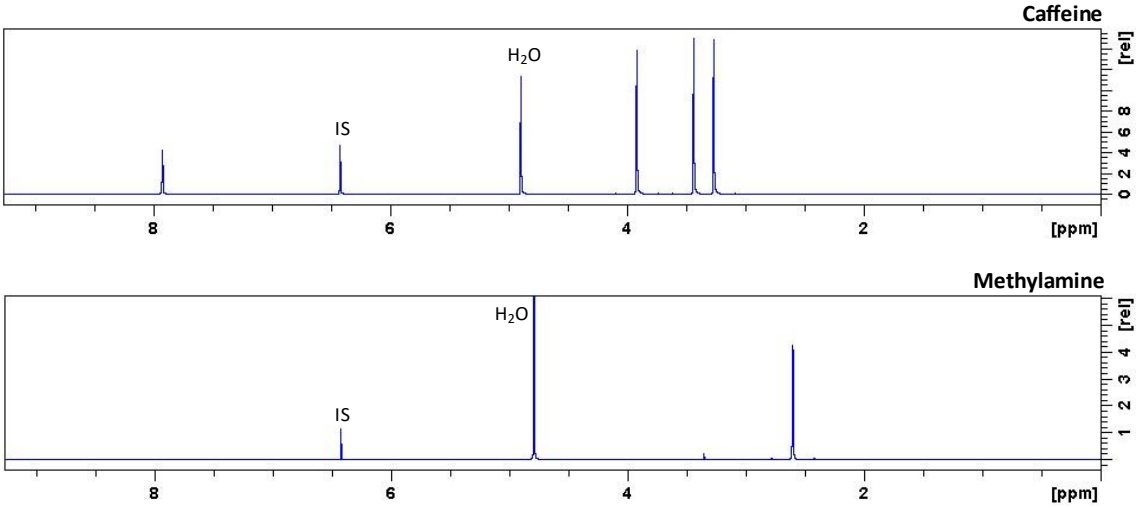

Figure S9. ^{1}H NMR spectra of caffeine and methylamine found in seized products.

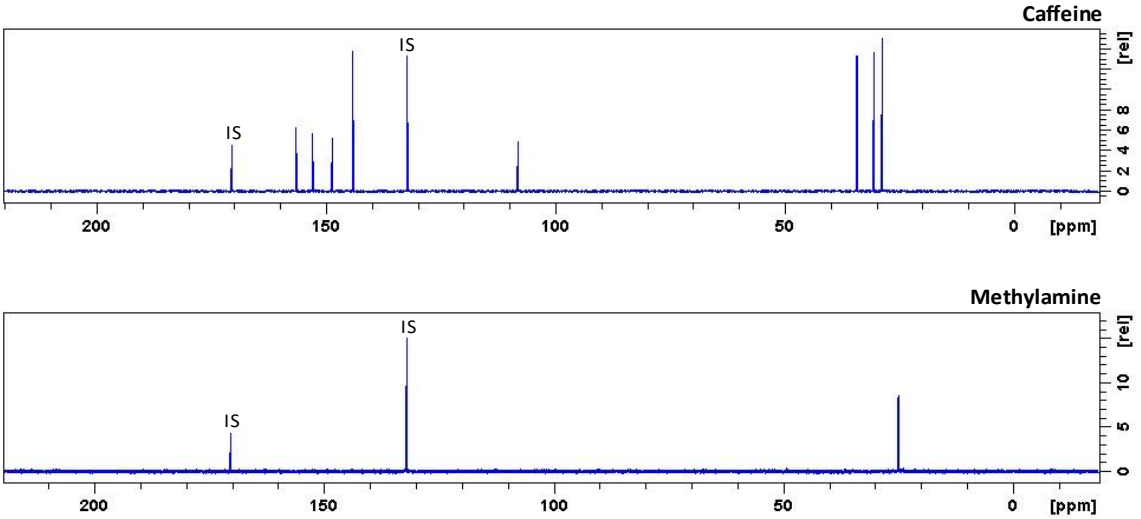

Figure S10. ^{13}C NMR spectra of caffeine and methylamine found in seized products.

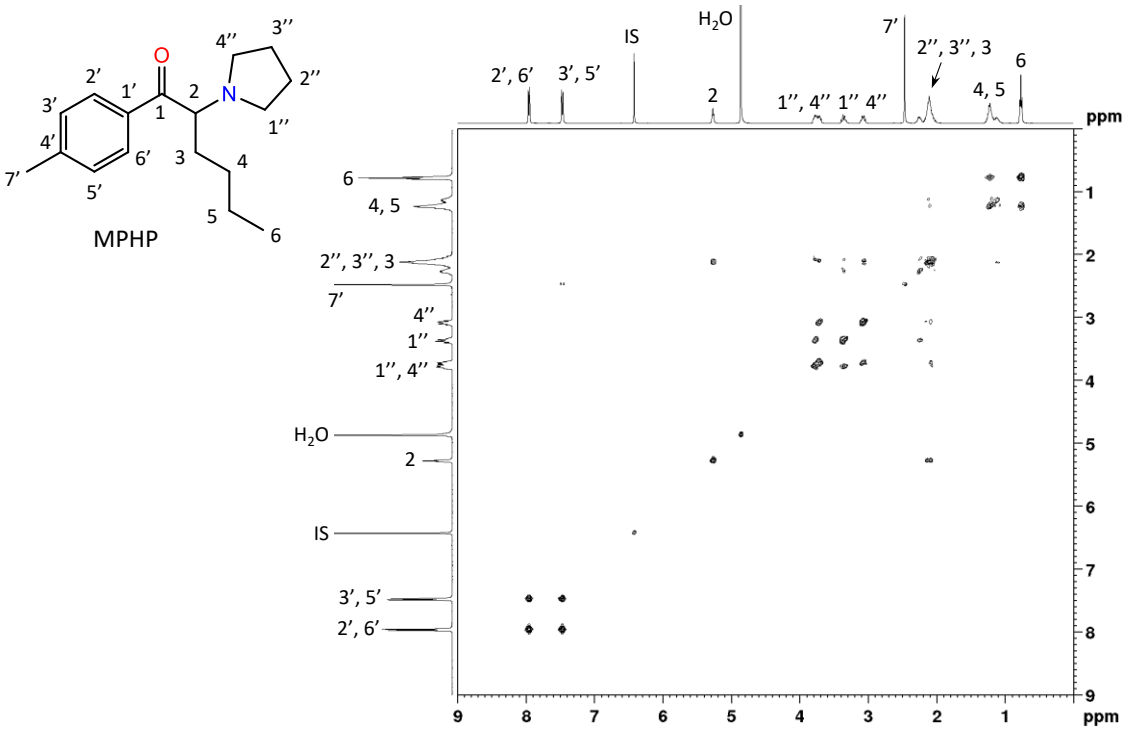
MPHP
IS
H2O
7'
2'', 3'', 3
6
2', 6'
3', 5'
2
1'', 4''
1'' 4''
4, 5
ppm

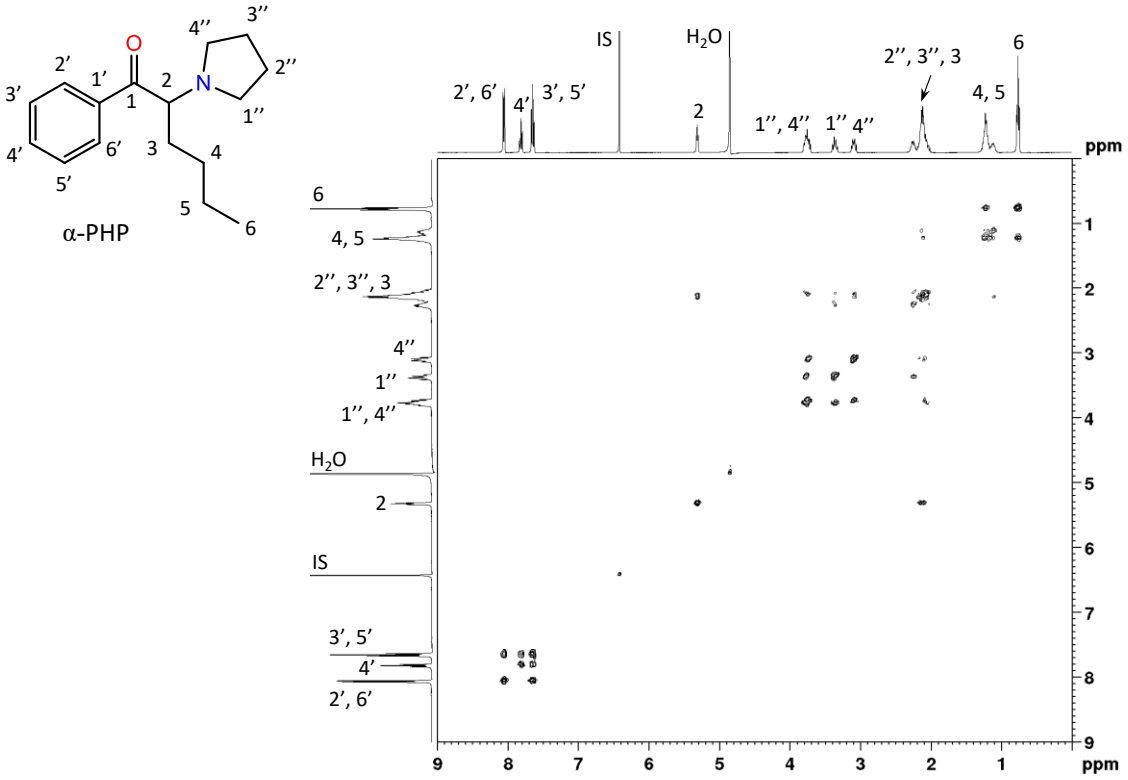
α-PHP
IS
H2O
2'', 3'', 3
6
2', 6'
4'
3', 5'
2
1'', 4''
1'' 4''
4, 5
ppm

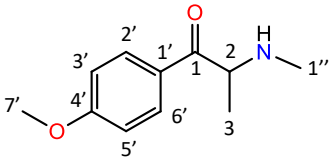

Methedrone

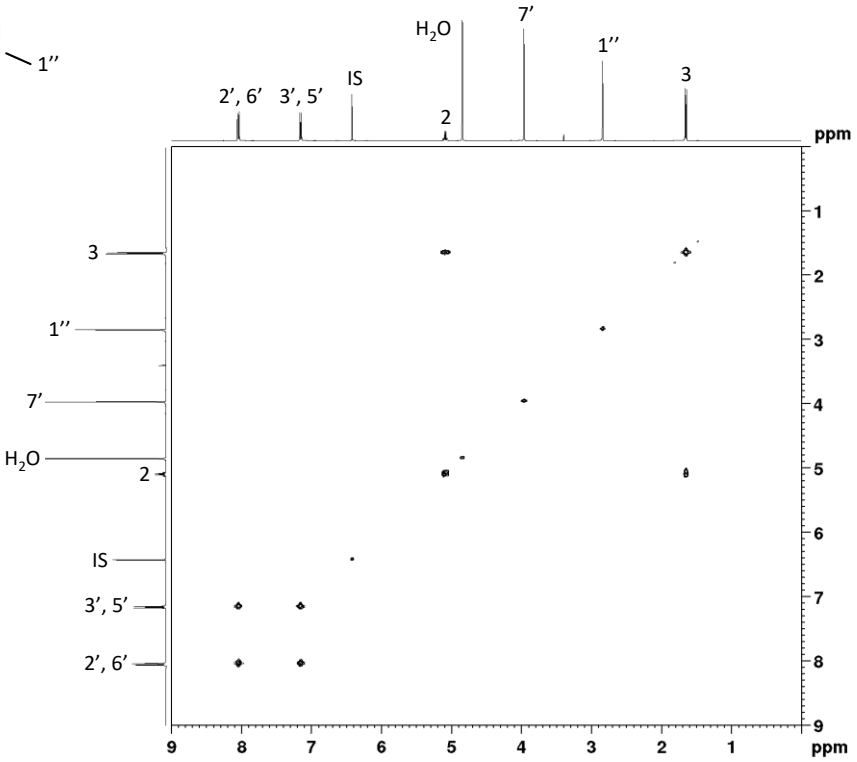

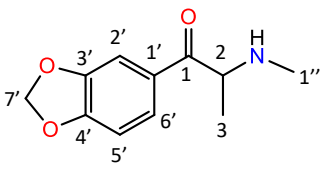

Methylone

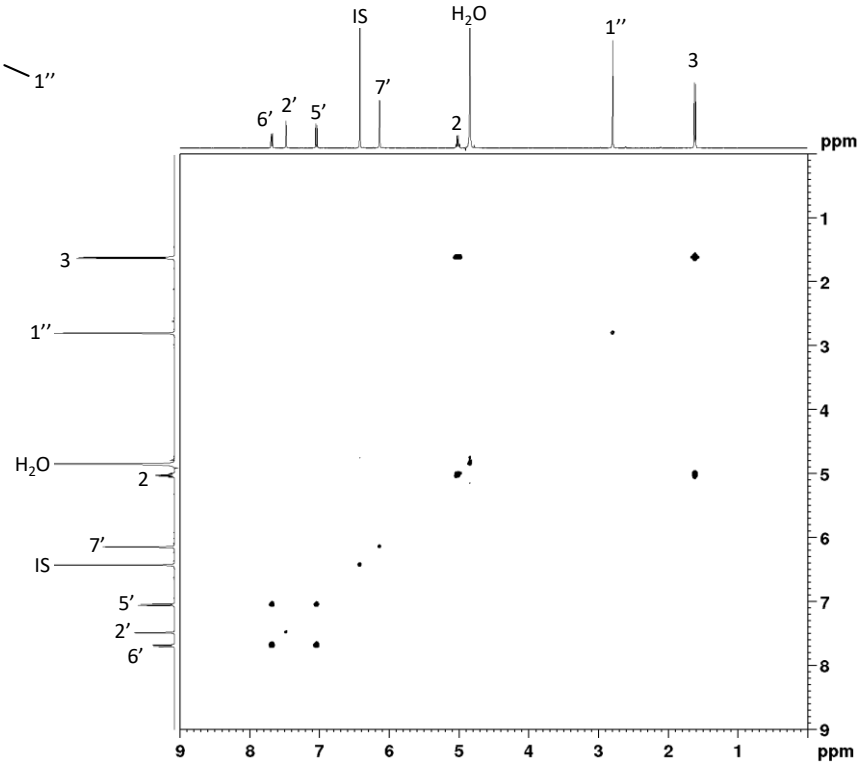

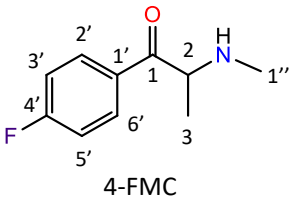

4-FMC

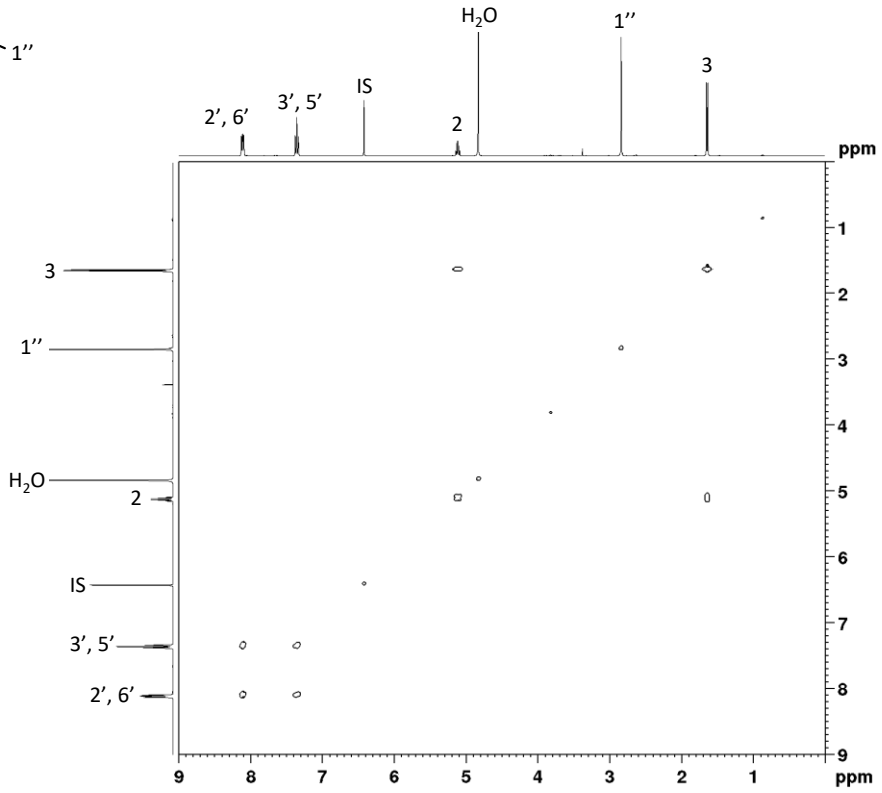

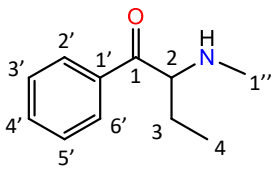

Buphedrone

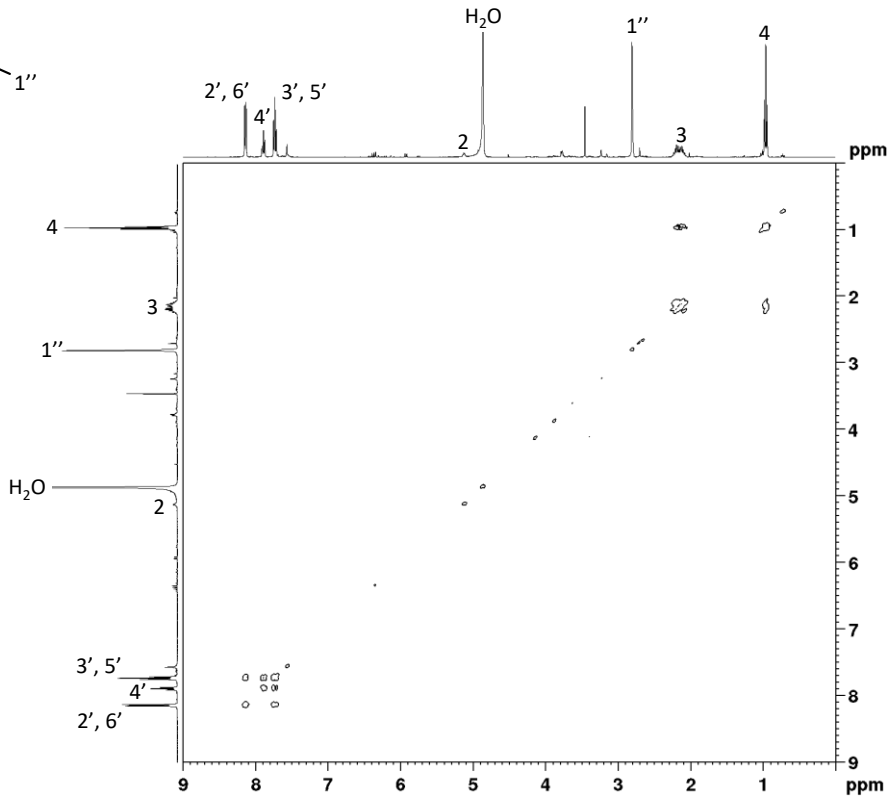

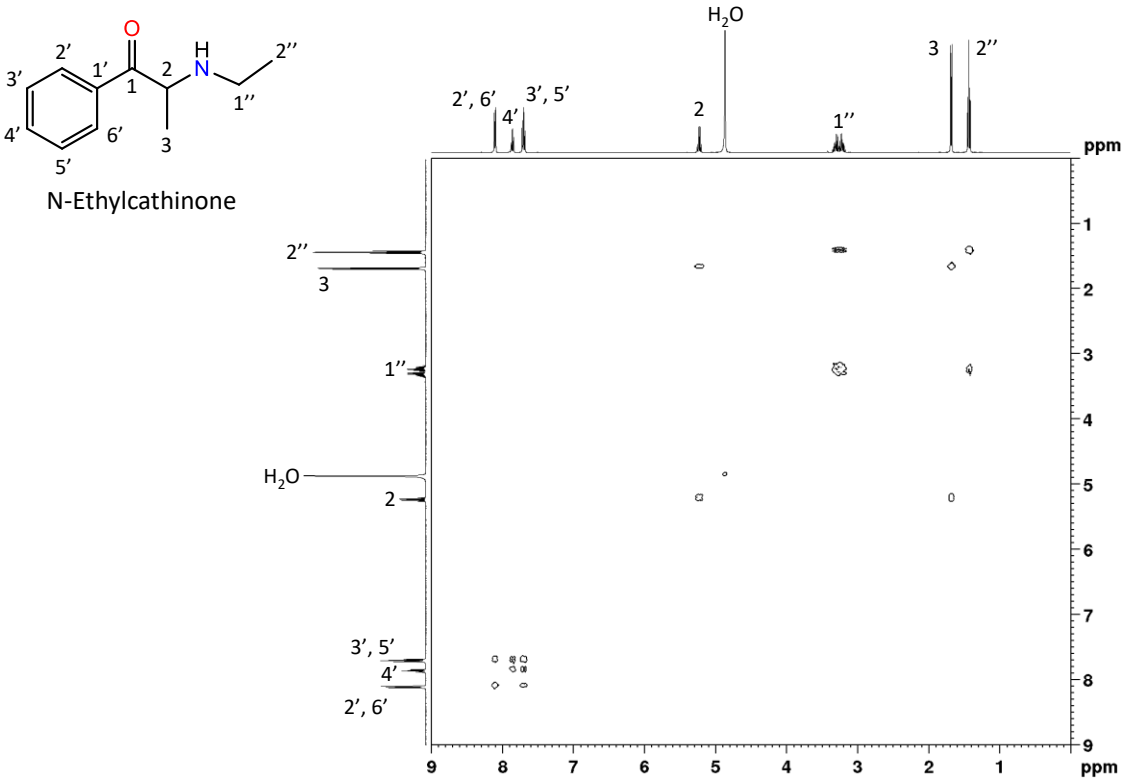

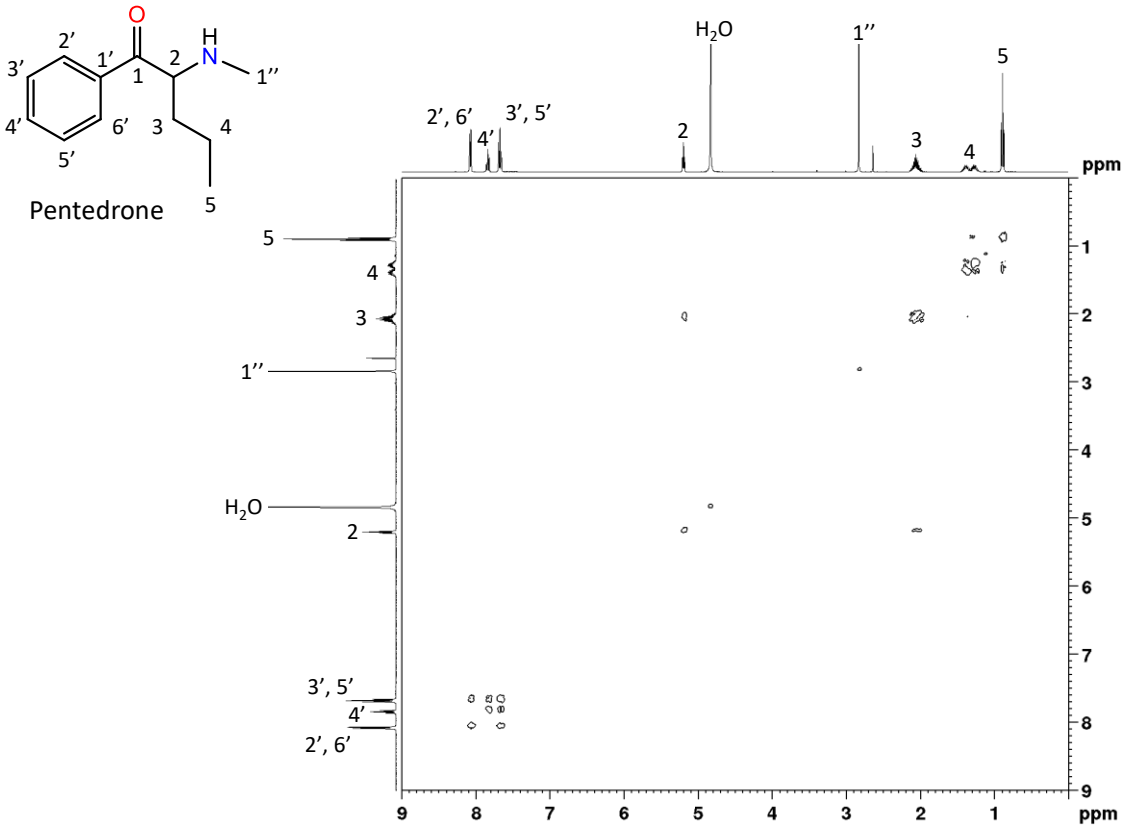

Figure S11. ^{1}H-^{1}H COSY NMR spectra of SCat found in seized materials.

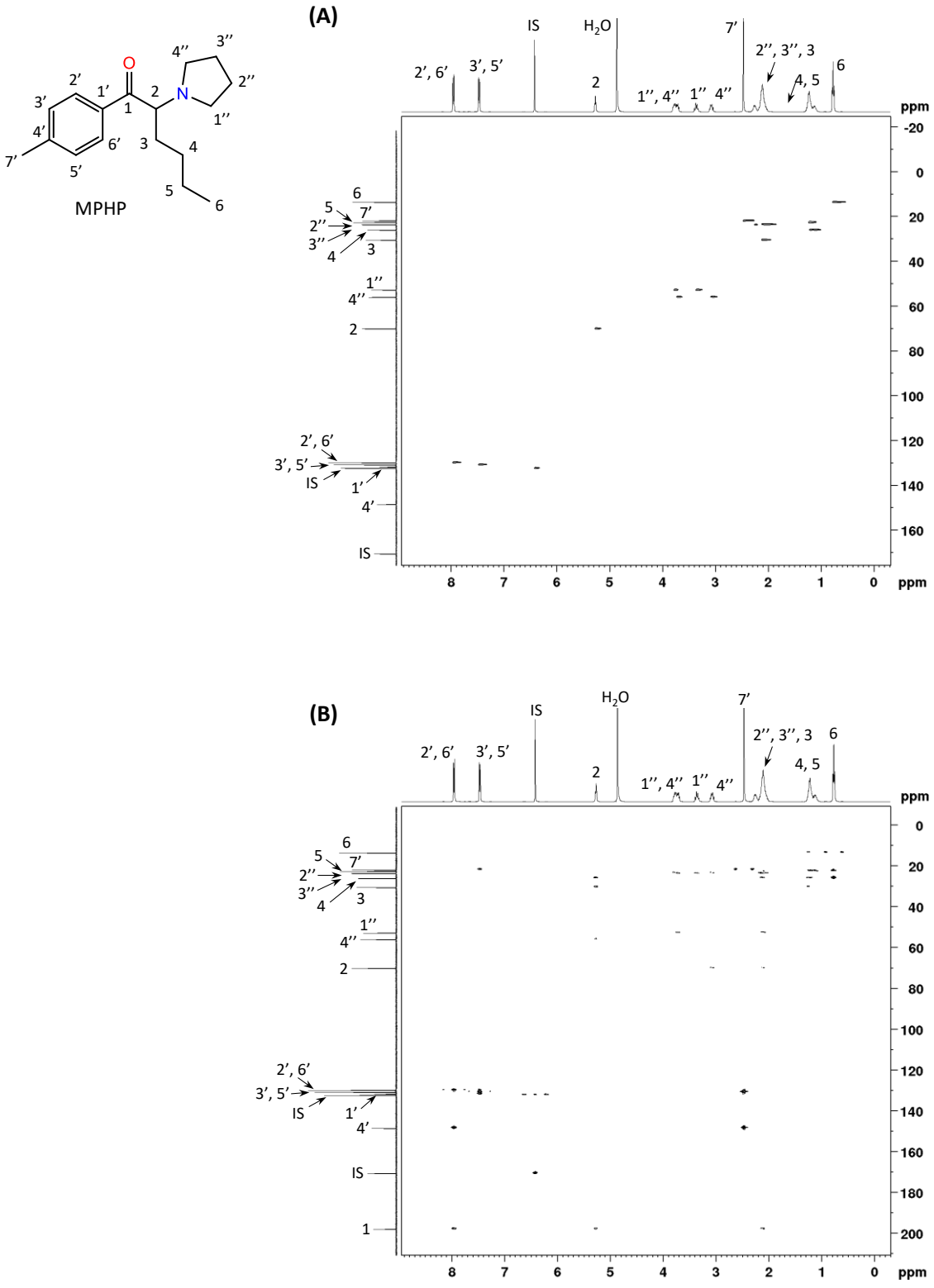

Figure S12. 2D NMR spectra of MPHP found in product 1: (A) ^{1}H-^{13}C HSQC and (B) ^{1}H-^{13}C HMBC NMR spectra.

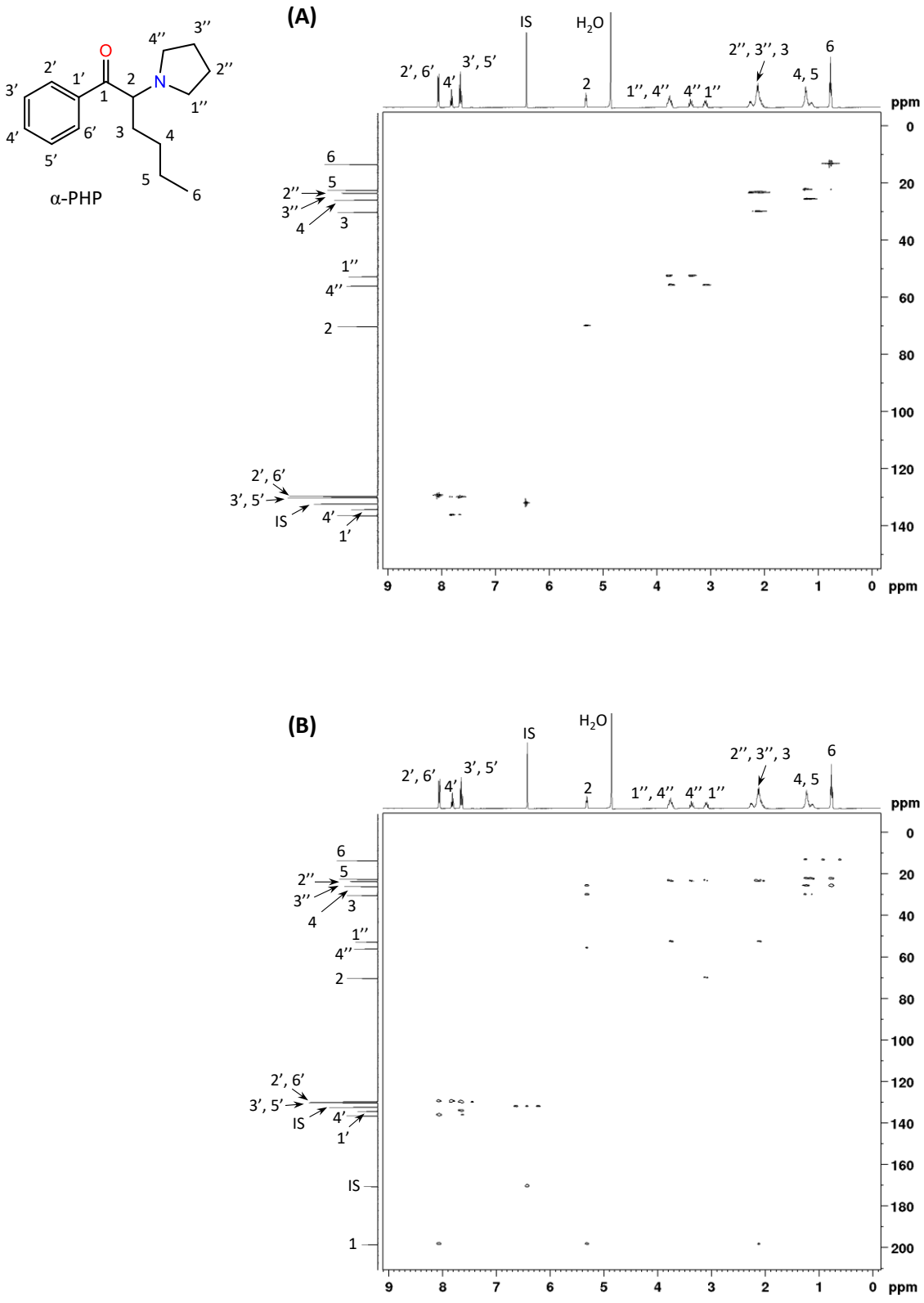

Figure S13. 2D NMR spectra of α-PHP found in product 2: (A) ^{1}H-^{13}C HSQC and (B) ^{1}H-^{13}C HMBC NMR spectra.

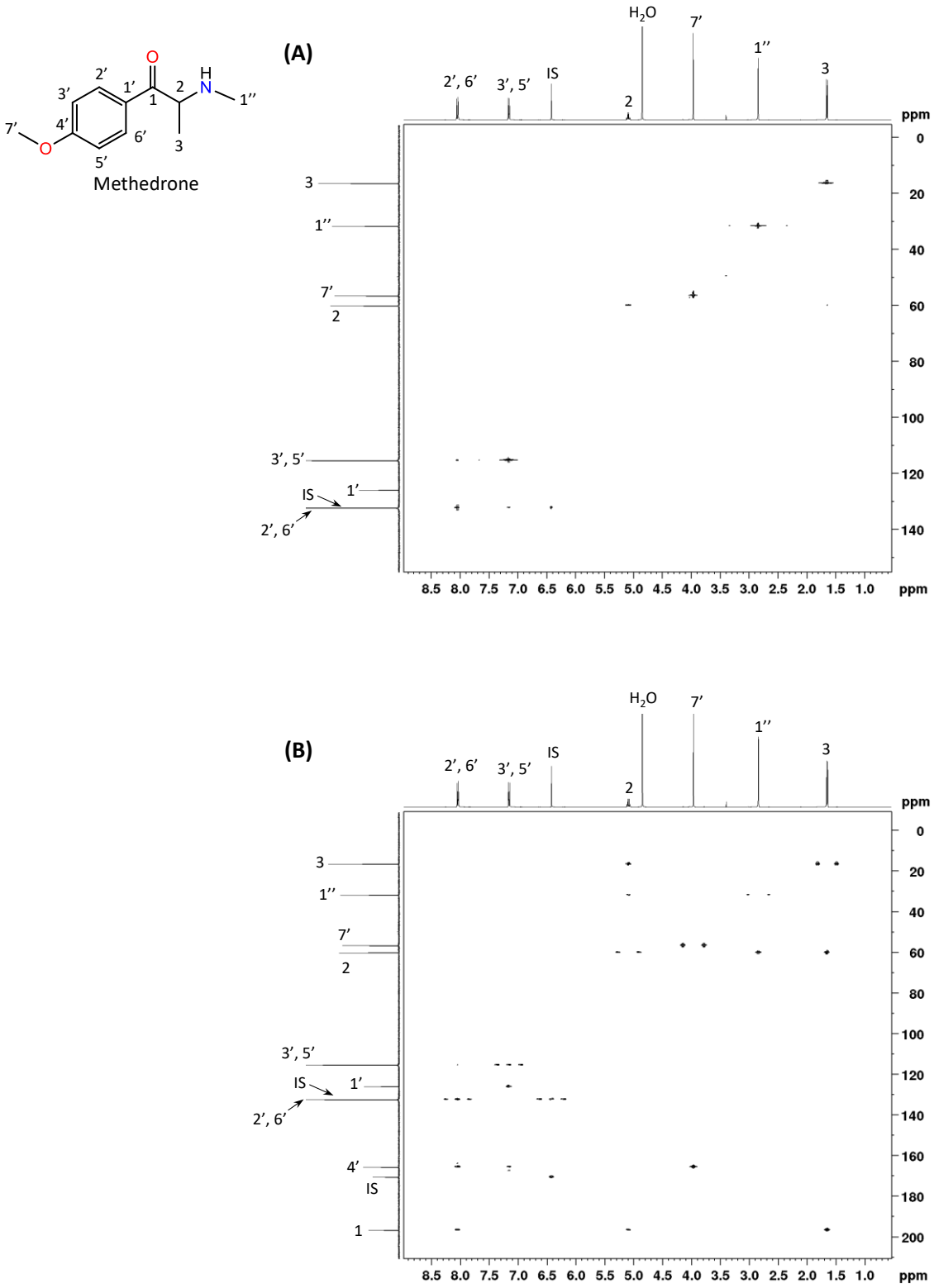

Figure S14. 2D NMR spectra of methedrone found in seized products: (A) ^{1}H-^{13}C HSQC and (B) ^{1}H-^{13}C HMBC NMR spectra.

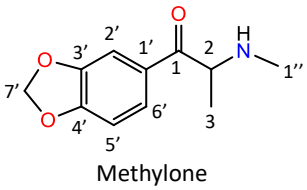

Methylone

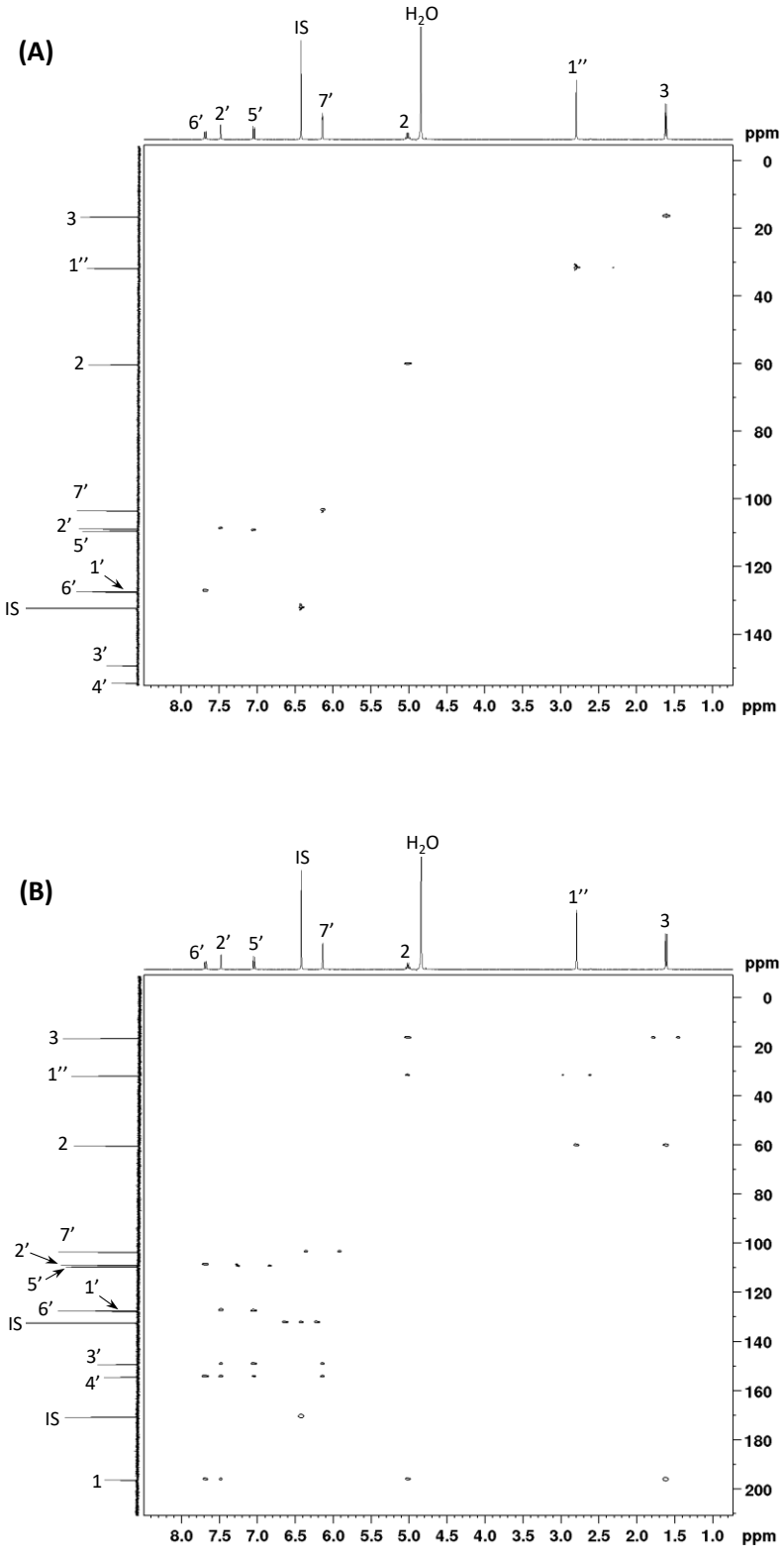

Figure S15. 2D NMR spectra of methylone found in seized products: (A) ^{1}H-^{13}C HSQC and (B) ^{1}H-^{13}C HMBC NMR spectra.

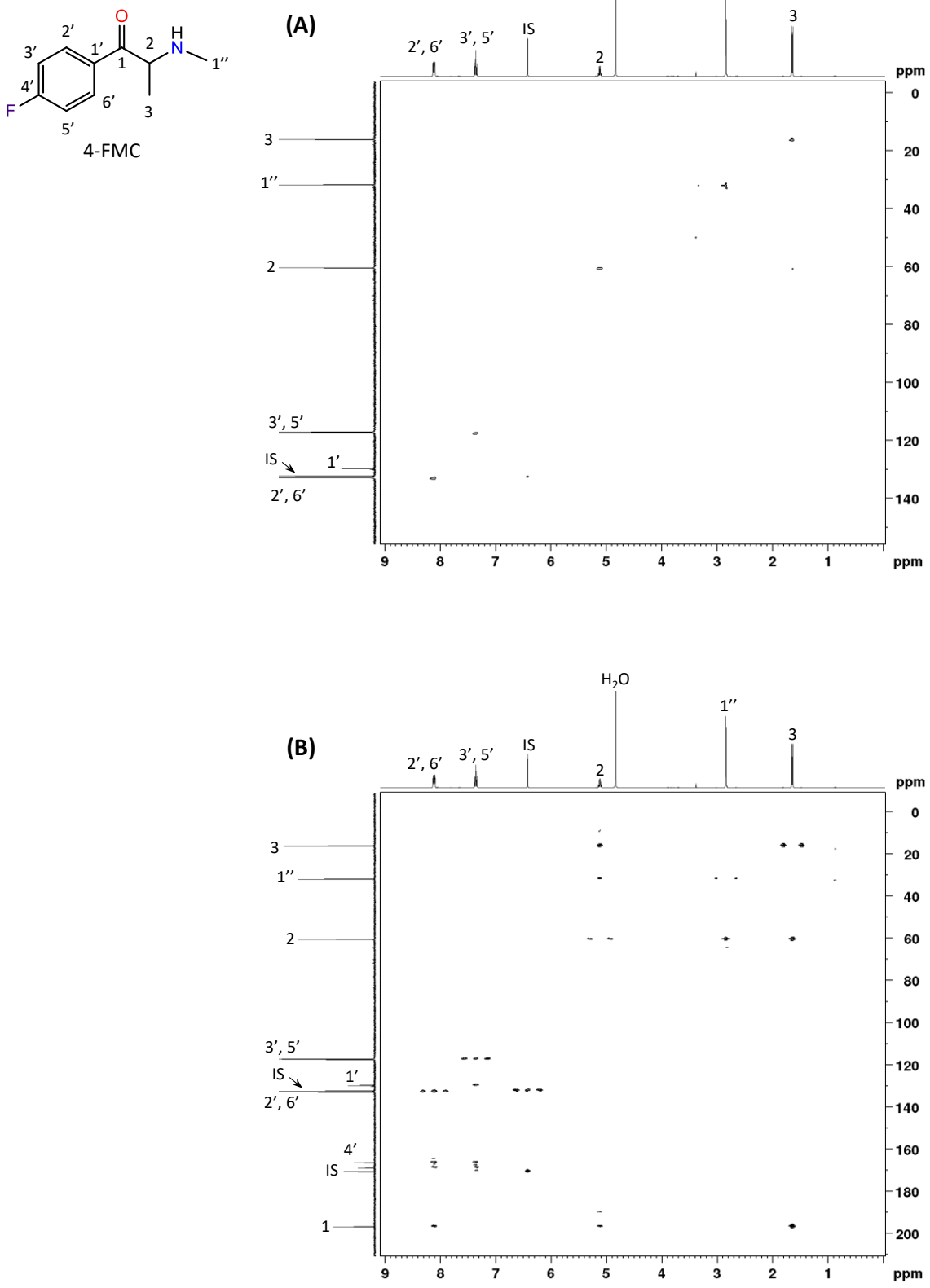

Figure S16. 2D NMR spectra of 4-FMC found in product 13: (A) ^{1}H-^{13}C HSQC and (B) ^{1}H-^{13}C HMBC NMR spectra.

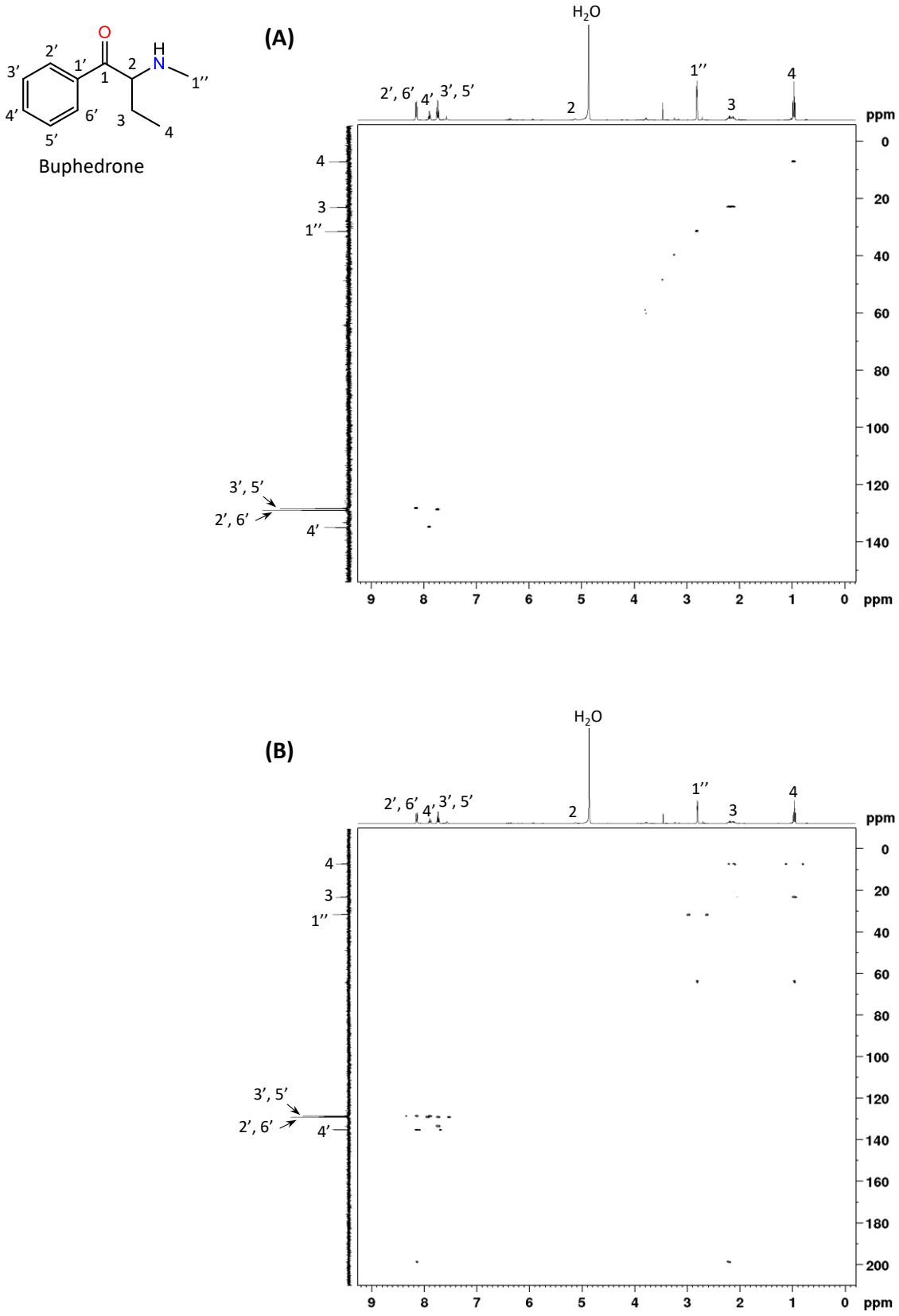

Figure S17. 2D NMR spectra of buphedrone found in seized products: (A) ^{1}H-^{13}C HSQC and (B) ^{1}H-^{13}C HMBC NMR spectra.

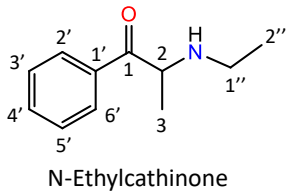

N-Ethylcathinone

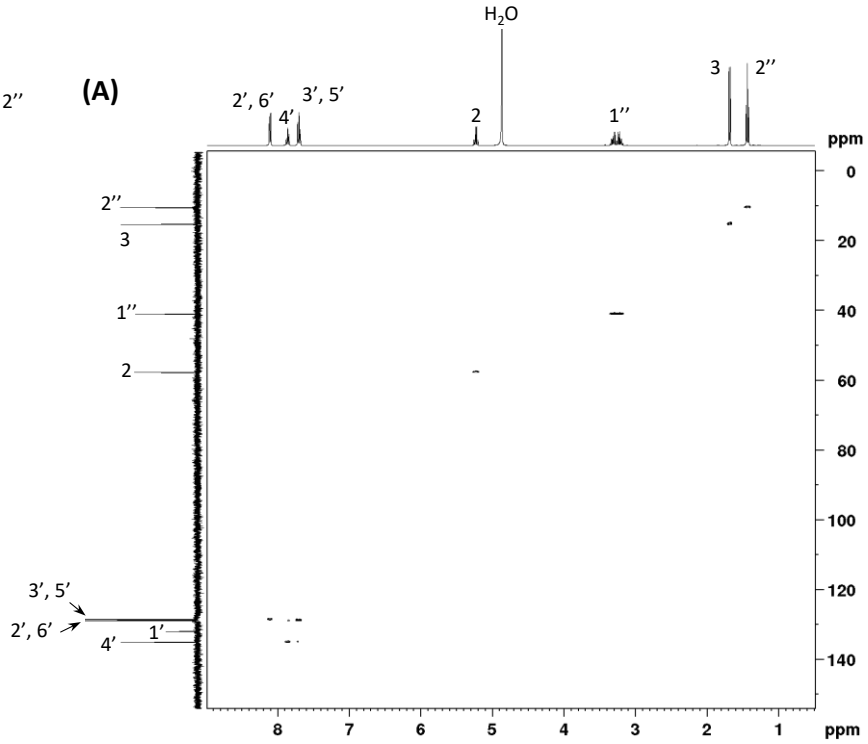

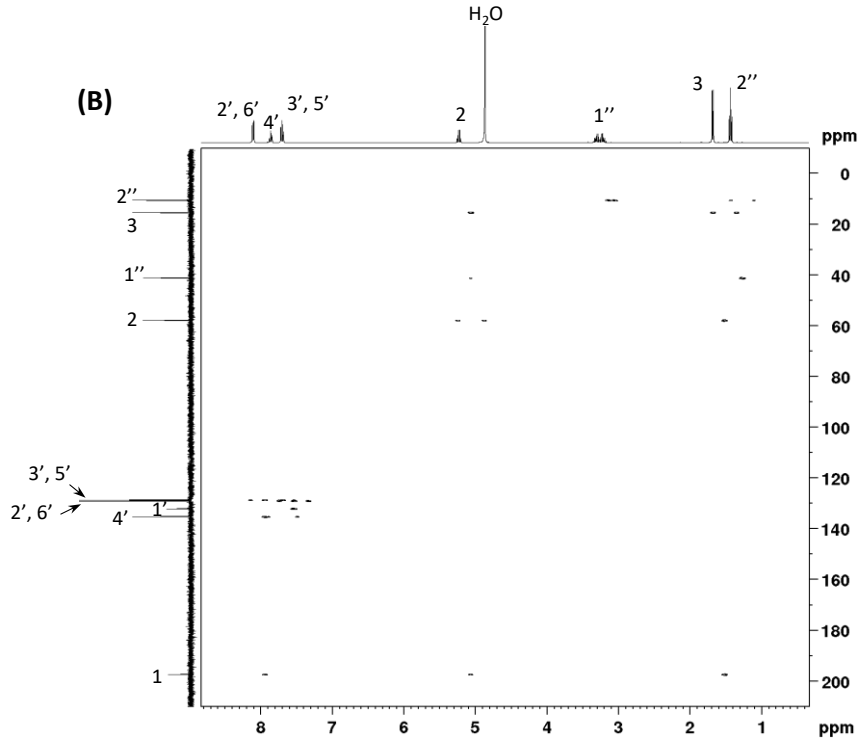

Figure S18. 2D NMR spectra of *N*-ethylcathinone found in seized products: (A) ^{1}H-^{13}C HSQC and (B) ^{1}H-^{13}C HMBC NMR spectra.

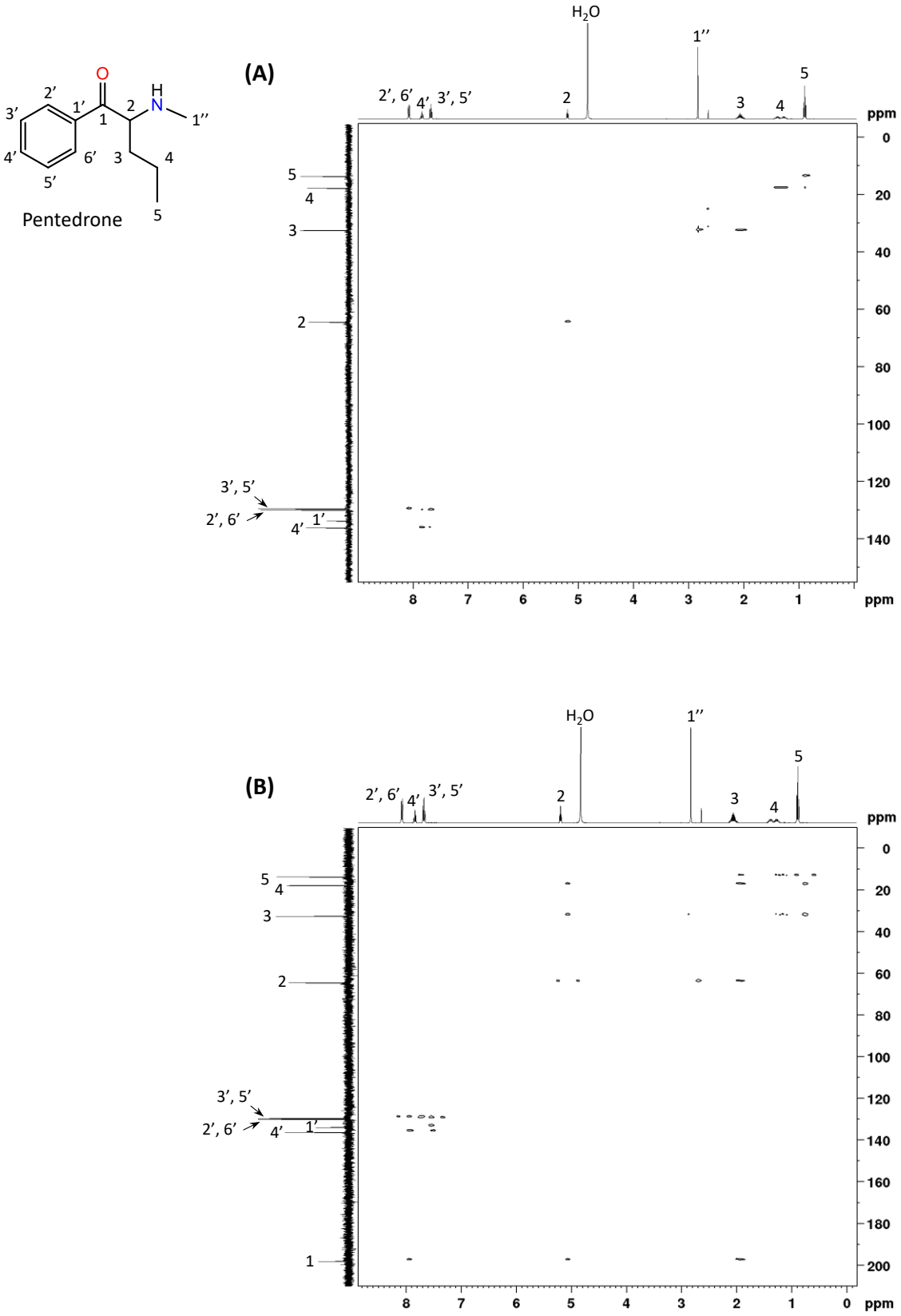

Figure S19. 2D NMR spectra of pentedrone found in seized products: (A) ^{1}H-^{13}C HSQC and (B) ^{1}H-^{13}C HMBC NMR spectra.

5. FTIR analysis of microcrystalline cellulose

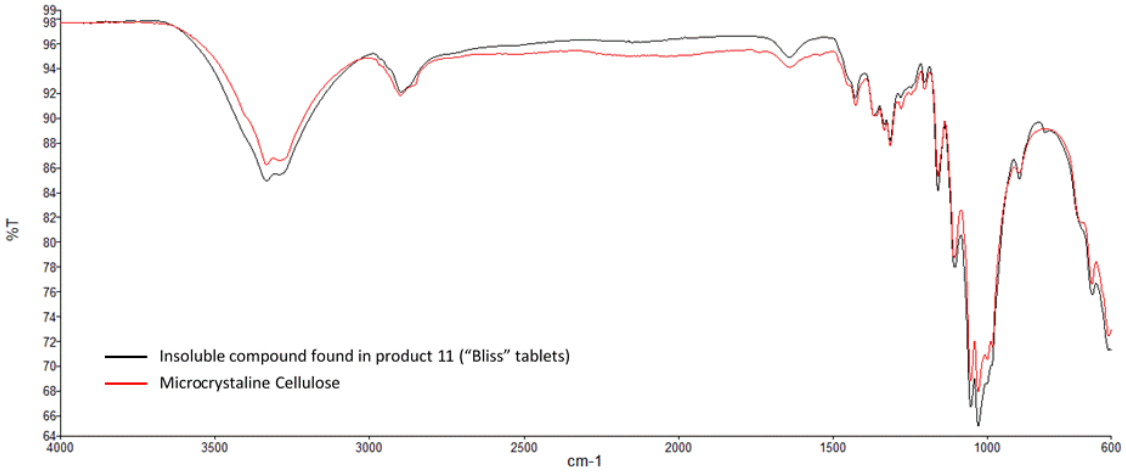

Figure S20. Comparison of the FTIR spectra of the insoluble substance found in product 11 ("Bliss" tablets) with microcristalline cellulose.

From Figure S20, it was possible to notice the following characteristics: the absorbance peaks in the 3400–3300 cm^{-1} regions are attributed to the stretching vibrations of the OH group. The peaks around 2900–2800 cm^{-1} correspond to CH stretching. The band located at 1639 cm^{-1} corresponds to vibration of water molecules adsorbed in microcellulose. The peaks observed in the range of 1420–1430 cm^{-1} were attributed to the symmetric CH_2 bending vibrations, while the absorbance bands at around 1030 cm^{-1} and 896 cm^{-1} were associated with the C-O stretching vibration and the C-H rocking vibration, respectively.

Determination of Synthetic Cathinones in Urine Samples by µSPEed®/ UHPLC-PDA methodology

Optimization of µSPEed® procedure

1. Nature of sorbent material and sample pH

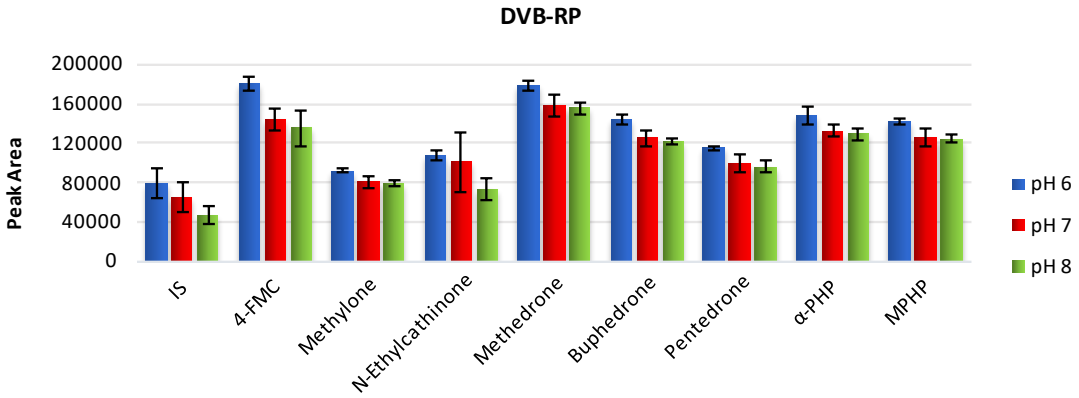

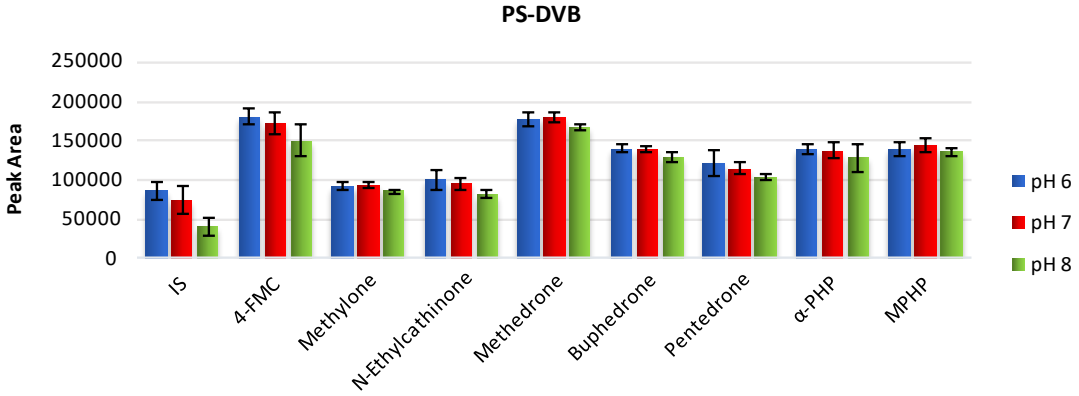

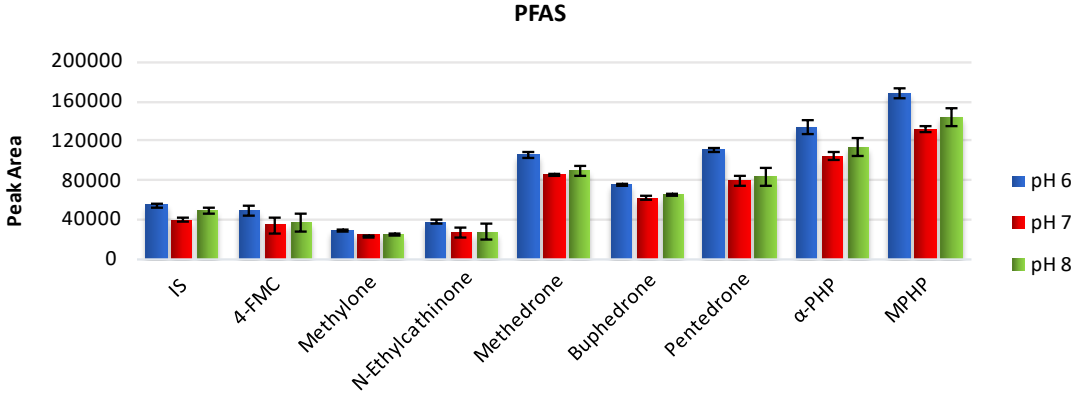

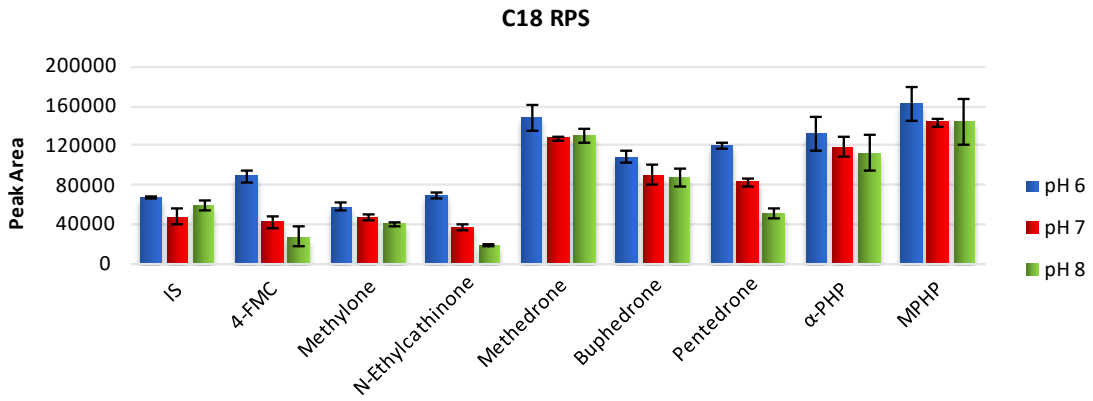
C18 RPS
Peak Area
200000
160000
120000
80000
40000
0
IS
4-FMC
Methylone
N-Ethylcathinone
Methedrone
Buphedrone
Pentedrone
α-PHP
MPHP
pH 6
pH 7
pH 8

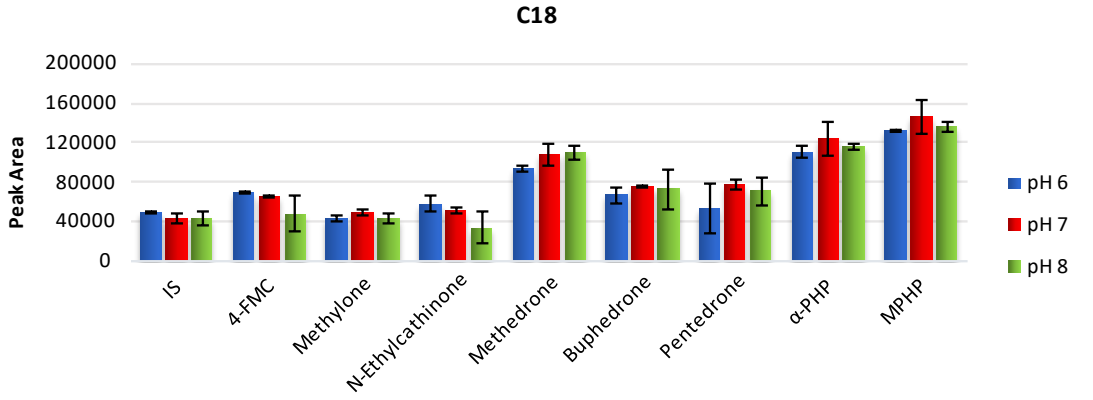
C18
Peak Area
200000
160000
120000
80000
40000
0
IS
4-FMC
Methylone
N-Ethylcathinone
Methedrone
Buphedrone
Pentedrone
α-PHP
MPHP
pH 6
pH 7
pH 8

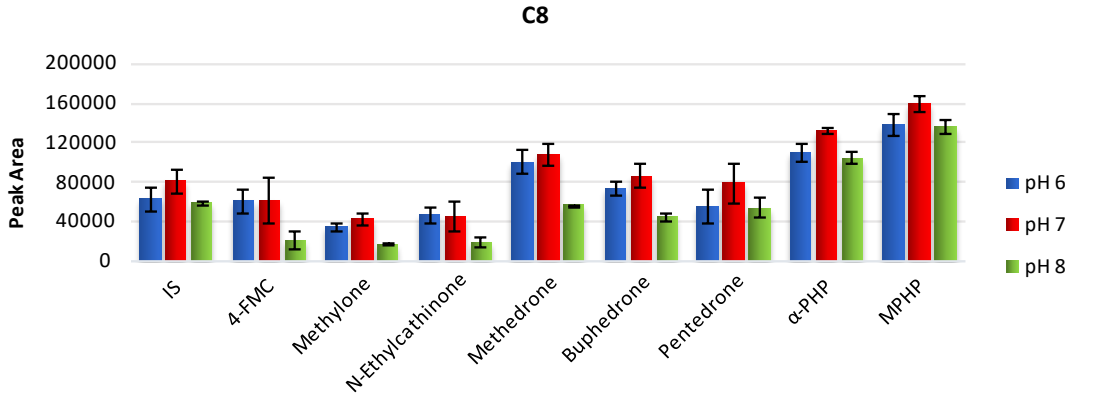
C8
Peak Area
200000
160000
120000
80000
40000
0
IS
4-FMC
Methylone
N-Ethylcathinone
Methedrone
Buphedrone
Pentedrone
α-PHP
MPHP
pH 6
pH 7
pH 8

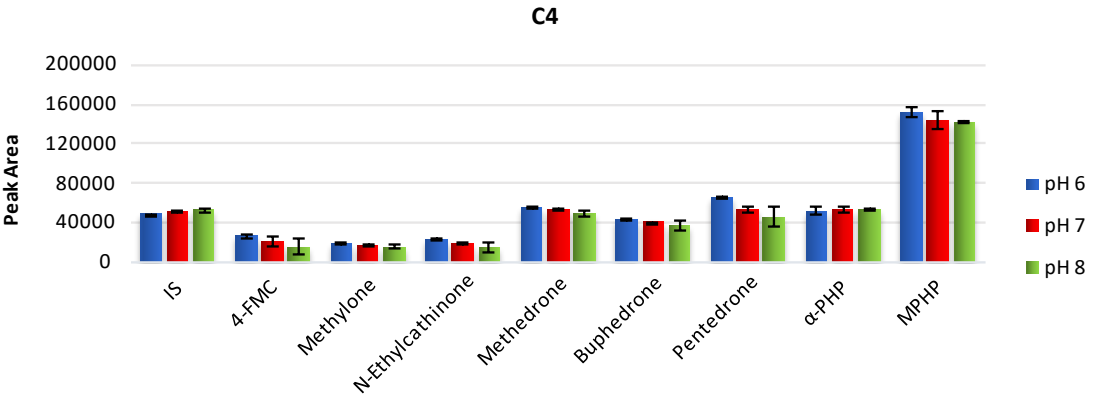
C4
Peak Area
200000
160000
120000
80000
40000
0
IS
4-FMC
Methylone
N-Ethylcathinone
Methedrone
Buphedrone
Pentedrone
α-PHP
MPHP
pH 6
pH 7
pH 8

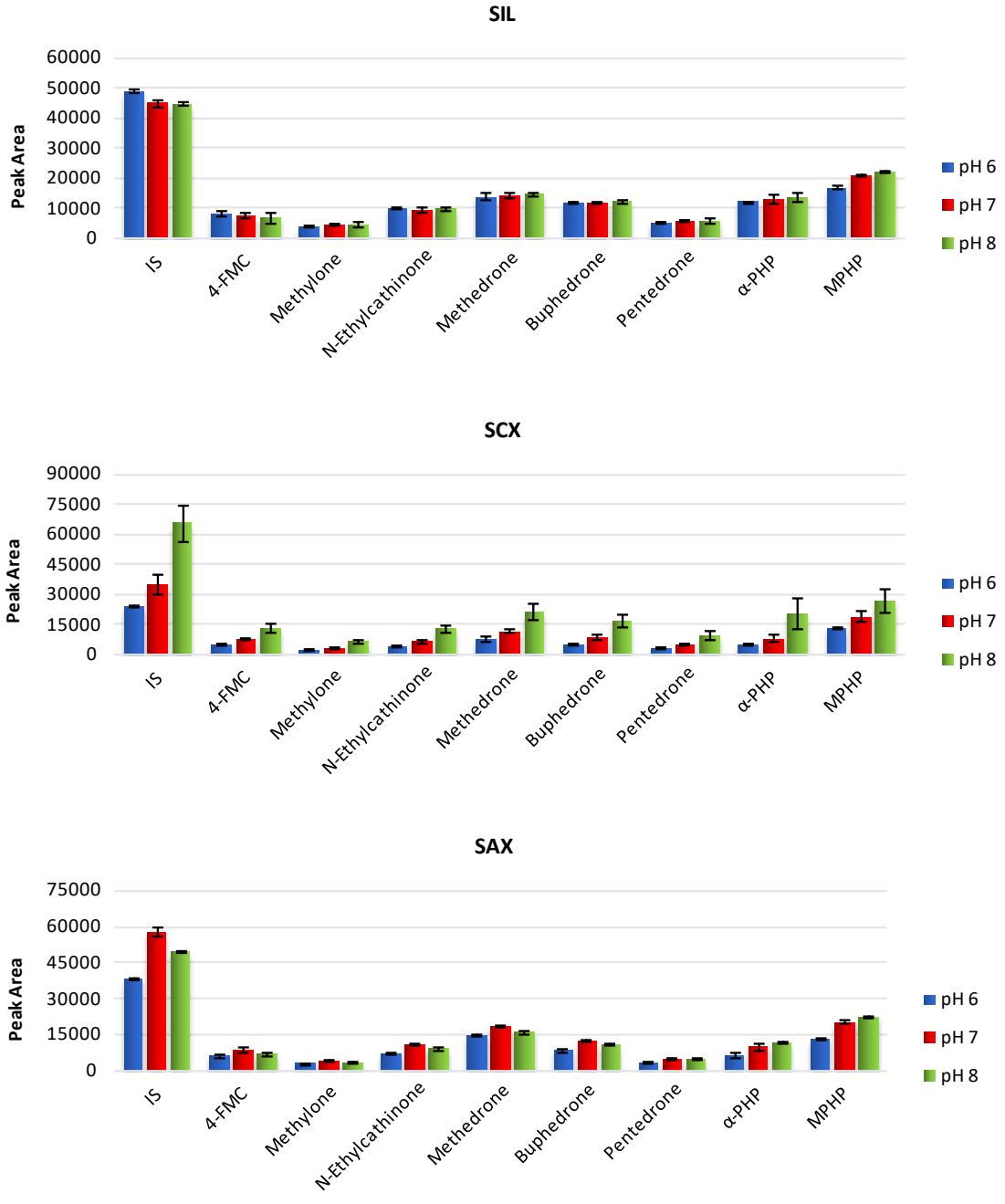

Figure S21. Comparison of the performance of each µSPEeD® sorbents and the influence of sample pH on the extraction of each SCat.

2. Number of extraction cycles and sample volume

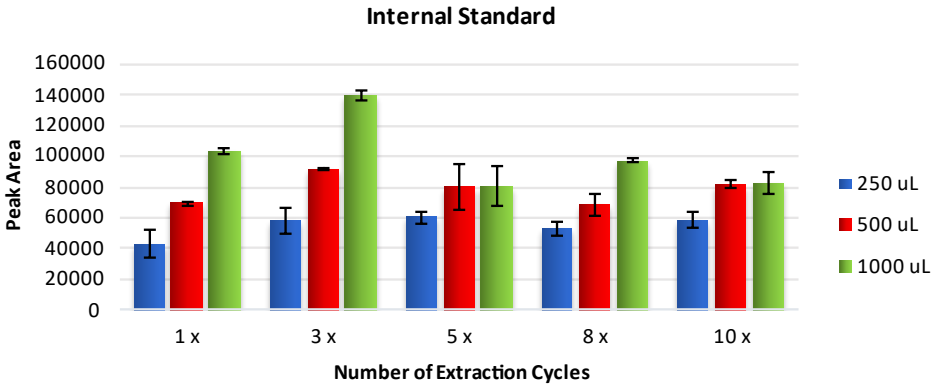

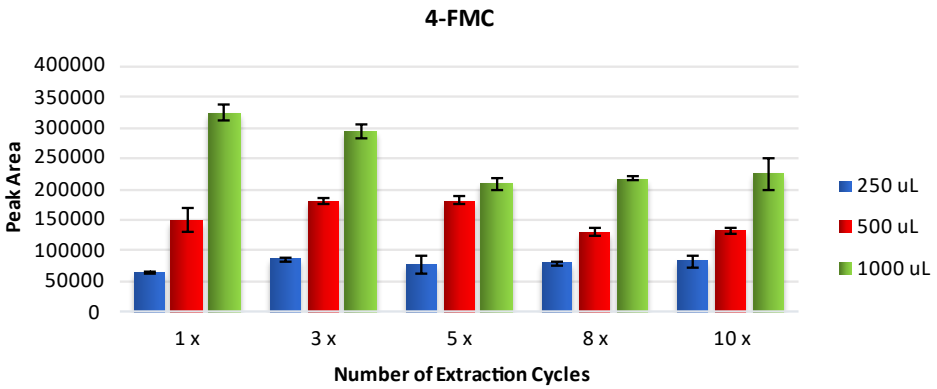

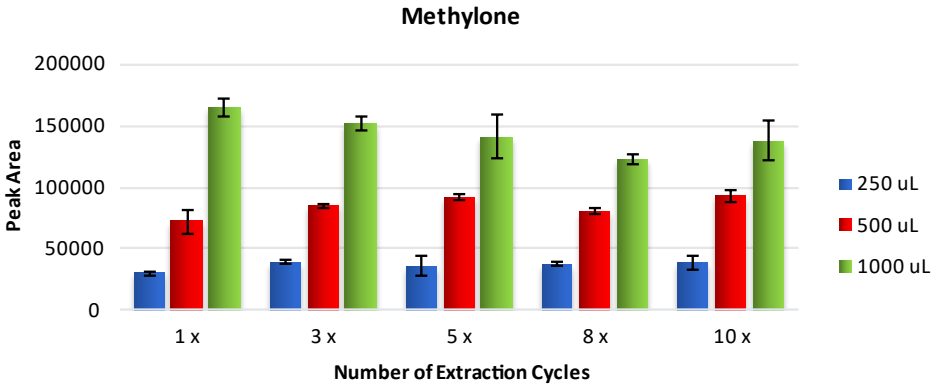

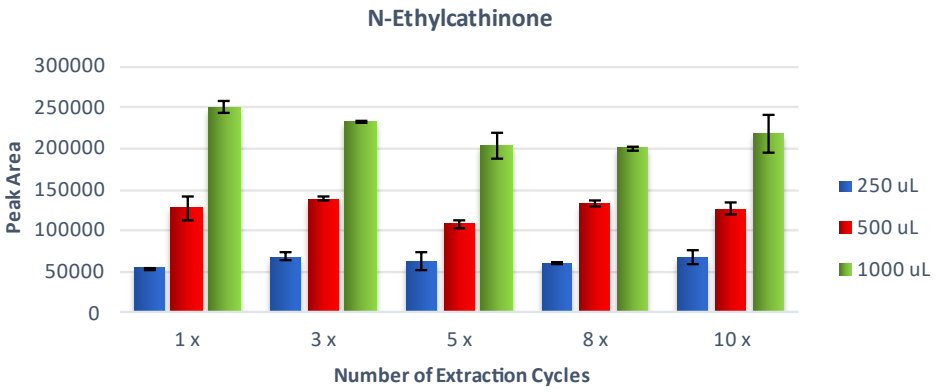
N-Ethylcathinone
300000
250000
200000
150000
100000
50000
0
Peak Area
1 x
3 x
5 x
8 x
10 x
Number of Extraction Cycles
250 uL
500 uL
1000 uL

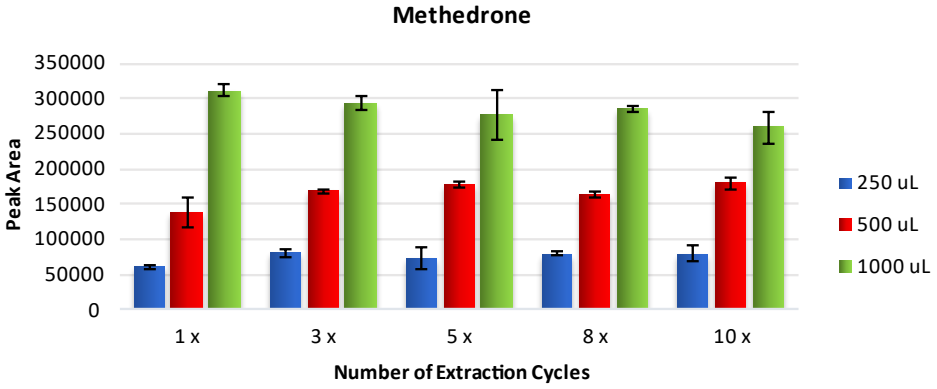
Methedrone
350000
300000
250000
200000
150000
100000
50000
0
Peak Area
1 x
3 x
5 x
8 x
10 x
Number of Extraction Cycles
250 uL
500 uL
1000 uL

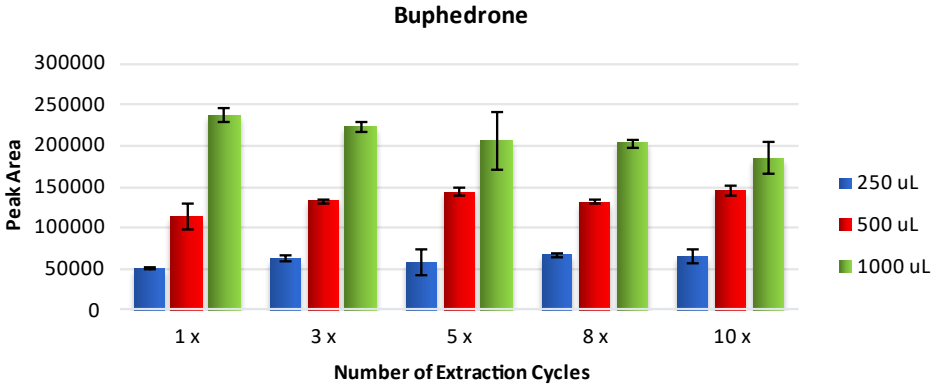
Buphedrone
300000
250000
200000
150000
100000
50000
0
Peak Area
1 x
3 x
5 x
8 x
10 x
Number of Extraction Cycles
250 uL
500 uL
1000 uL

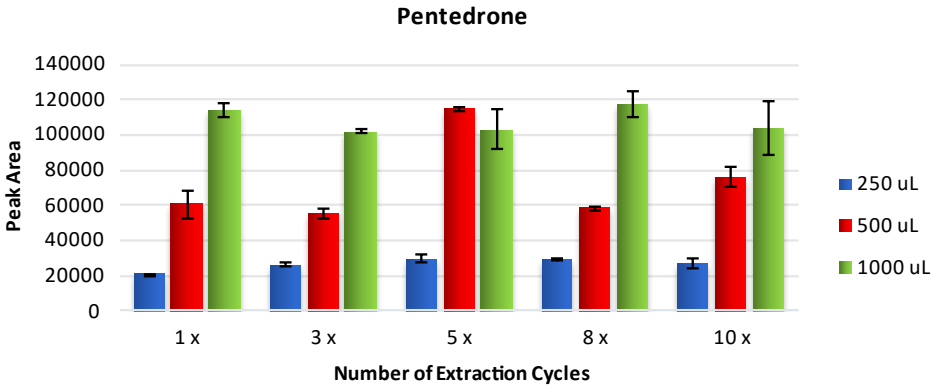
Pentedrone
140000
120000
100000
80000
60000
40000
20000
0
Peak Area
1 x
3 x
5 x
8 x
10 x
Number of Extraction Cycles
250 uL
500 uL
1000 uL

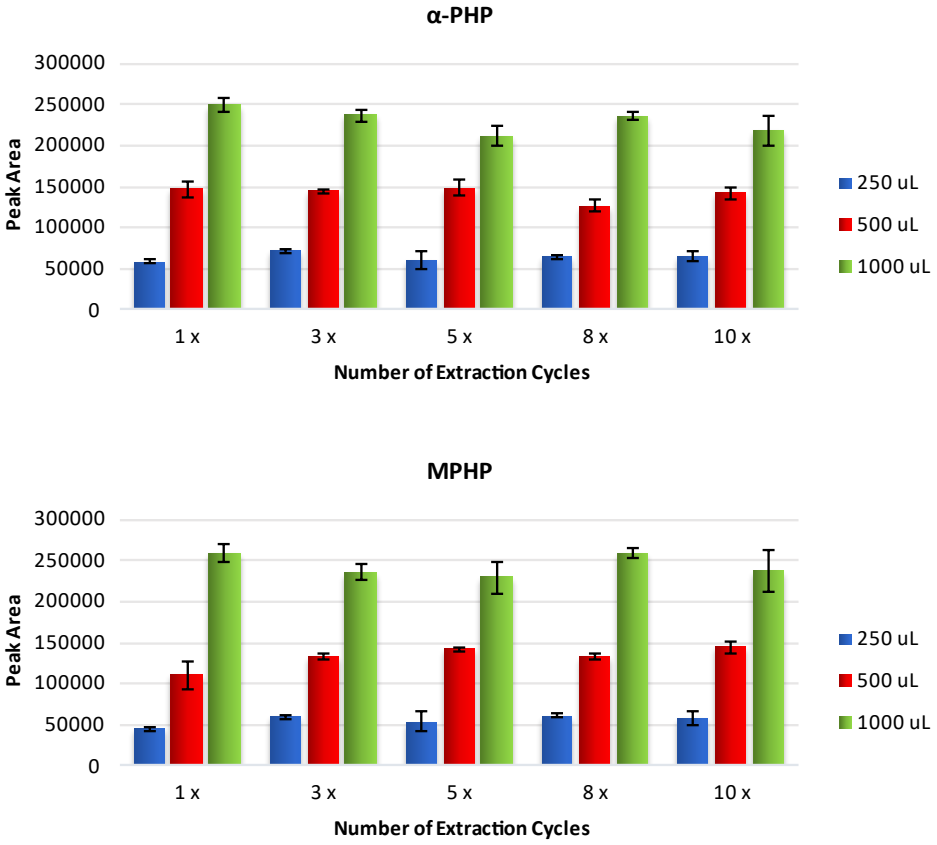

Figure S22. Influence of the number of extraction cycles and sample volume on µSPEeD® performance for each individual compound.

3. Washing conditions

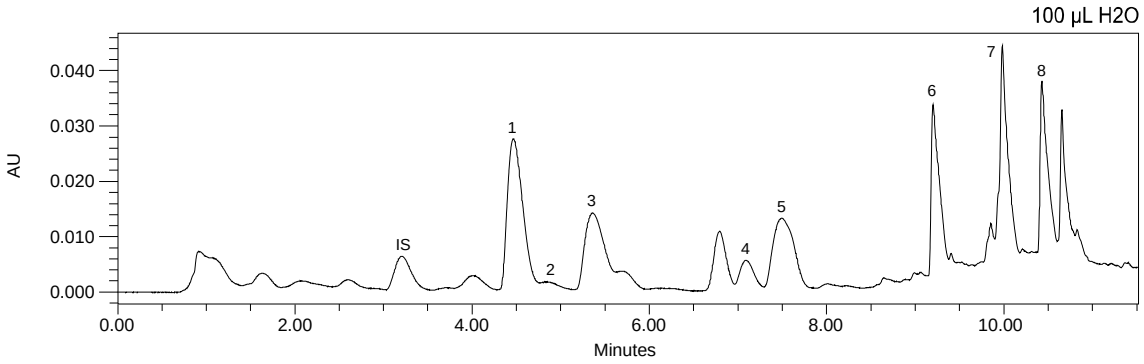

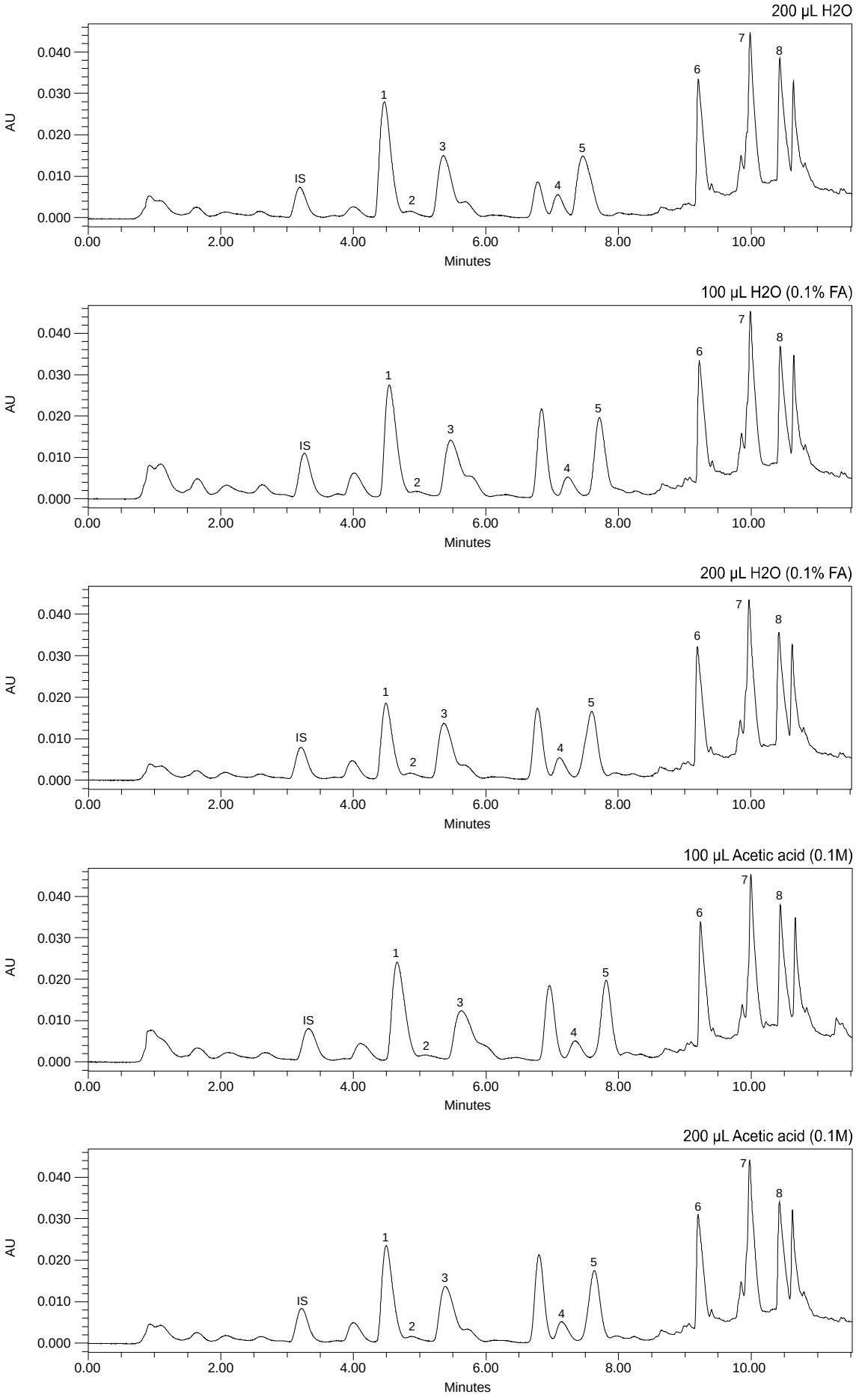
200 µL H2O
100 µL H2O (0.1% FA)
200 µL H2O (0.1% FA)
100 µL Acetic acid (0.1M)
200 µL Acetic acid (0.1M)
AU
Minutes
IS
1
2
3
4
5
6
7
8
0.000
0.010
0.020
0.030
0.040
0.00
2.00
4.00
6.00
8.00
10.00

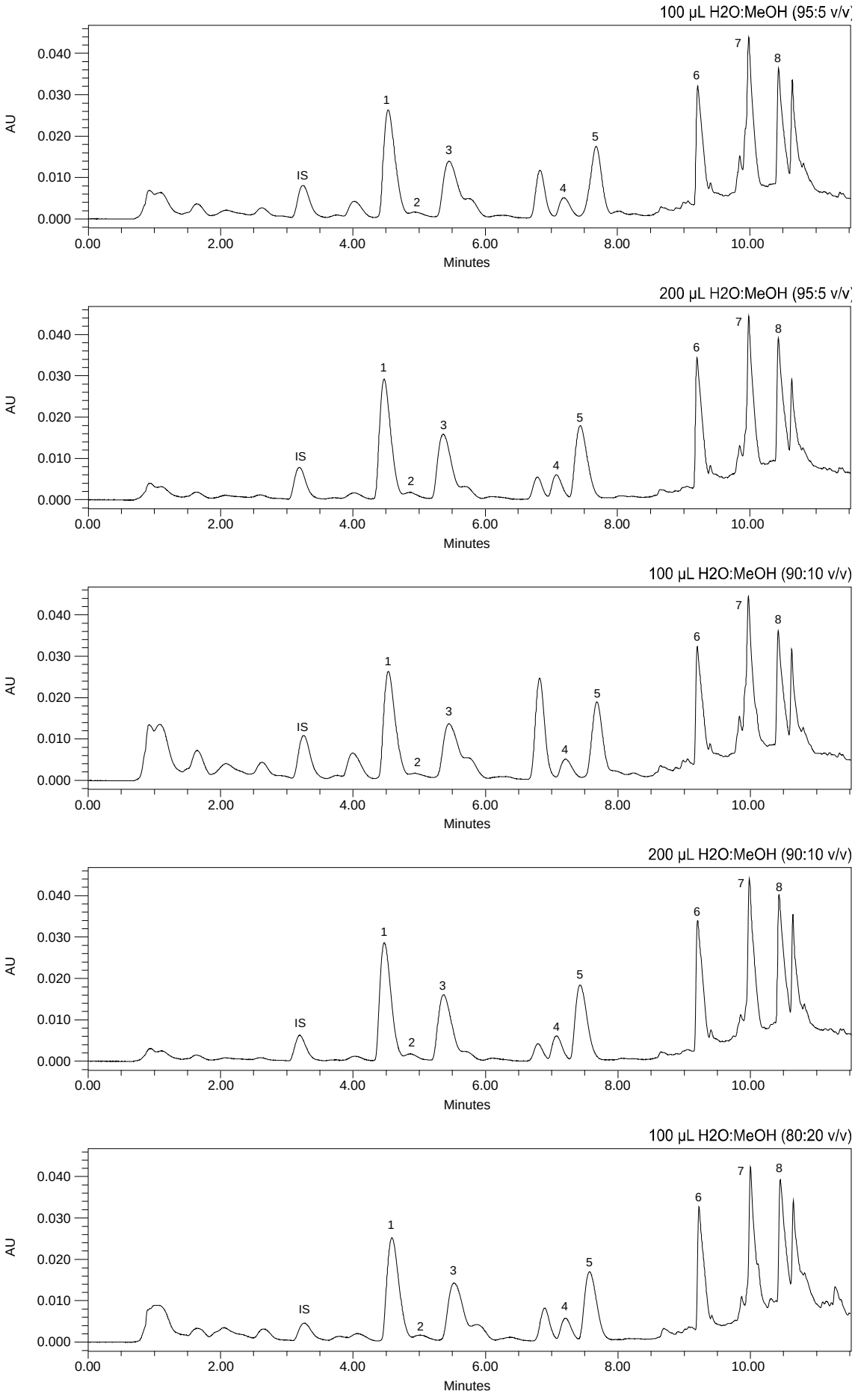
100 µL H2O:MeOH (95:5 v/v)
200 µL H2O:MeOH (95:5 v/v)
100 µL H2O:MeOH (90:10 v/v)
200 µL H2O:MeOH (90:10 v/v)
100 µL H2O:MeOH (80:20 v/v)
AU
Minutes
IS
1
2
3
4
5
6
7
8
0.000
0.010
0.020
0.030
0.040
0.00
2.00
4.00
6.00
8.00
10.00

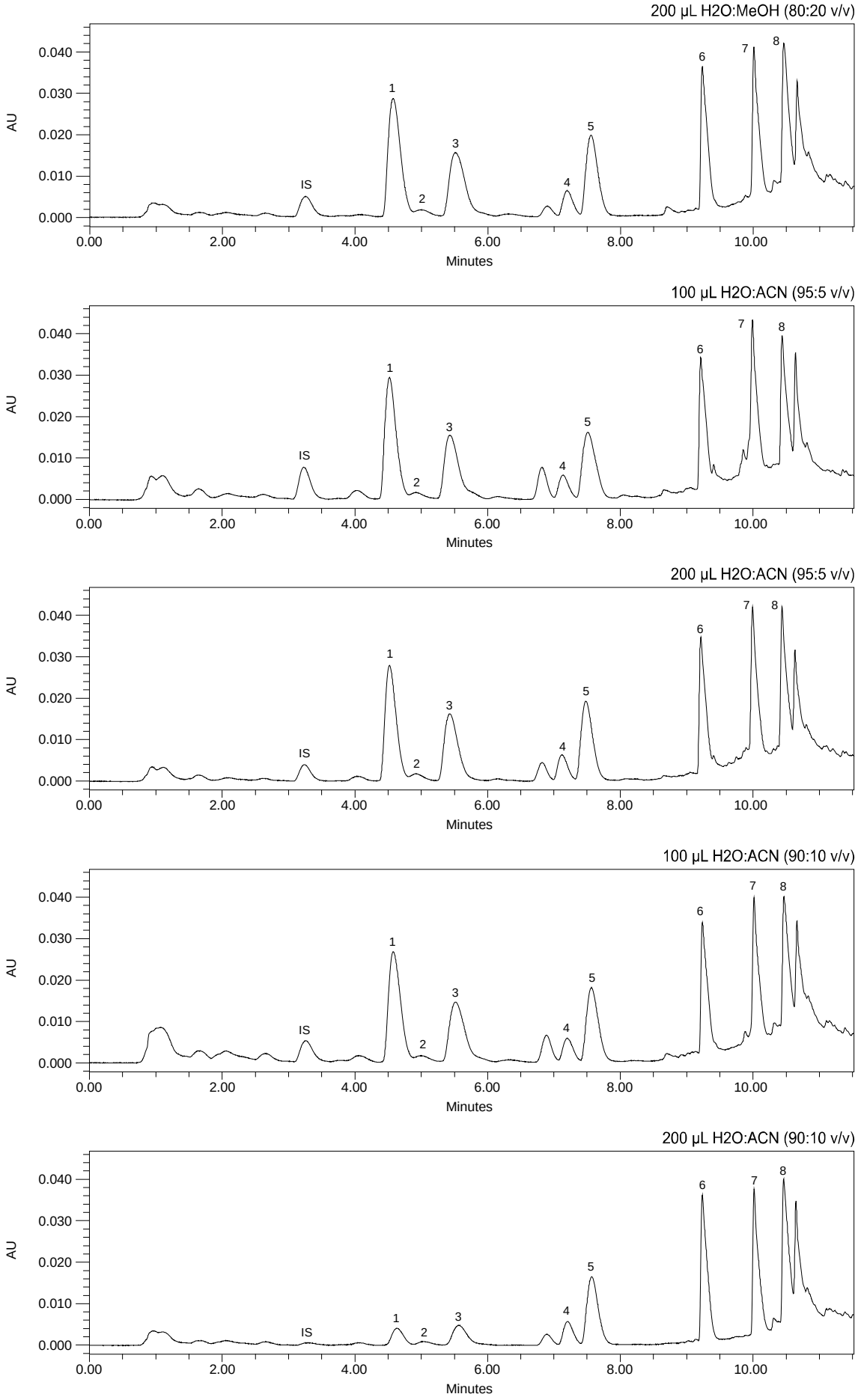
200 µL H2O:MeOH (80:20 v/v)
100 µL H2O:ACN (95:5 v/v)
200 µL H2O:ACN (95:5 v/v)
100 µL H2O:ACN (90:10 v/v)
200 µL H2O:ACN (90:10 v/v)
AU
Minutes
IS
1
2
3
4
5
6
7
8
0.000
0.010
0.020
0.030
0.040
0.00
2.00
4.00
6.00
8.00
10.00

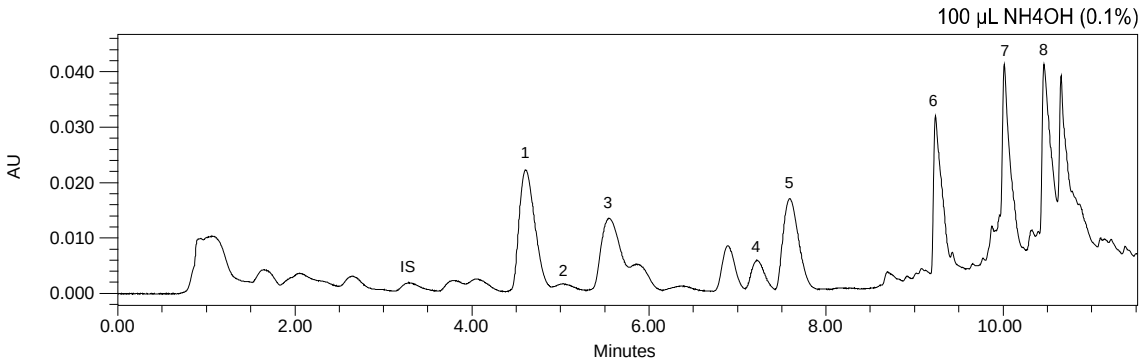
100 µL NH4OH (0.1%)
AU
0.040
0.030
0.020
0.010
0.000
IS
1
2
3
4
5
6
7
8
0.00
2.00
4.00
6.00
8.00
10.00
Minutes

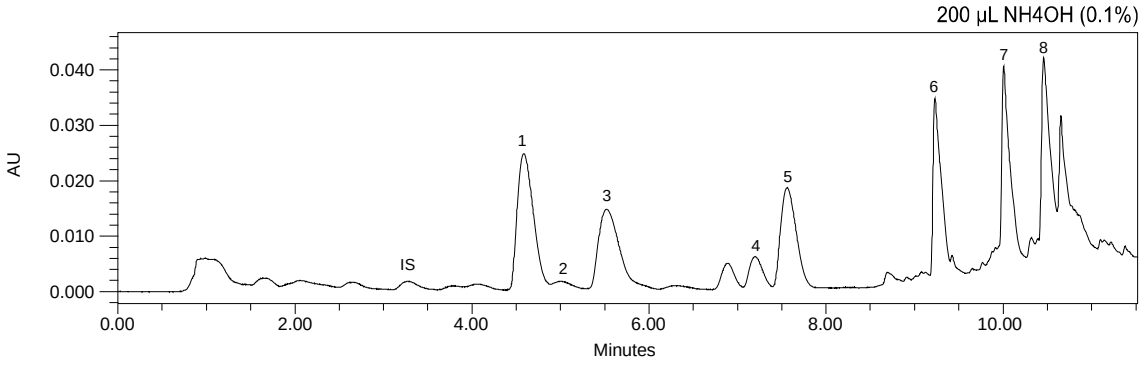
200 µL NH4OH (0.1%)
AU
0.040
0.030
0.020
0.010
0.000
IS
1
2
3
4
5
6
7
8
0.00
2.00
4.00
6.00
8.00
10.00
Minutes

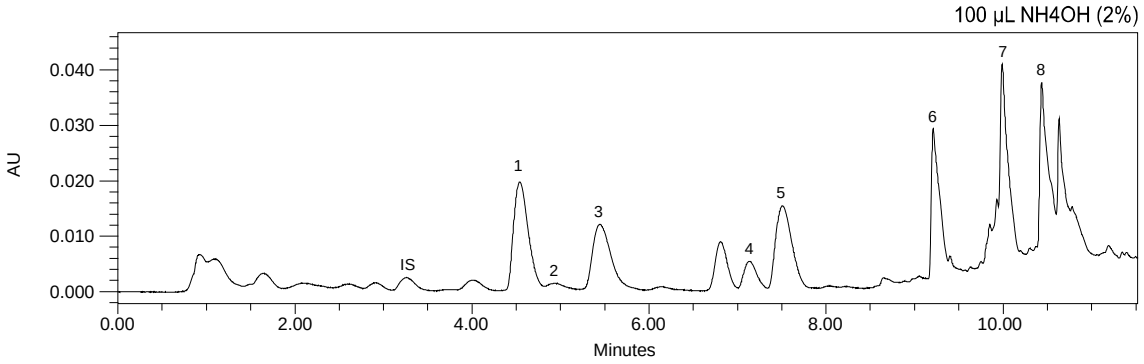
100 µL NH4OH (2%)
AU
0.040
0.030
0.020
0.010
0.000
IS
1
2
3
4
5
6
7
8
0.00
2.00
4.00
6.00
8.00
10.00
Minutes

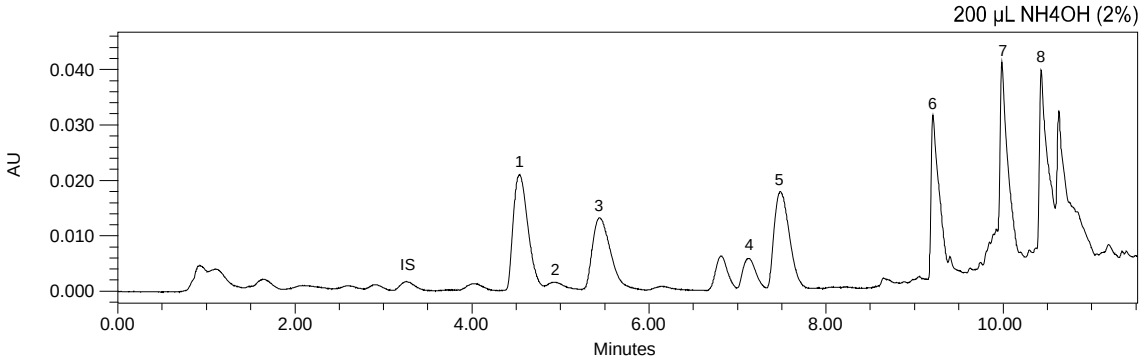
200 µL NH4OH (2%)
AU
0.040
0.030
0.020
0.010
0.000
IS
1
2
3
4
5
6
7
8
0.00
2.00
4.00
6.00
8.00
10.00
Minutes

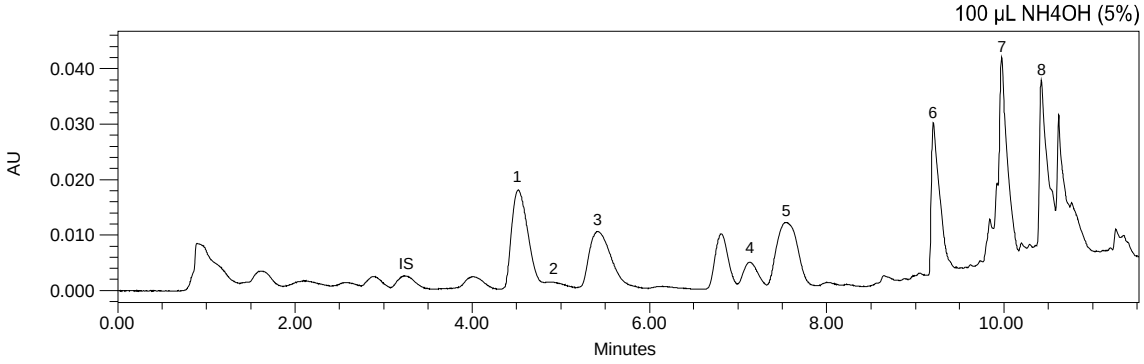
100 µL NH4OH (5%)
AU
0.040
0.030
0.020
0.010
0.000
IS
1
2
3
4
5
6
7
8
0.00
2.00
4.00
6.00
8.00
10.00
Minutes

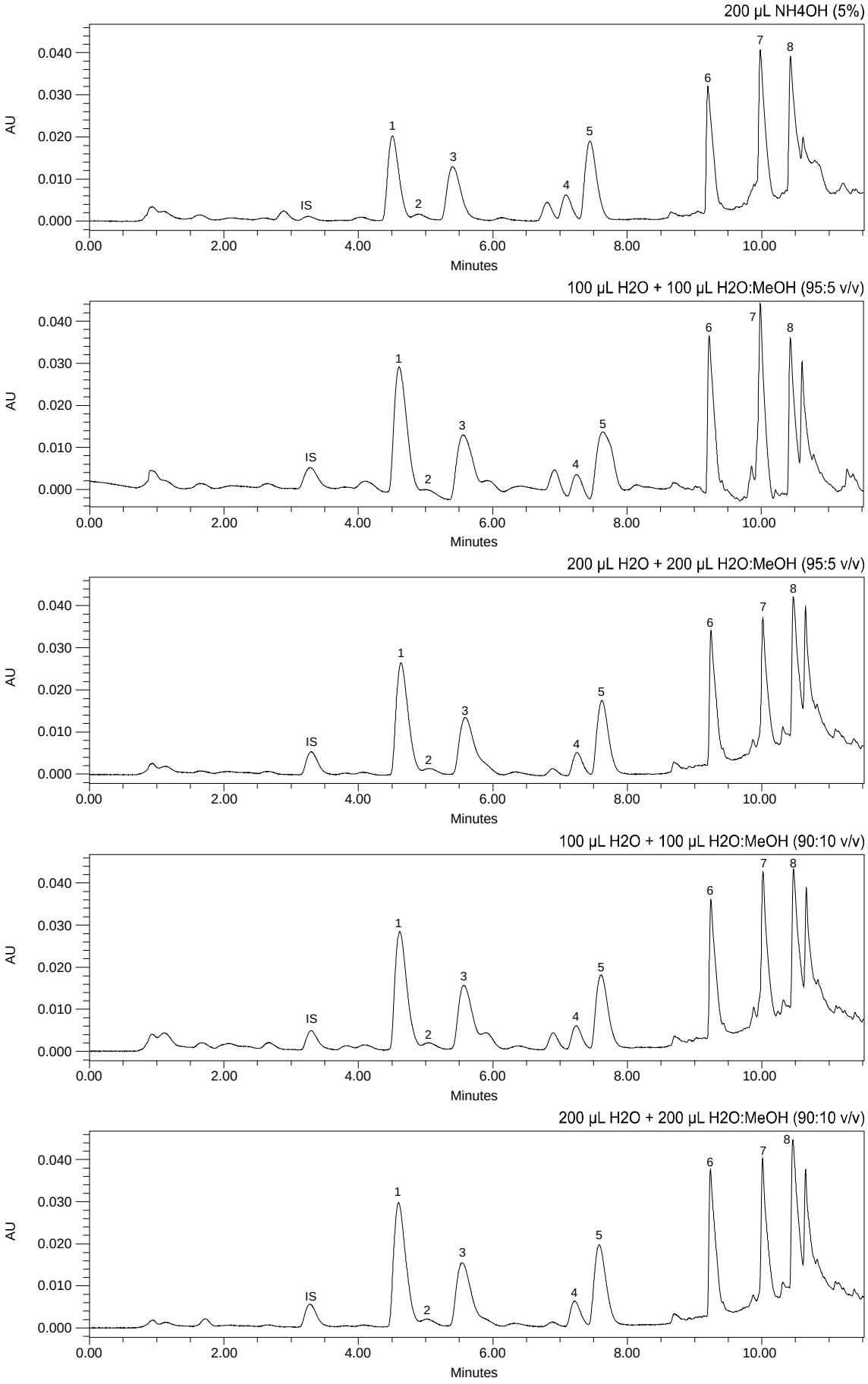
200 µL NH4OH (5%)
100 µL H2O + 100 µL H2O:MeOH (95:5 v/v)
200 µL H2O + 200 µL H2O:MeOH (95:5 v/v)
100 µL H2O + 100 µL H2O:MeOH (90:10 v/v)
200 µL H2O + 200 µL H2O:MeOH (90:10 v/v)
AU
Minutes
IS
1
2
3
4
5
6
7
8
0.000
0.010
0.020
0.030
0.040
0.00
2.00
4.00
6.00
8.00
10.00

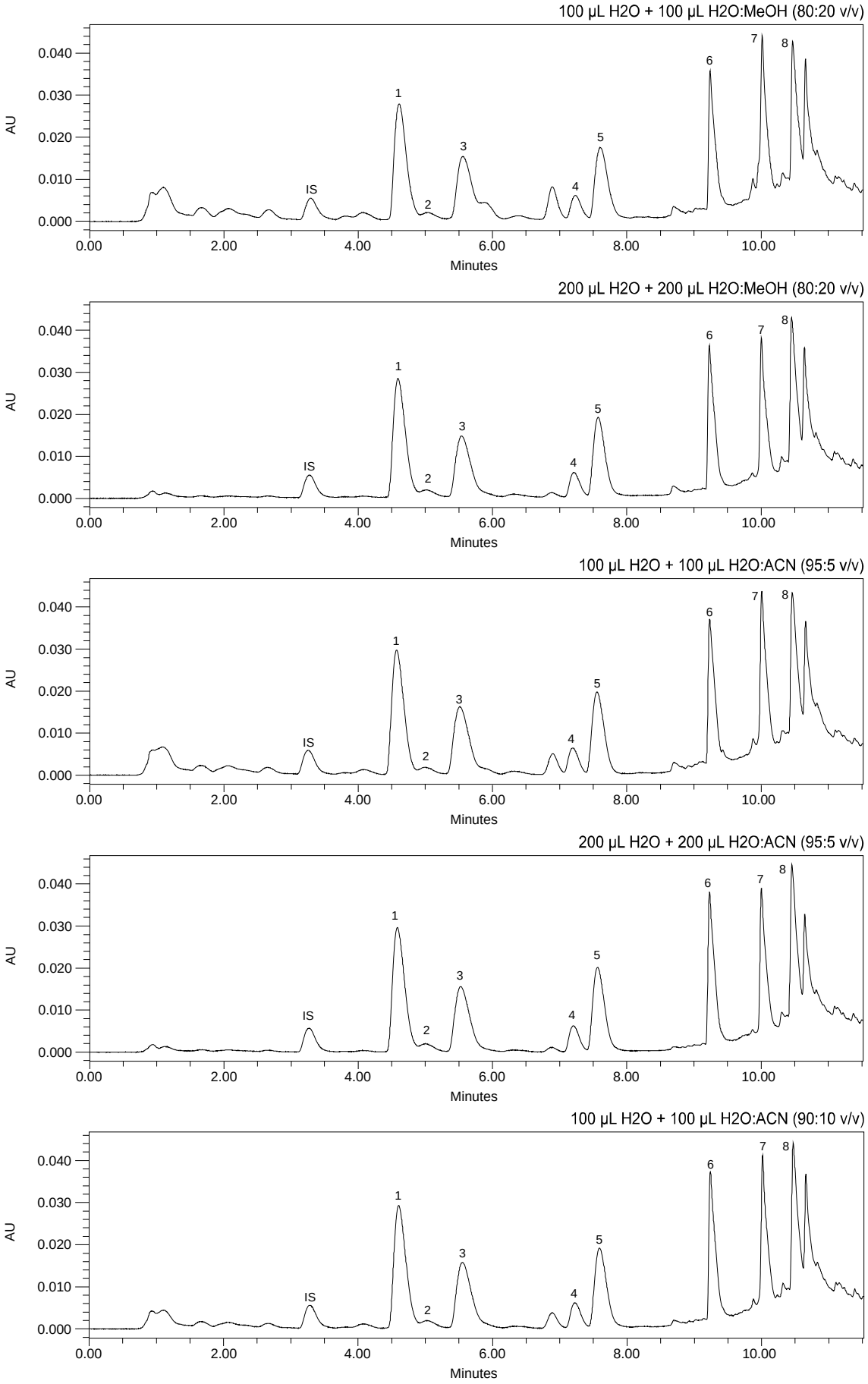
100 µL H2O + 100 µL H2O:MeOH (80:20 v/v)
200 µL H2O + 200 µL H2O:MeOH (80:20 v/v)
100 µL H2O + 100 µL H2O:ACN (95:5 v/v)
200 µL H2O + 200 µL H2O:ACN (95:5 v/v)
100 µL H2O + 100 µL H2O:ACN (90:10 v/v)
AU
Minutes
IS
1
2
3
4
5
6
7
8

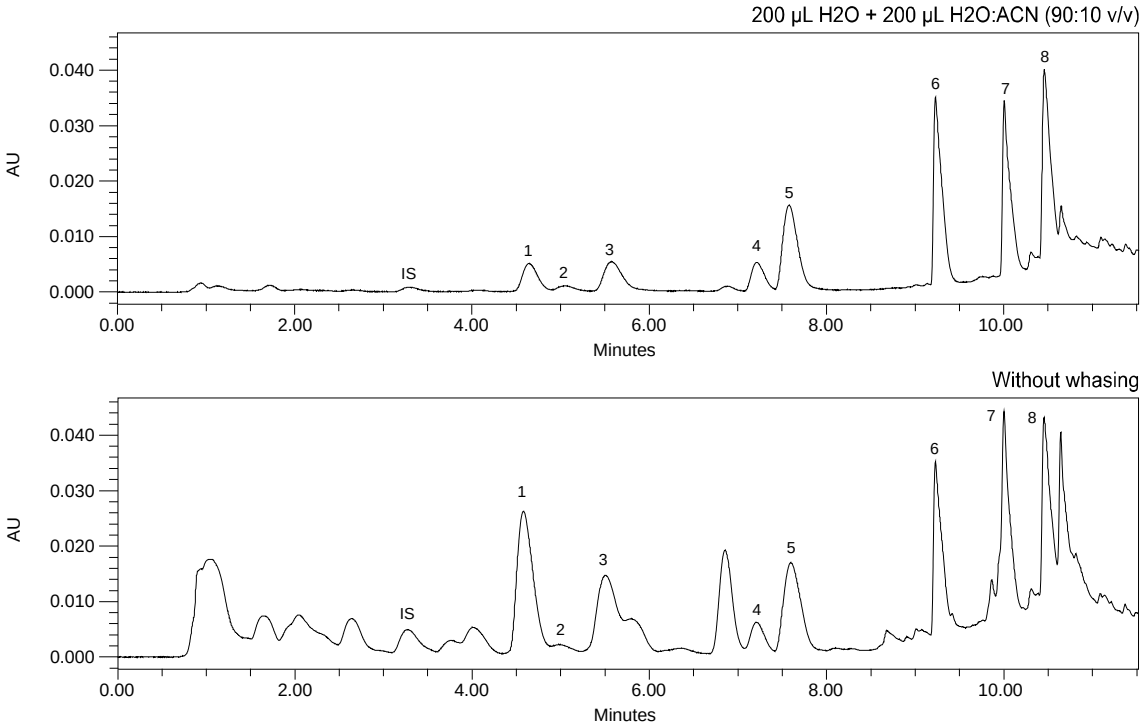

Figure S23. Chromatograms obtained during the study of the influence of the different washing conditions on µSPEeD®. Peak identification: (IS) internal standard, (1) 4-FMC, (2) methylone, (3) *N*-ethylcathinone, (4) methedrone, (5) buphedrone, (6) pentedrone, (7) α-PHP and (8) MPHP.

4. Influence of the Elution Conditions

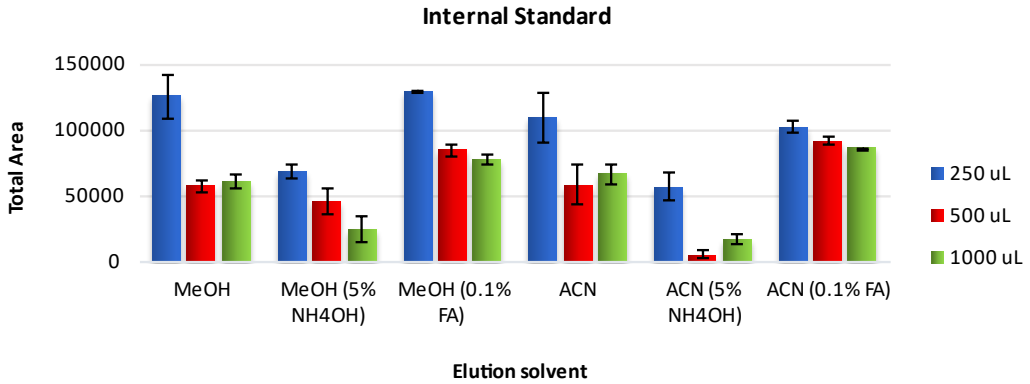

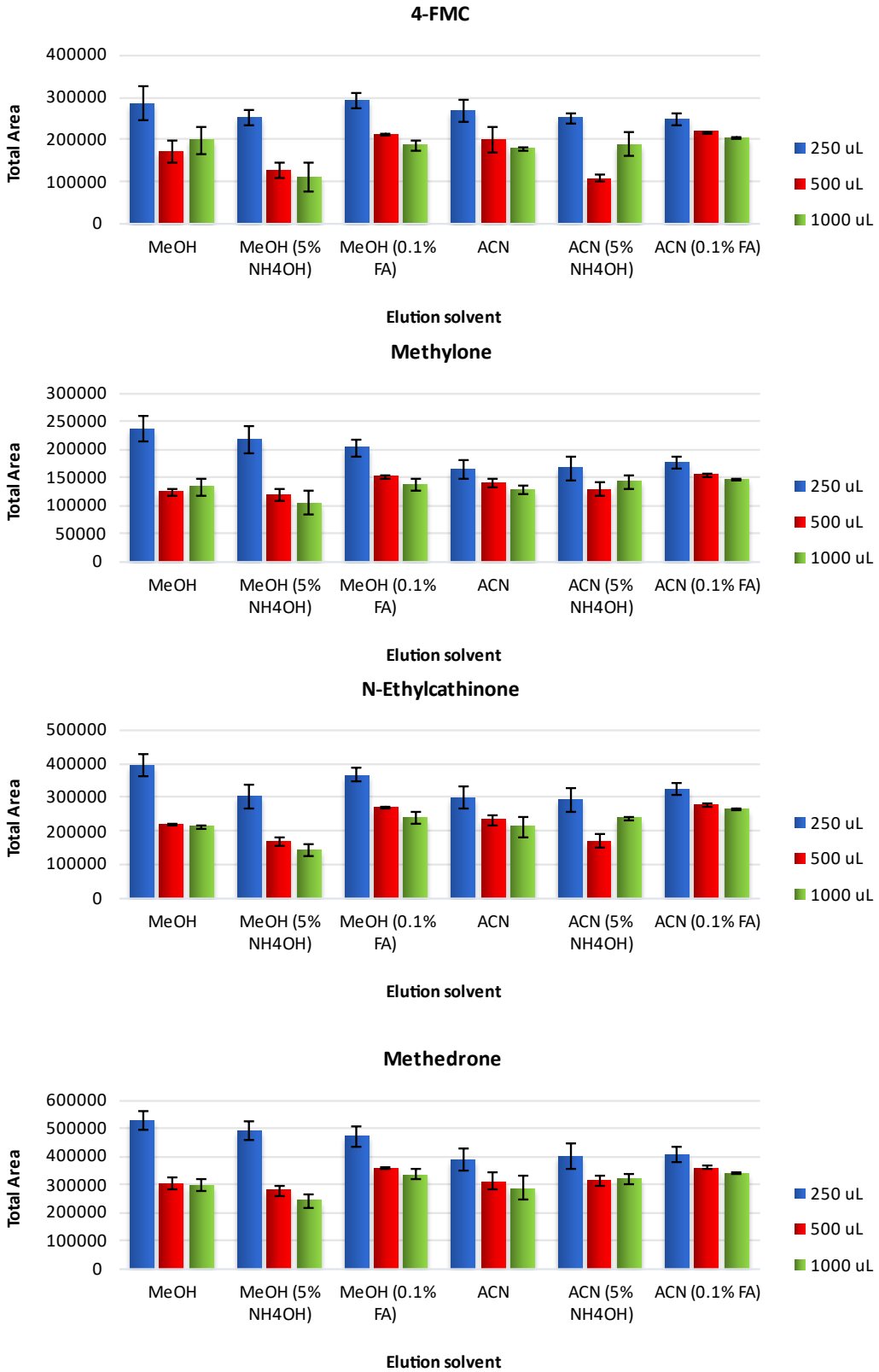
4-FMC
Total Area
400000
300000
200000
100000
0
MeOH
MeOH (5% NH4OH)
MeOH (0.1% FA)
ACN
ACN (5% NH4OH)
ACN (0.1% FA)
Elution solvent
250 uL
500 uL
1000 uL
Methylone
Total Area
300000
250000
200000
150000
100000
50000
0
MeOH
MeOH (5% NH4OH)
MeOH (0.1% FA)
ACN
ACN (5% NH4OH)
ACN (0.1% FA)
Elution solvent
250 uL
500 uL
1000 uL
N-Ethylcathinone
Total Area
500000
400000
300000
200000
100000
0
MeOH
MeOH (5% NH4OH)
MeOH (0.1% FA)
ACN
ACN (5% NH4OH)
ACN (0.1% FA)
Elution solvent
250 uL
500 uL
1000 uL
Methedrone
Total Area
600000
500000
400000
300000
200000
100000
0
MeOH
MeOH (5% NH4OH)
MeOH (0.1% FA)
ACN
ACN (5% NH4OH)
ACN (0.1% FA)
Elution solvent
250 uL
500 uL
1000 uL

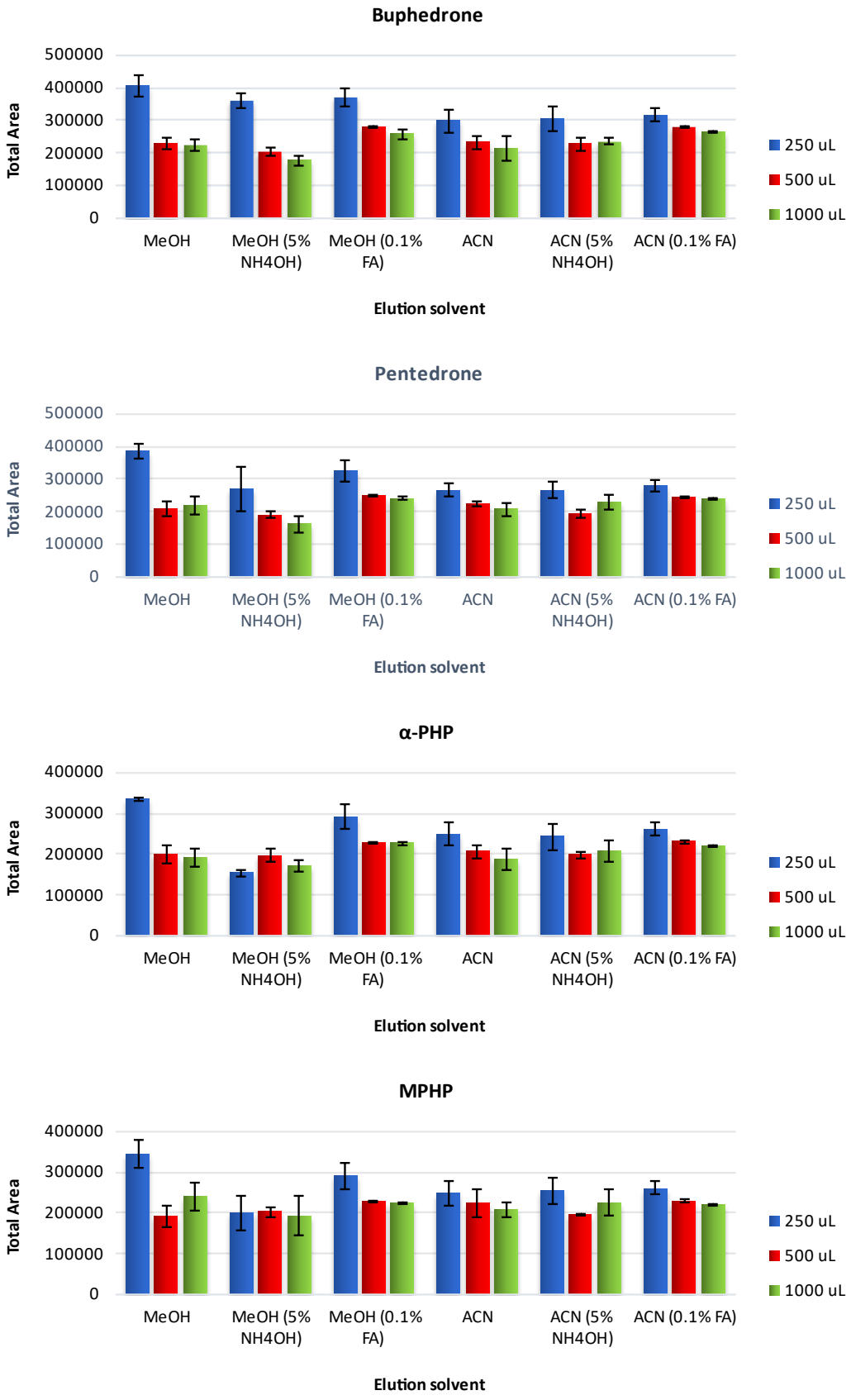

Figure S24. Influence of the elution conditions on the µSPEed® performance for each individual compound.

Validation of the analytical method

1. Selectivity

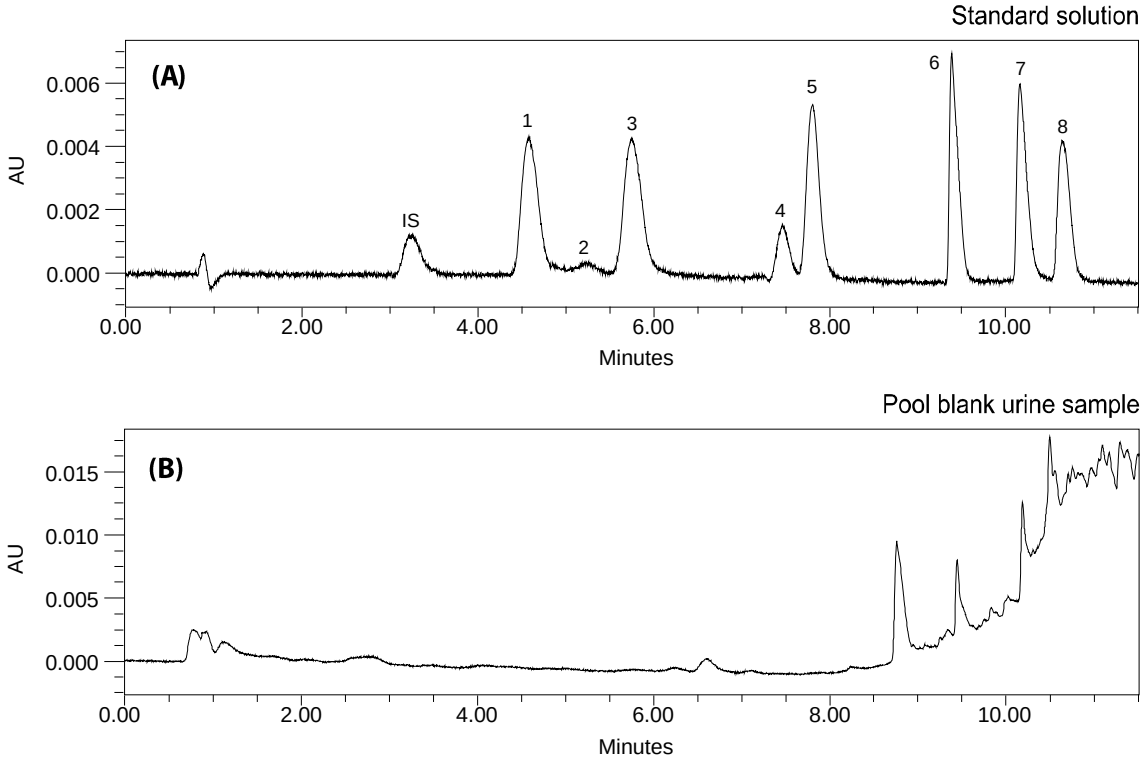

Figure S25. Chromatograms of a typical µSPEeD®–UHPLC/PDA procedure of a (A) SCat standard solution, and a (B) pooled blank urine sample. Peak identification: (IS) internal standard, (1) 4-FMC, (2) methylone, (3) *N*-ethylcathinone, (4) methedrone, (5) buphedrone, (6) pentedrone, (7) α-PHP and (8) MPHP. Some interferences present in blank urine samples coelute with pentedrone, α-PHP and MPHP.

2. Linearity - Statistical regression and residual analysis performed to access linearity

Statistical results of the linearity of 4-FMC

SUMÁRIO DOS RESULTADOS

Estatística de regressão	
R múltiplo	0.999326454
Quadrado de R	0.998653361
Quadrado de R ajustado	0.998384033
Erro-padrão	0.075162673
Observações	7

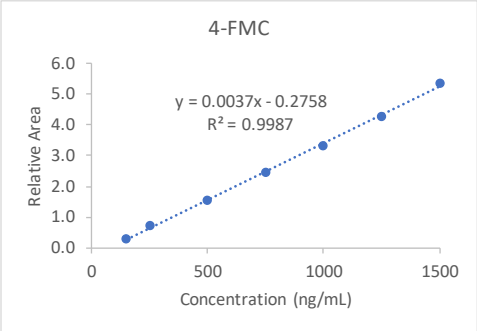

ANOVA

	gl	*SQ*	*MQ*	*F*	*F de significância*
Regressão	1	20.94777872	20.94777872	3707.947217	2.26056E-08
Residual	5	0.028247137	0.005649427		
Total	6	20.97602586			

	Coeficientes	*Erro-padrão*	*Stat t*	*valor P*	*95% inferior*	*95% superior*	*Inferior 95.0%*	*Superior 95.0%*
Interceptar	-0.275806791	0.054627009	-5.048908856	0.003936935	-0.416229989	-0.135383593	-0.416229989	-0.135383593
Variável X 1	0.003683029	6.04837E-05	60.89291599	2.26056E-08	0.003527551	0.003838508	0.003527551	0.003838508

RESULTADO RESIDUAL

Observação	*Y previsto*	*Residuais*
1	0.276647589	-0.004517852
2	0.644950509	0.086557886
3	1.565707808	-0.022460664
4	2.486465108	-0.040582962
5	3.407222407	-0.074197445
6	4.327979707	-0.048406593
7	5.248737006	0.103607631

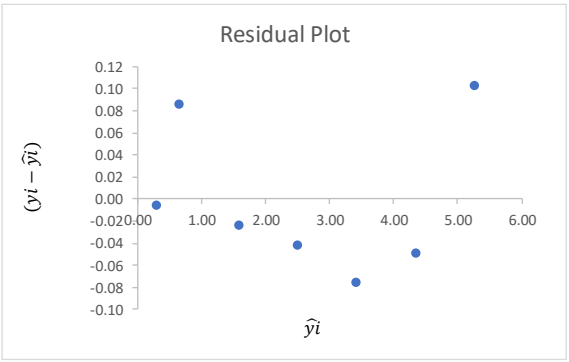

Statistical results of the linearity of Methylone

SUMÁRIO DOS RESULTADOS

Estatística de regressão	
R múltiplo	0.999221298
Quadrado de R	0.998443203
Quadrado de R ajustado	0.998131844
Erro-padrão	0.046195797
Observações	7

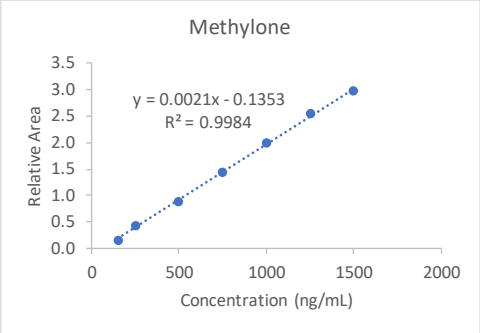

ANOVA

	gl	*SQ*	*MQ*	*F*	*F de significância*
Regressão	1	6.843313012	6.843313012	3206.723174	3.24863E-08
Residual	5	0.010670258	0.002134052		
Total	6	6.853983271			

	Coeficientes	*Erro-padrão*	*Stat t*	*valor P*	*95% inferior*	*95% superior*	*Inferior 95.0%*	*Superior 95.0%*
Interceptar	-0.135313948	0.033574355	-4.03027696	0.010018453	-0.221619575	-0.049008322	-0.221619575	-0.049008322
Variável X 1	0.002105084	3.71739E-05	56.62793634	3.24863E-08	0.002009525	0.002200642	0.002009525	0.002200642

RESULTADO RESIDUAL

Observação	*Y previsto*	*Residuais*
1	0.180448612	-0.032800666
2	0.390956985	0.037414265
3	0.917227919	-0.025653771
4	1.443498853	-0.006259044
5	1.969769786	0.026310666
6	2.49604072	0.058823154
7	3.022311653	-0.057834604

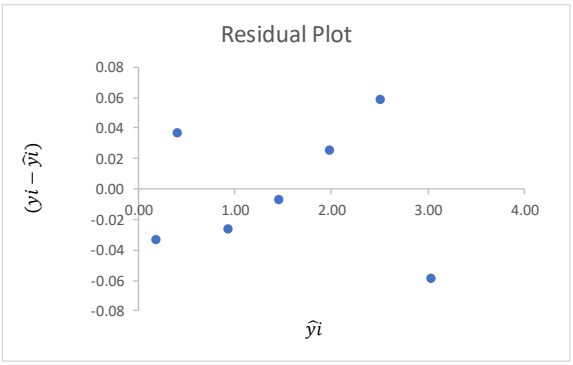

Statistical results of the linearity of *N*-Ethylcathinone

SUMÁRIO DOS RESULTADOS

Estatística de regressão	
R múltiplo	0.999518708
Quadrado de R	0.999037647
Quadrado de R ajustado	0.998845176
Erro-padrão	0.073595357
Observações	7

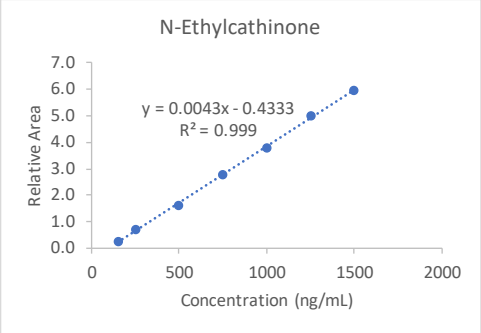

ANOVA

	gl	*SQ*	*MQ*	*F*	*F de significância*
Regressão	1	28.11371593	28.11371593	5190.598264	9.75808E-09
Residual	5	0.027081383	0.005416277		
Total	6	28.14079731			

	Coeficientes	*Erro-padrão*	*Stat t*	*valor P*	*95% inferior*	*95% superior*	*Inferior 95.0%*	*Superior 95.0%*
Interceptar	-0.43329996	0.05348791	-8.100895387	0.000464755	-0.570795008	-0.295804911	-0.570795008	-0.295804911
Variável X 1	0.004266731	5.92225E-05	72.04580671	9.75808E-09	0.004114495	0.004418968	0.004114495	0.004418968

RESULTADO RESIDUAL

Observação	*Y previsto*	*Residuais*
1	0.206709743	0.027489848
2	0.633382879	0.070431537
3	1.700065717	-0.101964451
4	2.766748555	-0.010506611
5	3.833431394	-0.069361264
6	4.900114232	0.077497304
7	5.96679707	0.006413638

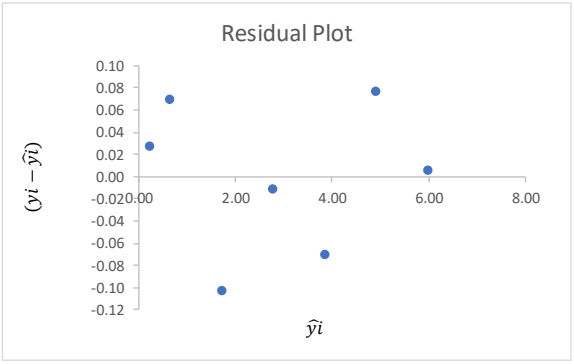

Statistical results of the linearity of Methedrone

SUMÁRIO DOS RESULTADOS

Estatística de regressão	
R múltiplo	0.99979842
Quadrado de R	0.999596881
Quadrado de R ajustado	0.999516258
Erro-padrão	0.054653828
Observações	7

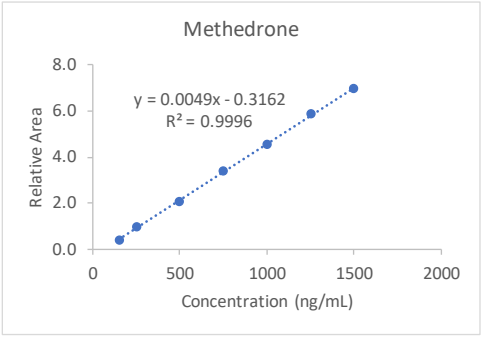

ANOVA

	gl	*SQ*	*MQ*	*F*	*F de significância*
Regressão	1	37.0342092	37.0342092	12398.29344	1.10796E-09
Residual	5	0.014935204	0.002987041		
Total	6	37.04914441			

	Coeficientes	*Erro-padrão*	*Stat t*	*valor P*	*95% inferior*	*95% superior*	*Inferior 95.0%*	*Superior 95.0%*
Interceptar	-0.316162789	0.039721514	-7.959484935	0.000504778	-0.418270191	-0.214055388	-0.418270191	-0.214055388
Variável X 1	0.004897086	4.39802E-05	111.3476243	1.10796E-09	0.004784031	0.00501014	0.004784031	0.00501014

RESULTADO RESIDUAL

Observação	*Y previsto*	*Residuais*
1	0.418400077	-0.031432209
2	0.908108654	0.067069153
3	2.132380097	-0.066892771
4	3.35665154	0.017027463
5	4.580922984	-0.002575812
6	5.805194427	0.056028484
7	7.02946587	-0.039224307

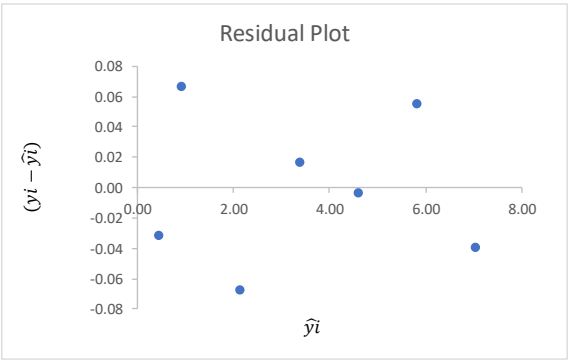

Statistical results of the linearity of Buphedrone

SUMÁRIO DOS RESULTADOS

Estatística de regressão	
R múltiplo	0.999519164
Quadrado de R	0.99903856
Quadrado de R ajustado	0.998846272
Erro-padrão	0.065238756
Observações	7

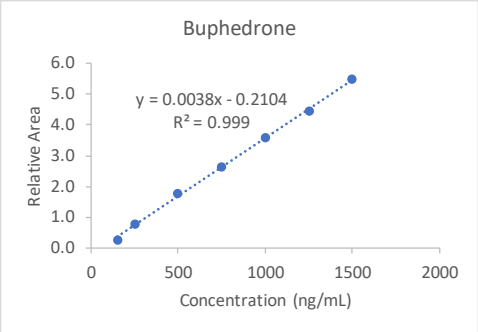

ANOVA

	gl	*SQ*	*MQ*	*F*	*F de significância*
Regressão	1	22.1126844	22.1126844	5195.533201	9.73494E-09
Residual	5	0.021280476	0.004256095		
Total	6	22.13396488			

	Coeficientes	*Erro-padrão*	*Stat t*	*valor P*	*95% inferior*	*95% superior*	*Inferior 95.0%*	*Superior 95.0%*
Interceptar	-0.210431973	0.047414468	-4.438138469	0.006776582	-0.332314742	-0.088549204	-0.332314742	-0.088549204
Variável X 1	0.00378405	5.24979E-05	72.08004718	9.73494E-09	0.0036491	0.003919	0.0036491	0.003919

RESULTADO RESIDUAL

Observação	*Y previsto*	*Residuais*
1	0.35717558	-0.088221877
2	0.735580616	0.031470495
3	1.681593204	0.076586025
4	2.627605792	0.014855794
5	3.573618381	0.021513054
6	4.519630969	-0.074891933
7	5.465643557	0.018688441

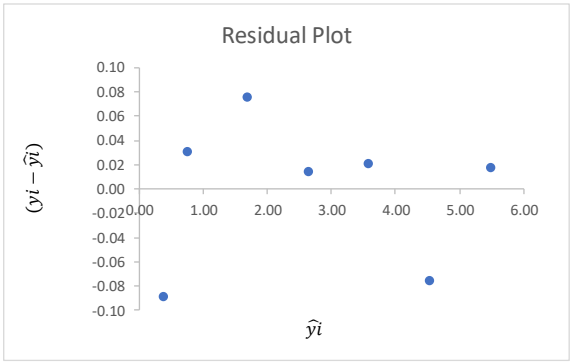

Statistical results of the linearity of Pentedrone

SUMÁRIO DOS RESULTADOS

Estatística de regressão	
R múltiplo	0.998651888
Quadrado de R	0.997305593
Quadrado de R ajustado	0.996766711
Erro-padrão	0.066871309
Observações	7

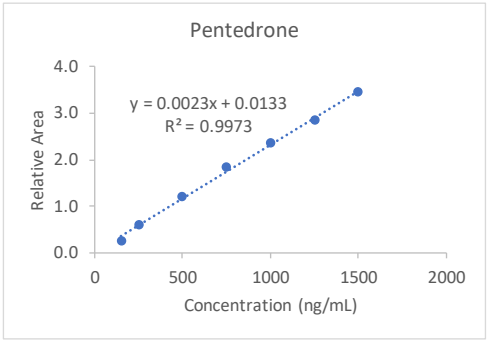

ANOVA

	gl	*SQ*	*MQ*	*F*	*F de significância*
Regressão	1	8.27588875	8.27588875	1850.695622	1.28072E-07
Residual	5	0.02235886	0.004471772		
Total	6	8.29824761			

	Coeficientes	*Erro-padrão*	*Stat t*	*valor P*	*95% inferior*	*95% superior*	*Inferior 95.0%*	*Superior 95.0%*
Interceptar	0.013340254	0.04860098	0.274485287	0.794691472	-0.111592543	0.138273052	-0.111592543	0.138273052
Variável X 1	0.00231496	5.38116E-05	43.01971202	1.28072E-07	0.002176633	0.002453287	0.002176633	0.002453287

RESULTADO RESIDUAL

Observação	*Y previsto*	*Residuais*
1	0.360584257	-0.091421648
2	0.592080259	0.019216405
3	1.170820264	0.03223307
4	1.749560269	0.092322496
5	2.328300274	0.023658984
6	2.907040279	-0.055622864
7	3.485780284	-0.020386443

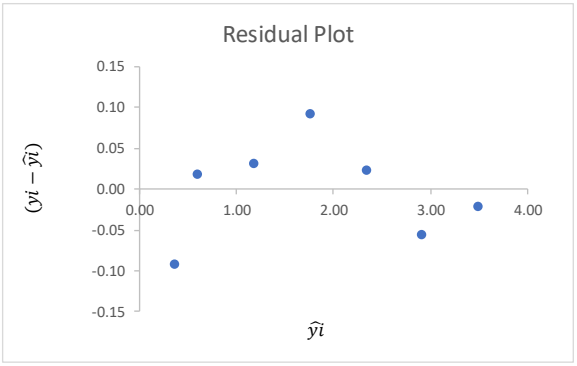

Statistical results of the linearity of α-PHP

SUMÁRIO DOS RESULTADOS

Estatística de regressão	
R múltiplo	0.998673012
Quadrado de R	0.997347785
Quadrado de R ajustado	0.996817342
Erro-padrão	0.066807834
Observações	7

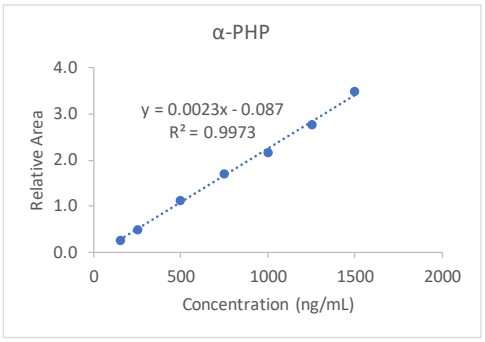

ANOVA

	gl	*SQ*	*MQ*	*F*	*F de significância*
Regressão	1	8.391945965	8.391945965	1880.216638	1.23115E-07
Residual	5	0.022316434	0.004463287		
Total	6	8.414262399			

	Coeficientes	*Erro-padrão*	*Stat t*	*valor P*	*95% inferior*	*95% superior*	*Inferior 95.0%*	*Superior 95.0%*
Interceptar	-0.087024952	0.048554848	-1.792302019	0.133069968	-0.211839163	0.037789258	-0.211839163	0.037789258
Variável X 1	0.002331135	5.37605E-05	43.3614649	1.23115E-07	0.00219294	0.002469331	0.00219294	0.002469331

RESULTADO RESIDUAL

Observação	*Y previsto*	*Residuais*
1	0.262645368	-0.001403405
2	0.495758915	0.003664171
3	1.078542782	0.03459609
4	1.66132665	0.031237138
5	2.244110517	-0.086564746
6	2.826894384	-0.06970875
7	3.409678252	0.088179502

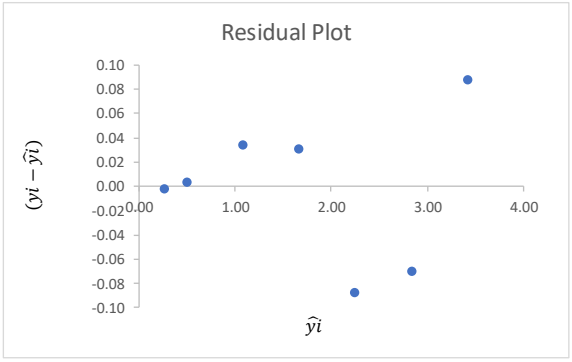

Statistical results of the linearity of MPHP

SUMÁRIO DOS RESULTADOS

Estatística de regressão	
R múltiplo	0.999117023
Quadrado de R	0.998234825
Quadrado de R ajustado	0.99788179
Erro-padrão	0.063902854
Observações	7

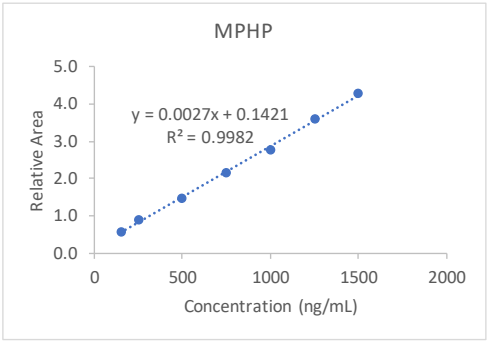

ANOVA

	gl	*SQ*	*MQ*	*F*	*F de significância*
Regressão	1	11.54663717	11.54663717	2827.580689	4.44756E-08
Residual	5	0.020417874	0.004083575		
Total	6	11.56705505			

	Coeficientes	*Erro-padrão*	*Stat t*	*valor P*	*95% inferior*	*95% superior*	*Inferior 95.0%*	*Superior 95.0%*
Interceptar	0.14212917	0.046443556	3.060255986	0.028093818	0.022742209	0.261516131	0.022742209	0.261516131
Variável X 1	0.002734412	5.14229E-05	53.17500061	4.44756E-08	0.002602225	0.002866599	0.002602225	0.002866599

RESULTADO RESIDUAL

Observação	*Y previsto*	*Residuais*
1	0.552290952	0.011080583
2	0.825732141	0.067811033
3	1.509335111	-0.038071988
4	2.192938082	-0.038757642
5	2.876541053	-0.0922602
6	3.560144023	0.054190967
7	4.243746994	0.036007248

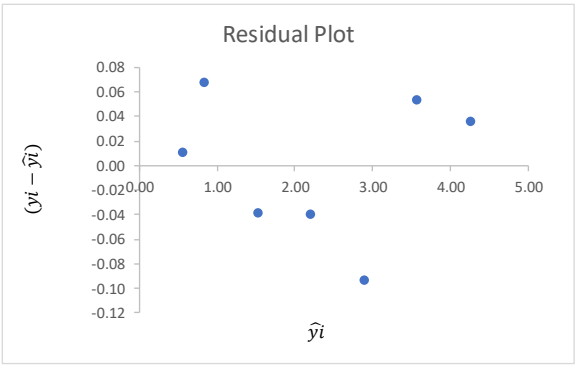

3. Matrix Effect

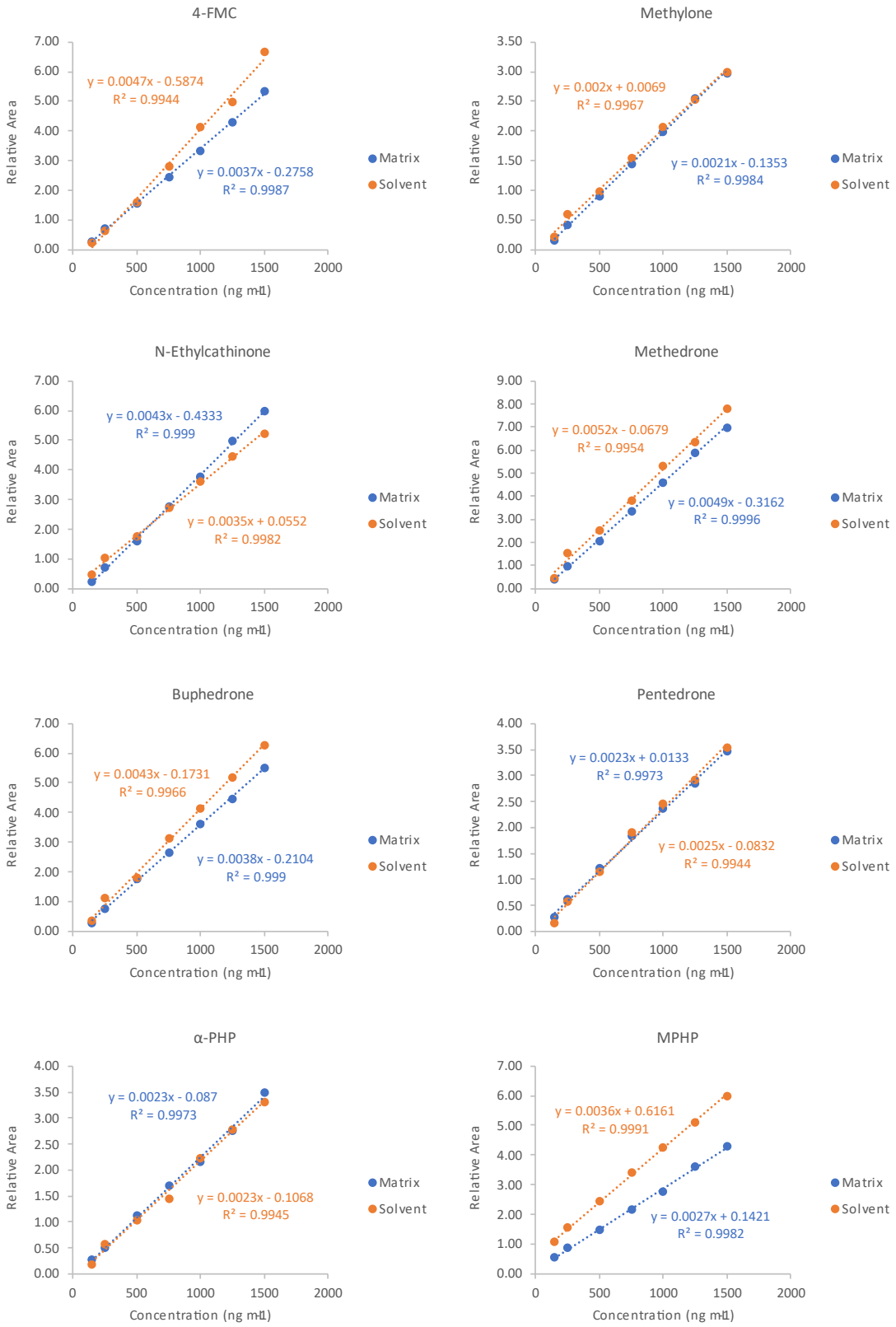

Figure S26. Calibration curves obtained for each SCat performed in matrix and in solvent for the matrix effect study.

4. SCat Stability

Table S1. Stability study performed at –80°C.

Time (days)	Low level							
	4-FMC	Methylone	*N*-Ethylcathinone	Methedrone	Buphedrone	Pentedrone	α-PHP	MPHP
1	100.0 ± 0.7	100.0 ± 1.2	100.0 ± 1.6	100.0 ± 0.8	100.0 ± 1.6	100.0 ± 1.1	100.0 ± 6.1	100.0 ± 5.8
7	93.1 ± 2.1	95.0 ± 3.0	104.8 ± 0.6	96.7 ± 1.4	103.0 ± 3.5	82.2 ± 18.2	83.5 ± 1.7	81.2 ± 7.8
15	95.8 ± 2.0	106.9 ± 1.7	106.1 ± 2.4	101.7 ± 2.8	105.9 ± 2.4	99.2 ± 2.2	102.2 ± 4.3	82.2 ± 4.8
30	92.3 ± 5.7	93.0 ± 7.2	109.9 ± 2.0	95.8 ± 1.7	99.0 ± 2.8	82.0 ± 3.8	98.2 ± 7.8	86.2 ± 10.4
60	99.0 ± 2.4	100.8 ± 18.0	114.7 ± 1.1	109.6 ± 9.6	99.7 ± 4.8	85.8 ± 6.3	80.1 ± 6.0	84.1 ± 12.0
90	96.4 ± 3.1	95.7 ± 10.1	106.4 ± 1.2	91.9 ± 0.4	100.6 ± 0.9	91.7 ± 8.9	83.1 ± 3.6	94.3 ± 9.3

Time (days)	Medium Level							
	4-FMC	Methylone	*N*-Ethylcathinone	Methedrone	Buphedrone	Pentedrone	α-PHP	MPHP
1	100.0 ± 4.3	100.0 ± 6.2	100.0 ± 3.9	100.0 ± 2.7	100.0 ± 1.6	100.0 ± 4.8	100.0 ± 12.5	100.0 ± 4.0
7	92.6 ± 2.8	86.2 ± 1.0	90.2 ± 1.5	98.8 ± 1.1	99.9 ± 1.0	80.1 ± 2.2	86.7 ± 1.5	93.8 ± 11.5
15	96.7 ± 4.3	91.3 ± 4.7	94.7 ± 5.6	103.8 ± 7.8	105.6 ± 9.2	85.8 ± 9.3	85.7 ± 8.1	97.5 ± 16.8
30	96.3 ± 0.9	95.8 ± 3.5	97.6 ± 1.9	108.1 ± 2.9	108.0 ± 1.4	103.3 ± 3.1	85.8 ± 1.6	106.4 ± 16.4
60	118.7 ± 3.0	111.9 ± 1.8	123.9 ± 16.8	126.5 ± 2.8	116.0 ± 9.3	115.9 ± 5.6	82.1 ± 7.8	87.3 ± 2.8
90	107.4 ± 2.1	95.7 ± 3.8	100.6 ± 3.0	97.3 ± 4.1	102.2 ± 3.8	102.5 ± 3.0	68.4 ± 4.0	83.9 ± 15.8

Time (days)	High Level							
	4-FMC	Methylone	*N*-Ethylcathinone	Methedrone	Buphedrone	Pentedrone	α-PHP	MPHP
1	100.0 ± 2.5	100.0 ± 9.3	100.0 ± 4.0	100.0 ± 8.8	100.0 ± 1.0	100.0 ± 5.2	100.0 ± 18.2	100.0 ± 4.4
7	83.9 ± 2.0	81.5 ± 3.5	83.6 ± 3.7	83.1 ± 3.2	100.1 ± 4.1	84.8 ± 13.3	79.7 ± 7.9	106.1 ± 6.7
15	91.8 ± 0.9	91.1 ± 1.4	90.3 ± 0.3	92.3 ± 0.5	113.7 ± 2.2	97.5 ± 2.1	83.7 ± 13.1	100.5 ± 4.6
30	94.6 ± 2.1	101.7 ± 0.5	99.1 ± 1.0	106.5 ± 1.8	108.1 ± 8.0	122.9 ± 5.8	90.6 ± 2.0	98.7 ± 7.4
60	113.5 ± 5.1	110.4 ± 8.7	82.7 ± 5.5	112.6 ± 6.9	115.3 ± 12.4	118.0 ± 15.8	83.2 ± 13.7	85.3 ± 4.7
90	77.0 ± 1.1	74.9 ± 0.4	74.4 ± 1.1	69.0 ± 2.8	86.3 ± 0.8	78.3 ± 0.9	85.7 ± 16.2	72.6 ± 2.9

Table S2. Stability study performed at –20°C.

Time (days)	Low level							
	4-FMC	Methylone	*N*-Ethylcathinone	Methedrone	Buphedrone	Pentedrone	α-PHP	MPHP
1	100.0 ± 0.7	100.0 ± 1.2	100.0 ± 1.6	100.0 ± 0.8	100.0 ± 1.6	100.0 ± 1.1	100.0 ± 6.1	100.0 ± 5.8
7	97.5 ± 3.5	102.9 ± 5.9	111.1 ± 2.2	105.5 ± 1.1	113.0 ± 2.1	86.9 ± 1.6	97.2 ± 3.3	93.2 ± 12.6
15	98.1 ± 0.6	104.0 ± 5.3	108.4 ± 1.8	97.1 ± 1.1	104.5 ± 2.7	83.9 ± 3.0	94.0 ± 4.7	81.6 ± 17.1
30	101.9 ± 4.7	106.1 ± 4.7	103.8 ± 7.3	103.5 ± 2.0	106.2 ± 0.9	84.2 ± 3.5	97.3 ± 2.2	87.2 ± 5.1
60	101.9 ± 5.1	98.7 ± 10.4	104.1 ± 5.0	119.9 ± 10.7	110.3 ± 5.3	103.6 ± 9.8	81.0 ± 5.4	88.0 ± 11.6
90	97.5 ± 3.9	98.4 ± 5.9	110.1 ± 3.0	94.8 ± 1.5	102.6 ± 5.3	101.3 ± 4.8	82.6 ± 3.7	52.0 ± 4.8

Time (days)	Medium Level							
	4-FMC	Methylone	*N*-Ethylcathinone	Methedrone	Buphedrone	Pentedrone	α-PHP	MPHP
1	100.0 ± 4.3	100.0 ± 6.2	100.0 ± 3.9	100.0 ± 2.7	100.0 ± 1.6	100.0 ± 4.8	100.0 ± 12.5	100.0 ± 4.0
7	84.1 ± 1.9	82.6 ± 1.3	83.8 ± 2.8	91.0 ± 3.4	89.9 ± 2.5	81.6 ± 2.3	89.6 ± 3.5	101.7 ± 3.8
15	90.2 ± 2.0	84.7 ± 2.0	90.1 ± 1.9	95.3 ± 2.4	96.4 ± 0.7	75.7 ± 1.3	91.2 ± 2.2	98.4 ± 8.4
30	110.0 ± 5.0	103.1 ± 6.7	111.0 ± 3.8	115.3 ± 6.6	116.3 ± 6.3	109.6 ± 7.5	108.8 ± 6.9	84.4 ± 4.9
60	120.2 ± 3.8	121.6 ± 4.4	116.3 ± 6.7	111.4 ± 3.5	117.3 ± 10.9	104.7 ± 13.2	119.4 ± 5.6	85.5 ± 5.4
90	92.3 ± 4.6	88.7 ± 5.2	92.3 ± 4.0	91.7 ± 2.1	94.8 ± 5.3	80.4 ± 3.8	65.7 ± 5.7	52.4 ± 5.6

Time (days)	High Level							
	4-FMC	Methylone	*N*-Ethylcathinone	Methedrone	Buphedrone	Pentedrone	α-PHP	MPHP
1	100.0 ± 2.5	100.0 ± 9.3	100.0 ± 4.0	100.0 ± 8.8	100.0 ± 1.0	100.0 ± 5.2	100.0 ± 18.2	100.0 ± 4.4
7	87.6 ± 0.3	96.4 ± 0.2	89.5 ± 1.5	100.0 ± 1.4	121.7 ± 1.2	113.3 ± 2.5	87.6 ± 1.6	94.5 ± 6.6
15	87.5 ± 1.1	89.6 ± 1.7	88.3 ± 1.4	89.6 ± 2.5	108.7 ± 2.1	94.2 ± 3.0	91.7 ± 3.7	93.2 ± 9.3
30	100.3 ± 2.7	105.3 ± 4.1	103.3 ± 3.8	106.8 ± 4.1	107.8 ± 17.7	112.4 ± 14.0	85.0 ± 5.6	83.1 ± 2.7
60	102.6 ± 14.0	120.9 ± 24.3	79.5 ± 7.4	113.2 ± 22.1	116.7 ± 10.2	111.2 ± 13.2	123.7 ± 4.1	80.4 ± 14.6
90	86.4 ± 3.8	84.3 ± 4.8	85.3 ± 4.1	79.2 ± 3.6	96.8 ± 4.6	108.8 ± 5.2	102.1 ± 13.1	59.9 ± 14.0

Table S3. Stability study performed at 4°C.

Time (days)	Low level							
	4-FMC	Methylone	*N*-Ethylcathinone	Methedrone	Buphedrone	Pentedrone	α-PHP	MPHP
1	100.0 ± 0.7	100.0 ± 1.2	100.0 ± 1.6	100.0 ± 0.8	100.0 ± 1.6	100.0 ± 1.1	100.0 ± 6.1	100.0 ± 5.8
7	93.7 ± 2.6	100.9 ± 3.9	106.4 ± 2.3	101.1 ± 2.6	104.8 ± 4.0	74.8 ± 3.3	97.4 ± 1.9	74.5 ± 8.9
15	97.9 ± 5.6	116.5 ± 4.1	112.5 ± 1.8	110.6 ± 5.7	116.4 ± 1.5	89.0 ± 2.3	110.1 ± 5.8	60.2 ± 4.4
30	95.3 ± 3.6	112.3 ± 11.3	109.7 ± 4.7	110.3 ± 2.6	109.6 ± 1.0	73.9 ± 2.3	95.8 ± 5.4	65.9 ± 1.7
60	98.3 ± 15.4	114.7 ± 16.2	102.8 ± 3.1	120.1 ± 2.1	115.9 ± 3.8	87.1 ± 8.6	101.1 ± 10.3	52.8 ± 4.5
90	71.4 ± 3.7	88.2 ± 5.3	88.8 ± 1.1	84.8 ± 3.8	85.6 ± 0.5	90.1 ± 10.7	98.4 ± 5.8	63.6 ± 4.4

Time (days)	Medium Level							
	4-FMC	Methylone	*N*-Ethylcathinone	Methedrone	Buphedrone	Pentedrone	α-PHP	MPHP
1	100.0 ± 4.3	100.0 ± 6.2	100.0 ± 3.9	100.0 ± 2.7	100.0 ± 1.6	100.0 ± 4.8	100.0 ± 12.5	100.0 ± 4.0
7	101.3 ± 3.0	104.7 ± 1.0	104.4 ± 2.6	120.3 ± 4.5	117.0 ± 2.4	95.0 ± 8.7	124.3 ± 3.0	85.0 ± 3.8
15	95.7 ± 1.9	108.1 ± 2.9	103.1 ± 2.6	126.7 ± 2.9	122.8 ± 0.3	102.5 ± 4.1	130.1 ± 3.5	93.7 ± 2.8
30	85.3 ± 2.4	101.3 ± 1.2	90.8 ± 0.6	113.7 ± 0.5	111.2 ± 2.0	111.9 ± 3.2	110.1 ± 1.6	93.7 ± 2.8
60	87.2 ± 3.5	110.4 ± 7.9	109.1 ± 3.9	129.0 ± 8.2	123.8 ± 6.2	122.4 ± 11.5	123.3 ± 7.6	69.2 ± 1.3
90	72.8 ± 3.5	110.9 ± 7.2	86.4 ± 3.6	117.3 ± 8.0	119.8 ± 6.6	111.2 ± 7.0	55.6 ± 6.1	39.4 ± 3.8

Time (days)	High Level							
	4-FMC	Methylone	*N*-Ethylcathinone	Methedrone	Buphedrone	Pentedrone	α-PHP	MPHP
1	100.0 ± 2.5	100.0 ± 9.3	100.0 ± 4.0	100.0 ± 8.8	100.0 ± 1.0	100.0 ± 5.2	100.0 ± 18.2	100.0 ± 4.4
7	96.0 ± 1.9	108.6 ± 4.8	101.0 ± 4.2	114.7 ± 2.8	137.0 ± 3.7	151.8 ± 4.4	108.5 ± 4.6	119.8 ± 2.5
15	86.4 ± 2.1	97.8 ± 3.1	89.5 ± 2.7	101.3 ± 4.3	120.9 ± 3.4	113.6 ± 1.4	86.7 ± 3.6	94.0 ± 4.1
30	91.7 ± 0.9	114.7 ± 2.1	99.4 ± 1.2	119.3 ± 1.0	143.2 ± 2.8	151.5 ± 4.5	123.9 ± 2.4	138.2 ± 0.9
60	101.5 ± 2.3	118.7 ± 26.6	84.9 ± 3.1	117.9 ± 16.9	148.1 ± 29.2	128.0 ± 18.6	146.1 ± 3.1	141.4 ± 0.4

90	51.7 ± 1.8	75.6 ± 3.9	59.6 ± 3.0	76.7 ± 5.1	89.6 ± 4.8	78.4 ± 3.9	46.3 ± 4.5	28.0 ± 2.6

Table S4. Stability study performed at room temperature.

Time (days)	Low level							
	4-FMC	Methylone	*N*-Ethylcathinone	Methedrone	Buphedrone	Pentedrone	α-PHP	MPHP
1	100.0 ± 0.7	100.0 ± 1.2	100.0 ± 1.6	100.0 ± 0.8	100.0 ± 1.6	100.0 ± 1.1	100.0 ± 6.1	100.0 ± 5.8
7	59.0 ± 0.7	73.0 ± 5.0	71.9 ± 0.8	81.2 ± 3.2	82.2 ± 2.6	49.5 ± 23.5	70.6 ± 6.1	15.3 ± 5.5
15	0.0 ± 0.0	64.6 ± 3.5	0.0 ± 0.0	80.9 ± 4.2	65.4 ± 1.8	68.1 ± 5.9	75.8 ± 3.8	45.7 ± 7.6
30	0.0 ± 0.0	0.0 ± 0.0	0.0 ± 0.0	0.0 ± 0.0	0.0 ± 0.0	0.0 ± 0.0	0.0 ± 0.0	50.9 ± 10.7

Time (days)	Medium Level							
	4-FMC	Methylone	*N*-Ethylcathinone	Methedrone	Buphedrone	Pentedrone	α-PHP	MPHP
1	100.0 ± 4.3	100.0 ± 6.2	100.0 ± 3.9	100.0 ± 2.7	100.0 ± 1.6	100.0 ± 4.8	100.0 ± 12.5	100.0 ± 4.0
7	21.9 ± 0.5	51.8 ± 1.5	27.5 ± 0.1	66.4 ± 0.6	54.7 ± 0.5	40.7 ± 0.4	85.5 ± 2.1	52.1 ± 1.9
15	0.0 ± 0.0	38.3 ± 1.1	0.0 ± 0.0	54.9 ± 0.4	37.9 ± 0.4	37.8 ± 4.0	96.3 ± 1.0	45.1 ± 3.1
30	0.0 ± 0.0	0.0 ± 0.0	0.0 ± 0.0	0.0 ± 0.0	0.0 ± 0.0	0.0 ± 0.0	0.0 ± 0.0	38.9 ± 6.7

Time (days)	High Level							
	4-FMC	Methylone	*N*-Ethylcathinone	Methedrone	Buphedrone	Pentedrone	α-PHP	MPHP
1	100.0 ± 2.5	100.0 ± 9.3	100.0 ± 4.0	100.0 ± 8.8	100.0 ± 1.0	100.0 ± 5.2	100.0 ± 18.2	100.0 ± 4.4
7	15.5 ± 0.5	50.4 ± 2.1	23.3 ± 1.0	59.7 ± 1.5	59.7 ± 0.9	52.1 ± 3.0	62.9 ± 1.4	44.3 ± 2.4
15	0.0 ± 0.0	31.7 ± 3.5	0.0 ± 0.0	44.0 ± 4.5	33.2 ± 3.3	74.7 ± 1.9	80.7 ± 8.8	61.0 ± 7.3
30	0.0 ± 0.0	0.0 ± 0.0	0.0 ± 0.0	0.0 ± 0.0	4.8 ± 1.0	0.0 ± 0.0	36.7 ± 1.4	22.6 ± 0.9

5. Analysis of real samples by GC-MS

Table S5. List of substances detected in urine samples by GC-MS.

Compounds	RT (min)	KI_{calc}	$KI_{Lit.}$	MF	MW	Ions (m/z)	Samples									
							2230	4514	6947	4184	3572	1295	4639	5248	5218	6754
Bupropion	16.17	1719	1756[a]	$C_{13}H_{18}ClNO$	239	**44**, 100, 77, 57						X				
α-PHP	17.95	1874	1880[b]	$C_{16}H_{23}NO$	245	**140**, 77, 105, 41	X	X		X	X	X	X	X		
EDDP	19.28	2000	2005[c]	$C_{20}H_{24}N$	278	**277**, 276, 262, 220			X	X			X			X
2''-oxo-α-PHP	19.34	2014	-	$C_{16}H_{21}NO_2$	259	**154**, 98, 86, 77	X	X		X	X	X	X	X		
Venlafaxine	19.60	2050	2056[a]	$C_{17}H_{27}NO_2$	277	**58**, 134, 91, 44									X	
Methadone	19.93	2109	2121[c]	$C_{21}H_{27}NO$	309	**72**, 165, 91, 294			X	X			X			X
Norvenlafaxine	19.97	2110	2108[a]	$C_{16}H_{25}NO_2$	263	**58**, 120, 52, 134									X	
Mirtazepine	20.51	2222	2323[a]	$C_{17}H_{19}N_3$	265	**195**, 208, 43, 180										X

Note: no compounds were detected in samples 752, 7088, 1829, 5584 and 2588. Bold numbers represent the base peak ion.

Abbreviations: EDDP - 2-ethylidene-1,5-dimethyl-3,3-diphenylpyrrolidine, MF - molecular formula, MW - molecular weight, KI_{calc} - Kováts retention index calculated, KI_{Lit} - Kováts retention index found in literature and RT - Retention time.

[a] NIST Mass Spectral Library 2014

[b] Sisco et al. [426]

[c] Phillips et al. [521]

Cytotoxicity Studies of Synthetic Cathinones in HepG2 cell line

1. Physicochemical properties of SCat

Table S6. Logarithmic values of the acid dissociation constant (pK_a) and the partition coefficient (Log P) of each SCat studied.

Compound	Chemical structure	pk_a*	Log P*
MPHP	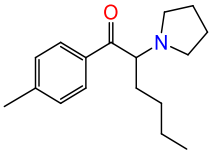	7.94	3.81
α-PHP	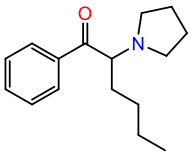	7.90	3.35
4-FMC	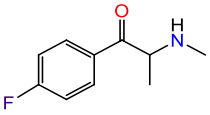	7.98	1.54
Methedrone	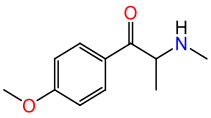	8.01	1.15
Methylone	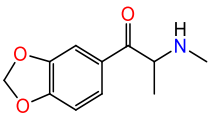	7.96	1.08
N-Ethylcathinone	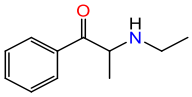	8.11	1.74
Buphedrone	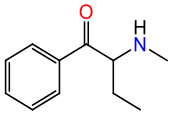	8.18	1.87
Pentedrone	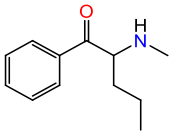	8.20	2.26

*pK_a and log P values were determined by MarvinSketch v.21.3 software (ChemAxon, Budapest, Hungary).